

# THE JOURNAL OF PHYSICAL CHEMISTRY

(Registered in U. S. Patent Office)

## CONTENTS

H. J. Marrinan and J. J. Hermans: Dimensions and Hydrodynamic Properties of Cellulosic Molecules in Dilute Solutions	385	B. J. Fontana and J. R. Thomas: The Configuration of Adsorbed Alkyl Methacrylate Polymers by Infrared and Sedimentation Studies	480
Makoto Suzuki and Philip J. Elving: Kinetics and Mechanism for the Electrochemical Reduction of Benzophenone in Acidic Media	391	W. I. Higuchi: Effects of Short Range Surface-Segment Forces on the Configuration of an Adsorbed Flexible Chain Polymer	487
L. E. Trevorow, W. E. Shinn and R. K. Steunenberg: The Thermal Decomposition of Plutonium Hexafluoride	398	Ernest Lustig: A Nuclear Magnetic Resonance Study of <i>syn-anti</i> Isomerism in Ketoximes	491
Leonard C. Labowitz and Edgar F. Westrum, Jr.: A Thermodynamic Study of the System Ammonium Fluoride-Water. I. The Heat Capacity and Thermodynamic Functions of Ammonium Fluoride Monohydrate	403	H. M. Huffman, M. E. Gross, D. W. Scott, and J. P. McCullough: Low Temperature Thermodynamic Properties of Six Isomeric Heptanes	495
Leonard C. Labowitz and Edgar F. Westrum, Jr.: A Thermodynamic Study of the System Ammonium Fluoride-Water. II. The Solid Solution of Ammonium Fluoride in Ice	408	H. O. Pritchard: The Kinetics of Dissociation of a Diatomic Gas	504
Burton Fine: Kinetics of Hydrogen Oxidation Downstream of Lean Propane and Hydrogen Flames	414	Wayne E. Bell, Ulrich Merten and M. Tagami: The Palladium-Chlorine System at High Temperature	510
P. B. Weisz and W. P. Kern: Hydrocarbon Synthesis on Pure Iron	417	Wayne E. Bell, M. C. Garrison and Ulrich Merten: Thermodynamic Properties of Gaseous Ruthenium Chlorides at High Temperatures	517
Leo Brewer, Thomas R. Simonson and Lee Karl J. Tong: A Vapor Phase Equilibrator for Activity Coefficient Determinations	420	Daniel Cubicciotti: The Equilibrium: $2/3\text{Bi}(l) + 1/3\text{Bi}_2(g) = \text{Bi}(g)$	521
Simao Mathias, Eurico de Carvalho Filho and Renato G. Cecchini: The Dipole Moments of Cyclohexanethiol, $\alpha$ -Toluenethiol and Benzenethiol	425	Edward P. Egan, Jr., and Basil B. Luff: Heat of Solution of Orthophosphoric Acid	523
Edward F. Casassa and Henryk Eisenberg: Partial Specific Volumes and Refractive Index Increments in Multicomponent Systems	427	Robert Reid and Robert Wheeler: Hydrogen Atom Excesses in Some Propane Flames	527
J. L. Bethune and Gerson Kegeles: Countercurrent Distribution of Chemically Reacting Systems. I. Polymerization	431	Martin Kilpatrick and Max W. Meyer: The Kinetics of the Reactions of Aromatic Hydrocarbons in Sulfuric Acid. II. Toluene, Pseudocumene and Hemimellitene	530
W. J. Thomas and I. A. Furzer: The Computation of the Path Difference Function for the Calculation of Diffusion Coefficients by the Gouy Method	438	W. A. Rosser, Jr., and H. Wise: The Rate of Reaction of Hydrogen with Nitrogen Dioxide	532
Armine D. Paul, Linda S. Gallo and Jean B. VanCamp: The Fluoride Complexing of Yttrium(III) in Aqueous Solution	441	Theodore P. Yin, Stuart E. Lovell and John D. Ferry: Viscoelastic Properties of Polyethylene Oxide in the Rubber-like State	534
Reinhard W. Hoffman and G. W. Brindley: Infrared Extinction Coefficients of Ketones Adsorbed on Ca-Montmorillonite in Relation to Surface Coverage (Clay-organic Studies, Part IV)	443	J. R. Ferraro and D. F. Peppard: An Infrared and Isopiestic Investigation of the Interaction between Tri- <i>n</i> -butyl Phosphate and Mono-(2-ethylhexyl)-phosphoric Acid	539
Marianne K. Bennett and W. A. Zisman: Synergistic Surface Tension Effects from Mixtures of Fluorinated Alcohols with Conventional Wetting Agents	448	R. A. Robinson, J. M. Stokes and R. H. Stokes: Potassium Hexafluorophosphate—an Associated Electrolyte	542
P. J. Proll, L. H. Sutcliffe and J. Walkley: Species of Cobalt(II) in Acetic Acid. I. Cobaltous Acetate in the Presence of Water and of Sodium Acetate	455	E. J. Smutny and A. Bondi: Ditertiary Butyl Ether: Strain Energy and Physical Properties	546
F. R. Duke and H. M. Garfinkel: Complex Ions in Fused Salts. Silver Halides	461	Oliver N. Salmon: High Temperature Thermodynamics of the Iron Oxide System	550
John M. Holland and John G. Miller: Hydrolysis of Alkyl Acetates in a Phosphate-Buffered Aqueous Medium	463	Richard G. Yalman: Kinetics of the Reaction between Hydrogen Peroxide and Aquo-(ethylenediamine-tetraaceto)-cobalt(II) and Evidence for the Formation of a Peroxidocobalt(III, III) Complex	556
S. M. E. Kellner and W. D. Walters: The Thermal Decomposition of <i>n</i> -Propylcyclobutane	466	Arvin S. Quist and Henry S. Frank: Ice VIII—An Acetone Hydrate?	560
R. S. Ondrejcin and T. P. Garrett, Jr.: The Thermal Decomposition of Anhydrous Uranyl Nitrate and Uranyl Nitrate Dihydrate	470	J. S. Waugh and F. A. Cotton: Interpretation of the Magnetic Resonance Spectrum of the Methylene Group in Certain Unsymmetrically Substituted Compounds	562
W. H. Reinmuth: Diffusion to a Plane with Langmuirian Adsorption	473	J. F. Harrod and J. Halpern: $\text{D}_2\text{O}$ Isotope Effects in the Catalytic Activation of Molecular Hydrogen by Metal Ions	563
Abbas Labbauf and Frederick D. Rossini: Heats of Combustion, Formation, and Hydrogenation of Fourteen Cyclomonocyclic Hydrocarbons	476	Emilian B. Weroniski: Polarographic and Coulometric Investigations on the Reduction Rate of Cobalt(II) Ions in the Presence of Cystine	564
		Jean H. Futrell: Secondary Processes in Gas Phase Radiolysis of Hydrocarbons	565
		James M. Peterson and Robert M. Mazo: Remarks on the Archibald Method of Molecular Weight Determination in the Ultracentrifuge	566

# THE JOURNAL OF PHYSICAL CHEMISTRY

(Registered in U. S. Patent Office)

W. ALBERT NOYES, JR., EDITOR

ALLEN D. BLISS

ASSISTANT EDITORS

A. B. F. DUNCAN

EDITORIAL BOARD

A. O. ALLEN  
C. E. H. BAWN  
J. BIGEISEN  
D. D. ELEY

D. H. EVERETT  
S. C. LIND  
F. A. LONG  
K. J. MYSELS

J. E. RICCI  
R. E. RUNDLE  
W. H. STOCKMAYER  
A. R. UBBELOHDE

E. R. VAN ARTSDALEN  
M. B. WALLENSTEIN  
W. WEST  
EDGAR F. WESTRUM, JR.

Published monthly by the American Chemical Society at 20th and Northampton Sts., Easton, Pa.

Second-class mail privileges authorized at Easton, Pa. This publication is authorized to be mailed at the special rates of postage prescribed by Section 131.122.

The *Journal of Physical Chemistry* is devoted to the publication of selected symposia in the broad field of physical chemistry and to other contributed papers.

Manuscripts originating in the British Isles, Europe and Africa should be sent to F. C. Tompkins, The Faraday Society, 6 Gray's Inn Square, London W. C. 1, England. Manuscripts originating elsewhere should be sent to W. Albert Noyes, Jr., Department of Chemistry, University of Rochester, Rochester 20, N. Y.

Correspondence regarding accepted copy, proofs and reprints should be directed to Assistant Editor, Allen D. Bliss, Department of Chemistry, Simmons College, 300 The Fenway, Boston 15, Mass.

Business Office: Alden H. Emery, Executive Secretary, American Chemical Society, 1155 Sixteenth St., N. W., Washington 6, D. C.

Advertising Office: Reinhold Publishing Corporation, 430 Park Avenue, New York 22, N. Y.

Articles must be submitted in duplicate, typed and double spaced. They should have at the beginning a brief Abstract, in no case exceeding 300 words. Original drawings should accompany the manuscript. Lettering at the sides of graphs (black on white or blue) may be pencilled in and will be typeset. Figures and tables should be held to a minimum consistent with adequate presentation of information. Photographs will not be printed on glossy paper except by special arrangement. All footnotes and references to the literature should be numbered consecutively and placed in the manuscript at the proper places. Initials of authors referred to in citations should be given. Nomenclature should conform to that used in *Chemical Abstracts*, mathematical characters be marked for italic, Greek letters carefully made or annotated, and subscripts and superscripts clearly shown. Articles should be written as briefly as possible consistent with clarity and should avoid historical background unnecessary for specialists.

Notes describe fragmentary or incomplete studies but do not otherwise differ fundamentally from articles and are subjected to the same editorial appraisal as are articles. In their preparation particular attention should be paid to brevity and conciseness. Material included in Notes must be definitive and may not be republished subsequently.

Communications to the Editor are designed to afford prompt preliminary publication of observations or discoveries whose

value to science is so great that immediate publication is imperative. The appearance of related work from other laboratories is in itself not considered sufficient justification for the publication of a Communication, which must in addition meet special requirements of timeliness and significance. Their total length may in no case exceed 1000 words or their equivalent. They differ from Articles and Notes in that their subject matter may be republished.

Remittances and orders for subscriptions and for single copies, notices of changes of address and new professional connections, and claims for missing numbers should be sent to the American Chemical Society, 1155 Sixteenth St., N. W., Washington 6, D. C. Changes of address for the *Journal of Physical Chemistry* must be received on or before the 30th of the preceding month.

Claims for missing numbers will not be allowed (1) if received more than sixty days from date of issue (because of delivery hazards, no claims can be honored from subscribers in Central Europe, Asia, or Pacific Islands other than Hawaii), (2) if loss was due to failure of notice of change of address to be received before the date specified in the preceding paragraph, or (3) if the reason for the claim is "missing from files."

Subscription rates (1961): members of American Chemical Society, \$12.00 for 1 year; to non-members, \$24.00 for 1 year. Postage to countries in the Pan-American Union \$0.80; Canada, \$0.40; all other countries, \$1.20. Single copies, current volume, \$2.50; foreign postage, \$0.15; Canadian postage \$0.10; Pan-American Union, \$0.10. Back volumes (Vol. 56-64) \$30.00 per volume; foreign postage, per volume \$1.20, Canadian, \$0.40; Pan-American Union, \$0.80. Single copies: back issues, \$3.00; for current year, \$2.50; postage, single copies: foreign, \$0.15; Canadian, \$0.10; Pan-American Union, \$0.10.

The American Chemical Society and the Editors of the *Journal of Physical Chemistry* assume no responsibility for the statements and opinions advanced by contributors to THIS JOURNAL.

The American Chemical Society also publishes *Journal of the American Chemical Society*, *Chemical Abstracts*, *Industrial and Engineering Chemistry*, International Edition of *Industrial and Engineering Chemistry*, *Chemical and Engineering News*, *Analytical Chemistry*, *Journal of Agricultural and Food Chemistry*, *Journal of Organic Chemistry*, *Journal of Chemical and Engineering Data*, *Chemical Reviews*, *Chemical Titles* and *Journal of Chemical Documentation*. Rates on request.

Robert E. Meyer: Self-Diffusion of Liquid Mercury . . . . .	567
Robert G. Charles: The Heat Stabilities of Bisacetylacetonethylenediimine and its Metal Chelates . . . . .	568
R. D. Shores and H. C. Moser: Reactions of Tritium Atoms with Frozen Hydrocarbons . . . . .	570
Horace A. Ory: The Rate of Thermal Decomposition of Dimethyl 2,2'-Azo-bis-iso-butylate . . . . .	571
Louis Watts Clark: The Effect of Aniline and its Derivatives on Oxanilic Acid . . . . .	572
Hidehiko Kido and W. Conrad Fernelius: Heat of Neu-	

tralization of Strong Acids by Strong Bases in Mixed Water-Dioxane Solutions . . . . .	574
A. M. Truchard, H. G. Harris and D. M. Himmelblau: Solubility and Thermodynamic Functions of Ethylene in Diethyl Sulfate . . . . .	575
COMMUNICATION TO THE EDITOR	
N. E. Weston and F. W. Billmeyer, Jr.: Specific Refractive Increment of Polypropylene in $\alpha$ -Chloronaphthalene . . . . .	576

---

---

# THE JOURNAL OF PHYSICAL CHEMISTRY

(Registered in U. S. Patent Office) (© Copyright, 1961, by the American Chemical Society)

VOLUME 65

MARCH 28, 1961

NUMBER 3

---

---

## DIMENSIONS AND HYDRODYNAMIC PROPERTIES OF CELLULOSIC MOLECULES IN DILUTE SOLUTIONS<sup>1</sup>

BY H. J. MARRINAN<sup>2</sup> AND J. J. HERMANS

*Cellulose Research Institute, State University College of Forestry, Syracuse 10, New York*

*Received April 13, 1960*

An analysis has been made of viscosity, sedimentation and light scattering data of some cellulose derivatives in dilute solutions, using results given in the literature. A molecular weight distribution of the well-known form  $M^{p-1} \exp(-\lambda M)$  was assumed, and the parameters  $y$  and  $\lambda$  were derived from the experimental  $M_n$  and  $M_w$  values. In addition, since the radius of gyration  $\rho$  enters into the hydrodynamic theories, quantities containing  $\rho$  must be averaged over the molecular weight distribution. To this end, a relation of the form  $\rho = kM^p$  is postulated and the value of  $p$  determined from the light scattering results. The expressions derived by Debye and Bueche and by Kirkwood and Riseman for intrinsic viscosity  $[\eta]$  and intrinsic sedimentation constant  $[S]$  are rewritten in a somewhat simplified form, which is independent of whether Gaussian statistics apply or not  $[\eta] = A\rho^2(1 + aM/\rho)^{-1}$ ;  $[S] = C(1 + cM/\rho)$  where  $A$ ,  $a$ ,  $C$  and  $c$  are constants. These equations become applicable to polydisperse samples when  $\rho^2$  in the expression for  $[\eta]$  is replaced by  $\langle \rho^2 \rangle_w$  while  $M/\rho$  in both equations is replaced by  $M_n \langle \rho^2 \rangle_w \langle \rho^3 \rangle_n^{-1}$ . These expressions greatly facilitate the application of the Debye-Bueche and Kirkwood-Riseman equations to experimental data. An assessment of the relative merits of various hydrodynamic expressions has been carried out using the experimental data of Huque, Goring and Mason in addition to those of Hunt, Newman, Scheraga and Flory. It is found that the modified Kirkwood-Riseman equations are compatible with the data and that the size of the monomer units derived from these data is quite acceptable. This is distinct from what was found in previous work using the same basic equations, and hence this difference must reside in the mathematical treatment.

### Introduction

In the earliest theories<sup>3</sup> of the hydrodynamics of polymer solutions the hydrodynamical interaction of the monomer units was ignored, and consequently such "free drain" theories may be regarded as limiting cases for structures of very low density. Brinkman<sup>4</sup> and, independently, Debye and Bueche<sup>5</sup> (DB) attempted to account for the hydrodynamical interaction by assuming that the polymer molecule could be represented by a sphere of uniform density to which a certain porosity is attributed. The results of the DB theory for intrinsic viscosity  $[\eta]$  and intrinsic sedimentation constant  $[S]$  may be written

$$[\eta] = (4\pi/3)(N_0 R_s^3/M)\Phi(\sigma) \quad (1)$$

$$[S] = M[6\pi R_s N_0 \psi(\sigma)]^{-1} \quad (2)$$

where  $R_s$  is the radius of the sphere,  $M$  the molecu-

lar weight of the polymer,  $N_0$  Avogadro's number and  $\Phi(\sigma)$  and  $\psi(\sigma)$  are functions of the "shielding ratio"  $\sigma$  which is defined by

$$\sigma^2 = 3P\zeta/(4\pi R_s \eta_0) \quad (3)$$

$P$  being the degree of polymerization,  $\zeta$  the frictional coefficient of a monomer unit and  $\eta_0$  the viscosity of the solvent.

Kirkwood and Riseman<sup>6</sup> (KR) used the more realistic model of a Gaussian string of beads, but in their averaging procedure had to use approximations. Their results are

$$[\eta] = N_0 \zeta P b^2 F(\lambda_0 P^{1/2}) / (36 \eta_0 m_0) \quad (4)$$

$$[S] = (m_0 \eta_0 / N_0 \zeta) (1 + 8 \lambda_0 P^{1/2} / 3) \quad (5)$$

where, in addition to the symbols defined previously,  $m_0$  is the molecular weight of the monomer unit,  $b$  the effective bond length,  $F(\lambda_0 P^{1/2})$  a function of the "shielding," tabulated by Kirkwood, Zwanzig and Plock,<sup>7</sup> and

$$\lambda_0 P^{1/2} = \zeta P^{1/2} (6\pi^3)^{-1/2} (\eta_0 b)^{-1} \quad (6)$$

For Gaussian chains, the mean square end-to-end distance is

(6) J. G. Kirkwood and J. Riseman, *ibid.*, **16**, 565 (1948).

(7) J. G. Kirkwood, R. W. Zwanzig and R. J. Plock, *ibid.*, **23**, 213 (1955).

(1) Presented at the meeting of the Am. Chem. Soc., Cleveland, Ohio, April, 1960.

(2) On leave from the British Rayon Research Association, Manchester, England.

(3) References in J. J. Hermans, "Flow Properties of Disperse Systems," North-Holland Publ. Co., Amsterdam, 1953, Ch. V, p. 219.

(4) H. C. Brinkman, *Proc. Akad. Amsterdam*, **50**, 618 (1947); *Physica*, **13**, 447 (1947); *Appl. Sci. Res.*, **A1**, 27 (1947).

(5) P. Debye and A. M. Bueche, *J. Chem. Phys.*, **16**, 573 (1948).

$$\bar{r}^2 = P b^2$$

and the parameter

$$x = \lambda_0 P^{1/2}$$

is proportional to  $M/\rho$  where  $\rho$  is the radius of gyration. Since  $\sigma^2$  in the DB theory is likewise proportional to  $M/R_s$ , it follows that the KR result for  $[\eta]$  may be given a form that closely resembles the DB formula

$$[\eta] = \gamma N_0 [(\bar{r}^2)^{3/2}/M] G(x) \quad (7)$$

where

$$\gamma = (6\pi^3)^{1/2}/36 \text{ and } G(x) = xF(x) \quad (8)$$

When eq. 7 is applied to molecules that show deviations from Gaussian statistics, the numerical value of the constant  $\gamma$  for such molecules need not necessarily be that given in eq. 8, nor will the form of the function  $G(x)$  be exactly the same as that found by Kirkwood and Riseman. However, when the deviations from Gaussian behavior are comparatively small, the application of eq. 7 should not lead to any serious error.

More recently Flory<sup>8</sup> and co-workers have advanced the equations (see also Sadron<sup>9</sup>)

$$[\eta] = X'(\bar{r}^2)^{3/2}/M$$

$$[S] = M[N_0(\bar{r}^2)^{1/2}Q']^{-1}$$

where  $X'$  and  $Q'$  are "universal constants," *i.e.*, they are the same for all polymers regardless of solvent and temperature. The root mean square end-to-end distance in these equations is  $\alpha$  times its unperturbed value  $(\bar{r}_0^2)^{1/2}$ , where  $\alpha$  is an expansion factor resulting from interactions between the monomer units.

While it has been shown that Flory's equations adequately represent the experimental data for many polymers, Newman and Flory found that the values of  $X'$  and  $Q'$  for cellulose trinitrate decrease markedly with decreasing molecular weight. In a more recent paper Hunt, Newman, Scheraga and Flory<sup>10</sup> have discussed the experimental data on cellulose trinitrate in terms of the equations of DB and KR, taking into account the polydispersity of the samples and the large experimental errors involved in this type of work. It was concluded that also the DB and KR expressions were unsatisfactory in explaining the hydrodynamic behavior as they lead to a value for the frictional coefficient of a monomer unit which is approximately one-fourth as large as that calculated on the basis of Stokes' formula.

In this paper a new approach to the assessment of the relative merits of the existing hydrodynamic equations is described. This approach enables one to make a more direct comparison between the various formulas, and this is illustrated for cellulose trinitrate using the experimental

data of Hunt, Newman, Scheraga and Flory<sup>10</sup> and those of Huque, Goring and Mason.<sup>11</sup>

The difference between the treatment of the experimental data by Hunt, *et al.*, and that presented here is merely a computational one, but it is nevertheless of importance as it leads to different conclusions. In essence, in this work the application of the DB and KR equations is made very much easier by using approximate expressions for the "shielding parameters"  $\Phi(\sigma)$ ,  $\psi(\sigma)$  and  $F(\lambda_0 P^{1/2})$ .

**Approximations to the DB and KR Expressions.**—To facilitate an application to polydisperse systems, the function  $\Phi(\sigma)$  in the DB theory of viscosity is approximated as

$$\Phi(\sigma) = (\sigma^2/10)(1 + k\sigma^2)^{-1} \quad (9)$$

where  $k$  is a constant. If  $k$  is given the value  $1/25$ ,  $\Phi(\sigma)$  becomes  $\sigma^2/10$  when  $\sigma$  is small and 2.5 when  $\sigma$  is large, these being the same limits as those of the DB function. However, for weight average molecular weights of cellulose trinitrate up to  $2.5 \times 10^6$  as encountered in this work, a better approximation to the actual  $\Phi(\sigma)$  is obtained with  $k = 0.0486$ . This is illustrated in Fig. 1 where it is seen that the agreement is to within about 5%.

Likewise the functions  $\psi(\sigma)$  in the DB theory of sedimentation and the function  $F(x)$  in the KR theory of viscosity may be approximated with similar accuracy (see Figs. 1 and 2) by

$$\psi(\sigma) = (2\sigma^2/9)(1 + 0.243\sigma^2)^{-1} \quad (10)$$

$$F(x) = (1 + 0.78x)^{-1} \quad (11)$$

The method by which the coefficients preceding the shielding parameters in the above equations were determined will be explained in a later section.

If it is assumed that  $R_s$  is proportional to the radius of gyration  $\rho$ , then  $\sigma^2$  and  $x$  are proportional to  $M/\rho$ . Hence the results of both the DB and the KR theories may be written

$$[\eta] = A\rho^2(1 + aM/\rho)^{-1} \quad (12)$$

$$[S] = (m_0\eta_0/N_0\zeta)(1 + cM/\rho) \quad (13)$$

where  $A$ ,  $a$  and  $c$  are constants. In the DB theory

$$A = (4\pi/30)N_0(R_s/\rho)^3\sigma^2\rho/M; \quad a = 0.0486\sigma^2\rho/M;$$

$$c = 0.243\sigma^2\rho/M \quad (14)$$

whereas in the KR theory

$$A = \gamma N_0(\bar{r}^2/\rho^2)^{3/2}x\rho/M; \quad a = 0.78x\rho/M; \quad c = (8/3)x\rho/M \quad (15)$$

We note, finally, that when Gaussian statistics apply, the approximation (12) becomes identical in form with an equation derived by Peterlin,<sup>12</sup> while the approximation (13) has the form derived from experiments with large-scale models by Kuhn and Kuhn.<sup>13</sup>

**Equations for Polydisperse Samples.** (a) **Viscosity.**—It follows from simple considerations that  $[\eta]$  is proportional to the weight average  $\langle\rho^2\rangle_w$  of  $\rho^2$  at the limit of free draining, and proportional to  $\langle\rho^3\rangle_n/\langle M\rangle_n$  at the limit of com-

(11) M. M. Huque, D. A. I. Goring and S. G. Mason, *Can. J. Chem.*, **36**, 952 (1958).

(12) A. Peterlin, *Proc. Akad. Ljubljana, Math. Phys. Sect.*, 59 (1950); *J. Polymer Sci.*, **5**, 473 (1950).

(13) H. Kuhn and W. Kuhn, *ibid.*, **5**, 519 (1950).

(8) (a) P. J. Flory, "Principles of Polymer Chemistry," Cornell Univ. Press, Ithaca, New York, 1953, p. 595 and following; (b) P. J. Flory and T. G. Fox, *J. Polymer Sci.*, **5**, 745 (1950); *J. Am. Chem. Soc.*, **73**, 1904, 1915 (1951); (c) L. Mandelkern and P. J. Flory, *J. Chem. Phys.*, **20**, 212 (1952).

(9) C. Sadron, *J. Polymer Sci.*, **3**, 812 (1948); *Nature*, **179**, 263 (1957).

(10) M. L. Hunt, S. Newman, H. A. Scheraga and P. J. Flory, *J. Phys. Chem.*, **60**, 1278 (1956).



pletely impenetrable particles. In view of eq. 12, this suggests that a good approximation for poly-disperse systems is

$$[\eta] = A\langle\rho^2\rangle_w [1 + a\langle M\rangle_n\langle\rho^2\rangle_w/\langle\rho^3\rangle_n]^{-1} \quad (16)$$

It follows that a plot of  $\langle\rho^2\rangle_w/[\eta]$  against  $\langle M\rangle_n\langle\rho^2\rangle_w/\langle\rho^3\rangle_n$  should be a straight line with slope  $a/A$  and intercept  $1/A$ . According to the Flory-Fox equation, such a plot should be a straight line which passes through the origin.

(b) **Sedimentation.**—The kind of averages that are appropriate in the expression for the intrinsic sedimentation constant depends on the technique used for recording the sedimentation process. As shown in the appendix, when Schlieren optics are used and the rate at which the peak of the band moves is recorded, we must extend eq. 13 as

$$[S] = (m_0\eta_0/N_0\zeta)[1 + cB\langle M\rangle_n\langle\rho^2\rangle_w/\langle\rho^3\rangle_n] \quad (17)$$

where  $B$  is a parameter which depends on the type of molecular weight distribution assumed. For the Schulz<sup>14</sup> type of distribution used in this work

$$B = (y + p)^{-2}\Gamma(3p + y)/\Gamma(2p + y + 1) \quad (18)$$

where  $\Gamma$  is the gamma function, and  $p$  and  $y$  will be defined in the next section.

Equation 17 shows that a plot of  $[S]$  against  $B\langle M\rangle_n\langle\rho^2\rangle_w/\langle\rho^3\rangle_n^{-1}$  should be linear with a finite intercept which in this case represents the intrinsic sedimentation constant of a "free drain" molecule and is the same as that of a single monomer unit. In the Flory-Mandelkern equation the intercept would be zero.

**Calculation of Averages.**—In order to derive the various averages needed in eq. 16 and 17, it has been assumed that the fractions of cellulose trinitrate investigated by Hunt, *et al.*, and by Huque, *et al.*, possess a molecular weight distribution of the Schulz type, *i.e.*, the number of molecules with molecular weight between  $M$  and  $M + dM$  is proportional to  $e^{-\lambda M}M^{y-1}dM$ , where  $\lambda$  and  $y$  are parameters which characterize the average molecular weight and the sharpness of the distribution. For this distribution  $M_n:M_w:M_z = y:(y + 1):(y + 2)$  and the values of  $y$  and  $M_z$  that have been calculated from the experimental values of  $M_n$  and  $M_w$  are shown in the second and third columns of Table I. In the work of Huque,

TABLE I

Sample	$y$	$10^{-4} M_z$	$10^{12} \langle\rho^2\rangle_w$	$10^{18} \langle\rho^3\rangle_n$
Data from ref. 8c	L-10	5.27	4.8	1.74
	L-8	4.0	9.1	4.76
	L-5	2.23	16.9	7.37
	H-2	1.42	35.1 <sup>a</sup>	17.05
	H-1	0.814	89.0	45.25
Data from ref. 9	T-8	1.0	102	58.7
	T-6	1.0	117	74.5
	M-3	1.0	147	127.0
	M	1.0	241.5	143.0
	M-2	1.0	238.5	164.5
	M-1	1.0	348	274.0
	H-2	1.0	375	298.0

<sup>a</sup>  $M_w/M_n$  assumed equal to 1.7 on basis of a  $M_w/M_n$  vs.  $M_n$  plot.

(14) G. V. Schulz, *Z. physik. Chem.*, **B43**, 25 (1939).

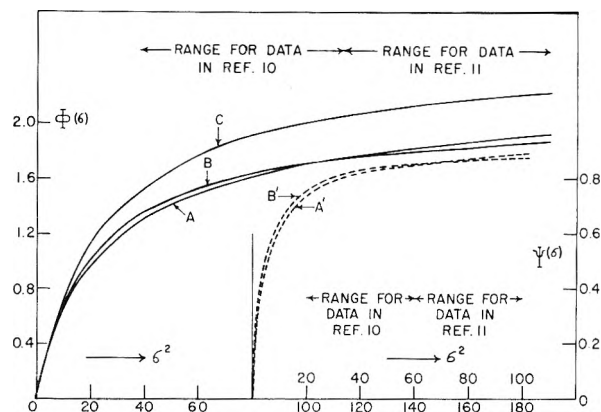


Fig. 1.—The shielding parameters  $\Phi(\sigma)$  and  $\Psi(\sigma)$  in the DB theory: (A) the function  $\Phi(\sigma)$  as given by DB; (B) approximated form with  $k = 0.0486$ ; (C) approximated form with  $k = 1/25$ ; (A') the function  $\Psi(\sigma)$  as given by DB; (B') approximated form with  $k = 0.243$ .

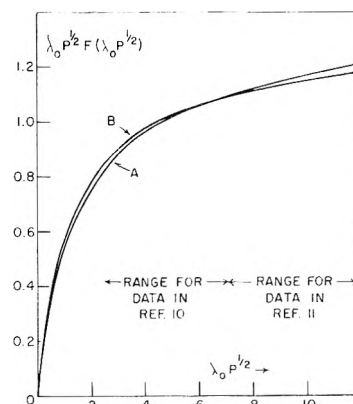


Fig. 2.—The shielding parameter  $\lambda_0 P^{1/2} F(\lambda_0 P^{1/2})$  in the KR theory of viscosity: (A) the function  $\lambda_0 P^{1/2} F(\lambda_0 P^{1/2})$  as given by KR; (B) approximated form with  $k = 0.78$ .

*et al.*, only  $M_w$  was measured and it was assumed that  $M_n:M_w:M_z = 1:2:3$ , *i.e.*,  $y = 1$ .

In addition, it has been assumed that the radii of gyration of the molecules are related to their molecular weights as

$$\rho = KM^p \quad (19)$$

where  $K$  and  $p$  are constants. It may be mentioned in this connection that according to Wall<sup>15</sup> all the computer results for random flights with excluded volume can be represented by eq. 19, but we believe it is uncertain whether the non-Gaussian relation between  $\rho$  and  $M$  in cellulose trinitrate is due to the excluded volume effect, and we do not attach any special significance to the specific form of eq. 19. Strictly speaking, molecules with the same value of  $M$  do not all have the same radius of gyration, but the effect that this might have on the averages has been neglected. To show that eq. 19 and the molecular weight distribution assumed are sufficient to represent the experimental data to within the experimental error, a comparison is made in Fig. 3 between the calculated values of  $\rho_z^2/M_z$  and the experimental ones. Other relationships between

(15) F. T. Wall, Lecture N. Y. Academy Sci., May 1960; F. T. Wall and J. J. Erpenbeck, *J. Chem. Phys.*, **30**, 634 (1959).

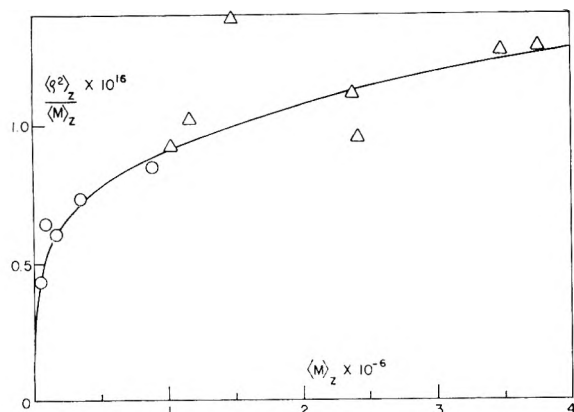


Fig. 3.—Dependence of  $\langle \rho^2 \rangle_z / M_z$  in  $\text{cm.}^2 / M$  on  $\langle M \rangle_z$ : O, Data of Hunt, *et al.*; Δ, data of Huque, *et al.* The solid line is a theoretical one, based on eq. 19.

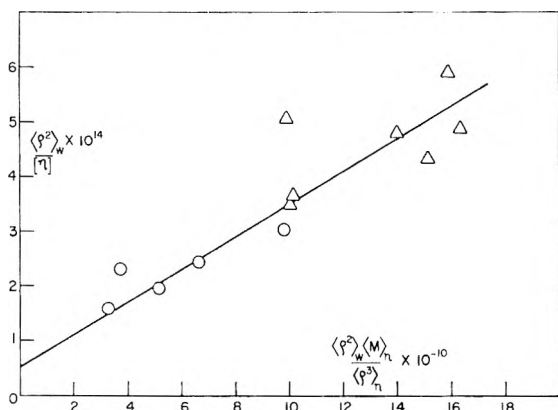


Fig. 4.—Viscosity data plotted in form  $\langle \rho^2 \rangle_w / [\eta]$  against  $\langle \rho^2 \rangle_w \langle M \rangle_n / \langle \rho^3 \rangle_n$ : O, data of Hunt, *et al.*; Δ, data of Huque, *et al.*

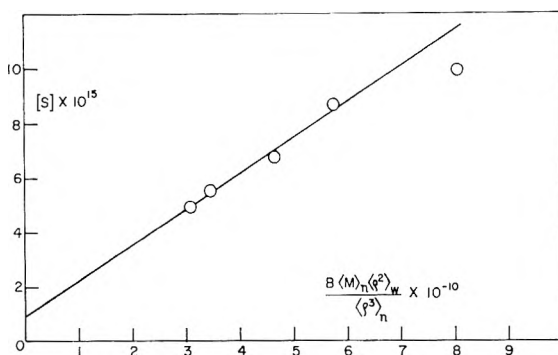


Fig. 5.—Sedimentation data of Hunt, *et al.*, plotted against  $B \langle M \rangle_n \langle \rho^2 \rangle_w / \langle \rho^3 \rangle_n$ .

$\rho$  and  $M$  could doubtless have achieved the same degree of agreement with experiment, and hence eq. 19 is best regarded simply as an interpolation formula.

The average radius of gyration derived from light scattering experiments is  $\rho_z^2$ . According to eq. 19 and our choice of molecular weight distribution, this should be given by

$$\rho_z^2 = K^2 \frac{\Gamma(2p + y + 2)}{\Gamma(y + 2)} \left( \frac{M_n}{y} \right)^{2p} \quad (20)$$

Since it follows, both from theoretical considerations and from the experimental data, that  $p$

does not differ much from  $1/2$ , eq. 20 is replaced by an expansion in terms of the parameter  $\xi = p - 1/2$ , omitting powers higher than the first, thus

$$\log \langle \rho^2 \rangle_z = 2 \log K + \log \left( \frac{y + 2}{y} M_n \right) + 2\xi \left[ \log \frac{M_n}{y} + 0.4343 \frac{d \ln \Gamma(y + 2)}{d(y + 2)} \right] \quad (21)$$

so that  $K$  and  $\xi$  can be found by plotting  $\log \langle \rho^2 \rangle_z - \log [(y + 2)M_n/y]$  against  $\log (M_n/y) + 0.4343 d \ln \Gamma(y + 2)/d(y + 2)$ . This gave  $p = 0.6125$  and  $K = 0.1969$  if  $\rho$  is expressed in Ångström units.

## Results

In Fig. 4 the values of  $\langle \rho^2 \rangle_w / [\eta]$  calculated from the experimental data are plotted against  $M_n \langle \rho^2 \rangle_w / \langle \rho^3 \rangle_n$ . The straight line drawn through the points does not extrapolate through the origin. From the slope and intercept, the quantities  $(R_s/\rho)^2$  and  $\zeta/\eta_0$  occurring in the DB theory and the quantities  $\bar{r}^2/\rho^2$  and  $\zeta/\eta_0$  occurring in the KR theory may be calculated (Table II).

TABLE II

Results from KR theory		Results from DB theory	
$(\bar{r}^2/\rho^2)_{\text{vis}}$	5.2	$(R_s/\rho)^2_{\text{vis}}$	0.761
$(\bar{r}^2/\rho^2)_{\text{sed}}$	6.3	$(R_s/\rho)^2_{\text{sed}}$	0.548
$(\zeta/\eta_0)_{\text{vis}}$	63.5 Å.	$(\zeta/\eta_0)_{\text{vis}}$	120.0 Å. = 55.0 Å. if $(R_s/\rho)^2 = 5/3$
$(\zeta/\eta_0)_{\text{sed}}$	53.0 Å.	$(\zeta/\eta_0)_{\text{sed}}$	53.0 Å.
$(R_m)_{\text{vis}}$	3.37 Å.	$(R_m)_{\text{vis}}$	6.38 Å. = 2.92 Å. if $(R_s/\rho)^2 = 5/3$
$(R_m)_{\text{sed}}$	2.81 Å.	$(R_m)_{\text{sed}}$	2.81 Å.

The intrinsic sedimentation constants  $[S]$  were calculated from the data of Hunt, *et al.*, using  $[S] = S\eta_0(1 - \bar{v}\rho_0)^{-1}$  where the partial specific volume of the polymer  $\bar{v} = 0.546$  cc./g., the density of the solvent  $\rho_0 = 0.8883$  g./cc. and the viscosity of the solvent  $\eta_0 = 0.004012$  poise.

In Fig. 5 values of  $[S]$  are plotted against  $B M_n \langle \rho^2 \rangle_w / \langle \rho^3 \rangle_n$  as suggested by eq. 17. The straight line drawn through the points may again be used to calculate  $\zeta/\eta_0$ ,  $R_s/\rho$  and  $\bar{r}^2/\rho^2$ , respectively. The results are given in Table II which shows, in addition, the radius of a monomer unit deduced from  $\zeta/\eta_0$  on the basis of Stokes' law. In the case of sedimentation, as distinct from that of the viscosity, the value deduced for  $\zeta/\eta_0$  does not depend on the value found for  $(R_s/\rho)^2$  or  $\bar{r}^2/\rho^2$ .

## Discussion

In order to determine the most appropriate value of  $k$  in the approximate form (eq. 9) of  $\Phi(\sigma)$  some knowledge of the range of  $\sigma^2$  values pertaining to the fractions studied in this work is a prerequisite. Since  $\sigma^2 = a M_n \langle \rho^2 \rangle_w / \langle \rho^3 \rangle_n / k$  the value deduced for  $\sigma^2$  for a given fraction depends on the value deduced for  $a$ , and thus on the slope and intercept in Fig. 4 in addition to the value assigned to  $k$ . Hence  $k$  was chosen so that the mean value deduced for  $\sigma^2$ , when used in the approximate form of  $\Phi(\sigma)$ , gave a value for this latter function which was equal to that of the function tabulated by Debye for this value of  $\sigma^2$ . This method also was used to determine the most appropriate approximations for  $\psi(\sigma)$  and  $F(x)$  in the molecular weight range covered in this

paper. The effect of this procedure is apparent in Figs. 1 and 2 where the graphs of the approximated forms of the shielding parameters coincide with the correct values for these functions at the mean values deduced for the "shielding ratios." These latter ratios were calculated as  $(\sigma^2)_{\text{vis}} = 115$ ,  $(\sigma^2)_{\text{scd}} = 60$ ,  $x_{\text{vis}} = 7.16$  and  $x_{\text{sen}} = 5.42$ . It is apparent that the values deduced from the KR theory of viscosity and sedimentation are in better agreement than those deduced from the DB theory and this is reflected in the values that have been determined for the various parameters shown in Table II.

The use of approximate expressions for the respective parameters  $\Phi(\sigma)$ ,  $\psi(\sigma)$  and  $F(x)$  leads to a possible error of approximately 5% for the range of molecular weights covered in this work. This additional error may be tolerated, not only because it is much smaller than the probable experimental error, but because the approximations introduce two important compensating factors. First, they allow the viscosity and sedimentation equations to be written in a form which is applicable to polydisperse samples and, second, they greatly facilitate application of the DB and KR equations.

It has been a general criticism of the DB and KR expressions that the frictional coefficient turns out to be very much smaller than that calculated by applying Stokes' law to a monomer unit. It may be surprising, therefore, that in this work, as shown in Table II, realistic values are obtained for the radius of the monomer unit. The reason for this difference is apparent when it is noted that here the frictional coefficient is deduced directly from either the slope and intercept of Fig. 4, or the intercept alone of Fig. 5, whereas in previous work recourse was made to the Mark-Houwink equation,  $[\eta] = KM^b$ , in order to determine the "average shielding ratio," which is related to the frictional coefficient. This latter method leads to values of the "shielding ratio" which are much too low, e.g., Flory and co-workers deduced from the Mark-Houwink equation a value for  $\lambda_0 P^{1/2}$  of 0.77, whereas the average value of  $\lambda_0 P^{1/2}$  for their fractions, as may be seen from Fig. 2, is about 4. Similarly their estimate of the value of  $\sigma^2$  is about one-fifth the true value. It is worth noting, however, that in deducing the above values Hunt, *et al.*,<sup>10</sup> improved the procedure originally recommended by Debye and Bueche, thereby making the discrepancy considerably less than it would have been according to earlier treatments.

Unfortunately, the experimental errors make the exact values of the intercepts in Figs. 4 and 5 somewhat uncertain. It can be seen in Fig. 4 that the line might have been drawn a little more steeply; but this would lead to a smaller intercept and therefore to larger values of  $\zeta$  and  $R_m$  instead of the low values found in previous work. That the difference between the values for  $\zeta$  deduced in this work and in previous work cannot be attributed to experimental error alone can be seen by observing that the previous values of  $\zeta$  would entail an extrapolation of the lines in Figs. 4 and 5 to an intercept at least four times bigger than that actually found. It will be noticed also in Fig.

5 that the point for the fraction of highest molecular weight (H-1) lies some way off the line drawn. This, however, is also apparent in the plot of the viscosity data in Fig. 4, and here the higher molecular weight fractions investigated by Huque, *et al.*, suggest that this point probably has a large experimental error associated with it. In fact, if the value of  $M_n \langle \rho^2 \rangle_w \langle \rho^3 \rangle_n^{-1}$  for fraction H-1 is reduced from 9.8 to 8.4, the point will lie on the lines drawn in both Figs. 4 and 5. These facts have been taken into consideration in drawing the straight line in Fig. 5.

The two values for the frictional coefficient deduced from the KR theories of viscosity and sedimentation, respectively, are in better agreement than those deduced from DB. It should be remembered that the KR and DB theories give identical results at the "free drain" limit. This explains why the value of  $\zeta/\eta_0$  derived from sedimentation is the same. It explains also why the intercept of the viscosity plot leads to a realistic value of  $\zeta/\eta_0$  when one inserts the value 5/3 of the DB theory for the ratio  $(R_s/\rho)^2$ ; compare Table II. In other words, the shortcomings of the DB theory are revealed by the slopes of the lines in Figs. 4 and 5, which are considerably larger than predicted. This is reflected in the small values of  $R_s/\rho$  calculated from these slopes.

Table II shows that  $\bar{r}^2/\rho^2$  as derived from the KR equation is close to the theoretical value 6 for Gaussian chains, even though the use of eq. 19 with  $p \neq 1/2$  implies deviations from Gaussian behavior. It is clear, therefore, that the non-Gaussian statistics are not revealed by plots such as those of Figs. 4 and 5.

Finally it may be mentioned that Hunt, *et al.*, carried out their investigation because they recognized that the well-known hydrodynamic equations did not appear to hold for stiff cellulosic chains. No claim is made that the agreement found here with the modified KR equations is conclusive evidence in favor of these equations over other well-known expressions. In view of the large experimental errors involved, this can be decided only by further experiments. We believe, however, that our procedure is physically significant and of sufficient interest to warrant its publication if only because it indicates what quantities must be measured to make such an analysis possible.

**Other Data Examined.**—In principle, for any given value of  $\rho$ , it should be possible to draw conclusions about the molecular shape from the dissymmetry of light scattering. In practice this procedure is complicated by polydispersity because this too affects the dissymmetry. When examining the dissymmetry data of Hunt, *et al.*, kindly put at our disposal by the authors, it was found that there were appreciable deviations from the dissymmetries predicted for monodisperse Gaussian chains, but that these deviations were due primarily to the polydispersity of the samples. To show this, the dissymmetries were calculated on the assumption that Gaussian statistics applied and that the molecular weight distribution was the "normal" one, *i.e.*, of the Schulz type with  $\gamma = 1$ . Even when these rather crude approximations

were made, the dissymmetries calculated were equal to the measured ones within experimental error.

Attempts were made to use data other than those mentioned so far, but investigations in which information on both the viscosity and the molecular dimensions (and, preferably, also the molecular weight distribution) has been obtained, are relatively scarce.

Outer, Carr and Zimm<sup>16</sup> did extensive work on polystyrene fractions, for which they assumed originally that  $M_w/M_n = 1.05$  (two of their fractions: 1.2), although they expressed some doubt as to whether the distribution was really that sharp. If it is assumed that  $M_w/M_n$  was 1.2 for those fractions which were polymerized under the same conditions and given the same fractionation procedure, then with butanone as solvent, it is found that a plot of  $\langle \sigma^2 \rangle_w / [\eta]$  vs.  $M_n \langle \rho^2 \rangle_w \langle \rho^3 \rangle_n^{-1}$ , although admittedly showing some scatter, is compatible with a straight line having a finite intercept. From this intercept, it follows on the basis of the KR theory that  $\zeta/\eta_0 = 32 \text{ \AA}$ . ( $R_m = 1.7 \text{ \AA}$ .) and  $\bar{r}^2/\rho^2 = 6.5$ . It should be added, however, that the extrapolation to the ordinate has to be done over a very large range, making the results rather doubtful.

Gralén's<sup>17</sup> sedimentation data for various celluloses in cuprammonium give a straight line plot for  $[S]$  vs.  $M_w^{1/2}$ . Assuming that  $M_w/M_n = 2$  and  $p = 1/2$ , this line leads to a value of  $\zeta/\eta_0 = 30 \text{ \AA}$ . or  $R_m = 1.6 \text{ \AA}$ .

Similarly, a plot of  $[S]$  vs.  $M_w^{1/2}$  for Mosimann's<sup>18</sup> data on nitrocellulose in acetone is linear with an intercept giving  $\zeta/\eta_0 = 40.0 \text{ \AA}$ . or  $R_m = 2.12 \text{ \AA}$ .

Ethylhydroxyethylcellulose was investigated by Manley.<sup>19</sup> A plot of  $[S]$  vs.  $BM_w^{1/2}$  (using molecular weights obtained from sedimentation) is a straight line with the same intercept as found from the data on cellulose trinitrate of Hunt, *et al.*, when plotted in the same way. If, however, one plots  $[S]$  vs.  $BM_n \langle \rho^2 \rangle_w \langle \rho^3 \rangle_n^{-1}$  one finds an intercept that is 4 times as large as that derived from Hunt's data when plotted in this fashion. This probably is due to the values of  $\rho$ ; Manley himself expresses doubt as to the accuracy of his light scattering data.

Hughes' data<sup>20</sup> on cellulose triacetate in chloroform cover only a small range of molecular weights

(16) P. Outer, C. I. Carr and B. H. Zimm, *ibid.*, **18**, 830 (1950).

(17) N. Gralén, "Sedimentation and Diffusion Measurements on Cellulose and Cellulose Derivatives," Inaugural Dissertation, Uppsala, 1944.

(18) H. Mosimann, *Helv. Chim. Acta*, **26**, 61 (1943).

(19) R. St. John Manley, *Arkiv. Kemi*, **44**, 519 (1956).

(20) H. Hughes, "A Physico-Chemical Investigation of Cellulose Triacetate in Chloroform," Thesis, Cambridge, England.

and show a large scatter when plotted according to Fig. 4. Similar difficulties were encountered when investigating the data of Holtzer, Benoit and Doty<sup>21</sup> concerning cellulose trinitrate in acetone. There is considerable scatter, which is reflected in the value  $10^{21}X'$ , *i.e.*, the constant in Flory's theory; it ranges from 1.41 to 2.42, showing little correlation with molecular weight.

### Appendix

When Schlieren optics are used in ultracentrifugation studies, one obtains a curve giving the gradient of the refractive index (which is proportional to the gradient of the weight concentration) as a function of the distance from the center of rotation. As long as the effect of diffusion is small, it is shown<sup>22</sup> easily that this curve is equivalent to a plot of  $c_0(s)$  vs.  $s$ , where  $s$  is the rate of sedimentation and  $c_0(s)ds$  is the weight fraction of solute with a sedimentation rate between  $s$  and  $s + ds$ .

Most authors measure the rate at which the maximum of this curve moves down the sedimentation cell, and this rate is equal<sup>22</sup> to the value of  $s$  for which  $c_0(s)$  has its maximum. To determine this value, we remember that  $s = a_0 + b_0M/\rho$  where  $a_0$  and  $b_0$  are constants. Using eq. 19, this may be written

$$s - a_0 = (b_0/k)M^{1-p} \quad (22)$$

Now, the weight fraction of polymer with molecular weight between  $M$  and  $M + dM$  is proportional to  $\exp(-\lambda M)M^y dM$ , so that it follows from eq. 22 that, apart from a constant

$$c_0(s) = \exp[-\lambda u^{1/(1-p)}] u^{(y+p)/(1-p)}; u = (k/b_0)(s - a_0)$$

The maximum of  $c_0(s)$  is found to be at

$$s = a_0 + (b_0/k)[(y + p)/\lambda]^{1-p} \quad (23)$$

We have found it convenient to express this as

$$s = a_0 + b_0BM_n \langle \rho^2 \rangle_w \langle \rho^3 \rangle_n^{-1} \quad (24)$$

which, on account of the relation between  $\rho$  and  $M$  assumed and the molecular weight distribution chosen, requires that

$$B = (y + p)^{1-p} \Gamma(y + 3p) / \Gamma(y + 2p + 1)$$

which is eq. 18 in the text.

This work was sponsored by the Office of Ordnance Research, U. S. Army.

**Acknowledgment** is made to Dr. P. J. Flory, whose criticism of our treatment has led to considerable improvements in the text.

(21) A. M. Holtzer, H. Benoit and P. M. Doty, *J. Phys. Chem.*, **58**, 624 (1954).

(22) J. W. Williams, K. E. Van Holde, R. L. Baldwin and H. Fujita, *Chem. Revs.*, **58**, 766 (1958); J. J. Hermans and A. M. Rijke, *J. Colloid Sci.*, **13**, 508 (1958).

# KINETICS AND MECHANISM FOR THE ELECTROCHEMICAL REDUCTION OF BENZOPHENONE IN ACIDIC MEDIA

BY MAKOTO SUZUKI AND PHILIP J. ELVING

*Department of Chemistry, The University of Michigan, Ann Arbor, Michigan*

*Received June 27, 1960*

The kinetic and mechanism factors in the electrochemical reduction of ketones have been investigated by observation of the following relations for the reduction of benzophenone and *p*-bromobenzophenone over the pH range of 2 to 7: variation of  $E_{1/2}$  with pH, ethanol concentration and drop-time; variation of current with time at various points on the polarographic waves; variation of the heterogeneous rate constant with pH, ethanol concentration and temperature. The pinacol produced by dimerization of the free radical formed in the first one-electron wave may form an insoluble [adsorbed?] film at the interface which has marked effects on the observed behavior. The wave I electron-transfer process is quite rapid, but the subsequent irreversible chemical process (dimerization) causes the net reaction to appear irreversible. The process producing the second one-electron wave (reduction of free radical to carbinol) is quasi-reversible. The combined wave, observed above ca. pH 5, is controlled at first by the wave II process; with increasing pH, control shifts to the wave I process. The cause of the heretofore unobserved slight pH-dependency of wave II is discussed.

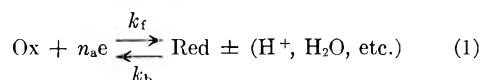
The polarography of benzophenone has been extensively studied and many details of its behavior are clear: In acidic media it yields at the dropping mercury electrode two well-defined reduction waves of about equal height, each corresponding to a one-electron reduction. The half-wave potential,  $E_{1/2}$ , of wave I becomes more negative with increasing pH to the extent of ca. 60 mv./unit pH;  $E_{1/2}$  of wave II is generally accepted as pH-independent. Below pH 2, wave II is masked by the hydrogen discharge wave. Above pH 5 or 6 the two waves merge into one, whose height approximately equals the sum of the wave heights at lower pH. At still higher pH, a new, more negative wave appears, whose height increases with increasing pH, while that of the merged wave decreases.

Based on such polarographic behavior and the results of coulometric measurement, the following electrochemical reduction mechanism of benzophenone is generally accepted, although authors differ in detail<sup>1-3</sup>: (a) In acidic media the first 1e wave represents the possibly reversible reduction of benzophenone to the carbinol free radical, which can dimerize to pinacol by secondary chemical reaction; the second 1e wave is the further reduction of the carbinol free radical to carbinol, which is assumed to proceed irreversibly. (b) The 2e combined wave involves reduction to carbinol through the free radical state. (c) The third wave in alkaline solution is attributed to reduction of metal ketyl<sup>1</sup> or carbinolate free radical ion.<sup>2</sup>

Although the reduction mechanism seems clear, the kinetics of the electrode reactions involved, especially in regard to their reversibility, have not yet been clarified. This is unfortunate, since the polarographic behavior of benzophenone seems to typify that of ketones in general.<sup>3</sup> Consequently, the kinetics of the electrochemical reduction of benzophenone and *p*-bromobenzophenone at pH 1 to 7 were studied by several methods, e.g., Koutecky analysis<sup>4</sup> of the irreversible polarographic wave, current-time relation during a single drop-life, etc.

## Discussion of the Results

**Dependence of  $E_{1/2}$  on Drop-time.**—The variation of  $E_{1/2}$  with drop-time,  $t$ , for the general half-cell electrode reaction



can be used as an experimental criterion of an irreversible process. Theoretically,  $E_{1/2}$  is related to  $t$  by

$$E_{1/2} = \frac{RT}{\alpha n_a F} \ln \frac{k^0}{\lambda_{1/2} D^{1/2}} + \frac{RT}{2\alpha n_a F} \ln t \quad (2)$$

where  $\alpha$  is the transfer coefficient,  $n_a$  the number of electrons involved in the rate-determining step,  $k^0$  the specific rate constant for the latter at potential  $E = 0$  vs. N.H.E.,  $\lambda$  a function of  $i/i_d$  ( $i$  is the current along the wave and  $i_d$  the diffusion current),  $D$  the diffusion coefficient of the reducible species, and  $R$ ,  $T$  and  $F$  have their usual meaning. The shift of  $E_{1/2}$  with  $t$  then can be calculated, provided  $\alpha n_a$  and  $k^0$  do not change with  $t$  and  $\alpha n_a$  is known

$$\Delta E_{1/2} = (RT/2\alpha n_a F) \ln (t_1/t_2) \quad (3)$$

Experimentally,  $\Delta E_{1/2}$  for wave I is 3 to 5 mv. (Table I,  $t = 4.8$  and 2.7), which is within measurement error. The minimum  $\Delta E_{1/2}$ , which would occur for  $\alpha n_a = 1$  and the times involved, is 8 mv. The shift of  $E_{1/2}$  for wave II with  $t$  is even less, from which  $E_{1/2}$  can be assumed to be independent of  $t$ . Consequently, both waves seem not to be completely irreversible by this criterion.

**Rate Constant Behavior.**—Plots of  $\log k_f$  vs.  $E$ , produced by analyzing wave I in 19% ethanol solution by the Koutecky procedure, are not straight lines, but show an inflection (Fig. 1), indicating that, even if the wave proceeds irreversibly, the electrode reaction is more complicated than the simple irreversible process, assumed by Koutecky<sup>4</sup> in deriving the equation for the irreversible polarographic wave. Similar plots for wave II are straight lines.  $\alpha n_a$  and  $\log k_0$  calculated by the Koutecky method are given in Table IIA;  $\alpha n_a$  for wave I is estimated from the slope of the lower segment in the  $\log k_f$  vs.  $E$  plot.

The upper segment of the  $\log k_f$ - $E$  plot for wave I in 19% ethanol is less steep at higher than at lower temperature.<sup>5</sup> If the subsequently proposed

(1) M. Ashworth, *Collection Czech. Chem. Commun.*, **13**, 229 (1948).

(2) M. Suzuki, *Mem. Coll. Agric. Kyoto Univ.*, **67**, 1 (1954).

(3) P. J. Elving and J. T. Leone, *J. Am. Chem. Soc.*, **80**, 1021 (1958).

(4) J. Koutecky, *Collection Czech. Chem. Commun.*, **18**, 597 (1953).

TABLE I  
 VARIATION OF KETONE  $E_{1/2}$  AND  $i_d$  WITH DROP-TIME (MERCURY HEIGHT)

Ketone concn., mM	EtOH volume, %	Hg ht., cm.	Drop time, <sup>a</sup> sec.	Wave I		Wave II		
				$i_d$ , $\mu$ a.	$E_{1/2}$ , v.	$i_d$ , $\mu$ a.	$E_{1/2}$ , v.	
A. Benzophenone (pH 2.9; ionic strength 0.40 M) <sup>b</sup>								
0.10	19.0	36	4.87	0.307	-0.928	0.311	-1.100	
		42	4.13	.340	-.929	.342	-1.099	
		49	3.63	.373	-.931	.380	-1.099	
		56	3.12	.403	-.932	.409	-1.099	
		64	2.76	.435	-.933	.440	-1.098	
.10	19.0	36	4.76	.320	-.929	.322	-1.100	
		42	4.09	.350	-.930	.354	-1.099	
		49	3.51	.392	-.930	.396	-1.099	
		56	3.03	.425	-.931	.425	-1.098	
		64	2.66	.457	-.932	.451	-1.098	
B. <i>p</i> -Bromobenzophenone (pH 2.1; ionic strength 0.40 M) <sup>b</sup>								
0.08	19.0	36	5.22	0.205	-0.819	0.206	-1.042	
		42	4.42	.222	-.820	.223	-1.042	
		49	3.71	.237	-.821	.240	-1.041	
		56	3.50	.256	-.822	.258	-1.043	
		64	2.95	.272	-.824	.275	-1.040	
.10	19.0	36	5.15	.257	-.817	.254	-1.040	
		49	3.74	.296	-.818	.296	-1.042	
		64	2.86	.340	-.819	.336	-1.041	
.10	28.5	36	5.16	.238	-.839	.240	-1.050	
		49	3.76	.274	-.840	.240	-1.052	
		64	2.86	.315	-.841	.320	-1.051	

<sup>a</sup> Drop-time measured at -0.92 v. (benzophenone) or -0.84 v. (bromobenzophenone). <sup>b</sup> The pH and ionic strength are those of the aqueous buffer solution before alcohol was added; the measured pH after EtOH addition was (A) 3.1, and (B) 2.4 for 19.0% alcohol and 2.5 for 28.5% alcohol.

TABLE II

VARIATION OF KINETIC DATA FOR THE BENZOPHENONE WAVES

 A. Effect of pH  
 (19.0% ethanol; ionic strength 0.4 M)

pH <sup>a</sup>	$\alpha n_a$	Wave I		Wave II		
		$\log k^0$	$E_{1/2}$ , v. vs. N.H.E.	$\alpha n_a$	$\log k^0$	$E_{1/2}$ , v. vs. N.H.E.
1.2	1.21	-14.9	-0.575			
2.1	1.21	-16.3	-.642	1.18	-20.0	-0.849
2.9	1.21	-17.4	-.696	1.18	-20.4	-.862
3.3	1.21	-18.0	-.722	1.18	-20.6	-.872
4.0	1.21	-18.9	-.768	1.18	-20.8	-.882

 B. Effect of pH  
 (38% ethanol; ionic strength 0.3 M)

pH	Wave	$\log \frac{k_t - E}{k^0}$ Slope, mv.		$\alpha n_a$	$\log k^0$	$E_{1/2}$ , v.
2.10 <sup>a</sup>	I	53	1.12		-17.0	-0.971
(2.60) <sup>b</sup>	II	65	0.91		-16.6	-1.114
2.95	I	53	1.12		-18.1	-1.028
(3.45)	II	65	0.91		-16.9	-1.134
3.85	I	45	1.31 (1.12) <sup>c</sup>		-21.7 (-19.0) <sup>c</sup>	-1.078
(4.35)	II	65	0.91		-17.2	-1.150
4.78	C <sup>d</sup>	56	1.06		-19.4	-1.146
(5.25)						
5.70	C	59	1.00		-19.2	-1.185
(6.20)						
6.82	C	62	0.95		-19.3	-1.246
(7.50)						

 C. Effect of ethanol content<sup>e</sup>

EtOH, volume %	9.5	14.5	19.0	28.5	38.0
Wave I: $\alpha n_a$	1.04	1.18	1.21	1.18	1.12
$\log k^0$	-14.4	-16.3	-16.9	-17.4	-17.4
Wave II: $\alpha n_a$	1.26	1.23	1.18	1.00	0.91
$\log k^0$	-20.7	-20.5	-20.1	-17.8	-16.6

<sup>a</sup> pH value of original aqueous buffer solution. <sup>b</sup> pH value after alcohol addition. <sup>c</sup>  $\log k^0$  value assuming  $\alpha n_a$  to be 1.12 (see text). <sup>d</sup> Combined wave. <sup>e</sup> pH and ionic strength of aqueous solution before dilution with ethanol: 2.6 and 0.4 M.

assumption that the inflection is due to pinacol film formation, is accepted, this would tend to indicate that the free radical produced is more stable at lower temperature. Values of  $\alpha n_a$  and of  $-\log k^0$ , estimated from the  $\log k_t - E$  plot, become numerically smaller with increasing temperature.

**Effect of Ethanol Content.**—The effect of organic solvent concentration on  $E_{1/2}$  has been reported to differ for reversible and irreversible organic electrode processes.<sup>6</sup> For a reversible process, the shift of  $E_{1/2}$  arises only from pH change caused by solvent addition; in an irreversible process the shift is determined mainly by changes in kinetics of the electrode process. The variation in  $E_{1/2}$  of benzophenone with EtOH content is given in Table III; for comparison,  $E_{1/2}$  values in 19% EtOH solutions having the same pH values as those measured at the various alcoholic contents are also listed. Obviously, the shift of  $E_{1/2}$  for wave I caused by pH is much smaller than that due to change in alcohol content, e.g., the shift is 25 mv. between pH 2.7 and 3.1 in 19% EtOH, but 105 mv. for the same pH change caused by variation in alcohol content. For wave II, the former shift is 8 mv.; the latter 41 mv. These data would indicate irreversible electrode reactions.

The  $\log k_t - E$  plot<sup>7</sup> for wave I approaches a

(5) In view of the probable temperature-dependence of the transfer coefficient, no attempt was made to calculate energies from the temperature coefficients of the rate constants.

(6) K. Schwabe, *Z. Elektrochem.*, **61**, 484 (1957).

(7) The plot of  $\log k_t$  vs.  $E$  has no physical meaning if Koutecky's assumptions, subsequently discussed, are not valid; however, analysis of the shape of current-potential curve is still useful. For example, it can markedly indicate the discontinuity of wave slope.

TABLE III  
 VARIATION OF  $E_{1/2}$  FOR BENZOPHENONE AND OF  $pH$  WITH ETHANOL CONTENT

Ethanol, vol. %	0	9.5	14.5	19.0	28.5	38.0
$pH^a$	2.6	2.7	2.8	2.9	3.0	3.1
$E_{1/2}$ (wave I), v.		-0.885	-0.898	-0.911	-0.953	-0.990
$E_{1/2}$ (wave II), v.		-1.068	-1.077	-1.090	-1.100	-1.109
$E_{1/2}$ (wave I in 19% EtOH), <sup>b</sup> v.		-0.925	-0.931	-0.938	-0.945	-0.951
$E_{1/2}$ (wave II in 19% EtOH), <sup>b</sup> v.		-1.101	-1.103	-1.104	-1.107	-1.109

<sup>a</sup> Original aqueous buffer solution was of  $pH$  2.6; the  $pH$  values given are those indicated by a glass electrode-calomel electrode pair. The  $pH$  measurement is, obviously, less meaningful with increasing ethanol content. <sup>b</sup> Benzophenone waves in 19% EtOH solution prepared from aqueous solution having the  $pH$  listed above.

straight line as the alcohol content increases. Values of  $\alpha n_a$  and  $\log k^0$  for both benzophenone waves at varying EtOH content are given in Table IIC;  $\alpha n_a$  for wave I at lower EtOH concentration is estimated from the straight-line portion of the plot.

**Analysis of Current-Time Curves.**—The Koutecky theory of irreversible processes predicts that, during the life of an individual drop, the instantaneous current  $i$  at the foot of the irreversible wave is approximately proportional to  $t^{1/3}$  ( $t$  is the time from the beginning of the drop formation).<sup>8-10</sup> Consequently, current-time curves for the benzophenone reduction were analyzed.

Since the  $i$ - $t$  relation during a drop-life can be expressed approximately as

$$i = \text{constant} \times t^a \quad (4a)$$

then

$$\log i = a \log t \quad (4b)$$

To evaluate  $a$ , it is only necessary to know the relative current magnitude at each time interval. Since measurement of the faradaic current at the early stages of the drop growth is very much affected by the charging current, correction for which is difficult, and by other factors which cannot be estimated theoretically,<sup>11</sup> measurements were made at 0.5-sec. intervals, starting 0.5 sec. after the beginning of drop growth.

The results for the two benzophenone waves at different alcohol contents and drop-times (mercury heights) are given in Fig. 2; for orientative purposes,  $i$ - $t$  plots are also presented for a typical diffusion-controlled reversible process (Cd(II) reduction) and a typical irreversible process (nitromethane reduction). In the Cd(II) reduction,  $i$  is proportional to  $t^{1/6}$  at any potential along the wave. In the nitromethane reduction,  $i$  is proportional to  $t^{2/3}$  at the foot of the wave, to  $t^{1/6}$  on the diffusion current plateau and to values between  $t^{2/3}$  and  $t^{1/6}$  in the intermediate potential range; these results are those theoretically expected for an irreversible process.

Wave I seems to be kinetic-controlled, regardless of alcohol content and mercury height. At higher Hg height, the change of  $\log i$ - $\log t$  slope with potential resembles that for an irreversible process; similar behavior has been observed for benzo-

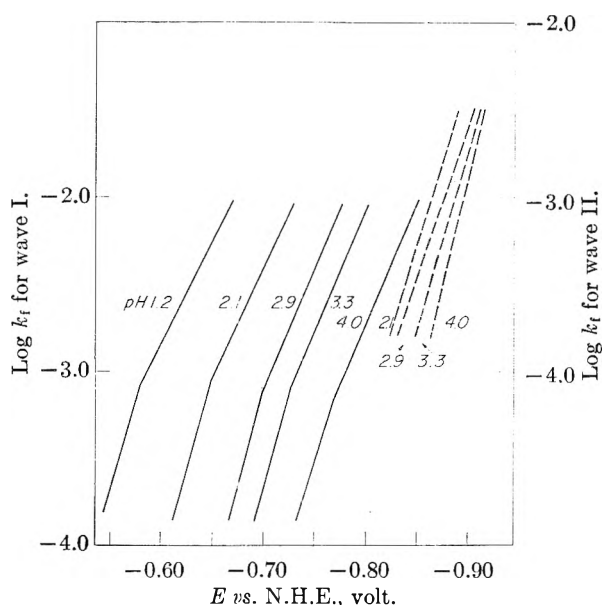


Fig. 1.—Effect of  $pH$  on the plot of  $\log k_f$  vs.  $E$  for the benzophenone reduction waves. Wave I, solid lines; wave II, dashed lines. The numbers near the lines refer to  $pH$  of the aqueous solution before ethanol addition. Solution composition, 0.1  $mM$  ketone; 19% ethanol; 0.4  $M$  ionic strength.

phenone in 0.1  $M$  LiOH.<sup>12</sup> However, even at the top of the wave the reaction is not purely diffusion-controlled as predicted by the Koutecky theory. At low EtOH content the log plot shows a convex slope at the foot of the wave; this and other aspects of the behavior of wave I are discussed in the following section.

Wave II is apparently entirely diffusion-controlled at higher Hg height, since the log slope is  $1/6$  at any potential along the wave except for the lower part of the wave in 38% EtOH, where partial kinetic-control is indicated; the latter may be due to the decrease in reaction rate by the EtOH film adsorbed on the electrode surface at high ethanol content.<sup>13</sup> At lower Hg height, all of wave II seems to be partially kinetic-controlled, even at lower EtOH content, although the reaction rate in 19% EtOH as indicated by the  $i$ - $t$  growth is higher than that in 38%. This kinetic control may be related to the peculiar  $i$ - $t$  curve shape subsequently discussed (Fig. 3). From such behavior, it is evident that the wave II process is not sufficiently rapid to make it diffusion controlled and that retardation of the reaction by an

(8) P. Kivalo, K. B. Oldham and H. A. Laitinen, *J. Am. Chem. Soc.*, **75**, 4148 (1953).

(9) P. Delahay, "New Instrumental Methods in Electrochemistry," Interscience Publishers, Inc., New York, N. Y., 1954, p. 81-82.

(10) I. Weber, *Collection Czech. Chem. Commun.*, **24**, 1420 (1959).

(11) For a discussion of these factors, see J. M. Markowitz and P. J. Elving, *Chem. Revs.*, **58**, 1047 (1958); *J. Am. Chem. Soc.*, **81**, 3518 (1959).

(12) J. Kuta and I. Smoler, *Collection Czech. Chem. Commun.*, **24**, 2208 (1959).

(13) M. Suzuki and P. J. Elving, *ibid.*, in press.



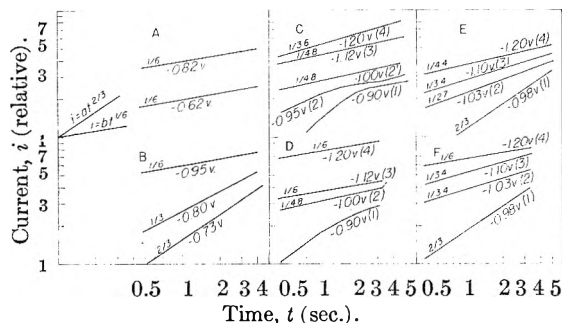


Fig. 2.—Plots of  $\log i$  vs.  $\log t$ , measured at various potentials, for: (A) 0.1  $M$  Cd(II) in 0.4  $M$  KCl ( $E_{1/2} = -0.65$  v.); (B) 0.1  $M$   $\text{CH}_3\text{NO}_2$  in pH 4.4 McIlvaine buffer plus added KCl (0.5% EtOH solution) ( $E_{1/2} = -0.77$  v.); and (C) to (F) 0.2  $M$  benzophenone in pH 2.6 McIlvaine buffer plus added KCl to 0.3  $M$  ionic strength. Potentials underneath the lines are those at which the relations were determined; fractions over the lines are the slopes of the lines (the slopes are not given for curved lines). (C) 19% EtOH,  $h$  (mercury height) = 44 cm.; (D) 19% EtOH,  $h = 64$  cm.; (E) 38% EtOH,  $h = 44$  cm.; (F) 38% EtOH,  $h = 64$  cm. Key to numbers following potentials: (1) foot of wave I; (2) upper part of wave I; (3) lower part of wave II; (4) upper part of wave II.

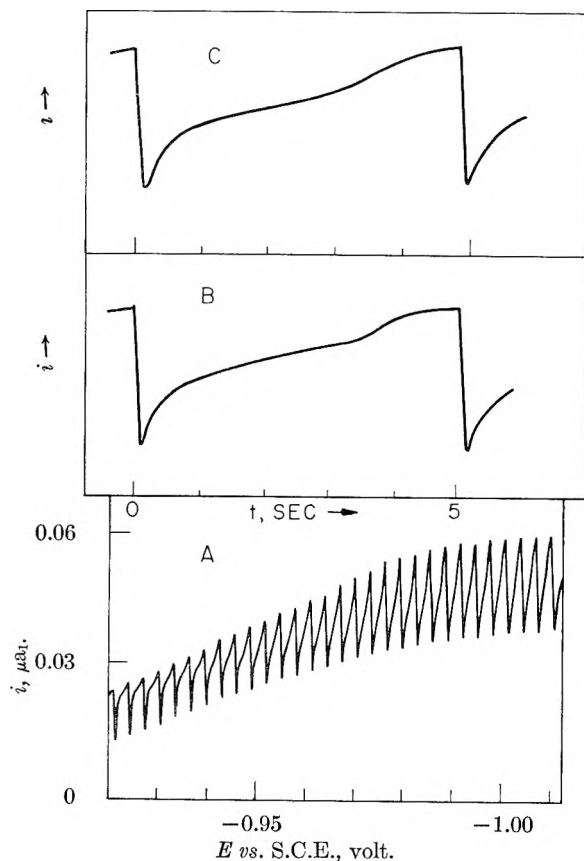


Fig. 3.—Benzophenone, 0.2  $mM$ , at pH 2.6 and 0.3  $M$  ionic strength (original solution), and 19.0% ethanol: A, rising portion of the first polarographic wave between ca. 0.5  $i_a$  and the limiting current; B, oscillographic current-time curve at  $-1.00$  v. ( $t = 5.0$  sec.); C, same as B except for the addition of ca. 0.001% Triton X-100.

ethanol film can change the electrode process from diffusion to partial kinetic control.

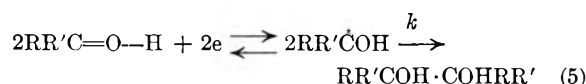
It can be concluded from the  $i-t$  curve analysis that wave I appears to be irreversible owing to the benzopinacol film formation, although the electron

transfer process itself is rapid. This phenomenon is more pronounced at lower alcoholic content because of the lesser solubility of benzopinacol in such solution.

The electrode process of wave II is diffusion-controlled at lower alcoholic content. At higher alcoholic content, it becomes partially kinetic-controlled owing to the retardation of the reaction rate by an adsorbed ethanol film. This suggests that the wave II process is not as rapid as a reversible one.

**Nature of the First Wave.**—The  $\log k_f-E$  and  $\Delta E_{1/2}-t$  relations observed indicate that the assumptions involved in the Koutecky theory are not valid in the case of the first ketone reduction process in acid solution, even if the reaction is irreversible. Koutecky assumes<sup>4</sup> that the process is controlled only by one rate-determining step and diffusion, that the product is soluble in solution or mercury, and that the backward reaction is negligible. Since the process giving rise to wave I involves only one electron, it is unlikely that two or more consecutive irreversible reactions are involved in the rate-determining step as in the case of nitromethane.<sup>13</sup> The unlikelihood of the backward reaction proceeding to any appreciable extent in the case of benzophenone is indicated by the failure to detect any anodic current by oscillographic observation of the anodic polarization of the electrode.<sup>2</sup>

The most probable discrepancy from Koutecky's assumptions is in failure of the product (carbinol free radical) to diffuse away from the electrode interface into the bulk solution due to its chemical reaction to form pinacol. In such a situation, if the rate of the dimerization reaction is very rapid, the net electrode process could appear to be irreversible, even if the electron transfer process is reversible as in



where  $k$  is the homogeneous rate constant for the dimerization reaction. The scheme of equation 5, reversible electron transfer followed by a very rapid irreversible dimerization reaction, has been analyzed mathematically by Koutecky and Hanus.<sup>14</sup> The equation of the polarographic wave is expressed as

$$\frac{(i/i_a)^3}{[1 - (i/i_a)]^2} = \frac{kC^*\lambda^3 t}{1.51} \quad (6)$$

where

$$\lambda = \exp[(n_a F/RT)(E^0 - E)] \quad (7)$$

and  $i$  is the mean current at the potential  $E$  along the wave,  $i_a$  the mean diffusion current,  $C^*$  the initial bulk concentration of the oxidant,  $t$  the drop time,  $E^0$  the standard oxidation-reduction potential for the reversible electron transfer reaction, and the other terms have their usual meaning. Relation (8) between current and potential then can be derived

$$3 \log (i/i_a) - 2 \log [1 - (i/i_a)] = \log (kC^*t/1.51) + 3E^0/0.0591 - 3E/0.0591 \quad (n_a = 1; 25^\circ) \quad (8)$$

The first and the second terms on the right-hand side are independent of  $E$ , provided that  $t$  is not appreciably changed by  $E$  along the wave. Thus, the left-hand side varies linearly with  $E$  with a slope of 19.7 mv.

On the other hand, if the electrochemical reaction leading to a free radical



proceeds irreversibly and the dimerization reaction has no effect on the electrode process, the current-potential relation should be<sup>15</sup>

$$E = \text{constant} - \frac{RT}{\alpha n_a F} \ln \frac{i}{i_d - i} \quad (10a)$$

$$= \text{constant} - \frac{0.0591}{\alpha} \log \frac{i}{i_d - i} [n_a = 1; 25^\circ] \quad (10b)$$

A plot of the log term *vs.*  $E$  should then give for wave I a straight line with a slope of 59.1/ $\alpha$  mv.

The experimentally obtained log plots are given in Fig. 4.

At low alcohol content the plot of  $\log [i/(i_d - i)]$  *vs.*  $E$  for benzophenone and *p*-bromobenzophenone is curved. With increasing EtOH content, the plot gradually becomes a straight line. On the other hand, the plot of  $\{3 \log (i/i_d) - 2 \log [1 - (i/i_d)]\}$  *vs.*  $E$  is curved in all EtOH contents investigated; however, at 38% EtOH it approximates a straight line for benzophenone reduction. Although, in general, a log plot does not accurately represent an electrode process, this behavior in log plots suggests that in low EtOH solution the electrode reaction proceeds according to neither of the schemes of equations 5 and 9, and in high EtOH solution may proceed according to that of equation 9. This assumption is reasonable, since in high alcoholic solution the electron transfer process is retarded by an adsorbed alcohol film,<sup>6,13</sup> and the rate of dimerization may be decreased due to the increased steady state concentration of pinacol resulting from its increased solubility. The failure of the plots for *p*-bromobenzophenone to become straight lines even in high EtOH solution may be attributed to the very low solubility of *p*-bromobenzopinacol.<sup>16</sup>

Thus, one may conclude from the above results that the electron transfer process for the first ketone reduction wave is neither reversible nor completely irreversible, but, as this reaction is followed by an irreversible chemical process, the net reaction appears to be completely irreversible. The rate of the irreversible chemical reaction depends on the solubility of the pinacol formed; with increasing alcohol content, the rate of the electron transfer process is retarded and the net reaction still appears to be irreversible, in which case the Koutecky treatment may be applicable to some extent. However, in the actual case some deviation from the Koutecky theory for simple irreversible processes should occur, because the reduction product dimerizes to form a film which is insoluble

(15) D. M. H. Kern, *J. Am. Chem. Soc.*, **76**, 4234 (1954).

(16) The solubilities of benzopinacol and *p*-bromobenzopinacol in alcoholic solution are not available. However, it is reasonable to suppose that, since *p*-bromobenzophenone is less soluble in alcoholic solution than benzophenone, *p*-bromobenzopinacol is less soluble than benzopinacol.

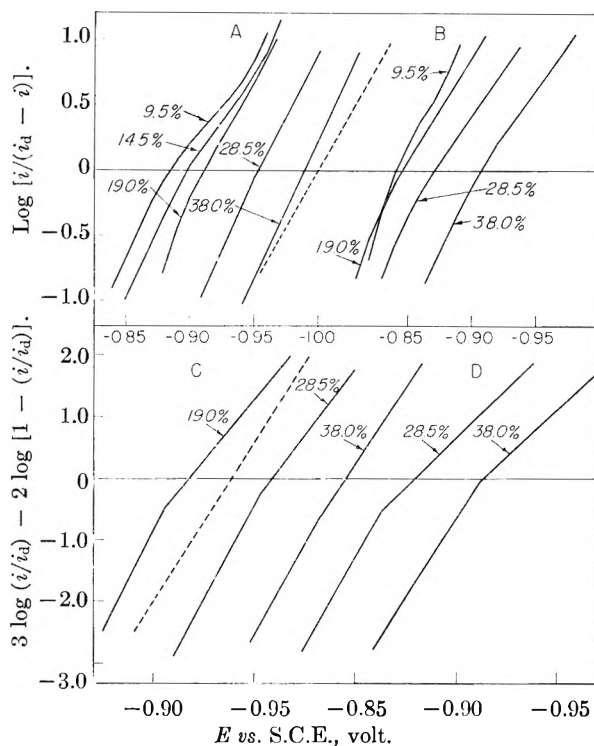


Fig. 4.—Effect of ethanol on the plots of current functions *vs.*  $E$  for wave I: A and C, benzophenone; B and D, *p*-bromobenzophenone. Solution composition, 0.1 mM ketone; 0.4 M ionic strength; pH 2.6; the percentages on the lines represent the ethanol concentration. The dotted lines represent the behavior expected for a reversible wave.

even in high EtOH content, as subsequently discussed.

**Presence of a Film Layer.**—There is considerable evidence for the formation at the electrode surface of a film layer during the reduction process, which produces wave I, due to the apparent low aqueous solubility of benzopinacol, *e.g.*, disappearance of the inflection in the  $\log k_t$ - $E$  plot with increasing alcohol content. This layer may be present as an adsorbed monolayer.

At low current (foot of the reduction wave), plots of  $\log k_t$ - $E$  for benzophenone approximately parallel each other. In this region the concentration of product formed at the interface is too low to form a film and consequently the electrode reaction proceeds smoothly. With increasing current, the product concentration becomes sufficiently high to form an insoluble film, which, by covering the electrode surface, may retard the reaction and hinder the current flow. Consequently, the  $\log k_t$ - $E$  plot shows an inflection. As benzopinacol is more soluble at higher EtOH content, film formation occurs there to a less extent and the  $\log k_t$ - $E$  relation tends toward a straight line.

Acetophenone and its pinacol are reported to be adsorbed on the mercury electrode surface; however, since these compounds are desorbed at -1.1 and -1.3 v. *vs.* S.C.E. in 0.1 M NaClO<sub>4</sub> solution and  $E_{1/2}$  of the acetophenone reduction is -1.5 v., the adsorbed film of either substance has no effect on the acetophenone reduction.<sup>17</sup> Attempts

(17) H. A. Laitinen and B. Mosier, *J. Am. Chem. Soc.*, **80**, 2363 (1958).

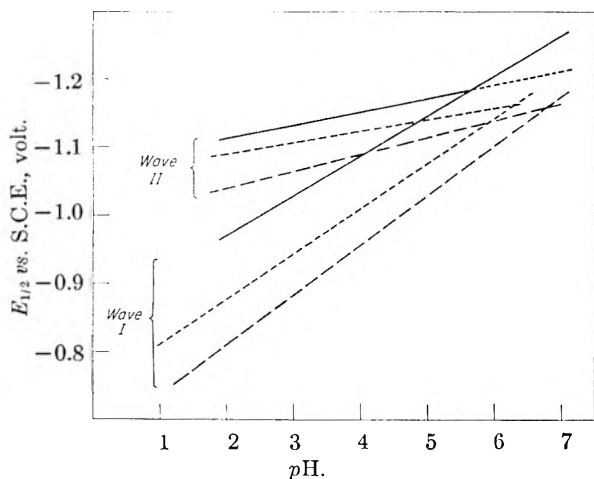


Fig. 5.—Variation of  $E_{1/2}$  with  $pH$ : solution composition, 0.1  $mM$  ketone; solid line, benzophenone in 38% EtOH; short dash line, benzophenone in 19% EtOH; long dash line,  $p$ -bromobenzophenone in 19% EtOH.

were made in the present study to detect adsorption and desorption of benzophenone and benzopinacol by alternating current polarography; a noticeable tensimetric wave could not be detected for either compound. This failure may be a result of the relatively low sensitivity of a.c. polarography for capacitance measurement.

Militating against the presence of a purely physically adsorbed layer of benzopinacol in the high alcohol content solutions used in the present work is the presumably greater adsorbability of ethanol as compared to benzopinacol. However, both adsorption of benzopinacol onto mercury and its low solubility in the solution may control film formation with the effect of adsorption being tempered by competition between the benzopinacol and ethanol for adsorption sites.

Further support for the postulated film layer is given by the current-time curves (Fig. 2). The fact that early in the drop-life the  $\log i$ - $\log t$  relation approximates a straight line with a slope of about  $2/3$  (the theoretical value for a purely kinetic controlled process) indicates that the electrode process is not hindered by the film at this stage. Later in the drop-life the current flow is obviously hindered. If this is due to the benzopinacol film formed with increased current, the effect of the film coverage must be more prominent the smaller the rate of increase in electrode area; this can be seen by comparing the curves at different mercury heights (Fig. 2C,D); the curvature is much more pronounced at lower height. At more negative potential, since film coverage should occur early in the drop-life, a discernible curvature in the log plot may not appear within the time range plotted.

A peculiar inflection in the  $i$ - $t$  curve at the upper part of wave I is identifiable with an anomalous shape in the polarograph recorder oscillation (Fig. 3). This possibly is due to the film decreasing the amount of electroactive material which reaches the electrode until the film is ruptured because of the drop expansion, which results in a burst of current due to the accumulated electroactive material. The change in capacity of the electrical double

layer due to film formation is likely a significant factor.

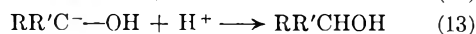
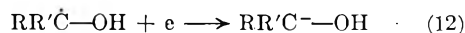
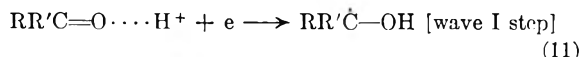
Addition of a surface-active substance (Triton X-100) is not very effective in eliminating the peculiar  $i$ - $t$  effect; this may be result from the rate of adsorption of Triton being much smaller than that of pinacol film formation or to the Triton being less successful in the competition for adsorption sites.

**Kinetics of the Reduction Wave.**—The Koutecky treatment, if applicable, would permit estimation of the kinetic parameters,  $\alpha n_a$  and  $k^0$ , from the  $\log k_f$ - $E$  plots in high EtOH concentration, where the plots approximate straight lines (Table IIB). If  $\alpha n_a$  at  $pH$  3.85, whose measurement involves some uncertainty due to the near coalescence of waves I and II, is assumed to be 1.12,  $\log k^0$  for both waves varies linearly with  $pH$  in both 19 and 38% EtOH, indicating linear dependence of the rate of the benzophenone reduction process upon hydrogen ion concentration. By extrapolating to  $pH$  0, the values of  $\log k^0$  are estimated

Ethanol, volume %	38%	19%
$\log k^0$ for wave I	-14.7	-13.3
$\log k^0$ for wave II	-15.9	-13.4

However, the value of  $\alpha n_a$  calculated from the plot slope (Table IIB) is too large ( $\alpha$  normally is between 0.7 and 0.3, and  $n_a$  for both waves is generally accepted to be 1), suggesting that the Koutecky treatment is not applicable in the present case, at least *in toto*. Consequently, the observed  $k^0$  values may be in error to some extent.

**Nature of the Second Wave.**—The electrochemical reaction mechanism of the second ketone wave in the acid solution is considered to be<sup>3</sup>



The rate of reaction 11 apparently becomes rapid; that of reaction 12 is much greater than the rate of dimerization of free radical, since, if it were not, the height of wave II would be less than that of wave I. If both reactions 12 and 13 proceed reversibly,  $E_{1/2}$  for wave II should depend on  $pH$  in a normal manner. Obviously, although the dependency of  $E_{1/2}$  for wave II on  $pH$  is less than that of wave I (Fig. 5), this dependency is contrary to the generally accepted  $pH$ -independence of the second wave.<sup>18</sup> This fact leads to the conclusion that reaction 13 participates to some extent in the potential-determining step, which is considered to be reaction 12.

It may be concluded from consideration of the slopes of the  $\log k_f$ - $E$  (Table IIB) and  $\log i$ - $\log t$  plots (Fig. 2), and of the shift of  $E_{1/2}$  with alcohol content (Table III) that wave II, *i.e.*, over-all reaction 12 and 13, is not a completely irreversible process. Existence of the backward reaction to some extent has been confirmed by oscillographic

(18) It is likely that previous investigators assumed that the variation in  $E_{1/2}$  with  $pH$  of wave II was due to experimental error. For example, the data for this wave in reference 3 is  $-1.151$  v. at  $pH$  4.1 and  $-1.169$  at  $pH$  4.8 (19% ethanol and ionic strength of 0.40  $M$ ).

observation.<sup>2</sup> Evidently, reaction 12 is a fairly rapid one, even though it might not be reversible, and reaction 13 is generally a very rapid reaction. It is, however, possible that the *pH*-dependency of wave II is associated with an acid-anion type of equilibrium involving the free radical and its protonated form, *i.e.*, there may be reduction of two competing forms.

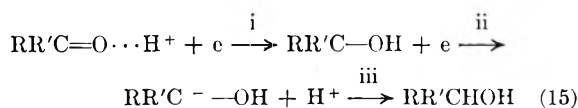
As stated in the earlier discussion of current-time curves, wave II is diffusion-controlled in 19% EtOH solution, but in 38% EtOH is partially kinetic-controlled at the lower part of the wave owing to retardation of the reaction rate by an ethanol film. Therefore, the rate constant,  $k_f$ , for wave II would have a value intermediate between those of a reversible process and a completely irreversible process. Assuming that the Koutecky procedure is applicable to the electrode process in 38% EtOH, the rate constant at  $E_{1/2}$  can be calculated from

$$k_{f(E_{1/2})} = \lambda_{1/2} D^{1/2} t^{1/2} \quad (14)$$

For the experimental conditions of Table IIB ( $D = 2.2 \times 10^{-6}$  cm.<sup>2</sup>/sec.,  $t = 3.30$  sec., *pH* 2.1 to 2.9),  $k_f$  at  $E_{1/2}$  is  $6.2 \times 10^{-4}$  cm./sec.; since the  $\log i$ - $\log t$  slope at the lower part of the wave is less than the  $2/3$  predicted by the Koutecky theory (Fig. 2), the actual rate constant may be somewhat greater. In 19% EtOH  $k_f$  should be much greater. For a reversible reaction the specific rate constant,  $k^0$ , calculated<sup>19</sup> for the  $D$  and  $t$  values specified, is *ca.*  $8 \times 10^{-3}$  cm./sec. As the actual wave II process is not completely reversible the actual rate constant at  $E_{1/2}$  for wave II in 19% EtOH would be between  $8 \times 10^{-3}$  and  $6.2 \times 10^{-4}$  cm./sec. Calculations for  $k_f$  at wave I  $E_{1/2}$  indicate it to have the same range.

The conclusion that the electron-transfer processes for ketone reduction are fairly rapid reactions, is supported by the recent study of benzophenone reduction in non-aqueous dimethylformamide solution,<sup>20</sup> although the circumstances in non-aqueous solution are somewhat different from those in aqueous solution.

**Nature of the Combined Wave.**—The electrochemical reaction mechanism of the combined ketone wave is considered to be<sup>3</sup>



In general, the natures of these reaction steps should approximate those of the first and second waves discussed. However, reaction i is not followed by an irreversible dimerization reaction as in the case of wave I in acidic solution, since the free radical immediately accepts a second electron; the net reaction involves two consecutive electron-transfer processes. Although the potential-determining step is obviously the first electron transfer process (process i, which corresponds to wave I in acidic media), the kinetic nature of the combined wave is not clear as the actual rate constant for each process is not available. In 38%

EtOH both electron-transfer processes are not as rapid as that of a reversible process. If the assumption is made that the net reaction is completely irreversible (actually, this might be not valid),  $\alpha n_a$  and  $\log k^0$  can be estimated by the Koutecky procedure (Table IIB). If  $\alpha n_a$  for each process is independent of *pH* and if  $k^0$  continues to shift linearly with *pH* as in acidic media (Table IIB),  $\log k^0$  for each reaction at higher *pH* can be calculated from the Table IIB data. From these values (Table IV) the hypothetical  $\log k_f$  for each process at  $E_{1/2}$  of the actual combined wave can be evaluated. Comparison of these values with those obtained from the combined wave indicates that the reaction rate is determined at *pH* 5.7 by process ii and at *pH* 6.8 by process i. This is reasonable, since with increasing *pH* process ii occurs at a much more negative potential than it might be itself. At *pH* 4.8, the measured  $\log k_f$  has a mean value of two processes, as might result from the merging of wave I into wave II. At higher *pH*, the wave I process probably occurs at a more negative potential than would wave II itself; consequently, process i as soon as it starts to occur, triggers process ii since the process i product is reducible at the potential of its formation. Consequently, the combined wave is mainly determined by process i.

TABLE IV  
MEASURED AND CALCULATED RATE CONSTANTS FOR BENZOPHENONE IN 38% ETHANOL

Aqueous buffer, <i>pH</i>	38% EtOH soln., <i>pH</i>	—Log $k^0$ —		Calcd. $\log k_f$ at $E_{1/2}$ of combined wave		Measd. values for combined wave	
		Wave I	Wave II	Wave I	Wave II	Log $k_f$	$E_{1/2}$ , v.
2.10	2.60	-17.0 <sup>a</sup>	-16.6 <sup>a</sup>				
2.95	3.45	-18.1 <sup>a</sup>	-16.9 <sup>a</sup>				
3.85	4.35	-19.0 <sup>a</sup>	-17.2 <sup>a</sup>				
4.78	5.25	-19.9 <sup>b</sup>	-17.5 <sup>b</sup>	-2.8	-3.6	-3.2	-0.904
5.70	6.20	-20.8 <sup>b</sup>	-17.8 <sup>b</sup>	-3.0	-3.3	-3.3	-0.943
6.82	7.50	-22.1 <sup>b</sup>	-18.3 <sup>b</sup>	-3.1	-2.8	-3.2	-1.004

<sup>a</sup> Measured value. <sup>b</sup> Calculated value.

## Experimental

**Chemicals.**—Benzophenone and *p*-bromobenzophenone were purified by recrystallization from ethanol (m.p. 48 and 81°, respectively); stock solutions (1 mM in ketone) were prepared by dissolving weighed amounts in reagent grade 95% EtOH. Other chemicals used were analytical reagent grade. McIlvaine buffers were used except at *pH* less than 2, where the HCl-KCl system was used; ionic strength of the test solution was adjusted to a definite value by adding KCl.<sup>21</sup> As the test solution contained a considerable amount of EtOH (added because of the limited solubility of ketone and to study the effect of ethanol concentration), *pH* and ionic strength in the test solution differ from those of the aqueous buffers used; *pH* and ionic strength values listed are those of the aqueous solution, unless otherwise mentioned.

Nitrogen used for deoxygenation was purified by bubbling it successively through alkaline pyrogallol solution, distilled water and, in the case of high alcoholic content test solution, a portion of the latter.

**Apparatus.**—A water-jacketed H-cell<sup>22</sup> containing a reference saturated calomel half-cell in one arm and an agar bridge plug was used at  $25 \pm 0.5^\circ$ . Reported potentials are *vs.* S.C.E. Since the cell solution resistance was

(21) P. J. Elving, J. M. Markowitz and I. Rosenthal, *Anal. Chem.*, **28**, 1179 (1956).

(22) J. C. Komyathy, F. Malloy and P. J. Elving, *ibid.*, **24**, 431 (1952).

(19) P. Delahay, *J. Am. Chem. Soc.*, **75**, 1430 (1953).

(20) A. C. Aten, Doctoral Thesis, The Free University of Amsterdam, 1959.

less than 500 ohms and the current less than 1  $\mu$ a., potentials were not corrected for  $iR$  drop.

Capillaries (Corning marine barometer tubing) used for the dropping mercury electrode had values of  $m = ca.$  1.2 mg./sec. and  $t = 3.5-4.5$  sec. at open circuit and 50 cm. pressure. The back pressure was about 1.8 cm.

A Beckman Model G pH meter was used for pH measurement.

**Current-measuring Procedures.**—Current-potential relations were measured by a Sargent Model XXI polarograph. Maximum recorder-pen deflection was taken as a measure of the true maximum current in a drop-life, use of which gives more precise results in calculations with the Koutecky equation than does the average current.<sup>8</sup> To verify this approach, maximum recorder current values were compared with those obtained using a cathode-ray oscilloscope (CRO). With no damping and a somewhat overshooting condition of the recorder pen, both values agreed within the measuring error; values of  $\alpha n_a$  and  $k^0$  obtained with this recorder technique coincide within experimental error with those measured with CRO technique. Currents obtained with the polarograph were checked occasionally with CRO observation.

Currents were measured at constant potential at 10 or 20-mv. steps along the wave and were corrected for residual current. To increase the accuracy of potential measurement, a potentiometer was used to set the span voltage of the polarograph to 500 mv. and the initial voltage to any desired potential.

Procedures for evaluating  $\alpha n_a$  and  $k^0$  by the Koutecky method from data for the polarographic wave have been described by Delahay.<sup>9</sup>

**Measurement of Current-Time Curves.**—Current-time curves during a drop-life were measured by the following oscillographic technique: polarizing potential is applied

to the dropping mercury electrode by a potentiometer. The ohmic voltage, produced by the current passing through a precision resistor (Leeds and Northrup decade box No. 4750) inserted in series with the cell in the electrolytic circuit, is fed to the input terminals of a Brown-recorder amplifier No. 76020, converted to a square wave voltage by the built-in converter, and then amplified. The output voltage produced by the gain-control of the amplifier is imposed on the vertical terminals of a DuMont No. 304H CRO and further amplified by the built-in d.c. amplifier to produce a sufficient deflection of the cathode-ray electron beam. Although the pattern obtained by this method is a distorted square wave having a frequency of 60 c.p.s., its amplitude is proportional to the magnitude of the d.c. current flowing through the electrolytic cell. By this amplifying method, the small potential of about 0.1 mv. which develops across the decade box can be sufficiently amplified to produce a considerable deflection (2 or 3 in.) on the CRO screen.

A capacitor contained in the CRO used can produce a time base of about 6 sec. for one cycle, which is sufficient to reproduce the  $i-t$  curve during one drop-life. This trace was recorded with a DuMont Type 296 CRO camera, using a diaphragm setting of f16 or f22, and Kodak Panatomic-X film (FX135). The shutter was set at "Bulb" speed and was opened during one entire sweep to record the whole  $i-t$  curve during one drop-life. The charging current was similarly recorded to permit correction of the faradaic current. The upper edge of the trace was measured to give the current.

**Acknowledgment.**—The authors wish to thank the U. S. Atomic Energy Commission, which helped support the work described.

## THE THERMAL DECOMPOSITION OF PLUTONIUM HEXAFLUORIDE<sup>1</sup>

BY L. E. TREVORROW, W. A. SHINN AND R. K. STEUNENBERG

*Chemical Engineering Division, Argonne National Laboratory, Argonne, Illinois*

*Received June 29, 1960*

Stoichiometric and equilibrium determinations were made of the thermal decomposition reaction of plutonium hexafluoride at temperatures from 150 to 400°. The reaction products under these conditions were gaseous fluorine and solid plutonium tetrafluoride. Below 300°, the equilibrium constants (moles PuF<sub>6</sub>/moles F<sub>2</sub>) were found to be higher than literature values. The sharp change in the relation between log  $K$  and  $1/T$  at 308° reported previously was not found in the present work. The relation between equilibrium constant and temperature is expressed by the equation  $\log K = -1331/T(^{\circ}\text{K.}) - 0.275$ .

### Introduction

The thermal decomposition reaction of plutonium hexafluoride is known to produce gaseous fluorine and a solid compound which is non-volatile at ordinary temperatures. On the basis of X-ray analysis, Weinstock and Malm<sup>2</sup> reported the solid compound as plutonium tetrafluoride. Other workers, however, have indicated some uncertainty regarding its identity. It was suggested that X-ray analysis may not constitute certain identification, since Mandelberg, *et al.*,<sup>3</sup> reported that a substance they identified as Pu<sub>4</sub>F<sub>17</sub> gave a diffraction pattern similar to that of plutonium tetrafluoride. Other work has also suggested the possibility of Pu<sub>4</sub>F<sub>17</sub>. The existence of plutonium pentafluoride has been postulated on the basis of thermodynamic estimates<sup>4</sup>

and some experimental evidence for it has been reported. It has not been isolated, however. Florin and co-workers<sup>5</sup> found the solid decomposition product to contain less fluorine than the pentafluoride. Thus it appeared that the solid decomposition product could be either plutonium tetrafluoride, or perhaps a plutonium compound analogous to one of the intermediate uranium fluorides, U<sub>4</sub>F<sub>17</sub>, U<sub>2</sub>F<sub>9</sub>, and UF<sub>5</sub>.

Since an identification of the solid product would involve distinguishing among a number of similar compounds, several independent methods were used to confirm the result.

Equilibrium constants for the reaction  $\text{PuF}_4 + \text{F}_2 \rightleftharpoons \text{PuF}_6$  were measured by Florin, *et al.*,<sup>5</sup> at several temperatures from 167 to 600°. They found the temperature dependence of the equilibrium constant to change rather abruptly at 308°, and suggested that this was the result of a phase change in the reacting material. Weinstock and

(1) Work performed under the auspices of the U. S. Atomic Energy Commission.

(2) B. Weinstock and J. G. Malm, *J. Inorg. Nuclear Chem.*, **2**, 380 (1956).

(3) C. J. Mandelberg, *et al.*, *ibid.*, **2**, 358 (1956).

(4) L. Brewer, *et al.*, "The Higher Fluorides of Plutonium," U. S. Atomic Energy Commission Report UCRL-633, March 20, 1950.

(5) A. E. Florin, I. R. Tannenbaum and J. F. Lemons, *J. Inorg. Nuclear Chem.*, **2**, 368 (1956).

Malm<sup>2</sup> also determined the equilibrium constant at 220°. Since these data appeared to be questionable, particularly at the lower temperatures, additional equilibrium constant determinations were made from 150 to 400°.

### Experimental

**Materials.**—Compressed fluorine was obtained from commercial sources; its purity had been determined previously to be over 99%. It was passed through a bed of sodium fluoride pellets at room temperature to remove possible traces of hydrogen fluoride. The plutonium tetrafluoride was obtained from the Rocky Flats facility through the U. S. Atomic Energy Commission. The helium used in the work was dried by passing it through a bed of Linde Molecular Sieves.

**Apparatus.**—Existing equipment in the laboratory was modified to provide sealed glove boxes suitable for the safe handling of powdered plutonium compounds. Two fume hoods were joined by a gasketed door. The sliding glass windows in the faces of the hoods were replaced by plastic panels which were equipped with glove ports and clamping bars to hold them in place. Air circulation was maintained in the hoods with suitable inlet and outlet filters to prevent any possible alpha contamination outside the hoods. The ventilation was adjusted to maintain a pressure about 0.7 inch of water below atmospheric within the hoods. Materials were transferred in and out of the hoods through a port fitted with a plastic sleeve which could be sealed and cut in such a way as to preserve the integrity of the enclosure. An oil diffusion pump with the associated vacuum gages was located inside the hood. Mechanical pumps were placed outside the hoods, but their exhausts were returned to the hoods *via* a copper line.

The apparatus was constructed of metal and was designed to operate either as a vacuum line or as a flow system. Those portions of the system in which plutonium fluorides were handled were assembled from Hoke No. 411A or 413A diaphragm valves and from nickel and Monel components welded together. The nickel and Monel sections of the vacuum line were pretreated with fluorine at pressures of 700 to 1200 mm. and temperatures of 300 to 350° for about 15 hours. The portion of the equipment in which plutonium hexafluoride was prepared, purified and handled was joined by a Teflon-gasketed flare connector to a vacuum service line. The latter consisted of 1/2-inch copper tubing and an arrangement of brass high-vacuum valves which permitted the use of the mechanical pump, the oil diffusion pump, dry traps and vacuum gages as needed.

In order to weigh samples of plutonium hexafluoride, small nickel vessels were fabricated from short lengths of 1/4-inch nickel tubing and 1/32-inch nickel sheet. Each vessel was fitted with a Hoke No. 1103 bellows valve and a flare connector by which it could be attached to the vacuum manifold. Teflon gaskets were used below 100° and copper gaskets were used at the higher temperatures. The volume of each weighing vessel was about 50 ml., and the total weight was about 150 g., which allowed them to be weighed on an ordinary analytical balance. A keyboard balance was used for ease of manipulation within the glove box.

Pressures below 1200 mm. were measured with a mercury manometer in conjunction with a Booth-Cromer pressure transmitter and self-balancing relay.<sup>6</sup> Pressures were measured above 1200 mm. with a Monel bourdon gage obtained from the American Chain and Cable Co. The bourdon gage was calibrated against a mercury manometer.

Temperatures were measured with a chromel-alumel thermocouple and a recording potentiometer. The thermocouple had been calibrated against a standard platinum resistance thermometer.

One of the problems associated with the equilibrium determinations is that the ratio of plutonium hexafluoride to fluorine in the equilibrium gas phase is small. Since the constant was derived from the amounts of plutonium hexafluoride and fluorine present in the gas phase, it was necessary to use a vessel of large volume in order to have sufficient plutonium hexafluoride for accurate weighing. As a conse-

quence, both the vessel volume and the equilibrium fluorine pressure were made as large as conveniently possible.

The equilibrium vessel, which was made from welded nickel components, had a diameter of about 3 inches and a volume of approximately 1.0 liter. A thermocouple well and a gas take-off tube extended down to the approximate geometric center of the vessel. This tube was closed by a Hoke No. 411A diaphragm valve welded to one end of the vessel. In order to obtain reliable operation at 400°, it was necessary to replace the stainless steel return spring by one made of Inconel "X". The entire assembly was enclosed in a cylindrical stainless steel heater shell which was flanged to accommodate covers at the ends. One cover was designed to permit access to the thermocouple well, the gas take-off tube and the valve, which was operated with an extension handle. The stainless steel heater shell was equipped with appropriate resistance heaters and insulation, and the temperature was controlled by a variable transformer.

A line from the valve on the gas take-off tube led to two U-traps in series, then to the vacuum line. The traps were made from 20-inch lengths of 1/4-inch nickel tubing coiled so as to produce four loops at the bottom of the U. The ends of the traps were fitted with Hoke No. 1103 bellows valves and flare connectors. The traps were of a size and weight that permitted them to be weighed on the analytical balance.

All the apparatus used for the vacuum work was tested prior to use with a helium leak detector.

**Procedure.**—Plutonium hexafluoride was prepared by passing fluorine over plutonium tetrafluoride at 550°. It was isolated by passing the gas stream through a trap cooled in Dry Ice and trichloroethylene, which condensed the product but not the fluorine. The hexafluoride was purified from the more volatile impurities such as hydrogen fluoride, occluded fluorine and carbon tetrafluoride by a procedure similar to that of Weinstock and Malm.<sup>2</sup> It was first frozen in a trap cooled by liquid nitrogen, allowed to warm slowly to room temperature and distilled into an adjoining trap cooled by Dry Ice and trichloroethylene. The latter trap was open to the diffusion pump during the distillation. This procedure was repeated several times on each batch of plutonium hexafluoride. The purity of the plutonium hexafluoride was confirmed by measuring its vapor pressure at the ice point, where it is about 16 mm.

The small nickel weighing vessels were treated with fluorine at 300 and at 400° until the rate of fluorine consumption became negligible. The weight change of the vessel during additional exposure of one hour to 300 mm. of fluorine pressure at the temperature to be used in the experiments was then measured to assure a negligible weight change due to fluorine uptake during the experiment.

The stoichiometry of the plutonium hexafluoride thermal decomposition reaction was determined from the weight changes accompanying the reaction, the change in the number of moles of gas present, and from chemical and X-ray analyses of the solid product.

For the weight change determinations, a sample of plutonium hexafluoride was distilled into one of the small vessels and weighed. The vessel was heated to decompose the hexafluoride, then cooled in liquid nitrogen and evacuated to remove the fluorine produced by the decomposition. After re-weighing, the vessel was evacuated at room temperature to remove the undecomposed plutonium hexafluoride. A third weighing allowed the weights of plutonium hexafluoride decomposed and solid residue to be calculated by difference.

For chemical analyses of the solid product, the vessels were opened with a tubing cutter and samples of the solid were weighed. The fluorine content was obtained from a pyrohydrolytic procedure followed by titration of the distillate with standard sodium hydroxide. The plutonium content was determined from the amount of solid plutonium dioxide remaining after the pyrohydrolysis.

The change in the total number of moles of gas present during the reaction was obtained from the ratio of final to initial pressures when the reaction occurred at constant volume. A portion of the system with a volume of about 100 ml. was filled with plutonium hexafluoride at a measured pressure and temperature. The sample was then condensed completely into a small vessel which formed a part of the original volume and it was isolated there by a valve. This vessel was heated to the desired temperature for a given time to decompose the hexafluoride. The system was cooled to room temperature, the valve was opened and the pressure and temperature were determined. These pressure and tem-

(6) S. Cromer, "The Electronic Pressure Transmitter and Self-Balancing Relay," U. S. Atomic Energy Commission Report, MDDC-803 (1947).



perature data together with the ideal gas law were then used to determine the ratio of final to initial moles of gas in the system.

For the equilibrium constant determinations, the large nickel vessel was charged with the solid decomposition product of plutonium hexafluoride by filling the vessel with the hexafluoride and heating it. The vessel could be charged in this manner with sufficient decomposition product for several equilibrium experiments. Fluorine was then added to the vessel at room temperature. The temperature and pressure of the fluorine were measured, and since the volume of the system was known, the amount of fluorine could be calculated. The vessel was brought to the equilibrium temperature both from higher and from lower temperatures to assure that equilibrium had been reached. After an equilibration period at temperature, the diaphragm valve was opened slightly and the equilibrium gas mixture was allowed to stream slowly from the vessel into the vacuum line at a rate of 15 to 100 ml. per minute. Flow rate variations in this range did not affect the results. The gas stream passed through the U-traps cooled in a Dry Ice-trichloroethylene mixture where the plutonium hexafluoride was condensed. When the vessel had been emptied, the traps were evacuated, warmed to room temperature and weighed. The increase in weight was assumed to be the equilibrium quantity of plutonium hexafluoride. The stoichiometric determinations had indicated that the ratio of plutonium hexafluoride to fluorine did not vary appreciably with the pressure, so no change in the equilibrium was expected during the evacuation of the vessel.

### Results

In the weight-change method of establishing the stoichiometry of the reaction, it was found that heating a sample of several hundred milligrams of plutonium hexafluoride for one hour at 60 to 100° resulted in the decomposition of only a few per cent. of the sample. In similar experiments at higher temperatures, about 80% of the sample decomposed in one hour at 200° and nearly 100% at 300°. Heating the solid thermal decomposition product during continuous evacuation at 100 to 150° for an hour resulted in no further weight change. The results of the weight-change experiments are presented in Table I. In all four experiments the ratio of fluorine to plutonium in the solid product was very close to 4.00. In the first three determinations the decomposition was allowed to proceed almost to completion. In the last experiment the reaction was quenched when about 60% of the plutonium hexafluoride had decomposed. The relatively large amount of plutonium hexafluoride was removed readily from the non-volatile decomposition product at room temperature to give the same result as the first three experiments. This observation suggests that stable complex compounds of plutonium hexafluoride and the solid decomposition product are not formed at temperatures of 25 to 150°.

TABLE I

WEIGHT CHANGE DATA FROM THE THERMAL DECOMPOSITION OF PLUTONIUM HEXAFLUORIDE

Temp., °C.	Wt. PuF <sub>6</sub> decomposed, g.	Wt. decomp. product, g.	Calcd. ratio F/Pu
300	0.3510	0.3147	4.08
300	.4178	.3717	3.95
300	.8681	.7726	3.96
200	.4958	.4416	3.97

Two samples of the decomposition product were analyzed chemically for plutonium and fluorine content. The results are given in Table II along with the theoretical values for PuF<sub>4</sub> and Pu<sub>4</sub>F<sub>17</sub>.

It is apparent that the percentages of plutonium and fluorine and the ratio are close to the values for plutonium tetrafluoride. In both analyses the sum of the plutonium and fluorine contents is close to 100%, indicating that the samples did not absorb appreciable amounts of atmospheric moisture as they were being weighed for analysis. Mandleberg, *et al.*,<sup>2</sup> reported that the radiation decomposition product of plutonium hexafluoride absorbed atmospheric moisture rapidly to form a hydrate of plutonium tetrafluoride. It is possible, however, that the crusty decomposition product formed at 300° in this work would be less reactive than the finely divided powder which Mandleberg obtained from the radiation decomposition at lower temperatures.

TABLE II

CHEMICAL ANALYSES OF THE SOLID THERMAL DECOMPOSITION PRODUCT OF PLUTONIUM HEXAFLUORIDE

Experiment	Fluorine, %	Plutonium, %	Atomic ratio F/Pu
1 <sup>a</sup>	24.3	75.6	4.05
2 <sup>b</sup>	24.6	76.0	4.06
PuF <sub>4</sub> (theor.)	24.1	75.9	4.00
Pu <sub>4</sub> F <sub>17</sub> (theor.)	25.3	74.7	4.25

<sup>a</sup> One-fourth of sample 1 was produced by decomposition of PuF<sub>6</sub> at 200°, the remainder was produced at 300°.

<sup>b</sup> Sample 2 was produced by decomposition of PuF<sub>6</sub> at 300°.

The results of the pressure measurements before and after the thermal decomposition of plutonium hexafluoride are shown in Table III. The results are expressed as the ratio of final to initial number of moles of gas in the system. Ratios are also given for hypothetical decomposition reactions. The experimental data agree more closely with the result expected if the product were plutonium tetrafluoride than with any of the other cases.

TABLE III

PRESSURE MEASUREMENTS BEFORE AND AFTER THE THERMAL DECOMPOSITION OF PLUTONIUM HEXAFLUORIDE

Ex-periment	Decomp. temp., °C.	Pressure, mm.		Temp., °K.		Pressure ratio <sup>a</sup>
		Initial	Final	Initial	Final	
1	300	105.0	108.0	299.0	299.7	1.03
2	300	95.0	96.8	302.2	304.7	1.01
3	370	78.1	80.7	294.7	296.2	1.04
Hypothetical decomposition reactions						
PuF <sub>6</sub> ⇌ PuF <sub>4</sub> + F <sub>2</sub>						1.000
PuF <sub>6</sub> ⇌ Pu <sub>4</sub> F <sub>17</sub> + 7/2 F <sub>2</sub>						0.875
PuF <sub>6</sub> ⇌ Pu <sub>12</sub> F <sub>9</sub> + 3/2 F <sub>2</sub>						.750
PuF <sub>6</sub> ⇌ PuF <sub>5</sub> + 1/2 F <sub>2</sub>						.500

<sup>a</sup> Calculated as  $P_{\text{final}} T_{\text{initial}} / P_{\text{initial}} T_{\text{final}}$ .

A final confirmation of the composition of the solid decomposition product was obtained by means of an X-ray powder pattern of the material. This material was a mixture about one-fourth of which was produced by decomposition of plutonium hexafluoride at 200°, and the remainder by decomposition at 300°. The pattern was identified as that of anhydrous plutonium tetrafluoride, with no other crystalline compounds evident.

In summary, the stoichiometry has been checked by measurement of weight change for the reaction at 300 and 200°; by chemical analysis of a residue



from decomposition of plutonium hexafluoride at 300°, and by chemical analysis of a mixture produced by decomposition at 200° and at 300°; by measurement of pressure change at constant volume before and after reaction at 300 and also at 370°; and finally by X-ray analysis on the mixture produced by decomposition at 200 and 300°.

In the equilibrium experiments, much longer periods were required for the system to reach equilibrium at the lower temperatures than at the higher ones. Less than two hours were required at 300°, 24 to 60 hours at 200°, and 150 to 300 hours at 150°. The time required to reach the equilibrium value at 150° is indicated graphically in Fig. 1.

The total pressure of gas used in the equilibrium measurements varied from 900 to 6000 mm. Within this range, there appears to be no dependence of the equilibrium constants upon the pressure of the system.

The results of the equilibrium experiments are compiled in Table IV. The equilibrium constant is defined as  $K = K_c = K_p = (\text{moles PuF}_6) / (\text{moles F}_2)$ . The values of  $\log K$  are shown as a function of  $1/T(^{\circ}\text{K.})$  in Fig. 2, where the data are represented as a single straight line. No evidence was found for a sharp change in the relation between  $\log K$  and  $1/T$  at 308° such as that described by Florin, *et al.*<sup>5</sup> The line in Fig. 2 results from fitting the data to a straight line by the method of least squares, assuming that the error of  $1/T$  is negligible compared to the error of  $\log K$ . The equation determined by this method is

$$\log K = -\frac{1331}{T(^{\circ}\text{K.})} - 0.275 \quad (1)$$

Values of  $\Delta F^0$  for the reaction  $\text{PuF}_4(\text{s}) + \text{F}_2(\text{g}) = \text{PuF}_6(\text{g})$  from 150 to 400° can be calculated from the equation

TABLE IV  
EQUILIBRIUM CONSTANT FOR THE REACTION  
 $\text{PuF}_4(\text{s}) + \text{F}_2(\text{g}) \rightleftharpoons \text{PuF}_6(\text{g})$

Initial temp., °C.	Time at equilibrium temp., hr.	Total pressure at equilibrium, mm.	Equilibrium temp., °C.	Equilibrium* constant $\times 10^4$
425	2.5	924	395 ± 0.5	50.5
25	3	902	393 ± .9	55.6
387	17	2320	336 ± .3	33.5
25	18	3150	342 ± .3	37.9
25	1	1920	302 ± 1	26.4
25	2.5	1910	303 ± 0.5	26.5
340	1	1920	301 ± 2	28.8
345	3	1920	302 ± 0.5	24.5
360	2	1920	301 ± .2	25.6
25	2.5	1920	302 ± .5	28.0
330	24.5	1920	300 ± .5	26.6
25	18.5	5030	251 ± .3	16.4
300	66	3690	251 ± .5	15.1
25	25	6250	199 ± .5	7.08
25	24.5	6250	202 ± .5	6.19
300	23	6250	200 ± .5	8.18
25	47.5	6250	200 ± .8	6.67
25	136	5620	152 ± 1	4.68
250	312	5460	150 ± 0.2	4.55

\*  $K = K_p = K_c = \text{moles PuF}_6 / \text{moles F}_2$ .

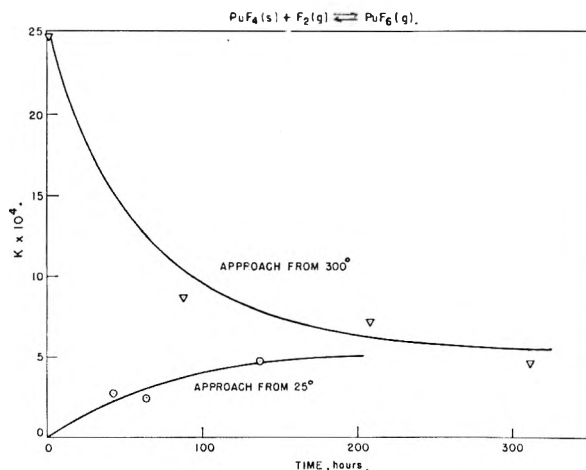


Fig. 1.—Approach to equilibrium at 150° for the reaction  $\text{PuF}_4(\text{s}) + \text{F}_2(\text{g}) \rightleftharpoons \text{PuF}_6(\text{g})$ .

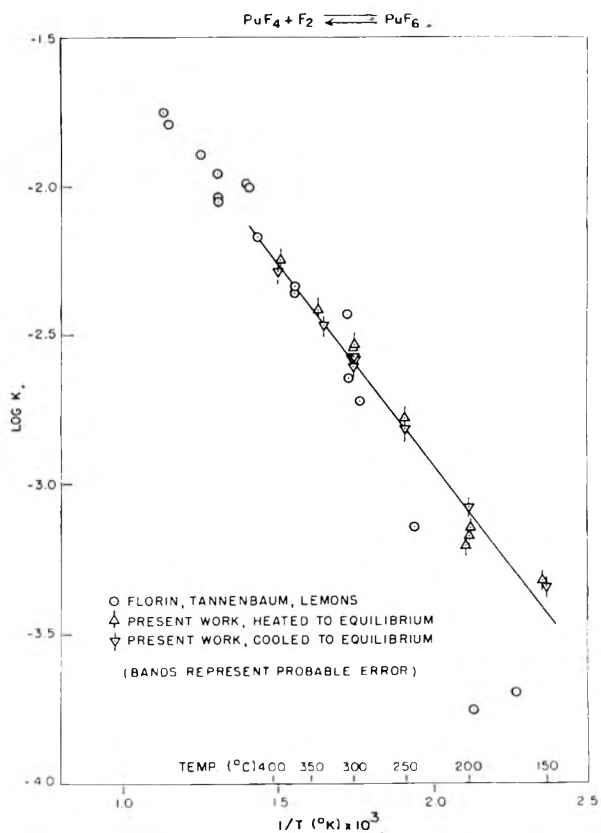


Fig. 2.—Relation between equilibrium constant and temperature for the reaction  $\text{PuF}_4 + \text{F}_2 \rightleftharpoons \text{PuF}_6$ .

$$\Delta F^0 = -RT \ln K = 6.09 \times 10^3 + 1.26 T(^{\circ}\text{K.}) \text{ cal./mole} \quad (2)$$

Using this equation, the value of  $\Delta F^0$  at 275° is calculated to be  $6.78 \pm 0.09$  kcal./mole. The mean value of  $\Delta H^0$  for the reaction has been determined from the slope of the line in Fig. 2 to be  $6.09 \pm 0.14$  kcal./mole. Using these values for the equation  $\Delta F^0 = \Delta H^0 - T\Delta S^0$ , the mean value of  $\Delta S^0$  for the reaction is  $-1.3 \pm 0.2$  cal. mole<sup>-1</sup> deg<sup>-1</sup>. The uncertainties listed are probable errors.

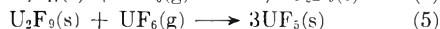
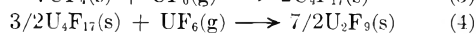
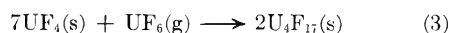
### Discussion

#### Stability of Intermediate Plutonium Fluorides.—

The interaction of plutonium hexafluoride with plutonium tetrafluoride differs greatly from that in the corresponding uranium system. When plutonium hexafluoride was heated to 200 or 300° in contact with plutonium tetrafluoride, no evidence was found for the formation of intermediate compounds, but fluorine was released. In the case of uranium, however, the intermediate fluorides formed by the interaction of uranium hexafluoride with the tetrafluoride show no appreciable dissociation into fluorine gas and the next lower compound.<sup>7</sup> The disproportionation of uranium intermediates produces only uranium hexafluoride and the next lower compound.

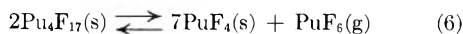
In the pressure change experiments (Table III), the total gas pressure over plutonium tetrafluoride formed in previous experiments never fell below that of the original plutonium hexafluoride metered into the vessel. This indication of the absence of a reaction between the hexafluoride and tetrafluoride to form the intermediate fluorides is in agreement with the observations of Weinstock and Malm.<sup>2</sup> Assuming that these are observations of a system at equilibrium, it is possible to estimate a limiting stability of the intermediate plutonium fluorides.

The formation of intermediate fluorides in the uranium system has been shown to proceed in a progressive fashion<sup>8</sup>



The pressures of uranium hexafluoride resulting from the disproportionation of the intermediates are in the order  $\text{UF}_5 > \text{U}_2\text{F}_9 > \text{U}_4\text{F}_{17}$ <sup>8</sup>; the stabilities are in the reverse order.

In the plutonium system the solid phase was shown to be plutonium tetrafluoride. If a minute amount of intermediate exists in the system, the equilibrium to be considered is then, by analogy with the uranium system



As an approximation, the disproportionation pressure of plutonium hexafluoride can be taken as 100 mm. at 298°K. (Table III). The equilibrium constant for the reaction in the plutonium system analogous to reaction 4 is then

$$K = p_{\text{PuF}_6} = 100/760 \text{ atm./mole PuF}_6(\text{g}) \quad (7)$$

and the corresponding free energy change is

$$F_{298}^0 = -RT \ln K \leq 1.2 \text{ kcal./mole PuF}_6(\text{g}) \quad (8)$$

The value for the corresponding uranium reaction is 19.2 kcal./mole  $\text{UF}_6(\text{g})$ .<sup>8</sup>

Thus, if it be assumed that the stabilities of any intermediate fluorides in the plutonium system lie in the same order as those of the uranium intermediates, the standard free energy change at 298°K. for the disproportionation of any plutonium fluoride intermediate between the tetrafluoride and the

hexafluoride is estimated to be equal to or less than 1.2 kcal./mole  $\text{PuF}_6(\text{g})$ .

TABLE V  
COMPARISON OF AQUEOUS WITH DRY-STATE FREE ENERGY CHANGES

(IV)-(VI) Reaction	$\Delta F_{298}^0$ , kcal./mole	Difference, kcal./mole
Aqueous couples		
$(1 M \text{HClO}_4) 2\text{H}_2\text{O} + \text{U}^{+4} \rightarrow$ $\text{UO}_2^{++} + 4\text{H}^+ + 2\text{e}^-$	15 <sup>a</sup>	33
$(1 M \text{HClO}_4) 2\text{H}_2\text{O} + \text{Pu}^{+4} \rightarrow$ $\text{PuO}_2^{++} + 4\text{H}^+ + 2\text{e}^-$	48 <sup>b</sup>	
Dry-state reactions		
$\text{UF}_4(\text{s}) + \text{F}_2(\text{g}) \rightarrow \text{UF}_6(\text{g})$	-64 <sup>c</sup>	70
$\text{PuF}_4(\text{s}) + \text{F}_2(\text{g}) \rightarrow \text{PuF}_6(\text{g})$	6.5	

<sup>a</sup> Calculated from  $E^0 = -0.32$  volt in 1 M  $\text{HClO}_4$ , given by Katz and Seaborg.<sup>9</sup> A value of  $\Delta F_{298}^0 = 15.4 \pm 1$  kcal./mole in 0.5 M  $\text{HClO}_4$  is quoted by L. Brewer, *et al.*,<sup>10</sup> based on potentials measured by Taylor and Smith.<sup>11</sup> <sup>b</sup> Calculated from data of Rabideau.<sup>12</sup> <sup>c</sup> Calculated from data listed in ref. 13.

#### Thermochemical Properties of the Uranium and Plutonium Fluorides.—

The results reported in this paper afford an opportunity to compare the heats or free energies of various reactions involving the uranium and plutonium fluorides. In Table V free energy data from this work are compared with values available in the literature for certain reactions of uranium and plutonium(IV) and (VI) fluorides. If it is assumed that the free energies of the hydrolysis reactions are roughly equal for uranium and plutonium tetrafluorides and for the two hexafluorides,<sup>4</sup> then a discrepancy of about 37.5 kcal./mole arises between the dry fluorination data and the data for aqueous reactions in Table V. This discrepancy leads to the conclusion either that the free energy data in Table V are erroneous in some respect, or that variations in the free energies of solution for uranium and plutonium tetrafluorides and hexafluorides are unexpectedly large.

Several types of experimental determinations would be helpful in resolving this discrepancy. Calorimetric determinations of the heat of formation of uranium hexafluoride and equilibrium measurements of the dissociation of uranium hexafluoride to fluorine and the tetrafluoride would be of great value. Similar data on the neptunium fluorides would permit an interesting comparison of the actinide series in this respect. Further work is also needed on reactions in the aqueous systems, particularly calorimetric determinations of heats of solution along with a thorough identification of the hydrolysis products.

**Acknowledgments.**—The authors wish to thank Prof. L. Brewer, Dr. A. E. Florin, Dr. M. J. Steindler and Dr. R. C. Vogel for comments and advice

(9) J. J. Katz and G. T. Seaborg, "The Actinide Elements," Methuen and Co., Ltd., London, 1957, p. 180.

(10) L. Brewer, *et al.* in "Chemistry of Uranium. Collected Papers," U. S. Atomic Energy Commission Report, TID-5290, p. 231 (1958).

(11) J. K. Taylor and E. R. Smith, *ref. 10*, p. 429.

(12) S. W. Rabideau, *J. Am. Chem. Soc.*, **78**, 2705 (1956).

(13) F. D. Rossini, *et al.*, "Selected Values of Chemical Thermodynamic Properties," U. S. Dept. of Commerce, National Bureau of Standards Circular No. 500 (1952).

(7) P. A. Agron, in "Chemistry of Uranium, Collected Papers," U. S. Atomic Energy Commission Report TID-5290, p. 610 (1958).

(8) J. S. Broadley and P. B. Longton, "The Reactions of  $\text{UF}_6$  with  $\text{UF}_4$ ," United Kingdom Atomic Energy Authority Report RDB(C)/TN-60 (1954).

on many aspects of the problem. The assistance of Mr. C. A. Seils and Mr. R. M. Clarke, who performed the chemical analyses, is also gratefully acknowledged.

## A THERMODYNAMIC STUDY OF THE SYSTEM AMMONIUM FLUORIDE-WATER. I. THE HEAT CAPACITY AND THERMODYNAMIC FUNCTIONS OF AMMONIUM FLUORIDE MONOHYDRATE

BY LEONARD C. LABOWITZ AND EDGAR F. WESTRUM, JR.

*Department of Chemistry, University of Michigan, Ann Arbor, Michigan*

*Received July 8, 1960*

Thermal analysis and solubility determinations on the  $\text{NH}_4\text{F}$ -rich side of the  $\text{NH}_4\text{F}$ - $\text{H}_2\text{O}$  eutectic indicate a peritectic temperature of  $246.0^\circ\text{K}$ . and a eutectic temperature of  $244.15^\circ\text{K}$ ., in contrast with  $256.4$  and  $246.7^\circ\text{K}$ ., respectively, reported by Yatlov and Polyakova. The existence of the compound  $\text{NH}_4\text{F}\cdot\text{H}_2\text{O}$  at  $245.7^\circ\text{K}$ . was established by application of the method of wet residues to the system  $\text{NH}_4\text{F}$ - $\text{NH}_4\text{I}$ - $\text{H}_2\text{O}$  at that temperature. The heat capacity of the monohydrate was determined from  $5$  to  $323^\circ\text{K}$ . The values of the saturation heat capacity,  $C_s$ , and the derived thermodynamic functions  $S^\circ$ ,  $H^\circ - H_0^\circ$ , and  $(F^\circ - H_0^\circ)/T$  at  $298.15^\circ\text{K}$ . are  $37.22$  cal./deg. mole,  $34.92$  cal./deg. mole,  $6146$  cal./mole, and  $-14.30$  cal./deg. mole, respectively. The enthalpy increment of the peritectic reaction is  $1360$  cal./mole at  $246^\circ\text{K}$ .

### Introduction

In the course of investigating the range of existence and the thermophysical properties of the solid solution of ammonium fluoride ( $\text{NH}_4\text{F}$ ) in ice reported by Brill and Zaromb,<sup>1,2</sup> thermal analysis measurements were carried out from  $230$  to  $290^\circ\text{K}$ . over the entire composition range of the system  $\text{NH}_4\text{F}$ - $\text{H}_2\text{O}$ . The results of these measurements in the monohydrate region of the system indicate that the eutectic and peritectic temperatures are so much closer together than the corresponding temperatures found by Yatlov and Polyakova<sup>3</sup> that it was not immediately evident whether the incongruently melting compound ammonium fluoride monohydrate ( $\text{NH}_4\text{F}\cdot\text{H}_2\text{O}$ ) reported by them really exists or whether the observed thermal halt was due to the eutectic transition alone. The present investigation involving equilibrium heat capacity determination by the adiabatic technique, Schreinemakers' wet residues analyses, and solubility determinations, was therefore undertaken. The existence of the compound ammonium fluoride monohydrate was established and its thermodynamic properties were determined.

### Experimental

**Preparation and Purity of Ammonium Fluoride.**—Ammonium fluoride was prepared by treating reagent hydrofluoric acid (48 wt. % aqueous HF) in a silver beaker with an excess of ammonia gas. The warm, strongly ammoniacal solution of ammonium fluoride obtained in this manner was transferred into a polyethylene bottle through a polyethylene funnel and a filter paper leached with hydrofluoric acid. Boiled distilled water was added to the filtrate to bring all of the crystals into solution at  $40^\circ$ . The bottle was then sealed and submerged in a large and well-insulated bath and allowed to cool gradually from  $40$  to  $0^\circ$  over a period of four days. Large clusters of acicular crystals resulted from this slow cooling-process. The crystals were separated from the mother liquor on a polyethylene Büchner funnel, rinsed with cold ammonia-saturated methanol, and packed into a polyethylene drying column. A stream of anhydrous ammonia gas was passed over the material for two days at room temperature. The dry crystals were then transferred to a silver beaker and evacuated for an hour in a vacuum desiccator to

remove excess ammonia gas. The product was stored in closed polyethylene bottles under an atmosphere of ammonia gas in a desiccator lined with paraffin and charged with calcium oxide. Analysis for  $\text{NH}_4^+$  by the Kjeldahl method<sup>4</sup> gave  $48.70 \pm 0.04$  (volumetric buret) and  $48.72 \pm 0.02$  (weight buret) wt. % (theoretical: 48.70). Analysis for  $\text{F}^-$  by the  $\text{PbFCl}$  gravimetric method<sup>5</sup> using the modified precipitation procedure of Kapfenberger<sup>6</sup> indicated  $51.32 \pm 0.03$  wt. %  $\text{F}^-$  (theoretical: 51.30). Interference of ammonium ion with the  $\text{PbFCl}$  precipitation<sup>7</sup> was eliminated by boiling the sample with dilute sodium hydroxide solution until the vapors evolved had no noticeable effect on the color of moist red litmus paper. The remaining alkaline solution was then neutralized with dilute hydrochloric acid in the presence of methyl orange indicator. To ascertain if the high chloride concentration resulting from this neutralization would interfere, the precipitation was carried out on a standard sample of sodium fluoride in the presence of a comparable amount of sodium chloride; the results were  $99.73\%$  of theoretical. The determination of water by the Karl Fischer method<sup>8</sup> gave  $0.004$  wt. %  $\text{H}_2\text{O}$  with the "dead stop" end-point technique. Using the procedure outlined for ammonium fluoride by Rosin,<sup>9</sup> none of the following contaminants were detected (the figures represent the sensitivity limits of the tests in wt. %): ignition residue  $< 0.002$ , acid fluoride ( $\text{NH}_4\text{HF}_2$ )  $< 0.05$ , chloride ( $\text{Cl}^-$ )  $< 0.002$ , nitrate ( $\text{NO}_3^-$ )  $< 0.01$ , silicofluoride (as  $\text{H}_2\text{SiF}_6$ )  $< 0.3$ , sulfate ( $\text{SO}_4^{2-}$ )  $< 0.010$ , heavy metals (as Pb)  $< \text{about } 0.002$ , and iron (Fe)  $< 0.003$ . The completeness of removal of methanol from the product was established by negative results with the spot test (sensitive to  $0.003$  wt. % methanol) developed by Eegriwe<sup>10</sup> and recommended by Feigl.<sup>11</sup> This method is based on the oxidation of methanol to formaldehyde with permanganate and subsequent color development with chromotropic acid (1,8-dihydroxynaphthalene-3,6-disulfonic acid). Furthermore, a weighed sample of reagent ammonium fluoride (which presumably had never been previously exposed to methanol) was treated with an approximately equal weight of methanol in a platinum dish, placed in a vacuum desiccator and evacuated. After 1.5 and 10

(4) I. M. Kolthoff and E. B. Sandell, "Textbook of Quantitative Analysis," Rev. Ed., The Macmillan Co., New York, N. Y., p. 1948, 562.

(5) G. Stark, *Z. anorg. Chem.*, **70**, 173 (1911).

(6) W. Kapfenberger, *Aluminium*, **24**, 428 (1942).

(7) R. P. Treadwell and W. T. Hall, "Analytical Chemistry," Vol. II, "Quantitative Analysis," 9th English Ed., John Wiley and Sons, New York, N. Y., 1942, pp. 397 and 739.

(8) I. M. Kolthoff and R. Belcher, "Volumetric Analysis," Vol. III, Interscience Publishers, Inc., New York, N. Y., 1957, p. 431.

(9) J. Rosin, "Reagent Chemicals and Standards," 3rd Ed., D. Van Nostrand Co., New York, N. Y., 1955, p. 38.

(10) E. Eegriwe, *Mikrochim. Acta*, **2**, 329 (1937).

(11) F. Feigl, "Spot Tests," Vol. 2, Elsevier Publishing Co., Amsterdam, 1954, p. 244.

(1) R. Brill and S. Zaromb, *Nature*, **173**, 316 (1954).

(2) S. Zaromb and R. Brill, *J. Chem. Phys.*, **24**, 895 (1956).

(3) V. S. Yatlov and E. M. Polyakova, *Zhur. Obshchei Khim.*, **15**, 724 (1945).

hours of evacuation the weight of the dry residue agreed with the initial weight of the untreated ammonium fluoride within the limits of experimental accuracy. The retention by the residue of as little as 0.01 wt. % methanol could have been detected in this manner. To test for ammonium carbonate (actually a mixture of ammonium bicarbonate and ammonium carbamate), an aqueous solution of the sample was treated in a centrifuge tube with a slight excess of saturated aqueous thorium nitrate solution to precipitate  $F^-$ . The flocculent precipitate was centrifugally separated and the supernatant liquid tested by the dropwise addition of 1 *N* HCl. Effervescence, indicating the presence of as little as 0.05 wt. % ammonium carbonate, could have been detected with a 10X magnifying glass. The product gave a negative result. For calorimetric measurements, wet residue studies and solubility determinations, only the ammonium fluoride prepared and analyzed in the manner described above was employed. For some of the thermal analysis measurements, however, reagent ammonium fluoride further purified by treatment with a stream of anhydrous ammonia gas was used. Analysis for  $NH_4^+$  by the Kjeldahl method gave  $48.67 \pm 0.04$  wt. %  $NH_4^+$ . Analysis for  $F^-$  by the Kapfenberger volumetric modification<sup>8</sup> of the Pb- $FCl$  method (the  $PbFCl$  precipitate is dissolved in dilute nitric acid, and the  $Cl^-$  content is determined by the Volhard method<sup>12</sup>) gave:  $51.33 \pm 0.03$  wt. %  $F^-$ . On the basis of these averages  $F^-/NH_4^+ = 1.0014$ . The thermal analysis results obtained with this purified commercial material coincide with those obtained with the specially prepared material.

**Thermal Analysis.**—The sample-container used for the thermal analysis measurements consisted of a silver cylinder of approximately 90-cc. capacity fitted with a motor-driven silver reciprocating stirrer (inserted through a Teflon bushing) and an entrant silver thermocouple well. The sample-container was suspended within a variable-pressure submarine placed in a constant-temperature refrigerating bath.<sup>13</sup> Cooling and warming rates were regulated by adjustment of bath temperature and of conduction gas pressure. The 55-g. samples were prepared in polyethylene bottles and transferred to the silver container. Temperature was measured to within 0.1° by means of a calibrated single-junction copper-constantan thermocouple and a millivolt range potentiometer. Potential readings were taken every minute or every half-minute.

**Solubility Determinations.**—Samples were enclosed in a small polyethylene bottle (equipped with a silver thermocouple well fitted through the cap) and suspended within a large test-tube in a bath about 5° below the eutectic temperature of the system for 4 to 5 hours. The samples were then equilibrated at the desired temperature for at least 9 hours with intermittent shaking. Samples of the aqueous solution were withdrawn with a hypodermic needle and analyzed for  $NH_4^+$  by the Kjeldahl method.

**Schreinemakers' Method of Wet Residues.**—The method of wet residues<sup>14</sup> was applied to the system  $NH_4F-NH_4I-H_2O$  at  $245.7 \pm 0.01^\circ K.$  to prove that a solid phase of composition  $NH_4F \cdot H_2O$  exists at that temperature. The samples were held in a small polyethylene bottle (with a silver thermocouple well and two lengths of 0.5 mm. dia. thin wall polyethylene tubing, for removing the liquid phase, passing through the cap) and suspended within a large test-tube in a constant temperature refrigerating bath. To separate the liquid phase from the wet residue, the tubes were blown clear of solid material, and the liquid was then sucked into a polyethylene receiver. The liquid phase and the wet residue were analyzed for  $NH_4^+$  by the Kjeldahl method and  $I^-$  by the method of Sadusk and Ball.<sup>15</sup> Fluoride interfered with the starch-iodine end-point and had to be inactivated by complexation with aluminum.

The reagent ammonium iodide used for wet residues studies gave the following analysis:  $NH_4^+ = 12.36$  wt. % by the Kjeldahl method (theoretical: 12.44);  $I^- = 87.63$  wt. % by gravimetric  $AgI$ <sup>12</sup> (theoretical: 87.56).  $I^-/NH_4^+ = 1.006$ .

**Adiabatic Calorimetric Measurements.**—The heat capac-

ity of ammonium fluoride monohydrate was measured by the adiabatic method from 5 to 323°K. The cryostat and circuits employed for this purpose are very similar to those previously described by Westrum, Hatcher and Osborne.<sup>16</sup>

Because of the corrosive nature of ammonium fluoride solutions, the calorimeter (laboratory designation W-19) was made of silver with the walls tapered slightly upward to allow for the expansion of the contents on freezing. A Monel cupola acted as a thermal dam during the soldering procedure and made it possible to seal the cap with 50-50 Pb-Sn solder without heating the contents. Thermal conductivity vanes were not used. Helium gas at a pressure of one atmosphere at 300°K. was used to provide thermal conduction between the calorimeter and its contents. The mass of the calorimeter is approximately 109 g. and the internal volume approximately 63.5 ml. The heat capacity of the calorimeter-heater-thermometer assembly was determined separately. The weight of Apiezon-T used for thermal contact between heater, thermometer and calorimeter was the same for both the calorimeter as run empty and when loaded with monohydrate, but corrections were applied for small differences in the amounts of helium and solder employed.

Temperature was measured with a 25-ohm platinum resistance thermometer inserted into the calorimeter by means of an entrant well. The thermometer was calibrated at the National Bureau of Standards by measuring its electrical resistance at the following fixed points on the International Temperature Scale: the boiling-point of oxygen, the ice-point, the steam-point, and the boiling point of sulfur. On the basis of these measured resistances the constants of the Callendar-Van Dusen equation were evaluated. Between 10 and 90°K. the thermometer was compared at 19 temperatures with the Bureau's platinum resistance temperature scale.<sup>17</sup> Between 4 and 10°K. a provisional temperature scale was established by using the value of  $dR/dT$  at 10°K., the resistance of the thermometer at 10°K., and the resistance of the thermometer at the boiling-point of liquid helium to evaluate the constants in the equation  $R = A + BT^2 + CT^6$  of Hoge and Brickwedde.<sup>17</sup> It is believed that the absolute values of the temperatures on this scale agree with the thermodynamic temperature scale to within 0.1° from 4 to 14°K., to within 0.02° from 14 to 90°K., and to within 0.03° from 90 to 373°K. Determinations of the temperature increments after correction for quasi-adiabatic drift are probably correct to within a millidegree.

Heat capacity measurements were made by determining the temperature rise produced by a measured input of electrical energy. Current and potential measurements were made on the electrical heater during the energy input and on the platinum resistance thermometer during the drift periods. The measurements of current and potential were made on an auto-calibrated White double potentiometer.

To load ammonium fluoride monohydrate, which is a two-phase mixture near room temperature, as much solid ammonium fluoride as possible was weighed into the calorimeter, and an additional weighed amount was rinsed in with water. The stoichiometric amount of water was determined by weight. The sample mass was 50.243 g. (*in vacuo*). The buoyancy corrections were based on the crystallographic density of 1.0092 g./cc. for ammonium fluoride determined by Wulff and Cameron,<sup>18</sup> and on the data of Heydweiller<sup>19</sup> for the densities of ammonium fluoride solutions.

## Results and Discussion

**Phase Equilibria in the Region of the Monohydrate.**—The only previous general study of the system  $NH_4F-H_2O$  is the work of Yatlov and Polyakova<sup>3</sup> who investigated the entire composition range from 246.7 to 353.2°K. by thermal analyses and solubility determinations and reported the existence of a previously unknown compound, ammonium fluoride monohydrate ( $NH_4F \cdot H_2O$ ), having an incongruent melting point

(12) W. C. Pierce and E. L. Haensch, "Quantitative Analysis," 3rd Ed., John Wiley and Sons, Inc., New York, N. Y., 1948.

(13) R. E. Dodd and P. L. Robinson, "Experimental Inorganic Chemistry," Elsevier Publishing Co., Amsterdam, 1954, p. 56.

(14) F. A. H. Schreinemakers, *Z. Physik. Chem.*, **11**, 75 (1893).

(15) J. F. Sadusk, Jr., and E. G. Ball, *Ind. Eng. Chem., Anal. Ed.*, **5**, 386 (1933).

(16) E. F. Westrum, Jr., J. B. Hatcher and D. W. Osborne, *J. Chem. Phys.*, **21**, 419 (1953).

(17) H. J. Hoge and F. G. Brickwedde, *J. Research Natl. Bur. Standards*, **22**, 351 (1930).

(18) P. Wulff and H. K. Cameron, *Z. physik. Chem., Abt. B*, **10**, 347 (1930).

(19) A. Heydweiller, *Ann. Phys.*, **37**, 739 (1912).

at 256.4°K. Their evidence for the existence of this compound consists of a halt in the cooling curve of a monohydrate-composition mixture at 256.4°K. and chemical analysis of the solid-phase obtained by maintaining an NH<sub>4</sub>F-H<sub>2</sub>O mixture of total system composition 28.5 mole % NH<sub>4</sub>F at 254.2 ± 1°K. with continuous stirring for four hours, filtering off the solid phase at 254.2°K., and rinsing off the adhering mother liquor with cold (254.2°K.) acetone. Analysis of the dry residue thus obtained was in good accord with the formula NH<sub>4</sub>F·H<sub>2</sub>O. Other previous investigations of this region of the system have been confined to determinations of the solubility of ammonium fluoride<sup>20-25</sup> over the temperature range 273.2 to 312.2°K. To conserve space the results of these studies are presented on the partial phase diagram in Fig. 1. A more extensive tabulation of these results has been prepared.<sup>26</sup>

Thermal analysis and solubility data from this study presented in Tables I and II, respectively, and in Fig. 1 are at variance with the findings of Yatlov and Polyakova<sup>3</sup> in that the present investigation indicates a peritectic transition at 246.0°K. and a eutectic transition at 244.5°K. Not only are both temperatures significantly lower than those previously reported, but they are so close together as to suggest doubt that both are not simply manifestations of the eutectic transition insofar as the observed thermal halts are concerned. However, the very sharp break of the solubility curve obtained in the present thermal analysis and solubility determinations strongly supports the existence of the peritectic transition.

TABLE I

THERMAL ANALYSIS DATA ON THE SYSTEM NH<sub>4</sub>F-H<sub>2</sub>O

Mole % NH <sub>4</sub> F in sample	T, °K.	Feature noted	Solid phase(s) present
18.86	245.3	F.p. <sup>a</sup>	α <sup>a</sup>
	244.5	Eutectic	α, NH <sub>4</sub> F·H <sub>2</sub> O
22.50	245.5	F.p.	α
	244.5	Eutectic	α, NH <sub>4</sub> F·H <sub>2</sub> O
23.02	245.7	F.p.	NH <sub>4</sub> F·H <sub>2</sub> O
	244.5	Eutectic	α, NH <sub>4</sub> F·H <sub>2</sub> O
28.08	246.0	Peritectic	NH <sub>4</sub> F, NH <sub>4</sub> F·H <sub>2</sub> O
	244.5	Eutectic	α, NH <sub>4</sub> F·H <sub>2</sub> O
79.87	246.0	Peritectic	NH <sub>4</sub> F, NH <sub>4</sub> F·H <sub>2</sub> O
100	230-290	None	NH <sub>4</sub> F

<sup>a</sup> F. p. = freezing point; α = solid solution.

(20) A. V. Novoselova and M. Ya. Averkova, *Zhur. Obshchei Khim.*, **9**, 1063 (1939).  
 (21) A. K. Zhdanov and M. A. Sarkazov, *Zhur. Fiz. Khim.*, **29**, 602 (1955).  
 (22) H. M. Haendler and A. W. Jache, *J. Am. Chem. Soc.*, **72**, 4137 (1950).  
 (23) J. E. Ricci and J. A. Skarulis, *ibid.*, **73**, 3618 (1951).  
 (24) H. M. Haendler and A. Clow, *ibid.*, **74**, 1843 (1952).  
 (25) W. M. Spurgeon, Ph.D. Dissertation, University of Michigan, 1942.

(26) Tabulation of the literature thermal analysis and solubility data on a consistent basis, more extensive tables of the thermodynamic properties of the ammonium fluoride-water system, and other details of this study have been deposited as Document Number 6421 with the ADI Auxiliary Publications Project, Photoduplication Service, Library of Congress, Washington 25, D. C. A copy may be secured by citing the document number and remitting \$2.50 for photoprints or \$1.75 for 35 mm. microfilm in advance by check or money order made payable to: Chief, Photoduplication Service, Library of Congress.

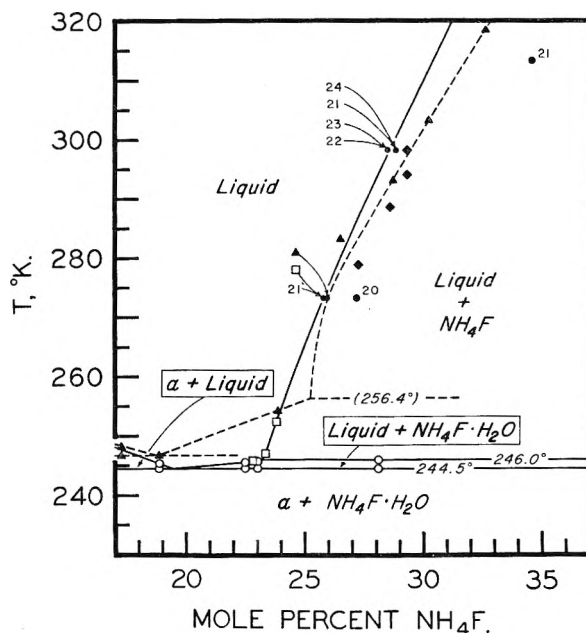


Fig. 1.—Partial phase diagram for the system NH<sub>4</sub>F-H<sub>2</sub>O. The data of this investigation are represented by ○ for thermal analysis determinations and □ for solubility determinations. Solubility data of Yatlov and Polyakova<sup>3</sup> are indicated by ▲, those of Spurgeon<sup>25</sup> by ◆, and other solubility points by reference numbers. The phase diagram of this investigation is indicated by solid lines and that of Yatlov and Polyakova by dashed lines. α represents a solid solution.

TABLE II

SOLUBILITY DETERMINATION ON THE SYSTEM NH<sub>4</sub>F-H<sub>2</sub>O

Mole % NH <sub>4</sub> F in liquid	T, °K.	Feature noted	Solid phase
25.63	273.2	Solubility	NH <sub>4</sub> F
23.80	252.4	Solubility	NH <sub>4</sub> F
23.31	247.0	Solubility	NH <sub>4</sub> F
22.84	245.7	Solubility	NH <sub>4</sub> F·H <sub>2</sub> O

**The Existence of the Phase NH<sub>4</sub>F·H<sub>2</sub>O.**—Application of the method of wet residues to the ternary system NH<sub>4</sub>F-NH<sub>4</sub>I-H<sub>2</sub>O at 245.7 ± 0.1°K. provides conclusive evidence that a solid phase of the composition NH<sub>4</sub>F·H<sub>2</sub>O does exist in the short range between the peritectic and the eutectic temperatures. The analyses are presented in Table III and the extrapolations to the composition of the anhydrous solid phase are shown in Fig. 2. Moreover, the eutectic temperature and the temperature of the incongruent melting point determined by adiabatic calorimetry are also in good agreement with the findings from thermal analysis and solubility determinations.

TABLE III

WET RESIDUES DATA FOR THE SYSTEM NH<sub>4</sub>F-NH<sub>4</sub>I-H<sub>2</sub>O AT 245.7 ± 0.1°K.

	Run no.	Liquid phase	Wet residue	Solid phase
Mole % NH <sub>4</sub> F	1	23.35	32.06	50.5
Mole % NH <sub>4</sub> I	1	0.771	0.534	
Mole % NH <sub>4</sub> F	2	24.02	33.81	49.8
Mole % NH <sub>4</sub> I	2	1.631	0.994	

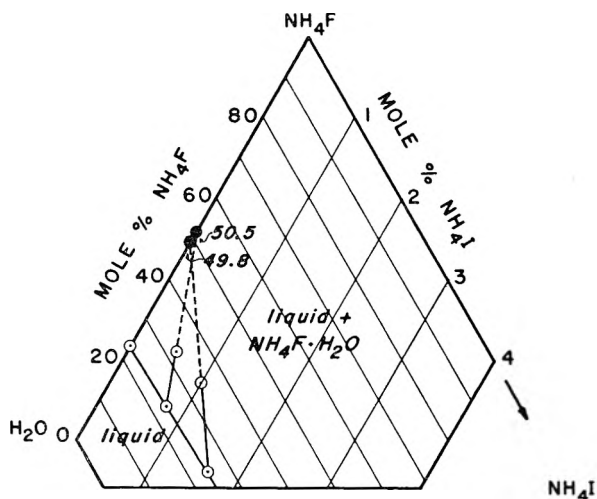


Fig. 2.—Ternary phase diagram of the system  $\text{NH}_4\text{F}$ - $\text{NH}_4\text{I}$ - $\text{H}_2\text{O}$  at  $245.7^\circ\text{K}$ .

**The Peritectic Temperature.**—No adequate explanation of the discrepancy between the peritectic temperature found by the present investigation and the one reported  $8^\circ\text{K}$ . higher by Yatlov and Polyakova<sup>3</sup> has been found. The possibility of a metastable equilibrium was considered initially but rejected after several years of experience in studying this system. It is to be noted, however, that studies of the temperature dependence of the dielectric constant of ammonium fluoride have resulted in a report of anomalous behavior in the region  $242$  to  $246^\circ\text{K}$ . by both Shul'vas-Sorokina and Evdokimov<sup>27</sup> and by Kamiyoshi.<sup>28</sup> Likewise, Simon, von Simson and Ruhemann<sup>29</sup> reported the existence of a "hump" in the heat capacity at  $243^\circ\text{K}$ . It is considered likely that the heat capacity hump and the dielectric constant anomalies may be attributable to the presence of water in the ammonium fluoride investigated. Proof that a thermal anomaly does not exist at this temperature was demonstrated by Benjamins and Westrum<sup>30</sup> who found no evidence of a phase transition in a high-purity sample of ammonium fluoride over the region  $6$  to  $309^\circ\text{K}$ . It is to be noted, however, that the reported anomalies, probably due to traces of water, have invariably been found in the vicinity of the peritectic temperature of the present investigation rather than at that reported by Yatlov and Polyakova. In order to confirm the results of thermal analysis by further equilibrium studies the heat capacity of ammonium fluoride monohydrate was determined over the range  $5$  to  $323^\circ\text{K}$ . with precise adiabatic calorimetry.

**Heat Capacity Results.**—The experimental heat capacity determinations are presented in Table IV in chronological order so that experimental temperature increments can usually be inferred from the adjacent mean temperatures. An analytically de-

termined curvature correction was applied to correct the observed values of  $\Delta H/\Delta T$  for the finite temperature increments employed in the measurements and yield the true or differential heat capacity. In addition a correction was made at the higher temperatures for the vaporization of water from the solution and for the heat capacity of water vapor in the small space over the liquid solutions. The vaporization corrections, detailed elsewhere,<sup>28</sup> were negligible below  $260^\circ\text{K}$ . and did not exceed  $0.1\%$  at the highest temperatures. Since the reported heat capacities of the condensed phases represent those under the saturation vapor pressure of the samples in the presence of a fraction of an atmosphere of helium pressure, they are represented by the symbol  $C_s$ . It is to be noted, however, that at least over the solid region these values are practically indistinguishable from the heat capacity at constant pressure. The results are expressed in terms of the defined thermochemical calorie (equal to  $4.1840$  absolute joules) and an ice-point of  $273.15^\circ\text{K}$ . The probable error of the heat capacities is estimated to be about  $0.1\%$  above  $25^\circ\text{K}$ ., increasing to  $1\%$  at  $10^\circ\text{K}$ . and to  $5\%$  at  $5^\circ\text{K}$ . The data are presented in Fig. 3.

TABLE IV

HEAT CAPACITY ( $C_s$ ) OF AMMONIUM FLUORIDE MONOHYDRATE

[ $\text{NH}_4\text{F}\cdot\text{H}_2\text{O}$ , mole weight =  $55.0574$  g., in cal./((deg. mole))]

$T$ , °K.	$C_s$	$T$ , °K.	$C_s$	$T$ , °K.	$C_s$
Series I					
		14.45	0.517	222.12	20.56
		15.83	0.666	230.94	21.16
219.36	20.31	17.35	0.860	239.23	22.36
223.72	20.64	19.06	1.078	243.95	65.22
230.95	21.16	20.99	1.339		
$\Delta H$ Run no. 1		23.20	1.646	Series V	
260.77	34.41	25.80	2.009	243.46	34.42
		28.86	2.427	244.83	385
Series II					
		32.26	2.879	245.05	1124
$\Delta H$ Run no. 2		35.91	3.344	245.23	1204
75.44	7.899	39.76	3.812	245.44	1114
81.44	8.584	43.85	4.292	245.78	666
88.55	9.362	48.27	4.814	246.31	253
95.81	10.08	52.98	5.360	247.90	63.9
103.75	10.88	Series IV			
112.33	11.70	56.38	5.761	250.42	38.14
120.80	12.48	62.04	6.404	253.02	35.28
128.98	13.23	68.65	7.148	255.73	34.41
137.40	13.96	75.38	7.894	258.46	34.33
		82.04	8.642	261.22	34.46
		88.77	9.391	263.94	34.62
Series III					
		$\Delta H$ Run no. 3		266.95	34.87
4.60	0.008	137.77	14.00	270.69	35.17
5.46	.019	145.88	14.67	275.28	35.58
6.60	.034	154.99	15.42		
7.63	.060	163.72	16.09	Series VI	
8.62	.094	172.00	16.76	272.98	35.36
9.62	.138	179.03	17.32	281.98	36.17
10.71	.214	186.28	17.91	291.09	37.07
11.92	.285	194.98	18.62	300.17	38.05
13.15	.387	203.62	19.27	309.34	39.15
		212.87	19.93	318.66	40.38

Because of the relatively slow rate of attainment of thermal equilibrium in the peritectic region where

(27) R. D. Shul'vas-Sorokina and V. G. Evdokimov, *Zhur. Ekspl. i. Teoret. Fiz.*, **8**, 762 (1938).

(28) K. Kamiyoshi, *Sci. Repts. Research Insts. Tohoku Univ.*, **A8**, 252 (1956).

(29) F. Simon, Cl. von Simson and M. Ruhemann, *Z. physik. Chem.*, **129**, 339 (1927).

(30) E. Benjamins and E. F. Westrum, Jr., *J. Am. Chem. Soc.*, **79**, 287 (1957).



TABLE V

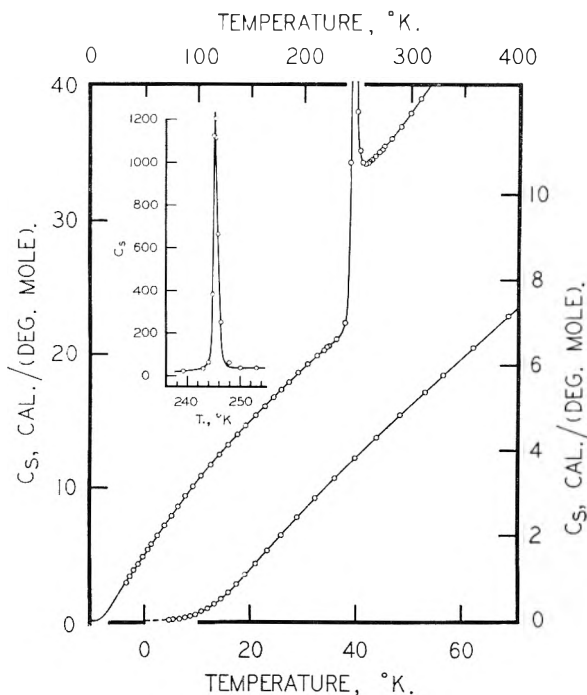
THERMODYNAMIC FUNCTIONS OF AMMONIUM FLUORIDE MONOHYDRATE

[NH<sub>4</sub>F·H<sub>2</sub>O, mole weight = 55.0574 g.]

$T$ , °K.	$C_s$ , cal./ deg. mole	$S^0$ , cal./ deg. mole	$H^0 - H_0^0$ , cal./mole	$-(F^0 - H_0^0)/T$ , cal./deg. mole
10	0.156	0.052	0.40	0.012
20	1.204	0.434	6.48	0.110
30	2.580	1.182	25.44	0.334
40	3.840	2.100	56.72	0.660
50	5.016	3.084	101.94	1.046
60	6.170	4.100	157.88	1.470
70	7.310	5.138	225.28	1.920
80	8.424	6.186	303.96	2.386
90	9.490	7.242	393.62	2.868
100	10.51	8.294	493.72	3.358
110	11.48	9.344	603.8	3.854
120	12.41	10.382	723.3	4.356
130	13.31	11.412	851.9	4.858
140	14.18	12.430	989.4	5.362
150	15.02	13.438	1135.4	5.868
160	15.82	14.432	1289.6	6.372
170	16.61	15.416	1451.8	6.876
180	17.40	16.388	1622.0	7.376
190	18.19	17.348	1799.8	7.876
200	18.98	18.302	1985.6	8.374
210	19.74	19.268	2179.4	8.868
220	20.42	20.182	2380.4	9.362
230	21.08	21.102	2587.6	9.852
240	20.54	22.026	2804.4	10.340
250	[38.58]	28.616	4421.8	10.928
260	34.40	29.996	4773.8	11.636
270	35.10	31.306	5121.0	12.340
280	35.98	32.598	5476.4	13.040
290	36.96	33.898	5841.2	13.756
300	38.02	35.150	6216.0	14.430
310	39.22	36.416	6602.2	15.118
320	40.54	37.682	7001.0	15.804
273.15	35.38	31.71	5232	12.56
298.15	37.22	34.92	6146	14.30

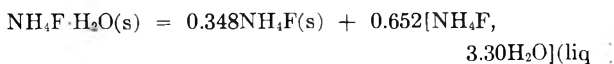
as much as 15 or more hours were required to obtain equilibrium drift, it was not possible to delineate the heat capacity as an exact function of temperature in this region. Hence, as a test of the measurements and the shape of the heat capacity curve as drawn through the peritectic region, several enthalpy-type determinations were made through the entire anomalous region. The results of two such runs yielded enthalpy increments over the region 230 to 260°K. of 2185.2 and 2186.2 cal./mole in excellent agreement with 2184.4 cal./mole obtained by a summation of the energies of nine consecutive heat capacity runs through this region despite the long time required for thermal equilibrium. The enthalpy value is also in good accord with the value 2182 cal./mole obtained by numerical quadrature of the  $C_s$  vs.  $T$  curve over this range.

**The Molal Thermodynamic Functions of NH<sub>4</sub>F·H<sub>2</sub>O.**—The molal heat capacities and the derived molal thermodynamic functions  $S^0$ ,  $H^0 - H_0^0$ , and  $(F^0 - H_0^0)/T$  are presented in Table V. The heat capacities in Table V represent the average of the nearly identical values read from a large scale

Fig. 3.—Heat capacity of NH<sub>4</sub>F·H<sub>2</sub>O.

smoothed curve and the values calculated from the polynomial curve fit by a digital computer used to evaluate the thermodynamic functions. The probable error in the derived thermodynamic functions is estimated to be less than 0.1% above 100°K. For the evaluation of these functions the heat capacity was extrapolated below 5°K. by means of a Debye  $T^3$  function.

**The Peritectic Reaction.**—The maximum thermal effect associated with the peritectic reaction was found by adiabatic calorimetry to be at  $245.3 \pm 0.1^\circ\text{K}$ . Practically the entire effect occurred within  $\pm 2^\circ$  of this temperature. However, there was some evidence of a pre-transitional increase in heat capacity and a noticeable tail on the high temperature side. To obtain the enthalpy of the peritectic reaction the essentially latent heat effect was obtained by subtracting the normal heat capacity of the substance (obtained by extrapolating the heat capacities from temperatures outside this range) from the measured heat capacities over the region 240 to 260°K. The extra heat capacity was then used to obtain the thermodynamic functions. The enthalpy and entropy associated with the peritectic reaction



at 245.3°K. giving the liquid solution containing 23.25 mole % NH<sub>4</sub>F, are 1360 cal./mole and 5.54 cal./deg. mole, respectively. The composition of the peritectic is estimated from the intersection of the solubility curves.

**Acknowledgment.**—The authors express their appreciation to H. Gary Carlson and Shu-Sing Chang for assistance in the calorimetry and to Elfreda Chang and Bruce H. Justice for collabora-



tion in the calculations and the digital computation program. The partial financial support of the Division of Research of the U. S. Atomic Energy Commission is gratefully acknowledged.

## A THERMODYNAMIC STUDY OF THE SYSTEM AMMONIUM FLUORIDE-WATER. II. THE SOLID SOLUTION OF AMMONIUM FLUORIDE IN ICE

BY LEONARD C. LABOWITZ AND EDGAR F. WESTRUM, JR.

*Department of Chemistry, University of Michigan, Ann Arbor, Michigan*

*Received July 14, 1960*

The existence, range and thermodynamic properties of the solid solution in the  $\text{NH}_4\text{F-H}_2\text{O}$  system have been established by thermal analysis, solubility determinations, Schreinemakers' method of wet residues and equilibrium adiabatic calorimetry. Some of the results are at variance with those reported by Yatlov and Polyakova, and the deviations have been explained when possible. Heat capacity measurements were made from 55 to 325°K. on systems of composition 0.5, 1.5, 4.6 mole % of  $\text{NH}_4\text{F}$ , and on the eutectic composition. No eutectic halt was observed in the case of the first two solutions, giving further confirmation of the existence of a solid solution at these concentrations. A theoretical relationship for the solidus curve is in accord with the experimental data obtained by the various methods.

### Introduction

The existence of solid solutions in which ice is the major component has long been a controversial subject. In 1920 Maass and Herzberg<sup>1</sup> investigated the system  $\text{H}_2\text{O}_2\text{-H}_2\text{O}$  by thermal analysis and reported the congruently melting compound  $\text{H}_2\text{O}_2 \cdot 2\text{H}_2\text{O}$  but did not analyze the solid phases. In 1940 Giguère and Maass<sup>2</sup> redetermined the freezing points, analyzed liquid and solid phases, and claimed that  $\text{H}_2\text{O}_2$  and  $\text{H}_2\text{O}$  formed two terminal and one intermediate solid solutions. Thermal analysis by Kubaschewski and Weber<sup>3</sup> supported the claim of Giguère and Maass and indicated that the range of the terminal solid solutions extended from 0 to 25 and from 90 to 100 wt. %  $\text{H}_2\text{O}_2$  at the respective eutectic temperatures. Mironov and Bergman<sup>4</sup> found distinct eutectic arrests at 1.0 and 97 wt. %  $\text{H}_2\text{O}_2$  and similarly showed that the intermediate solid solution does not exist over any appreciable concentration range. Foley and Giguère<sup>5</sup> utilized the method of wet residues with radioactive tracers and acknowledged the absence of solid solutions. Recent thermal analysis by Mironov<sup>6</sup> provides additional evidence for the absence of solid solutions in this system.

Although cesium ions are almost completely rejected, it is reported<sup>7</sup> that substantial amounts of fluoride are incorporated into ice crystallized from dilute solutions of cesium fluoride. Brill and Ender<sup>8</sup> indicate that electrically neutral molecules of hydrogen fluoride are incorporated into the ice. Although several studies of the dielectric and crystallographic properties of these

solid solutions have been made,<sup>9</sup> no investigation of the solubility limit has been reported. Balló<sup>10</sup> has reported the existence of solid solutions of ice in the systems acetic acid-, propionic acid- and *n*-butyric acid-water. This study has not been confirmed.

Interest in the existence of solid solutions of ammonium fluoride in ice was stimulated by a paper by Lonsdale<sup>11</sup> in which attention was directed to the fact that ice and ammonium fluoride are not only isomorphous but also show nearly identical Laue X-ray diagrams with strong, diffuse, star-shaped streaks attributable to thermal vibrations of the hydrogen nuclei ("proton jumps") and molecular rotation. Not only is the crystal structure of  $\text{NH}_4\text{F}$  like that of ice, but the atoms are similarly arranged; and the dimensions differ by only 3.7% ( $\text{N-H} \cdots \text{F}$ , 2.66 Å.;  $\text{O-H} \cdots \text{O}$ , 2.76 Å.).<sup>12</sup> The hydrogen bonding in  $\text{NH}_4\text{F}$  is also comparable to that in ice.<sup>13</sup> These similarities in the geometry and the binding forces of ice and  $\text{NH}_4\text{F}$  led Brill and Zaromb<sup>14</sup> to establish experimentally the existence of a solid solution of ammonium fluoride in ice by chemical analysis of the solid phase, thermal analysis, dilatometry, and measurements of resistivity and dielectric constants. A thermodynamic relation applied to the liquidus curve data of Yatlov and Polyakova<sup>15</sup> is in accord with solidus data of Brill and Zaromb and indicates a solubility limit of approximately 5 mole %  $\text{NH}_4\text{F}$  at 246.7°K. The dielectric<sup>13,16</sup> and the mechanical<sup>17</sup> relaxation properties

(1) O. Maass and O. W. Herzberg, *J. Am. Chem. Soc.*, **42**, 2569 (1920).

(2) P. A. Giguère and O. Maass, *Can. J. Research*, **18B**, 66 (1940).

(3) O. Kubaschewski and W. Weber, *Z. Elektrochem.*, **54**, 200 (1950).

(4) K. E. Mironov and A. G. Bergman, *Doklady Akad. Nauk S. S. R.*, **81**, 1081 (1951).

(5) W. T. Foley and P. A. Giguère, *Science*, **113**, 754 (1951); *Can. J. Research*, **29**, 123 (1951).

(6) K. E. Mironov, *Izvest. Sektora Fiz.-Khim. Anal. Inst. Obshchei Neorg. Khim., Akad. Nauk S. S. R.*, **26**, 215 (1955).

(7) E. J. Workman, *Science*, **119**, 73 (1954); E. J. Workman and W. Drost-Hansen, *Phys. Rev.*, **94**, 770 (1954).

(8) R. Brill and H. Ender, *Nature*, **176**, 925 (1955).

(9) H. Gränicher, C. Jaccard, P. Scherrer and Ad. Steinemann, *Disc. Faraday Soc.*, **23**, 50 (1957); Ad. Steinemann and H. Gränicher, *Helv. Phys. Acta*, **30**, 553 (1957); Ad. Steinemann, *ibid.*, **30**, 581 (1957); F. Truby, *Science*, **121**, 404 (1955).

(10) R. Balló, *Z. physik. Chem.*, **72**, 439 (1910).

(11) K. Lonsdale, *Nature*, **158**, 582 (1946).

(12) L. Pauling, "The Nature of the Chemical Bond," 3rd Ed., Cornell University Press, Ithaca, N. Y., 1960.

(13) S. Zaromb and R. Brill, *J. Chem. Phys.*, **24**, 895 (1956).

(14) R. Brill and S. Zaromb, *Nature*, **173**, 316 (1954).

(15) V. S. Yatlov and E. M. Polyakova, *Zhur. Obshchei Khim.*, **15**, 724 (1945).

(16) S. Zaromb, *J. Chem. Phys.*, **25**, 350 (1956); R. Brill, H. Ender and A. Feuersanger, *Z. Elektrochem.*, **61**, 1071 (1957).

(17) E. Walz and S. Magun, *Z. Physik*, **157**, 266 (1959).

of this solid solution have been described. Ammonium fluoride incorporated into the ice lattice greatly facilitates the dielectric relaxation in ice; the solute ions are capable of accelerating the rotation of ice molecules at a distance of 30 Å. or more from any ion. Yatlov and Polyakova<sup>15</sup> performed thermal analysis and solubility determinations on the  $\text{NH}_4\text{F}-\text{H}_2\text{O}$  system. They stated that the composition of the solid phase in the water-rich region of the system is pure ice, but this conclusion was presumably not based on chemical analysis.

The purpose of the present investigation is that of determining the range of existence and the thermophysical properties of this solid solution. Thermal analysis, Schreinemakers' method of wet residues,<sup>18</sup> and low temperature heat capacities and heats of transformation of several compositions within the  $\text{NH}_4\text{F}-\text{H}_2\text{O}$  system have been employed for this purpose.

### Experimental

**Materials.**—Specially prepared  $\text{NH}_4\text{F}$  (analysis:  $\text{F}^-/\text{NH}_4^+ = 1.000$ )<sup>19</sup> was employed for the wet residues studies and the calorimetry. For some of the thermal analysis measurements, purified reagent  $\text{NH}_4\text{F}$  ( $\text{F}^-/\text{NH}_4^+ = 1.001$ )<sup>19</sup> was used; the results were identical with those obtained with the prepared samples. Reagent  $\text{NH}_4\text{I}$  was used after chemical analysis.<sup>19</sup> Reagent  $\text{NH}_4\text{Cl}$  giving  $\text{NH}_4^+ = 33.71$  wt. % by the Kjeldahl method and  $\text{Cl}^- = 65.92$  wt. % by the Volhard method (theoretical: 33.73 wt. %  $\text{NH}_4^+$  and 66.27 wt. %  $\text{Cl}^-$ ) was used.

**Thermal Analyses.**—Cooling curves were made on 13 compositions in the system  $\text{NH}_4\text{F}-\text{H}_2\text{O}$  on the water-rich side of the eutectic. The apparatus and technique are described elsewhere.<sup>19</sup>

**Method of Wet Residues and Related Chemical Analyses.**—Ammonium ion was determined in all cases by the Kjeldahl method with methyl red as indicator using 0.1 *N*  $\text{NaOH}$  standardized against  $\text{KH}(\text{IO}_3)_2$  and against potassium biphthalate, and 0.1 *N*  $\text{HCl}$  standardized against  $\text{KI}$  plus  $\text{HgO}$ . All determinations were used as recommended<sup>20</sup> and checked against standard samples.

Fluoride was determined by three different methods. **Gravimetric  $\text{PbFCl}$ .** The precipitation procedure was carried out as recommended by Kapfenberger.<sup>21</sup> In all other respects the original method of Starck<sup>22</sup> was used. Ammonium ion interference<sup>23</sup> was eliminated before addition of the precipitating agent by boiling the sample with dilute sodium hydroxide solution until the vapors evolved had no noticeable effect on the color of moist red litmus paper. The solution was then adjusted to pH 4 with dilute hydrochloric acid. To ascertain whether the high chloride ion concentration resulting from this neutralization would interfere, the precipitation was carried out on reagent sodium fluoride in the presence of a comparable amount of sodium chloride and the results were consistently ( $\pm 0.1\%$ ) satisfactory. **Volumetric  $\text{PbFCl}$ :** instead of weighing the  $\text{PbFCl}$  precipitate, it was dissolved in dilute nitric acid, and its  $\text{Cl}^-$  content determined by the Volhard method. This modification of the original method of Starck<sup>22</sup> is known as the Kapfenberger method.<sup>21</sup> Determinations on a standard sample were also uniformly ( $\pm 0.06\%$ ) satisfactory in this case. **Indirect determination by difference:** in wet residues work where  $\text{NH}_4\text{F}$  had to be estimated in the presence of  $\text{NH}_4\text{I}$ , the  $\text{PbFCl}$  methods could not be

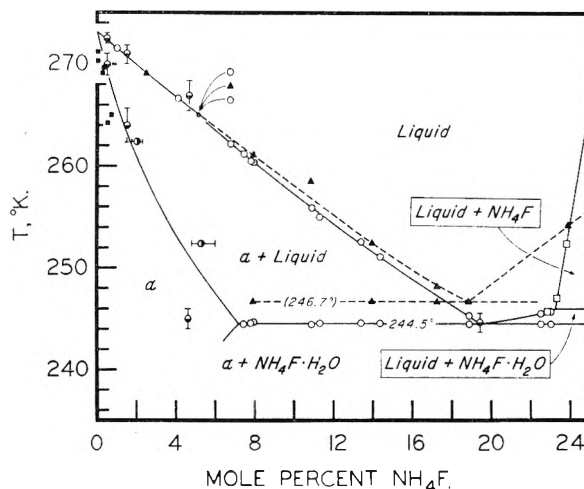


Fig. 1.—Phase diagram for the system  $\text{NH}_4\text{F}-\text{H}_2\text{O}$  from 0–24 mole %  $\text{NH}_4\text{F}$ . The solid solution is designated by  $\alpha$ . The data from this research are represented by  $\circ$  for thermal analysis,  $\square$  solubility measurements,  $\bullet$  wet residues results, and  $\bullet$  heat capacity determinations. The data of Zaromb and Brill<sup>13</sup> are given by  $\blacksquare$ , those of Yatlov and Polyakova<sup>15</sup> by  $\blacktriangle$ .

employed because of the possibility of forming  $\text{PbIF}$  and  $\text{PbCl}$ . In these cases, fluoride was estimated by difference:  $\text{eq. F}^- = \text{eq. NH}_4^+ - \text{eq. I}^-$ .

Chloride was determined by the Volhard method or by the gravimetric  $\text{AgCl}$  method.<sup>24</sup> To find out whether the presence of  $\text{F}^-$  would interfere with the end-point of the Volhard method,  $\text{Cl}^-$  was determined in  $\text{NH}_4\text{Cl}$  in the presence of  $\text{F}^-$ , giving 99.76% of theoretical  $\text{Cl}^-$ , and with  $\text{NH}_4\text{F}$  added, giving 99.64% of theoretical  $\text{Cl}^-$ . These results compare with 99.80% of theoretical  $\text{Cl}^-$  by the gravimetric  $\text{AgCl}$  method in the absence of  $\text{F}^-$ .

In the wet residues work on the solid solution  $\text{I}^-$  was determined gravimetrically as  $\text{AgI}$ .<sup>22</sup>

**Adiabatic Calorimetry.**—The heat capacities and heats of fusion of several  $\text{NH}_4\text{F}-\text{H}_2\text{O}$  mixtures were determined from about 55 to 325°K. by the adiabatic method. The apparatus and procedure employed are identical with those previously described,<sup>19</sup> with the exception that the samples in the present paper are all homogeneous solutions at 25° and could be poured from the polyethylene bottles in which they were prepared through a stainless steel funnel into the calorimeter.

### Results and Discussion

All data from the literature<sup>25</sup> and from the present investigation are presented in the phase diagram, Fig. 1.

**Thermal Analysis.**—The thermal analysis data are given in Table I. The liquidus curve obtained by the present investigation is not in close agreement with that of Yatlov and Polyakova.<sup>15</sup> The discrepancy between the two liquidus curves can be accounted for on the basis of the following analysis of  $\text{NH}_4\text{F}$  given by Yatlov and Polyakova: " $\text{NH}_3 = 45.65$  wt. %,  $\text{F} = 51.75$  wt. %,  $\text{F}/\text{NH}_3 = 1.06$ ." (Evidently the figure "1.06" for  $\text{F}/\text{NH}_3$  is a misprint and should read "1.016"

(24) W. C. Pierce and E. I. Haenisch, "Quantitative Analysis," 3rd Ed., John Wiley and Sons, Inc., New York, N. Y., 1948, p. 300.

(25) A summary of the thermal analysis and solubility data of previous investigations on a consistent basis, tables of the thermodynamic properties of the ammonium fluoride-water system, and other details of this study have been deposited as Document 6421 with the ADI, Auxiliary Publications Project, Photoduplication Service, Library of Congress, Washington 25, D. C. A copy may be secured by citing the document number and by remitting \$2.50 for photoprints or \$1.75 for 35 mm. microfilm in advance by check or money order made payable to: Chief, Photoduplication Service, Library of Congress.

(18) F. A. H. Schreinemakers, *Z. physik. Chem.*, **11**, 75 (1893).

(19) L. C. Labowitz and E. F. Westrum, Jr., *J. Phys. Chem.*, **65**, 403 (1961).

(20) I. M. Kolthoff and E. B. Sandell, "Textbook of Quantitative Analysis," Rev. Ed., The Macmillan Co., New York, N. Y., 1948.

(21) W. Kapfenberger, *Aluminium*, **24**, 428 (1942).

(22) G. Starck, *Z. anorg. Chem.*, **70**, 173 (1911).

(23) F. P. Treadwell and W. T. Hall, "Analytical Chemistry," Vol. II, "Quantitative Analysis," 9th English Ed., John Wiley and Sons, New York, N. Y., 1942, pp. 397 and 739.

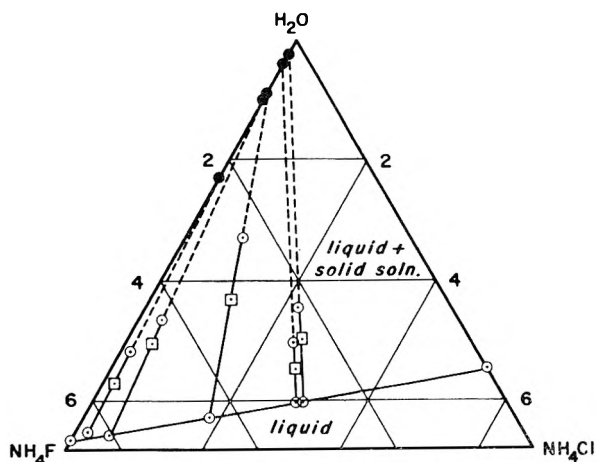


Fig. 2.—Ternary diagram for the system  $\text{NH}_4\text{F}-\text{NH}_4\text{Cl}-\text{H}_2\text{O}$  at  $262.4^\circ\text{K}$ . (in mole per cent.).

on the basis of the analytical data.) An  $\text{NH}_4\text{F}$  aqueous solution intentionally contaminated with  $\text{NH}_4\text{HF}_2$  to give  $\text{F}/\text{NH}_3 = 1.016$  (14.65 wt. %  $\text{NH}_4\text{F}$ , 0.35 wt. %  $\text{NH}_4\text{HF}_2$ ) was prepared. Although in this study it was found that the freezing point of an aqueous solution of pure  $\text{NH}_4\text{F}$  of 14.92 wt. % (7.80 mole %) was  $260.5^\circ\text{K}$ ., that of the above intentionally contaminated material with an apparent concentration of 14.92 wt. %  $\text{NH}_4\text{F}$  was  $261.0^\circ\text{K}$ . in exact agreement with the  $261.0^\circ\text{K}$ . reported by Yatlov and Polyakova. The addition of small amounts of ammonium bifluoride would be expected to elevate the freezing point of the solution because the  $\text{NH}_4\text{HF}_2-\text{H}_2\text{O}$  liquidus curve lies higher in temperature than the  $\text{NH}_4\text{F}-\text{H}_2\text{O}$  solubility curve, and the corresponding solubility surface in the water-rich region of the system  $\text{NH}_4\text{F}-\text{NH}_4\text{HF}_2-\text{H}_2\text{O}$  would rise with temperature in the direction  $\text{NH}_4\text{F}-\text{H}_2\text{O} \rightarrow \text{NH}_4\text{HF}_2-\text{H}_2\text{O}$ .

TABLE I

THERMAL ANALYSIS DATA ON THE SYSTEM  $\text{NH}_4\text{F}-\text{H}_2\text{O}$

Mole % $\text{NH}_4\text{F}$ in sample	Temp., $^\circ\text{K} \pm 0.1$	Feature	Solid phase(s)
1.000	271.5	F.p. <sup>a</sup>	$\alpha^a$
4.10	266.6	F.p.	$\alpha$
5.13	265.1	F.p.	$\alpha$
5.15	265.0	F.p.	$\alpha$
6.76	262.2	F.p.	$\alpha$
7.44	261.2	F.p.	$\alpha$
7.80	244.5	Eutectic	$\alpha, \text{NH}_4\text{F} \cdot \text{H}_2\text{O}$
	260.5	F.p.	$\alpha$
	244.6	Eutectic	$\alpha, \text{NH}_4\text{F} \cdot \text{H}_2\text{O}$
7.95	260.4	F.p.	$\alpha$
	244.7	Eutectic	$\alpha, \text{NH}_4\text{F} \cdot \text{H}_2\text{O}$
10.89	255.9	F.p.	$\alpha$
	244.5	Eutectic	$\alpha, \text{NH}_4\text{F} \cdot \text{H}_2\text{O}$
11.27	255.0	F.p.	$\alpha$
	244.6	Eutectic	$\alpha, \text{NH}_4\text{F} \cdot \text{H}_2\text{O}$
13.39	252.6	F.p.	$\alpha$
	244.6	Eutectic	$\alpha, \text{NH}_4\text{F} \cdot \text{H}_2\text{O}$
14.36	251.1	F.p.	$\alpha$
18.86	245.3	F.p.	$\alpha$
	244.5	Eutectic	$\alpha, \text{NH}_4\text{F} \cdot \text{H}_2\text{O}$

<sup>a</sup> Key: F.p. = freezing point;  $\alpha$  = solid solution.

**Method of Wet Residues.**—The method of wet residues was applied to the water-rich region of the systems  $\text{NH}_4\text{F}-\text{NH}_4\text{Cl}-\text{H}_2\text{O}$  and  $\text{NH}_4\text{F}-\text{NH}_4\text{I}-\text{H}_2\text{O}$  at  $262.4$  and  $252.4^\circ\text{K}$ ., respectively, to determine whether the composition of the solid phase which first separates on freezing is pure ice or the reported solid solution.<sup>12</sup> The results (Table II and Fig. 2) prove that the solid solution is indeed formed; and by plotting "mole % of  $\text{NH}_4\text{F}$  in the solid solution" vs. "mole % of  $\text{NH}_4\text{F}$  in the liquid solution" for each tie-line, it is possible to extrapolate to the  $\text{NH}_4\text{F}-\text{H}_2\text{O}$  solidus line at those temperatures. It was assumed that  $\text{NH}_4\text{Cl}$  and  $\text{NH}_4\text{I}$  were insoluble in the solid solution. On this basis the mole % of  $\text{NH}_4\text{F}$  in the  $\text{NH}_4\text{F}-\text{H}_2\text{O}$  solid solution is 2.0 at  $262.4 \pm 0.1^\circ\text{K}$ . and 5.3 at  $252.4 \pm 0.1^\circ\text{K}$ .

TABLE II  
WET RESIDUES DATA

Run no.	Liquid phase	Total system	Wet residue	Solid phase	
System $\text{NH}_4\text{F}-\text{NH}_4\text{Cl}-\text{H}_2\text{O}$ at $262.4 \pm 0.1^\circ\text{K}$ .					
Mole % $\text{NH}_4\text{Cl}$ in system $\text{NH}_4\text{Cl}-\text{H}_2\text{O}$ .. 5.45 <sup>26</sup>					
Mole % $\text{NH}_4\text{F}$	1	2.980	2.471	2.254	0.21
Mole % $\text{NH}_4\text{Cl}$	1	3.065	2.550	2.223	
Mole % $\text{NH}_4\text{F}$	2	3.070	2.800	2.611	.41
Mole % $\text{NH}_4\text{Cl}$	2	2.980	2.700	2.462	
Mole % $\text{NH}_4\text{F}$	3	4.459	3.152	2.442	.88
Mole % $\text{NH}_4\text{Cl}$	3	1.853	1.180	0.860	
Mole % $\text{NH}_4\text{F}$	4	6.080	4.681	4.346	.78
Mole % $\text{NH}_4\text{Cl}$	4	0.537	0.400	0.360	
Mole % $\text{NH}_4\text{F}$	5	6.364	5.572	5.064	1.80
Mole % $\text{NH}_4\text{Cl}$	5	0.181	0.152	0.129	
Mole % $\text{NH}_4\text{F}$ in system $\text{NH}_4\text{F}-\text{H}_2\text{O}$	..	6.67	By extrapolation = 2.0		
System $\text{NH}_4\text{F}-\text{NH}_4\text{I}-\text{H}_2\text{O}$ at $252.4 \pm 0.1^\circ\text{K}$ .					
Mole % $\text{NH}_4\text{I}$ in system $\text{NH}_4\text{I}-\text{H}_2\text{O}$ .. 10.03 <sup>27</sup>					
Mole % $\text{NH}_4\text{F}$	1	5.814	4.503	4.254	2.21
Mole % $\text{NH}_4\text{I}$	1	6.015	3.930	3.482	
Mole % $\text{NH}_4\text{F}$	2	10.46	8.541	8.212	4.13
Mole % $\text{NH}_4\text{I}$	2	2.099	1.493	1.341	
Mole % $\text{NH}_4\text{F}$ in system $\text{NH}_4\text{F}-\text{H}_2\text{O}$	..	13.40	By extrapolation = 5.3		

**Heat Capacity Data.**—Adiabatic calorimetry is a very powerful tool for the investigation of phase equilibria in binary systems because it is an equilibrium method and is capable of determining with high precision and accuracy the temperature and the enthalpy increments associated with phase transitions. It is, however, seldom employed for this purpose because of the time required to reach equilibrium. Heat capacities of 0.4916, 1.485, 4.603 and 19.39 mole %  $\text{NH}_4\text{F}$  solutions were determined by direct calorimetric measurements from 55 to  $325^\circ\text{K}$ . The results of the heat capacity measurements are presented in Table III in chronological order so that the approximate size of the temperature increments employed can usually be inferred from adjacent mean tempera-

(26) W. H. Rodebush, *J. Am. Chem. Soc.*, **40**, 1204 (1918).

(27) A. Smith and H. E. Eastlack, *ibid.*, **38**, 1500 (1916); T. R. Briggs, K. H. Ballard, F. R. Alrich and J. P. Wikswo, *J. Phys. Chem.*, **44**, 325 (1940).

TABLE III

HEAT CAPACITIES ( $C_p$ ) OF AQUEOUS SOLUTIONS OF AMMONIUM FLUORIDE [IN CAL./ (DEG. MOLE SOLUTION)]

$T, ^\circ K.$	$C_p$	$T, ^\circ K.$	$C_p$	$T, ^\circ K.$	$C_p$
0.4916 mole % $NH_4F$ ; 1 mole soln. = 18.110 g. soln.					
Series I					
	190.16	6.493	286.50	17.95	
	198.93	6.766	295.70	17.94	
53.34	2.041	207.47	7.029	305.36	17.94
58.23	2.239	215.81	7.286	315.22	17.94
64.24	2.483	224.45	7.564	325.04	17.96
70.33	2.713	233.52	7.852		
76.43	2.939	242.41	8.284		
83.10	3.189			Series VI	
90.23	3.441			141.12	5.050
Series II					
	237.61	8.035	159.42	5.584	
93.74	3.555	246.23	8.574	164.77	5.738
101.32	3.800	254.31	9.162	169.98	5.898
109.29	4.054	261.22	13.54	174.98	6.040
117.37	4.308	265.99	24.89	$\Delta H$ Run no. 1	
125.50	4.561	268.54	52.8		
133.66	4.817	270.33	149	Series VII	
142.08	5.071	271.78	540	277.89	17.97
150.76	5.329	272.46	1010	279.95	17.98
159.93	5.593	273.83	64.3	282.24	17.96
		280.36	17.96	284.99	17.96
Series III					
	287.73			287.73	17.95
163.67	5.702			290.48	17.95
172.53	5.968	277.51	18.01	296.50	17.93
181.32	6.222				
1.485 mole % $NH_4F$ ; 1 mole soln. = 18.259 g. soln.					
Series I					
	207.43	7.072		Series VII	
136.45	4.906	216.88	7.364	279.85	17.68
143.86	5.137			290.77	17.71
152.47	5.399			300.56	17.74
161.49	5.671	223.91	7.574	310.32	17.77
170.67	5.941	232.20	7.845	320.04	17.80
179.96	6.219	238.32	8.061		
188.89	6.502	242.18	8.272	Series VIII	
				243.65	8.530
Series II					
	244.54			244.54	10.13
57.41	2.216	237.15	8.006	245.33	11.76
62.73	2.434	240.88	8.147	246.11	11.46
69.02	2.675	243.62	8.461	246.94	13.18
75.16	2.906	245.21	10.86	248.39	13.72
81.74	3.156	247.70	11.78	$\Delta H$ Run no. 3	
88.60	3.405	252.60	14.27		
96.28	3.659			Series IX	
104.84	3.937			270.31	222
113.17	4.202	258.28	20.55	270.54	257
121.39	4.449	262.07	31.79	270.76	283
129.58	4.692	264.57	53.5	270.96	296
137.92	4.944	266.22	71.8	271.17	309
		267.33	106	271.39	288
Series III					
	268.39	143		271.63	259
$\Delta H$ Run no. 2	269.46	240		271.93	205
197.66	6.774	270.41	326	272.28	164
		272.36	94.4	273.89	20.65
4.603 mole % $NH_4F$ ; 1 mole soln. = 18.891 g. soln.					
Series IV					
	280.92			280.92	17.21
Series I	144.45	5.275	288.85	17.31	
55.23	2.169	153.31	5.550	297.87	17.37
60.40	2.383	162.14	5.812	307.37	17.44
66.38	2.626	170.78	6.060	317.15	17.53
72.69	2.864	179.38	6.328		

Series II				Series V		Series VII	
78.93	3.112			239.80	8.294	231.06	7.949
85.58	3.366	182.03	6.423	244.52	20.47	244.52	20.47
92.82	3.620	190.90	6.732	245.63	35.94	245.63	35.94
100.43	3.877	199.94	7.016	246.75	34.52	246.75	34.52
108.17	4.132	209.22	7.297	248.31	36.45	248.31	36.45
		218.74	7.585	250.90	42.13	250.90	42.13
		227.74	7.861	255.25	47.31	255.25	47.31
Series III				236.42	8.149	259.81	77.1
107.89	4.121			263.19	107	263.19	107
115.71	4.371			265.30	112	265.30	112
123.83	4.630			266.32	115	266.32	115
132.08	4.885	249.29	18.46	267.55	87.0	267.55	87.0
140.52	5.152	$\Delta$ Run no. 4		270.67	20.09	270.67	20.09
Eutectic composition: 19.39 mole % $NH_4F$ ; 1 mole soln. = 21.704 g. soln.							
		246.29	26.60	91.85	3.999	246.29	26.60
Series I				248.62	16.28	99.31	4.288
217.59	8.387	252.73	16.35	107.28	4.588	252.73	16.35
225.90	8.656	260.27	16.52	115.33	4.885	260.27	16.52
232.52	8.859	269.44	16.72	123.38	5.182	269.44	16.72
$\Delta H$ Run no. 5				278.58	16.89	131.73	5.481
255.67	16.42	287.91	17.06	140.34	5.778	287.91	17.06
		297.30	17.21	149.27	6.076	297.30	17.21
		306.60	17.37	158.53	6.384	306.60	17.37
Series II				315.82	17.52	167.69	6.706
233.53	8.888			176.67	7.058	315.82	17.52
239.97	9.186			185.55	7.413	239.97	9.186
243.53	14.55			194.50	7.709	243.53	14.55
244.80	613	65.15	2.833	203.76	8.000	244.80	613
244.95	5790	71.39	3.121	213.11	8.277	244.95	5790
$\Delta H$ Run no. 6				78.02	3.414	$\Delta H$ Run no. 7	
245.12	953	84.7	3.713				

tures. An analytically determined curvature correction was applied to the observed values of  $\Delta H/\Delta T$  to correct for the deviation occasioned by the finite temperature increments used in the actual measurements. A further correction has been

TABLE IV

ENTHALPY INCREMENTS IN THE  $NH_4F-H_2O$  SYSTEM

No. of runs	Exptl. temp. range, $^\circ K.$	$H_{230}^{230^\circ K.} - H_{230}^{230^\circ K.}$ cal./ (mole soln.)
0.4916 mole % $NH_4F$		
1 ( $\Delta H$ Run no. 1)	239.76-290.77	1927.6
10 $C_p$ runs	242.03-284.99	1930.1
Numerical quadrature of $C_p$ vs. $T$ curve		
		1926
1.485 mole % $NH_4F$		
1 ( $\Delta H$ Run no. 3)	239.79-285.44	1918.6
13 $C_p$ runs	242.77-273.83	1920.6
Numerical quadrature of $C_p$ vs. $T$ curve		
		1933
4.603 mole % $NH_4F$		
1 ( $\Delta H$ Run no. 4)	250.72-277.34	1856.9
12 $C_p$ runs	243.88-273.10	1860.2
Numerical quadrature of $C_p$ vs. $T$ curve		
		1864
$H_{230}^{230^\circ K.} - H_{230}^{230^\circ K.}$ cal./ (mole soln.)		
Eutectic composition: 19.39 mole % $NH_4F$		
1 ( $\Delta H$ Run no. 5)	235.01-252.21	1429.1
1 ( $\Delta H$ Run no. 7)	236.38-253.73	1428.1
8 $C_p$ runs		
(Inc. $\Delta H$ Run no. 6)	237.55-249.83	1428.8
Numerical quadrature of $C_p$ vs. $T$ curve		
		1419

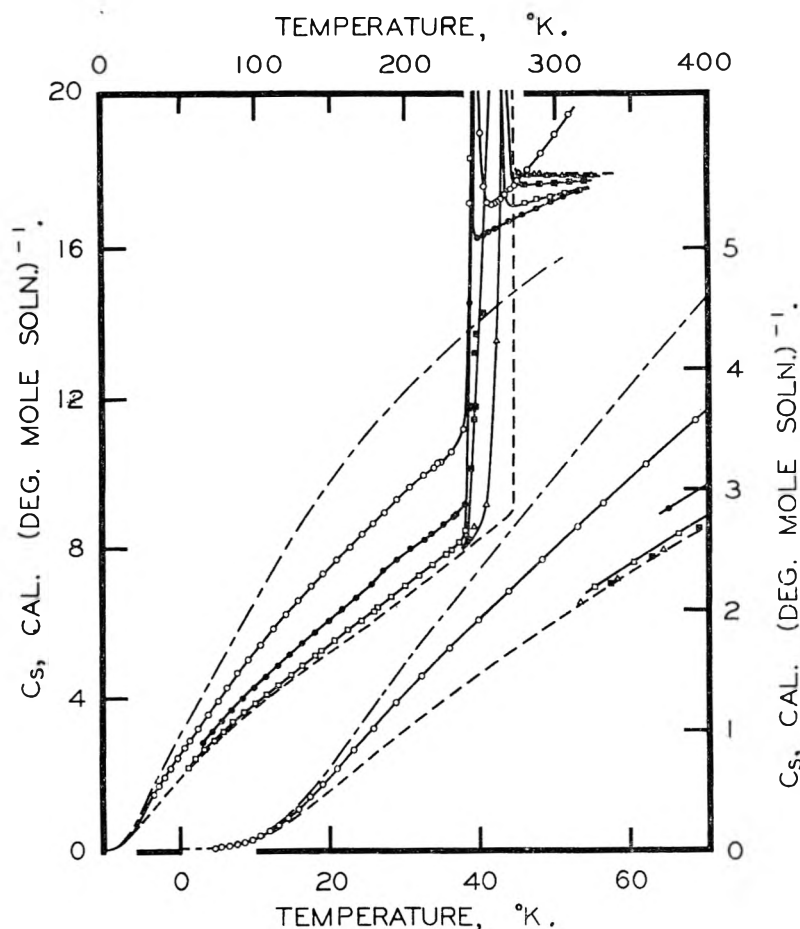


Fig. 3.—Low temperature heat capacities for the system  $\text{NH}_4\text{F}-\text{H}_2\text{O}$ . The various substances are represented as follows: ice<sup>29</sup>, ———;  $\text{NH}_4\text{F}$ <sup>28</sup>, - - - -; 0.4916 mole %  $\text{NH}_4\text{F}$ ,  $\Delta$ ; 1.485 mole %  $\text{NH}_4\text{F}$ ,  $\blacksquare$ ; 4.603 mole %  $\text{NH}_4\text{F}$  (eutectic),  $\bullet$ ;  $\text{NH}_4\text{F}\cdot\text{H}_2\text{O}$ ,  $\circ$ .

applied for the heat of vaporization of water and for the heat capacity of the water vapor over the solutions. At any given temperature,  $T$ , the heat capacity,  $C_s$ , corrected for vaporization is given by the equation

$$C_s = C_s (\text{apparent}) - n_v C_v - n_v \Delta E_v / RT^2$$

in which  $n_v$  = number of moles of water vapor within the calorimeter,  $C_s$  (apparent) = the observed heat capacity of the two-phase sample,  $C_v$  = molal heat capacity of water vapor at constant volume of temperature  $T$ ,  $\Delta E_v$  = molal energy of vaporization of water at constant volume at temperature  $T$ ,  $R$  = gas constant per mole. The derivation of this equation is presented elsewhere.<sup>25</sup> The probable error in the experimental heat capacities is estimated to be about 0.1%. The heat capacity data are presented at the saturation vapor pressure of the samples. For this reason the symbol  $C_s$  is used to represent the heat capacity. The vaporization correction seldom exceeds 0.1% and is completely negligible below 260°K. Therefore, the saturation heat capacities ( $C_s$ ) are virtually identical with the heat capacities at constant pressure ( $C_p$ ) usually tabulated. It should be noted that the heat capacities (and the derived thermodynamic functions) in this paper have been presented on a "per mole of solu-

tion" basis in order to provide for convenient comparison of different concentrations. One mole of solution is defined as the amount of solution for which the number of moles of  $\text{NH}_4\text{F}$  plus the number of moles of water is equal to unity.

In the heat capacity measurements outside of transition regions thermal equilibrium was usually attained within ten or twelve minutes after energy input. Within the fusion transition region, however, thermal equilibrium was usually not attained until ten or twelve hours after an energy input. Hence, it was not possible to delineate the heat capacity as an exact function of temperature in this region. Therefore, as a final test of the measurements and the calculation technique as well as the shape of the heat capacity curves drawn through the transition region, a number of enthalpy type runs were made over relatively large temperature intervals spanning the transition region. The results of these enthalpy runs are presented in Table IV and compared with the results obtained by the summation of the enthalpies of runs made with relatively small temperature increments through the transition region (and hence with long equilibrium times) as well as with numerical quadrature of the heat capacity *vs.* temperature curves as drawn through the fusion region. The results are seen to be in good agreement.

The heat capacities are presented graphically in Fig. 3 with the curves for  $\text{NH}_4\text{F}$ ,<sup>28</sup>  $\text{NH}_4\text{F}\cdot\text{H}_2\text{O}$ <sup>19</sup> and  $\text{H}_2\text{O}$ <sup>29</sup> included for comparison.

**Thermodynamic Functions.**—The smoothed heat capacities ( $C_s$ ) and the values of the derived thermodynamic functions, the enthalpy increment ( $S^0 - S_0^0$ ), and the enthalpy function ( $(H^0 - H_0^0)/T$ ) are given in Table V at selected temperatures and in more detail as a function of temperature elsewhere.<sup>25</sup> For comparison, the values for the ammonium fluoride monohydrate ( $\text{NH}_4\text{F}\cdot\text{H}_2\text{O}$ ), more fully discussed in the first paper of this series,<sup>19</sup> are also included. It will be noted that these values are presented on the basis of "per mole of solution." The heat capacities in Table V represent the average of the nearly identical values read from the smoothed curve and the values generated by a digital computer from a least squares polynomial fit to the data used for the integrations. Below the temperatures at which heat capacity measurements were made the

(28) E. Benjamins and E. F. Westrum, Jr., *J. Am. Chem. Soc.*, **79**, 287 (1957).

(29) W. F. Giauque and J. W. Stout, *ibid.*, **58**, 1144 (1936).

thermodynamic functions and heat capacities were obtained on the basis of the Kopp-Neumann rule<sup>30</sup> using the heat capacity data of Giauque and Stout<sup>29</sup> for ice and the heat capacity data for the monohydrate<sup>19</sup> as a basis for the interpolation. This is probably the most significant contribution to the probable error of the thermodynamic functions, but it contributes less than 0.2% above 100°K.

TABLE V  
THERMODYNAMIC FUNCTIONS OF AQUEOUS SOLUTIONS OF AMMONIUM FLUORIDE [IN CAL./(DEG. MOLE SOLUTION)]

Mole % NH <sub>4</sub> F	100°K.	150°K.	200°K.	298.15°K.
	<i>C<sub>s</sub></i>			
0.4916	3.758	5.305	6.797	17.94
1.485	3.780	5.319	6.843	17.73
4.603	3.862	5.445	7.015	17.38
19.39 (eut.)	4.318	6.101	7.881	17.23
50.00	5.255	7.510	9.492	18.61
	<i>S<sup>o</sup> - S<sub>0</sub><sup>o</sup></i>			
0.4916	3.119	4.939	6.668	16.05
1.485	3.130	4.957	6.696	16.05
4.603	3.183	5.053	6.830	16.14
19.39 (eut.)	3.439	5.534	7.534	16.83
50.00	4.147	6.719	9.151	17.46
	<i>(H<sup>o</sup> - H<sub>0</sub><sup>o</sup>)/T</i>			
0.4916	1.828	2.733	3.561	10.68
1.485	1.836	2.743	3.577	10.63
4.603	1.871	2.802	3.655	10.49
19.39 (eut.)	2.042	3.104	4.077	10.53
50.00	2.469	3.785	4.964	10.31

**The Fusion Transformation.**—The heat capacities of the aqueous solution of ammonium fluoride through the fusion transformation are presented graphically in Fig. 4, and the thermodynamics of this transformation are summarized in Table VI. Because of pre-transitional rise in heat capacity as well as a tail on the high temperature side, evaluation of the enthalpy and entropy increments for the fusion transformation required the extrapolation of the "normal" heat capacity curves for the solid and liquid phases to the temperature at which the apparent heat capacity was a maximum. This background heat capacity was approximated by drawing smooth curves tangent to the observed heat capacities at 240 and 280°K. for the three dilute solutions and between 240 and 260°K. for the eutectic and monohydrate solutions.

The eutectic and peritectic temperatures found by equilibrium calorimetry were in good agreement with the results of the thermal analysis and solubility-determination work of the present investigation. Despite repeated examinations for a thermal anomaly in the vicinity of the peritectic temperature reported by Yatlov and Polyakova, none was detected.

The absence of a thermal effect at the eutectic temperature for the 0.4916 and the 1.485 mole % NH<sub>4</sub>F solutions is conclusive evidence for the existence of the solid solution at these concentra-

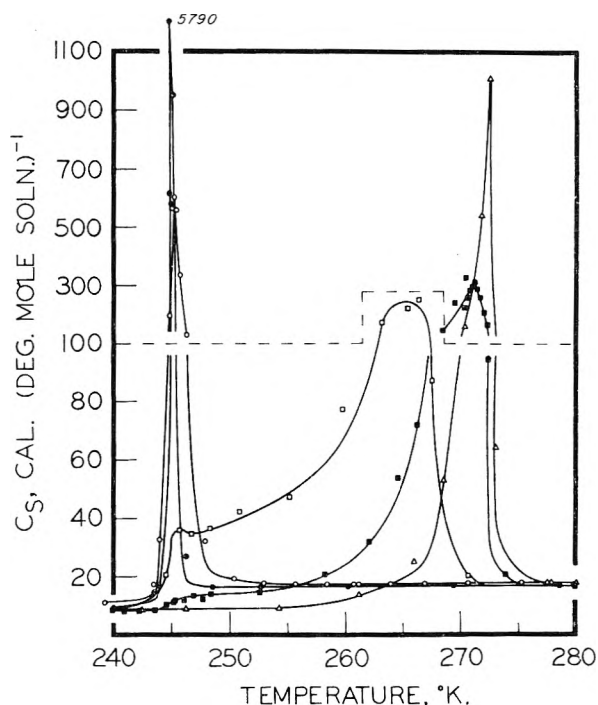


Fig. 4.—Heat capacities for aqueous solutions of NH<sub>4</sub>F in the fusion transformation region. 0.4916 mole % NH<sub>4</sub>F,  $\Delta$ ; 1.485 mole % NH<sub>4</sub>F,  $\blacksquare$ ; 4.603 mole % NH<sub>4</sub>F,  $\square$ ; 19.39 mole % NH<sub>4</sub>F (eutectic),  $\bullet$ ; NH<sub>4</sub>F·H<sub>2</sub>O,  $\circ$ .

tions. It would have been possible by the technique used here to detect an effect as small as three cal./(deg. mole soln.). Although a thermal effect was observed in the vicinity of the eutectic temperature for the 4.603 mole % NH<sub>4</sub>F sample, it is believed that this effect is not evidence of a true eutectic transition but is rather a consequence of the spectrum of non-equilibrium solid-solution-compositions frozen in as a result of cooling this particular sample too rapidly through the two-phase region. Although it was the operational policy to cool samples very slowly through the two-phase temperature region, examination of the data record shows that this practice was not observed prior to the fusion transformation measurements on the 4.603 mole % NH<sub>4</sub>F sample; equilibrium solid solution concentration, therefore was probably not achieved in this experiment.

**Theoretical Solidus Curve.**—Zaromb and Brill<sup>13</sup> derived an expression for the solidus curve by utilizing the Clapeyron equation, the liquidus curve of Yatlov and Polyakova,<sup>15</sup> and simplifying assumptions (such as the constancy of the heat of fusion). The temperature dependence of the heat of fusion of ice ( $\Delta H_f$ ) is considerable and may be represented by the following analytical expression over the range of interest

$$\Delta H_f \text{ (cal./mole)} = -6997 + 63.68T - 0.1586T^2$$

This reproduces the experimentally observed values for the heat of fusion of ice within 0.2%. By incorporating this into the differential Clapeyron type equation<sup>31</sup> and integrating, the relationship

(30) R. H. Fowler and E. A. Guggenheim, "Statistical Thermodynamics," Cambridge University Press, New York, N. Y., 1939, p. 568.

(31) A. Eucken, "Lehrbuch der chemischen Physik," Akad. Verlagsgesellschaft, Leipzig, II, 1950, p. 85.

TABLE VI  
THERMODYNAMICS OF THE FUSION TRANSFORMATION

	0.4916	1.485	4.603	(Eutectic)	
Mole % NH <sub>4</sub> F				19.39	50.00
Onset temp., <i>T</i> , °K.	270	264	245 <sup>a</sup>	243.7	243.7
Temp. of Max. <i>C<sub>s</sub></i> , <i>T</i> , °K.	272.5	270.9	266.3	244.9	245.3
Final temp., <i>T</i> , °K.	272.5	271	268	245.6	247.4
Extra enthalpy increment ( $\Delta H$ ) cal./(mole soln.)	1468	1445	1292	1048	680
Extra entropy increment ( $\Delta S$ ) cal./(deg. mole soln.)	5.46	5.38	5.03	4.33	2.77

<sup>a</sup> But note discussion in text.

$$\log(N_1/N_s) = -1530(1/T_0 - 1/T) + 32.02 \log(T_0/T) - 0.03467$$

was obtained.  $N_1$  = mole fraction of H<sub>2</sub>O in the liquid phase,  $N_s$  = mole fraction of H<sub>2</sub>O in the solid phase,  $\Delta H_f$  = the heat of fusion of ice,  $R$  = the gas constant,  $T_0$  = the melting point of pure ice,  $T$  = the freezing point of the solution. The solidus curve calculated on the basis of this equation and on the liquidus data of the present investigation is in much better agreement with

other findings of this study (cf. Fig. 1) than is the curve calculated by Brill and Zaromb which did not take into account the temperature dependency of  $\Delta H_f$ .

**Acknowledgment.**—The authors express their appreciation to Professor Lee O. Case for his many helpful suggestions, and to H. Gary Carlson, Bruce H. Justice and Shu-Sing Chang for assistance in the calorimetric investigation. The financial support of the Division of Research of the U. S. Atomic Energy Commission is gratefully acknowledged.

## KINETICS OF HYDROGEN OXIDATION DOWNSTREAM OF LEAN PROPANE AND HYDROGEN FLAMES

BY BURTON FINE

*Lewis Research Center, National Aeronautics and Space Administration, Cleveland, Ohio*

*Received August 1, 1960*

The decay of hydrogen was measured downstream of lean, flat, premixed hydrogen and propane-air flames seated on cooled porous burners. Experimental variables included temperature, pressure, initial equivalence ratio and diluent. Sampling of burned gas was done through uncooled quartz orifice probes, and the analysis was based on gas chromatography. An approximate treatment of the data in which diffusion was neglected led to the following rate expression for the zone downstream of hydrogen flames  $d[\text{H}_2]/dt = 1.7 \times 10^{10} [\text{H}_2]^{3/2} [\text{O}_2] e^{-8100/RT}$  mole/(l.) (sec.). On the basis of a rate expression of this form, the specific rate constant for the reaction downstream of hydrogen flames was about three times as great as that determined downstream of propane flames. This result was explained on the basis of the existence of a steady state between hydrogen and carbon monoxide in the burned gas downstream of propane flames.

### Introduction

Within the past few years, numerous studies have been reported which involve the sampling of the burned gas downstream of flat flames.<sup>1-3</sup> Such studies have shown that, even for fuel-lean flames, a significant part of the total combustion process takes place in this downstream zone, the temperature of which is practically constant for a reasonably large distance. This has afforded a means of studying the velocity of various chemical reactions at elevated temperatures.

This paper presents results on the consumption of molecular hydrogen downstream of lean, flat propane-oxygen and hydrogen-oxygen flames with nitrogen and argon as diluents.

### Apparatus and Procedure

**Description of Combustion System.**—Two burners were used, of similar design but different size. The smaller burner had a porous circular plate of sintered copper shot 2 inches in diameter and 1/4 inch thick, which was sintered to a copper jacket. A cooling coil of 3/16-inch-outside-diameter copper tubing was likewise sintered into the base

of the plate. The other burner had a sintered plate 4 inches in diameter and 5/16 inch thick. The top surfaces of both burner plates were machined and then etched with dilute nitric acid to obtain maximum smoothness. The burners were set in the base of a low-pressure combustion chamber connected to a plenum chamber and vacuum pump. The pressure in the chamber was controlled by balancing the pumping with a variable air bleed.

The hydrogen, argon and oxygen used in these experiments were obtained in tanks from stock and used without further purification. Laboratory service air was used as combustion air. The various constituents of the initial mixture were metered separately through calibrated critical-flow orifices and then mixed in flow.

**Measurement of Temperature.**—The temperature of the flame and, presumably, of the downstream zone, was controlled by controlling the stream velocity ahead of the burning mixture. This temperature was taken as being equal to the flame temperature calculated from an energy balance which included the quantity of heat removed by the cooling water.<sup>4</sup> For corresponding flames, temperatures calculated in that way agreed well with temperatures obtained by measurement with coated thermocouples.<sup>3,5</sup> In particular, the substantial decrease in the temperature of rather lean hydrogen-air flames with decreasing pressure at constant burning velocity reported in ref. 3 was reproduced.

(1) R. Friedman and J. A. Cyphers, *J. Chem. Phys.*, **23**, 1875 (1955).

(2) C. P. Fenimore and G. W. Jones, *J. Phys. Chem.*, **61**, 651 (1957).

(3) W. E. Kaskan, *Combustion and Flame*, **2**, 286 (1958).

(4) J. P. Botha and D. B. Spalding, *Proc. Roy. Soc. (London)*, **A225**, 71 (1954).

(5) W. E. Kaskan, "Sixth Symposium (International) on Combustion," Reinhold Publ. Corp., New York, N. Y., 1957, p. 134.



**Sampling and Analysis.**—Gas samples were withdrawn through an uncooled quartz probe. This was drawn down to a tip containing an orifice about  $25\mu$  in diameter. The probe was fitted to a brass tube which passed out the bottom of the combustion chamber. A flexible connection led from the base of the tube to a vacuum line where gas samples were collected. The probe was supported on an outer hollow shaft whose height could be changed by a micrometer screw. The height of the probe tip above the center of the burner was measured through a window in the combustion chamber with a cathetometer.

Samples were collected in 300-ml. bottles which were immediately pressurized to 1 atmosphere for analysis. The final pressure in the sampling line was always less than 1/10 of the pressure in the combustion chamber.

Analyses were performed on a Perkin-Elmer Vapor Fractometer, model 154 B. The use of a molecular sieve separation column and argon as the carrier gas gave satisfactory analyses for nitrogen and oxygen and particularly sensitive results for hydrogen. Because of the small size of the samples, analyses for water vapor were not performed.

For simplicity, concentrations were generally expressed relative to the concentration of nitrogen. For the range of equivalence ratios covered the approximate relation

$$r_{H_2} = \frac{x_{H_2}}{x_{N_2}} \approx 1.4x_{H_2} \quad (1)$$

where  $x$  is mole fraction, was found to hold. In analyzing for hydrogen downstream of flames with argon used as the diluent, no argon peak was obtained. However, the composition could be estimated by comparing the peaks for hydrogen and oxygen with peaks for known mixtures.

The quantity of hydrogen found in the burned gas ranged from about 0.001 to 1 mole %, the levels of concentration increasing with increasing temperature and equivalence ratio and decreasing with increasing pressure. It was found that the concentration of hydrogen always exceeded the value calculated for equilibrium, but that the degree of excess for any point in the downstream zone increased strongly with decreasing pressure and decreased somewhat with increasing temperature.

Values found for the mole fraction of oxygen in the burned gas are in good agreement with those expected for each initial mixture. However, for initial conditions of low pressure, low burning velocity and high equivalence ratio, it was necessary to use the larger burner; otherwise the observed oxygen concentration was much too high. Furthermore, when argon was used as a diluent, analysis of the burned gas always showed a few per cent. of nitrogen. These circumstances indicated that the ambient atmosphere, containing air and combustion products, tended to be swept into the center of the downstream zone. Detailed verification that such transverse diffusion did occur was presented in a previous report.<sup>6</sup> Even with a proper choice of burner, the effect of this transverse diffusion was to obscure the very shallow oxygen decay profile that would be expected to accompany the hydrogen decay.

### Results and Discussion

The experimental data consisted of determinations of the change in hydrogen concentration with distance in the burned gas for 20 different conditions. Results are summarized in Table I, which shows the initial conditions for each run, the calculated flame temperature, the initial burning velocity, the mole fraction of oxygen in the burned gas calculated on the basis of complete combustion of hydrogen to water, and important quantities in the chemical kinetic treatment. It was found that, for all runs except one, plots of  $r_{H_2}^{-1/2}$  against  $Z$ , the distance downstream of the burner, gave straight lines for all values of  $Z$ . For the one exception, the curvature was sufficiently small that a reasonable average slope could be obtained. Figure 1 shows several decay curves plotted in this form, and values of  $\Delta r^{-1/2}/\Delta Z$  are shown in the table.

(6) B. Fine, NASA TN D-198, 1959.

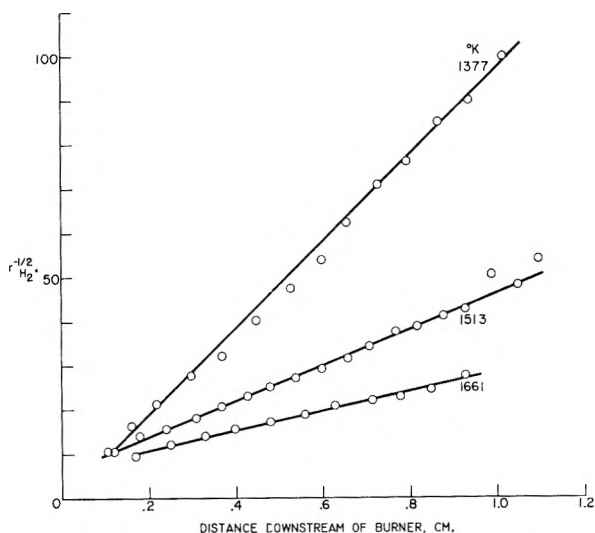


Fig. 1.—Decay of hydrogen from hydrogen-air flame. Data correspond to entries 1, 2 and 5 of table.

In order to derive a rate constant from concentration-distance data, one should consider the effect of diffusion in the flow direction; for hydrogen, this effect can be very important. An attempt was made to treat diffusion in terms of the theory of Hirschfelder and Curtiss,<sup>7</sup> but this led to non-linear differential equations which could not be solved in a satisfactory fashion, possibly because of insufficient precision in the data. It was found that the only simplification which allowed general analysis of the data was that of neglecting diffusion entirely. Thus, the treatment of the data is only approximate.

If diffusion is neglected, the data indicate that the hydrogen order is about  $3/2$ . Orders of reaction for hydrogen significantly greater than 1 have been previously inferred from measurements on the gross properties of hydrogen-oxygen burner flames.<sup>8,9</sup> The general correlation of the data in terms of an Arrhenius plot is shown in Fig. 2, on the assumption that the oxygen order is unity. Several features of the plot are worthy of note. First, the assumption that the reaction is first order in oxygen appears to hold for the range of oxygen concentration shown in the table. Second, the specific rate constant in terms of volume concentration is independent of pressure and diluent as far as those quantities have been varied. Third, the activation energy is small and is about the same for both fuels. The most striking feature of the plot is the fact that the rate constant downstream of hydrogen flames is consistently higher than that for propane flames by a factor of about 3. This appears to be reasonably well explained on the basis that, downstream of lean propane flames, the ratio of the concentrations of carbon monoxide and hydrogen always corresponds to the water-gas equilibrium. The consumption of hydrogen

(7) J. O. Hirschfelder and C. F. Curtiss, "Third Symposium (International) on Combustion," The Williams & Wilkins Co., Baltimore, Md., 1949, p. 121.

(8) A. E. Potter, Jr., and A. Berlad, "Sixth Symposium (International) on Combustion," Reinhold Publ. Corp., New York, N. Y., 1957, p. 27.

(9) B. Fine, *Combustion and Flame*, **4**, 243 (1960).

TABLE I  
CORRELATION OF SAMPLING DATA FOR HYDROGEN DECAY DOWNSTREAM OF FUEL-LEAN FLAMES

No.	Burner, in.	Fuel	Diluent	Pressure, atm.	Temp., °K.	Stream velocity of unburned mixture, cm./sec.	$z_{O_2}$	$\Delta r^{-1} \Delta Z$	Specific rate constant, $k \times 10^{-9}$
1	2	H <sub>2</sub>	N <sub>2</sub>	0.41	1513	30	0.054	41	1.24
2				0.41	1661	56	.054	23	1.22
3				1.00	1645	30	.037	135	1.40
4	4	H <sub>2</sub>	N <sub>2</sub>	0.25	1595	30	0.037	14	1.26
5				.41	1377	13.5	.054	100	.80
6				.25	1733	38	.027	6.4	1.42
7				.25	1494	25	.075	33	1.16
8				.25	1447	25	.095	48	1.04
9				.25	1300	18	.075	41	.76
10	2	H <sub>2</sub>	N <sub>2</sub>	1.00	1690	45	.037	74	1.64
11			N <sub>2</sub>	0.60	1609	35	.054	54	1.24
12			A	.41	1630	30	.075	46	1.18
13			A	.41	1444	20	.075	75	.96
14	4	H <sub>2</sub>	A	0.25	1680	15	.037	24	1.84
15	2	C <sub>3</sub> H <sub>8</sub>	N <sub>2</sub>	1.00	1790	12	.033	70	0.54
16	4	C <sub>3</sub> H <sub>8</sub>	N <sub>2</sub>	1.00	1870	16	.026	49	.72
17	2	C <sub>3</sub> H <sub>8</sub>	N <sub>2</sub>	1.00	1915	20	.033	39	.60
18			N <sub>2</sub>		1970	25	.033	27	.54
19			A		1870	14	.033	59	.60
20			A		2080	20	.033	37	.70

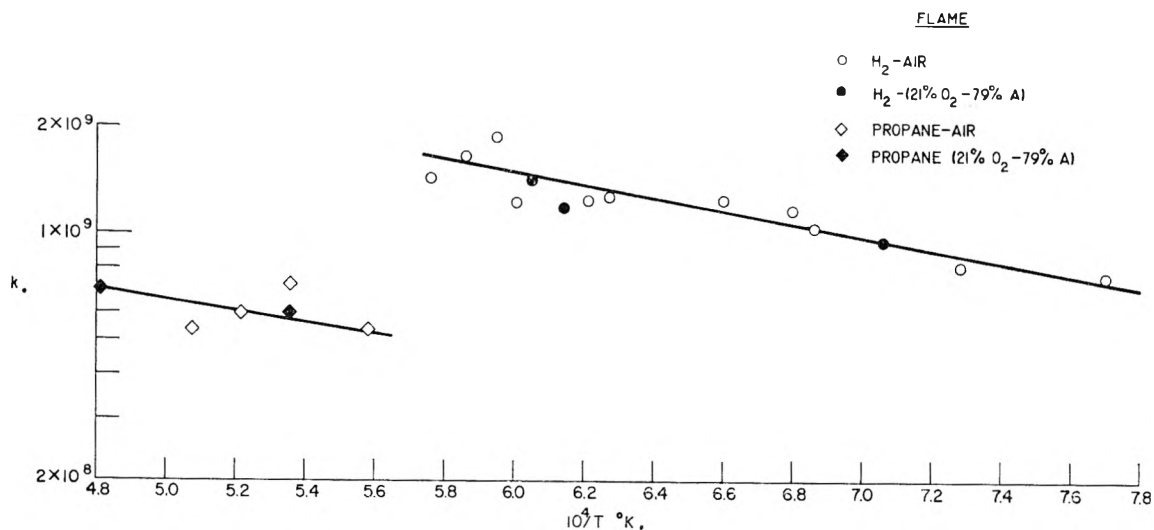


Fig. 2.—Plot of specific rate constant  $k$  against reciprocal absolute temperature:  $k = 1.7 \times 10^{10} e^{-8100/RT} \left( \frac{\text{moles}}{\text{liter}} \right)^{-3/2}$  sec.<sup>-1</sup> (equation for upper line).

is opposed by its formation at a relatively fast rate through the maintenance of a steady state between carbon monoxide and hydrogen. The observed lowering of the rate for propane flames agrees with that estimated from the ratio of equilibrium concentrations of carbon monoxide and hydrogen.

If the decay of carbon monoxide takes place only through the steady state between carbon monoxide and hydrogen, one would expect the same order and activation energy for both fuels. The fact that the activation energy obtained by Fenimore

and Jones for carbon monoxide, 24 kcal./mole, is much larger than that presently obtained for hydrogen can be explained by the fact that Fenimore and Jones assumed that carbon monoxide decay was first order. Thus, at constant oxygen concentration and pressure, the rate expression for a reaction order of  $3/2$  in hydrogen can be written

$$\frac{d \ln H_2}{dt} = \kappa [H_2]^{1/2} e^{-E/RT}$$

where  $\kappa$  is related to the specific rate constant and other symbols have their usual meanings. Since

the concentration of hydrogen in the burned gas depends on many factors, including the temperature of the downstream zone, one would expect that the

activation energy obtained would be different depending on whether the assumed hydrogen order was 1 or  $3/2$ .

## HYDROCARBON SYNTHESIS ON PURE IRON

By P. B. WEISZ AND W. P. KERN

Socony Mobil Oil Company, Inc., Research Department, Paulsboro Laboratory, Paulsboro, N. J.

Received August 8, 1960

Pure iron was observed gradually to develop activity for the production of paraffin hydrocarbons, from carbon monoxide and hydrogen, over a period of 350 hours of contact. The fraction of olefin hydrocarbons produced, however, was noted to decay to zero within about 150 hours of contact. Photoelectric measurements of the iron surface indicated only a small shift of work-function, photoelectric emission shifting toward longer wave lengths. The gradual shift in photoelectric properties parallels the slow transition of the catalytic properties.

### Introduction

Over the many years of investigation of iron as a synthesis catalyst for the conversion of carbon monoxide and hydrogen little attention has been given the behavior of pure iron. An important role of "promoter" additions, especially of alkali, has been indicated starting with the original work of Fischer and Tropsch,<sup>1</sup> for achieving practical synthesis catalysis. Moreover, Fischer and Tropsch suggested that alkali is an essential mechanistic factor for achieving the synthesis of molecules with more than one carbon number, the iron acting as hydrogenation catalyst for carbon monoxide, and alkali catalyzing condensation reaction steps.

The present report deals with a study employing iron introduced into the experiment as 99.99 (plus) % purity iron wire, without the aid of preparation techniques which may introduce other components. The gaseous products from repeated 20 hour contacts with a mixture of 1:1 CO-H<sub>2</sub> at 40 cm. pressure and 320° were studied over a period of several hundred hours. At the same time intervals the photoelectric properties of the surface were examined as a non-destructive tool which would indicate compositional changes occurring at the surface during the period of activity study.

### Experimental

The reactor vessel was designed to allow its use for catalytic contact with the reacting gases, as well as to offer part of the iron surface contained therein as the cathode of a photo-responsive tube geometry, which could be irradiated with the light from a Beckman monochromator, and the photoelectric response measured as a function of wave length.

The low photoelectric yield attainable from iron, especially in the presence of gas,<sup>2,3</sup> and the relatively low light intensity available after passage through a monochromator, and through a sighting passage of a surrounding furnace, made the conventional photo-current measurement a relatively unattractive prospect. Instead, a Geiger counter tube geometry, consisting of a pure iron cathode cylinder and coaxial pure iron anode wire was created as part of the reactor's total iron surface. The monochromator light beam could be directed onto the interior cathode surface, and with the gas fillings of the chemical experiment itself, the tube was operated as a photon counting Geiger counter.

In Fig. 1 is pictured the construction of the reactor tube constructed from Nonex glass, containing the bulk of the

catalytic iron in the form of a multiple honeycomb coil of 68 g. of 0.007" diameter iron wire (99.99 plus % highest purity iron from Swedish Iron and Steel Corp., New York City), presenting a geometric surface area of 2000 cm.<sup>2</sup>. This was wound around a 2 cm. diameter cylinder of the same iron, serving as a support as well as the photoelectric Geiger tube cathode. The axially suspended (0.007" iron) wire serves as anode. The ultraviolet transmitting window was blown to approximately 0.005" thickness from Corning 9741 glass.

This reactor tube was contained in a tubular furnace thermostatically controlled to a temperature of 320° during reaction periods. The furnace cylinder was provided with hole and side tube to allow proper injection of the monochromator beam.

The two gas leads to the reactor tube were attached to a glass circulating system comprising a glass bulb reservoir, a magnetically rotatable glass vane (with sealed-in iron bar) to provide continuous circulation of the gaseous content through the entire system, a mercury manometer and valving to allow evacuation to 10<sup>-4</sup> mm. pressure. The system, including the reactor itself, contained a volume of 2510 cm.<sup>3</sup>.

The Geiger tube electrodes were connected to a conventional (Instrument Development Co.—now Nuclear-Chicago Corporation) electronic quenching circuit and 64:1 scaler.

Hydrogen (Matheson Company, East Rutherford, N. J.) was used after passing it over reduced copper filings at 700° and liquid nitrogen cooled glass trap. Carbon monoxide was passed over the same purification train.

**Preparation of Iron Surface.**—The iron containing reactor tube was washed with large quantities of acetone and dried before sealing to the system. It was pumped to about 10<sup>-4</sup> mm. pressure over a period of 2 days; the iron was then oxidized in oxygen with 1 atm. oxygen for 20 minutes at 300°. The photoelectric response of the oxidized surface—taken with 5% O<sub>2</sub> in helium as the counting gas—is seen in Fig. 2A. Then the tube was pumped back to a vacuum, and reduced by filling the system to 1 atm. of hydrogen circulating over the iron at 420° for one hour and through a liquid nitrogen cooled trap before re-evacuation for several reduction cycles. This reduction was repeated beyond the state of no measurable hydrogen pressure drop, until no more change in the photoelectric spectral response of the surface occurred. The latter response was measured after each reduction cycle with the tube at room temperature and containing 10 mm. hydrogen pressure; Fig. 2B shows the response of the final surface. As previously pointed out by Brewer,<sup>4</sup> the photoelectric method is very sensitive to oxide (or oxygen) content and reveals changes toward the ultimate reduced state after pressure changes are no longer observable. Figure 2C shows the spectral response of the surface after room temperature exposure to 5% O<sub>2</sub> in 1 atm. helium for 15 minutes obtained in a previous preliminary experiment.

**Catalytic Reaction.**—After evacuation at room temperature, a 50/50 mixture of hydrogen and carbon monoxide were admitted to the system, to a total pressure of 3 cm. A

(1) F. Fischer and N. Tropsch, *Ber. deut. Chem. Ges.*, **56**, 2428 (1923).

(2) A. K. Brewer, *J. Am. Chem. Soc.*, **53**, 74 (1931).

(3) A. K. Brewer, *ibid.*, **54**, 1888 (1932).

(4) J. T. Kummer and P. H. Emmett, *ibid.*, **75**, 5177 (1953).

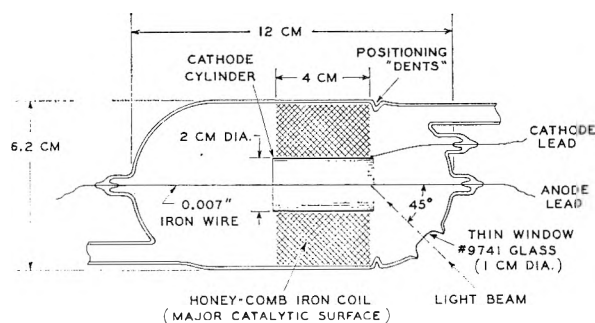


Fig. 1.

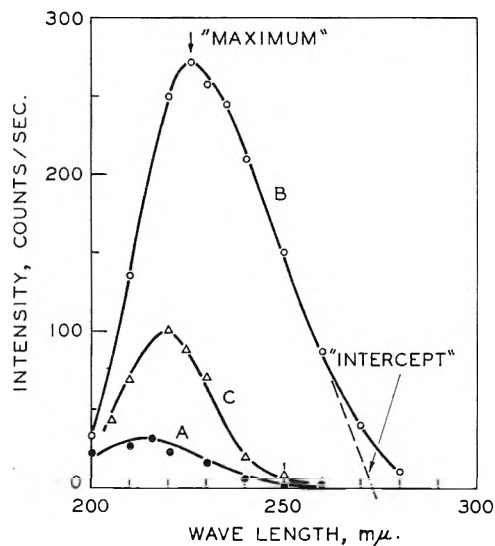


Fig. 2.

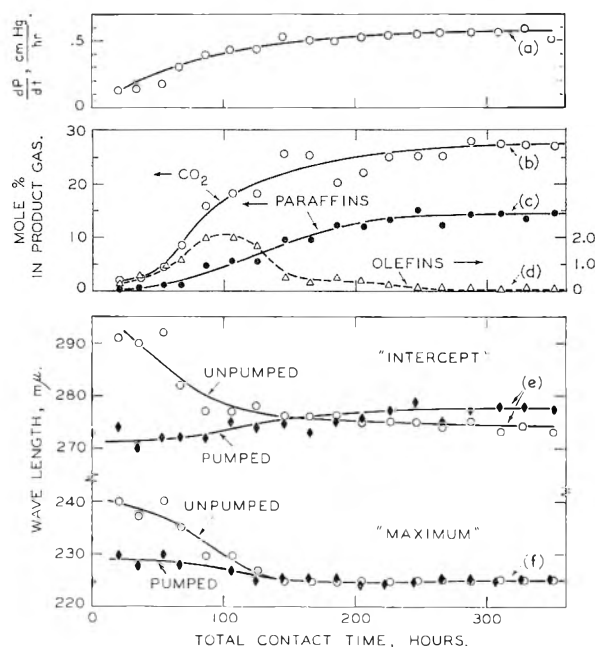


Fig. 3.

photoelectric response was taken, and the reactor heated to 320°. Additional gas mixture was added to a total pressure of 40 cm. Reaction was allowed to proceed for 20 hours with the circulating vane operating. The pressure drop was followed for that period. Thereafter, a gas sample was drawn from the system for mass spectrometer analysis, the

reaction tube cooled to room temperature, and pressure pumped back to 3 cm., a photoelectric response taken (*i.e.* in the presence now of any product species made), the system evacuated, and the same cycle of operations repeated. The set of measurements was carried out over a total catalytic contact time of 380 hours.

**Results of Catalytic Contact.**—Figure 3 summarizes the following results of the catalyst runs for each reaction interval: (a) the average rate of pressure change; (b) the concentration of CO<sub>2</sub>, (c) of total paraffin hydrocarbons, (d) of total olefin hydrocarbons in the product gas, (e) the wave length "intercept" and (f) of the wave length of the "maximum" of the photoelectric response spectrum of the iron surface, both measured in the absence as well as presence of reaction products (pumped, and unpumped).

Furthermore Table I shows the composition of paraffin and olefin components for the same reaction intervals.

TABLE I  
COMPOSITION OF HYDROCARBON COMPONENTS IN PRODUCT GASES

Total contact time, hr.	Mole % in product gas						
	Paraffins <sup>a</sup>			Olefins			
	C <sub>1</sub>	C <sub>2</sub>	C <sub>3</sub>	C <sub>2</sub>	C <sub>3</sub>	C <sub>4</sub>	C <sub>5</sub>
19.5	0.2	T	T	0.1	0.1	0.1	0.1
35	.5	0.1	T	.3	.2	.1	.1
53.5	.7	.2	0.1	.4	.3	.1	.1
66.5	.9	.2	T	.6	.4	.1	.1
86	3.6	.9	0.2	1.0	.7	.2	.1
105.5	4.2	.9	.3	1.0	.6	.2	.2
125	4.4	1.0	.1	0.8	.6	.2	.1
145.5	9.1	1.1	T	.2	.2	T	T
166	8.3	1.2	T	.2	.1	T	0
185.1	10.3	1.6	0.3	.2	.2	0	0
205	9.8	1.6	.3	.2	.2	0	0
226	11.5	1.5	.3	.1	.1	0	0
247	13.3	1.3	.3	T	.1	0	0
266	11.2	1.5	.3	T	.1	0	0
287	12.0	1.7	.4	T	.1	0	0
310	12.6	1.5	.3	0.1	T	0	0
329	11.3	1.5	.4	.1	0.1	0	0
351	12.5	1.6	.4	.1	0	0	0

<sup>a</sup> Only trace quantities of C<sub>4</sub>-paraffins were detected, and no reliably detectable amounts of C<sub>5</sub>-paraffin were observed.

**The Surface after Reaction Contact.**—After the catalytic contact, the surface was subjected to contact with hydrogen alone, to observe any continued production of hydrocarbon products due to interaction with the surface composition, and to test for the presence of iron carbide by examination of the products of hydrogen reduction. Methane production alone did continue. Figure 4 shows the mass spectrometer analysis of the hydrogen gas after successive contacts for 20 hour intervals at 270, 320 and 420°, as indicated along the abscissa. Water was the only other observed product (no quantitative amounts recorded).

The reduction, as indicated by Fig. 4, generated methane equivalent in carbon content to 52 cm. pressure of CO in the volume of the reaction system. For the sum of all reaction runs, the calculated carbon balance shows a deficiency of 59 ± 4 cm. pressure equivalent of CO. Thus most of this deficiency is accounted for by carbon remaining on the iron, and which was successfully reduced to methane with perhaps a small additional unreduced or irreducible carbonaceous material remaining on the catalyst. The photoelectric response of this surface remained identical to that after reaction contact; moreover, the addition of oxygen (air) at room temperature did not cause a distinct change in photoelectric response of this surface. In fact, even a contact with O<sub>2</sub> at 300°, for one hour, produced a spectral shift of only about -5 mμ of the maximum. These results are consistent with the conclusion that a clean iron surface had not been attained by the above hydrogen contacts.

### Discussion

The gas analyses reveal progressive development of activity of an initially unreactive surface. The

rate of development is fastest within the first 100 hours, and tapers off thereafter to possibly a constant activity. Hydrocarbons of larger carbon numbers begin to be detectable as the activity rises. After about 200 hours a nearly constant level of catalytic behavior is approached.

A qualitative change in the nature of the products, and therefore presumably in the nature of the catalytically active solid, is observed between 50 and 150 hours, during which time olefin product concentration reaches a peak but subsequently decays to essentially zero.

If we accept the hypothesis that olefinic hydrocarbons are generated prior to their saturated form,<sup>4</sup> then the product observations indicate gradual development of increasing hydrogenative activity as a catalytic characteristic of the surface change.

During the course of the qualitative surface changes, the course and concentrations of total C<sub>3</sub>, C<sub>4</sub>, C<sub>6</sub> hydrocarbon concentrations, individually, as shown in Table I, indicate that the ability to synthesize increasingly larger chains is arrested during the development of increased hydrogenation activity. Furthermore, the active disappearance of C<sub>4</sub> and C<sub>6</sub> olefins past the 100 hour contact time, in the absence of detectable C<sub>4</sub> and C<sub>6</sub> paraffins indicates an actual increased inhibition of chain growth.

The photoelectric behavior of the pumped surface parallels this gradual change of surface properties for the first 200 hours. The long wave length intercept changes, by a relatively small absolute amount, toward larger wave length, indicating a somewhat lower work-function. The location of the observed maximum also changes by a small amount (toward shorter wave length) during this contact period. The qualitative progression of the nature of the surface parallels the course of catalytic behavior. Also the relative effect of product molecules on the photoelectric nature of the surface (unpumped *vs.* pumped response) also reflects a qualitative change of surface property during the initial phase.

Beyond this, a quantitative interpretation of the response patterns, measured in absence of high vacuum techniques or of gases of highly controlled composition, is probably not justified. However, no major amount of surface appears to be in the oxide form, since a very rapid drop in photoelectron intensity and sharp increase of work-function would

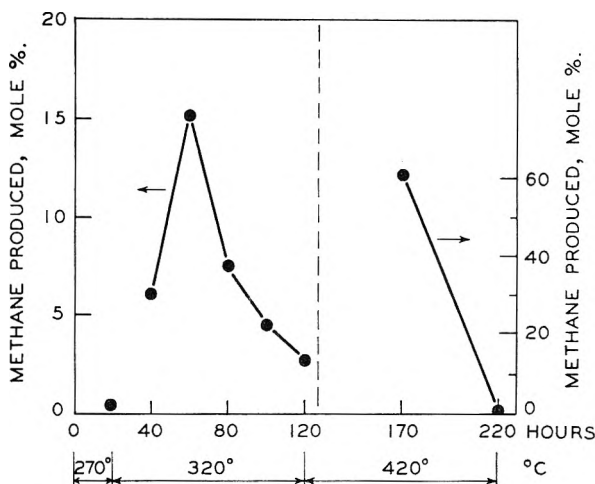


Fig. 4.

result. The opposite behavior in the shifts (pumped surface) of long wave length intercept and of the location of the observed maximum would, however, be consistent with development of a composite or heterogeneous structure. The observations do not exclude the possibility of some surface oxygen-iron bonding. However, considering the small changes in the photoelectric spectrum no more than an estimated 10% (and probably much less) of the surface atoms could be involved.

The presence of large amounts of iron carbide is indicated by the hydrogenation subsequent to the synthesis use of the iron. However, the production of such carbide does not indicate its participation as an intermediate in the synthesis. We prefer not to seek to identify the chemical nature of the catalyzing surface in terms of bulk chemical terminology.

One may conclude that "pure" iron, after contact with CO and H<sub>2</sub>, is capable of forming a surface composition which will produce addition of carbon units to form hydrocarbon beyond methane, and that promoters may act to favor production and maintenance of a state of surface which with pure iron is approached somewhat during the transitory period around 100 hours contact time in these experiments.

We are indebted to Prof. P. H. Emmett for helpful and stimulating discussions of the results and findings in this work.

# A VAPOR PHASE EQUILIBRATOR FOR ACTIVITY COEFFICIENT DETERMINATIONS

BY LEO BREWER, THOMAS R. SIMONSON AND LEE KARL J. TONG

*The Department of Chemistry, University of California, Berkeley 4, California*

Received August 9, 1960

A vapor phase distributor has been designed that allows rapid and accurate determinations of activity coefficients of volatile solutes. It has been used to determine the activity coefficient of mesityl oxide in a variety of aqueous salt solutions, but it can be applied to many types of solutions. A deviation from Henry's Law of 20% has been found for saturated mesityl oxide solutions. The distribution of iodine between water and carbon tetrachloride has been studied. It has been confirmed that the variation of distribution ratio with iodine concentration is entirely consistent with expected regular solution behavior and is not due to new species such as  $I^+$  or  $I_2$ .

## Introduction

Activity coefficients of organic solutes in aqueous salt solutions are commonly determined by the equilibration of the solute between the aqueous salt solutions and an organic phase, such as carbon tetrachloride or the pure organic solute (*e.g.*, solubility determinations), or sometimes through direct vapor pressure determinations. The first two methods involve errors due to emulsification of the organic phases and are complicated by deviations from Henry's Law in the organic phase or in the aqueous phase. The third method has been difficult to apply accurately. Friedman<sup>1</sup> also has pointed out that complete thermodynamic data cannot be obtained from solubility measurements since one cannot determine the effect of variation of solute concentration upon the solute activity coefficient.

Jones and Kaplan<sup>2</sup> have described an equilibrator for the distribution of volatile substances by way of the vapor phase, which avoids the difficulties of the other methods. Their method is applicable to solutes of relatively low vapor pressure. The Jones and Kaplan equilibrator is inconvenient in that the entire apparatus must be kept in motion. The equilibrator used in the present work is of a different design in that no movement of the main part of the distribution apparatus is required.

## Experimental

**Apparatus.**—The principle of the apparatus is illustrated in Fig. 1. Bulbs 1, 4, 5 and 6 contain mercury. Bulbs 2 and 3 contain the solutions between which a volatile substance is to be distributed. If pressure is applied on bulb 6, that pressure is transmitted through the mercury into bulb 4 and causes compression of the gas in bulb 4. This compressed gas travels by two paths. It pushes down on the liquid in bulb 2 until the liquid has risen in the arm between bulb 1 and 2 to a height equal to the height of liquid in bulb 3. Any further compression is relieved by bubbling through bulb 3. In actual operation pressure is applied at bulb 6 while suction is applied at bulb 5 and then this is reversed by applying pressure at bulb 5 and suction at bulb 6. The result of this alternating suction and pressure is to cause gas to bubble from 4 through 3 to 1 and then to bubble from 1 through 2 and back to 4 again. The source of the alternating pressure and suction is the oscillation of two bulbs of mercury which are connected with one another and are oscillated by a pulley system.

In the actual apparatus, there are two bulbs in series in place of bulb 3. The salt solution is placed in bulb 2 and water in bulbs 3a and 3b. Mesityl oxide is added to bulb 3a and the alternating pressure and suction started. The gas in the system bubbles through bulbs 3b, 3a and 2 and

around again until analyses indicate that equilibrium has been reached when the mesityl oxide concentration in bulbs 3a and 3b has become the same. Bulbs 1, 2, 3a, 3b, 4, 5 and 6 are arranged compactly on a wooden platform which is immersed in a thermostat. The two oscillating bulbs are outside of the thermostat and the alternating pressure and suction is transmitted by gas pressure through rubber tubing to bulbs 5 and 6 and through them into the apparatus. Bulbs 2, 3a and 3b have ground glass stoppers which may be removed to take samples.

The rate of distribution depends upon the rate of bubbling which can be regulated by the height through which the bulbs oscillate and by the rate of oscillation. A variable speed d.c. motor with a gear reducer was used to operate the pulley. Equilibrium could be approached from either side by putting mesityl oxide initially in any one of bulbs 2, 3a or 3b. Within the analytical uncertainty of 0.1%, equilibrium is attained in less than 12 hours. The materials used as solutes in this study, mesityl oxide and iodine, have lower vapor pressures than water. Thus it might seem surprising that one could expect to reach equilibrium with respect to the solute without transporting large amounts of solvent and thus diluting the salt solutions that are being compared with water. However, the success of this method does not depend upon the actual value of the partial pressure of the material being transported but depends upon the Henry's law constant, the ratio of partial pressure to concentration, or upon a corresponding quantity,  $K$ , which is defined as the ratio of concentration in the liquid phase to concentration in the gaseous phase using moles per liter for both phases.

If one sets up the differential equations for the transport of material from one bulb to the next due to saturation of the gas bubbling through each bulb, one finds that the concentration of solute varies in an oscillatory manner in its approach to its equilibrium value. Thus the concentration in the second bulb,  $c_2$ , is given by

$$c_2 = e^{-2V/2K} \left[ \frac{1}{3} (2c_2^0 - c_1^0 - c_3^0) \cos(\sqrt{3} V/2K) + \frac{1}{3} (c_1^0 - c_3^0) \sin(\sqrt{3} V/2K) \right] + (c_1^0 + c_2^0 + c_3^0)/3$$

where the  $c^0$  values are initial concentrations in the three bulbs,  $K$  has been defined above, and  $V$  is the ratio of the volume of gas bubbled through each bulb to the volume of solution in the bulb. This equation is given for equal volumes of solution in each bulb and equal values of  $K$  for each solution. A similar but more complicated expression results when  $K$  is different for each solution.

The equation takes a simpler form when one solution is saturated and thus maintains a constant concentration. This occurs for the solute when excess solute is present and for the solvent when no salt or other non-volatile solute is present in one of the bulbs and all volatile solutes are at low concentrations. Thus if  $c_1^0$  is now the concentration of solvent in the first bulb, which contains no salt, and  $c_2$  is the concentration of solvent in the second bulb

$$\ln \left( \frac{c_1^0/K_1 - c_2/K_2}{c_1^0/K_1 - c_2^0/K_2} \right) = \frac{V}{K_2}$$

$V$  is the same as above. The  $c$  and  $K$  values apply to the solvent. Examination of these equations shows that a solute like mesityl oxide will approach equilibrium more rapidly than will water. The value of  $K$  is  $4 \times 10^4$  for

(1) H. L. Friedman, *J. Phys. Chem.*, **59**, 161 (1955).

(2) G. Jones and B. B. Kaplan, *J. Am. Chem. Soc.*, **60**, 1600, 1855 (1928).



pure water, 620 for mesityl oxide in dilute aqueous solution, and 81 for iodine in dilute aqueous solution. A value of  $V$  of 1000 or a volume of gas 1000 times larger than the volume of solution in a bulb is sufficient to bring the mesityl oxide concentrations to closer than 99.9% of the equilibrium values. The same value of  $V$  will transport only 2.7 grams of water per liter of solution from pure water to a 2  $M$  NaCl solution.

The above equations assume saturation of each gas bubble by the volatile constituents of the solution. One can derive similar equations based on reasonable rates of saturation of the bubbles and reach similar conclusions. The observed rates for mesityl oxide solutions indicate rapid rates of saturation, and thus equilibrium is attained within the analytical accuracy of 0.1% before sufficient water can distill to have any significant effect. This source of error is largest for concentrated salt solutions. Distillation of water dilutes the salt solution by less than 1%. Such a dilution of a 5  $M$  NaCl solution would decrease the activity coefficient of mesityl oxide by less than 0.2%. The final salt concentration was used and any error in the equilibrium value of the activity coefficient due to water distillation is less than the analytical error. There was no error from spray as no test for halide ion could be detected in the water bulbs when halide salt solutions were used. This method appears to be quite generally applicable to distribution of solutes between immiscible phases such as  $CCl_4$  and water or between miscible phases such as alcohol and water or water and aqueous salt solutions as long as the Henry's law constant for the solute is large enough to permit approach to equilibrium within analytical uncertainty for the solute before appreciable amounts of solvent have been transported.

**Materials.**—Mesityl oxide was chosen to test the apparatus as its activity coefficient was desired for interpretation of kinetic studies. The mesityl oxide was prepared by distillation from purified Eastman Kodak diacetone containing 0.01% iodine.<sup>3</sup> The water layer was separated and the mesityl oxide was washed once with half-saturated sodium chloride solution containing 0.1  $M$  NaOH and then successively with half-saturated sodium chloride solutions with a ten-fold reduction in sodium hydroxide each time until the salt solution contained only  $10^{-4}$   $M$  NaOH. Calcium chloride hydrate and calcium hydroxide were added to the mesityl oxide and the saturated calcium chloride solution withdrawn. Drying was completed with anhydrous calcium chloride. The washing and drying operations were done quickly to minimize condensation, hydration and isomerization reactions. The presence of products of the condensation reactions considerably reduces the solubility of the resulting material. The dry mesityl oxide was fractionally distilled at 50 mm. discarding the low boiling fraction of low refractive index and the highest boiling fraction. The mesityl oxide then was slowly frozen and the lowest melting portion was discarded. The mesityl oxide was then fractionally distilled at 50 mm. again discarding the fraction of low boiling point and low refractive index and the very highest boiling fraction. The final material had a refractive index  $n_D$  1.443 at 25°. Comparison with the data given by Stross, Monger and Finch<sup>4</sup> for mesityl oxide and iso-mesityl oxide indicates that our final product had less than a per cent. of iso-mesityl oxide. The freshly made mesityl oxide was used at once to prepare 0.25  $M$  aqueous solutions, as the pure mesityl oxide reacts with oxygen and undergoes other reactions on standing. The aqueous solutions did not form peroxides and were quite stable although they decreased in strength due to volatility losses.

The sodium perchlorate solution was prepared by neutralization of perchloric acid. The other salt solutions were prepared from reagent grade salts. The salt solutions were close enough to neutrality to ensure no appreciable hydration of mesityl oxide to diacetone alcohol.

**Analyses.**—The mesityl oxide was determined by bromination as described by Pressman, Brewer and Lucas.<sup>5</sup> At high concentrations of mesityl oxide, the separation of a mesityl oxide dibromide phase removed some of the mesityl oxide from the aqueous phase and low bromination results

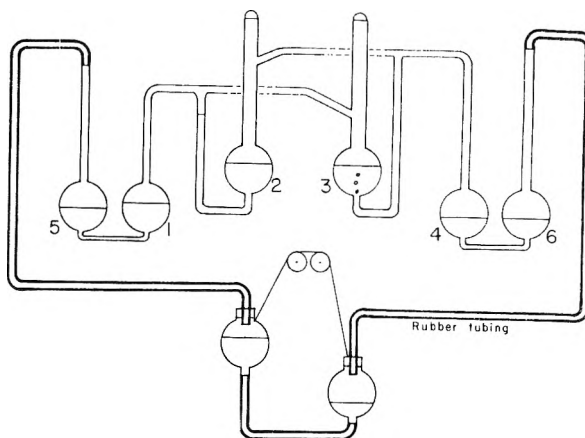


Fig. 1.—Illustration of principle of distribution apparatus.

were obtained unless a considerable excess of bromine was used or unless the mixture was shaken. The salt solutions were analyzed by evaporating to dryness below the boiling point of the saturated solution and weighing the residue. The analysis was accurate even for salts such as sodium acetate. Testing of the residue showed that only  $10^{-4}$  mole of acetic acid escaped per liter of 2.5  $M$  sodium acetate solution. As the salt solutions were handled volumetrically, they were kept in an air thermostat inasmuch as some concentrated salt solutions expand as much as 0.1% per degree. The halide solutions were checked by the Volhard titration.

**Equilibration Procedure.**—The procedure for adding salt and mesityl oxide to the bulbs has been described above. The time for equilibration could be considerably reduced from the normal 10–12 hours by adding mesityl oxide to all bulbs, but with different concentrations in bulbs 3a and 3b. The test for equilibration was equality within the experimental reproducibility of 0.1% of mesityl oxide concentrations in bulbs 3a and 3b. The mesityl oxide was determined in the three bulbs using the special pipet described by Eberz and Lucas<sup>6</sup> to prevent loss of mesityl oxide by vaporization. The solution was forced up into the special pipet by nitrogen which was bubbled through mesityl oxide solution of about the same concentration as that in the equilibrator. This procedure ensured that the progress of the equilibrator toward equilibrium was not affected by the sampling. Nitrogen was used as the equilibrator gas although mesityl oxide does not form peroxides in the aqueous solution. Check runs with air and oxygen yielded distribution ratios differing not more than 0.2% from the ratios obtained with nitrogen. As the apparatus could be run continuously, two to three runs could be done every 24 hours. The ratio of the mesityl oxide molality in the water to that in the salt solution yields directly the activity coefficient of mesityl oxide in the salt solution when the mesityl oxide molality is low enough to allow assumption of Henry's law. Appreciable deviations from Henry's law were found even below 0.1  $M$ . As corrections can be applied for this deviation, it was possible to use molalities as high as 0.1  $M$  without loss in accuracy.

The apparatus had to be modified for the few test distributions of iodine between water and carbon tetrachloride as the mercury in bulbs reacted with the iodine. The mercury was replaced with saturated sodium nitrate solution for iodine runs.

Following each run, a known volume of salt solution was pipetted into a weighed bottle, weighed, and then evaporated to dryness to yield the weight of salt and weight of solvent (water plus mesityl oxide). The mesityl oxide concentration was known; thus the weight fractions of all components could be calculated. One can express molalities as moles per kilogram of water or as moles per kilogram of solvent (mesityl oxide plus water). The latter choice was adopted. The ratio,  $c/m$ , of the concentration in moles per liter to the molality is obtained directly from the ratio of weight of solvent to pipet volume.

The  $c/m$  ratios for dilute salt solutions containing 0.1  $M$  mesityl oxide are about 0.1% lower than for pure salt solutions. For some of the more concentrated salt solu-

(3) H. Hibbert, *J. Am. Chem. Soc.*, **37**, 1748 (1915).

(4) F. Stross, J. M. Monger and H. de V. Finch, *ibid.*, **69**, 1627 (1947).

(5) D. Pressman, L. Brewer and H. J. Lucas, *ibid.*, **64**, 1117 (1942).

(6) W. F. Eberz and H. J. Lucas, *ibid.*, **56**, 1230 (1934).



TABLE I  
*c/m* RATIOS FOR AQUEOUS MESITYL OXIDE SOLUTIONS AT 25°

<i>m</i>	0.1 <i>M</i> MO						0.02 <i>M</i> MO	
	0.25	0.5	1	1.5	2	2.5	4.5	5.5
NaAc	0.987	0.977	0.947	...	0.916	0.897		
KAc	.983	.973						
NaCl	.993	.988	.978	0.964	.952	0.940	0.907	0.887
KCl	.990	.984	.969					
NaBr	...	.985						
KBr	...	...	.961	.947	.931			
NaI	...	.978	.962					
NaNO <sub>3</sub>	...	.983	.968	.954	.939			

tions, the difference is considerably greater. For example, for 1.5 *M* NaCl at 25° containing 0.1 *M* MO, *c/m* is 0.6% smaller than for the pure salt solution.

The distribution ratio of mesityl oxide was determined volumetrically. This ratio was converted to the molality basis in terms of moles of mesityl oxide per kilogram of solvent by multiplying by the ratio of *c/m* values for the two solutions. The *c/m* values for the salt solutions studied are given in Table I.

### Discussion

**Deviation from Henry's Law.**—Pressman, Brewer and Lucas<sup>5</sup> have determined the activity coefficient of mesityl oxide in sodium perchlorate and sodium nitrate solutions by means of distribution experiments between carbon tetrachloride and the aqueous salt solutions. They have ascribed the variation of the distribution ratio of mesityl oxide between water and carbon tetrachloride with the mesityl oxide concentration to deviation from Henry's law in the carbon tetrachloride. This deviation becomes substantial for mesityl oxide concentrations in the CCl<sub>4</sub> greater than 0.2 mole/liter. Thus, the aqueous concentration must be kept below 0.0076 mole/liter to avoid corrections for deviations from Henry's law in the CCl<sub>4</sub> phase. By use of the vapor phase distribution method one need not apply any corrections for deviations from Henry's law until one has attained much higher concentrations. The ratio of the fugacity of mesityl oxide to its aqueous molality is 7% smaller in a 0.1 *M* solution and 20% smaller in a saturated solution of mesityl oxide (0.304 *M* or 0.302 mole/l. at 25°) than in very dilute solutions.

The activity coefficient of mesityl oxide (component 3) relative to the hypothetical solute standard state in water (component 1) can be expressed as a function of both salt (component 2) and mesityl oxide molality

$$\log \gamma_3 = k_{32}m_2 + k_{33}m_3 \quad (1)$$

was found to hold rather well. The *k*<sub>33</sub> term represents the deviation from Henry's law. The deviation from Henry's law may be found readily by use of the vapor phase distribution apparatus. If mesityl oxide is distributed between water and a salt solution and the distribution repeated at several mesityl oxide molalities, it is found that the mesityl oxide molality in the water to that in the salt solution increases as the mesityl oxide molality rises since the deviation from Henry's law changes more rapidly in water than in the salt solution. This is due to the smaller mesityl oxide molality in the salt solution than in the water. Thus the ratio of the mesityl oxide molalities in the solution at equilibrium does not give the activity coefficient

of mesityl oxide relative to the hypothetical solute standard state in pure water unless one corrects for the deviation from Henry's law. The value of -0.3 which was found for *k*<sub>33</sub> of equation 1 allows one to make this correction. If  $\gamma^* = (\text{MO})_w/(\text{MO})_s$  is the observed distribution ratio between water and a salt solution when there is a molality (MO)<sub>w</sub> in the water bulb and a molality (MO)<sub>s</sub> in the salt solution, the error in log  $\gamma^*$  due to deviation from Henry's law is -0.30.  $[(\text{MO})_w - (\text{MO})_s] = -0.30(\text{MO})_w(1 - 1/\gamma^*)$ . Thus

$$\log \gamma = \log \gamma^* - 0.30(\text{MO})_w(1 - 1/\gamma^*) \quad (2)$$

gives the relationship between the distribution coefficient,  $\gamma$ , obtained at low mesityl oxide molality and the coefficient,  $\gamma^*$ , obtained at high mesityl oxide molality for a given salt solution.

These corrections are illustrated in Table II where the results of three experiments at approximately the same salt molality but with different mesityl oxide molalities are presented. The quantities *k*<sub>32</sub> and *k*<sup>\*</sup><sub>32</sub> were obtained by dividing the respective log  $\gamma^*$  and log  $\gamma$  values by the sodium chloride molality. Because sodium chloride molalities were not quite the same, one must compare *k* values rather than  $\gamma$  values to reduce the observations to the same sodium chloride molality.

TABLE II  
 EFFECT OF HIGH MESITYL OXIDE MOLALITY UPON DISTRIBUTION BETWEEN WATER AND SALT SOLUTIONS

<i>m</i> <sub>NaCl</sub>	$\gamma^*$	<i>k</i> <sup>*</sup> <sub>32</sub>	(MO) <sub>w</sub>	$\frac{0.30(\text{MO})_w}{(1 - 1/\gamma^*)}$	log $\gamma$	$\gamma$	<i>k</i> <sub>32</sub>
1.467	1.873	0.186	0.133	0.0186	0.2539	1.795	0.173
1.517	1.941	.190	.162	.0236	.2648	1.840	.1745
1.619	2.060	.194	.209	.0323	.2816	1.912	.174

A series of experiments of the type illustrated in Table II indicated that log  $\gamma = -0.30m_{\text{MO}}$  or the second term of eq. 1 appears to adequately represent the variation of the mesityl oxide activity coefficient as a function of mesityl oxide molality for both water and salt solutions of mesityl oxide. It is of interest to compare the value of *k*<sub>33</sub> = -0.30 ± 0.005 with the value of *k*<sub>3,DA</sub> = -0.07 ± 0.01 obtained from the data of Pressman, Brewer and Lucas<sup>5</sup> for the effect of diacetone alcohol upon the activity coefficient of mesityl oxide in aqueous solution.

It will be noted that *k*<sup>\*</sup> varied by 0.008 corresponding to a 3% variation in  $\gamma^*$  and that *k*<sup>\*</sup> at the highest (MO)<sub>w</sub> differs from *k* by 0.020 corresponding to a 7% error in  $\gamma^*$  due to the deviation from Henry's law. The average deviation from the mean value of *k*<sub>32</sub> is only 0.0005 corresponding

TABLE III  
 SALTING-OUT COEFFICIENT  $k_{32}$  FOR MESITYL OXIDE AT 25.00°

$m$	NaAc	KAc	NaCl	KCl	NaBr	KBr	NaNO <sub>3</sub>	NaI	NaClO <sub>4</sub>
0.25	0.190	0.176	0.190	0.158	...	...	...	...	...
0.5	.191	0.179	.180	.159	0.117	...	0.056	0.03	...
1	.180		.174	.149		0.102	(.08)	0.024	0.022
1.5	...		.173			.104	.074		.025
2	.168		.170			.105	(.082)		.033
2.5	.164		.1695						
4.5			.1648						
5.5			.1638						

to 0.2% deviation in  $\gamma$ . Thus, it is seen that the use of eq. 1 and a value of  $k_{33} = -0.3$  allows an accurate correction for deviation from Henry's law. The correction for  $(MO)_W = 0.0015 M$  is 0.1% and for  $(MO)_W = 0.015 M$ , the correction is 1%. As mesityl oxide solutions of the order of 0.015  $M$  can be analyzed with an accuracy of 0.1%, activity coefficients accurate to 0.1% can be obtained if the 1% Henry's law correction is applied.

It is of interest to note that the linear dependence of  $\log \gamma_3$  upon  $m_3$  can be derived as a limiting equation from the regular solution equation<sup>7</sup>  $\log \gamma_3^0 = (B/RT)x_1^2$  where  $\gamma_3$  is the activity coefficient of mesityl oxide relative to the pure mesityl oxide standard state and  $x_1$  is the mole fraction of water. The derivation consists of transforming mole fraction to molality, changing the standard states and neglecting higher powers of molality. One can make some generalizations about the deviations from Henry's law that might be expected for the two homogeneous portions of a liquid system with a miscibility gap. One finds that the regular solution equation predicts an increasing deviation from Henry's law at a given concentration of solute if mixtures of liquids of increasing differences of internal pressure are examined. On the other hand, the maximum concentration of solute increases as the internal pressure difference decreases. If one compares the deviations from Henry's law for various solutes in their saturated solutions, one finds that the deviations increase as the internal pressure differences decrease and reach a maximum when the miscibility gap has just closed. For a two liquid mixture just below the critical mixing temperature one would predict a deviation from Henry's law of about a factor of two in the saturated solutions.

**Salting-out of Mesityl Oxide.**—In Table III the distribution data at 25° are presented in terms of the  $k_{32}$  values at rounded values of the salt molality. The correction for deviation from Henry's law has been applied. The NaNO<sub>3</sub> values in parentheses are from Pressman, Brewer and Lucas.<sup>5</sup> The variation of the  $k_{32}$  values with molality is small. The maximum variation is 0.03 even up to 5  $M$ . Interpolated values may be obtained readily within 0.002. A change in  $k_{32}$  of 0.002 for a 1  $M$  salt solution corresponds to 0.5% change in  $\gamma_3$ . The activity coefficients of mesityl oxide which are calculated from eq. 1 by use of the values of  $k_{32}$  obtained by interpolation in Table III together with use of the value of  $k_{33} = -0.30$  are activity

coefficients taken with respect to the solute standard state of mesityl oxide in pure water with molality units used throughout. A solution designated as 0.1  $M$  MO and 1  $M$  NaCl will contain 0.1 mole of MO and 1 mole of NaCl per 1000 grams of solvent (990.2 g. of H<sub>2</sub>O and 9.8 g. of MO). The data of Table III can be converted to volumetric units by use of the  $c/m$  values of Table I.

For NaCl below 2  $M$  the  $k_{32}$  values at 20° are 0.001 higher than those at 25°. The 1.003 ratio of  $\gamma_{20}/\gamma_{25}$ , corresponding to an enthalpy of transfer of 100 cal./mole, is just slightly larger than the experimental uncertainty. Between 4.5 and 5  $M$ ,  $\gamma_{20}/\gamma_{25} = 1.02$ , which corresponds to  $\Delta\bar{H} = 690 \pm 200$  cal./mole for  $MO(H_2O) = MO(5 M NaCl)$  with the same mesityl oxide molality in each solution. Pressman, Brewer and Lucas<sup>5</sup> obtained one determination of  $\gamma_{MO}$  at 30° in 1  $M$  NaClO<sub>4</sub> and one in 1  $M$  NaNO<sub>3</sub> which indicated a 3.5 to 4% reduction of  $\gamma_{MO}$  upon heating from 25 to 30°, corresponding to a  $\Delta\bar{H}$  of transfer of around 1400 cal./mole. Comparison with the present determinations indicates that their 1  $M$  NaNO<sub>3</sub> value at 25° is 2% high. As the change of  $\gamma$  with temperature is close to the limit of their CCl<sub>4</sub> distribution method, there is some question whether salt solutions such as 1  $M$  NaClO<sub>4</sub> and 1  $M$  NaNO<sub>3</sub> with low salting-out coefficients really do display appreciable temperature coefficients in contrast to the low temperature coefficient observed here for 1  $M$  NaCl.

Combination of our results with those of Pressman, Brewer and Lucas<sup>5</sup> yields the following order of decreasing salting-out coefficients: Ac<sup>-</sup>, Cl<sup>-</sup>, Br<sup>-</sup>, NO<sub>3</sub><sup>-</sup>, I<sup>-</sup>, CO<sub>4</sub><sup>-</sup> and Na<sup>+</sup>, K<sup>+</sup> and H<sup>+</sup>. This is in general agreement with order reported in the literature<sup>8</sup> for other substances. Comparison of the  $k$  values of mesityl oxide in salt solutions with the  $k$  values of the related diacetone alcohol as determined by Akerlof<sup>9</sup> shows that the  $k$  values of diacetone alcohol in NaCl, KCl, NaBr and KI are about 75% of the corresponding  $k$  values of mesityl oxide.

Haugen and Friedman<sup>10</sup> have verified experimentally for nitromethane solutions the theoretical relationship between the coefficient  $k_{32}$  which characterizes the effect of an electrolyte 2

(7) J. H. Hildebrand and R. L. Scott, "The Solubility of Nonelectrolytes," Third Edition, Reinhold Publ. Corp., New York, N. Y., 1950.

(8) Pressman, Brewer and Lucas<sup>5</sup> present a summary of literature references in their footnotes 6 and 7. F. A. Long and W. F. McDevitt, *Chem. Revs.*, **51**, 119 (1952), have reviewed later work.

(9) G. Akerlof, *J. Am. Chem. Soc.*, **51**, 984 (1929).

(10) G. R. Haugen and H. L. Friedman, *J. Phys. Chem.*, **60**, 1363 (1956).

upon  $\gamma_3$  and the coefficient  $k_{23}$  which characterizes the effect of component 3 upon  $\gamma_2$ , the mean activity coefficient of the electrolyte. The application of the cross differentiation equation<sup>11</sup>

$$\nu_2 \left( \frac{\partial \log \gamma_2}{\partial m_3} \right)_{m_1} = \nu_3 \left( \frac{\partial \log \gamma_3}{\partial m_2} \right)_{m_1}$$

to eq. 1 yields  $2(\partial \log \gamma_2 / \partial m_3)_{m_1} = k_{32}$  or  $\log \gamma_2 = 1/2 k_{32} m_3$  for those 1-1 electrolyte solutions for which  $k_{33}$  and  $k_{32}$  are essentially independent of  $m_2$ . For those solutions which show appreciable variation of  $k_{32}$  with  $m_2$ , it is necessary to express  $k_{32}$  as a power series in  $m_2$  before differentiating eq. 1.

We may now apply this result to predict the effect of mesityl oxide upon the activity coefficient of electrolytes. For a 2 M NaCl solution, we calculate that the addition of 0.1 M mesityl oxide increases the mean activity coefficient of NaCl by 2%. Similar results may be obtained for the other salt solutions.

**Iodine Distributions.**—To illustrate the use of the equilibrator for distribution between two immiscible solvents, the distribution of iodine between water and carbon tetrachloride was measured as a function of iodine concentration. This distribution has been studied directly by many observers. Most of them have noted an increase of the distribution ratio or ratio of concentration in carbon tetrachloride to concentration in water as the iodine concentration was increased. Winther<sup>12</sup> attributed this trend to formation of  $I^+$  in dilute solutions. Hildebrand and Scott<sup>7</sup> have pointed out that such an effect can be expected on the basis of expected deviation from Henry's law in the carbon tetrachloride phase. Using the internal pressures given by Hildebrand and Scott, one can calculate that

$$\ln \gamma = 2(59)^2(5.6)^2(0.01147) / (97)(1.987)(298)(0.9885) = 0.0435$$

where  $\gamma$  is the activity coefficient of  $I_2$  in a saturated  $CCl_4$  solution,  $x_1 = 0.01147$ , at 25° relative to the hypothetical solute standard state of  $I_2$  in  $CCl_4$ . Thus, the regular solution equation would predict a 4.4% increase in the distribution constant as the iodine concentration is increased from low values to saturation. Winther and others had observed variations of 7 to 10%. A possible explanation that one should consider is the possibility of varying emulsification of some of the  $CCl_4$  phase in the aqueous phase. The vapor phase equilibrator provides all of the same conditions of direct contact of the two phases in that both phases are saturated with respect to water and  $CCl_4$ , but it is impossible for any of the  $CCl_4$  phase to appear in the water bulb as long as there is no temperature gradient. Thus one can check the emulsification theory.

Table IV presents the results of such a check.<sup>13</sup> The values in parentheses are calculated from solubility measurements.<sup>14</sup> These distribution ratios

(11) H. A. C. McKay, *Trans. Faraday Soc.*, **49**, 237 (1953).

(12) C. Winther, *Z. physik. Chem.*, **B3**, 299 (1929).

(13) These determinations were made by Thomas L. Allen for an undergraduate special problem. The aqueous solutions were made  $10^{-4}$  N in  $H_2SO_4$  to inhibit hydrolysis.

are considerably higher than most determinations in the literature. Only the data of Linhart<sup>15</sup> (after correction for hydrolysis) and the data of Davies and Gwynne<sup>16</sup> yield distribution ratios over 90 and some values in the literature range as low as 80. This would clearly seem to indicate that the aqueous phases did contain appreciable amounts of the  $CCl_4$  phase in all determinations other than the two mentioned. The trend to higher values of the distribution ratio with increasing iodine reported here and also that reported by Davies and Gwynne<sup>16</sup> is in fair agreement with the 4% increase predicted above on the basis of a regular solution equation calculation.

TABLE IV

DISTRIBUTION OF $I_2$ BETWEEN $CCl_4$ AND $H_2O$ AT 25°	
$I_2$ in $CCl_4$ (moles/l.)	Distribution ratio
0.013	89.8
.045	90.6
.054	91.6
.065	93.1
.073	91.1
(.119)	(91.0)

Keefe and Allen<sup>17</sup> and DeMaine<sup>18</sup> have observed the spectrum of  $I_4$  in  $CCl_4$ . The stability of the spectrally characterized  $I_4$  is much too small to account for the trend of distribution ratio with iodine concentration. Davies and Gwynne<sup>16</sup> state that Hildebrand and Scott<sup>7</sup> explain the variation of distribution ratio by an association of the iodine in the carbon tetrachloride. The use of the term "association" is most unfortunate here and is certainly not in the spirit of Hildebrand's regular solution treatment. The regular solution treatment is based upon the unbalance of weak London forces and it would not be profitable for most purposes to describe these weak interactions in terms of associated molecules. There also would not appear to be any basis for Winther's contention that the trend of distribution ratios is due to  $I^+$  formation in the aqueous solutions. The regular solution treatment is more than adequate to account for the entire observed effect.

The two examples of distribution of mesityl oxide and of iodine illustrate the wide possibilities for the use of the vapor phase equilibrator for distribution of solutes between miscible or immiscible phases. The apparatus is particularly valuable for the high accuracy of the data and for its ability to yield more nearly complete thermodynamic data for multicomponent systems than can be obtained easily by other methods.

(14) Values in the literature of the solubility of  $I_2$  in  $CCl_4$  vary over a range of 4%. The value chosen here is that of Jakowkin, which was accepted by Hildebrand and Scott<sup>7</sup> in their Table I on page 208 as the best value. The recent determination of the solubility of iodine in water by L. I. Katzin and E. Gebert, *J. Am. Chem. Soc.*, **77**, 5814 (1955) was used to obtain the distribution ratio. The solubility of iodine in both dry and wet  $CCl_4$  must be accurately determined before an accurate comparison with the distribution data can be made.

(15) G. A. Linhart, *J. Am. Chem. Soc.*, **40**, 158 (1918).

(16) M. Davies and E. Gwynne, *ibid.*, **74**, 2748 (1952).

(17) R. M. Keefe and T. L. Allen, *J. Chem. Phys.*, **25**, 1059 (1956).

(18) P. A. D. DeMaine, *Can. J. Phys.*, **35**, 573 (1957).

# THE DIPOLE MOMENTS OF CYCLOHEXANETHIOL, $\alpha$ -TOLUENETHIOL AND BENZENETHIOL

BY SIMÃO MATHIAS, EURICO DE CARVALHO FILHO AND RENATO G. CECCHINI

*Departamento de Química, Faculdade de Filosofia, Ciências e Letras, Universidade de São Paulo, São Paulo, Brazil*

*Received August 22, 1960*

The three compounds listed in the title above were carefully purified and the boiling points, densities, refractive indices and dielectric constants were determined. The dipole moments of these compounds in the pure liquid state and in benzene solution at 25° were calculated according to different methods.

## Introduction

The present study is concerned with the dipole moments of the three substances cyclohexanethiol,  $\alpha$ -toluenethiol and benzenethiol. Due to the position of the thiol group in these molecules, it was thought that an examination of the dipole moments of these compounds might disclose some interesting aspects related to their molecular structure. Determinations of dipole moments for the first two compounds were not found in the literature and, as far as the benzenethiol is concerned, the two values that have been reported are somewhat divergent.

In the present work the three substances were carefully purified and the pertinent physical properties measured. Following the same line as in a previous work,<sup>1</sup> the three equations of Debye,<sup>2</sup> Onsager<sup>3</sup> and Yasumi and Komooka<sup>4</sup> for the determination of the dipole moment from data in the liquid state were applied and the results compared among themselves and with the values obtained in benzene solution. Such comparisons are valuable as they allow the testing of the relative validity of such equations.

## Experimental Part

**Preparation and Purification of Substances.**—Cyclohexanethiol was prepared according to the method described by Stanek,<sup>5</sup> by condensation of cyclohexyl bromide with thiourea in amyl alcohol solution, separation of the thiuronium salt, and subsequent saponification of this product with an alcoholic solution of sodium hydroxide.

The preliminary purification was made by changing it into the lead mercaptide and liberating the thiol by decomposition of the mercaptide with dilute hydrochloric acid according to the method described by Borgstrom, Ellis and Reid.<sup>6</sup>

The final purification was done by submitting the dried thiol to successive fractional distillations in a column according to the method described in a previous work.<sup>7</sup>

$\alpha$ -Toluenethiol and benzenethiol were commercial products supplied by Eastman Kodak Company. They were first distilled under reduced pressure in a Claisen apparatus and then, after drying over calcium chloride, submitted to successive fractional distillations as previously described.

The benzene used for the preparation of the solutions was kept for many days over phosphorus pentoxide and then distilled through a fractionating column. Absence of thiophene was tested with ninhydrin,<sup>8</sup> b.p. 77.2° at 698.1 mm.,  $n_D^{25}$  1.4979. The benzene was stored over phosphorus pentoxide and small portions distilled when necessary.

**Determination of Physical Properties.**—The determination of the boiling temperatures and the degree of purity  $\Delta t$  of the substances studied in the present work were done according to the ebulliometric method of Swietoslawski as recently described.<sup>1</sup>

Density and refractive index measurements were performed as reported in a previous work.<sup>7</sup>

For the determination of the dielectric constants of the pure liquids an apparatus based on the heterodyne beat method<sup>1</sup> was used. The dielectric constants of the solutions were measured with a resonance apparatus<sup>9,10</sup> which has been in use for many years in this Laboratory. A slight modification was introduced in order to improve its stability and protect the instrument from outside electrical influences, by introducing between the input of the high potential and the ground a 0.1  $\mu$ F. capacitor. The apparatus, including the dielectric cell and its connections, was completely and rigidly screened. The dielectric cell, similar to the one described in a recent paper,<sup>1</sup> had a replaceable capacity, when filled with dry air, of about 98  $\mu$ F.

The estimated error in the dielectric constant measurements with the heterodyne beat apparatus was lower than 0.04%; with the resonance apparatus, lower than 0.1%.

## Results and Discussion

The physical properties of cyclohexanethiol,  $\alpha$ -toluenethiol and benzenethiol are reported in Tables I and II.

TABLE I

PHYSICAL PROPERTIES OF CYCLOHEXANETHIOL,  $\alpha$ -TOLUENETHIOL AND BENZENETHIOL

Substance	$\overline{B.P.}$ °C.	$\overline{Mm.}$	$\Delta t$ , °C.	$d_4^{25}$	$n_D^{25}$	$\epsilon_{25}$
Cyclohexanethiol	78.0	57.0	0.03	0.94393	1.49105	5.420
$\alpha$ -Toluenethiol	195.9	699.9	.02	1.05088	1.57372	4.705
Benzenethiol	165.4	698.4	.02	1.07264	1.58718	4.382

TABLE II

REFRACTIVE INDICES AT 25° OF CYCLOHEXANETHIOL,  $\alpha$ -TOLUENETHIOL AND BENZENETHIOL

Wave length, Å.	Cyclohexanethiol	$\alpha$ -Toluenethiol	Benzenethiol
$\infty$	(1.47554)	(1.54658)	(1.55633)
6678	1.48746	1.56720	1.57959
5893	1.49099	1.57357	1.58696
5876	1.49105	1.57372	1.58718
5016	1.49711	1.58500	1.60042
4713	1.50008	1.59079	1.60733
4471	1.50311	1.59653	1.61430

Comparable values for the first two compounds were not found in the literature. In the case of benzenethiol, the values listed in Table I, with the exception of the dielectric constant, agree with the ones reported by Timmermans<sup>11</sup> and Rossini, *et*

(9) S. Mathias, *J. Phys. Chem.*, **57**, 344 (1953).

(10) K. E. Calderbank and R. J. W. LeFèvre, *J. Chem. Soc.*, 1951 (1948); R. J. W. LeFèvre, "Dipole Moments," Methuen & Company, Limited, London, 1953, third edition, p. 47.

(1) S. Mathias and E. Carvalho Filho, *J. Phys. Chem.*, **62**, 1427 (1958).

(2) P. Debye, "Polar Molecules," The Chemical Catalog Co., Inc., New York, N. Y., 1929.

(3) L. Onsager, *J. Am. Chem. Soc.*, **58**, 1486 (1936).

(4) M. Yasumi and H. Komooka, *Bull. Chem. Soc. Japan*, **29**, 407 (1956).

(5) J. Stanek, *Chem. Listy*, **46**, 383 (1952); *C. A.*, **47**, 4296 (1953).

(6) P. Borgstrom, L. M. Ellis, Jr., and E. E. Reid, *J. Am. Chem. Soc.*, **51**, 3649 (1929).

(7) S. Mathias, *ibid.*, **72**, 1897 (1950).

(8) F. Feigl, "Spot Tests in Organic Analysis," Elsevier Publishing Co., Amsterdam, 1956, fifth edition, p. 427.

*al.*<sup>12</sup> The boiling point, calculated from the tables of Stull,<sup>13</sup> is 0.6° lower than the value indicated in Table I. The refractive indices at 25° for a number of wave lengths, required for the calculation of  $n_{\infty}$ , are listed in Table II. The compounds studied in the present work were obtained in a satisfactory degree of purity as indicated by the values of  $\Delta t$  in Table I.

The results of the measurements in benzene solution at 25° are summarized in Table III.

TABLE III

DIELECTRIC CONSTANT AND SPECIFIC VOLUME OF BENZENE SOLUTIONS OF CYCLOHEXANETHIOL,  $\alpha$ -TOLUENETHIOL AND BENZENETHIOL AT 25°

$w_2$	$\epsilon_{12}$	$v_{12}$
Cyclohexanethiol		
0.000000	(2.276)	(1.14460)
.009586	2.301	1.14394
.021376	2.238	1.14301
.030286	2.360	1.14232
.039813	2.389	1.14157
.046157	2.404	1.14108
$\alpha$ -Toluenethiol		
0.000000	(2.271)	(1.14465)
.010438	2.292	1.14267
.020409	2.310	1.14073
.029639	2.330	1.13892
.040366	2.350	1.13685
.049704	2.369	1.13500
Benzenethiol		
0.000000	(2.274)	(1.14470)
.019663	2.307	1.14047
.029826	2.325	1.13828
.038777	2.338	1.13636
.048619	2.356	1.13425
.057564	2.371	1.13232

The three columns show, respectively, the weight fraction of the solute  $w_2$ , the dielectric constant of the solution  $\epsilon_{12}$ , and the specific volume of the solution  $v_{12}$ . The numbers in parenthesis are extrapolated values.

Table IV contains the values of molar polarizations at infinite dilution  $P_2$ , calculated according to the method of Halverstadt and Kumler<sup>14</sup>; the molar refractivities for the sodium-D line  $R_D$ ; the electronic polarizations  $P_E$ , taken as equal to the molar refractivity for infinite wave length  $R_{\infty}$ ; the sum of the atomic plus orientation polarization  $P_{A+O}$ , and the apparent dipole moments in benzene solution of the three compounds studied. For the calculation of the apparent dipole moments the values of  $R_D$  were used.

From the three substances studied in the present work, benzenethiol is the only one that has been

(11) J. Timmermans, "Physico-Chemical Constants of Pure Organic Compounds," Elsevier Publishing Co., Inc., New York, N. Y., 1950.

(12) F. D. Rossini, K. S. Pitzer, R. L. Arnett, R. M. Braun and G. C. Pimentel, "Selected Values of Physical and Thermodynamic Properties of Hydrocarbons and Related Compounds," Carnegie Press, Carnegie Institute of Technology, Pittsburgh, Pennsylvania, 1953.

(13) D. R. Stull, *Ind. Eng. Chem.*, **39**, 517 (1947).

(14) I. F. Halverstadt and W. D. Kumler, *J. Am. Chem. Soc.*, **64**, 2988 (1942).

measured in benzene solution by Hunter and Partington<sup>15</sup> and by Lumbroso and Marschalk.<sup>16</sup> The value reported by the former authors is 1.33  $D$  and by the latter authors 1.19  $D$ .

TABLE IV

MOLAR POLARIZATIONS (IN MOLE) AND APPARENT DIPOLE MOMENTS (IN  $D$ ) IN BENZENE SOLUTIONS OF CYCLOHEXANETHIOL,  $\alpha$ -TOLUENETHIOL AND BENZENETHIOL AT 25°

Substance	$P_2$	$R_D$	$P_E$	$P_{A+O}$	$\mu$
Cyclohexanethiol	98.38	35.66	34.70	63.68	1.73
$\alpha$ -Toluenethiol	81.14	38.97	37.46	43.68	1.44
Benzenethiol	65.36	34.52	33.03	32.33	1.23

The dipole moments of these compounds, calculated from the dielectric constant of the pure liquids according to the equations of Debye,<sup>2</sup> Onsager<sup>3</sup> and Yasumi and Komooka,<sup>4</sup> are listed in Table V.

TABLE V

DIPOLE MOMENTS (IN  $D$ ) OF CYCLOHEXANETHIOL,  $\alpha$ -TOLUENETHIOL AND BENZENETHIOL IN THE LIQUID STATE AT 25°

Substance	Debye	Onsager	Yasumi-Komooka
Cyclohexanethiol	1.38	1.64	1.73
$\alpha$ -Toluenethiol	1.17	1.32	1.41
Benzenethiol	1.02	1.13	1.23

As in the case of the alkanethiols,<sup>1</sup> these results show that the dipole moments calculated by Debye's equation are lower and by Yasumi-Komooka's equation higher than the values obtained by Onsager's equation.

An examination of the values for the dipole moments listed in Tables IV and V shows an agreement between the solution values and the ones obtained in the pure liquid state by applying Yasumi and Komooka's equation.

It is interesting to point out that, while the apparent dipole moment of cyclohexanethiol in benzene solution (1.73  $D$ ) is higher than the corresponding values for 2-propanethiol (1.55  $D$ ) and for 1-methyl-1-propanethiol (1.57  $D$ ), where the SH group is linked to a secondary carbon atom, the values obtained in the pure liquid state for cyclohexanethiol (1.38, 1.64 and 1.73  $D$ ) show a very close agreement with the corresponding values for 2-propanethiol (1.32, 1.64 and 1.74  $D$ ) and for 1-methyl-1-propanethiol (1.36, 1.65 and 1.75  $D$ ).<sup>1</sup>

From the results obtained both in benzene solution and in the pure liquid state, one can see that the dipole moments decrease in the order cyclohexanethiol,  $\alpha$ -toluenethiol and benzenethiol. The same gradation is observed in the values of the dipole moments in benzene solution of analogous compounds, where the SH group is replaced by OH, Cl or Br, as shown by the results joined in Table VI.

The lower values of the dipole moments when the polar groups are directly bound to the benzene ring are in accord with the shorter internuclear distances of the C-X bonds (Table VII).

While it is possible to understand, at least qualitatively, why the dipole moment should decrease in

(15) E. C. E. Hunter and J. R. Partington, *J. Chem. Soc.*, 2812 (1932).

(16) H. Lumbroso and C. Marschalk, *J. chim. phys.*, **49**, 385 (1952).

TABLE VI

APPARENT DIPOLE MOMENTS OF SOME ALCOHOLS, CHLORIDES AND BROMIDES IN BENZENE SOLUTION

X =	OH	Cl	Br
C <sub>6</sub> H <sub>11</sub> X	1.7-1.9 D <sup>a</sup>	2.1-2.3 D <sup>a</sup>	2.1-2.3 D <sup>a</sup>
C <sub>6</sub> H <sub>5</sub> CH <sub>2</sub> X	1.67 <sup>b</sup>	1.82-1.85 <sup>a</sup>	1.85-1.87 <sup>a</sup>
C <sub>6</sub> H <sub>5</sub> X	1.45 <sup>b</sup>	1.57-1.60 <sup>a</sup>	1.51-1.56 <sup>a</sup>

<sup>a</sup> L. G. Wesson, "Tables of Electric Dipole Moments," The Technology Press, Massachusetts Institute of Technology, Cambridge, Mass., 1948. <sup>b</sup> A. H. Boud, D. Cleverdon, G. B. Collins and J. W. Smith, *J. Chem. Soc.*, 3793 (1955).

the order cyclohexanethiol,  $\alpha$ -toluenethiol and benzenethiol,<sup>17</sup> an attempt to interpret the experi-

(17) See for instance G. I. Brown, "An Introduction to Electronic Theories of Organic Chemistry," Longmans, Green and Co., London, 1958.

TABLE VII

INTERNUCLEAR DISTANCES OF C-X BONDS (IN Å.)<sup>a</sup>

X =	S	O	F	Cl	Br
Paraffinic	1.81	1.43	1.38	1.77	1.94
Aromatic	..	1.36	1.30	1.70	1.85

<sup>a</sup> "Tables of Interatomic Distances and Configuration in Molecules and Ions," Special Publication No. 11, The Chemical Society, London, 1958.

mental results reported in the present work by applying methods and approximations afforded by the molecular orbital theory may lead to a more satisfactory approach.

**Acknowledgment.**—The authors gratefully acknowledge the financial assistance given to this Laboratory by the Rockefeller Foundation (New York) and the Conselho Nacional de Pesquisas (Rio de Janeiro).

## PARTIAL SPECIFIC VOLUMES AND REFRACTIVE INDEX INCREMENTS IN MULTICOMPONENT SYSTEMS<sup>1</sup>

BY EDWARD F. CASASSA AND HENRYK EISENBERG

*Mellon Institute, Pittsburgh, Pennsylvania*

*Received August 23, 1960*

Partial specific volumes and specific refractive index increments of proteins and polyelectrolytes in aqueous solution with a simple salt are discussed in relation to possible definitions of independent thermodynamic components. As suggested elsewhere, it is sometimes useful to define components by equating inner and outer salt concentrations in a dialysis equilibrium experiment and assigning any excess or deficiency of salt ions in the three-component phase as part of the macromolecular component. Since by need or by custom, protein solutions may be dialyzed against the solvent, volume and refractive index changes corresponding to addition of the non-diffusible component are often measured in a way relating directly to such a definition of components: that is, as the protein concentration is changed the chemical potential of the salt component is held at least approximately constant. A consideration of available data indicates that in some three-component systems thermodynamic interaction between salt and the macromolecular species is great enough for volume and refractive index changes to be significantly affected. It is important, therefore, that the partial volumes and refractive index increments applied in thermodynamic analysis of ultracentrifuge and light scattering data be defined and interpreted in consistent fashion. An earlier discussion of sedimentation equilibrium is extended to the special case of sedimentation in a density gradient produced by the distribution of a heavy salt. It is shown how an unambiguous molecular weight for the polymeric species can be obtained from equilibrium measurements without explicitly evaluating the interaction with the supporting electrolyte.

### Introduction

The usefulness of ultracentrifugation and light scattering as techniques for the physicochemical investigation of macromolecular solutes depends in great part on the independent measurement of the partial specific volume and the specific refractive index increment. Aside from their intrinsic interest as physical properties, both enter into the interpretation of centrifuge measurements while the determination of the refractive increment makes possible absolute determinations of molecular weight by light scattering. In two-component solutions (one solute and one solvent) the definition of these quantities is subject to no ambiguity. In multicomponent systems, on the other hand, the definition of independent components to be used in thermodynamic formulations is largely a matter of convenience<sup>2,3</sup>; but whatever the conventions chosen, it is essential that all the experimental quantities involved and the relations used be consistent with

them. These considerations give rise to some rather subtle problems that have not always been fully appreciated. In some circumstances the uncritical acceptance of simple relations established for two-component systems may lead to serious errors in interpretation of experimental data or sometimes to failure to discern small effects that can furnish information about thermodynamic interactions in complex systems.

These remarks apply with particular force to studies of materials of biological interest since the systems encountered almost always contain at least three components. Aqueous protein solutions, for example, are frequently buffered or at least may contain an added salt. A further complication is the fact that preparative procedures often involve dialysis against the solvent medium with consequent redistribution of diffusible species across the membrane. As we have pointed out elsewhere<sup>3</sup> this circumstance, when its implications are understood correctly, actually becomes an advantage in simplifying the analysis of light scattering and ultracentrifugal measurements.

Rather full discussions of the question of defining

(1) This study was supported by a grant (NSF-G7608) of the National Science Foundation.

(2) G. Scatchard, *J. Am. Chem. Soc.*, **68**, 2315 (1946).

(3) E. F. Casassa and H. Eisenberg, *J. Phys. Chem.*, **64**, 753 (1960).



components in interpreting light scattering from dialyzed solutions have been given recently in a paper by Scatchard and Bregman<sup>4</sup> and in reference 3. Here, after considering the partial volume and refractive increment of a macromolecular solute in relation to useful definitions of components, we apply our conclusions in carrying further the discussion of sedimentation equilibrium given in reference 3. As in the earlier paper, we are concerned with a system of three components, of which one is non-diffusible: specifically the solution comprises water (component 1), a protein or polyelectrolyte (component 2), and a uni-univalent salt (component 3).

### Partial Specific Volume

In measurements of partial specific volume of a solute one usually compares solution and solvent densities and thus obtains directly the apparent partial volume  $\phi$  of solute from the change produced by a finite concentration increment. Conceptually one visualizes adding the solute component 2 in some completely definite, and possibly actually available, form (dry isoionic protein or the stoichiometric composition  $X_Z P$  of an alkali metal salt of the polyacid  $H_Z P$ , for example) to the solvent mixture consisting of components 1 and 3. Upon addition of  $g_2$  grams of component 2 to  $g_s$  grams of solvent of density  $\rho_s$ , the volume of the system changes by  $\Delta V$  and the density by  $\Delta\rho$ . The apparent partial specific volume of component 2 in these terms is

$$\phi = \frac{\Delta V}{g_2} = \frac{1}{\rho} \left( 1 - \frac{g_s \Delta\rho}{g_2 \rho_s} \right) = \frac{1}{\rho} \left[ 1 - \frac{(1 + m_3 M_3 / 1000) \Delta\rho}{w_2 \rho_s} \right] \quad (1)$$

where  $w_2$  is the solute concentration in grams per gram of water,  $m_3$  is the molality of the salt, and  $M_3$  is its formula weight. By substituting into equation 1 the weight fraction  $z = g_2 / (g_s + g_2)$ , one obtains an alternative form

$$\phi = \frac{1}{\rho_s} \left( 1 - \frac{\Delta\rho}{z\rho} \right) = \frac{1}{\rho_s} \left( 1 - \frac{\Delta\rho}{c} \right) \quad (2)$$

in which  $c$  is the concentration of component 2 in grams per milliliter of solution.

If the common laboratory practice of dialyzing solutions against the solvent has been adopted, it must be recognized that the distribution of small ions between solution and dialysate is affected by the presence of the macromolecular species. In the thermodynamic formalism for experiments carried out in this way, it is useful<sup>3,4</sup> to equate the molality of salt in the dialysate with that in the solution and to assign any excess (or deficiency) of diffusible ions to component 2. If component 2\*, as we shall designate the component defined in this way, were added to the solution at osmotic equilibrium there would occur no redistribution of diffusible species across the membrane. This convention is generally useful only if the numbers of diffusible ions included are independent of the concentration of the macromolecular species over a fairly wide concentration range and are also independent of pressure. Fortu-

nately these requirements hold to a good approximation in the few systems<sup>5-7</sup> adequately studied, and one may therefore discuss a partial specific volume for component 2\* in a concentration series equilibrated by dialysis, or equivalently prepared by dilution with dialysate.<sup>3,4</sup> Thus, conceptually one can add to the solution at constant pressure,  $g_2^*$  grams of component 2\*, the new mass being related to  $g_2$  by

$$g_2^* = g_2(1 + \xi) = g_2(1 + \sum \nu_{2i}^* M_i / M_2 - \sum \nu_{2i} M_i / M_2)$$

The numbers of moles of diffusible ions of molecular weight  $M_i$  included by each definition in one mole of the macromolecular component are designated  $\nu_{2i}$ ,  $\nu_{2i}^*$ ; and  $g_2 / M_2$  is the number of moles, the same in both cases, added to the system. For component 2\*, equations 1 and 2 are still valid in terms of the corresponding density change  $\Delta^* \rho$  and the weight concentrations  $w_2^*$ ,  $c^*$

$$\phi^* = \frac{1}{\rho^*} \left[ 1 - \frac{(1 + m_3 M_3 / 1000) \Delta^* \rho}{w_2^* \rho_s} \right] = \frac{1}{\rho_s} \left( 1 - \frac{\Delta^* \rho}{c^*} \right) \quad (3)$$

Since the volumes  $\phi$  and  $\phi^*$  have been defined in the usual fashion for apparent extensive properties, the true partial volume  $\bar{v}_2$  is given by  $\bar{v}_2 = \phi + w_2 (d\phi/dw_2)$ , and the analogous relation holds for  $\phi^*$ .

In the two procedures just described densities and concentrations are treated consistently. Sometimes however, though the solution is dialyzed and its density compared with that of dialysate, the weight concentration arbitrarily used in calculations does not correspond to component 2\*. For example, in protein studies, concentrations are often based on nitrogen content multiplied by a factor to give a protein concentration corresponding presumably to the salt-free isoionic species, which we can regard as the component 2 to which equation 1 applied. Hence, the apparent partial volume calculated is

$$\phi' = \frac{1}{\rho_s} \left( 1 - \frac{\Delta^* \rho}{c} \right) \quad (4)$$

which corresponds neither to  $\phi$  nor to  $\phi^*$ .

The relation between  $\phi'$  and  $\phi^*$  is obtained by substituting  $c^* = c(1 + \xi)$  in equation 4 and eliminating  $\Delta^* \rho / c_2^*$  by equation 3

$$\phi' = \phi^* - \xi(1/\rho_s - \phi^*) \quad (5)$$

The expression of  $\phi^*$  or  $\phi'$  in terms of  $\phi$  involves the volume corresponding to the fractional mass increment  $\xi$ ; and therefore the partial volume of the ions (taken in neutral combinations) contributing to  $\xi$  is required. To use an example cited above, we consider component 2 as the completely ionized salt  $X_Z P$  of the anion  $P^{-Z}$ . Component 3 is the salt  $XY$ ;  $\nu_{2X} = Z$ ;  $\nu_{2Y} = 0$ ; and  $\nu_{2X}^* - \nu_{2X} = \xi M_2 / M_3$ . Then, adding  $g_2^*$  grams of component 2\* to the solvent is equivalent to adding  $g_2$  grams of  $X_Z P$  and  $\xi g_2$  grams (or  $\xi g_2 / M_3$  moles) of  $XY$ . If the partial specific volume of  $XY$  in the three-component system is  $\bar{v}_3$ , the corresponding volume change is  $\Delta V + \xi \bar{v}_3 g_2$  if  $\bar{v}_3$  is independent of the change in salt concentration. It follows that

(5) G. Scatchard, A. C. Batchelder and A. Brown, *ibid.*, **68**, 2320 (1946).

(6) U. P. Strauss and P. Ander, *ibid.*, **80**, 494 (1958).

(7) H. Eisenberg and E. F. Casassa, *J. Polymer Sci.*, in press.

(4) G. Scatchard and J. Bregman, *J. Am. Chem. Soc.*, **81**, 6095 (1959).



TABLE I

System	PARTIAL SPECIFIC VOLUMES <sup>a</sup> AT 25°					
	Concn.	$\Delta^* \rho \times 10^3$	$\xi \times 10^3$	$\phi$	$\phi^*$	$\phi'$
NH <sub>4</sub> PVS in 0.5 M <sup>b</sup> NH <sub>4</sub> Cl	0.1036 equiv./l.	5.67	-87.6	0.534	0.518	0.560
KPVS in 0.1 M <sup>b</sup> KCl	0.1124 equiv./l.	8.77	-76.5	.411	.413	.457
BSA in 0.1 M <sup>b</sup> NaCl	58.3 g./kg. H <sub>2</sub> O		+ 2.67	.7343	.7331	.7324

<sup>a</sup> The meaning of symbols and procedures for calculation are given in the text. <sup>b</sup> The solvent composition refers to dialysate. <sup>c</sup> Equivalents of sulfonate groups per liter.

$$\phi^* = \frac{\Delta V + \xi \bar{v}_3 g_2}{g_2(1 + \xi)} = \frac{\phi + \xi \bar{v}_3}{1 + \xi} \quad (6)$$

By combining equations 5 and 6, we obtain

$$\phi' = \phi - \xi \left( \frac{1}{\rho_s} - \bar{v}_3 \right) \quad (7)$$

For a protein system we might designate the isoionic protein as component 2; but in defining components by osmotic equilibrium with a solution of the salt XY, we would not generally have equal numbers of moles of X<sup>+</sup> and Y<sup>-</sup> included in the electrically neutral components 2\* because the protein may "bind" protons or hydroxyl ions as well as the salt ions. To be in equilibrium with a protein component of specified composition, the dialysate must in general contain the acid HY or base XOH in addition to the salt; and the system then includes four components if one wishes to consider varying independently the concentration of acid or base.<sup>4</sup>

Ordinarily, the concentration variable most easily measured is *c*; and though *c*\* is for many solutions determinable in principle by comparing weights of dried residues of solution and dialysate, practical difficulties might sometimes make the procedure unsatisfactory. For instance, in a protein system the loss of the volatile acid HY from the protein component might have to be considered even though no acid has been added. The apparent volumes  $\phi$  or  $\phi'$  are therefore the quantities obtained directly from most density measurements, but  $\phi^*$  may be a primary result if concentrations are based on dry weights.

In order to convey some idea of the magnitude of the differences which may exist among the three partial volume quantities defined here, experimental and calculated values for several systems are collected in Table I. The ammonium and potassium salts of poly-(vinyl sulfonic) acid (denoted as NH<sub>4</sub>PVS and KPVS) have been studied in this Laboratory.<sup>7</sup> Values of  $\phi'$  listed in the table for these salts were determined from density measurements in pycnometers. Then with these results and  $\xi$  from data on the distribution of chloride ion at dialysis equilibrium, equations 5 and 7 were used to calculate  $\phi$  and  $\phi^*$ . For bovine serum albumin (BSA) at ca. 5% concentration in 0.1 M sodium chloride,  $\phi$  was taken as 0.7343, the value found in water by Dayhoff, Perlmann and MacInnes<sup>8</sup>; and  $\phi'$  and  $\phi^*$  were calculated by equations 6 and 7. The value of  $\xi$  was obtained from membrane equilibrium measurements of Scatchard, *et al.*,<sup>5</sup> at the pH corresponding to a protein species of zero valence; that is, under such conditions that equal numbers of moles of Na<sup>+</sup> and Cl<sup>-</sup> are included in component 2\*. For isoionic albumin of the molecular weight 69,000, found

by Scatchard, *et al.*, this amount of binding corresponds to 3.2 moles of sodium chloride per mole of protein. Partial specific volumes of salts and densities of salt solutions required in calculations for Table I were obtained from equations and parameters given by Harned and Owen.<sup>9</sup>

The tabulated apparent volumes exemplify a variety of circumstances that may be encountered in practice. In the case of serum albumin  $\xi$  is positive, and the solution density is close to unity while  $\phi$  is smaller and of the order of twice  $\bar{v}_3$ . It follows that the partial volumes should fall in the order  $\phi > \phi^* > \phi'$ . If  $\xi$  is negative, so that salt is rejected by the macromolecular species, the order is reversed as in the case of the KPVS solution in potassium chloride. For NH<sub>4</sub>PVS in ammonium chloride,  $\xi$  is also negative; but the order of partial volumes is  $\phi^* < \phi < \phi'$ , the interchange of  $\phi^*$  and  $\phi'$  being a reflection of the fact that the partial specific volume of ammonium chloride (0.701) is greater than that of the polymer salt.

It is clear that in protein solutions in rather dilute salt, the differences among  $\phi$ ,  $\phi^*$  and  $\phi'$  are likely to be of the order of only a few tenths of a per cent., indistinguishable or nearly so as compared with absolute uncertainties of concentration determinations. It is possible though that comparative measurements attain a level of precision at which these differences become significant. Since ion binding to proteins is a mass-action phenomenon, increasing the salt concentration increases the effect; and in 1 M sodium chloride, the values of the partial volumes for serum albumin would exhibit differences of the order of a per cent. The tabulated values provide some indication of the possibility of determining  $\xi$  from the densities of dialyzed and undialyzed solutions.

In the comparisons made here, we have assumed that  $\phi$  is the same in water and in salt solution. In the work of Charlwood<sup>10</sup> on proteins no significant difference is evident, but accurate measurements have been made only in rather dilute salt. For proteins,  $\phi$  does generally increase markedly as the pH is varied away from the isoelectric point.<sup>10</sup>

### Refractive Index Increment

Specific and molar refractive index increments in a multicomponent system may be defined by considerations analogous to those utilized above: for example, by adding a mass of component 2, defined in any convenient way, to a system at constant temperature and pressure, we obtain the derivative  $\psi_2 \equiv (\partial n / \partial w_2)_{P, T, m} \equiv \Psi_2 / M_2$  or more precisely in practice, the apparent value  $\Delta n / w_2$ , where  $\Delta n$  is the

(9) G. S. Harned and B. B. Owen, "The Physical Chemistry of Electrolytic Solutions," Reinhold Publ. Corp., New York, N. Y., Third edition, 1958, Chapter 8.

(10) P. A. Charlwood, *J. Am. Chem. Soc.*, **79**, 776 (1957).

(8) M. O. Dayhoff, G. E. Perlmann and D. A. MacInnes, *J. Am. Chem. Soc.*, **74**, 2515 (1952).

increment in refractive index relative to the solvent system. Alternatively we could add component 2 at constant chemical potential  $\mu$  of the other components, considered as diffusible, to obtain  $\psi_2' \equiv (\partial n / \partial w_2)_{T, \mu} \equiv \Psi_2^* / M_2$ . These refractive increments are easily related by expressing the refractive index as a function of pressure, temperature and masses of all the other components in a fixed mass of the principal solvent, conveniently one kilogram of water

$$dn = \left( \frac{\partial n}{\partial P} \right)_{T, m} dp + \left( \frac{\partial n}{\partial T} \right)_{P, m} dT + \sum_{i=2,3} \left( \frac{\partial n}{\partial m_i} \right)_{P, T, m} dm_i$$

We then calculate the derivative with respect to  $m_2$  at constant temperature and potential of the other components. The first term of the result  $(\partial n / \partial P)_{T, m} (\partial P / \partial m_2)_{T, \mu}$  depends on the isothermal compressibility of the system and the osmotic pressure, but we shall assume it to be negligible. Accordingly for the three-component system we write

$$\Psi_2^* = \Psi_2 + \Psi_3 \left( \frac{\partial m_3}{\partial m_2} \right)_{\mu_3, T} \quad (8)$$

where  $(\partial m_3 / \partial m_2)_{\mu_3, T}$  is the number of moles of component 3 which we include in the formulation of component 2<sup>3</sup>. Putting this expression in terms of the specific increments  $\psi$  and recalling that  $M_2^* = M_2 (1 + \xi)$ , we obtain the relation

$$\psi_2^* \equiv \left( \frac{\partial n}{\partial w_2^*} \right)_{T, \mu_3} = \frac{\psi_2 + \xi \psi_3}{1 + \xi}$$

This will be recognized as analogous to equation 6 for the partial specific volume.<sup>11</sup> In studies of proteins and synthetic polymers it is usually convenient to use the specific increment for the macromolecular component but the molar quantity for component 3. In these terms equation 8 gives

$$\psi_2^* = \frac{\psi_2 + \zeta \Psi_3}{1 + \zeta M_3}$$

and

$$\psi_2' = \psi_2 + \zeta \Psi_3 \quad (9)$$

where  $\zeta \equiv (\partial m_3 / \partial w_2)_{m_2} = \xi / M_3$ .

As we showed in reference 3, the light scattering equation for a three-component system reverts formally to the simpler relation for two components when expressed in terms of  $M_2^*$ ,  $w_2^*$ ,  $\psi_2^*$ , that is, in terms of component 2\* (cf. also Stigter<sup>12</sup> and Vrij<sup>13</sup>). Since these quantities appear in the combination  $M_2^* (\psi_2^*)^2 w_2^* = M_2 (\psi_2')^2 w_2$ , knowledge of  $\zeta$  is not required for determining  $M_2$ .

In practice it is usual to employ specific refractive index increments  $\Delta n / c$  in terms of volume concentrations. One reason for doing this, aside from custom and the ease of measurement, is that empirically the specific increment in this form appears to be independent of  $c$  to quite high concentrations in

(11) Although we chose to use a physical argument in discussing the partial specific volume in order to arrive at equations 1 to 4 for the apparent values, relations among  $\bar{v}_1$ ,  $\bar{v}_2'$  and  $\bar{v}_2^*$  of the form of equations 5, 6 and 7, could equally well have been obtained by reasoning like that leading to equation 8. It must be noted, however, that  $\bar{v}_2' = \bar{v}_2^* (1 + \xi) - \xi / \rho$ , as determined by density changes and equation 4, is not the same as  $(\partial V / \partial w_2)_{\mu_3} = \bar{v}_2^* (1 + \xi)$ .

(12) D. Stigter, *J. Phys. Chem.*, **64**, 842 (1960).

(13) A. Vrij, Thesis, Utrecht, 1959, as quoted by Stigter.<sup>12</sup>

solutions of proteins and organic polymers.<sup>14</sup> This observation implies that to a good approximation the refractive index of a mixture is a linear function of the composition by volume

$$n = \sum_{i=1,2,3} n_i \bar{v}_i c_i$$

Since we consider only solutions rather dilute in components 2 and 3, the constants  $n_2$ ,  $n_3$ , need not correspond to the refractive indices of pure components. If the  $\bar{v}_i$  are independent of concentrations and if variations of  $c_2 \equiv c$  are made without varying the relative proportions of components 1 and 3; that is, at constant molality of salt, it can be shown<sup>15</sup> that

$$\psi_{2c} \equiv \left( \frac{dn}{dc} \right)_{m_3} = \bar{v}_2 (n_2 - n_s) \quad (10)$$

where  $n_s = (n_1 \bar{v}_1 c_1 + n_3 \bar{v}_3 c_3) / (\bar{v}_1 c_1 + \bar{v}_3 c_3)$  is the refractive index of the solvent. It follows that if the refractive index increment in one solvent a is known, it can be calculated for another solvent b from equation 10 and a measurement of  $n_{sb} - n_{sa}$ . In particular if the specific increment  $(\partial n / \partial c)_0$  in water is available, that in salt solution is

$$\psi_{2c} = \left( \frac{\partial n}{\partial c} \right)_0 - \bar{v}_2 (n_s - n_1) \quad (11)$$

For proteins in water  $\psi$  is positive; hence increasing the salt concentration, and thus  $n_s$ , should decrease  $\psi_{2c}$ .<sup>16</sup>

The most careful determinations of refractive increments for proteins are perhaps those of Perlmann and Longworth<sup>17</sup> who employed a differential prism method for direct measurements of small differences of refractive index. It is therefore of interest to examine some of their data in light of the discussion just given.

In two series of experiments these workers added successive small amounts of sodium hydroxide to solutions of bovine serum albumin and ovalbumin in water and followed the change in  $\Delta n$  with respect to pure water at a wave length of 5780 Å. and temperature of 0.5°. They found  $\Delta n / c$ ,  $c$  being the concentration in weight of isoionic protein, to increase linearly with the amount of added base in identical fashion for both proteins according to the relation

$$\frac{\Delta n}{c} = \left( \frac{\Delta n}{c} \right)_{u=0} (1 + 0.045u/c)$$

where  $u$  is the molarity of the base. They interpreted this as indicating a variation of the refractive increment with the charge of the protein ion. In advancing a different interpretation we can ignore the fact of chemical reaction between protein and base and regard the system as a mixture of three components—water, protein, sodium hydrox-

(14) In the case of solutions of simple salts,  $\Delta n / c$  exhibits a linear dependence on  $c^{1/2}$  to much higher concentration than does  $\Delta n / w$  with respect to  $w^{1/2}$ . Here, where we are concerned with dilute solutions of component 2, any variation in salt concentration attending variation in  $c_2$  is much too small for the square-root term to contribute to the variation in the refraction due to the salt.

(15) E. F. Casassa, *J. Phys. Chem.*, **60**, 926 (1956).

(16) Equation 11 cannot be regarded as universally valid. In polyphosphates [U. P. Strauss and P. L. Wineman, *J. Am. Chem. Soc.*, **80**, 2366 (1958)]  $\psi_{2c}$  decreases with increasing salt concentration qualitatively as predicted, but the observed effect seems much too great.

(17) G. E. Perlmann and L. G. Longworth, *ibid.*, **70**, 2719 (1948).

ide. If we know the total refractive increment  $\Delta n$  with reference to water and that for a solution of sodium hydroxide of the same *molality*, we can calculate the specific increment for protein as

$$\psi_{2c} = (\Delta n - \Delta n_{\text{NaOH}})/c$$

This expression implies no theory; it is simply a definition of  $\psi_{2c}$  for the process of adding isoionic protein to sodium hydroxide solution. Then for comparison we can calculate  $\psi_{2c}$  by substituting the measured value in water into equation 11. The results are exhibited in Table II. The experimental values of  $\psi_{2c}$  in the fourth column are now independent of sodium hydroxide concentration, except possibly at the highest concentrations; and the calculated values in the fifth column confirm that the concentration of sodium hydroxide is never great enough to cause a sensible decrease in  $\psi_{2c}$  through narrowing of the refractive index difference between protein and the solvent mixture.

Alternatively we can regard these systems as containing two components, water and a sodium protein salt to which, denoting the isoionic protein by Pr, we could assign formulas such as  $\text{Pr} \cdot (\text{NaOH})_y$  or  $\text{Pr} \cdot (\text{NaOH})_y - y\text{H}_2\text{O}$  with the composition given by the amount of base added. Using the experimental values of  $\Delta n$  and multiplying  $c$  for Pr by  $1 + 0.040 u/c$  to obtain the weight concentration of  $\text{Pr} \cdot (\text{NaOH})_y$ , we have calculated  $\psi_{2c}$  for this component as given in the sixth column of Table II. It so happens, as is evident from the empirical result of Perlmann and Longworth, that with the component defined in this way,  $\psi_2$  appears to be independent of the composition  $y$ . This calculation is like that of Perlmann and Longworth except that while they included the contribution of NaOH to  $\Delta n$ , they did not include its corresponding contribution to the weight concentration. Had we chosen, on the other hand, to regard the solute as  $\text{Pr} \cdot (\text{NaOH})_y - y\text{H}_2\text{O}$  and increased  $c$  by the factor  $1 + 0.22 u/c$ , we would have obtained a  $\psi_{2c}$  increasing linearly with the NaOH content at about half the rate reported by Perlmann and Longworth.

In carrying through the calculations on the systems containing base we estimated the molar refractive increment of sodium hydroxide in water as  $10.1 \times 10^{-3}$  l. mole<sup>-1</sup>. This figure was obtained from the limiting value at infinite dilution,  $9.50 \times 10^{-3}$  for the  $\text{Na}_D$  line at  $15^\circ$ .<sup>18</sup> The Gladstone-Dale rule and partial molar volumes calculated from data given by Harned and Owen<sup>9</sup> were used to convert to  $0.5^\circ$ ; but the wave length dispersion correction was omitted as unimportant.

Perlmann and Longworth also measured refractive increments against dialysate for solutions of ovalbumin, bovine serum albumin and human serum albumin, in sodium chloride, and compared the results with solutions dialyzed against water. Averaged values of  $\psi_{2c}' \equiv (\partial n / \partial c)_{us}$  that they obtained are reproduced in the second column of Table III. From equation 11 and the experimental  $\psi_2$  in water, we have calculated  $\psi_{2c}$  in salt and thence from equation 9, (neglecting the distinction between  $\psi_2$  and  $\psi_{2c}$ ) the moles of salt  $\zeta$  bound per gram of

TABLE II

EFFECT OF ADDED SODIUM HYDROXIDE ON THE REFRACTIVE INCREMENTS OF PROTEINS IN AQUEOUS SOLUTION<sup>a</sup>

Protein concn., g. ml. <sup>-1</sup> × 10 <sup>2</sup>	NaOH added, mole l. <sup>-1</sup> × 10 <sup>3</sup>	$\Delta n$ × 10 <sup>3</sup> (vs. H <sub>2</sub> O)	$\psi_{2c}$ protein	$\psi_{2c}$ protein (calcd., eq. 11)	$\psi_{2c}$ Na proteinate
Ovalbumin					
6.451	0	12.106	0.18766		
5.951	7.754	11.234	.1875	0.1876	0.1878
5.739	11.065	10.868	.1875	.1876	.1879
5.545	14.073	10.523	.1873	.1876	.1879
5.334	17.426	10.187	.1878	.1875	.1885
5.128	21.69	9.77	.1864	.1875	.1874
5.025	22.41	9.593	.1865	.1875	.1876
BSA					
4.740	0	9.015	0.19019		
4.340	8.502	8.239	.1905	0.1901	0.1904
4.077	10.041	7.885	.1909	.1901	.1908
3.782	20.302	7.35	.1904	.1900	.1903
3.606	23.349	7.036	.1905	.1900	.1909
3.525	25.722	6.978	.1927	.1900	.1923

<sup>a</sup> From data of Perlmann and Longworth.<sup>17</sup>

protein. Multiplication by the molecular weight of the protein—we used 67,000 for the serum albumins and 45,000 for ovalbumin—then gives the number of moles of salt bound per mole of protein as shown in the last column of Table III. In calculating the refractive increment of NaCl for the experimental conditions, 5780 Å. and  $0.5^\circ$ , we employed the extensive refractive index data at  $25^\circ$  of Kruis<sup>19</sup> interpolating to the desired wave length. Then with the aid of a value for the temperature dependence given by Perlmann and Longworth, we obtained finally

$$\psi_2 = 11.36 - 1.17m^{1/2}$$

at  $0.5^\circ$ . In converting molarities at  $0.5^\circ$  to molalities we again used partial volumes calculated from the parameters given by Harned and Owen.

TABLE III

SPECIFIC REFRACTIVE INDEX INCREMENTS FOR PROTEINS IN AQUEOUS SOLUTION<sup>a</sup>

System	$\psi_{2c}'$ , ml. g. <sup>-1</sup>	$\psi_{2c}$	$\zeta M_2$
Ovalbumin:			
in H <sub>2</sub> O	0.1871	0.1871	
in 0.1 M NaCl	.1874	.1863	4.5
BSA:			
in H <sub>2</sub> O	.1921	.1921	
in 0.1 M NaCl	.1938	.1913	5
in 0.5 M NaCl	.1948	.1881	26
Human serum albumin:			
in H <sub>2</sub> O	.1887	.1887	
in 0.5 M NaCl	.1918	.1847	26

<sup>a</sup> From data of Perlmann and Longworth.<sup>17</sup>

At best, the binding calculated from these refraction determinations can be regarded as revealing no more than an order of magnitude. The results depend on very small differences and there are some unexplained variations in the measurements. Also, we assumed the protein species to be uncharged so that the binding involves only sodium

chloride. Considering these uncertainties, the agreement with membrane distribution data and other measurements of Scatchard and co-workers<sup>5,20</sup> on serum albumin is gratifying. Perlmann and Longworth remarked correctly that the binding of the salt by serum albumin is reflected in an increase in  $\psi_{2c}'$  when sodium chloride is added to the protein in water. Independence of  $\psi_{2c}'$  of the concentration of salt (as in the case of ovalbumin) does not, on the other hand, indicate that there is no binding since in the absence of interaction  $\psi_{2c}'$  is equal to  $\psi_{2c}$ , and decreases with increasing amounts of salt, at least if the assumptions implied by equation 11 are valid.

#### Application to Sedimentation Equilibrium

In reference 3, we pointed out that the entity designated here as component 2\*, to a good approximation sediments independently of component 3 in an ultracentrifuge experiment; hence the equilibrium distribution in the centrifugal field depends on the molecular weight  $M_2^*$ . Formulated in terms of this component (homogeneous in molecular weight and density) the expression for sedimentation equilibrium reverts to the simple form applicable in a two-component system: *i.e.*

$$M_2^*(1 - \bar{v}_2^*\rho) \frac{\omega^2}{2RT} \left( \frac{d \ln m_2}{dx^2} \right)^{-1} = \frac{1}{1 + m_2 (\Sigma \nu_{2i}^*/m_i + \beta_{22}^*)} \quad (12)$$

where  $m_i$ ,  $m_2$  are molalities of species and components,  $M_2^*$  is the molecular weight of component 2\*,  $\beta_{22}^*$  is the derivative of the logarithm of its activity coefficient with respect to  $m_2$ ,  $x$  is the distance from the center of rotation, and  $\omega$  is the angular speed of the rotor.

The correct measurement of  $M_2^*$  in the centrifuge requires an accurate value of  $\bar{v}_2^*$  (or of  $\phi^*$ ) the determination of which in turn requires, in addition to density measurements, data on distribution of diffusible species across an osmotic membrane or equivalent information. It is easy to show, however, that a meaningful molecular weight for the macromolecular component can be obtained, even without knowledge of the  $\nu_{2i}^*$ . Let us suppose that a protein is dialyzed against the supporting electrolyte and the density of solution and dialysate is measured. Then by some means of analysis (*e.g.*, optical density, nitrogen content) the weight concentration corresponding to salt-free protein is determined and used to calculate the apparent partial volume. In other words,  $\phi'$  is calculated. The substitution of this value in equation 12 to determine an unknown molecular weight leads in fact to the molecular weight of the isoionic protein. To see this, we need merely use equation 5 and the relation  $M_2^* = M_2(1 + \xi)$  to find that

$$M_2^*(1 - \phi_2^*\rho) = M_2(1 + \xi) \left[ 1 - \frac{\rho}{1 + \xi} \left( \phi' + \frac{\xi}{\rho_s} \right) \right] \\ = M_2[1 + \xi(1 - \rho/\rho_s) - \phi'\rho]$$

In the limit as  $m_2$  approaches zero,  $\rho/\rho_s$  approaches unity and

$$M_2^*(1 - \bar{v}_2^*\rho) = M_2(1 - \phi'\rho) \quad (13)$$

It may be mentioned that the many discussions of "hydration" in two-component systems, in which it is shown that

(20) G. Scatchard and E. S. Black, *J. Phys. Chem.*, **53**, 88 (1949).

$$M_h(1 - \bar{v}_h\rho) = M_2(1 - \bar{v}_2\rho)$$

the subscript *h* denoting the hydrated species, are not pertinent to the present problem. Whether it is based on a physical model<sup>21</sup> or a thermodynamic argument,<sup>22</sup> the simple reasoning which leads to the conclusion that sedimentation is unaffected by hydration involves the assumption that the density of the adsorbed hydration layer is the same as that of the solvent in bulk. Obviously this assumption cannot apply in a multicomponent system in which the macromolecular solute interacts selectively with other species.

#### Equilibrium Sedimentation in a Density Gradient

Ordinarily, equilibrium centrifugation experiments are carried out at speeds of rotation so low that ordinary salts do not sediment appreciably; hence the concentration of component 3 remains uniform in spite of the redistribution of component 2\*. Interpretation is then simplified because  $M_2^*$  and  $\bar{v}_2^*$  are constant throughout the solution column if our thermodynamic approximations<sup>3</sup> are valid and if hydrostatic pressure effects can be neglected. Recently, however, Meselson, Stahl and Vinograd<sup>23,24</sup> have studied sedimentation of nucleic acids in the presence of concentrated cesium chloride. At a fairly high speed of rotation this heavy salt forms a density gradient, at some point of which the centrifugal and buoyant forces acting on the macromolecular species are in balance. The studies of the equilibrium distribution in the gradient have provided important information about these substances which, owing to their extremely high molecular weights, cannot be investigated by the ordinary equilibrium method.

For the three-component system, the ideas presented here concerning partial volumes and refractive index increments are readily applied in interpreting data obtained by this important new technique. With components defined by osmotic equilibrium, the distribution of component 2\* does not affect the distribution of the diffusible salt component; but the  $\nu_{2i}^*$  depend on the salt concentration and therefore vary with position in the cell. Although equation 12 is still valid at any position  $x$ , this means that  $M_2^*$ ,  $\bar{v}_2^*$  and  $\rho$  are also functions of  $x$ . It is still possible to use equation 13, however, in determining the molecular weight  $M_2$ , which of course does not vary with  $x$ . Three independent sets of observations are required for a complete analysis of results: (a) the sedimentation experiment on the polymeric material to measure its distribution in the dense electrolyte at equilibrium, (b) the sedimentation of the salt alone to determine its distribution in the centrifuge cell, and (c) measurement of density difference between solutions of the polymer and dialysate as a function of salt concentration in the dialysate in order to determine the apparent partial volume  $\phi'$  as a function of  $x$ .

If we can presume that it is possible to use such a

(21) J. T. Edsall in "The Proteins," Academic Press, Inc., New York, N. Y., 1953, Vol. IB, Chapter 7.

(22) H. K. Schachmann, "Ultracentrifugation in Biochemistry," Academic Press, New York, N. Y., 1959.

(23) M. Meselson, F. W. Stahl and J. Vinograd, *Proc. Natl. Acad. Sci., U. S.*, **43**, 581 (1957).

(24) M. Meselson and F. W. Stahl, *ibid.*, **44**, 671 (1958).

low polymer concentration that the concentration dependent term on the right-hand side of equation 12 is negligible, the only problem remaining is that of evaluating the quantity

$$(dm_2/dx^2)m_2^{-1} = (dw_2/dx^2)w_2^{-1} \approx (dc/dx^2)c^{-1}$$

in equation 12. The last equality becomes exact in the limit of small  $c$ . When light absorption by the polymer species can be measured,  $c$  can be determined directly as a function of  $x$ . If the datum obtained is the difference in refractive index between the solution and the reference solvent at the same level  $x$  (e.g., as by interferometry) the concentration is obtained from this difference  $\Delta n$ , by  $\Delta n = \psi'_2 w_2 = \psi_{2c}' c$  where  $\psi'_2$  and  $\psi_{2c}'$  are now functions of  $x$  through their dependence on salt concentration. It is thus necessary to measure the refractive increment of polymer solution referred to dialysate as a function of salt concentration. If the refractive index gradients rather than indices are measured, as is the case for the schlieren optical system, the concentration profile in the centrifuge can be obtained if  $\psi'_2$  or  $\psi_{2c}'$ , together with  $\Psi_3$  or  $\Psi_{3c}$ , are known, but in general a numerical integration is required.

We conclude, therefore, that even though the analysis of sedimentation equilibrium in a density gradient is complicated by the variation of salt concentration through the cell and therefore by the variation in interaction between salt and polymeric

component, it is still possible to determine a molecular weight unambiguously without explicit knowledge of the amount of salt bound. The above remarks are confined to the case of a *single macromolecular component*. For a macromolecular solute heterogeneous in molecular mass, the expressions for sedimentation equilibrium in terms of the starred components assume the form<sup>22-25</sup> applicable to a mixture of species of uniform partial volume in a single solvent, provided  $\bar{v}^*$  is the same for all solute components. The question of heterogeneity with respect to partial volume, which does arise in the case of nucleic acids, has been discussed recently by Baldwin.

NOTE ADDED IN PROOF.—It is pertinent to make note here of two emendations to the previous paper, reference 3.

First, the indicated derivation of the osmotic relation, equation 5, is faulty in not including the effect of pressure on the potential of component 2. The result given is correct, however, as a limiting law for dilute solutions (which is all we actually require). As well as yielding the proper limit for  $\Pi/m_2$  when  $m_2$  is zero, it gives the second virial coefficient correctly except for a term smaller than errors of measurement in protein solutions.

Finally, equation 8 of the same paper should read

$$\left(\frac{\partial n}{\partial c^*}\right)_{m_1}^2 \frac{H'V_m M^* c^*}{RT\Delta\tau} = \left(\frac{\partial n}{\partial c}\right)_{\mu_3}^2 \frac{H'V_m M c}{RV\Delta\tau} = 1 + \frac{c}{M} \left[ \sum_i \frac{v_{2i}^*}{m_i} + \beta_{22}^* \right]$$

(25) R. J. Goldberg, *J. Phys. Chem.*, **57**, 194 (1953).

(26) R. L. Baldwin, *Proc. Natl. Acad. Sci.*, **45**, 939 (1959).

## COUNTERCURRENT DISTRIBUTION OF CHEMICALLY REACTING SYSTEMS. I. POLYMERIZATION

By J. L. BETHUNE<sup>1</sup> AND GERSON KEGELES

*Department of Chemistry of Clark University, Worcester, Mass.*

*Received August 24, 1960*

Although the simple extraction behavior of systems undergoing chemical reactions has been widely studied, general quantitative predictions of the expected behavior of such systems during countercurrent distribution experiments have been lacking. The recent theories of Gilbert and Gilbert and Jenkins for the separation of schlieren peaks in ultracentrifugation and electrophoresis, assuming instantaneous chemical re-equilibration between species, have suggested the possibility of hitherto unexpected behavior in countercurrent distribution experiments as well. The present study, involving the use of a high speed digital computer to solve the material balance equations involved, serves to predict the expected behavior of certain polymerizing systems over a wide range of the parameters governing the equilibria. One prediction is that a system undergoing trimerization may show quite different behavior from that of a dimerizing system.

### Introduction

Most interpretations of the concentration *vs.* tube number patterns obtained from the process of countercurrent distribution have been based upon the assumption of constant partition ratios, which should be expected to hold for dilute solutions of solutes not undergoing chemical reactions.<sup>2-5</sup> One quantitative calculation,<sup>6</sup> showing the possible effect of dimerization upon the distri-

bution of penicillins, has been reported briefly. The results of this calculation, done for 24 transfers, indicated that the position of the individual penicillins in a countercurrent distribution train could not be predicted by the use of a partition ratio measured by simple extraction at a single concentration. Calculations have also been done,<sup>7</sup> with the aid of an analog computer, for cases of continuous countercurrent extraction, in which the effective partition ratio may be represented by a power series in concentration. Note has also been made of the effects on countercurrent distribution behavior of non-linear partition isotherms<sup>8</sup> as well as of such possible reactions as  $X_a Y_b \rightleftharpoons aX + bY$ .<sup>8</sup> For non-linear partition isotherms

(1) Submitted by J. L. Bethune to the Faculty of Clark University in partial fulfillment of the requirements for the degree of Doctor of Philosophy, June, 1961.

(2) S. Stene, *Arkiv Kemi, Mineral. Geol.*, **A18**, No. 18 (1944).

(3) B. Williamson and L. C. Craig, *J. Biol. Chem.*, **168**, 687 (1947).

(4) R. M. Bock, *J. Am. Chem. Soc.*, **72**, 4269 (1950).

(5) L. C. Craig and D. Craig in A. Weissberger, "Technique of Organic Chemistry," Vol. III, Interscience Publ., New York, N. Y., 1950.

(6) W. R. Boon, *Analyst*, **73**, 202 (1948).

(7) A. Acrivos and N. R. Amundson, *Ind. Eng. Chem.*, **45**, 467 (1953).

(8) E. H. Ahrens and L. C. Craig, *J. Biol. Chem.*, **195**, 763 (1952).

some qualitative conclusions have been drawn as to the shapes of the countercurrent distribution patterns, and in the case of the chemically reacting system, it was concluded that the reactants X and Y could be separated after a sufficient number of transfers, provided that they possessed different partition ratios. In the determination of distribution functions for polyglycol systems<sup>9</sup> by countercurrent distribution, the possibility of association between molecules of different molecular weights was investigated by distributing separately and in mixtures two polyglycol fractions which differed in number-average molecular weights. Since the sum of the individual curves agreed with the curve for the mixture, it was concluded that no interaction existed.

Simple extraction, as opposed to countercurrent distribution, has been widely used in inorganic chemistry for the interpretation of equilibria in complex systems.<sup>10-12</sup> Even in the case of a system in which chemical equilibrium has not been attained, the experimental results have been used to elucidate the relationships between the different species appearing in the system.<sup>13</sup> The mathematical relationships developed in this field are, however, not of a type useful in the calculation of countercurrent distribution patterns. The relationships are developed in terms of the extractability of the metal of interest.

Recent theoretical findings of Gilbert<sup>14-16</sup> and Gilbert and Jenkins<sup>17-18</sup> quantitatively predict the previously denied possibility of schlieren peak separations in electrophoresis and ultracentrifugation of systems undergoing instantaneous chemical re-equilibration. Countercurrent distribution experiments may usually be expected to reach chemical equilibrium at each stage prior to transfer,<sup>2-5</sup> and as previous publications have suggested the parallels between countercurrent distribution experiments and convective heat flow<sup>2</sup> and diffusion with forced convection,<sup>2-5</sup> as well as between chromatography<sup>2</sup> and moving boundary electrophoresis or sedimentation,<sup>14</sup> it was suspected that certain of the predictions<sup>14-18</sup> for reacting systems would find qualitative similarities in the field of countercurrent distribution.

In the present study, calculations are reported for the predicted countercurrent distribution behavior of solute systems undergoing polymerization to dimers or to trimers in both of the two phases.

### Calculation Procedure

In considering the relationships involved in the

(9) K. E. Almin and R. Lundberg, *Acta Chem. Scand.*, **13**, 1274 (1959).

(10) H. Irving, *Quart. Rev.*, **5**, 200 (1951).

(11) H. Irving, F. J. C. Rossotti and R. J. P. Williams, *J. Chem. Soc.*, 1955 (1906).

(12) A. E. Martell and M. Calvin, "Chemistry of the Metal Chelate Compounds," Prentice-Hall, Inc., New York, N. Y., 1952, p. 451 ff.

(13) G. Rudstam, *Acta Chem. Scand.*, **13**, 1481 (1959).

(14) G. A. Gilbert, *Disc. Faraday Soc.*, **13**, 239 (1953).

(15) G. A. Gilbert, *ibid.*, **20**, 68 (1955).

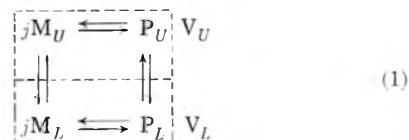
(16) G. A. Gilbert, *Proc. Roy. Soc. (London)*, **A260**, 377 (1959).

(17) G. A. Gilbert and R. C. Ll. Jenkins, *Nature, Lond.*, **177**, 853 (1956).

(18) G. A. Gilbert and R. C. Ll. Jenkins, *Proc. Roy. Soc. (London)*, **A263**, 420 (1959).

equilibration of chemically reacting solute systems between two phases, the following prior assumptions have been made: (1) the solvents are immiscible, (2) no volume changes occur as a result of either extraction or chemical re-equilibration of the solutes, (3) all solutions are thermodynamically ideal when described in terms of the proper reacting species, (4) in polymerization reactions, the monomer and only a single polymer species coexist at equilibrium, and (5) before a transfer, there is chemical as well as transport equilibrium.

For polymerization the following equilibria must then hold



where  $M_U$  and  $P_U$  represent, respectively, monomer and polymer in the upper phase of volume  $V_U$ , and  $M_L$  and  $P_L$  represent, respectively, monomer and polymer in the lower phase of volume  $V_L$  and  $j$  is an integer.

Equations 2 and 3 below then serve to describe the corresponding homogeneous equilibria, and equations 4 and 5 describe the phase distribution equilibria in terms of constants on the mass per unit volume scale

$$K_U = [P]_U/[M]_U^j \quad (2)$$

$$K_L = [P]_L/[M]_L^j \quad (3)$$

$$K_P = [P]_U/[P]_L \quad (4)$$

$$K_M = [M]_U/[M]_L \quad (5)$$

In these expressions all concentrations, indicated by brackets, are in mass per unit volume.

For any single equilibration stage, it is also possible to write an effective partition coefficient  $K_{n,r}^*$  as

$$K_{n,r}^* = \frac{\{[M]_{U,n,r} + [P]_{U,n,r}\} V_U}{\{[M]_{L,n,r} + [P]_{L,n,r}\} V_L} \quad (6)$$

where the subscripts refer to the upper and lower phases of the  $r$ th tube after  $n$  transfers. This may be re-written, using equations 2, 4, 5 and assuming  $V_U = V_L$ , in the form

$$K_{n,r}^* = \frac{K_M K_P (1 + K_U [M]_{U,n,r}^{j-1})}{K_P + K_U K_M [M]_{U,n,r}^{j-1}} \quad (7)$$

When  $j = 1$ , that is, isomerization,  $K_{n,r}^*$  is a constant for all  $n$  and  $r$  and, if both chemical equilibrium and distribution equilibrium are attained before transfer according to assumption 5, the solute will distribute binomially as a single band with a partition ratio

$$K^* = \frac{K_M K_P (1 + K_U)}{K_P + K_U K_M} \quad (8)$$

If, however,  $j$  is greater than one,  $K_{n,r}^*$  depends upon the total mass of solute in the tube, and since this depends upon every previous transfer which has changed the mass of solute in the tube, it is impossible to predict the shape of the pattern obtained after  $n$  transfers by use of the binomial expansion or any other form of mathematical



representation which is based upon a constant partition ratio.

Of the constants defined by equations 2 to 5 one is redundant, for

$$K_L = \frac{K_U K_M^j}{K_P} \quad (9)$$

As a result, in the calculations to follow, values are assigned only to  $K_U$ ,  $K_P$  and  $K_M$ . The calculations were done by solution of the appropriate form of the material balance equation which, assuming for convenience a unit volume of each phase, is

$$1 \times [M]_{U,n,r} + 1 \times [M]_{L,n,r} + 1 \times [P]_{U,n,r} + 1 \times [P]_{L,n,r} = C_{n,r} \quad (10)$$

where  $C_{n,r}$  is the total mass of solute in the  $r$ th tube after  $n$  transfers. By use of relations 2, 4 and 5, equation 10 may be re-written in the form

$$(K_U + K_U/K_P)M_{U,n,r} + (1 + 1/K_M)M_{L,n,r} - C_{n,r} = 0 \quad (11)$$

Equation 11 now relates the mass of monomer in the upper phase of a single tube, after equilibration between phases, to all the independent equilibrium constants. Provided that  $C_{n,r}$  has first been assigned, this quadratic (for dimerization,  $j = 2$ ) or cubic (for trimerization,  $j = 3$ ) equation can be solved for  $M_{U,n,r}$  and from (2), (4) and (5) the equilibrium concentrations of  $P_{U,n,r}$ ,  $P_{L,n,r}$  and  $M_{L,n,r}$  are then obtained. The solution begins for  $n = r = 0$ , since here  $C_{n,r}$  is the amount placed in the first tube of the train, and, if solute is introduced only once,  $C_{0,0}$  corresponds to the total amount of solute to be distributed. After calculation for  $n = r = 0$ , the total mass of solute in the upper phase, ( $M_{U,0,0} + P_{U,0,0}$ ), is moved to tube number one and the total mass of solute in the lower phase, ( $M_{L,0,0} + P_{L,0,0}$ ), remains behind in tube zero. This constitutes the first transfer and after it has been completed

$$C_{1,0} = M_{L,0,0} + P_{L,0,0} \quad (12)$$

and

$$C_{1,1} = M_{U,0,0} + P_{U,0,0} \quad (13)$$

for only fresh solvent is introduced into tube zero and there was only solute-free lower phase in tube one. This calculation according to the suitable form of equation 11 is then repeated for the  $C_{1,0}$  and  $C_{1,1}$  values of equations 12 and 13 and constitutes the equilibration preceding the transfer denoted by  $n = 2$ . Next, three new values  $C_{2,0}$ ,  $C_{2,1}$  and  $C_{2,2}$  can be computed in the same way. By repetition of this process, the entire countercurrent distribution patterns are obtained for every transfer up to  $n = n$ .

In part II of this series an expression for the equilibrium constant which governs the total concentrations of individual species in a single equilibration stage will be developed in terms of the species partition coefficients and upper phase equilibrium constant for a reacting system of the type  $A + B \rightleftharpoons C$ . If an over-all equilibrium constant,  $K_T$ , for a polymerization reaction of the type considered in this paper is derived by the same formal procedure, in terms of the individual equilibria

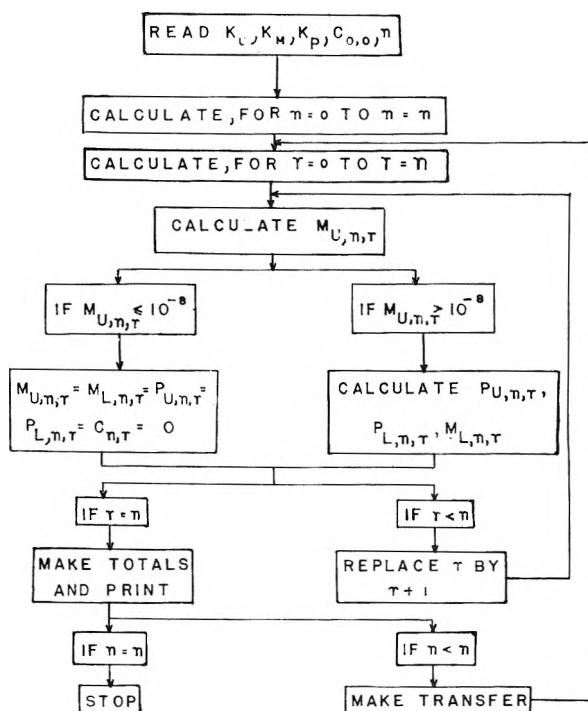


Fig. 1.—Flow diagram for Fortran programs.

$$K_T = \frac{K_U(1 + K_P)K_M^j}{(1 + K_M)^j K_P} \quad (14)$$

where  $K_T$  is the equilibrium constant

$$K_T = \frac{P_T}{M_T^j} \quad (15)$$

in which  $P_T$  and  $M_T$  are the masses of polymer and monomer in any one equilibration stage. This constant is useful in the comparison of any one set of the parameters  $K_U$ ,  $K_M$  and  $K_P$  with another.

Any one set of values of the parameters  $K_U$ ,  $K_P$ ,  $K_M$  and  $C_{0,0}$  for a single distribution experiment of  $n$  transfers involves the solution of approximately  $n(n + 1)/2$  quadratic or cubic equations. To investigate the behavior of different systems involving many different values of the parameters is impossible without the use of a high-speed computer.

The general structure of the programs which were written using the Fortran coding system before machine compilation on an I.B.M. 704 computer is shown in Fig. 1. Most of the results given in this paper were computed using programs of this type taking 2.5 minutes of machine time to compute and record the results for 50 transfers. Programs which result in the use of less computer time are being developed. All root extractions and exponentiations involved in the calculations were accomplished using an M.I.T. Computation Center library subroutine.

These programs were checked by three methods. The first check involved a comparison of results from the computer with desk calculator computations for six different sets of values of  $K_M$ ,  $K_P$ ,  $K_U$  and  $C_{0,0}$  for a small number of transfers. The desk calculator computations were done only to five significant figures and in no case did they differ from the computer values by more than 1 in the last place. The second check involved com-



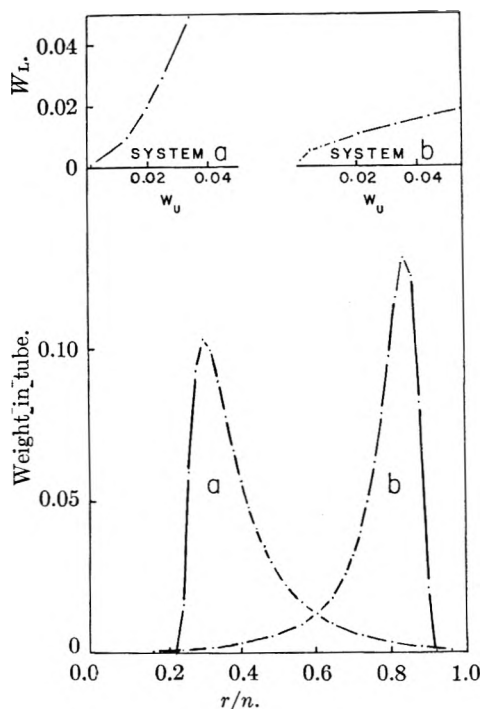


Fig. 2.—Countercurrent distribution patterns (below) and partition isotherms (above) for dimerizing systems.  $W_U$ —weight in upper phase;  $W_L$ —weight in lower phase.

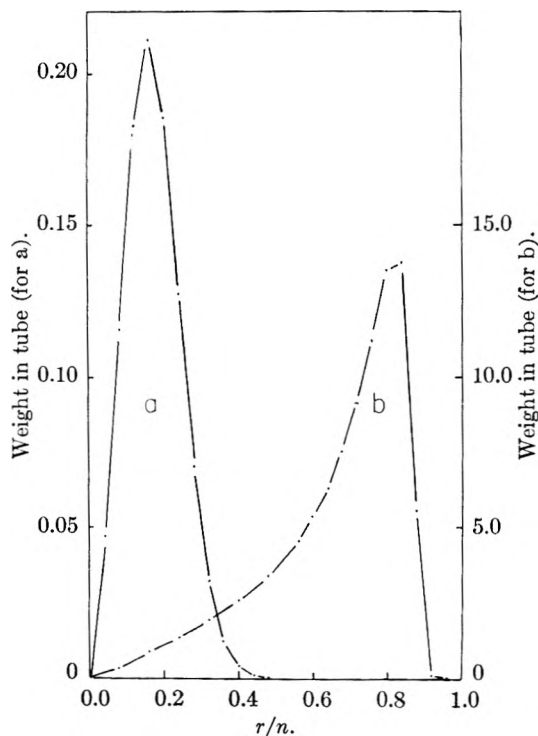


Fig. 3.—Countercurrent distribution patterns for a trimerizing system: the effect of concentration.

puter calculation of thirteen different cases, in which  $K_U$  took on the values of  $1.0 \times 10^4$ , 10 and  $1.0 \times 10^{-2}$ , and in which  $K_M = K_P$  and  $K_P$  took on values of 15.0, 1.5 and 0.15. These calculations, for any given  $K_P$ , for both dimerization and trimerization, give patterns which should agree with the pattern obtained by a binomial expansion

for a single solute with a partition ratio  $K_P$ , for, from (7), if  $K_M = K_P$

$$K_{n,r}^* = \frac{K_P^2(1 + K_U[M]_{U,n,r}^{j-1})}{K_P(1 + K_U[M]_{U,n,r}^{j-1})} = K_P$$

For purposes of comparison, tables of  $T_{n,r}$ , where

$$T_{n,r} = \frac{n!}{(n-r)! r!} \frac{K^r}{(K+1)^n}$$

were computed from  $K = 0.1$  to  $K = 4.0$  in steps of 0.005 for different numbers of transfers. The greatest deviation from the binomial expression was 6 parts in  $10^5$  when the concentration in a given tube reached a significant level, greater than  $6 \times 10^{-5}$ .

The third check involved summation, in the computer calculations, of all of the amounts of solute in all of the tubes after an equilibration and before a transfer. This sum should be constant and equal to  $C_{0,0}$ . The results were printed to seven decimal places and never differed, in any reported case, from  $C_{0,0}$  by more than 1 part in  $10^6$ .

### Results and Discussion

In all plots of distribution patterns the ordinate is the total weight per tube and the abscissas are tube numbers in terms of the reduced coordinate,  $r/n$ , where  $r$  is the tube number and  $n$  is the number of transfers. Plots in terms of this coordinate are useful in detection of abnormalities in distribution behavior, for in the ideal case the maximum in the pattern should occur always at the same value of  $r/n$ , and, with this plot, small shifts in the position of the maximum are easily detectable, as are changes in the over-all shape of the pattern. One effect of this type of plot should be noted. The area under the curve, as plotted, decreases as the number of transfers increases. If the area under the curve is 1 when  $n = 25$ , it is 0.5 when  $n = 50$ . Since the abscissal units are reduced coordinates, however, involving  $1/n$ , both areas represent the same total concentration in the apparatus.

In the following discussion, if a system 1 has parameters the values of which are  $K_{M(1)}$ ,  $K_{P(1)}$ ,  $K_{U(1)}$  and  $K_{T(1)}$  and a system 2 has parameters  $K_{M(2)}$ ,  $K_{P(2)}$ ,  $K_{U(2)}$  and  $K_{T(2)}$ , then system 1 will be called the inverse of system 2 if

$$K_{M(1)} = K_{P(2)}$$

$$K_{P(1)} = K_{M(2)}$$

$$K_{U(1)} \neq K_{U(2)}$$

$$K_{T(1)} = K_{T(2)}$$

**Dimerization.**—Calculations have been done for eighteen different sets of the parameters, with  $K_M$  ranging from 0.15 to 100.0,  $K_P$  from 0.1 to 15.0 and  $K_U$  from 1.0 to  $1.0 \times 10^4$ . The results conform to those predicted qualitatively from the shape of the partition isotherm.<sup>5,19</sup> Resulting distribution patterns are shown in Fig. 2, in which both patterns are for  $n = 50$ .

In Fig. 2 pattern a is for a system in which  $K_M = 15.0$ ,  $K_P = 0.15$ ,  $K_U = 10.0$  and  $K_T = 1.1 \times 10^2$ . Pattern b is for a system in which  $K_M = 0.15$ ,  $K_P = 15.0$ ,  $K_U = 1.0 \times 10^4$  and  $K_T = 1.8 \times 10^2$ . The partition isotherms are shown above each

(19) D. DeVault, *J. Am. Chem. Soc.*, **65**, 532 (1943).

pattern. That for pattern a is concave upward; that for b is concave downward, as is to be expected.<sup>5</sup> System b is very nearly the inverse of system a.

The results may be generalized, for these and all other cases where the polymer is present in significant amounts, in the following statement. When that edge of the pattern which lies in higher numbered tubes than the tube number of the maximum is hypersharpener, the polymer has a partition coefficient higher than that of the monomer, whereas if the edge lying in tubes of lower number than that of the maximum is hypersharpener, the polymer has a partition coefficient which is lower than that of the monomer.

It should be noted that the trailing edge in both patterns, in contrast to analogous cases in trimerization, shown below, fall smoothly and only a single inflection point appears at each side of the curve.

**Trimerization.**—Calculations have been done for fifty-six sets of the parameters, with  $K_M$  ranging from 1.0 to  $5.0 \times 10^4$ ,  $K_P$  ranging from  $1.0 \times 10^{-13}$  to 100.0 and  $K_U$  ranging from  $1.0 \times 10^{-12}$  to  $1.0 \times 10^8$ . The patterns resulting from many of these trimerization calculations are virtually indistinguishable from those in dimerization, at least in the limited range of transfer numbers considered here, if account is taken of the fact that in trimerization the polymer dilutes out more rapidly than in dimerization.

The generalization made for dimerization relating the appearance of the pattern to the partition coefficients also applies, and Fig. 3 illustrates the necessity of the qualification that the polymer must be present in significant amounts for the hypersharpener to be apparent. In both pattern a and pattern b of Fig. 3,  $n = 25$ ,  $K_M = 0.2$ ,  $K_P = 5.0 \times 10^4$  and  $K_U = 10.0$ . In pattern a,  $C_{0,0} = 1.0$  and in pattern b,  $C_{0,0} = 100.0$  weight units. For the system shown in a, after 25 transfers, in the entire train only 0.119% of the solute is in the form of trimer, while in the system shown in b, 41.78% is in the form of trimer, and here there is enough polymer present to hypersharpener the edge at higher tube numbers.

Figure 4 illustrates the effect of varying  $K_U$  while keeping  $K_M$ ,  $K_P$  and  $C_{0,0}$  constant. Here  $K_M = 15.0$ ,  $K_P = 0.15$ ,  $C_{0,0} = 1.0$  and  $n = 17$ . In pattern a,  $K_U = 1.0 \times 10^4$ , in b,  $K_U = 10.0$  and in c,  $K_U = 1.0 \times 10^{-2}$ . Here, as  $K_U$  decreases, more of the solute is in the monomeric form and, since  $K_M$  is larger than  $K_P$ , the maximum appears at higher tube numbers and the edge of the pattern at lower tube numbers is hypersharpener. The great difference from the results in dimerization is shown in pattern b, in which a third inflection point occurs at  $\sim 0.77$  on the  $r/n$  axis. If this pattern is compared with that of Fig. 2, a, where the parameters have the same values, the difference between the patterns which may be obtained from a trimerizing and a dimerizing system is seen. In Fig. 5, a, b and c, patterns for system b of Fig. 4 are given for  $n = 17, 25$  and 50. It is apparent that the effect persists, but even when the number of transfers is increased, no resolution

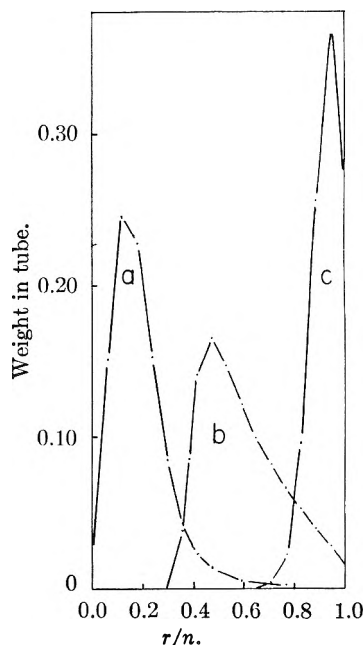


Fig. 4.—Countercurrent distribution patterns for trimerizing systems: the effect of varying  $K_U$ .

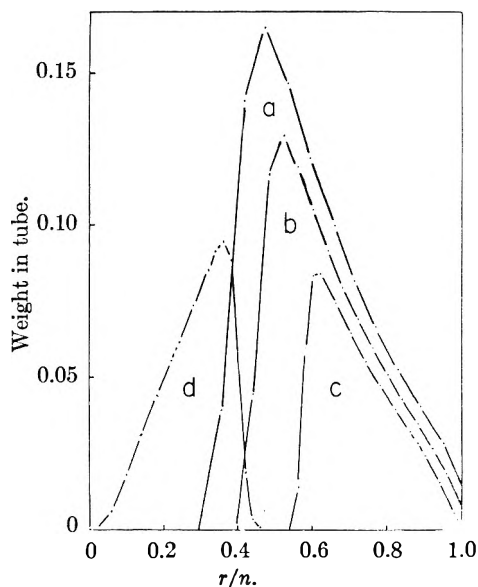


Fig. 5.—Countercurrent distribution patterns for trimerizing systems: the effect of varying  $n$  (a, b and c) and the inverse system (d).

is accomplished. Pattern d is for a 50 transfer distribution of a system having  $K_M = 0.15$ ,  $K_P = 15.0$  and  $K_U = 1.0 \times 10^4$ .  $K_T$  for this system is therefore 31.3, which is approximately the inverse of the system of patterns a, b and c, for which  $K_T = 61.3$ . The system of pattern d has the same values of the parameters as the dimerizing system in Fig. 2, b, to which it should be compared. The third inflection point in d is not as obvious as in a to c, but is present, at  $r/n \sim 0.15$ .

Figure 6 illustrates the influence of the association constant  $K_U$  upon the shape of the pattern for systems in which  $K_M$ ,  $K_P$  and  $C_{0,0}$  remain constant. Here  $n = 50$ ,  $K_M = 100.0$ ,  $K_P = 0.1$  and  $C_{0,c} = 1.0$ . In pattern a,  $K_U = 1000.0$ , in b,

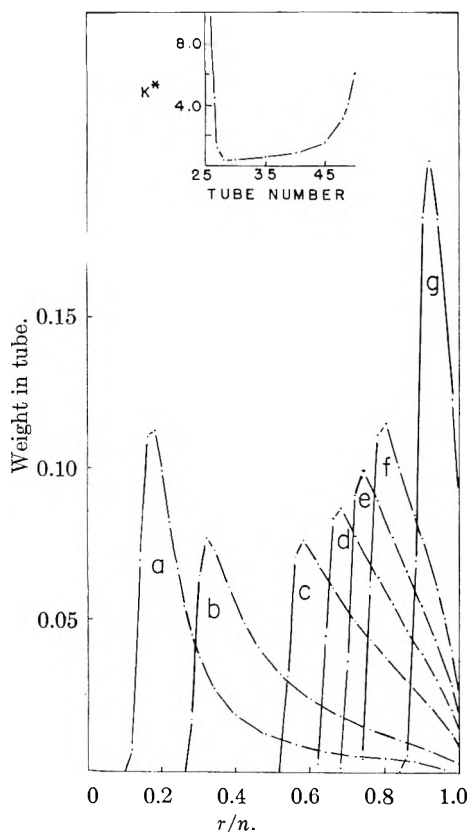


Fig. 6.—Partition ratio vs. tube number (above, for c) and countercurrent distribution patterns for trimerizing systems (below). The effect of varying  $K_U$  and an illustration of the diagnostic value of determining partition ratios across a zone.

$K_U = 100.0$ , in c,  $K_U = 10.0$ , in d,  $K_U = 4.0$ , in e,  $K_U = 2.0$ , in f,  $K_U = 1.0$  and in g,  $K_U = 0.1$ . In every pattern except g, the third inflection point is present, and, if the system for g were subjected to a larger number of transfers, it would appear here also.

These examples show that caution is necessary in the interpretation of patterns in countercurrent distribution experiments in which resolution is

apparently beginning. For example, Fig. 6, c might be interpreted as being composed of a large amount of a component with a partition ratio of about 1.0, and a smaller amount of another component with a partition ratio of about 4.0, but no matter how many transfers are applied, no resolution will occur. On the other hand, first differences of these patterns would show a clean distinction between patterns, e.g., 2,b for dimerization and 6,c for trimerization.

In the third paper of this series it will be shown that it is possible to obtain more information about such a system by the production of a front in the countercurrent distribution train, of the type formed in a cell during ultracentrifugation or moving boundary electrophoresis followed by an interpretation of the first-difference curve of this front, this curve corresponding to the schlieren pattern obtained from the ultracentrifuge or moving boundary electrophoresis equipment.

These results in general show that it is possible to arrive at a reasonable explanation of many bizarre countercurrent distribution patterns upon the basis of molecular associations which may take place during the distribution, rather than on the basis of thermodynamic non-ideality of individual constituents at concentrations where such non-ideality could not reasonably be expected.

Since countercurrent distribution is only one of a number of techniques which may be characterized as zone separation processes, similar results may be expected from these techniques when rapid reversible associations occur. So far these have not been predicted in any theory of, for example, chromatography,<sup>19</sup> although here, if a partition isotherm could be determined experimentally to a high enough degree of accuracy, the same type of pattern should result.

**Acknowledgments.**—This work was supported by U. S. Public Health Service Research Grant number A3508. All computations were carried out at the M.I.T. Computation Center as problem number N806, under the Co-operating Colleges of New England scheme.

## THE COMPUTATION OF THE PATH DIFFERENCE FUNCTION FOR THE CALCULATION OF DIFFUSION COEFFICIENTS BY THE GOUY METHOD

By W. J. THOMAS AND I. A. FURZER

*Chemical Engineering Department, Battersea College of Technology, London, England*

*Received August 29, 1960*

The path difference function defined by Kegeles and Gosting<sup>4</sup> has been computed in an electronic computer and is presented with steps of 0.0001 and 0.001 over different ranges of  $f(z)$ . The table will allow greater use of the Gouy method for the measurement of diffusion coefficients in the liquid state.

During the past fifteen years there has been considerable interest in the study of diffusion in the liquid state.<sup>1</sup> Three basic experimental techniques have been developed. The conductimetric method perfected by Harned and his co-workers<sup>2</sup> is capable

of precision measurement of the diffusion coefficient in dilute solutions. This region is of the greatest theoretical importance when considering electrolytes. The radioactive method is important for the measurement of self-diffusion coefficients. The third technique is based on optical interference and is known as the Gouy method.<sup>3</sup>

(1) P. A. Johnson and A. L. Babb, *Chem. Revs.*, **56**, 387 (1956).

(2) H. S. Harned and R. L. Nuttall, *J. Am. Chem. Soc.*, **71**, 1460 (1949).

(3) G. L. Gouy, *Compt. rend.*, **90**, 307 (1880).

TABLE OF  $f(z)$  AND  $\text{EXP}(-ZZ)$ 

$f(z)$	0	1	2	3	4	5	6	7	8	9
0.001	0.98792	0.98713	0.98637	0.98562	0.98489	0.98418	0.98349	0.98281	0.98214	0.98149
.002	.98085	.98021	.97959	.97898	.97837	.97778	.97719	.97661	.97604	.97547
.003	.97491	.97436	.97381	.97327	.97274	.97221	.97168	.97116	.97065	.97013
.004	.96963	.96913	.96863	.96813	.96764	.96716	.96667	.96619	.96572	.96524
.005	.96477	.96431	.96384	.96338	.96293	.96247	.96202	.96157	.96112	.96068
.006	.96024	.95980	.95936	.95893	.95850	.95807	.95764	.95722	.95679	.95637
.007	.95596	.95554	.95512	.95471	.95430	.95389	.95349	.95308	.95268	.95228
.008	.95188	.95148	.95108	.95069	.95029	.94990	.94951	.94912	.94873	.94835
.009	.94797	.94758	.94720	.94682	.94644	.94607	.94569	.94532	.94494	.94457
.010	.94420	.94383	.94346	.94310	.94273	.94237	.94200	.94164	.94128	.94092
.011	.94056	.94021	.93985	.93949	.93914	.93879	.93843	.93808	.93773	.93738
.012	.93704	.93669	.93634	.93600	.93565	.93531	.93497	.93463	.93429	.93395
.013	.93361	.93327	.93293	.93260	.93226	.93193	.93160	.93126	.93093	.93060
.014	.93027	.92994	.92961	.92929	.92896	.92863	.92831	.92798	.92766	.92734
.015	.92701	.92669	.92637	.92605	.92573	.92541	.92510	.92478	.92446	.92415
.016	.92383	.92352	.92320	.92289	.92258	.92226	.92195	.92164	.92133	.92102
.017	.92071	.92041	.92010	.91979	.91949	.91918	.91888	.91857	.91827	.91796
.018	.91766	.91736	.91706	.91676	.91646	.91616	.91586	.91556	.91526	.91496
.019	.91467	.91437	.91407	.91378	.91348	.91319	.91290	.91260	.91231	.91202
.020	.91173	.91143	.91114	.91085	.91056	.91027	.90999	.90970	.90941	.90912
.021	.90884	.90855	.90826	.90798	.90769	.90741	.90712	.90684	.90656	.90627
.022	.90599	.90571	.90543	.90515	.90487	.90459	.90431	.90403	.90375	.90347
.023	.90319	.90292	.90264	.90236	.90209	.90181	.90153	.90126	.90098	.90071
.024	.90044	.90016	.89989	.89962	.89934	.89907	.89880	.89853	.89826	.89799
.025	.89772	.89745	.89718	.89691	.89664	.89638	.89611	.89584	.89557	.89531
.026	.89504	.89477	.89451	.89424	.89398	.89371	.89345	.89319	.89292	.89266
.027	.89240	.89213	.89187	.89161	.89135	.89109	.89083	.89057	.89031	.89005
.028	.88979	.88953	.88927	.88901	.88875	.88849	.88824	.88798	.88772	.88747
.029	.88721	.88695	.88670	.88644	.88619	.88593	.88568	.88542	.88517	.88492
.030	.88466	.88441	.88416	.88390	.88365	.88340	.88315	.88290	.88265	.88240

In the Gouy method, monochromatic light is used to illuminate a fine slit, which is focussed by a lens through a diffusion boundary onto a photographic plate. As the diffusion proceeds from an initially sharp interface, the interference pattern seen on the plate slowly contracts. The method is particularly important as it allows measurements to be made in very small time intervals (minutes) as compared with the large intervals (days), required by the conductimetric and radioactive methods. The analysis of the interference pattern obtained with the Gouy method was first presented by Kegeles and Gosting<sup>4</sup> and almost simultaneously by Coulson, *et al.*<sup>5</sup> It was later refined by Gosting and Onsager.<sup>6</sup> The theory relates the spacing and intensity of the pattern to the diffusion coefficient. To make full use of the method one requires values of the path difference function  $f(z)$  which is defined as

$$f(z) = \frac{2}{\sqrt{\pi}} \int_0^z e^{-B^2} dB - \frac{2}{\sqrt{\pi}} Ze^{z^2} \quad (1)$$

Tables of this function were first presented by Kegeles and Gosting<sup>4</sup> with large unequal steps in  $f(z)$ . Robinson and Stokes<sup>7</sup> attempted to overcome the difficulty of interpolation by plotting the Function, and recording the results with coarse equal

steps in  $f(z)$ . They recommended that for  $f(z) > 0.03$ , linear interpolation could be used.

The table presented below gives values of  $f(z)$  in the working range  $0.001 < f(z) < 0.250$ . In the range  $0.001 < f(z) < 0.030$  the steps are equal at 0.0001, but in the range  $0.030 < f(z) < 0.250$  the steps are equal at 0.001. Linear interpolation can be used throughout both ranges. It is not usually required to operate at values of  $f(z) > 0.250$  and the table has been restricted for this reason. The complete table giving values of  $f(z)$  within the range  $0.001 < f(z) < 0.250$  and with steps of 0.0001 is given by Furzer.<sup>8</sup>

The diffusion coefficient is calculated from the table of the path difference function and the relevant equation quoted from Kegeles and Gosting<sup>4</sup> and Gosting and Morris.<sup>9</sup>

$$D = \frac{j_M^2 \lambda^2 b^2}{4\pi C_t^2 t} \quad (2)$$

$$C_t = \frac{Y_j}{e_j - z^2} \quad (3)$$

$$Z = \frac{x}{2(Dt)^{1/2}} \quad (4)$$

$$f(z) = \frac{j + \simeq 1/4}{j_M} \quad \text{for maxima} \quad (5)$$

$$f(z) = \frac{j + \simeq 3/4}{j_M} \quad \text{for minima} \quad (6)$$

The value of the constants which are  $1/4$  and  $3/4$

(4) G. Kegeles and L. J. Gosting, *J. Am. Chem. Soc.*, **69**, 2516 (1947).

(5) C. A. Coulson, J. T. Cox, A. G. Ogston and J. S. Philpot, *Proc. Roy. Soc. (London)*, **192A**, 386 (1948).

(6) C. J. Gosting and L. Onsager, *J. Am. Chem. Soc.*, **74**, 6066 (1952).

(7) R. A. Robinson and R. H. Stokes, "Electrolyte Solutions," Butterworths Scientific Publications, London, 1955.

(8) I. Furzer, Ph.D. Thesis, University of London, 1960.

(9) L. J. Gosting and M. S. Morris, *J. Am. Chem. Soc.*, **71**, 1998 (1949).

$f(z)$	0	$f(z)$	0	$f(z)$	0	$f(z)$	0
0.050	0.83868	0.100	0.74663	0.150	0.67107	0.200	0.60496
.051	.83658	.101	.74499	.151	.66967	.201	.60371
.052	.83449	.102	.74336	.152	.66827	.202	.60247
.053	.83241	.103	.74174	.153	.66687	.203	.60122
.054	.83035	.104	.74012	.154	.66540	.204	.59998
.055	.82830	.105	.73851	.155	.66410	.205	.59874
.056	.82626	.106	.73690	.156	.66271	.206	.59751
.057	.82424	.107	.73530	.157	.66133	.207	.59628
.058	.82223	.108	.73370	.158	.65996	.208	.59504
.059	.82024	.109	.73211	.159	.65858	.209	.59381
.060	.81825	.110	.73053	.160	.65721	.210	.59259
.061	.81628	.111	.72895	.161	.65585	.211	.59136
.062	.81432	.112	.72738	.162	.65449	.212	.59014
.063	.81237	.113	.72581	.163	.65313	.213	.58892
.064	.81043	.114	.72425	.164	.65177	.214	.58771
.065	.80850	.115	.72269	.165	.65042	.215	.58649
.066	.80658	.116	.72114	.166	.64907	.216	.58528
.067	.80468	.117	.71959	.167	.64772	.217	.58407
.068	.80278	.118	.71805	.168	.64638	.218	.58286
.069	.80090	.119	.71651	.169	.64504	.219	.58166
.070	.79902	.120	.71498	.170	.64370	.220	.58046
.071	.79715	.121	.71345	.171	.64237	.221	.57926
.072	.79530	.122	.71193	.172	.64104	.222	.57806
.073	.79345	.123	.71041	.173	.63971	.223	.57686
.074	.79161	.124	.70889	.174	.63838	.224	.57567
.075	.78978	.125	.70739	.175	.63706	.225	.57448
.076	.78796	.126	.70588	.176	.63574	.226	.57329
.077	.78615	.127	.70438	.177	.63443	.227	.57210
.078	.78435	.128	.70289	.178	.63312	.228	.57091
.079	.78256	.129	.70140	.179	.63181	.229	.56973
.080	.78077	.130	.69991	.180	.63050	.230	.56855
.081	.77899	.131	.69843	.181	.62920	.231	.56737
.082	.77722	.132	.69695	.182	.62790	.232	.56620
.083	.77546	.133	.69548	.183	.62660	.233	.56502
.084	.77371	.134	.69401	.184	.62531	.234	.56385
.085	.77196	.135	.69255	.185	.62401	.235	.56268
.086	.77023	.136	.69109	.186	.62272	.236	.56151
.087	.76849	.137	.68963	.187	.62144	.237	.56035
.088	.76677	.138	.68818	.188	.62015	.238	.55919
.089	.76506	.139	.68673	.189	.61887	.239	.55802
.090	.76335	.140	.68529	.190	.61760	.240	.55686
.091	.76164	.141	.68385	.191	.61632	.241	.55571
.092	.75995	.142	.68241	.192	.61505	.242	.55455
.093	.75826	.143	.68098	.193	.61378	.243	.55340
.094	.75658	.144	.67955	.194	.61251	.244	.55225
.095	.75491	.145	.67813	.195	.61125	.245	.55110
.096	.75324	.146	.67671	.196	.60998	.246	.54995
.097	.75158	.147	.67529	.197	.60873	.247	.54881
.098	.74992	.148	.67388	.198	.60747	.248	.54766
.099	.74827	.149	.67247	.199	.60621	.249	.54652

in eq. 5 and 6 vary with the fringe number and are given exactly by Gosting and Morris.<sup>9</sup>

The table has been checked at a number of points with standard probability tables, and the fifth significant figure is accurate to  $\pm 1$  integer unit. The variation is due to the round-off error in the computer programme.

The Ferranti Mercury Computer used, was programmed on the Auto-Code System.<sup>10</sup> Details of the prepared programme are given by Furzer.<sup>3</sup>

**Acknowledgments.**—The authors gratefully acknowledge the use of the computing facilities of the

University of London Computer Unit.

The present study represents part of the work carried out in preparation for a Ph.D. degree of the University of London on "Diffusion Studies in the Liquid State."

#### Nomenclature

$x$	Distance along the axis in direction of diffusion
$D$	diffusion coefficient
$t$	time
$Z$	reduced height as defined by eq. 4
$j_M$	total number of fringes
$j$	fringe number
$\lambda$	wave length
$b$	optical distance
$Y_j$	distance of fringe numbered $j$ from slit image
$C_i$	defined by eq. 3
$f(z)$	defined by eq. 5 and 6

(10) R. A. Brooker, B. Richards, E. Berg and R. H. Kerr, *The Manchester Mercury Autocode System*, The University of Manchester, 1959.

## THE FLUORIDE COMPLEXING OF YTTRIUM(III) IN AQUEOUS SOLUTION

BY ARMINE D. PAUL, LINDA S. GALLO AND JEAN B. VANCAMP

*Department of Chemistry, West Virginia University, Morgantown, W. Va.**Received August 26, 1960*

The fluoride complexing of  $Y^{+3}$  in perchlorate solution was studied potentiometrically by measuring the effect on the known ferric fluoride equilibria using the ferrous-ferric electrode. At  $25^\circ$  and an ionic strength of  $0.5 M$  the equilibrium quotients for the reactions  $Y^{+3} + HF = YF^{+2} + H^+$ ,  $YF^{+2} + HF = YF_2^+ + H^+$ , and  $YF_2^+ + HF = YF_3(aq) + H^+$  are 10.0, 2 and 2, respectively. Equilibrium quotients are also given at 15 and  $35^\circ$ . The stability of the yttrium fluoride complexes is compared with that of other trivalent ions. The decrease in stability of successive fluoride complexes of  $Y^{+3}$  is less than that for other trivalent ions.

During the past decade there has been accumulating a vast amount of quantitative and qualitative data pertaining to the complexing of metal ions with various ligands. The lanthanide ions have been fairly well studied in this respect, but little data is available concerning the complexing tendencies of other Group IIIB metal ions.

Complexing of  $Y^{+3}$  with organic ligands<sup>1</sup> has been studied more extensively than with inorganic ligands. Complexing with inorganic ligands has been limited to an estimation<sup>2</sup> of the hydrolysis constant, a study of sulfate complexing,<sup>3</sup> and a report that there is no evidence of chloride complexing from anion-exchange studies.<sup>4</sup>

The recent study<sup>5</sup> of the fluoride complexing of  $Sc^{+3}$  which reported that scandium fluoride complexes are more stable than those of other trivalent ions of similar radius led to the present study. Besides adding to the sparse complexing data available for  $Y^{+3}$ , it was felt that the study would answer the question of whether  $Y^{+3}$ , whose electronic structure is similar to  $Sc^{+3}$ , also exhibited the tendency of forming exceptionally stable fluoride complexes.

The complexing was studied potentiometrically by measuring the effect on the known ferric fluoride equilibria using the ferrous-ferric electrode according to the method first described by Brosset and Orring<sup>6</sup> and later successfully used by other workers.<sup>7-9</sup>

## Experimental

**Apparatus.**—The electrodes, measuring apparatus and general procedure are similar to those described elsewhere.<sup>7-9</sup> The half-cells were made from 200-ml. three-necked Pyrex flasks. The center neck contained a rubber stopper fitted with a stirrer. A two-hole rubber stopper accommodating the salt bridges occupied the second opening. The third opening also contained a two-hole rubber stopper, one hole of which provided the entrance for  $N_2$  to prevent oxidation, and the other provided the inlet for the NaF solution.

The temperature of the thermostat was controlled to  $\pm 0.1^\circ$ .

(1) J. Bjerrum, G. Schwarzenbach and L. G. Sillen, "Stability Constants of Metal-ion Complexes, with Solubility Products of Inorganic Substances. Part I: Organic Ligands," The Chemical Society, London, 1957.

(2) T. Moeller, *J. Phys. Chem.*, **50**, 242 (1946).

(3) F. H. Spedding and S. Jaffe, *J. Am. Chem. Soc.*, **76**, 882 (1954).

(4) K. A. Kraus, F. Nelson and G. W. Smith, *J. Phys. Chem.*, **58**, 11 (1954).

(5) J. W. Kury, A. D. Paul, L. G. Hepler and R. E. Connick, *J. Am. Chem. Soc.*, **81**, 4185 (1959).

(6) C. Brosset and G. Orring, *Svensk. Kem. Tid.*, **55**, 101 (1943).

(7) H. W. Dodgen and G. K. Rollefson, *J. Am. Chem. Soc.*, **71**, 2600 (1949).

(8) R. E. Connick and M. Tsao, *ibid.*, **76**, 5311 (1954).

(9) L. G. Hepler, J. W. Kury and Z. Z. Hugus, Jr., *J. Phys. Chem.*, **58**, 26 (1954).

**Procedure.**—Three half-cells, A, B and C contained the same initial concentrations of  $Fe(ClO_4)_2$ ,  $Fe(ClO_4)_3$  and  $HClO_4$ . Half-cell A contained in addition a known concentration of  $Y(ClO_4)_3$ . The ionic strength in each half-cell was adjusted to  $0.50 M$  with  $NaClO_4$  and the volumes in each half-cell were equal. Half-cells A and C and half-cells B and C were connected by sodium perchlorate-agar agar salt bridges.

After the initial zero potentials (about 0.2 mv.) became constant, aliquots of  $0.5 M$  NaF were added from a calibrated micropipet to half-cells A and B. The potentials of cells A-C and B-C were measured after each addition. The fluoride additions were continued until the  $YF_3$  precipitated, at which point the potential of cell A-C began to drift rapidly downward.

**Solutions.**—A solution of  $Y(ClO_4)_3-HClO_4$  was prepared by dissolving 99.9%  $Y_2O_3$  obtained from the Fielding Chemical Co. in a known quantity of  $HClO_4$ . The yttrium concentration calculated from the weight of  $Y_2O_3$  dissolved agreed with that obtained by precipitating  $Y^{+3}$  as  $Y(OH)_3$  and weighing as  $Y_2O_3$ . The acidity was determined by precipitating  $Y^{+3}$  as  $YF_3$  and titrating with standard NaOH to the phenolphthalein end-point.

The preparation and standardization of solutions of  $HClO_4$ ,  $NaClO_4$ , NaF and  $Fe(ClO_4)_2-Fe(ClO_4)_3-HClO_4$  is described elsewhere.<sup>7-9</sup>

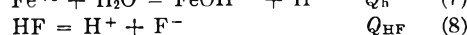
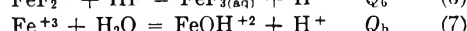
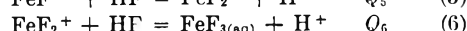
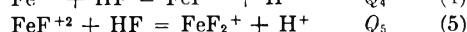
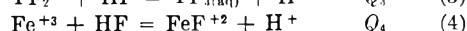
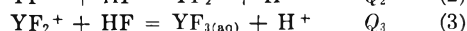
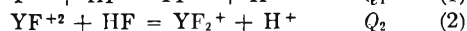
## Data and Calculations

Three experiments were performed at 15 and  $25^\circ$  and two at  $35^\circ$ . At each temperature the  $Y^{+3}$  concentration was varied approximately five-fold and the acidity a little more than threefold. Table I summarizes the initial conditions for each experiment. Typical data for a titration are presented in Table II together with calculated values of  $\bar{n}$  and  $(HF)/(H^+)$ .

TABLE I

	INITIAL EXPERIMENTAL CONDITIONS		
	$15^\circ, 25^\circ, 35^\circ$	$15^\circ, 25^\circ$	$15^\circ, 25^\circ, 35^\circ$
$Y(ClO_4)_3, M \times 10^4$	9.869	19.55	47.47
$HClO_4, M \times 10^2$	1.814	6.262	6.384
$NaClO_4, M$	0.4726	0.4224	0.4045
$Fe(ClO_4)_2, M \times 10^4$	3.752	3.725	3.619
$Fe(ClO_4)_3, M \times 10^4$	3.663	3.627	3.524
Highest $(\Sigma F^-), M \times 10^3$	2.953	7.246	9.346

The equilibria to be considered are



Moeller's<sup>2</sup> estimate of  $1 \times 10^{-7}$  for the hydrolysis constant of  $Y^{+3}$  allows one to neglect the species  $YOH^{+2}$  at the acidities used. The  $Q$ 's above are

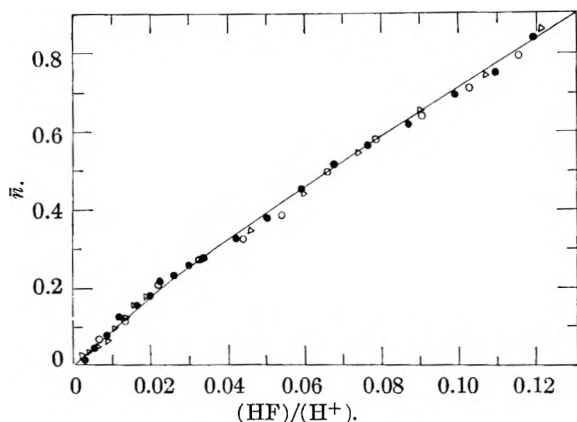


Fig. 1.—Fluoride complexing of Y(III) at 25°: O, initial conditions given in first column of Table I; ●, initial condition given in second column of Table I; Δ, initial conditions given in third column of Table I.

TABLE II

DATA FOR TYPICAL EXPERIMENT AT 25°

Initial concentrations are those in first column of Table I. Initial volume = 101.00 ml.; NaF = 0.5000 M

Ml. NaF added to cells A and B	$E_{A-c}$ (mv.)	$E_{B-c}$ (mv.)	$\bar{n}$	$(\text{HF})/(\text{H}^+)$ , $M \times 10^2$
0.0498	17.67	22.95	0.0709	0.562
.0996	32.08	40.38	.1217	1.316
.1494	43.57	54.73	.2131	2.181
.1992	53.71	66.07	.2732	3.194
.2490	63.21	76.41	.3250	4.393
.2988	69.94	85.18	.3861	5.417
.3486	76.67	92.22	.4982	6.595
.3994	82.93	99.19	.5798	7.850
.4482	88.20	105.55	.6412	9.036
.4980	93.18	110.07	.7128	10.27
.5478	97.86	113.78	.7947	11.54
.5976	101.77	116.60	.9988	12.70

equilibrium quotients expressed in concentrations (not activities). Values of  $Q_4$ ,  $Q_5$ ,  $Q_6$ ,  $Q_h$  and  $Q_{\text{HF}}$  used in these calculations are given by Connick, *et al.*<sup>10</sup>

The method for calculating  $Q_1$ ,  $Q_2$  and  $Q_3$  parallels that given in ref. 5. The average number of fluoride ions held by each yttrium ion is represented by  $\bar{n}$ .

$$\bar{n} = \frac{\Delta(\Sigma \text{F}^-)}{(\Sigma \text{Sc}^{+3})} \quad (9)$$

The quantity  $(\text{HF})/(\text{H}^+)$  can be calculated from the equation

$$(1 + (Q_b)/(\text{H}^+)(e^{PE/RT} - 1)) = Q_4(\text{HF})/(\text{H}^+) + \frac{Q_4 Q_5 (\text{HF})^2 / (\text{H}^+)^2 + Q_4 Q_5 Q_6 (\text{HF})^3 / (\text{H}^+)^3}{1 + Q_1(\text{HF})/(\text{H}^+) + Q_1 Q_2 (\text{HF})^2 / (\text{H}^+)^2 + Q_1 Q_2 Q_3 (\text{HF})^3 / (\text{H}^+)^3} \quad (10)$$

The relation between  $\bar{n}$ ,  $(\text{HF})/(\text{H}^+)$  and  $Q_1$ ,  $Q_2$  and  $Q_3$  is given by

$$\bar{n} = \frac{Q_1(\text{HF})/(\text{H}^+) + 2Q_1 Q_2 (\text{HF})^2 / (\text{H}^+)^2 + 3Q_1 Q_2 Q_3 (\text{HF})^3 / (\text{H}^+)^3}{1 + Q_1(\text{HF})/(\text{H}^+) + Q_1 Q_2 (\text{HF})^2 / (\text{H}^+)^2 + Q_1 Q_2 Q_3 (\text{HF})^3 / (\text{H}^+)^3} \quad (11)$$

From a plot of  $\bar{n}$  vs.  $(\text{HF})/(\text{H}^+)$ ,  $Q_1$ ,  $Q_2$  and  $Q_3$  were obtained by a process of curve fitting.

Figure 1 represents a plot of  $\bar{n}$  vs.  $(\text{HF})/(\text{H}^+)$  for the experiments at 25°. The solid curve was calculated using the  $Q$ 's listed in Table III. All

(10) R. E. Connick, L. G. Hepler, Z. Z. Hugus, Jr., J. W. Kury, W. M. Latimer and M. Tsao, *J. Am. Chem. Soc.*, **78**, 1827 (1956).

of the experimental points fall very close to the theoretical curve. The uncertainties in Table III represent the extent to which the  $Q$ 's can be varied without moving the curve more than 0.02  $\bar{n}$  unit. When  $Q_2$  and  $Q_3$  are of the same order of magnitude a rather wide variation is possible in fitting the curve and hence the uncertainties in  $Q_2$  and  $Q_3$  are larger than in other similar studies.

### Results

Table III lists the values obtained at  $\mu = 0.50 M$  for  $Q_1$ ,  $Q_2$  and  $Q_3$  at 15, 25 and 35°.

TABLE III

EQUILIBRIUM QUOTIENTS AT  $\mu = 0.5 M$ 

Temp., °C.	$Q_1$	$Q_2$	$Q_3$
15	$10.5 \pm 0.3$	$1.0 \pm 0.5$	$1 \pm 1$
25	$10.0 \pm 0.3$	$2 \pm 1$	$2 \pm 1$
35	$9.5 \pm 0.3$	$5 \pm 2$	$3 \pm 1$

Equilibrium quotients for reactions written in terms of  $\text{F}^-$  rather than  $\text{HF}$  were obtained by dividing  $Q_1$ ,  $Q_2$  and  $Q_3$  by the ionization constant of  $\text{HF}$  at  $\mu = 0.5$ .<sup>10</sup> These values together with the true equilibrium constants at  $\mu = 0$  are presented in Table IV. The latter values were calculated using the empirical relations for activity coefficient corrections given by Rabinowitch and Stockmayer<sup>11</sup> and Nasanen.<sup>12</sup>

TABLE IV

EQUILIBRIUM QUOTIENTS AT 25° FOR REACTIONS WRITTEN IN TERMS OF FLUORIDE ION

Reaction	$Q^1$ ( $\mu = 0.5$ )	$K$ ( $\mu = 0$ )
$\text{Y}^{+3} + \text{F}^- = \text{YF}^{+2}$	$8.5 \times 10^3$	$6.5 \times 10^4$
$\text{YF}^{+2} + \text{F}^- = \text{YF}_2^+$	$1.6 \times 10^3$	$5.4 \times 10^3$
$\text{YF}_2^+ + \text{F}^- = \text{YF}_3(\text{aq})$	$1.6 \times 10^3$	$4.0 \times 10^3$

The free energy, heat and entropy changes for reaction 1 were calculated and found to be  $-1.36 \pm 0.01$  kcal./mole,  $-0.93 \pm 0.55$  kcal./mole and  $1 \pm 2$  e.u., respectively. The rather large uncertainties in  $Q_2$  and  $Q_3$  prevent the calculation of meaningful thermodynamic quantities for reactions 2 and 3.

In addition to the equilibrium quotients presented in Table III,  $Q$  for the reaction  $\text{YF}_3(\text{aq}) + \text{HF} = \text{YF}_4^- + \text{H}^+$  was estimated to be about 10. It was necessary to take this reaction into consideration in order to fit only the last 3 or 4 points on the curve in Fig. 1. The uncertainty in these points is comparatively large since they represent measurements close to the precipitation point of  $\text{YF}_3$ . Hence the value of 10 should be considered only as a rough approximation.

### Discussion

If one assumes fluoride complexes to be purely ionic, their stability should be roughly proportional to the ionic radii, provided the ionic charges are equal. The ionic radii of  $\text{Y}^{+3}$  and  $\text{In}^{+3}$  are both  $0.95 \text{ \AA}$ .<sup>13</sup> Comparison of stability constants at  $\mu = 0$  shows that  $K$  for the formation of  $\text{YF}^{+2}$  is  $6.5 \times 10^4$  while that for  $\text{InF}^{+2}$  is  $4.3 \times 10^4$ .<sup>9</sup> Considering the first fluoride complex only, these

(11) E. Rabinowitch and W. H. Stockmayer, *ibid.*, **64**, 335 (1942).

(12) R. Nasanen, *Acta Chem. Scand.*, **4**, 140, 816 (1950).

(13) R. W. G. Wyckoff, "Crystal Structure," Interscience Publishers, Inc., New York, N. Y., 1951.



data are in good agreement with the ionic interpretation.

However if one compares the stability of the second and third fluoride complexes of  $Y^{+3}$  as given in Table III with corresponding data for other trivalent ions as given in Table V, an unusual

TABLE V  
EQUILIBRIUM QUOTIENTS FOR TRIVALENT FLUORIDES AT  
25° AND  $\mu = 0.5$

Reaction	Q	Ref.
$Fe^{+3} + HF = FeF^{+2} + H^+$	184	10
$FeF^{+2} + HF = FeF_2^+ + H^+$	10.3	10
$FeF_2^+ + HF = FeF_3(aq) + H^+$	1.0	10
$Al^{+3} + HF = AlF^{+2} + H^+$	1720	14
$AlF^{+2} + HF = AlF_2^+ + H^+$	131	14
$AlF_2^+ + HF = AlF_3(aq) + H^+$	8.5	14
$AlF_3(aq) + HF = AlF_4^- + H^+$	0.7	14
$Sc^{+3} + HF = ScF^{+2} + H^+$	1910	5
$ScF^{+2} + HF = ScF_2^+ + H^+$	233	5
$ScF_2^+ + HF = ScF_3(aq) + H^+$	14.6	5
$ScF_3(aq) + HF = ScF_4^- + H^+$	0.85	5
$In^{+3} + HF = InF^{+2} + H^+$	6.9	9
$InF^{+2} + HF = InF_2^+ + H^+$	0.5	9

trend becomes apparent. From Table V it can be seen that the stability of successive complexes of  $Fe^{+3}$ ,  $Al^{+3}$ ,  $Sc^{+3}$  and  $In^{+3}$  decreases by a factor of approximately 10. For the yttrium fluoride complexes, the decrease in stability of successive complexes is much less than this. As can be seen from Table III, the second and third fluoride complexes of  $Y^{+3}$  are of almost equal stability, and if Q for the reaction  $YF_3(aq) + HF = YF_4^- + H^+$

has any significance at all,  $YF_4^-$  is more stable than either  $YF_3(aq)$  or  $YF_2^+$ .

It appears that the tendency exhibited by  $Sc^{+3}$  for forming exceptionally stable fluoride complexes is also shown by  $Y^{+3}$  to some extent, particularly after one or two fluoride ions have been complexed.

The explanation of these discrepancies is not apparent. The crystal structure of  $YF_3$ <sup>15</sup> shows each yttrium atom to have 8 fluorine neighbors at 2.3 and another at 2.60 Å. The structure of  $Y(OH)_3$ <sup>16</sup> shows yttrium in the center of a regular trigonal prism with oxygen in the six corners and three more oxygens adjacent to the lateral faces of the prism. Assuming the radius of  $F^-$  to be 1.36 Å,<sup>13</sup> the radius ratio for  $Y^{+3}$  to  $F^-$  is 0.70, which is close to the minimum radius ratio of 0.732 proposed by Pauling<sup>17</sup> for coordination numbers 8 or 9. The crystal structures of  $YF_3$  and  $Y(OH)_3$  indicate that a coordination number of 9 exists even though the minimum radius ratio has not been satisfied. However when the larger water molecules surround the yttrium ions, perhaps the coordination sphere may become somewhat strained and hence replacement of water molecules by the smaller fluoride ions should relieve the strain and enhance the stability of the fluoride complexes. For yttrium ion, this apparently does not occur until at least two water molecules have been replaced.

(14) W. M. Latimer and W. L. Jolly, *J. Am. Chem. Soc.*, **75**, 1548 (1953).

(15) A. Zalkin and D. H. Templeton, *ibid.*, **75**, 2453 (1953).

(16) K. Schubert and A. Seitz, *Z. anorg. Chem.*, **264**, 116 (1947).

(17) L. Pauling, "The Nature of the Chemical Bond," Cornell University Press, Ithaca, N. Y., 1945, p. 382.

## INFRARED EXTINCTION COEFFICIENTS OF KETONES ADSORBED ON Ca-MONTMORILLONITE IN RELATION TO SURFACE COVERAGE. CLAY-ORGANIC STUDIES. PART IV<sup>1</sup>

BY REINHARD W. HOFFMANN AND G. W. BRINDLEY

Contribution No. 60-15 from the College of Mineral Industries, Department of Ceramic Technology, The Pennsylvania State University, University Park, Pennsylvania

Received August 29, 1960

Infrared spectra of one- and two-layer complexes of 2,5-hexanedione and 2,5,8-nonanetrione with calcium-montmorillonite were studied. The extinction coefficients for the absorptions of the adsorbed ketones were determined by a differential technique: The weight loss of a sample upon heating was related to the corresponding decrease in absorbance. The organic content and surface coverages of the clay-organic complexes were then determined using the extinction coefficients. The relation of the X-ray diffraction patterns to the surface coverage is discussed. The surface coverage at which the two-layer complex starts to form can be used as a relative measure of surface mobility. The extinction coefficients of the 1404, 1365 and 1312 ( $1325$ )  $cm^{-1}$  vibrations and that of the  $C=O$  stretching vibration decrease with increasing surface coverage. At values of the surface coverage approximating those at which the two-layer complex appears, there is a change in the observed rate of decrease. The rate of decrease and its inflection point are discussed in terms of decreasing clay-organic interaction. The use of these observations to arrive at a site energy distribution for the adsorption is discussed.

### Introduction

In previous studies,<sup>2,3</sup> adsorption isotherms for neutral aliphatic molecules adsorbed on clay surfaces from aqueous solutions have been determined

(1) Part III: L. G. Tensmeyer, R. W. Hoffmann and G. W. Brindley, *J. Phys. Chem.*, **64**, 1655 (1960).

(2) G. W. Brindley and M. Rustom, *Am. Mineralogist*, **43**, 627 (1958).

(3) R. W. Hoffmann and G. W. Brindley, *Geochim. et Cosmochim. Acta*, **20**, 15 (1960).

by measuring the depletion of the organic solutions. It is difficult to remove the clay from the liquid medium without altering the equilibrium amount of organic material adsorbed on the clay surface, since any washing or drying treatment of the clay causes a change in the organic content.

One of the objectives of these investigations has been to study the properties of clays in relation to the amount of organic material adsorbed, such as

for example the maximum amount of organic material contained in a one-layer complex, which could be used as a qualitative measure of the degree of packing and of the surface mobility of the adsorbed molecules. In order to study this it becomes essential to measure directly the amount of organic material retained by the clay after drying.

Infrared absorption spectroscopy provides an instrumental method for measuring quantitatively the amount of an organic material associated with a clay without destroying the sample. However, it is essential that a vibration be used whose extinction coefficient is independent of the amount adsorbed. The present investigation was concerned with 2,5-hexanedione and 2,5,8-nonanetrione as in previous work.<sup>1</sup> The extinction coefficients of the symmetrical methylene stretching vibration of these substances appear to be independent of the amount adsorbed, making this approach feasible.

There is however the experimental problem of establishing quantitatively the amount of organic material on the clay in order to measure the extinction coefficients in the first place. To solve this, a differential technique has been developed by which the extinction coefficients of the symmetrical methylene stretching vibrations were determined. The extinction coefficients of other vibrations, which are not obscured by the clay itself, are found to vary with the amount adsorbed, the significance of which will be considered.

### Experimental

I. **Materials.**—(a) 2,5-Hexanedione was obtained from Aldrich Chemicals Co. and was redistilled before use; b.p. 82.2–82.7° (17 mm.) (b) 2,5,8-Nonanetrione was prepared in this Laboratory<sup>1</sup>; m.p. 55°. (c) The preparation of the clay suspension containing 30 mg. of Ca-montmorillonite per ml. has been described previously.<sup>1</sup>

II. **Spectra.**—All spectra were recorded on a Perkin-Elmer Model 21 Spectrophotometer with NaCl optics using a resolution setting of 925. The spectra were recorded from 2 to 8.5  $\mu$ . The wave length drive was run very slowly often in the range of 1–2  $\mu$  per hour. The absorption frequencies were determined in a previous study,<sup>1</sup> where typical spectra are reproduced.

One- and two-layer complexes of the ketones with calcium montmorillonite were prepared by mixing 2 ml. of Ca-montmorillonite suspension (30 mg./ml.) and 0.5 ml. of a ketone solution of appropriate concentration in water. Two 1-ml. samples of the resulting suspension were dried on two glass slides. Teflon washers, with an open area of 3.75 cm.<sup>2</sup>, held the evaporating suspensions and fixed the shape of the resultant films which were dried together over P<sub>2</sub>O<sub>5</sub>. One slide was reserved for X-ray examination, the film of the other slide was carefully split off with a razor blade. For clay-organic complexes with low organic content a Teflon sheet instead of the glass slide was used to facilitate the separation of the clay film. The film was protected from atmospheric moisture by being placed between AgCl and NaCl windows separated by a Teflon spacer. The whole system was held tightly in a lucite sample holder.

For the reference beam a similar assembly was prepared containing either an AgCl window alone or an AgCl window with a film of pure Ca-montmorillonite.

III. **Determination of Extinction Coefficients.**—Preliminary experiments with complexes of 2,5,8-nonanetrione showed considerable changes in the extinction coefficients with different organic contents of the complexes: Clay organic films were prepared by drying suspensions on AgCl windows and apparent molar extinction coefficients were calculated by assuming that all the organic material in the initial suspension was incorporated in the resultant film. The extinction coefficients so obtained are definitely too small since some of the organic material fails to be incorporated in the final complex; this is particularly true for

complexes of 2,5-hexanedione, which evaporates partly during the drying process.

Whereas the extinction coefficients of most vibrations seem to vary with the amount of organic material on the clay, that of the symmetrical methylene stretching vibration at 2913 cm.<sup>-1</sup> showed only statistical variations over a wide range of complex compositions. It is assumed that its value is essentially constant and independent of the surface coverage or type of complex. This assumption is supported by the fact that this vibration is largely independent of the particular environment. Its frequency is not changed by transition from solution to the solid state (in case of 2,5,8-nonanetrione) or to the adsorbed state, whereas other frequencies show significant changes.<sup>1</sup> The extinction coefficient of this vibration may be used to determine quantitatively the amounts adsorbed as soon as the extinction coefficient is once determined.

Extinction coefficients can be determined by the following differential method: A clay-organic film loses some of its adsorbed material by heating. The weight loss can be related to the corresponding decrease in absorption intensity to arrive at the extinction coefficient

$$\epsilon = \frac{\Delta A S M}{\Delta W}$$

where  $\Delta A$  is the decrease in absorbance  $A = \log T_0/T$ ,  $S$  is the area of the film in cm.<sup>2</sup>,  $M$  is the molecular weight and  $\Delta W$  is the weight loss in mg.  $T_0$  and  $T$  are the intensity of the incident and transmitted light, respectively. The dimensions of  $\epsilon$  are therefore cm.<sup>2</sup> per millimole. The weight loss has to be corrected first for the weight loss due to water which is derived from the decrease in the H<sub>2</sub>O deformation vibration at 1625 cm.<sup>-1</sup>. The extinction coefficient of this vibration has been determined by the same method using a pure Ca-montmorillonite film.

The spectra of adsorbed water were recorded against an empty cell in the reference beam, those of the adsorbed organic compound against a film of Ca-montmorillonite thus balancing to some extent the absorption due to the clay and the adsorbed water. This permitted a more accurate measurement of the absorption of the symmetrical methylene stretching vibration as it is no longer a shoulder on the strong absorption of the OH stretching vibrations.

The following experimental procedure was employed: After the spectra of the adsorbed ketone and the adsorbed water were recorded the sample cell was transferred into a dry-box, the atmosphere of which was swept with nitrogen dried over a column of Linde molecular sieve A4 and subsequently over P<sub>2</sub>O<sub>5</sub>. The clay film and the windows of the cell were heated overnight in a small oven to 120°. Immediately before and after heating, the film (weighing between 10 and 20 mg.) was weighed to  $\pm 0.01$  mg. on a Cahn electrobalance M 10. All these operations were carried out in the dry-box to prevent any uncontrolled changes in the water content of the sample. Since rehydration of the clay film occurs rapidly, immediately after reweighing the absorbance of the adsorbed water is recorded on the instrument already pre-set to 1625 cm.<sup>-1</sup>. The spectrum of the adsorbed ketone is subsequently determined.

The extinction coefficient of the adsorbed water is calculated from the measurements of pure Ca-montmorillonite films. It is used to correct the weight loss of the clay-organic complexes for the loss of water. The weight loss due to evaporation of the organic compound together with the decrease in the methylene absorption enable the extinction coefficient to be derived. The extinction coefficients of other vibrations of the adsorbed molecule are now calculated by comparison of the relative intensities. Unfortunately the extinction coefficient of the symmetrical methylene stretching vibration is small compared with those of the other vibrations, and this limits its usefulness regarding the determination of the latter.

All the given extinction coefficients are apparent ones since they are not corrected for finite resolution of the spectrometer.<sup>4</sup>

IV. **Calculation of Surface Coverage.**—The adsorption of the ketones on the clay surface takes place when the Ca-montmorillonite is completely dispersed in suspension and during the drying process. It is assumed therefore that the total area (800 m.<sup>2</sup>/g.) derived from the dimensions of the unit cell of the crystal lattice is available for adsorption.

(4) D. A. Ramsay, *J. Am. Chem. Soc.*, **74**, 72 (1952).

The area occupied by one ketone molecule is calculated from a drawing using the interatomic distances and van der Waals radii of Pauling<sup>2</sup> and considering an orientation of the ketone molecules with the plane of their carbon chain parallel to the clay surface.<sup>3</sup> The areas thus obtained are 50.2 and 71.5 Å.<sup>2</sup> for 2,5-hexanedione and 2,5,8-nonanetrione, respectively.

The amount of ketones adsorbed is determined by the absorbance of the symmetrical methylene stretching vibration (see preceding paragraph). The amount of clay is calculated from the total weight of the film by subtracting the amount of organic material and the amount of water, the determinations of which are given above.

Surface coverage is derived by considering a clay-organic contact on one side only of the organic molecule so that a 50% coverage corresponds to a complete one-layer complex, 100% to a complete two-layer complex, provided that the molecules are completely mobile on the silicate surfaces.<sup>6</sup>

V. X-Ray Measurements.—From the clay film on the glass slide an X-ray diffraction pattern was obtained with a Philips Norelco diffractometer with filtered Cu K $\alpha$  radiation at 40 kv., 15 ma. During the X-ray measurement the sample was kept under an atmosphere dried over P<sub>2</sub>O<sub>5</sub> at 0°.

## Results

I. Extinction Coefficient for the H<sub>2</sub>O Deformation Vibration (1625–1655 cm.<sup>-1</sup>).—The extinction coefficient of the H<sub>2</sub>O deformation vibration at 1625 cm.<sup>-1</sup> for adsorbed water was determined as 38.5  $\pm$  5. A more accurate determination of this value was considered to be unrealistic, because the vibrational frequency of this absorption shifts toward higher frequencies up to 1655 cm.<sup>-1</sup> with increasing surface coverage of the clay by the ketones and is probably also accompanied by a change in the extinction coefficient. A similar frequency increase with increasing surface coverage has been observed by Benesi and Jones<sup>7</sup> for water adsorbed on silica gel. The uncertainty in the extinction coefficient of adsorbed water is not critical with regard to the determination of the extinction coefficients of the adsorbed organic material so long as the weight loss due to water is small compared with the total weight loss.

However it is more critical with regard to the determination of the surface coverage. Fortunately in the samples with low organic and high water content, the absorption of the H<sub>2</sub>O deformation vibration is close to 1625 cm.<sup>-1</sup>, where the determined extinction coefficient should be appropriate.

II. Extinction Coefficient for the Vibrations of the Adsorbed Ketones.—The extinction coefficients for the symmetrical methylene stretching vibration (2913 cm.<sup>-1</sup>) were determined as 18.6 (mean of 4 values, standard deviation 0.9) for 2,5-hexanedione and to 37.3 (mean of 3 values, standard deviation 0.4) for 2,5,8-nonanetrione. These values are regarded as accurate to  $\pm 7\%$  as the weight loss due to water was usually less than 15% of the total weight loss. Since the ratio of the methylene groups in the two molecules is 1:2, these values agree excellently. The extinction coefficients for the same vibrations in solution are in a similar close agreement, 27.4 and 54, respectively.<sup>1</sup>

The heating treatment did not result in major spectral changes of the adsorbed ketones. Condensation to 1-methyl-cyclopentenone-3 and its derivatives or polycondensation may occur to a small extent since the sample turns slightly brownish and the spectra of the heated samples reveal a small sharp absorption at 1608 cm.<sup>-1</sup> in 2,5-hexanedione and 1621 cm.<sup>-1</sup> in 2,5,8-nonanetrione, values which lie in the range of C=C stretching vibrations in conjugated cyclic ketones.<sup>8,9</sup> M. Fétizon<sup>10</sup> reported the same frequency (1621 cm.<sup>-1</sup>) for 1-methyl-cyclopentenone-3 which he found as a major contaminant in his 2,5-hexanedione.

This condensation is neglected in the determination of the extinction coefficients, as it does not change the number of the methylene groups at all for 2,5-hexanedione or only slightly for 2,5,8-nonanetrione.

The extinction coefficients of the 1404, 1365 and the 1312 cm.<sup>-1</sup> (1325 cm.<sup>-1</sup>, respectively) vibrations of adsorbed 2,5-hexanedione and 2,5,8-nonanetrione are plotted against surface coverage in Figs. 1 and 2, these being the only extinction coefficients which could be measured with sufficient accuracy. The organic content of the clay-organic complex had to be adjusted so that the 2913 cm.<sup>-1</sup> absorption could be measured accurately to determine the amount of ketone present. Inevitably the absorbance of the carbonyl stretching vibrations at 1705 and 1690 cm.<sup>-1</sup>, having much higher extinction coefficients, were far too large to be measured meaningfully. The absorptions between 1200 and 1300 cm.<sup>-1</sup> could be measured but in this case the base line had to be drawn rather arbitrarily so that their extinction coefficients have only a qualitative value. Several examples of the extinction coefficients are given in Tables I and II.

TABLE I  
EXTINCTION COEFFICIENTS OF DIFFERENT COMPLEXES OF  
2,5-HEXANEDIONE WITH Ca-MONTMORILLONITE

$\nu$ (cm. <sup>-1</sup> )	$\theta$ (%)				
	6	26	46	64	92
2990	....	....	....	7	15
2913	18.6	18.6	18.6	18.6	18.6
1704	....	468	>275	>260	>230
1690	1020	540	>360	>260	>230
1404	322	208	158	141	118
1365	423	297	202	204	205
1312	353	191	125	95	64
1275	33	32	39	35	33
1243	....	....	34	28	34
1202	....	....	34	7	18
X-ray	One	One	One	One	Two + (+ two) one

III. X-Ray Data.—The spacings of the one- and two-layer complexes were reported earlier.<sup>3</sup> The amount of each type of complex present is estimated from the X-ray diffraction patterns, as described by Greenland.<sup>11</sup> In Figs. 1 and 2 these data are compared with the surface coverage determinations for 2,5-hexanedione and 2,5,8-nonanetrione, respec-

(8) R. N. Jones, P. Humphries, E. Packard and K. Dobriner, *J. Am. Chem. Soc.*, **72**, 86 (1950).

(9) R. F. Furchgott, H. Rosenkrantz and E. Shorr, *J. Biol. Chem.*, **163**, 375 (1946).

(10) M. Fétizon, H. Fritel and P. Baranger, *Compt. rend.*, **238**, 2542 (1954).

(11) D. J. Greenland, *J. Soil Sci.*, **7**, 319 (1956).

(5) L. Pauling, "The Nature of the Chemical Bond," Third edition, Cornell University Press, Ithaca, N. Y., 1960.

(6) Compare J. W. Jordan, *J. Phys. Colloid. Chem.*, **53**, 296 (1949).

(7) H. A. Benesi and A. C. Jones, *ibid.*, **63**, 179 (1959).

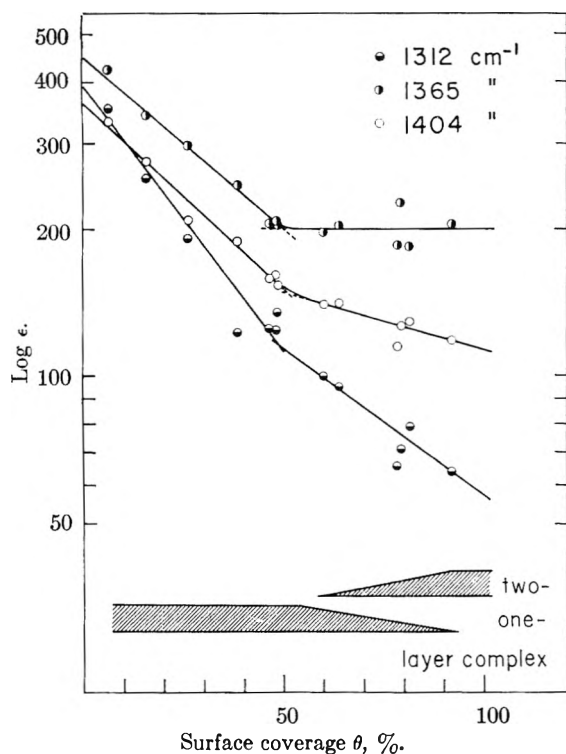


Fig. 1.—The dependence of extinction coefficients of adsorbed 2,5-hexanedione on surface coverage and type of complex.

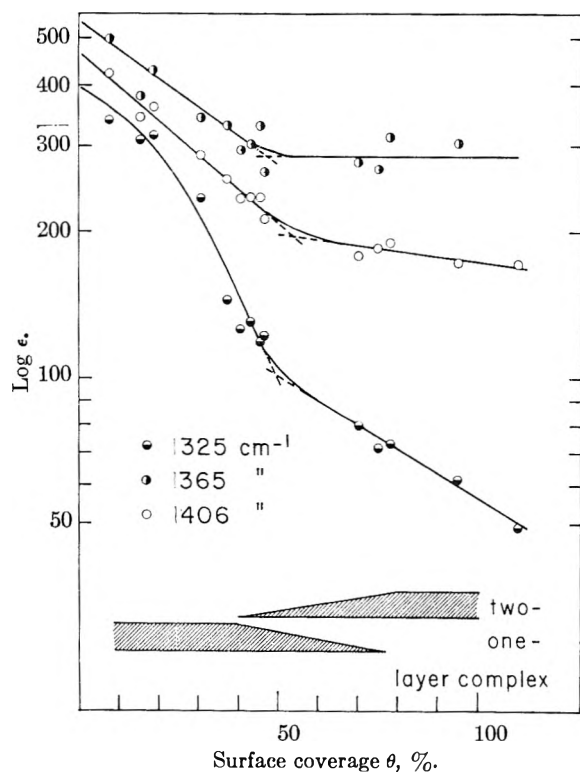


Fig. 2.—The dependence of extinction coefficients of adsorbed 2,5,8-nonanetrione on surface coverage and type of complex.

tively. The first appearance of the two-layer complex cannot be assigned precisely to a certain value of surface coverage, as only the presence of a larger amount of two-layer complex can be detected in

TABLE II  
EXTINCTION COEFFICIENTS OF DIFFERENT COMPLEXES OF  
2,5,8-NONANETRIONE WITH Ca-MONTMORILLONITE

$\nu$ ( $\text{cm}^{-1}$ )	$\theta$ (%)				
	7	30	43	70	95
2913	37.3	37.3	37.3	37.3	37.3
1704	..	500	>670	>330	>390
1690	1400	730	>670	>330	>390
1406	422	287	235	178	173
1365	498	341	302	287	304
1325	338	234	130	80	61
1268	Shoulder	Shoulder	67	Shoulder	Shoulder
1244	..	37	71	57	50
X-ray	One	One	One	Two + one	Two

the X-ray diffraction pattern. It can be assumed that traces of two-layer complex exist at lower surface coverage; only the *observed* phase region of the two-layer complex is marked in the figures.

The two-layer complex appears at 40% surface coverage for 2,5,8-nonanetrione and between 50 and 60% for 2,5-hexanedione. The latter value, by the definition of the surface coverage, (see Experimental section IV) is too high, as well as a surface coverage of 110% for a two-layer complex of 2,5,8-nonanetrione which shows no presence of free ketone in the X-ray pattern.

Therefore the surface coverage calculated in the manner described is probably too small by about 10%, which in turn may be due to an error in the calculated molecular cross-sections or to the uncertainty in the determination of the amount of water present.

## Discussion

### I. Layer Structure and Surface Coverage.—

If two clay plates, each having a surface coverage of 50%, settle out in contact with each other, they will form a one-layer complex only if the adsorbed molecules are completely mobile and able to key into each other. This is illustrated by Jordan<sup>6</sup> who reports for the *n*-alkylamines a transition from a one-layer complex to a two-layer complex at approximately 50% surface coverage. The appearance of two-layer complexes at lower surface coverages is an indication of a restriction of surface mobility.

For the adsorption of the ester of oleic acid and polyethylene glycol on Ca-Montmorillonite a value of 30% was found for the surface coverage at which a two-layer complex starts to form.<sup>2</sup> Comparing this with the above values of 40% for 2,5,8-nonanetrione and 50–60% for 2,5-hexanedione, it seems reasonable on the basis of the additivity of the Van der Waals forces that smaller molecules which are attached to the clay at fewer contact points should show a higher surface mobility. In the preceding study<sup>1</sup> it was concluded that the ketone molecules are not adsorbed in a random fashion, but that once a few molecules are adsorbed as nuclei, succeeding molecules are adsorbed in a manner similar to a crystallization process. Accordingly, a stage will be reached in the process of forming a one-layer complex, where the ketone-“crystallites” adsorbed on either side of the settling clay plates overlap to give an arrangement similar to a two-layer complex. The pressure exerted on the crystallites at the overlapping points will cause the

molecules to move until the crystallites key into each other and the final one-layer complex is formed. This motion can be thought of in either of two ways: (i) Single molecules may "jump" from one crystallite to the next one while the nuclei of the crystallites remain on the sites of high adsorption energy. (ii) Small crystallites may slide over sites of high adsorption energy by replacement of one molecule by its neighbor. In the second case again crystallites of large molecules will be more restricted in motion than those of short chain molecules.

**II. Infrared Absorption Intensities and Surface Coverage.**—The qualitative changes in the infrared spectra of the adsorbed ketones have already been discussed.<sup>1</sup> Both increases and decreases of extinction coefficients with different surface coverages are occasionally reported in the literature, mainly in recent years.

Eischens and co-workers<sup>12</sup> observed that desorption or oxidation of CO chemisorbed on Pt-surfaces lead to a non-linear decrease in the CO-absorbance, *i.e.*, to a change in the extinction coefficient. L. H. Little<sup>13</sup> reported a decrease in the extinction coefficient of ethylene chemisorbed on NiO and an increase after chemisorption on CuO with increasing surface coverage. Studies with many aromatic compounds and with butynediol adsorbed on AgI by Karagounis and Peter<sup>14,15</sup> have shown non-linear changes in relative intensities with changing surface coverage. They considered<sup>15</sup> the influence of the surface field on the aromatic ring adsorbed flat on the surface and concluded in agreement with their findings that the intensity of vibrations in the plane of the ring should be enhanced whereas out of plane vibrations should decrease.

De Boer<sup>16</sup> quotes that the ultraviolet absorption intensity of the first molecules of I<sub>2</sub> adsorbed on CaF<sub>2</sub> is up to 100 times larger compared with that of subsequently adsorbed molecules. He attributes this to adsorption on sites with electrostatic effects compared to subsequent adsorption due to van der Waals forces only. Folman and Yates<sup>17</sup> studied the adsorption of NH<sub>3</sub>, (CH<sub>3</sub>)<sub>2</sub>CO and CH<sub>2</sub>Cl<sub>2</sub> on porous glass. They observed exponential decreases in the extinction coefficient of the N-H stretching vibration and increase in that of the C-H stretching vibration with increasing surface coverage, and attributed these effects in accordance with De Boer<sup>16</sup> to asymmetric electric surface fields which polarize the adsorbed molecules leading to a different dipole change in the vibration, the square of which is proportional to the extinction coefficient. Molecules adsorbed at low surface coverages are adsorbed on the sites of highest adsorption energy, and therefore show the highest perturbation. Molecules adsorbed subsequently on sites of lower adsorption energy are less perturbed and have a smaller extinction coefficient. The resultant molar extinc-

tion coefficient is then the average over all molecular extinction coefficients.

This explanation given by Folman and Yates fits very well in the present situation since a similar exponential decrease in the extinction coefficient is found. Changes in the molecular arrangement should lead to a break in the log  $\epsilon(\theta)$ -function ( $\theta$  = surface coverage). The observed breaks (see Figs. 1 and 2) agree reasonably well with the appearance of the two-layer complex. The changes in slope of the log  $\epsilon(\theta)$ -function are as expected: In the one-layer complex the adsorbed molecule is perturbed by two clay-organic contacts; changes in adsorption energy lead to larger changes in the extinction coefficient than in the two-layer complex where the molecule is perturbed by only one clay-organic contact. The log  $\epsilon(\theta)$ -function has therefore a smaller slope in the two-layer complex.

The approach of Folman and Yates<sup>17</sup> does not consider the orientation of the vibration with regard to the surface. If it is assumed that the ketones are adsorbed with the plane of their aliphatic chain parallel to the clay surface,<sup>3</sup> then the vibrational vectors of the C-H deformation vibrations which are considered here, are also parallel to the surface. The decrease in extinction coefficient with increasing surface coverage shows that the highest perturbation leads to the highest absorption intensity. On the assumption that the vector of the electric surface field is perpendicular to the surface, these findings do not agree with the approach of Karagounis and Peter<sup>18</sup> who calculated the intensity change of an oscillator in an inhomogeneous electric field. They predict that vibrations with the vector of dipole change parallel to the surface should decrease in intensity with increasing field strength (in our case according to De Boer<sup>16</sup> with decreasing surface coverage) and that vibrations with their vector oriented perpendicular to the surface should increase, respectively.

The picture of Folman and Yates<sup>17</sup> indicates that the extinction coefficient is a function of the adsorbate-adsorbent interaction. The dependence of the extinction coefficient on the surface coverage could be used to derive a qualitative site energy distribution of the surface however resulting in a different site energy distribution for each vibration, according to how each vibration "sees" the adsorbent. This would be of particular interest in the clay-organic field because the best approach to determine site energy distributions—heat of wetting measurements<sup>19</sup>—is of limited application to clay-minerals, because of their large heat of swelling.<sup>20</sup> The approach based on extinction coefficients is very similar to that of heat of wetting measurements. If we define  $\epsilon_1$  as the apparent molar extinction coefficient of a molecule adsorbed on a surface element at a surface coverage of between  $\theta$  and  $\theta + d\theta$ , it is analogous to the differential heat of wetting which gives the heat of wetting of the same surface element. The integral heat of wetting is the sum over all "molecular" heats of wetting, whereas the observed extinction coefficient  $\epsilon$  is the mean

(12) R. P. Eischens, S. A. Francis and W. A. Pliskin, *J. Phys. Chem.*, **60**, 194 (1956).

(13) L. H. Little, *ibid.*, **63**, 1616 (1959).

(14) G. Karagounis and O. Peter, *Z. Elektrochem.*, **61**, 827 (1957).

(15) G. Karagounis and O. Peter, *ibid.*, **61**, 1094 (1957).

(16) J. B. De Boer, "Advances in Colloid Science," Interscience Publ. New York, N. Y., Vol. III, 1950, p. 1-66.

(17) M. Folman and D. J. C. Yates, *J. Phys. Chem.*, **63**, 183 (1959).

(18) G. Karagounis and O. Peter, *Z. Elektrochem.*, **63**, 1120 (1959).

(19) A. C. Zettlemoyer, *Chem. Revs.*, **59**, 974 (1959).

(20) J. J. Chessick and A. C. Zettlemoyer, "Advances in Catalysis," Vol. XI, Academic Press, New York, N. Y., 1959, pp. 263-299.

value of all "molecular" extinction coefficients  $\epsilon_i$  over  $\theta$ . Multiplying  $\epsilon$  with  $\theta$  therefore leads to an expression which corresponds to the integral heat of wetting but differs from it insofar as  $\theta$  is a function of the covered surface, whereas the heat of wetting is a measure of the uncovered surface. Just as differentiation of the integral heat of wetting with regard to  $\theta$  leads to the differential heat of wetting, so does differentiation of the expression  $\epsilon\theta$  yield the individual "molecular" extinction coefficient  $\epsilon_i$ :  $\epsilon_i = \epsilon + \theta(d\epsilon/d\theta)$ . A plot of  $\epsilon_i$  vs.  $\theta$  should be an indication of the site energy distribution as is an analogous plot of the differential heat of wetting.<sup>20</sup>

Chessick and Zettlemyer<sup>20</sup> attribute an exponential decrease in heat of wetting to a heterogeneous surface. Our observed exponential decrease in the extinction coefficients seems to indicate the same.

The observed decrease in the extinction coefficients is in some cases so large that the calculation of  $\epsilon_i$  in the described manner leads to negative values which of course have no physical meaning. The

derivation of  $\epsilon_i$  requires the same conditions as the determination of the site energy distribution from heat measurements.<sup>21</sup> The change in  $\epsilon$  should be due only to the different interaction of the adsorbate with the surface and not to any adsorbate-adsorbate interaction. Furthermore the adsorbed molecules should be distributed over the sites only according to the distribution of the adsorption energy. In our case where there is organic-organic interaction manifest in the spectra<sup>1</sup> it is probable that this causes a decrease of the  $\epsilon_i$  values by an unknown amount.

**Acknowledgment.**—Grateful acknowledgment is made to the donors of the Petroleum Research Fund, administered by the American Chemical Society for support of this research. The authors desire to thank Dr. L. G. Tensmeyer, Linde Company, Indianapolis Ind. for many helpful discussions.

(21) L. E. Drain and J. A. Morrison, *Trans. Faraday Soc.*, **48**, 316 (1952).

## SYNERGISTIC SURFACE TENSION EFFECTS FROM MIXTURES OF FLUORINATED ALCOHOLS WITH CONVENTIONAL WETTING AGENTS<sup>1</sup>

BY MARIANNE K. BERNETT AND W. A. ZISMAN

U. S. Naval Research Laboratory, Washington 25, D. C.

Received August 30, 1960

Aqueous solutions of any single, conventional hydrocarbon-derivative have surface tensions which never go below 26-27 dynes/cm., but certain synergistic mixtures of such wetting agents will depress the surface tension of water to around 22-24 dynes/cm. This investigation has demonstrated that small quantities of highly fluorinated insoluble alcohols, when added to conventional wetting agents, become solubilized in the micelles of the latter and can thus lower the surface tension of water well below any value obtainable by any mixture of unfluorinated compounds. These low surface tension values represent the closest possible packing of the fluorinated alcohol when adsorbed at the water-air interface. Where the solubilizing agent is not sufficiently water soluble, an increase in the solvent power of the continuous phase can be effected by adding a mutual solvent; the fluoro alcohol can then be solubilized to become effective in generating low surface tensions. Under the best conditions synergistic systems were produced having surface tensions of 15.2 dynes/cm. at 25° if a perfluoroalcohol was used, and 19.9 dynes/cm. if a  $\omega$ -monohydroperfluoroalkyl alcohol was used.

### Introduction

No single, pure, conventional wetting agent can lower the surface tension of its aqueous solution at 25° below 26 to 27 dynes/cm.<sup>2</sup> However, Miles and Shedlovsky<sup>3</sup> have shown that the surface tension of sodium dodecyl sulfate can be depressed considerably by the addition of small concentrations of dodecyl alcohol. Shedlovsky, Ross and Jacob<sup>4</sup> later reported a synergistic minimum surface tension of 22.6 dynes/cm. at 27° in a series of sodium dodecyl sulfonate solutions to which 0.5% dodecanol had been added. Burcik and Newman<sup>5</sup> found a minimum of 22.1 dynes/cm. at 25° when 7% dodecanol was present in solutions of sodium dodecyl sulfate.

Jarvis and Zisman,<sup>6</sup> in reviewing these and re-

lated investigations,<sup>7-15</sup> pointed out that the minimum surface tension at 25° obtainable by a mixture of a conventional wetting agent and a *n*-alkyl alcohol always falls between 22 and 24 dynes/cm. They explained the origin of this common synergistic minimum surface tension as follows: the sodium dodecyl sulfate is able to solubilize the insoluble dodecyl alcohol within its micelles; diffusion of the alcohol molecules from the micellar environment to the water-air interface results in an insoluble oriented monolayer consisting principally of dodecyl alcohol. The reported syner-

(6) N. L. Jarvis and W. A. Zisman, "The Stability and Surface Tension of Teflon Dispersions in Water," presented before Div. of Colloid Chemistry, A. C. S. Meeting, Atlantic City, Sept. 1959. NRL Report 5306, May 1959 (to be published).

(7) G. D. Miles, *J. Phys. Chem.*, **49**, 71 (1945).

(8) G. Nilsson and O. Lamm, *Acta Chem. Scand.*, **6**, 1175 (1952).

(9) O. Harva, *Rec. trav. chim.*, **75**, 101 (1956).

(10) A. Wilson, M. B. Epstein and J. Ross, *J. Colloid Sci.*, **12**, 345 (1957).

(11) J. Ross and M. B. Epstein, *J. Phys. Chem.*, **62**, 533 (1958).

(12) G. Nilsson, *ibid.*, **61**, 1135 (1957).

(13) W. M. Sawyer and G. M. Fowkes, *ibid.*, **62**, 159 (1958).

(14) A. N. Bose and V. K. Dixit, *Kolloid Z.*, **162**, 114 (1959).

(15) S. P. Harrold, *J. Phys. Chem.*, **63**, 317 (1959).

(1) Presented before the Division of Colloid Chemistry, American Chemical Society, at the 137th National Meeting in Cleveland, Ohio, April 11-14, 1960.

(2) E. K. Fischer and D. M. Gans, *Ann. N. Y. Acad. Sci.*, **46**, 373 (1946).

(3) G. D. Miles and L. Shedlovsky, *J. Phys. Chem.*, **48**, 57 (1944).

(4) L. Shedlovsky, J. Ross and C. W. Jacob, *J. Colloid Sci.*, **4**, 25 (1949).

(5) E. J. Burcik and R. C. Newman, *ibid.*, **9**, 498 (1954).



gistic minimum surface tension of from 22 to 24 dynes/cm. corresponds to the closest packing of the adsorbed monolayer of *n*-dodecyl alcohol. Jarvis and Zisman<sup>6</sup> pointed out that this minimum value should equal the free surface energy of any surface covered with close-packed *n*-alkyl chains, and showed it was equal to the critical surface tension of wetting ( $\gamma_c$ ) of a solid surface whose outermost composition consists of closely packed methyl groups.

A recent investigation by Bennett and Zisman<sup>16</sup> revealed that perfluoroparaffinic compounds having a hydrophilic terminal group adsorb from aqueous solution on clean polyethylene and, to a lesser extent, on polytetrafluoroethylene. This led them to propose that such fluorinated compounds, when added in low concentrations to an aqueous solution of a soluble aliphatic surface-active agent (such as sodium lauryl sulfate) would adsorb on the aliphatic chains of the polar molecules in the micelles formed by the latter compound and so would be solubilized. Some of these adsorbed fluorinated molecules would leave the micelles to diffuse into the liquid-air interface and thus lower the surface tension greatly. If the fluorinated molecule were a *n*-perfluoroalkanol, and if a high enough concentration of the fluorinated compound could in this way adsorb as a close-packed monolayer at the water-air interface, the minimum surface tension attainable would be expected to approximate the free surface energy of a close-packed film of perfluoromethyl groups. Since the value of  $\gamma_c$  of close-packed perfluoromethyl groups is approximately 6 to 8 dynes/cm.,<sup>17</sup> this would be the limiting synergistic minimum surface tension. If instead the compound were an  $\omega$ -monohydroperfluoroalkyl alcohol, the minimum surface tension would be expected to be around 15 dynes/cm.<sup>18</sup>

In this investigation the attempt was made to solubilize nearly insoluble surface-active perfluoro and  $\omega$ -monohydroperfluoro alcohols in micelles of a conventional, water-soluble, surface-active agent and to ascertain the minimum surface tension obtainable. The fluorinated alcohol (present in minor concentration) will hereafter be referred to briefly as the "wetting agent" and the conventional surface-active compound (the major additive agent) as the "solubilizing agent."

### Materials and Experimental Procedures

All but four of the pure solubilizing agents used have been described in a previous investigation.<sup>19</sup> The sodium myristyl sulfate and sodium cetyl sulfate used were specially prepared research samples free from any unsulfated alcohols which had been donated by L. Shedlovsky of the Colgate-Palmolive Company. The sulfosuccinates were specially purified research samples made available by J. K. Dixon of the American Cyanamid Company. The fluorinated polar compounds used have been described elsewhere by Ravner and co-workers<sup>20</sup> and by Bennett and Zisman.<sup>16</sup> In accordance with the established nomenclature,<sup>20</sup> the perfluoro

alcohols will be denoted as  $\phi'$ -alcohols and the  $\omega$ -monohydroperfluoro alcohols as  $\psi'$ -alcohols. Not previously used was the perfluoro *n*-decanol which was donated by J. W. Copenhaver of the Minnesota Mining and Manufacturing Company.

The aqueous solutions were prepared from water which had been triply distilled in a quartz still and had a conductivity when in equilibrium with the CO<sub>2</sub> in the air of  $1.0 \times 10^{-6}$  ohm<sup>-1</sup>. In order to dissolve the solute, it was found necessary in most instances to warm the solvent. When this measure did not suffice, a minor proportion of a mutual solvent such as methanol or isopropyl alcohol was added. The procedure employed by McBain and co-workers<sup>21</sup> of subsequently removing the alcohol solvent by evaporation or freeze-drying was tried but was not found advantageous. Instead, the small quantity of alcohol solvent was allowed to remain because the added surface tension depression of the dilute solutions used was insignificant. Where a combination of long chain solutes was employed, a mixture of water and methanol in a 1:1 ratio was used as solvent so as to increase the solvent power of the water.

Surface tensions were measured at 25° by the ring method using the Harkins and Jordan correction tables.<sup>22</sup> Since it was thought possible that metal ions from the platinum ring might react with the adsorbed monolayer formed by the fluorinated alcohols, which act as weak acids, the surface tensions of some solutions were also measured by the maximum bubble pressure method with the Cassel Tensiometer using glass tips<sup>23</sup>; results with the two methods differed by no more than  $\pm 1\%$ .

### Experimental Results and Discussion

Table I shows the experimental data obtained with combinations employing sodium di-*n*-octyl

TABLE I  
SURFACE TENSIONS OF AQUEOUS SOLUTIONS OF Na-di-*n*-OCTYL SULFOSUCCINATE AND HIGHLY FLUORINATED

Fluorinated alcohol	Total solutes, wt. %	Concentration Fluorinated alcohol, % of total solutes	ALCOHOLS AT 25°		Remarks
			Surface tension, dynes/cm. Soln. containing only NaOSS	Synergistic soln.	
$\psi'$ -C <sub>7</sub>	0.25	30.7	22.2	25.9	.....
$\psi'$ -C <sub>7</sub>	.25	18.2	23.3	25.9	.....
$\psi'$ -C <sub>7</sub>	.25	11.0	24.2	25.9	.....
$\psi'$ -C <sub>9</sub>	.50	10.0	19.9	24.3	.....
$\psi'$ -C <sub>9</sub>	.25	18.6	20.2	25.9	.....
$\psi'$ -C <sub>9</sub>	.25	14.5	20.6	25.9	.....
$\psi'$ -C <sub>9</sub>	.25	10.0	20.8	25.9	.....
$\psi'$ -C <sub>9</sub>	.25	4.6	23.0	25.9	.....
$\psi'$ -C <sub>11</sub>	.25	9.8	24.0	25.9	Some undissolved alc.
$\psi'$ -C <sub>11</sub>	.40	10.1	22.2	25.0	Some undissolved alc.
$\phi'$ -C <sub>8</sub>	.25	9.8	21.7	25.9	$\gamma$ drifts up with time

NOTE: C.m.c. of NaOSS = 0.30 g./l.<sup>23</sup>

sulfosuccinate (NaOSS) as the solubilizing agent and either of the two classes of fluorinated alcohols as the less soluble wetting agent. Table II gives the data obtained on using sodium lauryl sulfate (NaLS) as the solubilizing agent. Column 2 gives the sum of the concentrations of the solubilizing agent and the fluorinated wetting agent. Column 3 gives the concentration of the fluorinated additive expressed in weight per cent. of the total solutes. Columns 4 and 5 give the surface tension of the resulting solution and also that of the solution containing only the solubilizing agent in the same concentration as the total given in the second column. Comparison of these last two columns

(21) A. G. Brown, W. C. Thuman and J. W. McBain, *J. Colloid Sci.*, **8**, 491 (1953).

(22) W. D. Harkins and H. F. Jordan, *J. Am. Chem. Soc.*, **52**, 1751 (1930).

(23) E. F. Williams, N. T. Woodberry and J. K. Dixon, *J. Colloid Sci.*, **12**, 452 (1957).

(16) M. K. Bennett and W. A. Zisman, *J. Phys. Chem.*, **63**, 1911 (1959).

(17) E. F. Hare, E. G. Shafrin and W. A. Zisman, *ibid.*, **58**, 236 (1954).

(18) A. H. Ellison, H. W. Fox and W. A. Zisman, *ibid.*, **57**, 622 (1953).

(19) M. K. Bennett and W. A. Zisman, *ibid.*, **63**, 1241 (1959).

(20) P. D. Faurote, C. M. Henderson, C. M. Murphy, J. G. O'Rear and H. Ravner, *Ind. Eng. Chem.*, **48**, 445 (1956).



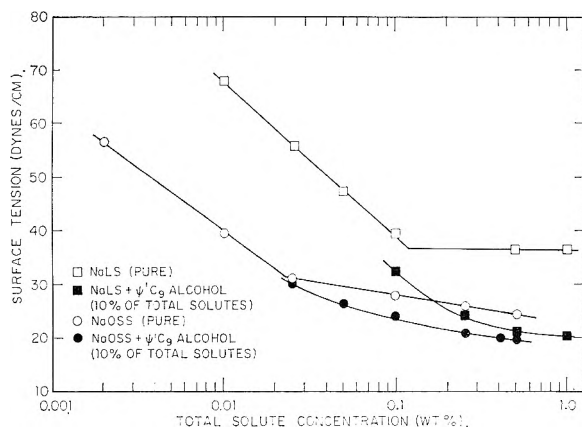


Fig. 1.—Surface tensions of aqueous solutions of either sodium lauryl sulfate or sodium di-*n*-octyl sulfosuccinate containing  $\psi'$ -nonyl alcohol.

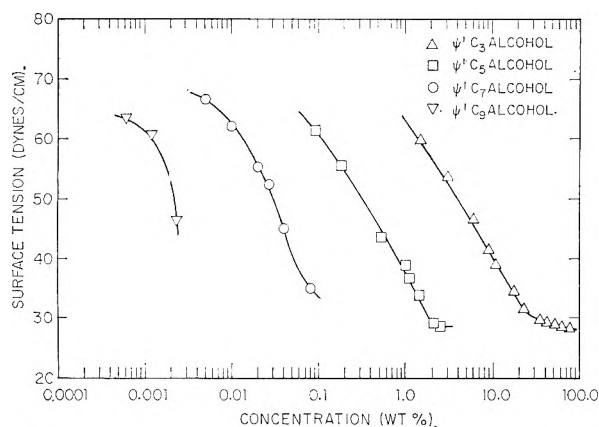


Fig. 2.—Surface tensions of  $\omega$ -monohydroperfluoro alcohols in aqueous solutions.

makes evident the surface tension depression effect of replacing some of the solubilizing agent by the fluorinated alcohol.

TABLE II

SURFACE TENSIONS OF AQUEOUS SOLUTIONS OF Na LAURYL SULFATE AND HIGHLY FLUORINATED ALCOHOLS AT 25°

Fluorinated alcohol	Concentration—		Syner- gistic soln.	Surface tension, dynes/cm.	Soln. containing only NaLS	Re- marks
	Total solute, wt. %	Fluorinated alcohol, % of total solute				
$\psi'$ -C <sub>3</sub>	1.0	10.1	20.3	36.4	..	
$\psi'$ -C <sub>9</sub>	0.5	10.1	21.6	36.4	..	
$\psi'$ -C <sub>9</sub>	.25	10.1	24.5	37.0	..	
$\psi'$ -C <sub>11</sub>	.5	10.7	27.0	36.4	a	
$\psi'$ -C <sub>11</sub>	.5	5.9	27.7	36.4	a	
$\psi'$ -C <sub>11</sub>	.25	11.1	32.7	37.0	a	
$\phi'$ -C <sub>6</sub>	1.0	10.3	26.3	36.4	a	
$\phi'$ -C <sub>6</sub>	0.5	10.3	30.7	36.4	a	
$\phi'$ -C <sub>8</sub>	1.0	7.0	21.8	36.4	a	
$\phi'$ -C <sub>8</sub>	1.0	5.0	23.1	36.4	a	
$\phi'$ -C <sub>8</sub>	0.5	5.0	26.2	36.4	a	
$\phi'$ -C <sub>10</sub>	0.5	10.3	30.2	36.4	a	

<sup>a</sup>  $\gamma$  drifts up with time.

It can be seen that the  $\psi'$ -nonanol ( $\psi'$ -C<sub>9</sub> alcohol), when used with either NaOSS or NaLS, is an effective surface tension depressant. When added in a concentration as small as 0.05% by weight (10% of the total solutes), it depressed the sur-

face tension below 20 dynes/cm., which is below the lowest value ever reported by any combination of conventional wetting agents alone. Figure 1 compares the curve of the surface tension of the aqueous solutions of NaOSS in which 10% of the total solute had been replaced by  $\psi'$ -C<sub>9</sub> alcohol and makes evident the large surface tension decrease caused by the added fluorinated alcohol. Combinations with NaLS as the solubilizing agent also prove that the  $\psi'$ -C<sub>9</sub> alcohol, when added in a concentration only one-tenth that of the total solutes, depressed the surface tension from 36.6 dynes/cm. to 20.3 dynes/cm. Figure 1 compares the synergistic depression in the surface tension *vs.* concentration curve of pure NaLS and NaOSS resulting from the addition of a minor concentration of  $\psi'$ -C<sub>9</sub> alcohol. It is seen that the synergistic effect begins at a concentration somewhat below the critical micelle concentration of the solubilizing agent. The c.m.c. of the mixed wetting agents is less sharply defined, which indicates that the c.m.c. of the solubilizing agent is altered by the addition of the fluorinated agent. Similar observations on the change of the c.m.c. by addition of paraffinic alcohols have been made previously.<sup>24</sup>

Since the  $\psi'$ -C<sub>9</sub> alcohol showed such promise as a synergistic surface tension depressant, measurements were made of the surface tensions of a series of pure  $\psi'$ -alcohols in aqueous solutions in various concentrations. Graphs are given in Fig. 2 of the surface tension *vs.* concentration for the first four members of the family of  $\psi'$ -alcohols; the  $\psi'$ -C<sub>9</sub> alcohol is too insoluble in water at 25° to lower the surface tension significantly. Because of the low solubility of the higher homologs and the fact that each solution had been prepared by warming the water to form a clear solution, these surface tension values at 25° drifted upwards with time of aging each solution. The time drift was particularly evident with the  $\psi'$ -C<sub>9</sub> and  $\psi'$ -C<sub>7</sub> alcohols except when observing the most dilute solutions. The rate of drift was smaller with the solutions of the  $\psi'$ -C<sub>5</sub> alcohol than with the higher homologs and it was almost negligible with the  $\psi'$ -C<sub>3</sub> alcohol solutions since this short-chain alcohol is the least adsorptive of them all, although some evaporation of its monolayer at the water-air interface does occur. ( $\psi'$ -C<sub>3</sub> alcohol is miscible with water in all proportions.) The lowest values of the surface tension recorded in Fig. 2 are therefore for initial values obtained on metastable solutions at 25°. These curves demonstrate the important fact that no pure  $\psi'$ -alcohol is soluble enough in water at 25° to depress the surface tension below 28 dynes/cm.; the solutions of  $\psi'$ -C<sub>7</sub> alcohol and  $\psi'$ -C<sub>9</sub> alcohol do not even reach values below 35 and 45 dynes/cm., respectively.

Inspection of Tables I and II shows that perfluoro *n*-octanol ( $\phi'$ -C<sub>8</sub> alcohol) is another effective synergistic surface tension depressant. Although the addition of this compound to each solubilizing agent caused the surface tension value of the resulting solution to drop considerably, it gradually drifted upwards until, after varying times

(24) S. H. Herzfeld, M. L. Corrin and W. D. Harkins, *J. Phys. Chem.*, **54**, 271 (1950).

according to the solution concentration, it appeared to be approaching the value exhibited by a solution containing only the solubilizing agent. Similar behavior was observed with  $\phi'$ -C<sub>6</sub> and  $\phi'$ -C<sub>16</sub> alcohols also, so that it is not believed that the time drift is caused by the tendency for the  $\phi'$ -alcohol to separate from mixed micelles to form alcohol homomicelles. This drift is illustrated in Fig. 3 which shows the behavior of a series of aqueous solutions of NaLS in various concentrations in which 5% by weight of the sulfate was replaced by  $\phi'$ -C<sub>8</sub> alcohol.

By changing the functional group of the fluorinated wetting agent from an alcohol to a carboxylic acid, the time drift in surface tension was eliminated; however, the change of functional group is a radical one since the perfluoro acids are very strong and are more soluble in water than the analogous perfluoro alcohols. Although the use of the  $\phi$ -C<sub>8</sub> acid as wetting agent in combination with either NaLS or NaOSS produced stable clear solutions, the resulting surface tension depression was only 5 compared to 15 dynes/cm. obtained with  $\phi'$ -C<sub>8</sub> alcohol. Previous investigations<sup>16,25,26</sup> have shown that the pure  $\phi$  acids in aqueous solution are soluble enough to be powerful surface tension depressants and form micelles in low concentrations. However, Klevens and Raison<sup>25</sup> found that a large proportion of the  $\phi$ -C<sub>8</sub> acid, at least 25% of the total solutes, was needed to appreciably lower the surface tension of solutions of NaLS. The  $\omega$ -monohydroperfluoro acids and their ammonium salts have also been shown previously<sup>16,27</sup> to be efficient surface tension depressants in aqueous solution and to form micelles at 20 and 25°. In mixed solutions of these compounds with the various solubilizing agents described here, only minor synergistic surface tension effects were observed. Therefore, it is concluded that such strong, fluorinated acids and their ammonium salts are not solubilized within the micelles of the solubilizing agents studied here, and no further studies of such compounds will be presented here.

Assuming a model in which the solubilizing agent (above its critical micelle concentration), forms spherical micelles with the polar groups outermost, it is possible that the fluorinated wetting agent is associated with the solubilizing agent to form spherical heteromicelles as indicated in Fig. 4. It had been established that the  $\psi'$ -C<sub>11</sub> alcohol is not as efficient a surface tension depressant as the  $\psi'$ -C<sub>9</sub> alcohol for either NaOSS or NaLS (Tables I and II). This was unexpected for it had seemed that the nearly equal chain lengths of the C<sub>11</sub> alcohol and the C<sub>12</sub> solubilizing agent would provide the best conditions for the adlineation of aliphatic chains in the spherical micelles. Since the  $\psi'$ -C<sub>9</sub> alcohol or  $\psi'$ -C<sub>7</sub> alcohol proved to be more effective, it would appear that a compromise is required for an optimum effect between obtaining maximum association by the chains adlineating between solubilizing and wetting agents and obtaining sufficient solubility of the wetting agent to allow mixed

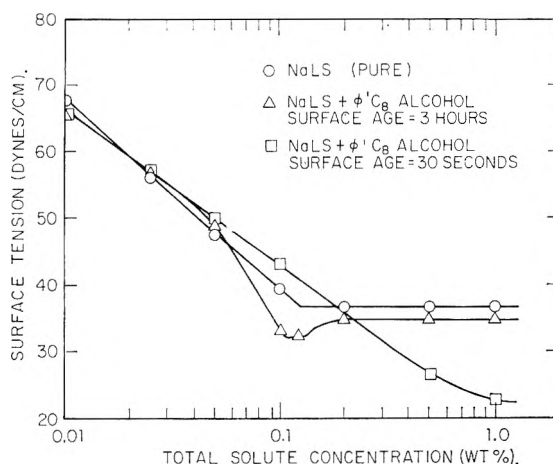


Fig. 3.—Surface tensions of aqueous solutions of sodium lauryl sulfate containing  $\phi'$ -octyl alcohol.

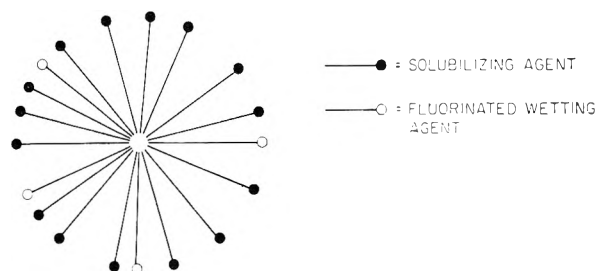


Fig. 4.—Model of mixed micelle.

micelles to form at all. Since  $\psi'$ -C<sub>7</sub> alcohol is the more soluble, it had to be added in larger proportions to be effective. Therefore,  $\psi'$ -C<sub>9</sub> alcohol is the most efficient surface tension depressant in this particular homologous series of alcohols.

The mechanism just described assumes that the solubilizing agent is present in a concentration higher than its c.m.c., since the micelles must be present in order to solubilize the fluorinated wetting agent. If the c.m.c. is too low, *i.e.*, if a given compound is too insoluble in water, it would not make a good solubilizing agent for the fluorinated agent because too few micelles would be present to have a significant effect in the solubility of the fluoroalcohol. Conversely, if the c.m.c. is too high, the quantity necessary to solubilize the fluoroalcohol would be so large as to become uneconomical. These points are exemplified in Table III. A homologous series of sulfosuccinates is used, from the di-*n*-lauryl to the di-*n*-butyl derivative. It can be seen that the higher homologs such as the di-*n*-lauryl and di-*n*-decyl sulfosuccinates are too insoluble at 25° to be useful.

The use of the more soluble lower homologs, however, proved to be very successful: by being able to solubilize enough fluorinated alcohol, they were capable of producing the lowest surface tensions achieved in this study. Thus, using NaBSS and  $\phi'$ -C<sub>8</sub> alcohol, the lowest value obtained was 15.2 dynes/cm. Although shortening the alkyl chains of the sulfosuccinate caused a lowering of the synergistic surface tension, the concentration of solubilizing agent required to produce this effect ultimately became very large; this high concentration in turn also necessitated the presence of a

(25) H. B. Klevens and M. Raison, *J. chim. phys.*, **51**, 1 (1954).

(26) H. M. Scholberg, R. A. Guenther and R. I. Coon, *J. Phys. Chem.*, **57**, 923 (1953).

(27) C. H. Arrington and G. D. Patterson, *ibid.*, **57**, 247 (1953).

TABLE III  
SURFACE TENSIONS OF AQUEOUS SOLUTIONS OF OTHER ALIPHATIC SOLUBILIZING AGENTS AND HIGHLY FLUORINATED ALCOHOLS AT 25°

Solution		Concentration		Surface tension, dynes/cm.			Remarks
Solubilizing agent S.A.	Fluorinated alcohol	Total solutes, wt. %	Fluorinated alcohol, % of total solutes	Synergistic soln.	Soln. containing only S.A.		
NaMS <sup>a</sup>	$\psi'$ -C <sub>11</sub>	0.20	20.0	27.5	37.3	Some solid residue: $\gamma$ drifts up with time	
NaMS <sup>a</sup>	$\psi'$ -C <sub>9</sub>	.20	20.2	23.7	37.3	Some solid residue; $\gamma$ drifts up with time	
NaLSS <sup>b</sup>	$\psi'$ -C <sub>11</sub>	.0125	10.0	40.7	45.4	Cloudy (both soln.)	
NaDSS <sup>c</sup>	$\psi'$ -C <sub>11</sub>	.0125	27.4	24.9	29.2	Ppt. forms on standing (both soln.)	
NaEHSS <sup>d</sup>	$\phi'$ -C <sub>8</sub>	1.0	22.9	17.6	26.3	$\gamma$ drifts up with time	
NaEHSS <sup>d</sup>	$\phi'$ -C <sub>8</sub>	1.0	27.8	17.6	26.3	$\gamma$ drifts up slowly with time	
NaHSS <sup>e</sup>	$\phi'$ -C <sub>8</sub>	1.0	24.3	16.7	28.8	$\gamma$ drifts up very slowly	
NaASS <sup>f</sup>	$\phi'$ -C <sub>8</sub>	4.0	19.5	15.4	29.8	.....	
NaBSS <sup>g</sup>	$\phi'$ -C <sub>8</sub>	8.0	17.8	15.2	33.2	.....	

<sup>a</sup> NaMS = Na myristyl sulfate. <sup>b</sup> NaLSS = Na di-*n*-lauryl-sulfosuccinate. <sup>c</sup> NaDSS = Na di-*n*-decyl-sulfosuccinate. <sup>d</sup> NaEHSS = Na di-(ethyl-hexyl)-sulfosuccinate (c.m.c. = 1.12 g./l.<sup>23</sup>). <sup>e</sup> NaHSS = Na di-*n*-hexyl sulfosuccinate (c.m.c. = 4.8 g./l.<sup>23</sup>). <sup>f</sup> NaASS = Na di-*n*-amyl-sulfosuccinate (c.m.c. = 19.2 g./l.<sup>23</sup>). <sup>g</sup> NaBSS = Na di-*n*-butyl-sulfosuccinate (c.m.c. = 67 g./l.<sup>23</sup>).

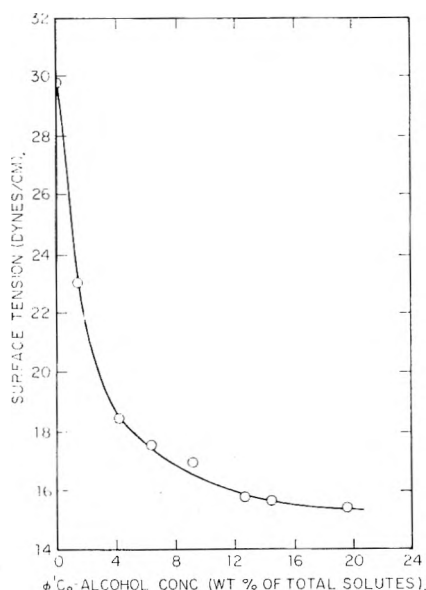


Fig. 5.—Surface tension of a 4% aqueous solution of sodium di-*n*-amyl sulfosuccinate containing various concentrations of  $\phi'$ -octyl alcohol.

comparatively large concentration of the fluorinated alcohol. Figure 5 demonstrates the dependence of the synergistic surface tension lowering on the concentration of the fluorinated alcohol present. By holding constant the concentration of total solutes and varying only the concentration of  $\phi'$ -C<sub>8</sub> alcohol replacing part of the NaASS, successively lower surface tensions were obtained, until a minimum value of 15.4 dynes/cm. was reached. However, the total concentration necessary to produce this lowest value was 4%, and about 20% of this amount, *i.e.*,  $2.25 \times 10^{-2}$  moles/l., consisted of the  $\phi'$ -C<sub>8</sub> alcohol.

A study was also made of the combination of NaASS and  $\phi'$ -C<sub>10</sub> alcohol in which the  $\phi'$ -C<sub>10</sub> alcohol concentration was held constant and the concentration of NaASS was varied. In order to solubilize the proper amount of  $\phi'$ -C<sub>10</sub> alcohol necessary to effect a sizable surface tension depression, a large amount of NaASS had to be used, as can be seen in the last row of Table V.

On comparing the results obtained with the vari-

ous sulfosuccinates combined with  $\phi'$ -C<sub>8</sub> alcohol (Table III), it becomes evident that if one wishes to depress the surface tension to not less than 17 dynes/cm., the most efficient combinations in terms of the concentration of both solubilizing and wetting agent are those involving either NaHSS or NaEHSS. When the same considerations are applied to the alkyl sulfate series, the most efficient combinations are provided by the NaLS. Where it is necessary to decrease the surface tension to its lowest possible value (about 15.2 dynes/cm.), a more soluble micelle-forming agent is required, such as NaASS. However, solutions have to be prepared in higher concentrations of the solubilizer, and the attendant concentrations of the fluorinated alcohols are also necessarily higher.

Inspection of Table III shows that combinations of higher homologs of the solubilizing agent with a  $\psi'$ -C<sub>11</sub> alcohol were not effective. Either the solubilizing agent or the wetting agent, or both, did not dissolve completely. Therefore, addition of a few per cent. by volume of a mutual solvent, methanol, was used to bring both addition agents into intimate molecular contact before adding water. The resulting solutions were clear and free of any precipitate or colloidal dispersions. Various combinations prepared by this procedure are given in Table IV. It can be seen that under such circumstances the  $\psi'$ -C<sub>11</sub> alcohol is about as efficient a synergist as the  $\psi'$ -C<sub>9</sub> alcohol when added to sodium myristyl sulfate (NaMS). The above is in good agreement with the suggested model of a spherical mixed micelle in which the molecules of the aliphatic solubilizing agent should be effective if sufficiently soluble in the aqueous solution. Table IV also shows that the addition of methanol or isopropyl alcohol as a mutual solvent resulted in lower surface tensions with NaLS and NaOSS in synergistic combinations. Thus, a value of 18.4 dynes/cm. was observed with the combination of NaOSS,  $\phi'$ -C<sub>8</sub> alcohol, and CH<sub>3</sub>OH and 19.1 dynes/cm. with the combination of NaLS,  $\phi'$ -C<sub>8</sub> alcohol and CH<sub>3</sub>OH. However, an increase in surface tension with time was always obtained with any combinations involving the  $\phi'$ -C<sub>8</sub> alcohol except when it was present in very high concentra-

TABLE IV

SURFACE TENSIONS OF AQUEOUS SOLUTIONS OF SOLUBILIZING AGENTS AND HIGHLY FLUORINATED ALCOHOLS PREPARED WITH MUTUAL SOLVENT AT 25°

Solubilizing agent, S.A.	Solution		Concentration		Surface tension, dynes/cm.		Remarks
	Fluorinated alcohol	Mutual solvent	Total solutes, wt. %	Fluorinated alcohol, % of total solutes	Synergistic soln.	Soln. containing only S.A.	
NaCS <sup>a</sup>	$\psi'$ -C <sub>9</sub>	CH <sub>3</sub> OH	0.1	15.0	30.2	36.5	Ppts., $\gamma$ drifts up with time
NaCS <sup>a</sup>	$\psi'$ -C <sub>11</sub>	CH <sub>3</sub> OH	.05	15.0	32.5	36.5	Ppts.
NaCS <sup>a</sup>	$\phi'$ -C <sub>8</sub>	CH <sub>3</sub> OH	.2	20.0	32.4	36.5	Ppts., $\gamma$ drifts up with time
NaCS <sup>a</sup>	$\phi'$ -C <sub>10</sub>	CH <sub>3</sub> OH	.1	18.2	32.4	36.5	Ppts., $\gamma$ drifts up with time
NaMS <sup>b</sup>	$\psi'$ -C <sub>9</sub>	CH <sub>3</sub> OH	.20	21.2	22.9	37.3	$\gamma$ drifts up with time
NaMS <sup>b</sup>	$\psi'$ -C <sub>11</sub>	CH <sub>3</sub> OH	.20	18.2	23.5	37.3	Surface detaches slowly
NaMS <sup>b</sup>	$\psi'$ -C <sub>11</sub>	CH <sub>3</sub> OH	.20	9.8	24.9	37.3	Surface detaches slowly
NaMS <sup>b</sup>	$\phi'$ -C <sub>8</sub>	CH <sub>3</sub> OH	.20	19.5	24.6	37.3	$\gamma$ drifts up with time
NaMS <sup>b</sup>	$\phi'$ -C <sub>10</sub>	CH <sub>3</sub> OH	.20	19.2	27.3	37.3	$\gamma$ drifts up with time
NaLS <sup>c</sup>	$\psi'$ -C <sub>11</sub>	CH <sub>3</sub> OH	.50	22.8	24.1	36.4	Surface detaches slowly
NaLS <sup>c</sup>	$\psi'$ -C <sub>11</sub>	Isoprop.	.50	21.6	23.0	36.4	Surface detaches slowly
NaLS <sup>c</sup>	$\phi'$ -C <sub>8</sub>	CH <sub>3</sub> OH	.50	21.6	19.1	36.4	$\gamma$ drifts up with time
NaLS <sup>c</sup>	$\phi'$ -C <sub>8</sub>	Isoprop.	.50	18.2	21.1	36.4	$\gamma$ drifts up with time
NaLS <sup>c</sup>	$\phi'$ -C <sub>8</sub>	$\phi'$ -C <sub>2</sub> alc.	.50	19.7	22.1	36.4	$\gamma$ drifts up with time
NaOSS <sup>d</sup>	$\phi'$ -C <sub>8</sub>	CH <sub>3</sub> OH	.50	18.7	18.4	24.3	$\gamma$ drifts up with time

<sup>a</sup> NaCS = Na cetyl sulfate. <sup>b</sup> Same as *a* in Table III. <sup>c</sup> NaLS = Na lauryl sulfate. <sup>d</sup> NaOSS = Na di-*n*-octyl sulfosuccinate.

TABLE V

SURFACE TENSIONS OF AQUEOUS SOLUTIONS OF SOLUBILIZING AGENTS AND HIGHLY FLUORINATED ALCOHOLS PREPARED WITH LARGE AMOUNTS OF MUTUAL SOLVENT AT 25°

Solvent: H<sub>2</sub>O:CH<sub>3</sub>OH = 1:1 ( $\gamma$  = 34.2 dynes/cm.)

Solubilizing agent, S.A.	Solution		Concentration		Surface tension, dynes/cm.		Remarks
	Fluorinated alcohol	Total solutes, wt. %	Fluorinated alcohol, % of total solutes	Synergistic soln.	Soln. containing only S.A.		
NaCS <sup>a</sup>	$\phi'$ -C <sub>10</sub>	0.1	21.7	23.6	34.2		
NaCS <sup>a</sup>	$\phi'$ -C <sub>10</sub>	.1	25.3	20.3	34.2	Gelatinous ppt. on long storage	
NaCS <sup>a</sup>	$\psi'$ -C <sub>11</sub>	.1	16.6	22.8	34.2		
NaCS <sup>a</sup>	$\psi'$ -C <sub>11</sub>	.1	26.2	22.8	34.2		
NaMS <sup>b</sup>	$\phi'$ -C <sub>10</sub>	.2	24.7	17.1	34.2	Gelatinous ppt. on long storage	
NaMS <sup>b</sup>	$\psi'$ -C <sub>11</sub>	.2	16.6	23.2	34.2		
NaMS <sup>b</sup>	$\psi'$ -C <sub>11</sub>	.2	25.9	23.2	34.2		
NaLS <sup>c</sup>	$\phi'$ -C <sub>10</sub>	.5	12.1	22.1	33.5		
NaLS <sup>c</sup>	$\phi'$ -C <sub>10</sub>	.5	22.2	19.5	33.5		
NaASS <sup>d</sup>	$\phi'$ -C <sub>10</sub>	6.0	3.6	16.8	28.8	Gelatinous ppt. on long storage	

NOTE: Surface tensions of all solutions rise with time, because of CH<sub>3</sub>OH evaporation.

<sup>a</sup> Same as *a* in Table IV. <sup>b</sup> Same as *a* in Table III. <sup>c</sup> Same as *c* in Table IV. <sup>d</sup> Same as *f* in Table III.

tions. (The cause will later be identified as evaporation of the  $\phi'$ -C<sub>8</sub> alcohol.)

Since it had been demonstrated that synergistic combinations of higher homologs were made possible by increasing the solvent power of the continuous phase, an even greater increase was effected by using a solvent consisting of water and methanol in a volume ratio of 1:1. Table V shows the surface tensions thus obtained. The surface tension of the solvent mixture by itself is 34.2 dynes/cm. at 25°, and the surface tensions of the pure solubilizing agents quoted in column 6 were measured in this same medium. The data show that very low surface tensions could thus be obtained using long-chain hydrocarbon derivatives which were too insoluble in pure water. Again  $\phi'$ -C<sub>10</sub> alcohol proved to be very effective; it could depress the surface tension of a long-chain hydrocarbon, NaMS, to a low value of 17.1 dynes/cm. and that of a short chain one, NaASS, to 16.8 dynes/cm. After long storage, a gelatinous phase separated out at the bottom of each solution; however, this phase could be redissolved by gently reheating the mixture.

The upward drift in surface tension with time during the measurements in all of these synergistic combinations was shown to result from the evaporation of the methanol from the solvent phase.

Using solutions containing only water as the solvent phase, the following experiments were intended to ascertain if the upward time drift in the surface tension with solutions of  $\phi'$ -C<sub>8</sub> alcohol mentioned earlier was caused by evaporation of adsorbed  $\phi'$ -C<sub>8</sub> alcohol molecules from the water-air interface. The  $\phi'$ -C<sub>8</sub> alcohol has a significantly higher vapor pressure than that of either  $\psi'$ -C<sub>9</sub> alcohol or  $\psi'$ -C<sub>7</sub> alcohol. This was demonstrated by suspending one crystal of  $\psi'$ -C<sub>9</sub> alcohol or a drop of either  $\psi'$ -C<sub>7</sub> or  $\phi'$ -C<sub>8</sub> alcohols close to but above the clean surface of water in a hydrophil tray. By using fine particles of Teflon powder to serve as "indicator powder" instead of the usual talc or lycopodium powder, the adsorptivity of each fluorinated alcohol vapor on the water and the resulting spreading of the adsorbed film was readily observed. It thus appears probable that because of its much higher vapor pressure, the  $\phi'$ -C<sub>8</sub> alcohol

monolayer evaporates faster from the surface of the water than the monolayers of the  $\psi$ -C<sub>7</sub> or  $\psi$ -C<sub>9</sub> alcohols. In agreement with this interference, the solution which lost its synergistic decrease in surface tension earliest was the one containing the lowest concentration of the perfluoroalkanol.

Accordingly, the storage stability of solutions containing various synergistic combinations was investigated. Surface tension measurements were made on several apparently stable solutions which had been stored in closed Pyrex flasks for 6 months at 20 to 25°. The surface tensions of these solutions did not change with aging under these conditions. Upon then leaving these flasks open to the atmosphere, the solutions which had reached equilibrium immediately, such as combinations of NaLS or NaOSS with the  $\psi$ -C<sub>9</sub> and  $\psi$ -C<sub>7</sub> alcohol, still acted the same; however, solutions which had originally exhibited time drifts, such as combinations containing the  $\phi$ '-C<sub>6</sub> and  $\phi$ '-C<sub>8</sub> alcohols, again exhibited time drifts which started at essentially the same low values as freshly prepared solutions. Therefore, all solutions prepared with these synergistic combinations were stable when kept in closed vessels, and the time drifts in surface tension observed with the solutions containing the perfluoroalkyl alcohol were caused by the evaporation of adsorbed perfluoro alcohol film from the surface of the water.

The lowest synergistic surface tension in the entire investigation (15.2) was attained with the  $\phi$ '-C<sub>8</sub> alcohol. Such a surface tension should correspond to that of water covered with an adsorbed monolayer of  $\phi$ '-C<sub>8</sub> alcohol in its closest possible packing. However, a stable monolayer of a liquid compound cannot be compressed below the equilibrium spreading pressure (e.s.p.). Therefore, the lowest steady-state surface tension attainable should be equal to the surface tension of pure water minus the value of the equilibrium spreading pressure of the  $\phi$ '-C<sub>8</sub> alcohol at 25°. In order to verify this hypothesis, the equilibrium spreading pressure of  $\phi$ '-C<sub>8</sub> alcohol and  $\phi$ '-C<sub>6</sub> alcohol each were measured by the method of Washburn and Keim<sup>28</sup> on a Langmuir-Adam film balance of Pyrex glass using a substrate of triply distilled water adjusted to *pH* 2 with sulfuric acid. A monolayer of eicosyl alcohol was used as the "piston film." For the  $\phi$ '-C<sub>6</sub> alcohol the e.s.p. determined at 25° is 46.2 dynes/cm. Using 72.0 dynes/cm. as the surface tension of water, a minimum surface tension of 25.8 dynes/cm. is obtained for  $\phi$ '-C<sub>6</sub> alcohol, in good agreement with the minimum surface tension of 26.3 dynes/cm., observed from the aqueous solution in which  $\phi$ '-C<sub>6</sub> alcohol was added as the wetting agent (see Table II). The e.s.p. value of  $\phi$ '-C<sub>8</sub> alcohol was more difficult to determine because of the necessary high collapse pressure of the piston film and the semi-solid state of the  $\phi$ '-C<sub>8</sub> alcohol. However, the calculated minimum surface tensions, 14-17 dynes/cm. are close to the observed values of 15.2-15.4 dynes/cm. Thus, it can be inferred that the synergistic minima found represent the lowest values theoretically attain-

able in an aqueous system by the adsorption of the respective fluoroalkanol.

A saturated aqueous solution of  $\phi$ '-C<sub>8</sub> alcohol had a surface tension at 25° only a few dynes/cm. lower than that of pure water. However, when a drop of pure  $\phi$ '-C<sub>8</sub> alcohol was spread on the surface of this solution, the surface tension was lowered to 21.3 dynes/cm. It will be noted that the surface tension did not go as low as 15.4 dynes/cm., the lowest synergistic surface tension reported in Fig. 5, because the evaporation of the fluorinated alcohol from the surface of the water was not being compensated for by the adsorption of  $\phi$ '-C<sub>8</sub> alcohol molecules from the solution phase; hence, a less closely packed film resulted. When the surface of a solution containing a synergistic combination of NaLS and  $\phi$ '-C<sub>8</sub> alcohol was scraped clean with sliding Teflon barriers in a Teflon hydrophil tray and the surface tension was measured immediately thereafter, the resulting value was 23 dynes/cm. which is not far from the minimum of 21.8 given in Table II. Repetition of the process of scraping the water surface clean of any adsorbed film always resulted in the same surface tension. Therefore, it is concluded that in an open system the rate at which the  $\phi$ '-C<sub>8</sub> alcohol molecules were able to be released from the mixed micelle and diffuse to and adsorb at the water-air interface could not compensate enough for the  $\phi$ '-C<sub>8</sub> alcohol molecules lost from the surface phase by evaporation to allow a steady-state equivalent to that of an adsorbed film at the equilibrium spreading pressure.

Some exploratory experiments were carried out with solubilizing compounds other than aliphatic anionic agents. Representative compounds examined were the cationic wetting agent, cetyl trimethylammonium bromide and the non-ionic wetting agent, nonylphenoxy polyoxyethylene-ethanol (Igepal CO-850). In addition the aromatic anionic agents, sodium *p*-decyl benzene sulfonate and sodium dinonylnaphthalene sulfonate, were also examined. The surface tension depressions through addition of fluorinated alcohols to any of these solubilizing agents were only a few dynes/cm. in each instance and thus did not compare favorably with those obtained by the NaLS or NaOSS; obviously further investigation of other homologs or compounds is required.

Instead of a conventional surface-active compound as the solubilizing agent, an amphipathic fluorinated compound can be used. A combination of the ammonium salt of the  $\psi$ -C<sub>9</sub> acid used with  $\psi$ -C<sub>9</sub> alcohol was quite effective as a synergistic combination for lowering the surface tension, but was too insoluble for optimum use. The  $\psi$ -C<sub>7</sub> alcohol was more soluble and proved to be equally efficient. Unfortunately, both combinations were not sufficiently soluble and eventually they formed gelatinous precipitates.

These studies have resulted in the following conclusions: (a) the nearly insoluble fluorinated alcohols can be solubilized in micelles of a conventional wetting agent. (b) Surface tension values much below 22 dynes/cm. can be obtained by addition of small concentrations of fluorinated alcohols

(28) E. R. Washburn and C. P. Keim, *J. Am. Chem. Soc.*, **62**, 1747 (1940).

to an aliphatic anionic wetting agent, the minimum surface tension obtainable with the synergistic combinations studied being 15.2 dynes/cm. (c) The lowest values represent the closest possible packing of the fluorinated alcohol when adsorbed at the water-air interface under their equilibrium spreading pressures. (d) The transitory low values of the  $\phi'$ -alcohols observed in open vessels, especially when low concentrations are used, are caused

by the evaporation of the fluorinated monolayer adsorbed at the water-air interface. In closed systems, the synergistic surface tensions are not transitory. (e) In cases where the anionic solubilizing agent is not sufficiently soluble in water, increasing the solvent power of the continuous phase by adding a mutual solvent makes it possible to solubilize the fluoroalcohols and so to obtain synergistic surface tension depressions.

## SPECIES OF COBALT(II) IN ACETIC ACID. PART I. COBALTOUS ACETATE IN THE PRESENCE OF WATER AND OF SODIUM ACETATE

By P. J. PROLL, L. H. SUTCLIFFE AND J. WALKLEY

*Department of Inorganic and Physical Chemistry, University of Liverpool, Liverpool, England*

*Received August 29, 1960*

The reversible variations of the visible spectrum of cobaltous acetate in anhydrous acetic acid with temperature and the effect of sodium acetate and of water have been studied over the temperature range 25 to 64°. From ion migration and spectrophotometric measurements the ionic species present under these conditions are postulated to be  $\text{CoOAc}^+$ ,  $\text{Co(OAc)}_2$ ,  $\text{Co(OAc)}_3^-$ ,  $\text{Co(OAc)}_4^{2-}$ , the latter pair being favored by the addition of sodium acetate and increase of temperature while the former pair are favored by the addition of water. Evidence is put forward for solvated  $\text{Co(OAc)}_2$  or  $\text{Co(OAc)}_4^{2-}$  being the reactive species in reactions in which cobaltous acetate is used as a catalyst.

### Introduction

It has previously been reported that several oxidation-reduction reactions between metal acetates in anhydrous acetic acid occur at measurable rates.<sup>1</sup> Two of these, namely, the cerous acetate-plumbic acetate<sup>2</sup> and the cobaltous acetate-plumbic acetate<sup>3</sup> reactions have been reported in detail. During the investigation of the latter an interesting postulation was necessary to explain the kinetic scheme, namely that a dimeric form of cobaltous acetate is present. In addition, the observations were made that (a) the kinetics of the reaction were affected by sodium acetate and by water, and (b) during the addition of sodium acetate or on heating the anhydrous solutions the pink-red color turned to blue—the heating effect being reversible.

Cobaltous acetate has been used by many workers in the field of autooxidation reactions as an important catalyst. However, little attention has been directed to the detailed role of this catalyst.<sup>4</sup> It was therefore decided to make a complete spectrophotometric investigation of cobaltous acetate in acetic acid under as wide a variety of conditions as possible. This first paper of the series deals with the solutions of the salt alone and in the presence of water and of sodium acetate. Future papers will deal with the effect of lithium bromide and chloride to this system since cobaltous bromide is an important autooxidation catalyst.

### Experimental

**Acetic Acid.**—Analytical reagent (A.R.) quality acetic acid was purified by refluxing with finely divided A.R. chromium trioxide along with a calculated amount of A.R.

acetic anhydride to remove the water, this amount being estimated from freezing point measurements.<sup>5</sup> After distillation, any excess water or acetic anhydride was determined by a spectrophotometric method<sup>6</sup> and removed. The acetic acid was then refluxed with commercial cobaltous acetate and fractionated with a column packed with Fenske helices.

**Cobaltous Acetate.**—Solutions of known concentrations were made by refluxing 99.95% pure cobalt sponge (Johnson Matthey Ltd.) with acetic acid purified as described above.

**Sodium Acetate.**—A.R. quality sodium acetate was recrystallized twice from anhydrous acetic acid and then dried under a vacuum for 24 hours at 100°.

**Ion Migration Experiments.**—The migration cell consisted of a W-shaped vessel having three compartments isolated from one another by sintered glass discs. The solution under investigation was placed in the central compartment and the solvent in the outer compartments. Five hundred v.d.c. was applied to platinum foil electrodes situated in the two outer limbs of the cell. Current was passed for 20 hours and then the polarity reversed, and current passed for a further 20 hours. The cobalt(II) concentrations in the anode and cathode compartments were determined spectrophotometrically.

**Spectrophotometry.**—All measurements were made by means of a Unicam S.P. 500 spectrophotometer fitted with a thermostated cell compartment enabling temperatures of all the solutions to be maintained to within  $\pm 0.05^\circ$ .

### Results and Discussion

**Ion Migration.**—Ion migration experiments on cobaltous acetate solutions<sup>3</sup> led to the conclusion that there are four likely species, namely,  $\text{CoOAc}^+$ ,  $\text{Co(OAc)}_2$ ,  $\text{Co(OAc)}_3^-$ ,  $\text{Co(OAc)}_4^{2-}$ . The first being favored by the addition of water and the last two by the addition of acetates or the application of heat.

**Spectrophotometry.**—The spectrum of cobaltous acetate in anhydrous acetic acid is shown in Fig. 1, at five temperatures in the range 25 to 64°. As can be seen it has a d-d transition band (526 to 538  $m\mu$ ) in the visible region and a charge transfer band (310  $m\mu$ ) in the ultraviolet region. The

(1) L. H. Sutcliffe and J. Walkley, *Nature*, **178**, 999 (1956).

(2) D. Benson and L. H. Sutcliffe, *Trans. Faraday Soc.*, **56**, 246 (1960).

(3) D. Benson, P. J. Proll, L. H. Sutcliffe and J. Walkley, *Disc. Faraday Soc.*, **29**, 60 (1960).

(4) H. S. Blanchard, *J. Am. Chem. Soc.*, **82**, 2014 (1960).

(5) De Visser, *Rec. trav. chim.*, **12**, 101 (1893).

(6) S. Bruckenstein, *J. Am. Chem. Soc.*, **78**, 1921 (1956).



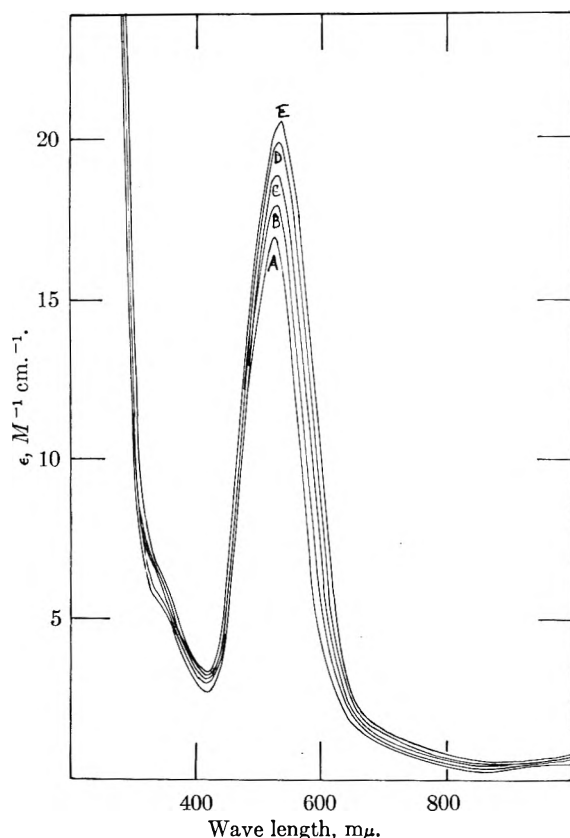


Fig. 1.—The absorption spectrum of cobaltous acetate in anhydrous acetic acid at the temperatures: A, 25.0°; B, 38.0°; C, 47.8°; D, 58.7°; E, 64.0°.

Beer-Lambert law is obeyed over the whole spectrum to within  $\pm 1\%$  over the concentration range  $5 \times 10^{-3}$  to  $5 \times 10^{-2} M$ . It was noticed, however, that different samples of cobaltous acetate did not always have the same maximum to minimum ratio; this ratio being variable from 5:1 to 10:1 depending on the method of purification of the salt. Commercial  $\text{Co}(\text{OAc})_2$  recrystallized at least three times had a large value of this ratio, as do crystals taken after refluxing cobalt metal sponge with acetic acid. These crystals are distinct from a powdery "sludge" which also appears in both cases. X-Ray photographs obtained by the Debye-Scherrer powder method show marked differences. The "sludge" photographs have the "crystal" photograph lines as well as some new ones. The line spacing does not appear to fit any regular shape and, in agreement with other workers' results for  $\text{Co}(\text{OAc})_2 \cdot 4\text{H}_2\text{O}$ , are consistent with a monoclinic structure.<sup>7</sup> We have therefore assumed that the "sludge" contains a different form of cobaltous acetate which may be a dimer or higher polymer in support of the kinetic evidence obtained previously.<sup>3</sup> It is interesting to note that variations in autooxidation rates of cumene depend on the mode of preparation of the cobaltous acetate catalyst used.<sup>4</sup> We also concluded that the dimer (higher aggregates may also be present) is formed on heating, and is affected in the same way as the monomer by heating or by the addition of sodium

(7) J. N. van Niekerk and F. R. L. Schoening, *Acta Cryst.*, **6**, 613 (1953).

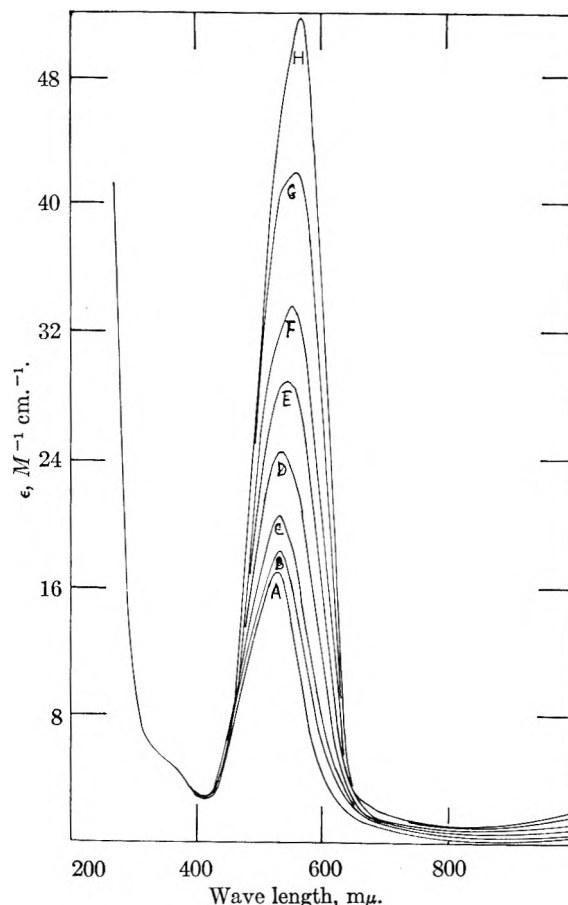


Fig. 2.—The absorption spectrum of cobaltous acetate in anhydrous acetic acid at 25° with sodium acetate at the concentrations: A, 0.000 *M*; B, 0.03131 *M*; C, 0.0625 *M*; D, 0.125 *M*; E, 0.185 *M*; F, 0.250 *M*; G, 0.368 *M*; H, 0.500 *M*.

acetate. The kinetic results suggest<sup>3</sup> that the dimer does not predominate and is in rapid equilibrium with the monomer.

Separate experiments show that although maximum to minimum ratio varies the value of the molar extinction coefficient at the absorption maximum  $\epsilon_{\text{max}}$  does not; the value  $\epsilon_{\text{min}}$  changes over the range 350 to 450  $m\mu$ . The results that follow are for a cobaltous acetate solution having a maximum to minimum ratio of  $\sim 5:1$ ; solutions with a ratio of 10:1 also showed the same effects, and give the same values of the extinction coefficient over all parts of the spectrum except in the vicinity of the minimum.

**The Effect of Sodium Acetate.**—The effect of added sodium acetate on the spectrum at 25° is shown in Fig. 2. In Fig. 3 a graph of  $\epsilon_{565m\mu}$  vs. sodium acetate concentration is shown at five temperatures between 25 and 64°. It can be seen from these two figures that there is a wave length shift from 526 to 565  $m\mu$ , this latter wave length being the limit to which the absorption maximum moves. Thus the new species of cobaltous formed by the addition of sodium acetate has a maximum intensity of absorption at 565  $m\mu$ . It may be noted here that heating the cobaltous acetate solution alone had the similar but less pronounced effect as the addition of sodium acetate, *i.e.*, the absorp-



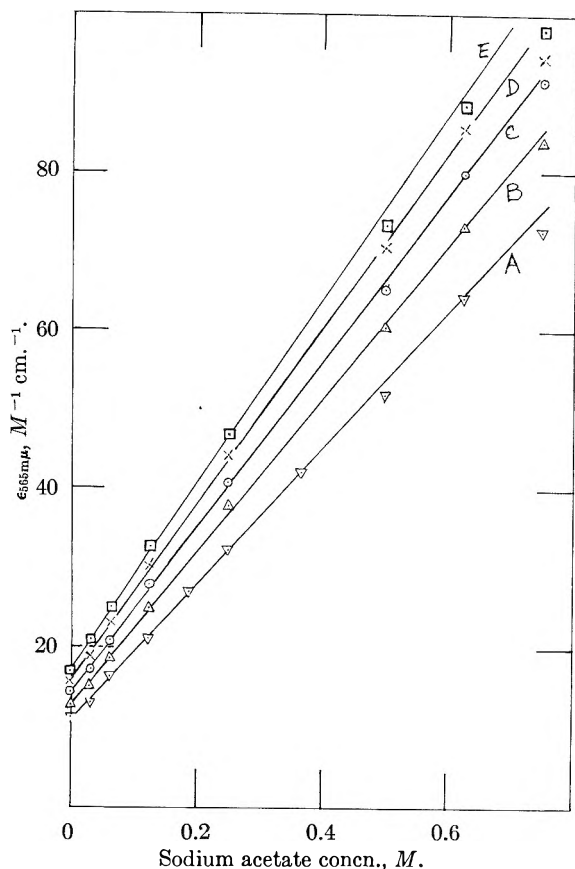
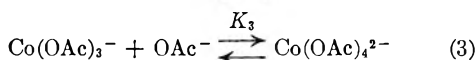
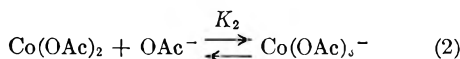


Fig. 3.—The plot of  $\epsilon_{565\text{m}\mu}$  against the concentration of sodium acetate at five temperatures: A, 25.0°; B, 38.0°; C, 47.8°; D, 58.7°; E, 64.0°.

tion intensity was increased and the maximum was shifted to longer wave lengths. In both cases the following equilibria are likely to be operative



from which it can be shown that the molar extinction coefficient  $\epsilon$  at any wave length is given by

$$\epsilon = \epsilon_2 + \epsilon_3 K_2 [\text{OAc}^-] + \epsilon_4 K_3 K_2 [\text{OAc}^-]^2$$

where  $\epsilon_2$ ,  $\epsilon_3$  and  $\epsilon_4$  are the extinction coefficients of  $\text{Co(OAc)}_2$ ,  $\text{Co(OAc)}_3^-$  and  $\text{Co(OAc)}_4^{2-}$ , respectively, at a given wave length. In the case of the sodium acetate addition we have

$$\epsilon = \epsilon_2 + \epsilon_3 K_2 K_A^{1/2} [\text{NaOAc}]^{1/2} + \epsilon_4 K_3 K_2 K_A [\text{NaOAc}]$$

where  $K_A$  is the dissociation constant of sodium acetate in acetic acid<sup>8</sup> which has a value  $(2.63 \pm 0.12) \times 10^{-7}$  at 25°. In the derivation of the above equation the plausible assumption is required that  $K_2 [\text{OAc}^-] (1 + K_3) \ll 1$ . The fact that the plot of  $\epsilon_{565\text{m}\mu}$  against sodium acetate concentration (Fig. 3) is linear indicates that the term involving  $[\text{NaOAc}]^{1/2}$  is not important. Hence it may be concluded that  $\text{Co(OAc)}_3^-$  is not present to any appreciable extent, or else that it has an absorption spectrum almost identical with that of  $\text{Co(OAc)}_2$ . It can be seen that  $\epsilon_4 K_3 K_2 K_A$

is given by the slope of Fig. 3 which has a value 83.2 at 25°. Assuming  $\epsilon_4$  to have a value of  $1700 \text{ M}^{-1} \text{ cm}^{-1}$  (estimated by extrapolation to high sodium acetate concentrations from data similar to that shown in Fig. 3) and  $K_A = 2.63 \times 10^{-7}$  at this temperature, then a value of  $1.9 \times 10^5$  is obtained for  $K_2 K_3$ . The free energy change calculated from this combined equilibrium constant is  $-7.2 \text{ kcal. mole}^{-1}$ , thus indicating that the suggested equilibria are likely to occur.

The predominance of  $\text{Co(OAc)}_4^{2-}$  over  $\text{Co(OAc)}_3^-$  is not unexpected since the experimental data suggest that the former species is of the stable tetrahedral type, being blue colored ( $\lambda_{\text{max}}$  is 565  $\text{m}\mu$ ), while all the remaining Co(II) species are probably of the stable red octahedral type ( $\lambda_{\text{max}}$  is 526  $\text{m}\mu$ ). From ligand field theory  $\lambda_{\text{max}}$  (tetrahedral) is greater than  $\lambda_{\text{max}}$  (octahedral) since the ligand field splitting for the tetrahedral configuration is less than that of the octahedral configuration. Furthermore, cobalt(II) is likely to form some tetrahedral complexes since the stabilization energy is not large.<sup>9</sup> The enthalpy associated with the combined term  $K_2 K_3 K_A$  is obtained from a plot of  $\log_{10} \epsilon_4 K_2 K_3 K_A$  against  $1/T^\circ \text{A}$ . as shown in Fig. 4A; the value obtained was  $1.8 \pm 0.1 \text{ kcal. mole}^{-1}$ . In the case of cobaltous acetate in pure anhydrous acetic acid, the expression for the observed extinction coefficient, neglecting the acetate ions released by the cobaltous acetate ( $\sim 10^{-2} \text{ M}$ ), becomes

$$\epsilon = \epsilon_2 + \epsilon_3 K_2 (K'_{\text{Ac}})^{1/2} + \epsilon_4 K_2 K_3 K'_{\text{Ac}}$$

because the acetic acid concentration remains constant: where  $K'_{\text{Ac}} = K_{\text{Ac}} [\text{HOAc}]$  and  $K_{\text{Ac}}$  is the dissociation constant of acetic acid. Again the second term on the right-hand side appears to be negligible. The heat change of the combined term  $K_2 K_3 K'_{\text{Ac}}$  is obtained from a graph of  $\log (\epsilon_{565\text{m}\mu} - \epsilon_2)$  against  $1/T^\circ \text{A}$ . (see Fig. 4B).  $\epsilon_2$  was assumed to have a value of  $8.5 \text{ M}^{-1} \text{ cm}^{-1}$  at 565  $\text{m}\mu$  which is the value obtained with 2% water present to reduce the contribution of the tetrahedral form to negligible proportions. The value obtained was  $5.6 \pm 0.2 \text{ kcal. mole}^{-1}$ . The procedure outlined above clearly provides a means of obtaining the dissociation constants and heats of dissociation of metal acetates in acetic acid by their effect on the spectrum of cobaltous acetate, providing one such constant is already known. The relative heats of dissociation may also be determined by this method; this will be the subject of a future paper.<sup>10</sup>

**The Effect of the Addition of Water.**—An exploratory study of the changes brought about by the addition of water has been made by Dean and Skirrow.<sup>11</sup> We have made a more detailed investigation and have interpreted the changes in terms of a dielectric effect. No electrolytes are strongly dissociated in acetic acid; therefore, it is reasonable to assume that the absorption maximum of cobaltous acetate in anhydrous acetic acid at 526  $\text{m}\mu$  (see Fig. 1 at 25°) is due to the entity  $\text{Co(OAc)}_2$ . When 50% v./v. water is present the extinction

(9) L. E. Orgel, Solvay Conference, Brussels, 1956.

(10) P. J. Proll and L. H. Sutcliffe, *Trans. Faraday Soc.*, in press.

(11) M. H. Dean and G. Skirrow, *ibid.*, **54**, 849 (1958).

(8) I. M. Kolthoff and S. Bruckenstein, *J. Am. Chem. Soc.*, **78**, 2974 (1956).

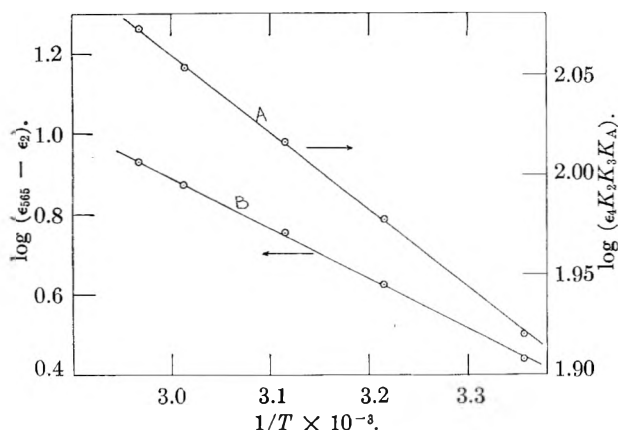


Fig. 4A.—The plot of  $\log \epsilon_4 K_2 K_3 K_A$  against  $1/T$  °A. for the addition of sodium acetate; B, the dependence of  $\log(\epsilon_{565} - \epsilon_2)$  on  $1/T$  °A.

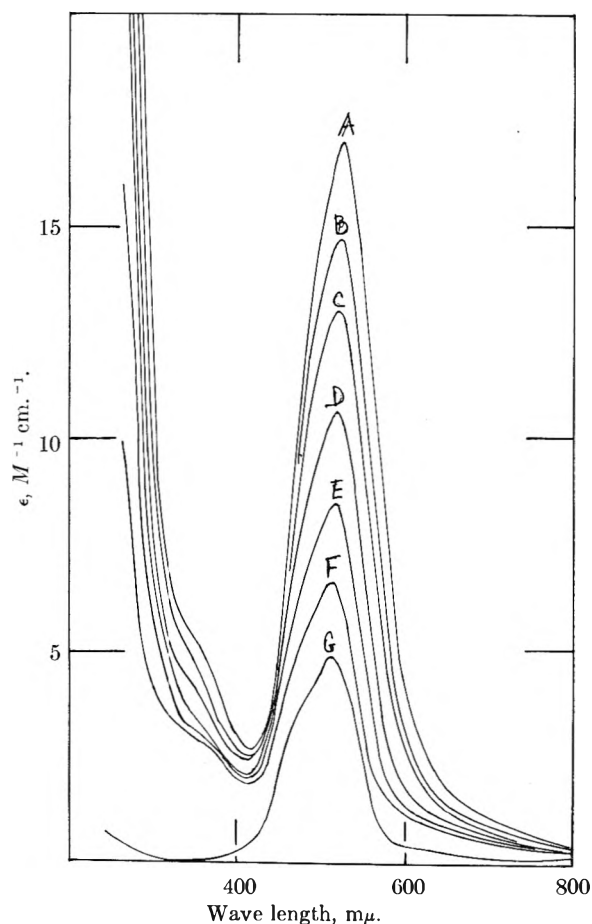
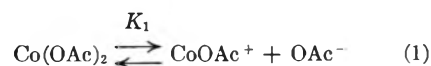


Fig. 5.—The effect of water on the spectrum of cobaltous acetate in acetic acid at 25°. The concentration of  $\text{Co(II)} = 1.96 \times 10^{-2} M$ . Water concentrations: A, 0.00% v./v.; B, 2.00% v./v.; C, 6.25% v./v.; D, 12.5% v./v.; E, 25.0% v./v.; F, 50.0% v./v.; G, 100.0% v./v.

coefficient drops from  $17.0$  to  $6.6 M^{-1} \text{ cm.}^{-1}$  and the absorption maximum of cobaltous acetate shifts slightly to  $515 m\mu$ . The absorption maximum of cobaltous perchlorate in water lies at  $510 m\mu$  and has an extinction coefficient of  $4.9 M^{-1} \text{ cm.}^{-1}$ . It has been shown that cobaltous acetate is not completely dissociated in water,<sup>12</sup> giving rise

(12) S. Bardan and S. Aditya, *J. Indian. Chem. Soc.*, **32**, 100 (1955).

to an appreciable concentration of  $\text{CoOAc}^+$ . From the above data one may conclude that the latter species has an absorption spectrum in the visible region similar to that of  $\text{Co}^{2+aq}$  and that the only equilibrium affected by the change of dielectric constant is



It can be shown that

$$K_1 = \frac{[\text{OAc}^-](\epsilon_2 - \epsilon)}{(\epsilon - \epsilon_1)}$$

where  $\epsilon$ ,  $\epsilon_1$  and  $\epsilon_2$  are the observed extinction coefficient and the extinction coefficients of  $\text{CoOAc}^+$  and  $\text{Co(OAc)}_2$ , respectively.  $[\text{OAc}^-]$  is the concentration of acetate ions produced by the above equilibrium, and is given by

$$[\text{OAc}^-] = \frac{c(\epsilon_2 - \epsilon)}{(\epsilon_2 - \epsilon_1)}$$

where  $c$  is the total cobalt(II) concentration. Therefore

$$K_1 = \frac{c(\epsilon_2 - \epsilon)^2}{(\epsilon_2 - \epsilon_1)(\epsilon - \epsilon_1)}$$

In deriving this expression it has been assumed that the concentration of acetate ions originating from the acetic acid is negligible.<sup>13</sup>  $K_1$  will be affected by the dielectric constant  $D$  according to the relationship<sup>14</sup>

$$\ln K_1^{-1} = \text{constant} - \frac{e^2 Z_A Z_B}{k T D r}$$

where  $e$  is the electronic charge,  $k$  is the Boltzmann constant,  $r$  is radius of solvated  $\text{Co(OAc)}_2$  and  $Z_A$  and  $Z_B$  are the charges on the two ions produced. Table I lists the data calculated from the extinction coefficient observed at the fixed wave length of  $510 m\mu$ , the position of the maximum absorption in pure water. Values of the dielectric constants of the mixtures were calculated from those of acetic acid and water obtained by Smyth and Rogers<sup>15</sup> and by Lange and Robinson,<sup>16</sup> respectively. The final column shows the good linear dependence of  $\log K_1^{-1}$  on  $D^{-1}$ . The average value at 25° for  $\Delta \log K_1^{-1} / \Delta(D^{-1})$  is 21.2 which corresponds to a rather high value of  $12 \text{ \AA.}$  for the radius of  $\text{Co(OAc)}_2$  when the product  $Z_A Z_B$  is taken to be  $-1$ . In applying this theory, the contribution of the tetrahedral form, namely,  $\text{Co(OAc)}_4^{2-}$ , has been neglected since at 25°, the concentration is the order of 0.1% and even at 64°, it will be less than 0.5% in anhydrous acetic acid. Also, as will be seen later, the addition of water reduces the amount of  $\text{Co(OAc)}_4^{2-}$ . The increase in concentration of the tetrahedral form with increase in temperature probably accounts for the larger deviation at the higher temperatures in the value of  $\Delta \log K_1^{-1} / \Delta(D^{-1})$ . The complexity of the system prevents an expres-

(13) H. S. Harned and G. L. Kazanjian, *J. Am. Chem. Soc.*, **58**, 1912 (1936).

(14) S. Glasstone, K. J. Laidler and H. Eyring, "The Theory of Rate Processes," McGraw-Hill Book Co., New York, N. Y., first edition, 1930, p. 430.

(15) C. P. Smyth and H. E. Rogers, *J. Am. Chem. Soc.*, **52**, 1824 (1930).

(16) E. Lange and A. L. Robinson, *ibid.*, **52**, 2811 (1930).

TABLE I

Temp., °C.	H <sub>2</sub> O % v. v.	$\epsilon_{565m\mu}$	$K_1, M^{-1}$	$\log K_1^{-1}$	$D^{-1}$	$\frac{\Delta \log K_1^{-1}}{\Delta(D^{-1})}$	
25.0	0.00	15.60	.....	.....	0.1620	..	
	2.08	14.22	$3.73 \times 10^{-4}$	3.428	.1300	..	
	4.17	13.20	$1.06 \times 10^{-3}$	2.974	.1090	21.4	
	6.25	12.70	$1.97 \times 10^{-3}$	2.706	.0945	20.0	
	12.5	10.53	$8.32 \times 10^{-3}$	2.080	.0667	21.2	
	25.0	8.41	$2.69 \times 10^{-2}$	1.570	.0412	20.8	
	50.0	6.50	$9.44 \times 10^{-2}$	1.250	.0236	22.4	
	74.0	6.37	$1.06 \times 10^{-1}$	0.977	.0169	21.6	
100.0	4.90	.....	.....	.....	.0127	..	
38.0	0.00	16.37	.....	.....	.1600	..	
	2.08	14.57	$5.69 \times 10^{-4}$	3.245	.1305	..	
	6.25	12.90	$2.56 \times 10^{-3}$	2.592	.0953	18.5	
	12.5	10.74	$9.20 \times 10^{-3}$	2.056	.0679	19.2	
	25.0	8.54	$2.86 \times 10^{-2}$	1.544	.0431	19.2	
	50.0	6.62	$9.17 \times 10^{-2}$	1.028	.0245	20.8	
	100.0	4.90	.....	.....	.....	.0136	..
	47.8	0.00	16.85	.....	.....	.1580	..
2.08		14.85	$6.58 \times 10^{-4}$	3.182	.1310	..	
6.25		13.20	$2.60 \times 10^{-3}$	2.586	.0966	17.3	
12.50		10.99	$9.23 \times 10^{-3}$	2.035	.0696	18.8	
25.00		8.85	$2.65 \times 10^{-2}$	1.578	.0447	18.9	
50.00		6.75	$9.34 \times 10^{-2}$	1.030	.0260	20.4	
100.00		4.90	.....	.....	.....	.0142	..
58.7		0.00	17.78	.....	.....	.1550	..
	2.08	15.54	$7.15 \times 10^{-4}$	3.146	.1290	..	
	6.25	14.06	$2.29 \times 10^{-3}$	2.640	.0978	16.2	
	12.50	11.81	$7.83 \times 10^{-3}$	2.107	.0710	17.8	
	25.00	9.31	$2.47 \times 10^{-2}$	1.608	.0461	18.2	
	50.00	6.90	$9.00 \times 10^{-2}$	1.046	.0277	20.4	
	100.00	4.90	.....	.....	.....	.0148	..
	64.0	0.00	18.30	.....	.....	.1540	..
2.08		15.96	$7.83 \times 10^{-4}$	3.107	.1295	..	
6.25		14.47	$2.24 \times 10^{-3}$	2.650	.0995	15.2	
12.50		12.12	$7.71 \times 10^{-3}$	2.113	.0722	17.3	
25.00		9.61	$2.35 \times 10^{-2}$	1.630	.0475	18.0	
50.00		7.00	$8.87 \times 10^{-2}$	1.051	.0279	20.2	
100.00		4.90	.....	.....	.....	.0253	..

Av. values of  $\Delta \log K_1^{-1}/\Delta(D^{-1})$

- at 25.0° = 21 ± 1
- at 38.0° = 20 ± 1
- at 47.8° = 19 ± 2
- at 58.7° = 18 ± 2
- at 64.0° = 18 ± 3

sion from being developed which takes into account the presence of the tetrahedral form.

From the results, it is evident that small concentrations of water do not cause preferential solvation of the Co(II) species unless the absorption spectra of say Co(OAc)<sub>2</sub>·4H<sub>2</sub>O and Co(OAc)<sub>2</sub>·4HOAc are identical in acetic acid. Since chemical reactivity differences between these species might be greater than optical differences we examined kinetic data obtained previously both by ourselves<sup>3</sup> and by other workers.<sup>11,17</sup> The effect of water on the non-catalytic reaction between cobaltous acetate and plumbic acetate could be represented as a dielectric effect and did not suggest specific solvation.<sup>3</sup> Systems in which cobaltous acetate was employed as a catalyst should be even more sensitive to water addition. Dean and Skirrow<sup>11</sup> and Bawn, Pennington and Tipper<sup>17</sup> have studied the cobaltous catalyzed decomposition of *t*-butyl hydroperoxide and the aerobic oxidation of trimethylethylene, respectively, in acetic acid with the addition of water. We have treated the addition of water as causing a change of dielectric constant in both cases. The

(17) C. E. H. Bawn, A. A. Pennington and C. F. H. Tipper, *Disc. Faraday Soc.*, **10**, 282 (1951).

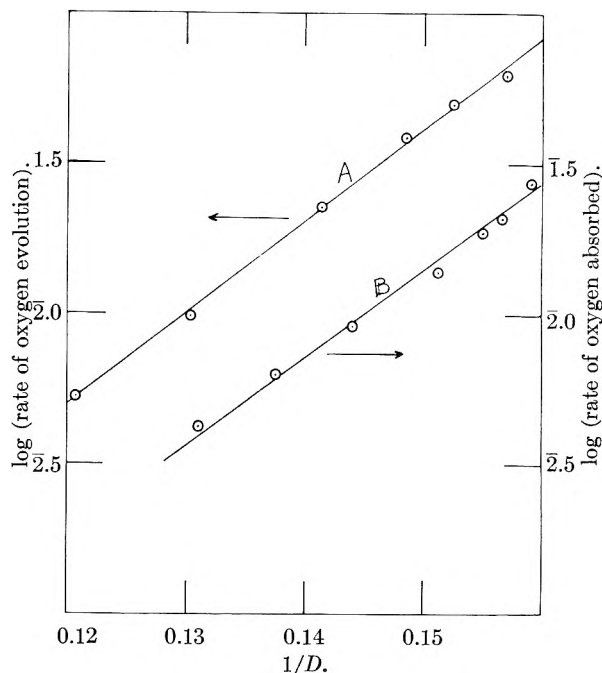


Fig. 6.—The results of (A) Dean and Skirrow<sup>11</sup> obtained at 55° and (B) Bawn, Pennington and Tipper<sup>17</sup> obtained at 40.5°, plotted as dielectric effects.

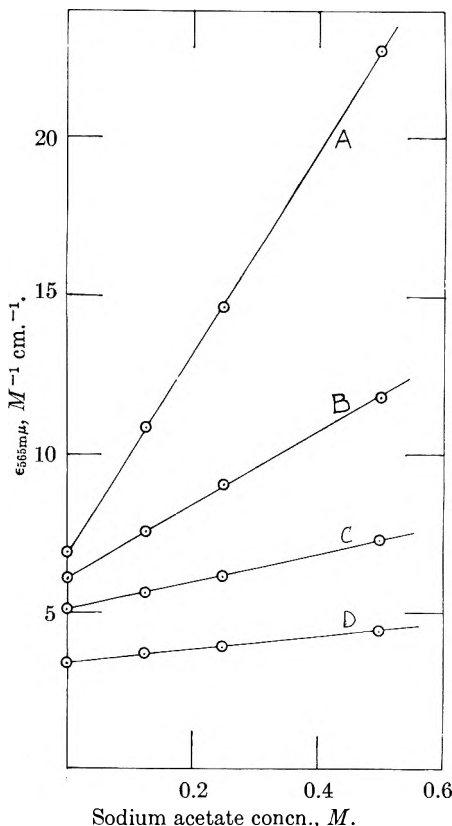


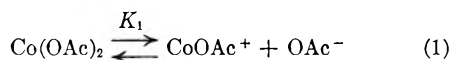
Fig. 7.—The dependence of the observed extinction coefficient at 565 mμ on the sodium acetate concentration in the presence of water at 25.0°. Water concentrations: A, 2.08% v/v.; B, 6.25% v/v.; C, 12.5% v/v.; D, 25.0% v/v.

two sets of data are shown in Fig. 6: it has been assumed that the organic substrate does not make a significant contribution to the dielectric constant.

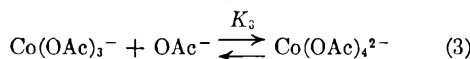
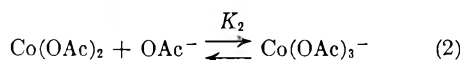
It can be seen from Fig. 6 that a good straight line is obtained in both cases and hence we conclude that no specific effects occur on the addition of water. Therefore, the reactive catalytic species of cobaltous acetate in these systems is most likely to be  $\text{Co}(\text{OAc})_2$  or  $\text{Co}(\text{OAc})_4^{2-}$ . The latter species is probably the more reactive since the addition of sodium acetate can increase the rate of reaction.<sup>3</sup>

Our findings are somewhat opposed to those of Katzin and Gebert<sup>18</sup> who studied the effect of water on the absorption spectra of solutions of cobaltous nitrate in *t*-butyl alcohol, acetone and dioxane. They consider that in their system the specific aquation effect is more important than the dielectric effect. Unfortunately, the experimental data quoted in their paper is inadequate for the application of our treatment.

**The Combined Effect of Sodium Acetate and Water.**—Since the main effect of water on the spectrum of cobaltous acetate in acetic acid is caused by the dielectric effect on the equilibrium



it was decided to test if the second equilibrium of the pair



was affected by water in the same manner. To this end sodium acetate up to 0.5 *M* and water up to 25% v./v. were added to cobaltous acetate in anhydrous acetic acid. The form of the dependence of the observed extinction coefficient on the sodium acetate concentration was found to be unchanged by water indicating that equilibria (2) and (3) were still operative. The experiments were carried out at three temperatures in the range 25 to 47.8°; Fig. 7 shows the results at 25°. Table II lists the data calculated from the slopes of the plots of the observed extinction coefficients at 565  $m\mu$  against sodium acetate concentrations for each fixed water concentration at temperatures of 25.0, 38.0 and 47.8°.

Values of the dielectric constant at these temperatures for acetic acid and water were obtained from the results of Smyth and Rogers<sup>15</sup> and Lange and Robinson,<sup>16</sup> respectively, by graphical extrapolation.

It can be seen from Table II, that increase in temperature decreases the value of  $\Delta \log \epsilon_4 K_2 K_3 K_A / \Delta(D^{-1})$  slightly. This would be expected from an increase in the ionic radius due to the larger vibrational energy of the ligands of  $\text{Co}(\text{OAc})_4^{2-}$  and its solvation shell. It is interesting to note that in this case  $Z_A Z_B$  is of opposite sign to that when only water is added to cobaltous acetate. This is expected since a dielectric constant change in the present case only affects equilibrium 3 which involves two negatively

(18) L. I. Katzin and E. Gebert, *J. Am. Chem. Soc.*, **72**, 5455 (1950).

TABLE II

Temp., °C.	H <sub>2</sub> O % v. v.	$\epsilon_4 K_2 K_3 K_A$	$\log \epsilon_4 K_2 K_3 K_A$	$D^{-1}$	$\frac{\Delta \log \epsilon_4 K_2 K_3 K_A}{\Delta(D^{-1})}$
25.0	0.00	83.2	1.920	0.162	..
	2.08	31.6	1.500	.130	13.1
	6.25	11.4	1.052	.0945	12.8
	12.50	4.4	0.644	.0667	13.3
	25.00	2.1	0.322	.0412	13.2
38.0	0.00	95.0	1.978	.160	..
	2.08	42.6	1.630	.1305	11.7
	6.25	17.0	1.230	.0953	11.6
	12.50	6.7	0.826	.0679	12.5
	25.00	3.55	0.550	.0431	12.2
47.8	0.00	103.6	2.015	.158	..
	2.08	52.8	1.720	.131	10.9
	6.25	21.4	1.330	.0966	11.1
	12.50	9.5	0.978	.0696	11.7
	25.00	4.7	0.672	.0447	11.7

Av. values of  $\Delta \log \epsilon_4 K_2 K_3 K_A / \Delta(D^{-1})$

at 25.0° = 13.0 ± 0.3

at 38.0° = 12.0 ± 0.5

at 47.8° = 11.4 ± 0.5

charged ions, while in the case of the addition of water only equilibrium 1 is concerned. The fact that the slope is less in the present case than in the former case at the same temperature may mean that the radius of solvated  $\text{Co}(\text{OAc})_4^{2-}$  is greater than that of solvated  $\text{Co}(\text{OAc})_2$ . The product  $K_2 K_3$  cannot be evaluated because  $K_A$  has not been determined for sodium acetate dissolved in acetic acid–water mixtures. In passing, it should be mentioned that the dielectric effect on the dissociation of sodium acetate is in the opposite direction compared with that on equilibrium 3. This fact eliminates the possibility that the addition of water to acetic acid solutions of cobaltous acetate and sodium acetate increases the concentration of  $\text{Co}(\text{OAc})_4^{2-}$  merely by the provision of more acetate ions.

### Conclusions

The main conclusions that have been reached in this work are that cobalt(II) exists to a slight extent in a polynuclear form in anhydrous acetic acid and that a tetrahedral form, namely,  $\text{Co}(\text{OAc})_4^{2-}$  having an absorption maximum at 565  $m\mu$ , is an important ionic species in acetic acid. The influence of water on the spectrum of cobaltous acetate under various conditions has been found to be attributable to the change of dielectric constant and any specific solvation effects, if they are present, must be masked. A value for the product of the equilibrium constants  $K_2$  and  $K_3$  for the change from the octahedral form (solvated  $\text{Co}(\text{OAc})_2$ ) to the tetrahedral form (solvated  $\text{Co}(\text{OAc})_4^{2-}$ ) at 25° is found to be  $1.9 \times 10^6$  corresponding to a free energy change of  $-7.2$  kcal. mole<sup>-1</sup>.

The authors wish to thank Miss J. M. Silcock of this University for obtaining the X-ray photographs and for advising us on their interpretation.

COMPLEX IONS IN FUSED SALTS. SILVER HALIDES<sup>1</sup>

BY F. R. DUKE AND H. M. GARFINKEL

*Institute for Atomic Research and Department of Chemistry, Iowa State University, Ames, Iowa**Received September 8, 1960*

The system  $\text{AgNO}_3\text{-KX}$  in sodium-potassium nitrate eutectic solvent has been investigated by following the electromotive force as a function of the concentration of either chloride or bromide ion. Since the silver nitrate electrode shows Nernst behavior, the deviations from such behavior have been ascribed to complex ion formation. Several determinations have been made at various temperatures and equilibrium constants and standard heats of reaction have been tabulated for the different species postulated.

## Introduction

The existence of complex ions in fused salts has been postulated by many investigators and indeed seems to be fairly well substantiated by their studies. These include freezing point depression,<sup>2</sup> spectrophotometry<sup>3</sup> and solubility data.<sup>4</sup>

Van Artsdalen<sup>5</sup> has shown by cryoscopic measurements that  $\text{NaCl}$  behaves ideally in  $\text{NaNO}_3$  up to about 6 mole % of  $\text{NaCl}$  and similarly it has been shown that the  $\text{KCl-KNO}_3$  system behaves ideally.<sup>6</sup> Moreover the applicability of the Nernst equation to silver-silver nitrate electrodes has been demonstrated by Flengas and Rideal<sup>7</sup> in molten  $\text{NaNO}_3\text{-KNO}_3$ . Laity<sup>8</sup> has shown in a thermodynamic analysis that for solutions having the transport properties of the  $\text{AgNO}_3\text{-NaNO}_3$  system the junction potential terms vanish from the expression for the e.m.f. and the system  $\text{AgNO}_3\text{-NaNO}_3$  is a regular solution. In this study a eutectic mixture of  $\text{NaNO}_3$  and  $\text{KNO}_3$  was used as the solvent. The electromotive force of a concentration cell was followed as a function of the concentration of the halide ion employed. This was done at various initial silver ion concentrations and several temperatures.

## Experimental

ACS reagent grade chemicals were used.  $\text{NaNO}_3$  and  $\text{KNO}_3$  were recrystallized from redistilled water.

The e.m.f. measurements were made on the concentration cell



where  $m$  is the molality of the ion indicated by the subscript and  $X$  is either chloride or bromide. The cell consisted of a Pyrex tube 10-in. long and 2.5-in. wide, fitted with a 300-ml. flask on the bottom and a 60/50 ground glass joint on top. The top of the cell had wells used to position the reference (left hand) half-cell, the indicator electrode, the thermocouple, the addition tube and the motor-driven Pyrex stirrer. The reference half-cell was a tube with a fine Pyrex-fitted disc, 10 mm. in diameter, partially fused to reduce diffusion. The electrodes were prepared by taking equal lengths of #22 gauge platinum wire and spot welding short pieces of #22 gauge silver wire (99.99+ % pure) to each. The silver wire in turn was wound into a loose helix.

(1) Contribution No. 923. Work was performed in the Ames Laboratory of the U. S. Atomic Energy Commission.

(2) E. R. Van Artsdalen, *J. Phys. Chem.*, **60**, 172 (1956).

(3) (a) D. M. Gruen, *J. Inorg. Nuclear Chem.*, **4**, 74 (1957); (b)

D. M. Gruen and R. L. McBeth, *J. Phys. Chem.*, **63**, 393 (1959).

(4) F. R. Duke and M. L. Iverson, *ibid.*, **62**, 417 (1958).

(5) E. R. Van Artsdalen, *J. Tenn. Acad. Sci.*, **29**, No. 2 (1954).

(6) E. Kordes, W. Bergman and W. Vogel, *Z. Electrochem.*, **65**, 600 (1951).

(7) S. N. Flengas and E. K. Rideal, *Proc. Roy. Soc. (London)*, **233A**, 443 (1956).

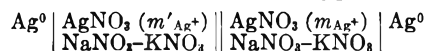
(8) R. W. Laity, *J. Am. Chem. Soc.*, **79**, 1849 (1957).

Then these electrodes were sealed into 3 mm. Pyrex tubing to position the electrodes.

When assembled this cell was positioned in a fused alkali nitrate bath. The bath was insulated on the side with successive layers of insulating materials and on top with a 1-in. transite cover with opening for the cell and other equipment. Temperatures were measured with a calibrated chromel-alumel thermocouple and were maintained at least  $\pm 1^\circ$  during a series of measurements. All e.m.f. measurements were made with a Type K Leeds and Northrup potentiometer.

## Results

For a concentration cell of the type



in which the solute concentration is so low that essentially all the current is carried by the solvent the e.m.f. is given by

$$E = \frac{2.30RT}{F} \log \frac{a_{\text{AgNO}_3}}{a'_{\text{AgNO}_3}} \quad (1)$$

where  $a'$  is the activity of the solute in the reference half-cell. If the ratio of the practical activity coefficient which are defined by

$$\gamma_{\text{AgNO}_3} = \frac{a_{\text{AgNO}_3}}{m_{\text{Ag}^+} m_{\text{NO}_3^-}} \quad (2)$$

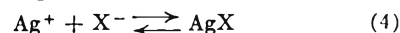
is constant as shown by Flengas and Rideal<sup>7</sup> then eq. 1 becomes

$$E = \frac{2.30RT}{F} \log \frac{m_{\text{Ag}^+}}{m'_{\text{Ag}^+}} \quad (3)$$

This equation was tested with the electrodes and set up as described above at  $366^\circ$ . The slope of the line in the above plot is 0.124 and the Nernst slope is 0.126.

However as  $\text{KCl}$  or  $\text{KBr}$  was added to the right-hand compartment, and  $m_{\text{Ag}^+} + m_{\text{X}^-}$  was of the order of  $10^{-5}$ , deviations from eq. 3 were noted that could not be accounted for simply by dilution. These deviations were ascribed to complex ion formation.

Consider the stepwise reactions



and



It is apparent that the total silver ion can be expressed as a sum.

$$T_{\text{Ag}^+} = [\text{Ag}^+] + [\text{AgX}] + [\text{AgX}_2^-] = m'_{\text{Ag}^+} \quad (6)$$

It  $T_{\text{Ag}^+} \ll T_{\text{X}^-}$  then

$$K_1 = \frac{[\text{AgX}]}{[\text{Ag}^+][\text{X}^-]}, \quad K_2 = \frac{[\text{AgX}_2^-]}{[\text{AgX}][\text{X}^-]} \quad (7)$$

Substituting for  $\text{AgX}$  and  $\text{AgX}_2^-$  into eq. 6 one obtains

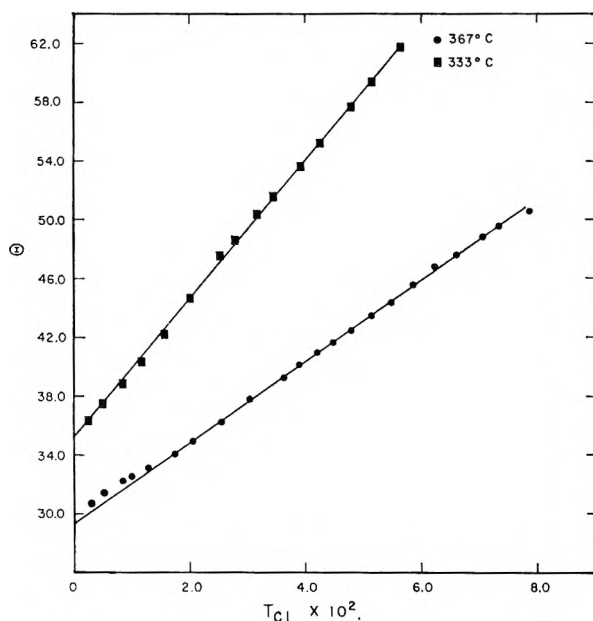


Fig. 1.—Plot to show linearity of the derived equation  $\theta = \frac{10^{-EF/2.3RT} - 1}{T_{Cl}} = K_1 + K_1K_2T_{Cl}$  for the silver nitrate system when KCl is added.

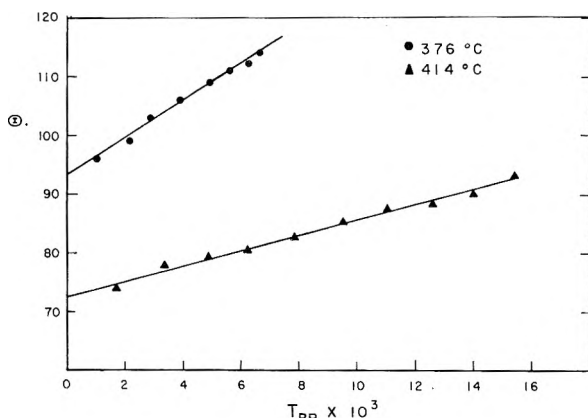


Fig. 2.—Plot to show linearity of the derived equation  $K_1 = K_1K_2T_{Br}$  for the silver nitrate system when KBr is added.

$$\frac{m'_{Ag^+}}{m_{Ag^+}} = 1 + K_1T_{X^-} + K_1K_2T_{X^-}^2 \quad (8)$$

Substituting for the left-hand side of eq. 8, then

$$10^{\frac{-\Delta EF}{2.30RT}} = 1 + K_1T_{X^-} + K_1K_2T_{X^-}^2 = \beta \quad (9)$$

where  $\Delta E$  is equal to the difference of the Nernst potential from that when KCl is added. Some typical data for these systems with bromide or chloride are shown in Table I.

Now if  $10^{-\Delta EF/2.3RT}$  is plotted *vs.*  $T_{X^-}$  then  $\lim d\beta/dT_{X^-} = K_1$ ; and  $(10^{-\Delta EF/2.3RT} - 1)/T_{X^-}$  plotted *vs.*  $T_{X^-}$  should yield a straight line with  $K_1$  equal to the intercept and  $K_1/K_2$  equal to the slope. Some typical plots are shown in Figs. 1 and 2 where the method of averages<sup>9</sup> was used to get the best straight line. These constants could also be extracted by graphically differentiat-

(9) R. Livingston, "Physico Chemical Experiments," The Macmillan Co., New York, N. Y., 1948, p. 40.

TABLE I  
ELECTROMOTIVE FORCE AS FUNCTION OF HALIDE ION

$t = 333^\circ$ $\frac{m'_{Ag^+}}{m_{Ag^+}} = 0.838 \times 10^{-3}$		$t = 367^\circ$ $\frac{m'_{Ag^+}}{m_{Ag^+}} = 0.579 \times 10^{-3}$		$t = 374^\circ$ $\frac{m'_{Ag^+}}{m_{Ag^+}} = 0.845 \times 10^{-3}$	
$T_{Cl^-} \times 10^2$	$-\Delta E(v.)$	$T_{Cl^-} \times 10^2$	$-\Delta E(v.)$	$T_{Cl^-} \times 10^2$	$-\Delta E(v.)$
0.248	0.0045	0.264	0.0043	0.267	0.0039
.533	.0095	.643	.0101	0.57	.0083
.846	.0148	.845	.0133	1.02	.0148
1.17	.0202	.994	.0155	1.41	.0201
1.55	.0262	1.31	.0199	1.76	.0249
1.98	.0330	1.74	.0257	2.2	.0309
2.50	.0408	2.04	.0297	2.75	.0373
.277	.0444	2.54	.0360	3.18	.0423
3.15	.0495	3.06	.0424	3.52	.0462
3.45	.0532	3.63	.0489	4.16	.0532
3.92	.0589	3.92	.0522	4.67	.0585
4.27	.0631	4.23	.0555	5.00	.0619
4.80	.0691	4.50	.0582	5.32	.0649
5.15	.0729	4.80	.0613	5.78	.0694
5.64	.0781	5.15	.0648	6.34	.0743
		5.50	.0682	6.92	.0794
		5.88	.0718	7.52	.0842
		6.25	.0754	8.24	.0900
		6.64	.0787	9.03	.0960
		7.06	.0824	9.75	.1012
		7.36	.0848		
		7.85	.0885		

#### B. Bromide

$t = 375^\circ$ $\frac{m'_{Ag^+}}{m_{Ag^+}} = 0.737 \times 10^{-3}$		$t = 376^\circ$ $\frac{m'_{Ag^+}}{m_{Ag^+}} = 1.04 \times 10^{-3}$		$t = 414^\circ$ $\frac{m'_{Ag^+}}{m_{Ag^+}} = 0.562 \times 10^{-3}$	
$T_{Br^-} \times 10^3$	$-\Delta E(v.)$	$T_{Br^-} \times 10^3$	$-\Delta E(v.)$	$T_{Br^-} \times 10^3$	$-\Delta E(v.)$
1.26	0.0066	1.05	0.0054	0.170	0.0070
2.07	.0107	2.16	.0109	.335	.0136
2.91	.0148	2.90	.0146	.485	.0191
3.78	.0190	3.93	.0195	.619	.0239
4.53	.0225	4.94	.0241	.784	.0295
5.41	.0264	5.62	.0272	.935	.0346
6.18	.0298	6.14	.0294	1.10	.0399
7.00	.0333	6.65	.0315	1.26	.0441
				1.40	.0481
				1.54	.0527

ing the plot of  $10^{-\Delta EF/2.3RT}$  *vs.*  $T_{X^-}$  with a tangentmeter at a series of halide ion concentrations. The plot of the slope *vs.*  $T_{X^-}$  should yield a straight line with intercept  $K_1$  and slope  $2K_1K_2$ .

The data compiled by Blander<sup>10,11</sup> and explained on the basis of the quasi-lattice model were treated in a similar manner. The constants calculated from his data are included in Table II along with those of this investigation. By means of the van't Hoff equation  $\Delta H$  for the various reactions was calculated and the values are tabulated (Table III). The values in parentheses were calculated from two points only. It is estimated that  $K_1$  is determined with a precision of about 3% and  $K_2$  with a precision of about 15% although the uncertainty in  $K_2$  in the bromide system is somewhat larger.

It is interesting to note the large decrease in total complexing as one goes from pure  $KNO_3$

(10) M. Blander, F. F. Blankenship and R. F. Newton, *J. Phys. Chem.*, **63**, 1259 (1959).

(11) M. Blander, *ibid.*, **63**, 1262 (1959).

TABLE II

STABILITY CONSTANTS (MOLAL <sup>-1</sup> )		Temp., °C.	$K_1$ $\times 10^{-1}$	$K_1K_2$ $\times 10^{-2}$	$K_2$ $\times 10^{-1}$
KNO <sub>3</sub> <sup>a</sup>	Ag <sup>+</sup> , Cl <sup>-</sup>	370	5.00	8.60	1.70
		436	2.80	3.33	1.19
Na-KNO <sub>3</sub>	Ag <sup>+</sup> , Cl <sup>-</sup>	333	3.53	4.72	1.34
		374	2.80	2.50	0.893
Na-KNO <sub>3</sub>	Ag <sup>+</sup> , Br <sup>-</sup>	376	9.33	31.1	3.33
		414	7.23	13.3	1.84

<sup>a</sup> Constants calculated from data of Blander, *et al.*

TABLE III

HEATS OF REACTION		Solvent	$-\Delta H$ (kcal./mole)
Reaction			
Ag <sup>+</sup> + Cl <sup>-</sup> = AgCl		KNO <sub>3</sub> <sup>a</sup>	7.96
AgCl + Cl <sup>-</sup> = AgCl <sub>2</sub> <sup>-</sup>			4.92
Ag <sup>+</sup> + Cl <sup>-</sup> = AgCl		NaNO <sub>3</sub> -KNO <sub>3</sub>	4.40
AgCl + Cl <sup>-</sup> = AgCl <sub>2</sub> <sup>-</sup>			7.73
Ag <sup>+</sup> + Br <sup>-</sup> = AgBr		NaNO <sub>3</sub> -KNO <sub>3</sub>	5.94
AgBr + Br <sup>-</sup> = AgBr <sub>2</sub> <sup>-</sup>			13.9

<sup>a</sup> Heats calculated from data of Blander, *et al.*

as solvent to a eutectic mixture of NaNO<sub>3</sub>-KNO<sub>3</sub> as shown by the product  $K_1K_2$ . This trend will

be further investigated as a function of the solvent cation.

## HYDROLYSIS OF ALKYL ACETATES IN A PHOSPHATE-BUFFERED AQUEOUS MEDIUM

By JOHN M. HOLLAND AND JOHN G. MILLER

*Department of Chemistry of the University of Pennsylvania, Philadelphia, Penna.*

*Received September 8, 1960*

The hydrolyses of methyl and ethyl acetates have been studied at 30° in aqueous medium maintained in the pH range of 6.2 to 6.9 by sodium phosphate buffer. The hydrolyses occurred at a measurable rate; the reaction was found to be first order in both ester and phosphate dianion. The specific rate constant for ethyl acetate hydrolysis, determined at seven different concentrations of ester and phosphate dianion, and at a total ionic strength of 1.6, was  $1.00 \pm 0.10 \times 10^{-3}$  l. mole<sup>-1</sup> hr.<sup>-1</sup>. The rate constant extrapolated to zero ionic strength was approximately  $1.8 \pm 0.1 \times 10^{-3}$  l. mole<sup>-1</sup> hr.<sup>-1</sup>. For methyl acetate the hydrolytic rate constant, determined at three different concentrations of reactants and a total ionic strength of 1.5, was  $1.75 \pm 0.05 \times 10^{-3}$  l. mole<sup>-1</sup> hr.<sup>-1</sup>. The course of the reaction was followed by titrimetric determinations of increasing concentration of phosphate monoanion. A mechanism has been proposed which includes a rate-determining nucleophilic attack by phosphate dianion on the carbonyl carbon of the ester followed by a relatively rapid hydrolytic decomposition of the intermediate acetyl phosphate monoanion into acetate and phosphate monoanions.

Several years ago during an investigation of the effects of various solvents on the alkaline hydrolysis esters, it was found in this Laboratory that phosphate-buffered hydrolyses of several formates and acetates proceeded at a measurable rate in aqueous dioxane solution and in the pH range 7.6 to 8.8.<sup>1</sup> Although the work was of a semiquantitative nature, the results could be equated to a second-order rate expression involving ester and phosphate dianion concentrations. This present study was undertaken to demonstrate that ester hydrolysis does occur with reproducible second-order kinetics in a neutral phosphate-buffered aqueous medium, where the catalytic effects of hydronium and hydroxyl ions are minimal.

The exclusion of organic solvents limited this work to those alkyl acetates with sufficient water-solubility to ensure homogeneity; *i.e.*, methyl and ethyl acetates. The hydrolyses of phenyl and *p*-nitrophenyl acetates in phosphate buffers, but otherwise uncatalyzed, has been reported recently by several investigators,<sup>2a-e</sup> and in two of these studies<sup>2c,e</sup> kinetic measurements of *p*-nitrophenyl acetate hydrolysis in phosphate buffer have been reported. In each case the reaction was followed by determining either the disappearance of ester<sup>2d</sup>

or the appearance of hydrolysis products.<sup>2a,b,c,e</sup> In the investigation reported here, we have followed the course of the hydrolyses through the alteration of the phosphate buffer content.

### Experimental

**Reagents: Ethyl Acetate.**—J. T. Baker Reagent Grade ethyl acetate was treated by the method of Fieser.<sup>3</sup> A sample of the distilled material had an  $n_D^{25}$  of 1.3700 (lit. value<sup>4</sup>  $n_D^{25,2}$  1.37012). Examination of a sample by gas chromatography uncovered no impurities.

**Methyl Acetate.**—Fisher-Certified methyl acetate was treated by the method of Hurd and Strong,<sup>5</sup>  $n_D^{25}$  of sample, 1.3589 (best literature values are 1.3588<sup>6a</sup> and 1.35938<sup>6b</sup>). Gas chromatography indicated the presence of impurities in both reagent and redistilled materials, with reduction in peaks with the latter.

An approximately 2.5 M solution of NaH<sub>2</sub>PO<sub>4</sub> was made up and stored in a 250-ml. volumetric flask using freshly opened Mallinckrodt granular NaH<sub>2</sub>PO<sub>4</sub>·H<sub>2</sub>O and freshly-boiled distilled water.

Anhydrous dibasic sodium phosphate, Na<sub>2</sub>HPO<sub>4</sub>, B. & A. Reagent Grade, and Mallinckrodt, granular, Analytical Reagent, was dried to constant weight at 105° and weighed amounts made up in a calibrated 500-ml. volumetric flask with freshly-boiled distilled water. The molarity of this solution was calculated (*ca.* 0.5 M).

Sodium hydroxide was made up in a liter Pyrex bottle in concentrated (50 wt. %) solution with freshly-boiled distilled water to which was added a small amount of barium hydroxide. Dilute solutions (0.05 to 0.1 N) were prepared periodically from this stock solution and kept in a Pyrex

(1) G. A. Gallagher, Dissertation, Univ. of Pa., 1954; *C.A.*, **48**, 10413b (1954).

(2) (a) T. C. Bruice and G. L. Schmir, *J. Am. Chem. Soc.*, **79**, 1663 (1957); (b) T. C. Bruice and G. L. Schmir, *ibid.*, **80**, 148 (1958); (c) T. C. Bruice and R. Lapinski, *ibid.*, **80**, 2265 (1958); (d) W. P. Jencks and J. Carriuolo, *ibid.*, **82**, 675 (1960); (e) W. P. Jencks and J. Carriuolo, *ibid.*, **82**, 1778 (1960).

(3) L. F. Fieser, "Experiments in Organic Chemistry," 3rd Ed., D. C. Heath and Co., Boston, Mass., 1955, p. 287.

(4) Zawidski, *Z. physik. Chem.*, **35**, 140 (1900).

(5) C. D. Hurd and J. S. Strong, *Anal. Chem.*, **23**, 542 (1951).

(6) (a) J. C. Munch, *J. Am. Chem. Soc.*, **48**, 994 (1926); (b) I. J. Krehma and J. W. Williams, *ibid.*, **49**, 2408 (1927).



bottle equipped with a drying tube containing Ascarite. Each fresh solution was standardized with reagent grade potassium acid phthalate.

Reagent grade sodium chloride was dried at about 110° for 30 minutes before weighed amounts were transferred to reaction flasks.

**Procedure.**—The homogeneous reaction solution was made up by transferring by calibrated delivery pipets both phosphate solutions, freshly-boiled distilled water, and ester, and then distilled water to the mark of the 100-ml. volumetric flask. For each series of runs a blank solution containing all but the ester was also made up. All of these transfers were carried out in a thermostat which was maintained at  $30.00 \pm 0.1^\circ$ . In those runs requiring the addition of sodium chloride to maintain the desired ionic strength, the salt was weighed into each volumetric flask before any solution was added.

When transfer was completed, the flasks were shaken vigorously for about 30 seconds and returned to the bath. Ten-ml. aliquots were then withdrawn from reaction and blank solutions and the  $\text{NaH}_2\text{PO}_4$  content of each determined by titration with sodium hydroxide using a Leeds & Northrup, Model 7664, pH meter.

Ten-ml. aliquots of the reaction solution were then pipetted into 18 mm. Pyrex tubes partially immersed in salt-ice water. The tubes were immediately corked to prevent evaporation of ester until they were sealed. After sealing they were placed in the bath and were removed at recorded times for determination of  $\text{NaH}_2\text{PO}_4$  content. The blank solution was kept in the stoppered volumetric flask, and aliquots were removed from time to time during the run for determination of  $\text{NaH}_2\text{PO}_4$  content. In no instance did this value vary by more than 0.5%; an average of these values was used as a base point in calculating the steady increase in  $\text{NaH}_2\text{PO}_4$  content found in the reaction aliquots. Before each titration the pH meter was standardized with NBS phosphate buffer in the pH 6.8–6.9 region. A set of three samples was usually analyzed consecutively; the readjustment required after each was quite small, less than 0.05 pH unit.

Whether the buffered reaction solution is affected to any degree by being in contact with Pyrex glass over an extended period of time (some of the samples remained in the bath for nine months) is not known. The reaction is sensitive, however, to traces of strong acid, since an almost instantaneous increase of 2 to 5% in phosphate monoanion content was noted in preliminary runs where volumetric flasks and delivery pipets had been cleaned with chromic acid and then rinsed a dozen times with distilled water. Subsequently, volumetric flasks were cleaned with a nonionic detergent (Triton X-100). Chromic acid rinse of delivery pipets was followed by one in alcoholic KOH and then a dozen rinses with distilled water. This revision in procedure eliminated the initial upsurge in monoanion content. The Pyrex tubes were simply rinsed about a dozen times with water.

**Calculations.**—Equating increase in phosphate monoanion, which is measured, to consumption of dianion and ester, the second-order rate expression has been used to plot the course of the reaction. In Table I data for Run 6 are listed.

TABLE I  
THE HYDROLYSIS OF ETHYL ACETATE IN AQUEOUS PHOSPHATE BUFFER AT 30°

<i>t</i> , hr.	<i>x</i> <sup>a</sup>	<i>k</i> (l. mole <sup>-1</sup> hr. <sup>-1</sup> )
0.3	0.00072	.....
54.9	.00281	0.00130
335.8	.01099	.00088
674.2	.02082	.00089
968.6	.02881	.00091
1399.3	.03834	.00091
2094.3	.05115	.00092

<sup>a</sup> The *x* values are equal to the increments in  $[\text{NaH}_2\text{PO}_4]$  in mole l.<sup>-1</sup>.

## Results

Run data and results are listed in Table II. Runs 11 and 12 were made to determine the effect of ionic strength on the rate of reaction. It should be

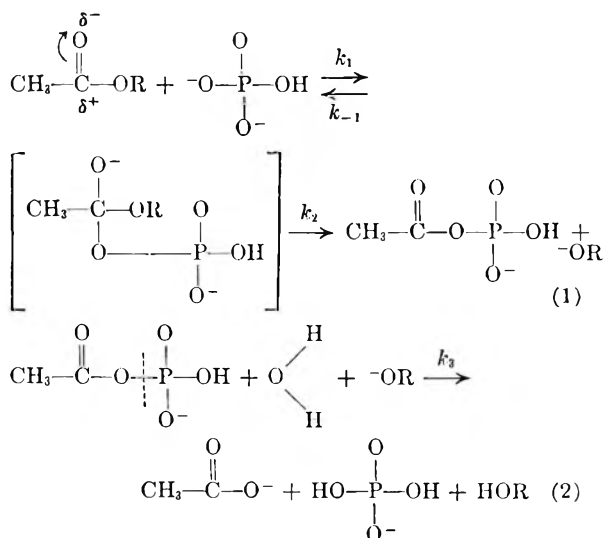
noted that the pH values listed take into consideration the dilution effect on phosphate buffer solutions; *i.e.*, these estimated values are about 0.2 pH unit lower than those measured for 10-ml. aliquots diluted to about 100 ml.

An attempt was made to measure ester hydrolysis in water alone at a neutral pH, but in the absence of buffer the medium gradually became acidic and triggered acid-catalyzed hydrolysis. It was found, however, that during the first two weeks of this blank run only about 0.4% of the ester had hydrolyzed; thereafter the rate accelerated rapidly.

## Discussion

The *k* values listed in Table II for the hydrolysis of ethyl acetate in solutions with a total ionic strength of 1.6 are constant within the range of experimental error. These constants have been obtained with varying concentrations of reactants. Equimolar amounts of each phosphate have been employed except in one case, run 13, where the ratio of di- to monoanion was 2, and the initial pH of the reaction solution was about 6.9, rather than 6.6–6.7 for the other runs. This variation in phosphate ratio had no noticeable effect on the rate. Close agreement in rate constants has been found with the three methyl acetate hydrolysis runs.

The reaction mechanism which best fits these data is believed to be a two-stage one, involving (1) nucleophilic attack by phosphate dianion on the partially polarized carbonyl carbon of the ester, followed by a splitting off of alkoxide ion and the formation of the relatively stable acetyl phosphate monoanion. In the second step, acetyl phosphate monoanion is hydrolyzed with P—O bond fission and the formation of acetate and monovalent phosphate anions and alcohol



assuming  $k_1 \ll k_{-1} \ll k_2, k_3$ ; then rate =  $k_1$  [ester]  $[\text{HPO}_4^{2-}]$

Step (1): Phosphoric acid and inorganic phosphates have been reacted with acetyl chloride,<sup>7</sup> with isopropenyl acetate,<sup>8</sup> and with acetic anhydride.<sup>9</sup> In each case one of the products was the mixed anhydride, acetyl phosphate. The addition

(7) F. Lipmann and L. C. Tuttle, *J. Biol. Chem.*, **153**, 571 (1944).

(8) E. R. Stadtmann and F. Lipmann, *ibid.*, **185**, 549 (1950).

(9) A. W. D. Avison, *J. Chem. Soc.*, 732 (1955).

TABLE II  
 HYDROLYSIS OF ALKYL ACETATES AT 30° IN PHOSPHATE BUFFERS

Run no.	Approximate initial concn. (mole/l.) Na <sub>2</sub> HPO <sub>4</sub>	Approximate initial concn. (mole/l.) NaH <sub>2</sub> PO <sub>4</sub>	Ester	NaCl	Initial ionic strength	$k \times 10^3$ , l. mole <sup>-1</sup> hr. <sup>-1</sup>	% reaction	Approx. pH of medium at start	Approx. pH of last sample
Ethyl acetate hydrolysis									
1	0.1	0.1	0.1	None	0.4	1.81	37	6.70	6.35
2	.1	.1	.1	1.2	1.6	1.02	41	6.60	6.30
3	.05	.05	.1	1.4	1.6	1.10	38	6.60	6.30
4	.1	.1	.05	1.2	1.6	1.01	46	6.65	6.45
5	.1	.1	.05	1.2	1.6	1.06	45	6.60	6.40
6	.1	.1	.4	1.2	1.6	0.92	51	6.60	6.10
7	.1	.1	.4	1.2	1.6	.87	70	6.60	6.00
8	.25	.25	.1	0.6	1.6	.95	42	6.60	6.45
9	.25	.25	.1	0.6	1.6	.95	39	6.60	6.50
10	.4	.4	.1	None	1.6	1.06	58	6.65	6.50
11	.1	.1	.1	0.8	1.2	1.13	23	6.60	6.45
12	.1	.1	.1	.4	0.8	1.35	25	6.70	6.50
13	.4	.2	.1	.2	1.6	1.11	45	6.90	6.75
Methyl acetate hydrolysis									
14	.125	.125	.125	1.0	1.5	1.72	38	6.70	6.40
15	.125	.125	.375	1.0	1.5	1.75	58	6.70	6.10
16	.375	.375	.125	None	1.5	1.73	73	6.65	6.45

of phosphate dianion to a saturated alkyl acetate would occur less readily than any of these reactions, and this has been confirmed by this study. As an example of the extreme slowness of the reactions, run 4 (Table II) required 7000 hours to reach 46% completion.

The postulated mechanism is similar to that proposed by Bruice and Lapinski<sup>2c</sup> for general base catalysis of *p*-nitrophenyl acetate by nucleophilic reagents, including HPO<sub>4</sub><sup>=</sup>, AcO<sup>-</sup>, CN and others, although the base catalyst was assumed to be regenerated after hydrolysis of the intermediate.

Step (2): Koshland<sup>10</sup> has studied kinetically the hydrolysis of acetyl phosphate in aqueous solution over a wide pH range and has reported that at a pH of 7.2 (phosphate buffer) about 80% was hydrolyzed within six hours at a temperature of 39°, and that the rate of disappearance of acetyl phosphate was first order and almost steady in the pH region 5–10. Isotopic experiments have demonstrated that hydrolytic cleavage of acetyl phosphate takes place at the P–O bond in this region,<sup>11,12</sup> a finding verified by Bunton and co-workers<sup>13</sup> who conducted an extensive kinetic and isotopic study of the hydrolysis of organic dihydrogen phosphates. They attributed the rapid hydrolysis of the phosphate monoanion to its special ability to form complexes with water through hydrogen bonding. Although acetyl phosphate was not examined, their findings indicated that the rate of hydrolysis was little affected by the nature of the organic group.

No search was made for an accumulation of an appreciable amount of the postulated acetyl phosphate anion in view of the findings of Koshland<sup>10</sup> and Bunton<sup>13</sup> that the rate of hydrolysis ( $k_3$  in our scheme) is far more rapid than the rate of formation which we have measured ( $k_1$ ). Furthermore, Bunton<sup>13</sup> reported that the presence of strong nucleo-

philes, such as halide ions, markedly increased the hydrolysis rates of organic dihydrogen phosphates. Large concentrations of NaCl have been employed in our study to maintain the high ionic strength of the medium, a factor which would further reduce the stability of acetyl phosphate in the reaction solution.

The gradual drift toward a lower pH as the reaction proceeds (Table II) is an indication of the changing phosphate buffer ratio as dianion is consumed and additional monoanion generated. Spot calculations were made at points in several of the runs. They show that the decreases in pH measured experimentally closely parallel ( $\pm 0.05$ – $0.10$  pH units) those found by applying the equilibrium constant

$$K = \frac{[H^+][HPO_4^-]}{[H_2PO_4^-]} = 6.2 \times 10^{-8}$$

Little or no general acid or specific hydronium ion catalysis is indicated in our results. Such catalysis would require a dependence of reaction rate on concentrations of phosphate monoanion and hydronium ion. Comparison of the observed rate for run 10 with that for run 13, where initial concentrations of monoanion and hydronium ion (as calculated from the initial pH of the reaction solution) were reduced by 50% (Table II), shows no difference within the limits of experimental error. Furthermore, the method we employed for following the course of the reaction demonstrated that the concentrations of these ions increased steadily as hydrolysis proceeded, while the reaction rate remained constant. Recent investigations by Bruice<sup>2c</sup> and Jencks<sup>14</sup> have disclosed that hydrolysis rates of *p*-nitrophenyl acetate in phosphate-buffered solutions were first order in both ester and phosphate dianion.

**Effect of Ionic Strength on Reaction Rates.**— Because this reaction is extremely slow, it has been

(10) D. E. Koshland, Jr., *J. Am. Chem. Soc.*, **74**, 2286 (1952).

(11) R. Bentley, *ibid.*, **71**, 2765 (1949).

(12) J. H. Park and D. E. Koshland, Jr., *J. Biol. Chem.*, **233**, 986 (1958).

(13) C. A. Bunton, *et al.*, *J. Chem. Soc.*, 3574 (1958).

(14) W. P. Jencks and J. Carriuolo, *J. Am. Chem. Soc.*, **82**, 1778 (1960).

necessary to use relatively large amounts of phosphate buffers and the ionic strength has been maintained at a very high level. At an ionic strength of this magnitude one might expect the reaction rate to be affected, and this effect has been measured by making single studies at ionic strengths of 0.4, 0.8 and 1.2 (runs 1, 12 and 11, resp., Table II). Findings point to a definite retardation of the reaction rate with increasing ionic strength of the

medium. A linear extrapolation of these data yields the value of  $1.8 \times 10^{-3}$  l. mole<sup>-1</sup> hr.<sup>-1</sup> for the reaction rate at zero ionic strength. It should be noted that the decrease in ionic strength over the course of a run is quite small. The calculated decrease in the ionic strength of the more lightly buffered run 7 after 70% completion amounts to 0.1 unit (about 6%); for the heavily buffered run 10 after 58% completion it is 0.05 units or about 3%.

## THE THERMAL DECOMPOSITION OF *n*-PROPYLCYCLOBUTANE<sup>1,2</sup>

BY S. M. E. KELLNER AND W. D. WALTERS

Department of Chemistry of the University of Rochester, Rochester, N. Y.

Received September 9, 1960

The thermal decomposition of *n*-propylcyclobutane has been studied in the temperature range 400–456° and at initial pressures from 5.4–495 mm. The products in the early stages of the reaction are almost exclusively ethylene and 1-pentene. The decomposition is a homogeneous first-order reaction which is not inhibited by nitric oxide, propylene or toluene. The temperature dependence of experiments with 5.4–117 mm. initial pressure gave an activation energy of  $61.6 \pm 0.6$  kcal./mole for the decomposition. The first-order rate constant can be expressed as  $k = 3.4 \times 10^{15} e^{-61,800/RT}$  sec.<sup>-1</sup>.

### Introduction

The saturated aliphatic hydrocarbons are known to decompose to a large extent by free radical processes,<sup>3</sup> whereas the members of the cyclobutane series studied so far have been found<sup>4,5</sup> to undergo a single ring cleavage reaction to give ethylene and a substituted ethylene. The decompositions of the cyclobutanes are of first order and are not inhibited by the addition of propylene, toluene or nitric oxide. It was of interest to study the thermal decomposition of *n*-propylcyclobutane to see whether with the increased length of the aliphatic side chain the molecule would undergo the simple ring cleavage of the smaller cyclobutanes or would decompose in a manner similar to that of the saturated aliphatic hydrocarbons. In the former case it was hoped that further data could be obtained regarding the effect of the size and nature of the side chain constituent on the rate of decomposition of the cyclobutane ring.

### Experimental

**Materials and Apparatus.**—The *n*-propylcyclobutane was prepared from ethyl cyclobutyl ketone by a Wolff-Kishner reduction as modified by Huang-Minlon.<sup>6</sup> The ethyl cyclobutyl ketone was prepared from cyclobutane-carboxylic acid and propionic acid by a catalytic procedure similar to that of Zelinskii and Kazanskiĭ.<sup>7</sup> The *n*-propylcyclobutane was fractionated in a 75 cm. Lecky-Ewell column at a reflux ratio greater than 7:1. Fractions III, IV and VI were used for kinetic studies. The boiling points at 749 mm. pressure

were: III, 99.8°; IV, 99.8°; VI, 100.1° (literature value<sup>7</sup> 99 to 100° at 736.2 mm.). Carbon-hydrogen analysis<sup>8</sup> yielded the following percentages: IV, C = 85.6, H = 14.3; VI, C = 85.3, H = 14.7 (theoretical, C = 85.63, H = 14.37). The refractive indices  $n_D^{20}$  were: IV, 1.412; VI, 1.412 (lit.<sup>7</sup>  $n_D^{19}$  1.4119). The density of VI was  $d_4^{19}$ , 0.746 (lit.<sup>7</sup>  $d_4^{19}$ , 0.7440). Minimum mole per cent. purities determined by gas chromatography were: III, 99.9; IV, 99.2; VI, 99.9. The infrared absorption curves for III, IV and VI, which showed strong absorption peaks at 3.50 and 6.85  $\mu$  and medium peaks at 7.24, 7.44, 7.56, 7.83, 7.98, 10.98 and 11.36  $\mu$ , were essentially identical and gave no evidence of impurities. The samples were usually dried over anhydrous CaSO<sub>4</sub> before use. As a further check on the possible effects of trace impurities on the kinetic results, special treatments were given the samples for some experiments, as described later.

The cyclobutane, methylcyclobutane, and part of the ethylcyclobutane from earlier investigations<sup>4,5</sup> were purified further for the present study by gas chromatography.

A sample of 1-pentene (N.B.S.) with a stated purity of 99.3  $\pm$  0.4 mole % was used without further purification. Samples of propylene (Ohio, 99.5%), ethylene (Ohio, 99.5%), ethylene oxide (Dow Chemical, specially purified), and nitric oxide (Matheson, 98.7%) were purified by repeated low temperature vacuum distillation, end fractions being discarded. Toluene (Brothers Chemical, reagent grade) was dried over anhydrous CaSO<sub>4</sub>. All samples were degassed immediately before use.

The vacuum system and the apparatus for temperature control were similar to those used in a previous study.<sup>9</sup> Pressure measurements for pressures above 32 mm. were made with a heated 3 mm. bore capillary mercury manometer. For the low pressure measurements a 20 mm. bore mercury manometer read with a Gaertner cathetometer was used. Most of the experiments were carried out in an unpacked 360 ml. cylindrical Pyrex reaction vessel (U), but a 110-ml. spherical Pyrex vessel (SU) was used for the majority of the experiments above 175 mm. The effect of the nature of the surface was tested by the use of a 330-ml. cylindrical unpacked Pyrex vessel (UC) with the inside walls coated with KCl. A packed vessel (P) which was filled with thin-walled Pyrex glass tubes had a surface-to-volume ratio 30 times greater than the plain 360-ml. vessel. The temperature was measured with a platinum, platinum-13% rhodium thermocouple connected to a Leeds and Northrup type K-2 potentiometer. The thermocouple was standardized repeat-

(1) This work was supported by a grant from the National Science Foundation.

(2) Abstracted from the Ph.D. Thesis submitted by S. M. E. Kellner, who held an E. H. Hooker fellowship during 1958–1959.

(3) E. W. R. Steacie, "Atomic and Free Radical Reactions," 2nd edition, Reinhold Publ. Corp., New York, N. Y., 1954, Chapter IV.

(4) C. T. Genaux, F. Kern and W. D. Walters, *J. Am. Chem. Soc.*, **75**, 6196 (1953).

(5) (a) M. N. Das and W. D. Walters, *Z. physik. Chem.*, **15**, Bohnhoffer Gedenkband, 22 (1958); (b) R. E. Wellman and W. D. Walters, *J. Am. Chem. Soc.*, **79**, 1542 (1957).

(6) (a) Huang-Minlon, *ibid.*, **68**, 2487 (1946); (b) D. Todd in "Organic Reactions," Vol. 4, John Wiley and Sons, Inc., New York, N. Y., 1948, p. 378.

(7) N. Zelinskii and B. A. Kazanskiĭ, *Ber.*, **60**, 1101 (1927).

(8) Performed by W. Manser, "Mikroanalytisches Laboratorium," E. T. H., Zürich, Switzerland.

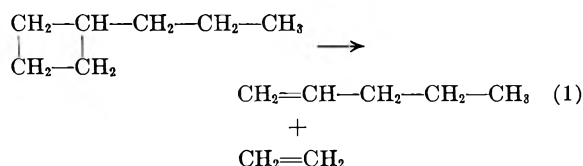
(9) E. R. Johnson and W. D. Walters, *J. Am. Chem. Soc.*, **76**, 6266 (1954).

edly at the melting point of zinc (419.5°) obtained from the National Bureau of Standards.

**Analysis of Reaction Products.**—The reaction products were separated on the basis of volatility and analyzed by infrared absorption spectrometry, mass spectrometry, absorption in sulfuric acid and gas chromatography. The fraction volatile at  $-196^\circ$  was very small (less than 1% of the total products) and was shown mass spectrometrically to be mostly methane.<sup>10</sup> The fraction volatile at  $-115^\circ$  gave an infrared absorption curve with peaks at 3.28, 5.25, 5.31, 5.38, 6.84, 6.94, 7.10 and 10.75  $\mu$  and marked absorption between 9.3 and 11.9  $\mu$ . The spectrum agreed well with one obtained for pure ethylene on the same instrument (Perkin-Elmer model 21 with a 1 meter gas cell) in this Laboratory and with infrared curves for ethylene in the literature.<sup>11</sup> The infrared absorption spectrum of the fraction volatile at  $-65^\circ$  was in good agreement with our spectrum of pure 1-pentene and with spectra in the literature,<sup>11</sup> (showing principal peaks at 3.28, 3.41–3.47, 6.09, 6.86, 10.04 and 10.98  $\mu$ ) but different from those of *cis*- and *trans*-2-pentene.<sup>11</sup> The infrared curve of the fraction condensable at  $-65^\circ$  was identical with that of *n*-propylcyclobutane.

The composition of the separated fractions of reaction products was determined by gas chromatography by comparison with standard synthetic mixtures. It was found that on an average 98% of the fraction volatile at  $-115^\circ$  corresponded to ethylene. This identification was confirmed by the absorbability of 95% of this fraction in activated sulfuric acid.<sup>12</sup> Of the fraction volatile at  $-65^\circ$ , 98% was found by gas chromatography to be pentene-1. The chromatograms of the fraction condensable at  $-65^\circ$  showed that it consisted of *n*-propylcyclobutane with not more than 2% of other components. The ethylene and *n*-propylcyclobutane fractions contained small amounts of 1-pentene; the pentene fraction contained traces of ethylene and *n*-propylcyclobutane. The retention times of small peaks on the chromatograms indicated the presence of small percentages of propylene and 1-butene in the ethylene and pentene fractions.

Gas buret measurements were used in conjunction with the quantitative gas-chromatographic analyses of the separated fractions to obtain a mass balance. The results for several typical experiments calculated as millimeters of pressure in the reaction vessel at the reaction temperature are shown in Table I. The data indicate that the only important reaction taking place is represented by



For the experiments shown in Table I, 1-butene, propylene and non-condensables averaged only 0.008, 0.019 and 0.014 times the corresponding pressure increases. These trace products are probably attributable to the slight secondary decomposition of 1-pentene. Less than 2% of a pure sample of 1-pentene decomposed when kept in the reaction vessel for a time equivalent to 35% decomposition of *n*-propylcyclobutane.

The products and stoichiometry of the thermal decomposition of *n*-propylcyclobutane do not seem to be affected by the reaction temperature, the surface-to-volume ratio, or the initial pressure of reactant over the range, experimental conditions studied. The pressure increase is very nearly equal to the pressure of ethylene formed, which in turn is about equal to the pressure of pentene-1 in the products. It appears, therefore, that the pressure increase is a good measure of the rate of the reaction.

(10) The mass-spectrometric analysis was kindly supplied by Mr. R. C. Wilkerson of the Celanese Corporation of America.

(11) Infrared Spectral Data, American Petroleum Institute Research Project 44, Carnegie Institute of Technology, Pittsburgh, Pennsylvania; Curves 18 and 530 for ethylene, curves 24, 145 and 356 for 1-pentene, curves 357 and 814 for *cis*-2-pentene, and curves 358 and 817 for *trans*-2-pentene.

(12) W. J. Gooderham, *J. Soc. Chem. Ind. (London)*, **57**, 388T (1938).

TABLE I

COMPARISON OF THE PRESSURE CHANGE IN THE DECOMPOSITION OF *n*-PROPYLCYCLOBUTANE WITH THE PRESSURES OF THE PRODUCTS

Vessel <sup>a</sup>	$P_0$ , <sup>b</sup> mm.	$\Delta P$ , <sup>c</sup> mm.	THE PRODUCTS		
			$P_E$ , <sup>d</sup> mm.	$P_P$ , <sup>d</sup> mm.	$P_{PCB}$ , <sup>d</sup> mm.
Temp., 450°					
U	9.73	3.32	3.36	3.32	
U	78.9	29.5	26.8	26.2	53.6
U	88.1	30.5	29.1	28.0	59.1
P	123.8	42.8	41.9	37.5	
P	143.3	49.5	52.4	53.3	
SU	457	149	150 <sup>e</sup>	148 <sup>e</sup>	300
Temp., 440°					
P	173.2	57.7	59.1 <sup>e</sup>	56.0 <sup>e</sup>	116
Temp., 410°					
P	95.6	33.0	33.0	33.2	
P	152.6	41.7	41.7	38.0	

<sup>a</sup> Vessel P is a 300-ml. packed bulb with surface to volume ratio thirty times that of U which is a 360-ml. unpacked Pyrex vessel. SU is a 110 ml. unpacked bulb. <sup>b</sup>  $P_0$  is the initial pressure of *n*-propylcyclobutane. <sup>c</sup>  $\Delta P$  is the measured pressure increase in the reaction bulb, corrected for dead space. <sup>d</sup>  $P_E$ ,  $P_P$  and  $P_{PCB}$  stand for the pressures of ethylene, 1-pentene, and unreacted *n*-propylcyclobutane in the reaction mixture. <sup>e</sup> The pressures of the products given are those of the separated fractions as measured in the gas buret.

## Results and Discussion

**Homogeneity and Order of the Reaction.**—In view of the data mentioned above, pressure-time curves were used to determine the rates of reaction under various conditions. The pressure-time curves exhibited no induction period and had the general appearance expected for a first-order reaction. Several types of evidence established a first-order behavior for the pyrolysis. A ninety-fold change in the initial pressure did not affect significantly the time for 25% decomposition ( $t_{1/4}$ ). Some typical values at 450° are given in Table II. Plots of  $\log(P_0/(2P_0 - P_t))$  vs. time were linear up to 20–25% decomposition. The ratio of quarter time to eighth-time ( $t_{1/4}/t_{1/8}$ ) for 51 experiments averaged 2.12, which is close to the theoretical value of 2.15 for a first-order reactions.<sup>13</sup>

The rate of the decomposition is apparently not influenced by the nature or the amount of the surface of the reaction vessel since neither coating the walls with KCl nor packing the vessel changed the quarter-time (see Table II). The decomposition, therefore, seems to be a homogeneous gas-phase reaction.

In order to test whether any trace impurities were influencing the rate of the decomposition, experiments were carried out with different fractions from the original distillation of the *n*-propylcyclobutane and also with samples subjected to various additional treatments as indicated in the representative experiments shown in Table II. No significant differences in the rates were observed for the different samples.

**Influence of Temperature.**—The temperature dependence of the pyrolysis was studied in an un-

(13) The slight deviations from linearity beyond 20% in the plots of  $\log(P_0/(2P_0 - P_t))$  vs. time and of the ratio ( $t_{1/4}/t_{1/8}$ ) from the theoretical value of 2.15 can be explained on the basis of the slight decomposition of 1-pentene.

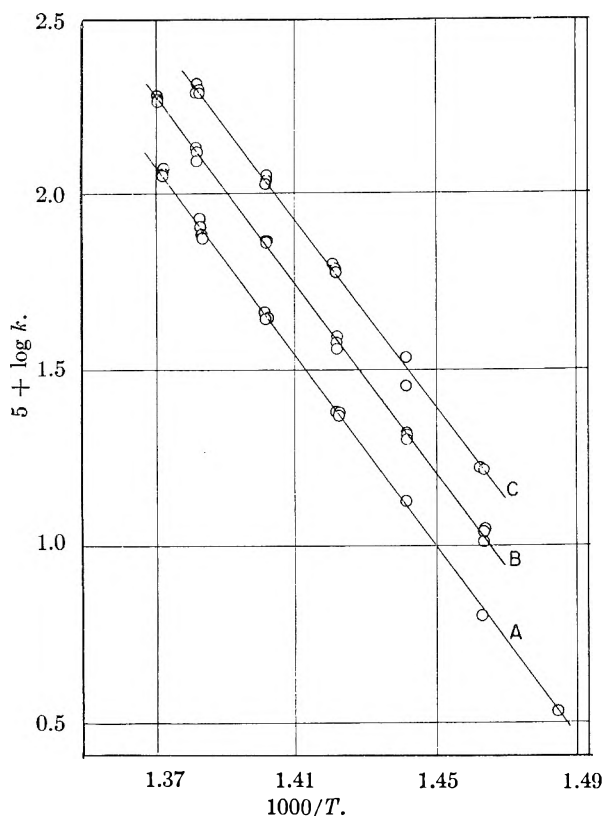


Fig. 1.—Temperature dependence of the first-order rate constant for the pyrolysis of *n*-propylcyclobutane: A, unpacked vessel, initial pressure 65–117 mm.; B, unpacked vessel, initial pressure 5–11 mm., curve displaced upwards 0.2 log unit; C, packed vessel, initial pressure 50–175 mm., curve displaced upwards 0.4 log unit.

TABLE II

DECOMPOSITION OF *n*-PROPYLCYCLOBUTANE AT 450° UNDER DIFFERENT EXPERIMENTAL CONDITIONS

$P_0$ , mm.	$t/4$ , min.	Sample <sup>a</sup>	$P_0$ , mm.	$t/4$ , min.	Sample <sup>a</sup>
Unpacked reaction vessel					
5.45	6.1	VI	178 <sup>b</sup>	5.9	VI
9.61	5.8	VI(1)	197	5.8	III
11.2	5.7	VI	257	5.8	VI(5)
77	6.0	VI	304 <sup>b</sup>	5.6	VI
80	5.9	IV	335	5.6	VI
103	5.9	IV	495 <sup>b</sup>	5.8	VI(4)
123 <sup>b</sup>	5.7	VI(4)			
Packed reaction vessel (P) <sup>c</sup>					
32	5.9	III(2)	87	5.8	III(3)
55	6.1	IV	107	6.1	III
71	5.7	III(2)	143	5.7	VI
85	5.8	III			
KCl coated vessel (UC)					
54–108	6.0 <sup>d</sup>	IV			

<sup>a</sup> Numbers in parentheses indicate the treatments of *n*-propylcyclobutane prior to decomposition: (1) treated with sodium; (2) purified by gas chromatography; (3) KOH; (4) pre-pyrolyzed; (5) treated with Linde molecular sieve 4A. <sup>b</sup> Experiment performed in a 110-ml. spherical vessel; in other cases, an unpacked 360-ml. cylindrical vessel was ordinarily used. The 257 mm. experiment was performed in a 320-ml. vessel in a second reaction system. <sup>c</sup> For description see the Experimental section. <sup>d</sup> Value at 450° obtained from graph of data of experiments from 449 to 453°. The other experiments were within 0.5° of 450°, but small corrections were applied whenever necessary.

packed Pyrex vessel between 410 and 456° in the range 4.7–11.2 mm. initial pressure and between 400° and 456° in the range 65–117 mm. Rate constants were calculated from quarter-times and eighth-times using the integrated first-order equation, and in a few instances rate constants were obtained from the slopes of graphs of  $\log(P_0/(2P_0 - P_t))$  vs. time. The experimental data, which are shown in Fig. 1, were used to determine the activation energy from the Arrhenius equation  $k = A \exp(-E/RT)$  in two ways: (1) by graphical determination of the slope of the best straight line through the points of a plot of  $\log k$  vs.  $1/T$ ; (2) by least squares analysis of the experimental points on an I.B.M. model 650 electronic computer. Similarly the activation energy was obtained for the experiments in the packed vessel between 410 and 450° over a range of initial pressures from 50–175 mm. The values of the activation energy determined by the two methods were in good agreement. The slopes of the graphs in Fig. 1 for the three different series of experiments are practically identical. The average value of the activation energy in the unpacked vessel was found to be  $61.6 \pm 0.6$  kcal./mole. Using this activation energy and known rate constants, the frequency factor was calculated. The first-order rate constant could thus be expressed as

$$k = 3.4 \times 10^{15} \exp(-61,600/RT) \text{ sec.}^{-1}$$

The fact that the activation energies for the decomposition of *n*-propylcyclobutane in the packed and unpacked vessels agree within 1 kcal./mole provides some additional indication that the decomposition in the unpacked vessel is homogeneous. If an appreciable fraction of the decomposition occurred by a heterogeneous reaction of lower activation energy, the activation energy observed in the packed bulb would be expected to be lower than that in the unpacked vessel.

**Effect of Added Substances.**—Propylene, toluene and nitric oxide are known to inhibit many free radical chain reactions,<sup>14</sup> whereas ethylene oxide in some cases leads to radical-induced reactions.<sup>15</sup> Experiments were carried out with each of these substances added separately to the reaction system. The data are summarized in Table III. It is evident from the last column of the table that the rate is approximately the same in the presence of radical chain inhibitors and radical sources. Thus, there is no indication of the occurrence of a decomposition involving long chains.

**Discussion.**—On the basis of the products formed, the first-order character, the homogeneity, and the lack of evidence for a chain mechanism the decomposition of *n*-propylcyclobutane resembles the decompositions of the alkylcyclobutanes previously studied and it may be another example of a unimolecular reaction. Efforts to obtain evidence for a biradical intermediate in the decomposition were unsuccessful. No isomerization product of

(14) (a) F. O. Rice and O. L. Polly, *J. Chem. Phys.*, **6**, 273 (1938); (b) L. A. K. Staveley and C. N. Hinshelwood, *Proc. Roy. Soc. (London)*, **154A**, 335 (1936); (c) M. Swzarc, *J. Chem. Phys.*, **17**, 431 (1949).

(15) C. J. M. Fletcher and G. K. Rollefson, *J. Am. Chem. Soc.*, **58**, 2135 (1936).

TABLE III

EFFECT OF ADDED SUBSTANCES UPON THE DECOMPOSITION OF *n*-PROPYLCYCLOBUTANE AT 450 ± 0.2°

<i>P</i> <sub>PCB</sub> , mm. <sup>a</sup>	Added gas	<i>P</i> <sub>A</sub> , mm. <sup>b</sup>	<i>t</i> / <sub>4</sub> , min.
105.6	Propylene	51.6	6.1
100.9	Toluene	31.3	6.0
69.1	Nitric oxide	0.5	5.6
88.3	Nitric oxide	2.0	5.6
6.52	Ethylene oxide	0.16	5.7-5.8
70-107	None	...	5.9 <sup>c</sup>

<sup>a</sup> *P*<sub>PCB</sub> means initial pressure of *n*-propylcyclobutane.  
<sup>b</sup> *P*<sub>A</sub> means pressure of added gas. <sup>c</sup> Average of 11 experiments.

*n*-propylcyclobutane could be detected and no indication of the formation of oximes or nitroso compounds by addition of nitric oxide to an intermediate radical or biradical was found.

The frequency factor for a unimolecular reaction can be expressed as

$$A = \kappa e(kT/h) \exp(\Delta S^\ddagger/R)$$

where  $\kappa$  is the transmission coefficient and  $\Delta S^\ddagger$  is the entropy of activation.<sup>16</sup> Taking  $\kappa$  as unity,  $\Delta S^\ddagger$  can be calculated from experimental values of *A*. The value of  $\Delta S^\ddagger$  calculated for the decomposition of *n*-propylcyclobutane at 450° is 8.9 cal./deg. mole. The positive value of  $\Delta S^\ddagger$  seems reasonable for a ring breaking reaction involving the loosening of some of the bonds in the formation of the activated complex.

The values for the activation energy and entropy of activation for the decomposition of *n*-propylcyclobutane are similar to the corresponding quantities for cyclobutane and the alkyl cyclobutanes studied earlier<sup>4,5</sup> ( $E_{\text{act}} = 61.2\text{--}62.5$  kcal./mole,  $\Delta S^\ddagger = 8\text{--}9$  e.u.) and suggest a similarity in the mechanism of decomposition. The relative rates at 450° for cyclobutane, methylcyclobutane, ethylcyclobutane and *n*-propylcyclobutane as determined in the present study under identical experimental conditions in the same apparatus are in the ratios 1.00:1.54:1.24:1.57. These values which confirm the ratios obtained previously<sup>4,5</sup> for the first three compounds indicate that the difference in rate produced by the substitution of an alkyl group for a hydrogen on the ring is relatively small. The results for the first three alkyl-sub-

(16) S. Glasstone, K. J. Laidler and H. Eyring, "The Theory of Rate Processes," McGraw-Hill Book Co., New York, N. Y., 1941, p. 295.

stituted cyclobutanes show an alternation rather than a monotonic change in rate with increase in size of the side chain and indicate that more than a single factor is involved. In these reactions a molecule of an alkylethylene is produced along with a molecule of ethylene. Thermodynamic data seem to indicate that the enthalpies (and free energies) of hydrogenation of ethylene and the lower substituted ethylenes may alternate to some extent in the same way as the rates of decomposition of the corresponding cyclobutanes.<sup>17</sup> To determine whether a Baker-Nathan order ( $H < \{CH_3\} > C_2H_5 > i-C_3H_7 > t-C_4H_9$ ) may exist for alkyl substituents,<sup>18</sup> the decomposition of isopropylcyclobutane will be investigated.

It is of interest that substitution for a hydrogen atom on the cyclobutane ring by a methyl, ethyl or *n*-propyl group has a very much smaller effect on the rate of decomposition of cyclobutane than the influence of  $\alpha$ -methyl substitution in the elimination of hydrogen halides from alkyl halides or in the elimination of olefins from esters.<sup>19</sup>

No fall-off in the first-order rate constant for the thermal decomposition of *n*-propylcyclobutane was observed at the lowest initial pressure reached in this study (5 mm.) although the rate constant for cyclobutane at 5 mm. initial pressure is 12-15% below its high pressure value. This difference in behavior is not unexpected. Both the Rice-Ramsperger-Kassel theory and the Slater theory of unimolecular reactions predict that with other factors held constant the first-order rate constant for the more complex molecule will show a more gradual fall-off beginning at a lower pressure.<sup>20</sup>

**Acknowledgment.**—The authors wish to thank the Esso Foundation for the grant to the Department of Chemistry which provided the gas chromatograph used in this work. They also wish to thank Mr. Carl Whiteman, Jr., for assistance in making the infrared measurements and in setting up the least squares computer program.

(17) R. W. Taft, Jr., and M. M. Kreevoy, *J. Am. Chem. Soc.*, **79**, 4011 (1957); E. J. Prosen and F. D. Rossini, *J. Research Natl. Bur. Standards*, **56**, 269 (1946).

(18) Recent spectroscopic data for aliphatic carbonyl derivatives seem to show a Baker-Nathan order. See C. N. R. Rao, J. Ramachandran and G. K. Goldman, *Tetrahedron Letters*, No. 2, 1 (1960).

(19) A. Maccoll, "Theoretical Organic Chemistry, The Kekulé Symposium," Butterworths, London, 1959, p. 230.

(20) For a comparison of methylcyclopropane with cyclopropane, see J. P. Chesick, *J. Am. Chem. Soc.*, **82**, 3277 (1960).

# THE THERMAL DECOMPOSITION OF ANHYDROUS URANYL NITRATE AND URANYL NITRATE DIHYDRATE<sup>1</sup>

BY R. S. ONDREJCIN AND T. P. GARRETT, JR.

*Savannah River Laboratory, E. I. du Pont de Nemours & Co., Aiken, South Carolina*

*Received September 12, 1960*

The thermal decomposition of anhydrous uranyl nitrate followed first-order kinetics *in vacuo* at temperatures from 250 to 450°. Amorphous uranium trioxide was the only non-volatile product of decomposition. No intermediate compounds were observed. The thermal decomposition of uranyl nitrate dihydrate occurred as two independent reactions following first-order kinetics: dehydration to form anhydrous uranyl nitrate and denitration to form uranium trioxide. The decomposition was studied both *in vacuo* and at atmospheric pressure under nitrogen, at temperatures from 250 to 400°. Intermediate and final decomposition products were identified. The specific reaction rate constants were measured for the dehydration and denitration reactions. From these data, the heats and entropies of activation were calculated.

## Introduction

Normally, uranium from spent reactor fuels is processed to form uranyl nitrate hexahydrate, which is thermally decomposed in a complex series of reactions<sup>2</sup> to yield uranium trioxide. The trioxide is reduced with hydrogen to uranium dioxide and then hydrofluorinated to uranium tetrafluoride. Conditions of thermal decomposition affect the reactivity of the trioxide and hence the efficiency of the reduction and hydrofluorination.

Table I shows the products possible from the thermal decomposition of uranyl nitrate hexahydrate.

$\alpha$ -UO <sub>3</sub>	UO <sub>3</sub> (A) <sup>a</sup>	$\alpha$ -UO <sub>3</sub> ·2H <sub>2</sub> O
$\beta$ -UO <sub>3</sub>	UO <sub>3</sub> · $\frac{1}{2}$ H <sub>2</sub> O	$\beta$ -UO <sub>3</sub> ·2H <sub>2</sub> O
$\gamma$ -UO <sub>3</sub>	$\alpha$ -UO <sub>3</sub> ·H <sub>2</sub> O	
$\delta$ -UO <sub>3</sub>	$\beta$ -UO <sub>3</sub> ·H <sub>2</sub> O	
$\epsilon$ -UO <sub>3</sub>	$\gamma$ -UO <sub>3</sub> ·H <sub>2</sub> O	
	$\delta$ -UO <sub>3</sub> ·H <sub>2</sub> O	

<sup>a</sup> Amorphous.

The nomenclature used for the allotropes of uranium trioxide was that suggested by Hoekstra and Siegel.<sup>3</sup> Other notations have been used by various authors.<sup>4-7</sup> In Hoekstra and Siegel's system,  $\gamma$ UO<sub>3</sub> is Dawson's<sup>4</sup> UO<sub>3</sub>(I), and  $\delta$ -UO<sub>3</sub> is Dawson's cubic phase, UO<sub>3</sub>(II). The  $\alpha$ -UO<sub>3</sub> is identical to UO<sub>3</sub>(I) described by Katz and Rabinowitch.<sup>5</sup> The  $\alpha$ - and  $\beta$ -monohydrates correspond, respectively, to Dawson's UO<sub>3</sub>·0.8H<sub>2</sub>O and UO<sub>3</sub>·H<sub>2</sub>O. There is no variation in the nomenclature for  $\gamma$ - and  $\delta$ -monohydrates. Infrared data indicate that the dihydrates have only one true water of hydration, while the mono- and hemihydrates probably are not true hydrates.<sup>8,9</sup>

(1) The information contained in this article was developed during the course of work under contract AT(07-2)-1 with the U. S. Atomic Energy Commission. Presented to the Boston Meeting of the American Chemical Society, April 1959.

(2) B. A. J. Lister and R. J. Richardson, "The Preparation of Uranium Trioxide by Thermal Decomposition of Uranyl Nitrate." Atomic Energy Research Establishment, Harwell, AERE C/R 1874, October 18, 1954.

(3) H. R. Hoekstra and S. Siegel, *Proc. U. N. Intern. Conf. Peaceful Uses Atomic Energy*, 2nd, Geneva, 28, 231 (1958). P/1548.

(4) J. K. Dawson, E. Wait, K. Alcock and D. R. Chilton, *J. Chem. Soc.*, 3531 (1956).

(5) J. J. Katz and E. Rabinowitch, "The Chemistry of Uranium," Natl. Nuclear Energy Ser., Div. VIII, Vol. 5, McGraw-Hill Book Co., New York, N. Y., 1951, pp. 277-285.

(6) P. Perio, *Bull. soc. chim. France*, 776 (1953).

(7) J. J. Katz and D. M. Gruen, *J. Am. Chem. Soc.*, 71, 2106 (1949);

These oxides are usually prepared by various treatments of uranyl nitrate or its hydrates, inferring that the mechanism of the thermal decomposition is extremely complex. The usual product of the thermal decomposition of UO<sub>2</sub>(NO<sub>3</sub>)<sub>2</sub>·6H<sub>2</sub>O is  $\gamma$ -UO<sub>3</sub>, which has variable reduction characteristics with H<sub>2</sub>.<sup>10</sup> A better understanding of the mechanism of decomposition could lead to a prediction of the process conditions necessary to produce UO<sub>3</sub> that would be reduced consistently under a given set of conditions.

## Experimental

Anhydrous uranyl nitrate was synthesized from uranium trioxide and nitrogen dioxide by the method of Gibson and Katz.<sup>11</sup> The product was analyzed for nitrogen by the Devarda modification of the Kjeldahl procedure. The nitrogen content of the product varied from 6.4-6.7 weight % corresponding to 90-95 weight % anhydrous uranyl nitrate. The remainder of the material consisted of unreacted uranium trioxide.

Uranyl nitrate dihydrate was prepared from reagent-grade uranyl nitrate hexahydrate that was placed in a vacuum desiccator over sulfuric acid for a minimum of 48 hours.<sup>12,13</sup> Analysis of the dihydrate showed the salt contained 55.3 weight % uranium which agreed with the theoretical value of 55.4 weight %. X-Ray diffraction showed only the dihydrate in the product.

The thermal decompositions were carried out in an all-glass system. Approximately 10-gram samples of each salt were heated in a reaction tube immersed in a molten metal bath. Two runs were made at each of four temperature levels over the range of 250-400°. In addition, one run with anhydrous uranyl nitrate was made at 450°. Gaseous products from the reactions were condensed in traps cooled with liquid nitrogen.

The condensed gaseous products taken periodically during the thermal decomposition were transferred to a storage bulb, weighed and the pressures measured at room temperature with a high sensitivity Bourdon gauge.<sup>14</sup> The samples were analyzed by infrared and mass spectroscopy. The liquid from hydrated samples remaining in the trap was weighed and titrated for acid content. The water of hydration was calculated from the liquid weight and acid content.

Decomposition at atmospheric pressure was carried out by flushing the system at a rate of 30 ml./min. with dried nitrogen. Under these conditions the gaseous products were not

(8) J. J. Katz and E. Rabinowitch, "Chemistry of Uranium," Natl. Nuclear Energy Ser. Div. VIII, Vol. 7, McGraw-Hill Book Co., New York, N. Y., 1951, p. 746.

(9) R. E. DeMarco, National Lead Co., private communication.

(10) C. W. Kuhlman, Jr., and B. A. Swinehart, *Ind. Eng. Chem.*, 50, 1774 (1958).

(11) G. Gibson and J. J. Katz, *J. Am. Chem. Soc.*, 73, 5436 (1951).

(12) A. J. King, R. Pfeiffer and W. Zeek, "Thermal Stability of the Hydrates of Uranyl Nitrate," Syracuse University, New York, N. Y., NYO 6313, August 1, 1957.

(13) J. J. Katz and G. T. Seaborg, "The Chemistry of the Actinide Elements," John Wiley and Sons, New York, N. Y., 1957, p. 193.

(14) R. A. W. Hill and R. A. Hamilton, *Research*, 7, 855 (1954).



removed from the reaction area immediately, so as to simulate the conditions normally found in the production of uranium trioxide. The pressure above the reaction remained within a few mm. of atmospheric pressure.

**Results**

In the vacuum denitration of  $UO_2(NO_3)_2$  the number of moles of this compound remaining at time  $t$  was derived from analyses of the gaseous products as shown in Table II.

TABLE I

THERMAL DECOMPOSITION OF  $UO_2(NO_3)_2$  UNDER VACUUM

Temp., °C.	Run I		Run II	
	Reaction time, min.	$-\log [UO_2-(NO_3)_2]^a$	Reaction time, min.	$-\log [UO_2-(NO_3)_2]^a$
250	0	1.85	0	1.55
	20	1.96	30	1.77
	60	2.12	90	1.95
	180	2.52	150	2.14
	360	3.26	210	2.42
			330	2.64
300	0	1.52	0	1.48
	10	1.60	10	1.52
	20	1.72	20	1.62
	30	1.85	30	1.72
	60	1.85	60	1.98
	120	2.68	122	2.52
350	0	1.42	0	1.45
	6	1.53	6	1.55
	10	1.68	16	1.81
	17	1.90	30	2.09
	30	2.20	48	2.35
	60	2.72		
450	0	1.46		
	14	2.10		
	23	2.76		
	40	3.40		

<sup>a</sup> Quantity of compound is expressed in moles.

Uranyl nitrate dihydrate was thermally decomposed under vacuum and under nitrogen at one atmosphere. From the analyses of the condensed gaseous products, the number of moles of water and uranyl nitrate present at any given time were calculated as shown in Table III.

Least squares analyses were made on each set of data in Tables II-III. The slopes of the lines were used to calculate the specific reaction rate constants shown in Table IV. The denitration reactions of both uranyl nitrate and uranyl nitrate dihydrate follow apparent first-order kinetics as does the dehydration of the dihydrate. The overall thermal decomposition of uranium nitrate dihydrate proceeds by way of two first-order mechanisms: the first, dehydration to the anhydrous nitrate; the second, denitration to the amorphous trioxide.

The data in Table IV show that the reaction rates at atmospheric pressure are much greater than those under vacuum. Gaseous decomposition products are probably removed under vacuum as rapidly as produced. At atmospheric pressure some of the gaseous products are not removed immediately and may be acting as catalytic agents.

Since the Arrhenius equation is an empirical relationship of the reaction rate constant-temperature dependence, the data in Table IV were plotted

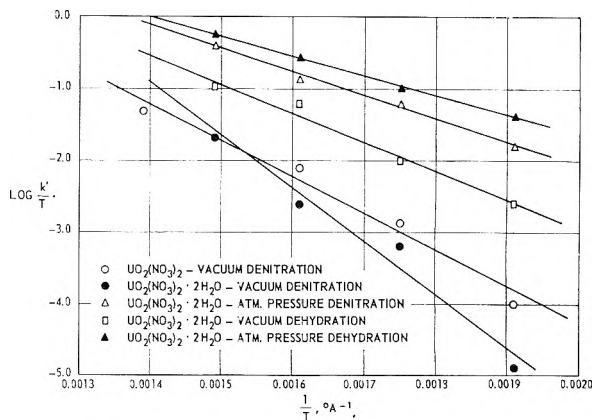


Fig. 1.—Thermal decomposition of uranyl nitrate and uranyl nitrate dihydrate.

TABLE III

THERMAL DECOMPOSITION OF  $UO_2(NO_3)_2 \cdot 2H_2O$

Pres- sure	Temp., °C.	Run I		Run II			
		Reac- tion time, min.	$-\log [H_2O]^a$	$-\log [UO_2-(NO_3)_2]^a$	Reac- tion time, min.	$-\log [H_2O]^a$	$-\log [UO_2-(NO_3)_2]^a$
Vacuum	250	0	1.21	1.58	0	1.25	1.56
		20	1.43	1.59	20	1.80	1.60
		60	1.95	1.66	60	2.82	1.66
		120	..	1.72	120	..	1.72
		180	..	1.79	180	..	1.75
		240	..	1.86	240	..	1.93
	300	..	1.89	300	..	1.99	
	300	0	1.24	1.36	0	1.32	1.38
		15	1.61	1.38	15	1.84	1.42
		30	2.10	1.46	30	2.34	1.54
		45	..	1.59	45	..	1.70
		75	..	1.74	75	..	1.87
		350	0	1.31	1.61	0	1.34
	400	0	1.20	1.45	0	1.23	1.50
		7	1.65	1.66	5	1.52	1.63
		18	2.92	2.10	12	2.37	1.70
		24	..	2.34	18	..	1.90
		250	0	1.12	1.42	0	1.40
Atmos- pheric		10	1.87	1.73	10	1.81	1.69
	15	2.31	2.00	16	2.02	1.90	
	25	3.16	2.52	24	2.77	2.32	
	300	0	1.18	1.61	0	1.18	1.48
	4	1.55	1.80	3	1.32	1.56	
	8	2.12	2.60	6	1.85	2.13	
350	15	..	..	15	2.60	2.61	
	0	1.38	1.62	0	1.44	1.64	
	3	2.36	1.99	3	1.89	1.90	
	6	2.82	2.43	6	2.38	2.24	
	400	0	..	..	0	..	..
	3	1.70	1.71	3	1.51	1.69	
4	2.11	1.89	5	2.16	2.25		
6	2.82	2.38	7	2.42	2.70		

<sup>a</sup> Quantity of compound is expressed in moles.

according to absolute reaction rate theory on the basis of equation 1

$$k' = \frac{kT}{h} e^{-(\Delta H^* - T\Delta S^*)/RT} \quad (1)$$

Plotting  $\log k'/*T$  vs.  $1/T$  as shown in Fig. 1, the slopes of the lines are  $-\Delta H^*/2.30R$ , with the intercepts equal to  $\Delta S^*/2.30R + 4.48$ . The

TABLE IV  
SPECIFIC REACTION RATES OF URANYL NITRATE

	Temp., °C.	$k', \text{min.}^{-1}$		
		Vac., anhydrous	Vac., dihydrate	Atm., dihydrate
Denitration	250	0.0083	0.0028	0.11
	300	.021	.014	.22
	350	.048	.032	.28
	400	...	.068	.55
	450	.12	...	..
Dehydration	250		.044	.18
	300		.074	.25
	350		.19	.45
	400		.22	.69

equations of the lines in Fig. 1 were calculated by the least squares method and the heats and entropies of activation were calculated from them. These values are shown in Table V.

TABLE V  
HEATS AND ENTROPIES OF ACTIVATION

Process	Hydration state	$\Delta H^*$ , kcal./mole		$\Delta S^*$ , e.u.	
		Vac.	Atm.	Vac.	Atm.
Denitration	Anhydrous	23.5	..	7.0	...
Denitration	Dihydrate	33.4	14.8	22.0	-0.3
Dehydration	Dihydrate	18.6	12.8	3.1	-2.5

The least reliable data are those derived from the vacuum denitrations. The estimated accuracy of the values for  $\Delta H^*$  in Table V is  $\pm 15\%$ . The calculated standard deviation of the plotted points affects  $\Delta S^*$  by 5 to 10%.

**Products and Intermediates.**—The effects of temperature and pressure on the final products of the thermal decomposition of anhydrous uranyl nitrate and uranyl nitrate dihydrate are summarized in Table VI.

TABLE VI  
FINAL DENITRATION PRODUCTS

Salt	Temp., °C.	Pressure	Product
$\text{UO}_2(\text{NO}_3)_2$	250-450	Vac.	$\text{UO}_3(\text{A})$
	500	Vac.	$\text{UO}_3(\text{A}) + \text{U}_3\text{O}_8$
$\text{UO}_2(\text{NO}_3)_2 \cdot 2\text{H}_2\text{O}$	250	Vac.	$\text{UO}_3(\text{A}) + \alpha\text{-UO}_3$
	300-400	Vac.	$\text{UO}_3(\text{A})$
$\text{UO}_2(\text{NO}_3)_2 \cdot 2\text{H}_2\text{O}$	250-450	Atm.	$\gamma\text{-UO}_3$
	500	Atm.	$\gamma\text{-UO}_3 + \beta\text{-UO}_3$

The salts that were decomposed at atmospheric pressure were blanketed with nitrogen. The final products were identified from established X-ray diffraction patterns,<sup>4,15,16</sup> infrared analyses,<sup>17</sup> and chemical analyses of the completely amorphous (A) compounds.

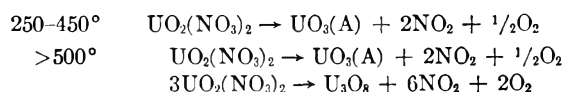
Typical chemical analyses of the amorphous products were 83.0, 83.1 and 83.1 weight % ura-

nium. Uranium trioxide is 83.2 weight % uranium. Small amounts of occluded nitrates detectable by Kjeldahl determinations caused the low experimental values.

Alpha- $\text{UO}_3$  is the normal end product of the dehydration of the hemihydrate of uranium trioxide. Since the hemihydrate is not formed above 250°, a substantial portion of the denitration must have occurred below this temperature. Heating at an increased rate would minimize the initial formation of the hemihydrate.

Reactions accounting for the decomposition of anhydrous uranyl nitrate under vacuum are shown in Table VII.

TABLE VII  
DECOMPOSITION REACTIONS ANHYDROUS URANYL NITRATE  
UNDER VACUUM



The vacuum denitration of uranyl nitrate dihydrate produced a compound with distinct X-ray diffraction and infrared absorption patterns not identifiable from data in the literature.

From previous experimental work and other data,<sup>18</sup> the compound was assumed to be a uranyl hydroxynitrate. To confirm this identification, uranyl hydroxynitrate was synthesized by adding "active" amorphous uranium trioxide<sup>11</sup> to an aqueous solution of uranyl nitrate. Vacuum dehydration at 30-35° of the solution produced a compound with the same X-ray diffraction pattern as the intermediate in denitration. The synthesized product had a rhombic structure. Analysis showed that titratable hydroxyl groups were present. Water of crystallization was determined by the Karl Fisher Reagent method and uranium by ignition; analysis showed 12 weight % water and 58.4 weight % U vs. 12 weight % water and 59.1 weight % U for a trihydrate of uranyl hydroxynitrate. Dehydration of this compound under vacuum at room temperature produced a compound that was amorphous to X-ray diffraction, but showed an infrared pattern, with hydroxyl groupings, not previously reported in the literature. Hydration of the dehydrated compound at room temperature changed the diffraction pattern from that of the trihydrate. The water solubility of the compounds formed proved the various allotropes of uranium trioxide were absent. This final compound was analyzed for water and uranium. The results agreed reasonably well with the values for uranyl hydroxynitrate tetrahydrate: uranium, 56.0 weight % vs. 56.5 weight %; water, 16 weight % vs. 17 weight %. Listed in Table VIII are the main diffraction lines of these hydrates and their relative intensities, plus the infrared absorption patterns for the hydrates and the anhydrous compound.

Differentiation is not made between the hydrates on the infrared pattern because the only variation is a slight increase in the size of the 3390 and 1626

(15) ASTM X-Ray Powder Data, File Card No. 2-0276.

(16) J. R. Bridge, C. W. Melton, C. M. Schwartz and D. A. Vaughan, Battelle Memorial Institute, BMI-1110, July 12, 1956.

(17) J. W. Nehls—Savannah River Laboratory, Aiken, S. C., private communication.

(18) R. H. Moore, "Factors Affecting the Reactivity of Uranium Trioxide," Interim Progress Report, Hanford Works HW-31670, April 29, 1954.

TABLE VIII  
X-RAY DIFFRACTION AND INFRARED ABSORPTION PATTERNS  
OF URANYL HYDROXYNITRATES

Tetrahydrate <i>d</i>	<i>I/I</i> <sub>0</sub>	Trihydrate <i>d</i>	<i>I/I</i> <sub>0</sub>	Hydrate		Anhydrous	
				Wave no., cm. <sup>-1</sup>	Charac- teristic	Wave no., cm. <sup>-1</sup>	Charac- teristic
7.15	70	6.33	55	3390	s, b		
6.52	60	5.68	55	1626	m		
6.30	85	5.58	100	1613	s	1613	s
5.19	35	5.28	80	1515	vs	1515	vs
4.70	45	5.20	75	1381	s, sp	1381	s, sp
4.49	40	5.01	70	1266	s	1266	s
4.33	100	4.81	70	1026	s	1026	s
3.83	35	4.08	70	943	vs	943	vs
3.56	35	3.75	70	845	vs	845	vs
3.24	70	3.52	75	803	s, sp	803	s, sp
2.16	50			749	w	749	w
				742	m, sp	742	m, sp

bands for the tetrahydrate as compared to the trihydrate.

The trihydrate, anhydrous uranyl hydroxynitrate and  $\alpha$ -uranium trioxide monohydrate were identified by infrared and X-ray diffraction as intermediates in the denitration of uranyl nitrate dihydrate under vacuum. Equations that account for these reactions are shown in Table IX.

TABLE IX  
DECOMPOSITION REACTIONS-URANYL NITRATE DIHYDRATE  
UNDER VACUUM

250°	Primary Reactions
	$\text{UO}_2(\text{NO}_3)_2 \cdot 2\text{H}_2\text{O} \rightarrow \text{UO}_2(\text{NO}_3)_2 + 2\text{H}_2\text{O}$
	$\text{UO}_2(\text{NO}_3)_2 \rightarrow \text{UO}_3(\text{A} + \alpha) + 2\text{NO}_2 + \frac{1}{2}\text{O}_2$
	Secondary Reactions
	$\text{UO}_2(\text{NO}_3)_2 \cdot 2\text{H}_2\text{O} \rightarrow \text{UO}_2(\text{OH})\text{NO}_3 + \text{H}_2\text{O} + \text{HNO}_3$
	$\text{UO}_2(\text{OH})\text{NO}_3 + 3\text{H}_2\text{O} \rightarrow \text{UO}_2(\text{OH})\text{NO}_3 \cdot 3\text{H}_2\text{O}$
	$\text{UO}_2(\text{OH})\text{NO}_3 \cdot 3\text{H}_2\text{O} \rightarrow \alpha\text{-UO}_3 \cdot \text{H}_2\text{O} + 2\text{H}_2\text{O} + \text{HNO}_3$
	$\alpha\text{-UO}_3 \cdot \text{H}_2\text{O} \rightarrow \text{UO}_3(\text{A}) + \text{H}_2\text{O}$
300-400°	$\text{UO}_2(\text{NO}_3)_2 \cdot 2\text{H}_2\text{O} \rightarrow \text{UO}_2(\text{NO}_3)_2 + 2\text{H}_2\text{O}$
	$\text{UO}_2(\text{NO}_3)_2 \rightarrow \text{UO}_3(\text{A}) + 2\text{NO}_2 + \frac{1}{2}\text{O}_2$

Thermal decomposition of uranyl nitrate dihydrate at atmospheric pressure produced either  $\gamma\text{-UO}_3$  between 250 and 400° or  $\gamma + \beta\text{-UO}_3$  at 500° as the final product. From 525 to 550° the final product was  $\beta\text{-UO}_3$ . Amorphous anhydrous uranyl hydroxynitrate was found as the only intermediate. The equations in Table X summarize the reactions of uranyl nitrate dihydrate at atmospheric pressure.

TABLE X  
DECOMPOSITION REACTIONS URANYL NITRATE DIHYDRATE  
AT ATMOSPHERIC PRESSURE

250°	$\text{UO}_2(\text{NO}_3)_2 \cdot 2\text{H}_2\text{O} \rightarrow \text{UO}_2(\text{NO}_3)_2 + 2\text{H}_2\text{O}$
	$\text{UO}_2(\text{NO}_3)_2 \rightarrow \gamma\text{-UO}_3 + 2\text{NO}_2 + \frac{1}{2}\text{O}_2$
	$\text{UO}_2(\text{NO}_3)_2 \cdot 2\text{H}_2\text{O} \rightarrow \text{UO}_2(\text{OH})\text{NO}_3 + \text{H}_2\text{O} + \text{HNO}_3$
	$\text{UO}_2(\text{OH})\text{NO}_3 \rightarrow \gamma\text{-UO}_3 + \text{HNO}_3$
300-450°	$\text{UO}_2(\text{NO}_3)_2 \cdot 2\text{H}_2\text{O} \rightarrow \text{UO}_2(\text{NO}_3)_2 + 2\text{H}_2\text{O}$
	$\text{UO}_2(\text{NO}_3)_2 \rightarrow \gamma\text{-UO}_3 + 2\text{NO}_2 + \frac{1}{2}\text{O}_2$
500°	$\text{UO}_2(\text{NO}_3)_2 \cdot 2\text{H}_2\text{O} \rightarrow \text{UO}_3(\gamma + \beta) + 2\text{NO}_2 + \frac{1}{2}\text{O}_2 + 2\text{H}_2\text{O}$
525-550°	$\text{UO}_2(\text{NO}_3)_2 \cdot 2\text{H}_2\text{O} \rightarrow \beta\text{-UO}_3 + 2\text{NO}_2 + \frac{1}{2}\text{O}_2 + 2\text{H}_2\text{O}$

The results presented show that by proper choice of conditions the thermal decomposition of uranyl nitrate dihydrate will produce a product that is primarily  $\beta\text{-UO}_3$ ,  $\gamma\text{-UO}_3$  or amorphous uranium trioxide. The  $\beta$ -phase is produced by the rapid decomposition of the dihydrate at temperatures above 500° at atmospheric pressure,  $\gamma$ -phase over the temperature range of 250-450°. Decomposition of the dihydrate in the temperature range of 300-450° under vacuum always produces amorphous uranium trioxide. Above 500° the product is contaminated with  $\text{U}_3\text{O}_8$ . Below 300° some  $\alpha$ -phase uranium trioxide is formed.

**Acknowledgment.**—The authors are indebted to Drs. C. H. Ice and R. C. Milham for technical advice, Drs. W. R. Cornman and J. W. Nehls for X-ray diffraction and infrared absorption patterns, and Mrs. B. S. Russell for chemical analyses.

## DIFFUSION TO A PLANE WITH LANGMUIRIAN ADSORPTION

By W. H. REINMUTH

Department of Chemistry of Columbia University, New York, N. Y.

Received September 13, 1960

A theoretical treatment is given of semi-infinite linear diffusion to a stationary plane with Langmuirian adsorption at the boundary. The fraction of the surface covered is a function of two variables  $C^*/a$  and  $a^2Dt/I_m^2$  where  $C^*$  is the solution concentration of surfactant,  $a$  is the solution concentration which would correspond to half coverage,  $\Gamma_m$  is the surface concentration of surfactant at full coverage,  $D$ , the diffusion coefficient of the surfactant and  $t$ , time. Comparisons of exact theory with approximate treatments are given and discussed. A formal solution to the same problem at an expanding plane is included.

Many workers have concerned themselves with the effects of surface active agents on electrode processes.<sup>1</sup> Delahay and Trachtenberg<sup>2</sup> in particular

(1) For a review see: W. H. Reinmuth in C. N. Reilly, ed., "Recent Advances in Analytical Chemistry and Instrumentation," Interscience Publishers, Inc., New York, N. Y., 1960.

(2) P. Delahay and I. Trachtenberg, *J. Am. Chem. Soc.*, **79**, 2355 (1957); **80**, 2094 (1958).

emphasized the influence of the rate of diffusion of these species on the observed results. Delahay and Fike<sup>3</sup> later attempted to solve the differential equations describing semi-infinite linear diffusion to a plane boundary with Langmuirian adsorption by an unstated method with the aid of an electronic

(3) P. Delahay and C. T. Fike, *ibid.*, **80**, 2628 (1958).

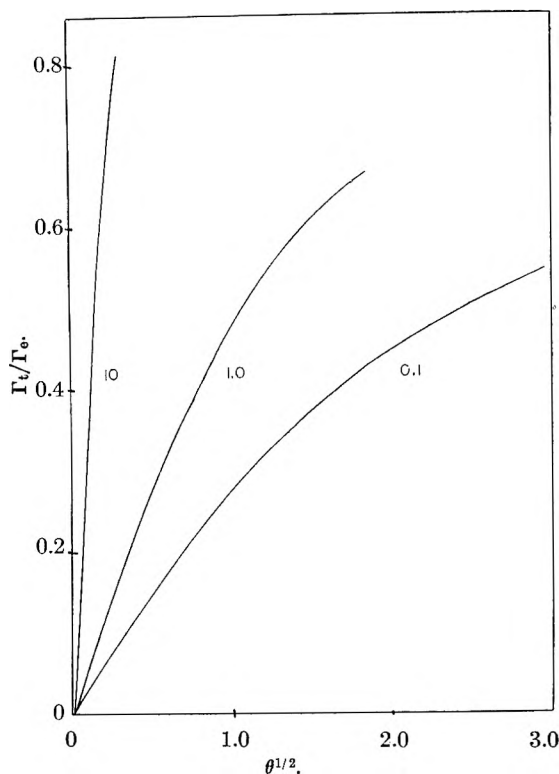


Fig. 1.—Fractional coverage of the boundary as a function of time for representative values of  $\psi$ .  $\Gamma_\infty$  is surface concentration at equilibrium.

computer. However, the form of their solutions, as we mentioned,<sup>1</sup> indicated that their method was invalid. Testa and Reinmuth<sup>4</sup> also made a numerical solution. More recently, in the course of other work, we have applied a method which gives solutions in series form. The purpose of the present paper is to describe that method and some of the results achieved by its application. For the sake of completeness the formal solution at an expanding plane is included, although no calculations have been performed for this case.

### Theory

It is assumed that the adsorbing species obeys Fick's laws of linear diffusion and has a constant diffusion coefficient,  $D$ ; further, that the initial concentration of the species in solution,  $C^*$ , is homogeneous. It can then be shown readily from Duhamel's theorem<sup>5</sup> that at the electrode surface

$$C = C^* - (D/\pi)^{1/2} \int_0^t (\partial C/\partial x)(t - \tau)^{-1/2} d\tau \quad (1)$$

where  $C$  is the solution concentration at the boundary at any time  $t$ ;  $x$  is the distance from the boundary; and  $\tau$  is an integration variable. It is assumed that at the boundary Langmuir's isotherm is obeyed in the form

$$\Gamma_t/\Gamma_m = C/(C + a) \quad (2)$$

where  $\Gamma_t$  is the instantaneous surface concentration corresponding to solution concentration  $C$ ,  $a$  is the isotherm constant, and  $\Gamma_m$  is the surface concentration corresponding to complete coverage.

(4) A. C. Testa and W. H. Reinmuth, unpublished work.

(5) H. S. Carslaw and J. C. Jaeger, "Conduction of Heat in Solids," Oxford University Press, London, 1947, p. 57.

It is also assumed that the adsorbed species does not react at the boundary or pass through it so that the material flux at the boundary equals the rate of adsorption

$$d\Gamma_t/dt = D(\partial C/\partial x)_{x=0} \quad (3)$$

Equations 1, 2 and 3 can be combined to give an integral equation for  $\Gamma_t$  in the form

$$a\Gamma_t/(\Gamma_m - \Gamma_t) = C^* - (\pi D)^{-1/2} \int_0^t (d\Gamma_\tau/d\tau)(t - \tau)^{-1/2} d\tau \quad (4)$$

It is convenient to define three dimensionless parameters

$$\mu = \Gamma_t/\Gamma_m; \psi = C^*/a; \theta = 4\pi a^2 D t/\Gamma_m^2 \quad (5)$$

Equation 4 can then be written in the form

$$\mu/(1 - \mu) = \psi - 2 \int_0^\theta (d\mu/d\rho)(\theta - \rho)^{-1/2} d\rho \quad (6)$$

Because equation 6 contains only two parameters in addition to  $\mu$ , it is apparent that its solution must be of the form

$$\mu = f(\psi, \theta) \quad (7)$$

However, Delahay and Fike<sup>3</sup> present theoretical results in the form

$$\mu = f(\psi, t, D/\Gamma_m) \quad (8)$$

The functional dependence of their results must be incorrect *a priori* because no combination of their stated variables can yield a dimensionless  $\mu$ . Since these authors give no indication of their method of solution, it is unclear whether the difficulty could be resolved by redefinition of their variables. The results given by the same authors for the expanding plane electrode are invalid for the same reason.

The method of solution of equation 6 is given in Appendix I.

In principle, the solution for an expanding plane electrode, the commonly used approximation of the dropping mercury electrode, follows the same lines as that for the stationary plane, with the modification that a different form of Fick's law must be applied. The details for this case are given in Appendix II.

### Results and Discussion

The series solution converges rapidly for small values of  $\theta$ . Results for three representative values of  $\psi$  are given in Fig. 1. They were all calculated with the aid of a ten term expansion. As might be expected, the rate of attainment of equilibrium is more rapid as  $\psi$ , the motivating force to adsorption, becomes larger. Results computed by the present method were within calculational error of those obtained by numerical solution of equation 6.<sup>4</sup>

The fractional coverage of the surface at equilibrium depends on  $\psi$ . For given equilibrium coverage, however, the time required to reach an appreciable fraction of that coverage is inversely proportional to the bulk solution concentration of the surfactant. For example, assuming  $\psi = 1$  *i.e.*, (half coverage at equilibrium),  $17\text{\AA}^2$  as the area of an adsorbed molecule, and  $5 \times 10^{-6}$  cm.<sup>2</sup>/sec. as the diffusion coefficient, the times required to reach quarter coverage for  $10^{-3}$ ,  $10^{-4}$ ,  $10^{-5}$  and  $10^{-6}M$  solutions are  $2 \times 10^{-2}$ ,  $2$ ,  $2 \times 10^2$ , and  $2 \times 10^4$  sec.,

respectively. The extreme times required at low concentrations are determined largely by the rate of diffusion to the electrode rather than by the adsorption equilibrium. This may be shown by assuming the same molecular area and diffusion coefficient as above but assuming  $a = 0$ . The time required for quarter coverage with a  $10^{-6}M$  solution is still  $1 \times 10^4$  sec.

It is of interest to compare the results of exact theory with those obtained by approximate methods. When equilibrium strongly favors the adsorbed form, the solution concentration of the surfactant at the boundary is reduced nearly to zero until the surface is completely coated. By substituting for equation 2 the condition

$$C_{(z=0)} = 0 \quad (9)$$

and solving the resulting set of equations 3, 4, 9 it can be shown that in this limiting case

$$\mu = \psi\theta^{1/2}/\pi \quad (10)$$

This is the same as the first term in the expansion for the case in which Langmuir's isotherm is obeyed. In Fig. 2, curve A exact theory (solid line) is compared with the approximation of equation 10 (dashed line) for the condition  $\psi = 10$ . The agreement is excellent up to about half-coverage. The approximation becomes even better as  $\psi$  becomes larger, and, even for smaller  $\psi$ , indicates the initial slope of the coverage *vs.* time relation.

For small values of  $\psi$  Langmuir's isotherm can be replaced by a linear approximation

$$\Gamma/\Gamma_m = C/a \quad (11)$$

The solution to the problem under this condition has been given by Delahay and Trachtenberg.<sup>2</sup> In the notation of the present work their result is

$$\mu = \psi - \psi \exp(\theta/4\pi) \operatorname{erfc}(\theta/4\pi)^{1/2} \quad (12)$$

In Fig. 2 curve B exact theory (solid line) is compared with this approximation (dashed line) for the condition  $\psi = 0.1$ . Again the agreement is excellent at short times and discrepancy becomes appreciable only at about 50% of equilibrium coverage. For smaller  $\psi$  the approximation is improved. It should be noted that there is some ambiguity involved in the choice of constants when approximating Langmuirian adsorption with a linear isotherm. In the present case, for example, with  $\psi$  chosen equal to 0.1 for each isotherm the predicted equilibrium coverage becomes 0.091 for Langmuirian adsorption but 0.1 for linear adsorption. As Fig. 2 indicates this leads to discrepancies between the two at long times. If the  $\psi$ 's are so chosen that the limiting values are equal, then the discrepancy shows up at short times. Appropriate choice of parameters for approximation is therefore dictated by where the error is of lesser importance.

Methods for experimentally achieving the mathematically assumed conditions merit some discussion. It would be a difficult operation at best to introduce an initially clean surface into a solution of surfactant without introducing convection. However, if the surface is a conductor, the same effect can often be achieved by applying a large anodic or cathodic potential to the electrode until time zero. Under such conditions desorption occurs in the presence of electrolytes due to preferential adsorption

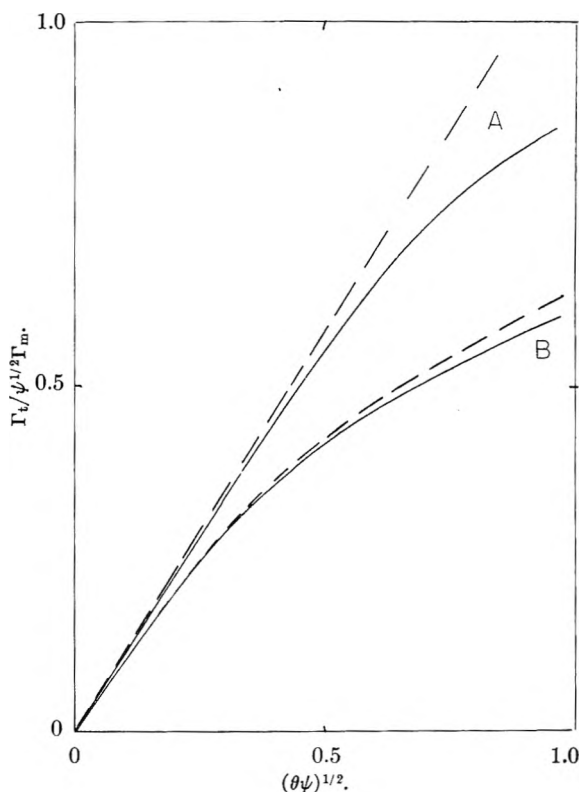


Fig. 2.—Comparison of exact theory with approximate methods. Curve A: solid line, exact theory; dashed line, complete adsorption; both for  $\psi = 10$ . Curve B: solid line, exact theory; dashed line, linear isotherm; both for  $\psi = 0.1$ .

of the latter on the surface. If desorption is not complete at accessible potentials, this can be taken into account theoretically by appropriate selection of  $a_0$  for the expansion (see Appendix I).

The mathematical treatment given here can be readily adapted to cases in which the adsorbate undergoes chemical or electrochemical reaction at the boundary or the adsorption process itself is slow. Preliminary results for these cases<sup>6</sup> indicate that the convergence of the series is much less rapid, however. Detailed discussion will be given elsewhere.

### Appendix I

**Stationary Plane.**—Equation 6 of the text can be solved by assuming the solution to be of the form

$$\mu = \sum_0^{\infty} a_i \theta^{i/2} = \sum \quad (A1)$$

From this it follows that

$$d\mu/d\theta = (2\theta)^{-1} \sum_1^{\infty} j a_i \theta^{i/2} \quad (A2)$$

Substituting equations A1 and A2 into equation 6 and defining the new integration variable,  $v = \rho/\theta$ , gives

$$\sum_0^1 \left(1 - \sum_0^1\right) = \psi - \theta^{-1/2} \sum_1^{\infty} j a_i \theta^{i/2} \int_0^1 v^{i/2-1} (1-v)^{-1/2} dv \quad (A3)$$

(6) P. Levy and W. H. Reimuth, unpublished work.

But

$$\int_0^1 v^{j/2-1} (1-v)^{-1/2} dv = B_{(j/2, 1/2)} \quad (\text{A4})$$

where  $B$  is the  $\beta$  function. Therefore

$$\theta^{1/2}(1+\psi) \sum_0^\infty = \psi \theta^{1/2} - \left(1 - \sum_0^\infty\right) \sum_1^\infty j a_j \theta^{j/2} B_{(j/2, 1/2)} \quad (\text{A5})$$

The coefficients  $a_j$  can be readily evaluated by equating terms with equal powers of  $\theta$  in equation A5. The first coefficient,  $a_0$ , is determined by the initial state of the system and is zero if there is no adsorption at time zero. In this case the second coefficient is

$$a_1 = \psi/\pi \quad (\text{A6})$$

and following coefficients are given by the recurrence formula

$$j a_j B_{(j/2, 1/2)} = -a_{j-1} + \sum_2^{j-1} i a_i a_{j-i} B_{(i/2, 1/2)} \quad (\text{A7})$$

### Appendix II

**Expanding Plane.**—For an expanding plane the analog of equation 1 of the text is

$$C = C^* - (3D/7\pi)^{1/2} \int_0^y (\partial C/\partial h)(y-\tau)^{-1/2} d\tau \quad (\text{A8})$$

where

$$y = t^{1/3}, h = xt^{2/3} \quad (\text{A9})$$

The analog of equation 3 of the text is

$$d\Gamma/dt = D(\partial C/\partial h)y^{2n} - 2\Gamma/3y^{3n} \quad (\text{A10})$$

Combining equations A8, A9 and A10 with equation 2 of the text yields

$$\mu = (1-\mu)\psi - \int_0^\alpha [7(\partial\mu/\partial\beta) + 2\mu/\beta]\beta^{2n} (\alpha-\beta)^{-1/2} d\beta \quad (\text{A11})$$

where

$$\alpha = (21\pi a^2 D/\Gamma_m^2)^{1/3} y \quad (\text{A12})$$

The solution of equation A11 is assumed to be of the form

$$\mu = \sum_0^\infty b_j \alpha^{3j/14} \quad (\text{A13})$$

Substitution into equation A11 and simplification gives

$$\rho(1+\psi) \sum_1^\infty b_j \rho^j = \rho\psi - \left(2 - \sum_1^\infty b_j \rho^j\right) \sum_1^\infty (2 + 3j/2) b_j \rho^j B_{(3j+4)/14, 1/2} \quad (\text{A14})$$

where  $\rho = \alpha^{3/14}$ , and it is assumed that  $b_0 = 0$ . Equating coefficients of equal powers of  $\rho$  allows the calculation of the  $b$ 's.

$$b_1 = 2\psi/7\mu \quad (\text{A15})$$

and following  $b$ 's are given by the recurrence formula

$$b_i(2 + 3j/2) B_{(3j+4)/14, 1/2} = -b_{j-1} + \sum_2^{j-1} (2 + 3i/2) b_i b_{j-i} B_{(3i+4)/14, 1/2}$$

## HEATS OF COMBUSTION, FORMATION, AND HYDROGENATION OF 14 SELECTED CYCLOMONOÖLEFIN HYDROCARBONS<sup>1</sup>

BY ABBAS LABBAUF AND FREDERICK D. ROSSINI<sup>2</sup>

*Chemical and Petroleum Research Laboratory, Carnegie Institute of Technology, Pittsburgh 13, Pennsylvania*

*Received September 19, 1960*

Measurements were made of the heat of combustion, in the liquid state at 25°, of 14 selected cyclomonoölefin hydrocarbons, with 5 to 8 carbon atoms per molecule. From these and appropriate other data were calculated values of standard heats of formation, hydrogenation and isomerization as appropriate, for the liquid state at 25°. The relation between energy content and molecular structure of these compounds is discussed. Values were calculated for the heat of formation, for both the liquid and gaseous states at 25°, for all the 1-normal alkyl cyclopentenes and all the 1-normal alkylcyclohexenes.

### I. Introduction

Preceding reports<sup>3-5</sup> have provided essentially complete data and information leading to the calculation of values of heats of formation, combustion, hydrogenation and isomerization as appropriate, for all aliphatic monoölefin hydrocarbons. Because of the scientific and technical importance of the cyclomonoölefin hydrocarbons, and the lack of data on them, it was desired that similar data and information should be obtained on this class of

hydrocarbons. Accordingly, the present investigation was carried out to obtain experimental data on 14 selected cyclomonoölefin hydrocarbons and to analyze the data in terms of the relation of energy content to molecular structure.

### II. Apparatus and Experimental Procedures

The experimental values of this investigation are based on the absolute joule as the unit of energy. Conversion to the defined thermochemical calorie is made by using the relation 1 calorie = 4.184 (exactly) joules. For internal consistency with other investigations from the Laboratory, the molecular weight of carbon dioxide was taken as 44.010 g./mole.

In this investigation, the chemical and calorimetric apparatus and procedure were the same as described by Browne and Rossini,<sup>6</sup> except that a new design of combustion bomb was used. The new bomb, made of Illium, is of the inverted type, as shown in Fig. 1. The rise of temperature in each experiment was near 2°, with the final temperature being

(1) This investigation was supported in part by a grant from the National Science Foundation. Submitted by Abbas Labbauf in partial fulfillment of the requirements for the degree of Doctor of Philosophy in Chemistry at the Carnegie Institute of Technology.

(2) University of Notre Dame, Notre Dame, Indiana.

(3) Sr. M. C. Loeffler and F. D. Rossini, *J. Phys. Chem.*, **64**, 1530 (1960).

(4) H. F. Bartolo and F. D. Rossini, *ibid.*, **64**, 1685 (1960).

(5) J. D. Rockenfeller and F. D. Rossini, *ibid.*, **65**, 267 (1961).

(6) C. C. Browne and F. D. Rossini, *ibid.*, **64**, 727 (1960).



near 30°, the temperature of the jacket of the calorimeter. The amount of reaction in each hydrocarbon combustion experiment was determined from the mass of carbon dioxide formed in the combustion, as previously described.<sup>6</sup> The bomb had an internal volume of 340 ml. One ml. of water was placed in the bomb prior to each combustion experiment. The pressure of the oxygen for combustion was made 30 atmospheres (calculated to 25°).

The compounds measured in the present investigation were API Research hydrocarbons, made available through the American Petroleum Institute Research Project 44 from materials purified by the American Petroleum Institute Research Project 6. The API Research samples had the values of purity given in Table I. Description of the purification and determination of purity of these samples has already been given.<sup>7-12</sup> As a result of the methods of purification, the impurities in these samples are substantially all isomeric, and the amounts are believed to be such as to have an insignificant effect on the results.

TABLE I  
PURITY OF THE HYDROCARBONS MEASURED

Compound	Purity, mole %
Ethenylcyclopentane (vinylcyclopentane)	99.92 ± 0.08
3-Cyclopentyl-1-propene (allylcyclopentane)	99.90 ± .10
Methylenecyclopentane	97.5 ± .5
Ethylidenecyclopentane	99.94 ± .05
Ethenylcyclohexane (vinylcyclohexane)	99.95 ± .04
Ethylidenecyclohexane	99.87 ± .06
Cyclopentene	99.975 ± .020
1-Methylcyclopentene	99.89 ± .08
3-Methylcyclopentene	(99.5 ± .4) <sup>a</sup>
4-Methylcyclopentene	99.8 ± .1
1-Ethylcyclopentene	99.5 ± .2
Cyclohexene	99.978 ± .020
1-Methylcyclohexene	99.86 ± .08
1-Ethylcyclohexene	99.90 ± .09

<sup>a</sup> Estimated.

The ampoules for containing the liquid hydrocarbon material were made of soft glass, as previously described and filled and sealed likewise.<sup>4,6</sup>

The methods of determining the absolute and relative heats of combustion and heats of isomerization have already been described.<sup>3-8,13</sup>

### III. Data of the Present Investigation

The results of the calorimetric combustion experiments with benzoic acid to determine the energy equivalent of the standard calorimetric system are given in Table II. NBS Standard benzoic acid, No. 39g, was used, with the value of 26,433.8 joules per gram mass for the heat of combustion of this sample under the conditions of the standard bomb process at 25°, with appropriate corrections for the differences between the actual and standard bomb processes. The symbols in Table II are as previously defined.<sup>5</sup>

A summary of the results of the calorimetric combustion experiments on the 14 hydrocarbons is given in Table III. In the 69 experiments referred to in Table III, the following ranges were observed in the several calorimetric quantities:

(7) A. J. Streiff, E. T. Murphy, V. A. Sedlak, C. B. Willingham and F. D. Rossini, *J. Research Natl. Bur. Standards*, **37**, 331 (1946).

(8) A. J. Streiff, J. C. Zimmerman, L. F. Soule, M. T. Butt, V. A. Sedlak, C. B. Willingham and F. D. Rossini, *ibid.*, **41**, 323 (1948).

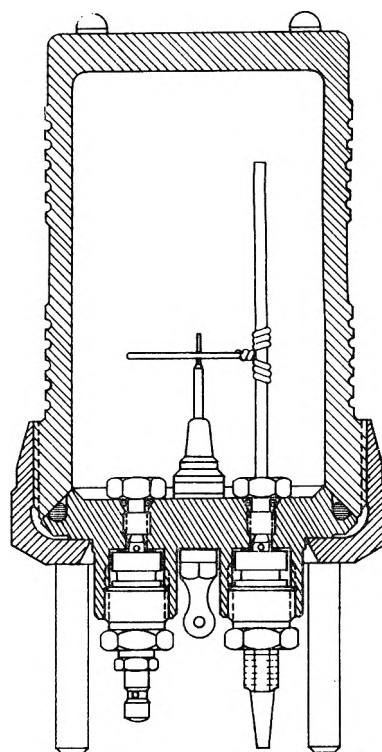
(9) A. J. Streiff, A. R. Hulme, P. A. Cowie, N. C. Krouskop and F. D. Rossini, *Anal. Chem.*, **27**, 411 (1955).

(10) A. J. Streiff, L. H. Schultz, A. R. Hulme, J. A. Tucker, N. C. Krouskop and F. D. Rossini, *ibid.*, **29**, 361 (1957).

(11) American Petroleum Institute Research Project 6. Carnegie Institute of Technology, Pittsburgh, Pennsylvania. Unpublished.

(12) A. J. Streiff, F. D. Rossini and others, Chemical and Petroleum Research Laboratory, Carnegie Institute of Technology, Pittsburgh, Pennsylvania. Unpublished.

(13) D. M. Speros and F. D. Rossini, *J. Phys. Chem.*, **64**, 1723 (1960).



BOMB ASSEMBLY

Fig. 1.—Inverted-type calorimetric combustion bomb (No. 1106, Parr Instrument Company, Moline, Illinois).

mass of carbon dioxide formed, 2.62466 to 2.94731 g.;  $k$ , 0.001600 to 0.001701/min.<sup>-1</sup>;  $K$ , 0.000736 to 0.001242 ohm;  $U$ , -0.000253 to 0.000258 ohm;  $\Delta R_c$ , 0.181187 to 0.204010 ohm;  $\Delta r_1$ , 0.000332 to 0.000388 ohm;  $\Delta r_2$ , 0.000007 to 0.000036 ohm. The foregoing symbols, and those in Table III, are as previously defined.<sup>6</sup>

In Table IV are presented the resulting values of the standard heats of combustion, for the liquid state at 25°, for the 14 compounds. The symbols have been defined previously.<sup>6</sup>

### IV. Data of Other Investigations

Previous data have been reported for the heats of combustion of cyclopentene,<sup>14</sup> cyclohexene<sup>14-17</sup> 1-methylcyclohexene,<sup>15,16</sup> 1-ethylcyclohexene<sup>16</sup> and ethenylcyclohexene.<sup>17</sup> Table V gives a comparison of the earlier data, reduced to modern form as appropriate and necessary, with the data of the present work. It is seen that the earlier modern work is in good agreement with the present investigations, but the others appear to be quite low.

### V. Heats of Formation, Hydrogenation and Isomerization from the Present Work

Table VI gives the values of the standard heats of formation and hydrogenation for the 14 hydrocarbons in the liquid state at 25°. The values of heats of formation were derived from the values of heats of combustion in Table IV combined with the

(14) E. J. Prosen, F. Yenchiu and F. D. Rossini, National Bureau of Standards, unpublished; see M. B. Epstein, K. S. Pitzer and F. D. Rossini, *J. Research Natl. Bur. Standards*, **42**, 379 (1949).

(15) P. W. Zubow, *J. Russ. Phys. Chem. Soc.*, **30**, 926 (1898); **33**, 708 (1901); **35**, 815 (1903). See also: W. Swietoslawski, *J. Am. Chem. Soc.*, **42**, 1092 (1920).

(16) W. Roth and K. von Auwers, *Liebigs Ann. Chem.*, **407**, 145 (1915).

(17) F. Stohman and Langbein, *J. prakt. Chem.*, **48**, 447 (1893).

TABLE II  
 RESULTS OF THE CALIBRATION COMBUSTION EXPERIMENTS WITH BENZOIC ACID

Expt.	Mass of benzoic acid, g.	$k$ , min. <sup>-1</sup>	$K$ , ohm	$U$ , ohm	$\Delta R_c$ , ohm	$q_i$ , j.	$q_n$ , j.	$E_i$ , j./ohm	Dev. from the mean, j./ohm
1	1.53899	0.001610	0.000980	0.000126	0.196862	69.68	2.09	206,981	- 5
2	1.54606	.001589	.000945	.000125	.197733	71.40	2.38	207,024	+39
3	1.54703	.001607	.000925	-.000053	.197904	71.55	2.38	206,975	-11
4	1.54975	.001595	.000915	-.000053	.198235	71.33	1.49	206,987	+ 1
5	1.54429	.001600	.000947	.000160	.197588	71.10	2.68	206,939	-47
6	1.54032	.001603	.000956	-.000038	.198289	71.56	1.79	207,009	+23
7	1.53905	.001609	.000940	-.000046	.196870	71.03	1.79	206,986	0
Mean value								206,986	
Standard deviation of the mean									±10

TABLE III

SUMMARY OF THE RESULTS OF THE CALORIMETRIC COMBUSTION EXPERIMENTS ON FOURTEEN HYDROCARBONS IN THE LIQUID STATE AT 30°

Compound	No. of expt.	Range of $B$ , ohm/g. CO <sub>2</sub>	Mean value of $B$ , ohm/g. CO <sub>2</sub>	Stand. dev. of the mean, ohm/g. CO <sub>2</sub>
Ethenylcyclopentane (vinylcyclopentane)	5	0.0694143 to 0.0694608	0.0694369	±0.0000076
3-Cyclopentene-1-propene (allylcyclopentane)	5	.0696126 to .0696460	.0696350	± .0000058
Methylcyclopentane	5	.0688558 to .0688920	.0688723	± .0000066
Ethylidencyclopentane	5	.0690718 to .0691054	.0690922	± .0000058
Ethenylcyclohexane (vinylcyclohexane)	5	.0693143 to .0693281	.0693222	± .0000041
Ethylidencyclohexane	5	.0691105 to .0691248	.0691188	± .0000024
Cyclopentene	5	.0683040 to .0683345	.0683192	± .0000053
1-Methylcyclopentene	5	.0685372 to .0685574	.0685487	± .0000040
3-Methylcyclopentene	5	.0688000 to .0688213	.0688071	± .0000039
4-Methylcyclopentene	5	.0688966 to .0689449	.0689188	± .0000085
1-Ethylcyclopentene	5	.0690550 to .0690743	.0690684	± .0000054
Cyclohexene	4	.0685232 to .0685393	.0685306	± .0000031
1-Methylcyclohexene	5	.0687006 to .0687200	.0687090	± .0000040
1-Ethylcyclohexene	5	.0690558 to .0690908	.0690747	± .0000057

TABLE IV

VALUES<sup>a</sup> OF THE STANDARD HEATS OF COMBUSTION IN THE LIQUID STATE

Compound	$-\Delta E_B$ at 30°, kcal./mole	$-\Delta E_C$ at 30°, kcal./mole	$-\Delta H_C$ at 30°, kcal./mole	$-\Delta H_C$ at 25°, kcal./mole
Ethenylcyclopentane (vinylcyclopentane)	1058.15 ± 0.25	1058.06 ± 0.25	1059.97 ± 0.25	1060.27 ± 0.25
3-Cyclopentyl-1-propene (allylcyclopentane)	1212.77 ± .23	1212.40 ± .23	1214.51 ± .23	1214.87 ± .23
Methylcyclopentane	899.62 ± .19	899.32 ± .19	900.83 ± .19	901.08 ± .19
Ethylidencyclopentane	1052.90 ± .19	1052.57 ± .19	1054.38 ± .19	1054.69 ± .19
Ethenylcyclohexane (vinylcyclohexane)	1207.32 ± .18	1206.95 ± .18	1209.06 ± .18	1209.42 ± .18
Ethylidencyclohexane	1203.78 ± .14	1203.41 ± .14	1205.52 ± .14	1205.88 ± .14
Cyclopentene	743.66 ± .14	743.15 ± .14	744.35 ± .14	744.55 ± .14
1-Methylcyclopentene	895.39 ± .14	895.10 ± .14	896.60 ± .14	896.85 ± .14
3-Methylcyclopentene	898.76 ± .13	898.47 ± .13	899.98 ± .13	900.22 ± .13
4-Methylcyclopentene	900.22 ± .24	899.93 ± .24	901.44 ± .24	901.68 ± .24
1-Ethylcyclopentene	1052.42 ± .19	1051.96 ± .19	1054.02 ± .19	1054.32 ± .19
Cyclohexene	895.15 ± .12	894.65 ± .12	896.37 ± .12	896.62 ± .12
1-Methylcyclohexene	1047.06 ± .16	1046.73 ± .16	1048.54 ± .16	1048.85 ± .16
1-Ethylcyclohexene	1203.01 ± .23	1202.64 ± .23	1204.75 ± .23	1205.11 ± .23

<sup>a</sup> The uncertainties in this table are twice the standard deviation.

appropriate values for the heats of formation of water and carbon dioxide.<sup>18</sup> The values of heats of hydrogenation were derived from these heats of formation and the heats of formation of the appropriate paraffin hydrocarbons.<sup>18,19</sup>

From the values of the heats of formation in Table VI, values of heats of isomerization may be readily obtained for three groups of compounds, for the liquid state at 25°, in kcal./mole

1-Methylcyclopentene, 0.00; 3-methylcyclopentene, 3.37 ± 0.22; 4-methylcyclopentene, 4.83 ± 0.29; methylenecyclopentane, 4.23 ± 0.27.

1-Ethylcyclopentene, 0.00; ethylidencyclopentane, 0.37 ± 0.28; ethenylcyclopentane(vinylcyclopentane), 5.95 ± 0.34.

1-Ethylcyclohexene, 0.00; ethylidencyclohexane, 0.77 ± 0.31, ethenylcyclohexane(vinylcyclohexane), 4.31 ± 0.33.

## VI. Heats of Formation of the 1-Normal Alkyl Cyclopentenes and Cyclohexenes

For the members of any normal alkyl series of compounds, the relation proposed by Rossini<sup>20</sup>

(18) F. D. Rossini, K. S. Pitzer, R. L. Arnett, R. M. Braun and G. C. Pimentel, "Selected values of physical and thermodynamic properties of hydrocarbons and related compounds," API Research Project 44. Carnegie Press, Pittsburgh, Pa., 1953.

TABLE V  
 COMPARISON WITH THE DATA OF OTHER INVESTIGATIONS

Compound (liquid)	Previous investigators	Year	Derived value of $\Delta H_c^\circ$ at 25°, kcal./mole	Difference from the value of $\Delta H_c^\circ$ at 25° of the present work, kcal./mole
Ethenylcyclopentane (vinylcyclopentane)	Roth <sup>16</sup>	1915	1206.7	-2.7 ± ?
Cyclopentene	Prosen, Yenchius and Rossini <sup>14</sup>	1944	744.46 ± 0.17	-0.09 ± 0.31
	Zubow <sup>15</sup>	1903	889.9	-6.7 ± ?
Cyclohexene	Roth and von Auwers <sup>16</sup>	1915	891.0	-5.6 ± ?
	Stohman and Langbein <sup>17</sup>	1893	890.7	-5.9 ± ?
	Prosen, Yenchius and Rossini <sup>14</sup>	1944	896.20 ± 0.21	-0.42 ± 0.35
1-Methylcyclohexene	Zubow <sup>15</sup>	1903	1034.0	-14.8 ± ?
	Roth and von Auwers <sup>16</sup>	1915	1046.9	-1.9 ± ?
1-Ethylcyclohexene	Roth and von Auwers <sup>16</sup>	1915	1202.2	-2.9 ± ?

TABLE VI

 VALUES<sup>a</sup> OF THE STANDARD HEATS OF FORMATION,  $\Delta H_f^\circ$ , AND HYDROGENATION,  $\Delta H_h^\circ$ , FOR THE LIQUID STATE AT 25°

Compound	$\Delta H_f^\circ$ , kcal./mole	$\Delta H_h^\circ$ , kcal./mole
Ethenylcyclopentene (vinylcyclopentane)	- 8.00 ± 0.26	-31.08 ± 0.38
3-Cyclopentyl-1-propene (allylcyclopentane)	-15.77 ± .25	-29.44 ± .39
Methylenecyclopentane	- 4.82 ± .21	-28.26 ± .29
Ethylidenecyclopentane	-13.58 ± .21	-25.50 ± .32
Ethenylcyclohexane (vinylcyclohexane)	-21.22 ± .21	-29.50 ± .43
Ethylidenecyclohexane	-24.76 ± .18	-25.96 ± .41
Cyclopentene	1.02 ± .15	-26.33 ± .23
1-Methylcyclopentene	- 9.05 ± .16	-24.03 ± .26
3-Methylcyclopentene	- 5.68 ± .15	-27.40 ± .25
4-Methylcyclopentene	- 4.22 ± .25	-28.86 ± .32
1-Ethylcyclopentene	-13.95 ± .21	-24.93 ± .32
Cyclohexene	- 9.28 ± .14	-28.06 ± .24
1-Methylcyclohexene	-19.42 ± .19	-26.03 ± .31
1-Ethylcyclohexene	-25.53 ± .25	-25.19 ± .45

<sup>a</sup> The uncertainties in this table are twice the standard deviation.

may be used to represent the values of the heats of formation

$$\Delta H_f^\circ = A + Bm + \Delta \quad (1)$$

 Here  $A$  is a constant characteristic of the end group,  $B$  is the constant increment per  $\text{CH}_2$  group,  $m$  is the number of carbon atoms in the normal alkyl group attached to a carbon atom of a given end group, and  $\Delta$  may, within certain limits, be taken as zero for values of  $m$  of 2 and greater. This means that, when values for the first three members of a given series are known, the values for all the higher members can be calculated.<sup>3</sup>

From the values in Table VI, the following equations may be derived for the liquid state at 25°

$$\Delta H_f^\circ = -1.74 - 6.106m \text{ kcal./mole; for all the 1-normal alkyl cyclopentenes with}$$

$$m > 1 \quad (2)$$

$$\Delta H_f^\circ = -13.31 - 6.106m \text{ kcal./mole; for all the 1-normal alkyl cyclohexenes with}$$

$$m > 1 \quad (3)$$

## VII. Discussion

From the values of heats of isomerization given above, the following comments may be made regarding the relative stability of the compounds in the several groups of isomers: 1-Methylcyclopentene is more stable (3.4 kcal./mole) than 3-methylcyclopentene, which is more stable (1.5 kcal./mole)

than 4-methylcyclopentene. 1-Methylcyclopentene is more stable (4.2 kcal./mole) than methylenecyclopentane. 1-Ethylcyclopentene is slightly more stable (0.4 kcal./mole) than ethylidenecyclopentane, which is more stable (5.6 kcal./mole) than ethenylcyclopentane. 1-Ethylcyclohexene is slightly more stable (0.8 kcal./mole) than ethylidenecyclohexane, which is more stable (3.5 kcal./mole) than ethenylcyclohexane.

Considering ethylcyclopentene and its several isomers, including ethylidene- and ethenylcyclopentenes or the corresponding isomers of ethylcyclohexene, one can make the following statements: With respect to energy content, the molecule becomes more stable as the double bond moves from outside the ring (ethenyl) to the edge of the ring (ethylidene) and into the ring in the 1-position. Movement of the double bond around the ring from the 1-position to the 3-position to the 4-position is in the direction of lesser stability.

 The foregoing observations are in accord with the work of Turner and Garner<sup>21,22</sup> in 1957. Furthermore, these conclusions are in accord with the generalization made by Rossini<sup>23</sup> in 1940 regarding

TABLE VII

COMPARISON OF THE HEATS OF HYDROGENATION OF TEN CYCLOMONOOLEFINS WITH THOSE OF THE STRUCTURALLY ANALOGOUS ALIPHATIC MONOOLEFINS, IN THE LIQUID STATE, AT 25°

I Cyclomonoolefin	II Aliphatic monoolefin	$\Delta H_h^\circ(\text{II}) - \Delta H_h^\circ(\text{I})$ , kcal./mole
1-Methylcyclopentene	2-Methyl-2-pentene	-1.02 ± 0.63
3-Methylcyclopentene	4-Methyl- <i>cis</i> -2-pentene	-0.40 ± .56
4-Methylcyclopentene	<i>cis</i> -2-Hexene	2.00 ± .64
Methylenecyclopentane	2-Ethyl-1-butene	1.02 ± .66
1-Ethylcyclopentene	2-Methyl-2-pentene	-0.12 ± .69
Ethylidenecyclopentane	2-Methyl- <i>trans</i> -2-pentene	0.04 ± .69
Ethenylcyclopentane	2-Methyl-1-pentene	1.70 ± .74
1-Ethylcyclohexene	2-Methyl-2-pentene	0.14 ± .82
Ethylidenecyclohexane	3-Methyl- <i>trans</i> -2-pentene	.50 ± .78
Ethenylcyclohexane	2-Methyl-1-pentene	.12 ± .81

monolefin hydrocarbons, namely, that, with regard to energy content, increase in the stability of the molecule is produced by having the double bond near the center of the molecule and by having the maximum number of carbon atoms attached to each of the doubly bonded carbon atoms, excluding steric hindrance of the attached groups.

It is of interest to compare the heats of hydro-

 (19) D. D. Wagman, J. E. Kilpatrick, W. J. Taylor, K. S. Pitzer and F. D. Rossini, *J. Research Natl. Bur. Standards*, **34**, 143 (1945).

 (20) F. D. Rossini, *ibid* **13**, 21 (1934).

 (21) R. B. Turner and R. H. Garner, *J. Am. Chem. Soc.*, **79**, 253 (1957).

 (22) R. B. Turner and R. H. Garner, *ibid.*, **80**, 142 (1958).

 (23) F. D. Rossini, *Chem. Revs.*, **27**, 1 (1940).

genation of the cyclomonoolefins measured in the present investigation with the heats of hydrogenation of aliphatic monoolefins which are structurally analogous, with respect to the attachments to, and orientation about, the double bond. Table VII

gives such a comparison. It is to be noted that in the ten pairs of compounds, the corresponding heats of hydrogenation differ by an average, without respect to sign, of only  $\pm 0.66$  kcal./mole, with the maximum difference being only 2.0 kcal./mole.

## THE CONFIGURATION OF ADSORBED ALKYL METHACRYLATE POLYMERS BY INFRARED AND SEDIMENTATION STUDIES

BY B. J. FONTANA AND J. R. THOMAS

California Research Corporation, Richmond, California

Received September 19, 1960

The number of attached segments of a poly-(alkyl methacrylate) molecule adsorbed from solution onto silica was determined directly by infrared spectrometry. Use is made of the shift of 22 to 30  $\text{cm}^{-1}$  of the normal carbonyl vibration frequency at about 1740  $\text{cm}^{-1}$  caused by hydrogen bonding to the surface hydroxyl groups. The extinction coefficient for adsorbed carbonyl is established by study of the adsorbed mono- and di-esters. The effect of adsorption on the spectrum of the silica surface hydroxyls in the region of 3670 to 3420  $\text{cm}^{-1}$  confirms the adsorption mechanism depicted. The fraction of attached segments,  $p$ , is found to be about 0.36 at high coverage and is only slightly dependent upon surface coverage. It is independent of a 3.6-fold change in molecular weight and 1.3-fold change in polymer voluminosity. These results agree only partially with the predictions of the statistical theories of polymer adsorption for strong interactions. The apparent fit of the adsorption data to the Langmuir isotherm is discussed. Estimates of the film thicknesses of several polymers adsorbed on carbon black particles are made from sedimentation studies.

### Introduction

Studies of the adsorption of polymers from solution onto solid surfaces indicate that adsorption occurs at a number of points along the molecular chain. The polymer chain segments between the points of adsorption presumably loop into the surrounding solution. These conclusions were first arrived at by Jenckel and Rumbach<sup>1</sup> to account for the fact that more polymer is adsorbed than can be accounted for by a monolayer. In two recent studies attempts have been made to obtain direct quantitative information on the state of adsorbed polymer. Using values for the area occupied on a liquid-air interface by a monomeric unit of polyvinyl acetate and the measured adsorption on iron surfaces, Koral, Ullman and Eirich<sup>2</sup> concluded that the polymer film was of the order of 10–20 molecules thick. Comparison with measurements of the adsorption by the monomeric analog, ethyl acetate, suggested values about twice as high. From a comparison of the adsorption of polyisobutylene on carbon black with an estimate of the available adsorption sites, Binford and Gessler<sup>3</sup> concluded that these polymers were completely extended on the surface.

A statistical analysis of polymer adsorption by Simha, Frisch and Eirich<sup>4,5</sup> resulted in a form of the adsorption isotherm which in principle allows the determination of the number of adsorbed segments per molecule. In the few instances where this equation has been applied to actual adsorption data<sup>3,6</sup> (for polyhydrocarbons on carbon black), the number of adsorbed segments per macromolecule appears to be of the order of one to three.

The theory further predicts that the number of adsorbed segments will be proportional to the square root of the molecular weight in the case of weak boundary forces and directly proportional to the molecular weight when the boundary forces are appreciably greater than  $kT$ . This latter prediction will be tested directly in the present work.

The above summary is not exhaustive; however, it serves to illustrate the need for unambiguous information regarding the state of adsorbed macromolecules. This paper describes a direct experimental determination of the number of segments attached to a silica surface for an adsorbed poly-(alkyl methacrylate). The results of a study to determine directly the thickness of adsorbed polymer films from the sedimentation rates of polymer coated carbon black particles is also reported.

**Theoretical Approach for Determination of the Number of Attachments.**—The adsorption of a poly-(alkyl methacrylate) obviously will involve attachment of the polar ester group to the solid surface. In particular, when the solid surface has OH groups available, the adsorption will certainly proceed *via* H-bond formation with the carbonyl oxygen atoms of the ester. Studies<sup>7,8</sup> in the homogeneous liquid phase have shown that the characteristic stretching vibration frequency of ester carbonyl groups ( $\nu \sim 1700$   $\text{cm}^{-1}$ ) is shifted to lower frequencies when H-bonding occurs. Such a shift ( $\Delta\nu = 14$  to 29  $\text{cm}^{-1}$ ) then must occur as a result of the adsorption of the poly-(alkyl methacrylate). The unadsorbed carbonyl groups in the "free" loops of the adsorbed polymer molecule should exhibit only the normal ester carbonyl vibration frequency. A direct measure of the number of adsorbed groups is possible, then, provided that (1) the unperturbed and H-bonded carbonyl frequencies can be resolved in the infrared spec-

- (1) E. Jenckel and B. Rumbach, *Z. Elektrochem.*, **55**, 612 (1951).
- (2) J. Koral, R. Ullman and F. R. Eirich, *J. Phys. Chem.*, **62**, 541 (1958).
- (3) J. S. Binford and A. M. Gessler, *J. Phys. Chem.*, **63**, 1376 (1959).
- (4) R. Simha, H. L. Frisch and F. R. Eirich, *ibid.*, **67**, 584 (1953).
- (5) H. L. Frisch, *ibid.*, **69**, 633 (1955).
- (6) G. Kraus and J. Dugone, *Ind. Eng. Chem.*, **47**, 1809 (1955).

- (7) M. L. Josien and J. Lascombe, *J. chim. phys.*, **52**, 162 (1955).
- (8) P. G. Puranik, *J. Chem. Phys.*, **26**, 601 (1957).

trum of the adsorbed polymer molecule and (2) an estimate of the extinction coefficient for the adsorbed carbonyl can be made.

This requires that the infrared spectrum be observed directly on the equilibrium system: polymer (in solution)  $\rightleftharpoons$  polymer (adsorbed). Recently, Terenin and Filimonov<sup>9</sup> have studied the frequency shifts upon adsorption of simple organic molecules onto silica, etc., from carbon tetrachloride solutions. Changes were found in the first overtone frequencies of the C-H band of ethyl ether and of the N-H band of aromatic amines when the ether or amine was adsorbed on the solid phase. The success of such observations depends simply upon having sufficiently small particles with high surface area. Contact with the liquid phase actually aids in decreasing light scattering from the solid particles.

In the homogeneous liquid phase, H-bond formation of hydroxyl groups with esters, results in a large frequency shift of the fundamental O-H stretching vibration at about 3620  $\text{cm}^{-1}$ . Many of the studies on gas-solid adsorption<sup>10</sup> have been concerned with the analogous shift in either the first overtone or fundamental OH stretching frequency. Terenin and Filimonov<sup>9</sup> demonstrated such an effect in their liquid-solid adsorption systems. We have also made some use of this effect in the polymer studies.

### Experimental

**Materials.** PLMA.—The polymer designated PLMA was prepared by the thermal polymerization of a partially fractionated commercial (Rohm and Haas) "lauryl methacrylate." The final product had a composition corresponding closely to a  $\text{C}_{12}$  alkyl side chain.

**PAM-VP.**—The polymer designated PAM-VP was prepared by the procedure described in Australian patent no. 216911 from commercial (Rohm and Haas) "stearyl methacrylate" and N-vinyl-2-pyrrolidone. Analysis indicated the product was a copolymer of alkyl methacrylate and vinylpyrrolidone in the monomer ratio 5 to 1.

The polymers were fractionated by the usual solvent precipitation techniques, the precipitated fractions being redissolved and reprecipitated by appropriate temperature control. The fractions were always less than 10% of the original material. Molecular weights were determined from intrinsic viscosity measurements in benzene based on previous calibrations from ultracentrifuge sedimentation rates (see Table I.)

TABLE I  
CHARACTERIZATION OF POLYMER FRACTIONS

Polymer fraction	$[\eta]$ at 25°					Mol. wt. $\times 10^{-4}$
	Iso-octane	n-Dodecane	Tetrachloroethane	Benzene	Decalin	
PLMA-3	72	74	83	92	95	330
PLMA-7	173	172	177	217	228	1190

The esters, *n*-dodecyl isobutyrate, and di-*n*-dodecyl 3,3-dimethylglutarate were synthesized by standard methods. Narrow (17%) heart distillation cuts were used in the adsorption experiments. The di-*n*-butyl oxalate and succinate esters were Eastman Grade and used as received.

The solid adsorbent was the non-porous silica Cab-O-Sil from G. L. Cabot, Inc. According to the manufacturer, the particle diameter is 0.015–0.020  $\mu$  with a surface area

(9) A. Terenin and V. Filimonov, "Hydrogen Bonding," D. Hadzi, Editor, Pergamon Press, Inc., New York, N. Y., 1959, pp. 545–554.

(10) R. P. Eischens, S. A. Francis and W. A. Pliskin, *J. Chem. Phys.*, **22**, 1786 (1954); *J. Phys. Chem.*, **60**, 194 (1956). For a recent comprehensive review, see R. P. Eischens and W. A. Pliskin, "Advances in Catalysis," Vol. X, D. D. Eley, et al., Editors, Academic Press, Inc., New York, N. Y., 1958, pp. 1–56.

( $\text{N}_2$  adsorption) of 175–200  $\text{m}^2/\text{g}$ . The silica was stored *in vacuo* over Drierite desiccant before use.

Aerosol O.T. (Sodium di-2-ethylhexyl sulfosuccinate) was purified by removing a methanol-soluble fraction. The fluorotoluene was Eastman White Label.

Humphrey-Wilkinson, Inc. *n*-dodecane (minimum 95% purity) was dried over calcium hydride, then percolated through silica gel. *cis*-Decalin obtained by fractionation of Du Pont decalin was similarly treated. The purified solvents were stored under dry nitrogen. The measured densities at 25° were 0.744 and 0.892  $\text{g}/\text{cm}^3$  for the dodecane and decalin, respectively.

**Determination of Adsorption Isotherms.**—Adsorption isotherms were determined from the concentration change before and after adsorption. From 20 to 200 mg. of silica was shaken with about 9 cc. of solution for 6–10 hours at room temperature ( $25.5 \pm 1.5^\circ$ ). Accurate temperature control is not necessary in view of the very small heats of adsorption, in general, for polymers. (See, for example, ref. 1 and 2.) After equilibration, the mixtures were centrifuged directly for analysis of the supernatant solution. Analyses were carried out by means of infrared spectrometry using the carbonyl absorption peak at about 5.8  $\mu$ . Appropriate calibrations were made for each system with solutions of known concentration. A Perkin-Elmer Model 21 infrared spectrometer with  $\text{CaF}_2$  prism was used throughout the present work. Automatic slit programming was employed corresponding to spectral slit widths of 9 and 3  $\text{cm}^{-1}$  at 2.7 and 5.7  $\mu$ , respectively. The wave length was calibrated *versus* polystyrene standards.

**Spectra of Adsorbed Species.**—In order to make quantitative spectral measurements, it was necessary to work with known weights of adsorbent per unit area in the light beam. This was accomplished relatively simply because of a fortunate property of Cab-O-Sil. Upon centrifuging the equilibrium adsorption mixtures, the silica settled as a stable gel containing approximately 6 to 7% solid. The latter composition was determined accurately in each case by draining off the supernatant solvent completely and weighing the residual gel. A portion of the gel (usually about 0.1 g.) was then weighed onto the polished face of a 1-inch diameter NaCl disk. By careful manipulation, a second identical disk could be placed on top of the first to result in the uniform spreading of the sample over the total 1-inch diameter area. Very gentle clamping of the NaCl plates resulted in some loss of the solvent phase by "bleeding" out of the gel; however, the distribution of the solid phase remained unaffected. These preparations were stable for at least several hours as evidenced by lack of spectral changes and were very transparent; light scattering was negligible. The reproducibility of the weight of the solid phase per unit area in the spectrometer light beam was at least  $\pm 10\%$ , which was adequate for our purpose. It was convenient for the purposes of this investigation to express the extinction coefficients on a simple weight basis; hence, we define

$$\epsilon_w = \frac{\log I/I_0}{\text{g./cm.}^2} = \frac{D}{\text{g./cm.}^2}$$

To avoid possible confusion with surface adsorption, note that the values of  $\text{g./cm.}^2$  (or  $\text{mg./cm.}^2$ ) given throughout this paper always refer to the denominator in the above equation.

The relation to the usual molar extinction coefficient  $\epsilon_M$  is

$$\epsilon_M = \frac{\epsilon_w \times M}{1000}$$

where the carbonyl equivalent weight is used for the molecular weight,  $M$ , in the case of the diesters and polymers.

To balance out the infrared absorption of the unadsorbed species and/or the solvent, a continuously variable thickness NaCl cell was used in the reference beam of the spectrometer. To eliminate the effect of the solvent alone, the variable cell containing pure solvent was adjusted to cancel the hydrocarbon overtone peak at about 2.4  $\mu$ . The very intense hydrocarbon peaks must be avoided for this purpose because the high light energy absorption renders the spectrometer insensitive. To eliminate the effect of the "free" carbonyl, the canceling must obviously be done at the carbonyl absorption peak using an appropriate solution. In the case of monomer adsorption, the free car-

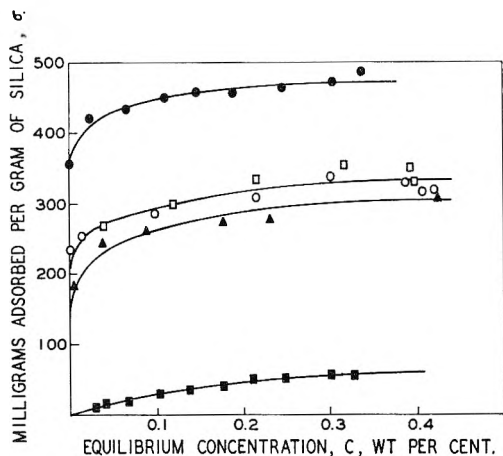


Fig. 1.—Adsorption isotherms on silica from dodecane at 25.5°C: ●, PAM-VP; ○, PLMA-3; □, PLMA-7; ▲, PLMA-3 from decalin; ■, dodecyl isobutyrate.

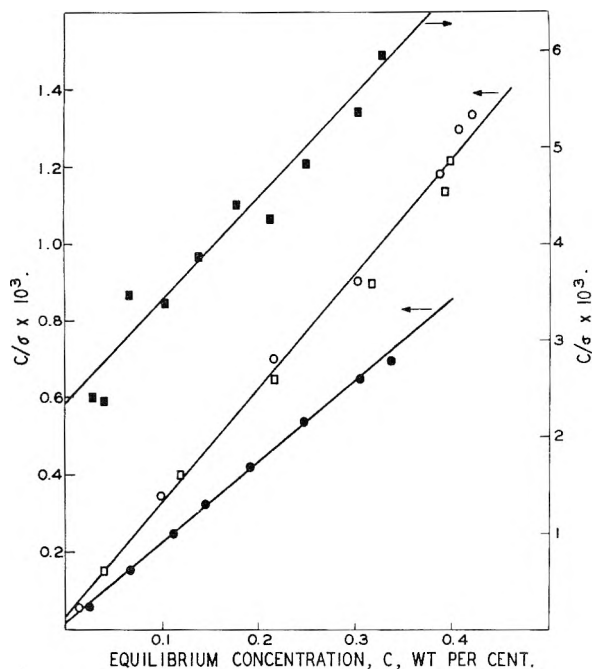


Fig. 2.—Langmuir plot of  $c/\sigma$  vs.  $c$ ; symbols same as for Fig. 1.

bonyl is due only to the equilibrium concentration of monomer in the liquid phase. Hence, a solution of just the equilibrium concentration of monomer is required for complete canceling. In the case of polymer adsorption, free carbonyl will be due to both the equilibrium concentration and the carbonyl in the free loops of adsorbed polymer. Hence, the appropriate concentration of polymer to use in the variable cell for complete cancellation of both solvent and free carbonyl could be found only after preliminary trial and error. Actually, accurate simultaneous cancellation of the effects of solvent and carbonyl or even of carbonyl alone was not necessary. Mismatching of the carbonyl cancellation by as much as 10 to 20% ordinarily produced negligible effects on the measured infrared absorbance of the bound carbonyl. It was found, however, that in the case of the polymers in view of the greater overlapping of the free and bound carbonyl peaks that cancellation was best carried out about 10  $\text{cm}^{-1}$  off of the peak on the high frequency side.

**Determination of Film Thickness.**—In principal, the thickness of an adsorbed polymeric film can be estimated by observing the influence of the film upon the sedimentation rate of a particle of known size. We used this tech-

nique to estimate the film thickness of adsorbed poly-(alkyl methacrylate) and of the copolymer of alkyl methacrylate and vinylpyrrolidone in the following fashion.

A small sample of Eimer and Amend Carbon Black G was stirred with 50 cc. of 2.0% PAM-VP in benzene with a high-speed Sorval Omnimixer. This sample was centrifuged to remove large aggregates. A small volume of this solution was carefully floated in a centrifuge tube on a larger volume of 0.5% of PAM-VP in *p*-fluorotoluene. This sample was centrifuged in a clinical centrifuge until the carbon black transferred well down from the benzene layer into the *p*-fluorotoluene layer. A narrow band of the *p*-fluorotoluene was removed with a micropipet and constituted the starting sample of carbon black. This technique allows one to obtain a sample of carbon black particles with narrow size distribution. *p*-Fluorotoluene was chosen because its density is very nearly unity, making it easy to layer on the benzene solution and also because the polymer densities are very nearly that of *p*-fluorotoluene. In subsequent centrifugations, to determine particle size, the polymer film thus contributes nothing to the effective mass of the sedimenting particle.

The sample of fractionated carbon black dispersed in PAM-VP solution was quite stable to coagulation and could be kept unchanged for several weeks. An aliquot of this sample was diluted tenfold with a solution of Aerosol OT in *p*-fluorotoluene. This sample was aged from 0.5 to 3 days before centrifuging in a Spinco centrifuge to determine particle size. Neither variations in aging time nor variations in the Aerosol OT concentration from 5 to 20% changed the particle size as determined from its sedimentation rate. This behavior indicated that the polymer film had been completely displaced by an Aerosol OT film. By similar centrifugation of a tenfold dilution in 0.5% PAM-VP in *p*-fluorotoluene of an aliquot of the fractionated carbon black sample, the polymer film thickness could be estimated. In like fashion, centrifugation of a tenfold dilution of the fractionated carbon black sample in 0.5% PLMA in *p*-fluorotoluene yielded a film thickness for this polymer. The evidence that PLMA displaces the PAM-VP film under these conditions rests upon the change in measured film thickness for these two polymers.

The carbon black particle diameters averaged 650 Å. as determined from sedimentation rates in the Aerosol OT solutions. It was assumed that the Aerosol OT film was small. Electron microscope examination of the carbon black suspensions showed that a large number of single particles of about the above size were contained in the sample and that they were roughly spherical. Larger aggregates of irregular size were also always present to some extent. In the sedimentation velocity determinations, the optical density gradient was used to determine the sedimenting boundary; and it is believed that this was determined primarily by the single particles.

## Results

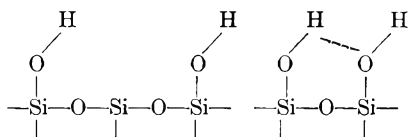
**Adsorption Isotherms.**—The adsorption data for the polymer fractions are depicted in Fig. 1. Included also are the data for the saturated analog of the PLMA monomer, *n*-dodecyl isobutyrate. Values of the adsorption,  $\sigma_0$ , at total coverage obtained from the slopes of the Langmuir  $c/\sigma$  vs.  $c$  plots of Fig. 2 agree reasonably with the apparent extrapolation of the  $\sigma$  vs.  $c$  isotherms. A 3.6-fold change in molecular weight of the PLMA had a negligible effect on the adsorption. The 1.3-fold increase in polymer voluminosity in changing to decalin as solvent had only a small effect on the adsorption. The insertion of vinylpyrrolidone segments in PAM-VP, however, increased the adsorption markedly.

It is of interest to compare the  $\sigma_0$  values for the PLMA polymer and monomer (*n*-dodecyl isobutyrate). Provided that each monomeric segment of the polymer and the monomer occupy the same area per site of attachment to the solid surface, then the  $\sigma_0$  ratio should be a measure of



the fraction of attached segments for the adsorbed polymer. This fraction is about 0.24. This value should be increased if the ester occupies a greater area per site of attachment than the polymer, and decreased if the opposite is true. The adsorbed ester apparently occupies an area of about  $100 \text{ \AA}^2$  per molecule, which is appreciably greater than the approximately  $36 \text{ \AA}^2$  estimated from a molecular model. This may be a manifestation of the steric hindrance effect discussed by Mackor and Van der Vaals<sup>11</sup> for the adsorption of rod-shaped molecules. The area of coverage may be also limited by the area of the silica surface available per hydroxyl group available for H-bonding.

**Nature of the Silica Surface.**—The surface of silica presumably consists to a large degree of hydroxyl groups bound by covalent links to silicon.<sup>9,12</sup> The hydroxyl groups appear both free and hydrogen bonded as depicted



Corresponding strong infrared absorptions were observed at  $3670 \text{ cm}^{-1}$  (sharp) and  $3410 \text{ cm}^{-1}$  (broad), respectively, after equilibrating the silica with pure solvent only. Two small peaks at  $1864$  and  $1626 \text{ cm}^{-1}$  are also characteristic of the silica. The free OH peak normally occurs at about  $3749 \text{ cm}^{-1}$  on dry silica; the shift to  $3670 \text{ cm}^{-1}$  observed here is due to interaction with the solvent.<sup>12</sup> A similar effect has been noted with carbon tetrachloride on silica.<sup>13</sup> As is to be expected, heating *in vacuo* reduced the bound OH peak at  $3410 \text{ cm}^{-1}$  and the bound water peak at  $1626 \text{ cm}^{-1}$ ; however, it was not practical to attempt the present experiments with silica treated in this fashion. Brief exposure to the atmosphere revives these peaks. Under the experimental conditions used here, the bound OH peak at  $3410 \text{ cm}^{-1}$  was found to be reproducible,  $\epsilon_w = 97 \pm 9$  expressed as  $\text{D/g. SiO}_2/\text{cm}^2$ .

**Adsorbed Mono- and Diesters.**—Adsorbed *n*-dodecyl isobutyrate, as the analog of the individual PLMA polymer segments, was studied in order to obtain an estimate of the extinction coefficient for carbonyl bound to the silica surface. The expected shift in the ester carbonyl vibration frequency upon H-bonding to the silica surface was observed ( $\Delta\nu = 30 \text{ cm}^{-1}$ ). The normal peak at  $1745 \text{ cm}^{-1}$  due to the equilibrium concentration of ester in the solvent phase can be eliminated as described above, leaving only the new bound carbonyl peak at  $1715 \text{ cm}^{-1}$ . In accord with the H-bonding mechanism of carbonyl attachment to the surface presumed to be functioning here, it is observed that the free hydroxyl peak of the silica virtually disappears; and the intensity of the bound hydroxyl peak is markedly increased. Exactly similar results were obtained with the

adsorbed diester, di-*n*-dodecyl 3,3-dimethyl glutarate. The spectral evidence in this case indicated that each diester molecule was virtually always attached to the surface by both carbonyl oxygen atoms even at low surface coverage.

The measured extinction coefficients are listed in Table II. A constant and essentially identical value of  $\epsilon_M$  for the adsorbed carbonyl is observed for the mono- and diesters, independent of surface coverage,  $\theta$ . The values of  $\epsilon_M$  (Table III) for "free carbonyl," that is, for the esters in solution in *n*-dodecane, differ considerably from that for the adsorbed carbonyl. H-bonding should cause both a change in intensity and frequency of the normal carbonyl infrared absorption. Such effects are observed in homogeneous solutions.<sup>14</sup>

TABLE II

EXTINCTION COEFFICIENTS FOR ADSORBED MONO- AND DI-ESTERS

$\sigma = \text{mg. adsorbed ester per gram of silica; } \theta = \text{fraction of surface covered; } \epsilon_M = \text{D/meq. of ester per cm}^2$ .

Ester	$\sigma$ , mg./g.	$\theta$	Adsorbed	Bound OH
			$\epsilon_M$ at $1715 \text{ cm}^{-1}$	$\epsilon_M$ at $3410 \text{ cm}^{-1}$
<i>n</i> -Dodecyl isobutyrate	31	0.38	446	569
	55	.69	446	466
	75	.94	440	366
	(80)	(1)	..	(343) <sup>a</sup>
Di- <i>n</i> -dodecyl 3,3-dimethyl glutarate	32	0.34	462	294
	57	.61	443	309
	86	.92	468	337
	(93)	(1)	..	(343) <sup>a</sup>
			Av. 451	Av. (343) <sup>a</sup>

<sup>a</sup> Extrapolated value.

TABLE III

EXTINCTION COEFFICIENTS FOR ESTERS IN SOLUTION

Ester	Solvent	$\nu$ , $\text{cm}^{-1}$	$\Delta\nu/2$ , $\text{cm}^{-1}$	$\epsilon_M$
<i>n</i> -Dodecyl isobutyrate	<i>n</i> -C <sub>12</sub> H <sub>26</sub>	1745	13	653
Di- <i>n</i> -dodecyl 3,3-dimethyl glutarate	<i>n</i> -C <sub>12</sub> H <sub>26</sub>	1745	15	542
PLMA-3,7	<i>n</i> -C <sub>12</sub> H <sub>26</sub>	1736	23	400
Methyl methacrylate <sup>15</sup>	CCl <sub>4</sub>	1727	..	672
Poly-(methyl methacrylate) <sup>15</sup>	CHCl <sub>3</sub>	1729	..	354
Di- <i>n</i> -butyl oxalate	<i>n</i> -C <sub>12</sub> H <sub>26</sub>	1753	13	408
Di- <i>n</i> -butyl succinate	<i>n</i> -C <sub>12</sub> H <sub>26</sub>	1747	13	626

An attempt was also made to calculate an  $\epsilon_M$  for the enhancement of the bound hydroxyl peak at  $3410 \text{ cm}^{-1}$  due to hydrogen bonding of the surface hydroxyls by carbonyl. A difficulty arises due to the necessity of correcting for the remaining surface hydroxyls which are H-bonded to each other. The correction subtracted from the observed  $\log I/I_0$  was

$$g. \text{ SiO}_2/\text{cm}^2 \times \epsilon_w(\text{OH}) \times (1 - \theta)$$

where  $\epsilon_w(\text{OH}) = 97$  (see previous section on Nature of the Silica Surface). Quantitative information on the nature of the silica surface would be required in order to make a more rigorous correction. The  $\epsilon_M$  values obtained in this way were not con-

(11) E. L. Mackor and J. H. Van der Vaals, *J. Coll. Sci.*, **7**, 535 (1952); E. L. Mackor, *ibid.*, **6**, 492 (1951).

(12) R. S. McDonald, *J. Am. Chem. Soc.*, **79**, 850 (1957).

(13) L. M. Roev, V. N. Filimonov and A. N. Terenin, *Optika i Spektroskopiya*, **4**, 328 (1958).

(14) N. S. Bayliss, A. R. H. Cole and L. H. Little, *Australian J. Chem.*, **8**, 26 (1955).

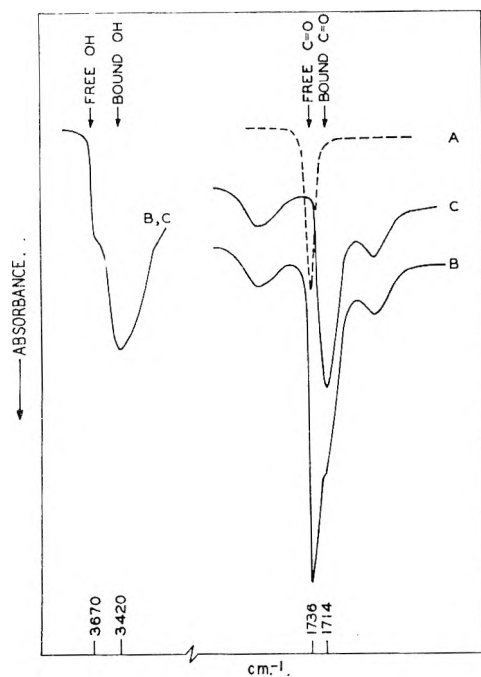


Fig. 3.—Infrared spectrum of PLMA in solution and adsorbed on silica: A, in dodecane solution, 0.101 wt. %; B, equilibrium adsorption system on silica ( $\theta = 0.71$ ,  $\sigma = 234$  mg./g.,  $c = 0.000$ ); with pure solvent in reference cell; C, same as B, but with PLMA solution in reference cell.

stant with surface coverage for the monoester but appeared approximately constant for the diester (see Table II). Both sets of values surprisingly extrapolate to the same value at total coverage ( $\theta = 1$ ). This extrapolated value will be assumed to be the best value. We will use this value only for approximate comparison with information obtained from the carbonyl data.

**Extinction Coefficient for Adsorbed Polymer Carbonyl.**—We wish to assume that the  $\epsilon_M$  for adsorbed polymer carbonyl will be identical with that observed for the adsorbed mono- and diesters. It is pertinent, therefore, to inquire into the reason for the large difference in  $\epsilon_M$  for free carbonyl of the monomer (*n*-dodecyl isobutyrate) and polymer (PLMA) as noted in Table III. A similar difference has also been reported for poly-(methylmethacrylate) and its monomer.<sup>15</sup> Observed band widths (Table III) at half intensity,  $\Delta\nu_{1/2}$ , suggest that the differences are largely due to band broadening. It appears reasonable to relate this effect to structural hindrances that tend to bring the carbonyl groups into proximity. An apparently relevant phenomenon is that of the effect of structure on the ratio of the first and second dissociation constants of dicarboxylic acids. The latter have been used by Gane and Ingold<sup>16</sup> to calculate an apparent distance,  $r$ , between the ionic centers on the dibasic anions. Some typical values of  $r$  are given in Table IV. It is evident that the  $r$  values are qualitatively consistent with the observed  $\epsilon_M$  values for the corresponding esters of Table III. The steric effect suggested here must occur to a large degree in a poly-(alkyl methacry-

late) which can be considered to be made up of units of a 2,2,4,4-tetra-substituted glutaric acid.

TABLE IV

SEPARATION OF CHARGE IN DIBASIC ANIONS <sup>18</sup>	
Acid	$r$ (Å.)
3,3-Di- <i>n</i> -propylglutaric	3.12
Oxalic	3.37
Malonic	3.43
3,3-Di-methylglutaric	3.58
Methylsuccinic	3.83
Succinic	5.58
Glutaric	7.11

It seems reasonable then to assume that upon adsorption the alignment of the carbonyl groups in an ordered, H-bonded array on the surface will play the major role in determining the absolute value of the extinction coefficient for the adsorbed carbonyl group. Indeed, this is borne out perfectly in a comparison of the mono- and diesters themselves. There, although the  $\epsilon_M$  values for free carbonyl differ markedly, the  $\epsilon_M$  values for adsorbed carbonyl are identical. It seems justifiable then to use the same value for adsorbed polymer carbonyl.

**Adsorbed Polymer PLMA.**—A typical spectrum for adsorbed poly-(alkyl methacrylate) is shown in Fig. 3. The new peak due to adsorbed carbonyl is not resolved as in the case of the simple esters but now appears as a distinct shoulder under the normal carbonyl peak. This is the result of the latter being broader and shifted slightly to a lower frequency for free polymer as compared to free monomer. However, appropriate cancellation with polymer solution in the reference cell, as described above, results in the isolation of the 1714  $\text{cm}^{-1}$  peak. It is pertinent to note that because of the very steep initial rise of the adsorption isotherm in the case of polymers (Fig. 1), it is possible to have considerable adsorbed polymer in equilibrium with a practically undetectable concentration of free polymer in solution. Such is the case in the example of Fig. 3. This means that in this case, the peak at 1736  $\text{cm}^{-1}$  observed with the adsorbed polymer must be due essentially entirely to "free" carbonyl groups in the unadsorbed segments of the adsorbed polymer molecules. Note that there is no change observed in the frequency over that for free carbonyl in solution. Note also that the adsorbed carbonyl vibration frequencies for the polymer and monomer are identical. The effect of adsorption on the spectrum of the surface hydroxyls was exactly the same as observed for the monomer.

In order, now, to calculate the  $\text{g./cm}^2$  for adsorbed, that is, directly attached segments (in terms of weight of polymer), we assume, as discussed above, the molar extinction coefficient for adsorbed carbonyl to be the same as observed for the monomer; whence (where the carbonyl equivalent weight of PLMA = 273)

$$\epsilon_w = 451 \times 1000/273 = 1650$$

It is not feasible to use the observed absorbance at 1736  $\text{cm}^{-1}$  for the "free" carbonyl because of the difficulty of correcting for the contribution of the steep shoulder of the 1714  $\text{cm}^{-1}$  peak. It is

(15) R. R. Hampton and J. E. Newell, *Anal. Chem.*, **21**, 914 (1949).

(16) R. Gane and C. K. Ingold, *J. Chem. Soc.*, 2153 (1931).

TABLE V  
DETERMINATION OF THE FRACTION OF ADSORBED SEGMENTS

Polymer (solvent)	Adsorbed polymer mg./g. silica $\sigma$	Fraction of surface covered, $\theta$	Mg. silica per cm. <sup>2</sup>	Mg. polymer/cm. <sup>2</sup>		Total adsorbed polymer	Fraction of adsorbed carbonyl groups <sup>a</sup> $p$
				From C=O data	From OH data		
PLMA-3 (Dodecane)	314	0.95	0.67	0.073	0.073	0.210	0.35
	234	.71	1.28	.107	.105	.298	.36
			1.23	.102	.110	.289	.35
			1.29	.069	.068	.155	.44
	120	.36	1.44	.077	.067	.173	.44
52	.16	1.57	.032	.012	.082	.39	
PLMA-3 (Decalin)	272	.96	1.03	.100	.115	.272	.37
	181	.64	0.97	.081	.089	.176	.46
1.04			.079	.088	.188	.42	
PLMA-7 (Dodecane)	292	.96	0.97	.105	.125	.283	.37
	216	.71	1.28	.103	.116	.278	.37
			1.10	.059	.064	.111	.53

<sup>a</sup> Based on the carbonyl data.

simpler to obtain the "total adsorbed polymer" in each case from the known weight of silica on the NaCl plate and the measured adsorption,  $\sigma$ . Then the desired quantity, the fraction  $p$  of adsorbed segments or carbonyl groups, is

$$p = \frac{\text{wt. of attached polymer segments/cm.}^2}{\text{wt. of total adsorbed polymer/cm.}^2}$$

The data obtained in this manner are given in Table V. It should be understood that "segment" refers here to the monomeric ester unit. Included are comparative values for the g./cm.<sup>2</sup> obtained from the hydroxyl data. Correction for the initially present H-bonded surface hydroxyls was applied in a manner exactly analogous to that used in originally evaluating  $\epsilon_M$  for bound hydroxyl from the mono- and diester experiments. The agreement, except at the very lowest surface coverage, is better than expected. The agreement suggests that our assumption regarding the extinction coefficient for adsorbed carbonyl is not seriously in error.

It appeared pertinent to ensure that none of the effects being observed might be due to H-bonding between free polymer and any H<sub>2</sub>O which might be displaced from the silica surface. Accordingly, it was observed that the spectrum of a polymer solution equilibrated with a second phase of liquid water was identical with that of the original free polymer.

**Adsorbed Polymer PAM-VP.**—Solutions of this copolymer of alkyl methacrylate and vinylpyrrolidone show, besides the main infrared absorption peak due to ester carbonyl, an additional absorption (appearing as a shoulder on the main peak) at about 39 cm.<sup>-1</sup> lower frequency due to the pyrrolidone carbonyl. The latter spans the ester carbonyl frequency shift of 22 cm.<sup>-1</sup> upon adsorption onto silica, so that one cannot resolve the free pyrrolidone groups from adsorbed ester groups in an adsorption experiment. Hence, no estimates can be made of the fraction,  $p$ , of adsorbed carbonyl groups. However, it is of interest to note that the adsorbed polymer, PAM-VP, shows a new well resolved peak at about 72 cm.<sup>-1</sup> below the free ester carbonyl peak. This can only be due to adsorbed pyrrolidone carbonyl groups and

represents a 33 cm.<sup>-1</sup> shift of the free pyrrolidone frequency. This indicates that the highly polar pyrrolidone groups are indeed involved in the attachment of the polymer to the silica surface.

**Film Thickness Estimation.**—A number of uncertainties make a precise determination of the adsorbed film thickness by the sedimentation velocity technique impossible. In the treatment of our data, we assume that the sedimenting particles are spherical and that the adsorbed polymer films influence the sedimentation velocity in the manner of a solvent impenetrable shell of constant thickness. Experimentally, the two most serious uncertainties concern the identity of the film coating the particle and the determination of the sedimenting boundary which tends to become diffuse with polydisperse particles. The increase in sedimentation constant when PAM-VP coated particles are treated with Aerosol OT and PLMA solutions suggests strongly that the films have exchanged in the manner desired. The particle fractionation technique described previously gave particle size distributions sufficiently narrow to allow reasonable estimates of the sedimenting boundary to be made.

Proceeding as described, film thicknesses of  $25 \pm 10 \text{ \AA}$ . (four determinations) for PLMA and  $210 \pm 40 \text{ \AA}$ . (five determinations) for PAM-VP were obtained.

## Discussion

**The Fraction of Adsorbed Segments.**—On the average for the PLMA fractions, about 36% of the segments are attached to the surface at high coverage, showing that the polymer is highly extended on the silica surface. This is in accord with the qualitative results of the statistical theory of polymer adsorption of Simha-Frisch-Eirich<sup>4</sup> as extended by Frisch<sup>5</sup> for strong interactions between polymer and surface. For adsorption due to hydrogen bonding where  $\Delta H = 5-6 \text{ kcal./mole}^{17}$  or  $8-10 kT$ , this result appears reasonable. For this case, the independence of the fraction of segments attached upon polymer molecular weight observed over a 3.6-fold change is also in accord

(17) G. C. Pimentel and A. L. McClellan, "The Hydrogen Bond," W. H. Freeman, San Francisco, Cal., 1960, pp. 348 *et seq.*

with Frisch's treatment. It is surprising, however, that the number of attachments is so little influenced by the degree of coverage. We find at most a 30% change in  $p$  over the range of  $\theta = 0.16$  to  $\theta = 0.96$ . Frisch's treatment for strong boundary forces results in the expression  $p = \nu/t = \text{constant} (1 - \theta)\alpha_0/R$ , where  $\nu$  = the number of attached segments,  $\theta$  = the fraction of the surface covered,  $\alpha_0$  = the probability that if a segment touches an unoccupied site, it adheres,  $t$  = total number of segments, and  $R$  = range over which the boundary forces operate.

While our data indicate some tendency for  $p$  to increase at low surface coverage, the change is smaller than anticipated from the Frisch relation. Higuchi<sup>18</sup> has modified the statistical analysis of Simha, Frisch and Eirich<sup>4</sup> to allow the determination of the effect upon  $p$  (our  $p$  is Higuchi's  $P(0)$ ) of the net attractive surface-segment energy,  $\epsilon$ , over the entire range from weak to strong forces. This analysis indicates that  $p$  is an S-shaped function of  $\ln [\alpha_0 K_0 (1 - \theta)]$ , where  $K_0 = \exp(\epsilon/kT)$ , and  $\alpha_0$  and  $\theta$  are as before (Fig. 2, ref. 18).  $p$  varies slowly with surface coverage at very low  $\epsilon$  ( $\sim 0$ ) and very high  $\epsilon$  ( $> 5kT$ ) while in the intermediate range of  $\epsilon$  the rate of change of  $p$  with  $\theta$  is of the same order as predicted by the Frisch relation. The small dependence of  $p$  upon  $\theta$  found here is in agreement with Higuchi's treatment for strong interactions. The fact that  $p$  is essentially constant as the amount of polymer on the surface varies suggests that the adsorbed polymer configuration is determined to a considerable degree by intramolecular interactions and not by interactions with other molecules. It must be concluded, therefore, that under the conditions of our experiments, concentration levels are not attained at which polymer-polymer interactions on the surface become operative. Koral, *et al.*,<sup>2</sup> showed that substitution (by partial hydrolysis) of more polar groups in poly-(vinyl acetate) resulted in increased adsorption on iron powder, but that the maximum adsorption levels off rapidly after the first introduction ( $\sim 13\%$ ) of polar groups. This would appear to be additional evidence of the importance of intramolecular interactions in influencing the state of an adsorbed polymer molecule.

The theoretical treatments suggest that  $p$  must be close to unity for the strong polymer-surface interactions which are operative in the present experiments. The lower value which is observed might be due to steric effects associated with polymer backbone inflexibility or possibly reflects a lack of surface uniformity and availability of properly spaced adsorption sites. Intramolecular excluded volume effects, which are ignored in the theoretical treatments, might also cause  $p$  to be less than unity.

The theoretical treatments presuppose that the adsorption is reversible. As is commonly observed, the desorption of polymer is extremely slow. This is not an indication of irreversibility but is to be expected in view of the statistical improbability of a polymer molecule desorbing all of its points

of attachment at once. Equilibrium must exist for the adsorption-desorption of individual segments. Otherwise, the  $c$  versus  $\sigma$  isotherms should appear as a straight line parallel to the  $c$  axis. Accordingly, the simple esters studied were observed to equilibrate extremely rapidly *via* either adsorption or desorption.

No difference in  $p$  is apparent for PLMA adsorbed from the solvents, *n*-dodecane and *cis*-decalin, wherein the ratio of intrinsic viscosities of PLMA is 1.3. In view of the greatly extended state of the adsorbed polymer revealed here, it is not surprising that increasing the voluminosity of the polymer in the solvent phase has no apparent effect on the mode of attachment of the polymer to the solid surface. Unfortunately, the stringent requirements for a solvent suitable for studies, such as have been made here, preclude comparison of solvents with a greater difference in solvent power.

**Film Thickness.**—For PLMA with  $p = 0.36$ , one would estimate a film thickness the order of 20 to 40 Å. The value of 25 Å, determined from the carbon black sedimentation studies is in good agreement with this value and further demonstrates the extended nature of adsorbed PLMA on polar surfaces. It should be noted that the sedimentation data were taken at 0.5% polymer concentration, a condition which gives high surface coverage (Fig. 1).

A copolymer, such as PAM-VP, which contains a small fraction of groups more strongly adsorbed than the ester group would be expected to give thicker films than an ester homopolymer, due to preferential adsorption of the more strongly adsorbed groups. Sedimentation data on PAM-VP indicate a film thickness of about  $210 \pm 40$  Å, which is consistent with this explanation. This value is considerably higher than would be expected from the relative saturation values of PAM-VP and PLMA isotherms, however. (Isotherms on carbon black gave a similar relative saturation value to that indicated on Cab-O-Sil in Fig. 1.) Possibly, this large film thickness reflects the incorporation of the strongly adsorbed vinyl pyrrolidone in runs or blocks in the copolymer.

**The Adsorption Isotherm.**—As shown in Fig. 2, the adsorption data appear to fit the Langmuir isotherm. Similar empirical fitting of polymer adsorption data to the Langmuir expression has been reported in several instances.<sup>1-3,19</sup> The Simha-Frisch-Eirich (SFE) isotherm,<sup>5</sup> as corrected by Frisch and Simha<sup>20</sup> and simplified by ignoring lateral interactions between polymer segments, is  $[\theta/\nu(1 - \theta)] = kc$ . When  $\nu = 1$ , this equation reduces to the Langmuir isotherm. It is apparent then that there is no point in attempting to evaluate  $\nu$  by fitting data to the SFE isotherm if the data are adequately described by the Langmuir equation. Frisch and Simha<sup>21</sup> discuss the difficulty in attempting to differentiate between the Langmuir and SFE isotherms from

(19) J. F. Hobden and H. H. G. Jellinek, *J. Polymer Sci.*, **11**, 365 (1953).

(20) H. L. Frisch and R. Simha, *J. Chem. Phys.*, **27**, 702 (1957).

(21) H. L. Frisch and R. Simha, *J. Phys. Chem.*, **58**, 507 (1954).

(18) W. I. Higuchi, *J. Phys. Chem.*, **65**, 487 (1961).

the experimental data. In effect, the equations are insensitive to values of  $\nu$  except at extremely low concentrations where it is ordinarily not possible to obtain accurate data. The recent data on the adsorption of polystyrene on carbon of Frisch, *et al.*,<sup>22</sup> illustrate this difficulty clearly. The latter authors found that their data fit the Frisch and Simha isotherm better when an *a priori* assumed value of  $\nu = 50$  was used rather than  $\nu = 1$  (for a polystyrene of molecular weight 301,000). However, this yields a value of 900 Å.<sup>2</sup> area per adsorption site, which appears an order of magnitude too large in view of the probable area of not over 60 Å.<sup>2</sup> per segment as estimated from the data of Van der Vaarden.<sup>23</sup>

It still seems surprising that the adsorption data should reasonably fit the Langmuir isotherm in our case where  $\nu$  is so very large. For the

(22) H. L. Frisch, M. Y. Hellman and J. L. Lundberg, *J. Polymer Sci.*, **38**, 441 (1959).

(23) M. J. Van der Vaarden, *J. Coll. Sci.*, **6**, 443 (1951).

polymers PLMA-3 and PLMA-7,  $\nu \cong 470$  and 1660, respectively. One might question whether the apparent fit to the Langmuir equation is entirely accidental. Simha, Frisch and Eirich<sup>4</sup> point out that their isotherm is identical in form with the result for the adsorption of a  $\nu$ -mer with complete dissociation into "monomer" on the surface. This would appear to suggest that even in the case of the adsorption-desorption equilibrium of a polymer molecule, the equilibrium is basically a competition only between the individual adsorbing segments. We have studies in progress which may elucidate further the fundamental nature of the adsorption isotherm for polyfunctional molecules.

**Acknowledgments.**—The authors wish to acknowledge the coöperation of Dr. D. G. Rea and Mr. H. M. White of our Spectroscopic Laboratory and are grateful to Drs. O. L. Harle and W. I. Higuchi for helpful discussion.

## EFFECTS OF SHORT RANGE SURFACE-SEGMENT FORCES ON THE CONFIGURATION OF AN ADSORBED FLEXIBLE CHAIN POLYMER

BY W. I. HIGUCHI<sup>1</sup>

California Research Corporation, Richmond, California, and The School of Pharmacy, University of Wisconsin, Madison, Wisconsin

Received September 21, 1960

Following the model for the statistics of deposition of a flexible polymer chain from solution developed by Simha, Frisch and Eirich,<sup>2</sup> equations were formulated which describe the segment density distribution as a function of a short range interaction parameter  $K$ . Calculations for  $P(0)$ , the fraction of anchor segments, were carried out over a wide range of  $K$  and the chain size. The calculations show that if anchoring of a segment is accompanied by a net change in potential energy,  $\epsilon$ , equivalent to that of about  $4kT$  or more resulting from interactions of unspecific types,  $P(0)$  may be essentially unity, *i.e.*, the entire chain may be found collapsed to the surface. In the range  $0 \leq \epsilon \lesssim 4kT$ , the changes in  $P(0)$  may be very large, corresponding to the change from a chain predominantly existing in the solution "phase" to that which is collapsed to the surface. The recent experimental determination of  $P(0)$  by Fontana and Thomas for the system-poly(alkyl methacrylate) adsorption onto silica—is found to be consistent with the present treatment of the problem, for the case of large  $\epsilon$ .

### Introduction

The theoretical aspect of the problem of the adsorption of flexible non-ionic high polymers onto solids from their solutions has been examined and discussed in rather great detail by Simha, Frisch and Eirich,<sup>2</sup> Frisch and Simha,<sup>3</sup> and Frisch.<sup>4</sup> The model employed by these investigators in their quantitative discussions assumes that the adsorbed polymer chains are characterized by a Gaussian distribution of end-to-end distances. Knowledge of the average configuration of the polymer containing a statistically significant number of segments then permits the application of statistical thermodynamics to the derivation of the adsorption isotherm equation. However, even for the simplified model, because of the complexity of the situation, it is extremely difficult to enter the various interactions into a suitable equation

with the expectation of finding a satisfactory quantitative description of the system within the limitations of the model.

The configuration of the flexible chain at the interface is a very important facet of the over-all problem, as well as being interesting in itself. The present communication is concerned with the effects of short range forces between the polymer segment and the active surface sites on the polymer configuration. Frisch<sup>4</sup> has already treated the two limiting cases: very weak attractive forces (energies  $\ll kT$ ) and very strong attractive forces (energies  $\gg kT$ ). It appeared to us that the region in between these extremes should be important for many real systems.

### Theory

Assume that the polymer chain in solution is characterized<sup>5</sup> by its  $l$  segments of length  $A$  and a Gaussian distribution of end-to-end distances. Then with the adsorbing surface at  $Z = 0$  in the  $x$ - $y$  plane and anchoring the first segment of the chain to the surface, the chain segment density,

(1) The School of Pharmacy, University of Wisconsin, Madison, Wisconsin.

(2) R. Simha, H. L. Frisch and F. R. Eirich, *J. Phys. Chem.*, **57**, 584 (1953).

(3) (a) H. L. Frisch and R. Simha, *ibid.*, **58**, 507 (1954); (b) H. L. Frisch and R. Simha, *J. Chem. Phys.*, **27**, 702 (1957).

(4) H. L. Frisch, *J. Phys. Chem.*, **59**, 633 (1955).

(5) Conventions of Frisch, *ref. 4*, are used whenever possible.

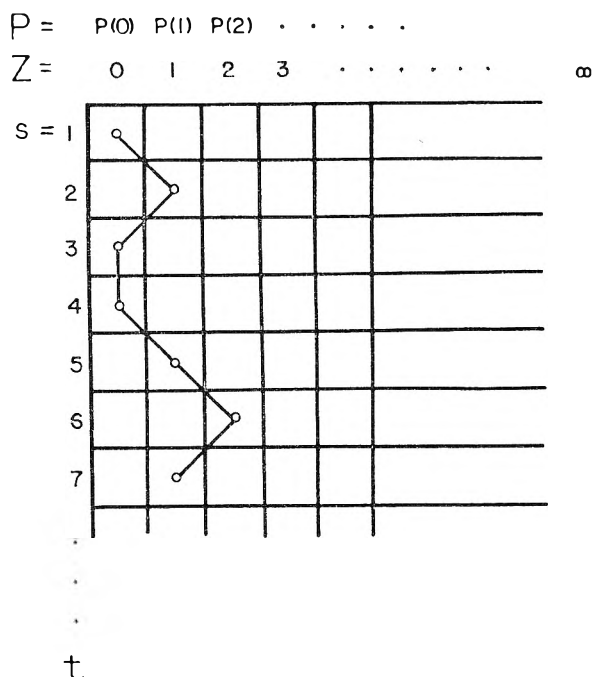


Fig. 1.—A typical beginning of an adsorbed polymer chain of  $t$  segments in the modified random walk representation (see text).

$P(Z)$ , may be calculated for the adsorbed polymer. Here  $P(Z)$  is defined as the fraction of  $t$  located between  $Z$  and  $Z + dZ$ . The coordinate  $Z$  is in units of  $A$ . This treatment for large  $t$  gives<sup>2-4</sup>

$$P(0) = \frac{2\alpha_0(1-\theta)}{(\pi ft)^{1/2}} - 0 \left(\frac{1}{t}\right) \quad (1)$$

which is the expression for the fraction of  $t$  existing as anchors for the polymer chain. In the equation  $\alpha_0$  is an accommodation coefficient (the probability of a successful contact between an active site on the surface and a segment),  $\theta$  is the fraction of sites covered, and  $f$  is the segment "diffusion" coefficient<sup>4</sup> which includes the effects of the restrictions of valence angles and bond rotation on the molecular configuration.

To the extent that the discussion in this article will be quantitative, it will be limited to examining  $P(0)$ , although a general expression for  $P(Z)$  will be presented and discussed.

Equation 1 is expected to apply to the case where no net interaction exists between the segment and the surface sites. It is a consequence only of the geometric restriction placed upon the polymer chain.

For the case of very weak attractive forces Frisch<sup>4</sup> obtained

$$P(0) = \frac{2\alpha_0(1-\theta)}{(\pi ft)^{1/2}} (1 + \lambda + \dots) \quad (2)$$

where  $\lambda = \epsilon/kT$ ,  $\epsilon$  is the net attractive surface-segment energy, and  $k$  and  $T$  have their usual meanings. More exactly,  $\epsilon$  is the depth of a square well potential located at  $0 \leq Z \leq R$  where  $R$  is the order of  $A$  for short range forces. It represents an average or "smoothed" potential energy decrease for the segment in  $0 \leq Z \leq R$  relative to the segment located at  $Z > R$ . The less specific the interaction of the surface-segment rela-

tive to the solvent-segment the closer  $\epsilon$  would be to the actual energy of anchoring (*i.e.*, the minimum in the real potential energy curve).

Because of the mathematical approximations, equation 2 is strictly valid for the model when  $\epsilon \ll kT$ . Under these conditions  $P(Z)$ , which determines the extension of the polymer in the  $Z$ -direction and the density of the segments, remains<sup>4</sup> essentially the same as that for  $\epsilon = 0$ .

Frisch<sup>4</sup> has also analyzed the case for  $\epsilon \gg kT$  and found that in the limit  $\epsilon \rightarrow \gg kT$ ,  $P(0) \rightarrow 1$ ,  $P(Z) \rightarrow 0$  for  $Z > R$ , *i.e.*, all  $t$  segments collapse to the surface layer and serve as anchors.

An alternative approach but which essentially retains Frisch's physical model will now be presented. This will permit using standard procedures for numerically computing  $P(0)$  for any  $\epsilon$  and large  $t$ .

For the calculations it will be assumed as before<sup>4</sup> that excluded volume effects may be neglected. This point will, however, be examined later in the discussion of the results. Also only short range interactions (range the order of one segment length) will be considered.

Let us begin (see Fig. 1) with the first segment ( $s = 1$ ) of the polymer chain in  $Z = 0$ . The second segment ( $s = 2$ ) has the choice of residing in  $Z = 0$  or in  $Z = 1$  (as it does). Then the third segment ( $s = 3$ ) has the choice to reside in  $Z = 2$  or  $Z = 0$  (as it does). This continues to  $s = t$ . The process is called random walk<sup>6</sup> with a perfectly reflecting barrier if the probabilities for  $\Delta Z = +1$  is unity and  $\Delta Z = 0$  is zero at  $Z = 0$ . If, on the other hand, the probabilities for  $\Delta Z = +1$  and  $\Delta Z = 0$  are equal, the corresponding expression for  $P(0)$  is, as will be seen later, equation 1 with  $\alpha = 1$  and  $\theta = 0$ .

The effect of short range forces may be accounted for by suitable choice of the probabilities for a  $\Delta Z$  transition at  $Z = 0$  and  $Z = 1$ , maintaining equal probabilities of  $\Delta Z = +1$  and  $\Delta Z = -1$  for all other  $Z$  values.

The walk process may be described by the following differential equation under the usual limiting conditions<sup>6</sup>

$$\frac{\partial w}{\partial t} = f \frac{\partial^2 w}{\partial Z^2} \text{ for } Z \geq 2 \quad (3)$$

where  $w = w(Z, t)$  is the end-to-end distribution function integrated over all  $x$  and  $y$ .<sup>7</sup> The behavior at  $Z = 0$  and  $Z = 1$  follows the conditions

$$\left(\frac{\partial w}{\partial t}\right)_{z=0} = \frac{2fK}{K+1} w_{z=1} - \frac{2f}{K+1} w_{z=0} \quad (4)$$

$$\left(\frac{\partial w}{\partial t}\right)_{z=1} = \frac{2f}{K+1} w_{z=0} + f w_{z=2} - 2f w_{z=1} \quad (5)$$

$$f \left(\frac{\partial w}{\partial Z}\right)_{z=2} = \left(\frac{\partial w}{\partial t}\right)_{z=0} + \left(\frac{\partial w}{\partial t}\right)_{z=1} \quad (6)$$

It is visualized, as indicated by these equations, for simplicity's sake that there are three regions,  $Z = 0$ ,  $Z = 1$  and  $Z \geq 2$ .

The present approach differs from Frisch's<sup>4</sup> in that the attractive forces are accounted for by the use of conditions 4, 5 and 6 rather than by their

(6) S. Chandrasekhar, *Revs. Modern Phys.*, **15**, 1 (1943).

(7) This differs from the  $w(Z, t)$  of the previous workers, ref. 1-4, by the integration.



direct incorporation into equation 3 with  $Z \geq 0$ . The other boundary conditions remain the same,<sup>4</sup> viz.

$$\left. \begin{aligned} w, \frac{\partial w}{\partial t} &\rightarrow 0 \text{ as } Z \rightarrow \infty, t > 0 \\ \text{and} \\ w &\rightarrow \delta(Z) \text{ as } t \rightarrow 0 \end{aligned} \right\} \quad (7)$$

A few remarks on the meaning of conditions 4, 5 and 6 are necessary. The first term on the right side of 4 is the "rate" at which the  $(t + 1)^{\text{st}}$  segments are going to  $Z = 0$  from the  $t^{\text{th}}$  segments in  $Z = 1$ . The second term in 4 is the "rate" at which the  $(t + 1)^{\text{st}}$  segments are going to  $Z = 1$  from the  $t^{\text{th}}$  segments in  $Z = 0$ . In condition 5 the first two terms on the right side are the "rates" at which  $(t + 1)^{\text{st}}$  segments are coming into  $Z = 1$  from  $Z = 0$  and  $Z = 2$ , respectively, and the third term represents the "rate" of segments leaving  $Z = 1$ . Condition 6 simply represents mass balancing. The quantity  $K$  accounts for the effect of forces on these "rates," i.e., the larger  $K$  is the less the tendency for the  $\Delta Z$  (0 to 1) and the  $\Delta Z$  (1 to 2) steps while the greater the tendency for  $\Delta Z$  (0 to 0) and the  $\Delta Z$  (1 to 2) steps. A detailed examination of  $K$  will be given in the Discussion section.

To find a solution to the problem it becomes necessary to make an approximation. From condition (4) it is clear that

$$\left(\frac{\partial w}{\partial t}\right)_{z=0} \ll \frac{2fK}{K+1} w_{z=1} \approx \frac{2f}{K+1} w_{z=0} \text{ for large } t \quad (8)$$

From this it follows that for large  $t$

$$w_{z=0} \approx Kw_{z=1} \quad (9)$$

It can be shown that the effect of not neglecting  $(\partial w/\partial t)_{z=0}$  in equation 8, in the first approximation, is to effectively decrease  $f$  by the order of  $(K^2 + 3K + 1)/(K^2 + 2K + 1)$  which is always sufficiently close to unity for our purposes.

Employing equation 9, equation 3 may be solved<sup>3</sup> to give

$$w = \frac{2}{(K+1)^2(b-a)} \left[ \exp\{a(Z-2) + a^2ft\} \operatorname{erfc} \left\{ \frac{(Z-2)}{2(ft)^{1/2}} + a(ft)^{1/2} \right\} - \exp\{b(Z-2) + b^2ft\} \operatorname{erfc} \left\{ \frac{(Z-2)}{2(ft)^{1/2}} + b(ft)^{1/2} \right\} \right] \quad (10)$$

for  $Z \geq 2$

$$\begin{aligned} \text{with } a &= \frac{1}{2} + \frac{1}{2} \left(1 - \frac{8}{(K+1)^2}\right)^{1/2} \\ \text{and } b &= \frac{1}{2} - \frac{1}{2} \left(1 - \frac{8}{(K+1)^2}\right)^{1/2} \end{aligned}$$

Thus

$$w_{z=2} = \frac{2}{(K+1)^2(b-a)} \left[ \exp(a^2ft) \operatorname{erfc}\{a(ft)^{1/2}\} - \exp(b^2ft) \operatorname{erfc}\{b(ft)^{1/2}\} \right] \quad (11)$$

Now  $(\partial w/\partial Z)_{z=2}$  may be obtained from equation 10 by differentiation and combined with 4, 5, 6, 9 and 11 to give

$$w_{z=0} = \frac{1}{(1+1/K)(b-a)} \left[ (1-a) \exp(a^2ft) \operatorname{erfc}\{a(ft)^{1/2}\} - (1-b) \exp(b^2ft) \operatorname{erfc}\{b(ft)^{1/2}\} \right] \quad (12)$$

(8) H. S. Carslaw and J. C. Jaeger, "Conduction of Heat in Solids," Oxford University Press, London, 1959, p. 306.

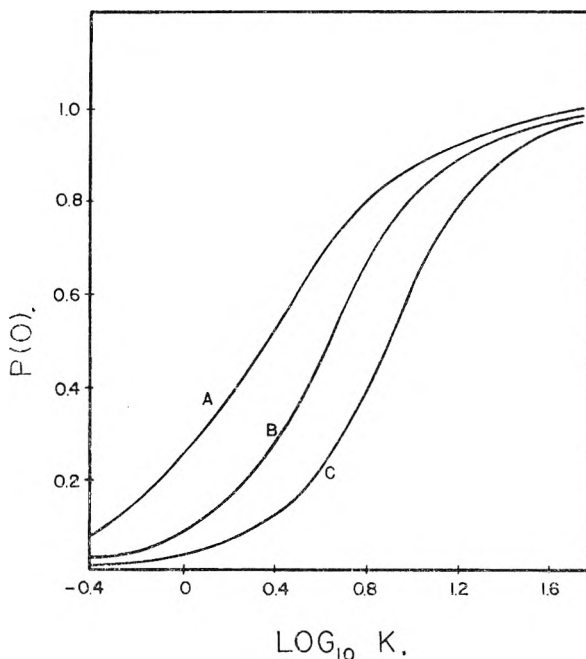


Fig. 2.—A plot of  $P(0)$ , the fraction of the total number of segments  $t$  that are anchors, against the site-surface interaction parameter  $K$ . A, B and C correspond to  $t = 1 \times 10^2, 1 \times 10^3$  and  $1 \times 10^4$ , respectively.

Now  $P(0)$  is related to  $w_{z=0}$  by<sup>2-4,9</sup>

$$P(0) = \frac{1}{t} \int_1^t w_{z=0} dt \quad (13)$$

It can be easily shown that equation 13 reduces to equation 1 for  $K = 1$ , provided  $\alpha_0 = 1$  and  $\theta = 0$  in equation 1. Also when  $K = 0, P(0) = 0$ .

### Results of Calculations and Discussion

In Fig. 2 are given the results of  $P(0)$  calculations for three  $t$  values of  $1 \times 10^2, 1 \times 10^3$  and  $1 \times 10^4$  which should be representative of most real systems of interest (MW range of  $1 \times 10^4$  to  $1 \times 10^6$  or so). The calculations were carried out by a graphical method with equations 12 and 13, and an  $f$  value of  $1/6$ . This  $f$  value would correspond to a free chain (no valence angle restrictions and no bond rotation barriers).

In passing, it is worthwhile to mention an alternative interpretation of the meaning of the results of Fig. 2 with  $f = 1/6$ . If the concept of the statistical chain element of W. Kuhn<sup>10</sup> is introduced to characterize the polymer chain, then  $f = 1/6$  will include the restriction of valence angles and bond rotation. In this interpretation the number,  $t'$ , of the statistical chain elements (of length  $A'$ ) would be less than  $t$  for a given polymer chain according to the following conditions<sup>10</sup>

$$\left. \begin{aligned} t' &= t/n \\ A' &= \text{r.m.s. length of } n \text{ segments of length } A \\ &\quad \text{where } n \text{ is large enough to make orienta-} \\ &\quad \text{tion of one element independent of the} \\ &\quad \text{next} \\ At &= A't' \end{aligned} \right\} \quad (14)$$

It is clear that in some respects the statistical chain element analysis would be more consistent

(9) In eq. 12  $w_{z=0}$  is the same as  $p(r)$  used by the previous workers. See ref. 7.

(10) See P. J. Flory, "Principles of Polymer Chemistry," Cornell University Press, Ithaca, N. Y., 1953.

with the model of random flight. However, in the present discussion,  $A$  and  $t$  will be used as before<sup>2-4</sup> to describe the polymer chain for the reason that a clearer relationship between the variables can be seen with this choice.

The long range effect on  $P(0)$  of increasing  $f$  while holding  $K$  constant would be essentially the same as proportionally increasing  $t$  (see equation 12). For linear polymers involving the tetrahedral carbon linkages  $f$  is the order of 2 to 4 times greater than  $f$  for the free chain. This would correspond to about a 10 to 20% downward shift in the results of Fig. 2. For more inflexible polymers the increase in  $f$  would be greater.

The effect of solvent on  $P(0)$  while holding  $K$  constant is to *effectively* either increase or decrease  $f$  depending on whether the solvent is a good one or a poor one, and on whether there is a high concentration of other polymer chains nearby (intermolecular excluded volume effects). The discussion up until now has assumed the Flory theta solvent, *i.e.*, the net effect of solvent-segment and segment-segment interactions was to permit the random walk calculation of the configuration to be the correct one with  $f$  providing the valence angle and bond rotation restrictions only. The Flory type treatment<sup>10</sup> involving the expansion factor, alpha, may be used to estimate<sup>11</sup> the effective change in  $f$  caused by solvents. For linear polymers the effects of solvents are about the same order as in the three-dimensional cases,<sup>10</sup> as perhaps expected. For not too extreme solvents the effective changes in  $f$  over the  $f$  for theta solvent is generally the order of 2 or so, even for moderate coverages. At very high coverages, when both inter- and intramolecular excluded volume effects could become very serious, the effective  $f$  will be much larger.

It appears that  $K$ , itself, might be the most important  $P(0)$  determining factor, especially at low to moderate coverages. Particularly for the high molecular weight polymer chains,  $K$  has a very large influence on  $P(0)$ . For example (Fig. 2), taking the  $t = 1 \times 10^4$  chain, while at  $K = 1$ ,  $P(0)$  is  $\sim 0.03$ ; at  $K = 3$ ,  $P(0) = 0.13$ —a fourfold effect; and at  $K = 10$ ,  $P(0) = 0.6$ —a twenty-fold effect. At  $K \gtrsim 30$ , polymer chains are essentially collapsed to the surface. The character of an adsorbed film undergoes drastic changes in the region of  $1 \sim K \sim 30$ . The segment density distribution,  $P(Z)$ , which could be calculated along the same lines as the  $P(0)$  calculation by means of equations 11 and 13, should reflect these changes. The adsorbed film thickness, however defined, should be considerably smaller for  $K = 30$  than for  $K = 1$ .

The meaning of  $K$  now requires discussion. From equations 4 and 5 it is seen that  $K$  is a kind of distribution coefficient for  $Z = 0$  and  $Z = 1$ . When the  $t^{\text{th}}$  segment is in  $Z = 0$  the quantity  $K/K + 1$  represents the probability of anchoring for the  $(t + 1)^{\text{st}}$  segment; while  $1/K + 1$  represents the probability for not anchoring. Now we have also chosen  $K/K + 1$  to represent the probability

of anchoring of the  $(t + 1)^{\text{st}}$  segment when the  $t^{\text{th}}$  segment is in  $Z = 1$  with again letting  $1/K + 1$  represent the probability for not anchoring. Strictly the same probabilities should not be used for the two processes, or, alternatively, different  $K$ 's should be used. The problem arises because even though the potential energy change for anchoring may be the same in the two processes, the degree of orientational freedom associated with anchoring differs (neglecting restrictions of valence angle and bond rotation). However, the effect is small enough to be unimportant<sup>12</sup> for the present discussion and thus the simple derivation will be retained.

We may write

$$\text{and } \left. \begin{aligned} K &= \alpha_0 K_0 (1 - \theta) \\ K_0 &= \exp(\epsilon/kT) \end{aligned} \right\} \quad (15)$$

and  $\alpha_0$ ,  $\theta$  and  $\epsilon$  have already been defined. For  $\epsilon/kT \ll 1$  this gives

$$P(0) = \frac{2\alpha_0(1-\theta)}{(\pi ft)^{1/2}} \left(1 + \frac{3}{2}\lambda + \dots\right) \quad (16)$$

which differs somewhat from equation 2 in the coefficient for  $\lambda$ .

Frisch has discussed<sup>4</sup> some probable values for  $\epsilon$  (adsorption from solutions) when the site-segment interaction involves dispersion type forces, weak dipole-dipole forces, or strong dipole-dipole forces. In general when only dispersion type forces or weak dipole forces are involved

$$\epsilon \lesssim kT$$

However, when anchoring occurs with a net formation of a hydrogen bond or other strong dipolar interaction  $\epsilon$  may easily exceed several  $kT$ .<sup>4</sup> This may occur, for example, if the segment contains a carbonyl or a comparably basic group, the active site involves an acidic proton (*e.g.*, hydrated silica) and the solvent is an aliphatic hydrocarbon.

If  $\alpha_0$  may be assumed to be the order of unity and if  $\theta$  is not too large

$$K \sim \exp\left(\frac{\epsilon}{kT}\right) \text{ or somewhat less} \quad (17)$$

It is seen that  $K \sim 7$  for  $\epsilon = 2kT$ ,  $K \sim 20$  for  $\epsilon = 3kT$ , and  $K \sim 150$  for  $\epsilon = 5kT$ . In the last case the entire polymer chain may be lying collapsed at the interface.

While the long range effects of the valence angle and bond rotation restrictions were considered above, the effects of these restrictions on  $P(0)$  arising near the surface are more difficult to assess. It is clear that these effects or correlation between two successive segments is most important for large  $P(0)$ . With the aid of expressions 14, it is seen that the worst conceivable deviation from the  $P(0)$  values given by Fig. 2 corresponds to

$$P(0,t) = \frac{1}{n} P(0,t') \quad (18)$$

Condition 18 is a somewhat improbable estimate

(12) More detailed derivations of equation 12 with allowance given to the anisotropy of the "diffusion" coefficient in  $Z = 0$  and  $Z = 1$  leads to somewhat larger  $P(0)$  values for the same  $K$ , corresponding to a leftward shift of the curves of Fig. 2 by about 0.1 in  $\log K$  for large  $K$ .

(11) Unpublished results employing a one-dimensional modification of Flory's method.

of  $P(0)$ , however, as it is reasonable to expect much of the effects of correlation to cancel. In any case the entire polymer chain would collapse to within  $A'$  of the surface as  $P(0,t')$  for the polymer given by Fig. 2 approaches unity.

A significant point with regard to equation 15 and the curves of Fig. 2 is that  $P(0)$  may be very sensitive to  $\theta$  over a certain range of  $\theta$ . In considering the thermodynamics of chain adsorption<sup>2,3</sup> the number of anchoring segments  $\nu = P(0)t$  is an important factor. It is seen that for  $\theta$  going from 0 to 0.9,  $\nu$  may vary over a wide range ( $\sim$ a factor of ten) if, say  $K \sim 10$  at  $\theta = 0$  (or  $K \sim 1$  at  $\theta = 0.9$  if  $K_0$  remains constant). Any isotherm equation should take this variation of  $\nu$  into account if agreement with experiments is to be expected.

#### Comparison of Calculations with Data

Recently Fontana and Thomas<sup>13</sup> have carried out some very interesting experiments bearing on the problem of the configuration of adsorbed polymers. They were able to directly determine  $P(0)$  for poly-(alkyl methacrylate), PLMA, adsorbed onto silica by infrared spectrometry.

Their investigation showed that, for this system,  $P(0)$  is relatively independent of  $\theta$  over a wide range of  $\theta$ . Since it is clear from their work that the mechanism of adsorption involves hydrogen bonding between the surface hydroxyl groups on

(13) B. J. Fontana and J. R. Thomas, *J. Phys. Chem.*, **66**, 480 (1961).

the silica and the carbonyl groups on the polymer,  $\epsilon$  is very likely relatively large ( $>5kT$ ) for this case. Thus, their data is consistent with the idea that this system is operating at the upper regions of the curves in Fig. 2 where  $P(0)$  is relatively insensitive to  $\theta$ .

These investigators found, however, that the relatively constant value for  $P(0)$  was not unity but instead about 0.4. This, as the authors point out, most probably is a result of the combination of polymer backbone inflexibility and availability of properly spaced adsorption sites. It is to be expected that as  $P(0)$  approaches a value as high as 0.4 the chain becomes relatively rigid (as compared to the solution configuration) and surface site spacing and surface uniformity requirements become more critical. Furthermore, under these conditions both intermolecular and intramolecular overlapping of portions of the chains will lead to smaller  $P(0)$  because of steric effects. Alternatively it may be stated that at  $P(0) = 0.4$  the entire PLMA chain is collapsed to the surface to the extent that equation 18 might be more appropriate.

**Acknowledgments.**—The author wishes to acknowledge the very helpful suggestions and discussions concerning the problem with Drs. O. L. Harle, J. R. Thomas and B. J. Fontana. He also gives thanks to Professor R. L. Scott for his critical examination of the methods employed in this article.

## A NUCLEAR MAGNETIC RESONANCE STUDY OF *syn-anti* ISOMERISM IN KETOXIMES

BY ERNEST LUSTIG

*Division of Physical Chemistry, National Bureau of Standards, Washington 25, D.C.*

*Received September 21, 1960*

Isomerism of the *syn-anti* kind has been detected for the first time in several aliphatic ketoximes and ketoxime ethers and is indicated by the presence of two resonance lines for the protons on carbon atoms next to the  $>C=NOH$  or  $>C=NOR$  group. The separation of these two lines depends on (a) the presence of aromatic compounds, acids or bases in the oxime solution, and (b) on the concentration. A differential ring-current effect and the presence of oxime ions are assumed to be responsible for these separations. Steric effects and internal hydrogen-bonding seem to account for the apparent absence of a second isomer in some cases.

### Introduction

The separation of geometrical isomers and the behavior of oximes has been a subject for controversy.<sup>1</sup> Although the chemical behavior of these substances gives valuable clues to their isomerism, only direct methods for determining molecular structure can reliably establish the non-linearity of the  $C=NO-$  group which gives rise to this isomerism. Several X-ray diffraction studies have shown that the  $CNO$  angle is  $113 \pm 2^\circ$ . The only oxime for which the structure of both isomers has been determined is *p*-chlorobenzaldoxime.<sup>2</sup> In the *anti* form, the oxygen atom was found to lie closer to the

ring than in the *syn* form. This result confirms earlier assumptions about the structure of these two aldoxime isomers.

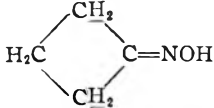
Nuclear magnetic resonance is a valuable technique complementary to the preceding, since hydrogen atoms (or fluorine atoms) in the neighborhood of the oxime group can be probes for detecting asymmetry in oxime molecules of the  $R_2C=NOH$  type, as well as in alternative isomeric structures of the  $R'R''C=NOH$  type. Phillips<sup>3</sup> has recently reported work on aliphatic aldoximes ( $RHC=NOH$ ). The fact that the spectra show two multiplets, separated by about 0.6 p.p.m., for the aldehydic hydrogen atoms, was ascribed to the simultaneous existence of *syn* and *anti* isomers; he also assigned

(1) J. Meisenheimer and W. Theilacker, "Stereochemie des Stickstoffes," in "Stereochemie" (K. Freudenberg, ed.), F. Deuticke, Leipzig and Vienna, 1933.

(2) B. Jerslev, *Nature*, **166**, 741 (1950); **180**, 1410 (1958).

(3) W. D. Phillips, *Ann. N. Y. Acad. Sci.*, **70**, 817 (1958).

TABLE I  
PROTON RESONANCE SEPARATIONS FOR SYMMETRICAL KETOXIMES AND O-ALKYL ETHERS

Compound	Ref.	Multiplicity of H line	Separation, c./sec.	Solvent	Concn. g./100 ml. of soln.
(I) $(\text{CH}_3)_2\text{C}=\text{NOH}$		1	5	Benzene	10
(II) <sup>a</sup> $(\text{CH}_3\text{CH}_2)_2\text{C}=\text{NOH}$	5	4	15	Benzene	10
(III) $[(\text{CH}_3)_2\text{CH}]_2\text{C}=\text{NOH}$		7	54	Benzene	20
			51	Carbon tetrachloride	
(IV) <sup>a</sup>					
	6	3	7	Benzene	10
(V) $(\text{C}_6\text{H}_5\text{CH}_2)_2\text{C}=\text{NOH}$	7	1	15	Acetone	10
(VI) $(\text{CH}_3)_2\text{C}=\text{NOCH}_3$	8	1	1.5	Benzene	10
(VII) $(\text{CH}_3)_2\text{C}=\text{NOC}_2\text{H}_5$	8	1	1.5	Benzene	10

<sup>a</sup> See Fig. 1 for spectrum.

the multiplet at higher field to the *anti* form. (See Appendix.)

The simultaneous existence, in some unsymmetrical ketoximes ( $R'' \neq R'$ ), of the two forms, also suspected for a long time,<sup>1</sup> has been demonstrated for the first time by the present study. Although the present n.m.r. spectra give evidence of this conclusion in some cases, the separations corresponding to the proton resonances are much smaller than, and of different origin from, those assumed in aldoximes.<sup>3</sup> In the latter, the position of the  $-\text{HC}=\text{NOH}$  resonance in the spectrum seems to depend directly on the  $\text{H} \dots \text{O}$  distance. It now appears possible to demonstrate *syn-anti* isomerism in ketoximes and to use proton resonance to monitor the separation of *syn* and *anti* isomers.

It was originally thought that the differences in the electronic environment of hydrogen atoms on the carbon adjacent to the  $>\text{C}=\text{NOH}$  group, differences resulting from the non-linearity of this group, might be sufficient to give rise to an observable chemical shift, *e.g.*, for one methyl group in acetoxime with respect to the other. As has now been observed, however, the frequency of the resonance lines of these protons differs only when certain solvents are used, and the separation of the lines depends on concentration. Measurable separations were found in "aromatic" solvents, such as benzene, thiophene, furan, and their derivatives, and in solutions of naphthalene in carbon tetrachloride and carbon disulfide. In pyridine solutions separations were also observed, but because of the basic nature of pyridine, there may have been an additional effect due to  $\text{OH}^-$  (see below). The magnitudes of these splittings were found to depend on the field strength, so that spin-spin coupling is excluded.

### Experimental

All data were taken with a Varian 60 mc./sec. n.m.r. spectrometer, except for a few measurements made at 24.3 mc./sec. to check the field dependence. The scale of the spectra was established directly on the recorder trace by the side-band technique. All measurements were made at room temperature and on undegassed material. Some spectra are shown in Fig. 1.

The oximes were obtained from the following sources: (a) gift; 2,4-dimethyl-3-pentanone oxime (diisopropyl ketoxime) III,<sup>4</sup> from Prof. D. E. Pearson, Vanderbilt Univer-

(4) Roman numerals designate the compounds listed in Tables I-III.

sity; (b) commercial sources: acetoxime I, from Eastman; butanone oxime VIII, from Matheson, Coleman, and Bell; acetophenone oxime, from Eastman; (c) prepared in this Laboratory: all other oximes (see Tables I and III for references). The compound  $\text{CF}_3\text{-C}(=\text{NOH})\text{-C}_6\text{H}_5$ , 2,2,2-trifluoroacetophenone oxime, which is not described in the literature, was prepared by refluxing 12.3 ml. of the ketone with 100 ml. of a 1:1 methanol-water mixture containing 10 g. of  $\text{NH}_2\text{OH}\cdot\text{HCl}$  and 14 g. of  $\text{NaOAc}\cdot 3\text{H}_2\text{O}$ , for two hours; 50 ml. of liquid were then distilled off. The residue (which had separated into two layers) was poured into cold water, whereupon the oxime was precipitated. After recrystallization from ligroin, it melted at 75°.

TABLE II  
METHYL SEPARATIONS FOR ACETONE OXIME

Solvent	Concn., g./100 ml. of soln.	Separation, c./sec.
Benzene	20	4.1
	10	4.9
	5	5.5
	1	6.2
Toluene	5	4.4
Nitrobenzene	5	1.3
Naphthalene (about 30% soln. in $\text{CS}_2$ )	5	1.5
Furan	5	3.2
Thiophene	5	4.3
Benzene-carbon tetrachloride mixtures <sup>a</sup>	$n = 7$	10
	5	10
	3	10
	1	10

<sup>a</sup> Prepared by placing 1 g. of acetone oxime in a 10-ml. volumetric flask, adding  $n$  ml. of benzene, and diluting to volume with  $\text{CCl}_4$ .

### Results and Discussion

In symmetrical ketoximes (see Table I), it was observed that the resonances of protons on carbon atoms adjacent to the  $>\text{C}=\text{NOH}$  group appeared in the spectrum twice, with equal intensity. This may be expected, since the two radicals bound to this group are not equivalent because of the non-linearity of the  $>\text{C}=\text{NOH}$  group. With the exception of III, such a "splitting" occurred in the

(5) E. W. Bousquet, "Organic Syntheses," Coll. Vol. 2, McGraw-Hill Book Co., New York, N. Y., 1943, p. 313.

(6) D. C. Iffland, G. X. Criner, M. Coral, F. J. Lotspeich, Z. B. Papanastassiou and S. M. White, Jr., *J. Am. Chem. Soc.*, **75**, 4044 (1953); private communication from Prof. Iffland.

(7) E. Beckmann, *Ber.*, **19**, 988 (1886).

(8) A. I. Vogel, W. T. Cresswell, G. H. Jeffrey and J. Leicester, *J. Chem. Soc.*, 514 (1952).

TABLE III

SEPARATIONS<sup>a</sup> FOR UNSYMMETRICAL METHYL KETOXIMES,  
CH<sub>3</sub>-C(=NOH)-R

Compound	R	Ref.	CH <sub>3</sub> separation	CH <sub>2</sub> separation
(VIII) <sup>b</sup>	CH <sub>3</sub> -CH <sub>2</sub>		6.2	17.0
(IX) <sup>b</sup>	C <sub>6</sub> H <sub>5</sub> -CH <sub>2</sub>	22	6.1	19.2
(X)	CH <sub>3</sub> -CH <sub>2</sub> -CH <sub>2</sub>	5	6.3	? <sup>c</sup>
(XI)	(CH <sub>3</sub> ) <sub>2</sub> -CH-CH <sub>2</sub>	9	4.9	? <sup>c</sup>
(XII)	CH <sub>2</sub> Cl	10	0	0
(XIII)	(CH <sub>3</sub> ) <sub>2</sub> CH	5	0	..
(XIV)	CH <sub>3</sub> -CH <sub>2</sub> -CH(CH <sub>3</sub> )	5	0	..
(XV)	(CH <sub>3</sub> ) <sub>2</sub> C=CH	11	2.5	..
(XVI)	(C <sub>6</sub> H <sub>5</sub> ) <sub>2</sub> -CH	12	0	..
(XVII)	(CH <sub>3</sub> ) <sub>3</sub> C	13	0	..
(XVIII)	COOR'(R' = H, CH <sub>3</sub> , or C <sub>2</sub> H <sub>5</sub> )	14, 15, 16	0	..

<sup>a</sup> In 10% benzene solution. <sup>b</sup> See Fig. 1 for spectrum.  
<sup>c</sup> Obscured by spin-spin splittings.

presence of aromatic compounds only (see Table II), or when the oxime molecule itself had an aromatic substituent. Thus the presence of the phenyl group in 1-phenyl-2-propanone oxime (phenylacetone oxime, IX) was sufficient to cause separation of resonance lines. No splittings were found in any of a large number of non-aromatic solvents tested. All parent ketones in the present study exhibit a single resonance for the corresponding protons, regardless of solvent and concentration.

Other factors which affect the separation are (see Table II): the type of aromatic ring present, the nature of the substituent, and the ratio of aromatic compound to oxime. Measurements at 24.3 mc./sec. show that the separation of the CH<sub>3</sub> peaks in acetoxime (I) is diminished in all cases by a factor 24.3/60.

It is difficult to understand why for -CH=NOH protons the shifts are at least thirty times larger than for, say, -C(CH<sub>3</sub>)=NOH protons (if one disregards the solvent effects described). The fact that the corresponding O...H distances are smaller for aldoximes than for ketoximes, suggests only that the neighboring effect of oxygen is expected to be larger in aldoximes. A more quantitative interpretation seems not possible at present.

At any rate, all these observations are similar to those for proton shifts of chloroform in aromatic solvents.<sup>17</sup> The origin of the proton shift with respect to pure chloroform has been explained as follows: a complex (e.g., CHCl<sub>3</sub>-C<sub>6</sub>H<sub>6</sub>) is formed, having the CH bond of CHCl<sub>3</sub> lying approximately along the C<sub>6</sub>-axis of the ring. The proton of CHCl<sub>3</sub> experiences the effect of the magnetic field of the ring, which results from the circulation of  $\pi$ -electrons. Thus a shift of the CHCl<sub>3</sub> resonance signal is

- (9) P. Karrer and P. Dinkel, *Helv. Chim. Acta*, **36**, 122 (1953).
- (10) R. Scholl and G. Matthiaopoulos, *Ber.*, **29**, 1550 (1896).
- (11) C. Harries and R. Gley, *Ber.*, **32**, 1330 (1899); C. Harries, *Ann.*, **330**, 185 (1903); L. Kahovec and K. W. F. Kohlrusch, *Monatsh.*, **83**, 615 (1952).
- (12) R. Stoermer, *ibid.*, **39**, 2288 (1906).
- (13) O. Piloty and A. Stock, *ibid.*, **35**, 3093 (1902).
- (14) V. Meyer and A. Janny, *ibid.*, **15**, 1525 (1882).
- (15) L. Piaux, *Bull. soc. chim. biol.*, **6**, 412 (1924).
- (16) G. Ponzio and G. Ruggieri, *Gazz. chim. ital.*, **55**, 453 (1925).
- (17) L. W. Reeves and W. G. Schneider, *Can. J. Chem.*, **35**, 251 (1957); M. Charton-Koehlin and M. A. Leroy, *J. chim. phys.*, **56**, 850 (1959); Z. Pajak and F. Pellán, *Compt. rend.*, **251**, 79 (1960).

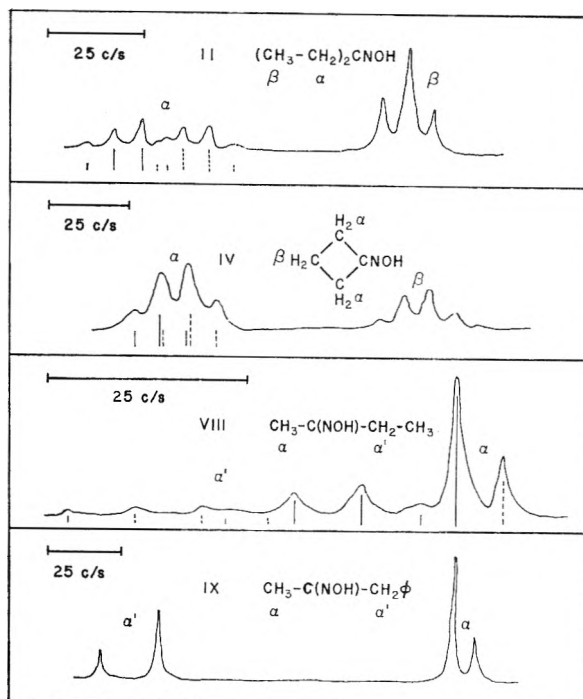


Fig. 1.—Spectra of some oximes in *p* % benzene solution: *p* is 10 for II and IV, 15 for VIII, and 7.5 for IX. In the spectrum of IV, the left quadruplet appears to be a superposition of two triplets; in the spectrum of cyclobutanone (not shown), the resonance of the  $\alpha$ -protons is a triplet.

observed. In the more general case, the shift increases with the mole fraction of aromatic compound present and decreases for compounds, such as nitrobenzene, having electron-withdrawing substituents. The effect is of the order of 40 c./sec. at 40 mc./sec.; theoretical calculations<sup>17,18</sup> indicate that it should be field dependent.

In the present study, the oxime molecule is presumed to experience the magnetic field of a ring compound. Such  $\epsilon$  field<sup>19</sup> is cylindrically symmetrical and, since the molecule is asymmetrical (the  $>C=NO-$  group is not linear) in any complex, the various parts of the oxime molecule would lie in regions of different field strength. It is this difference of local field which is assumed to cause the observed separations. The decrease in separation for the ethers VI and VII (see Table I) indicates that the hydroxyl hydrogen atom may be involved in complex-formation. Further studies on the nature of the complex will have to be concerned with the details of the benzene field<sup>19</sup> and the self-association of oximes<sup>20</sup> by hydrogen bonds. Oxime ethers are not hydrogen-bonded, and their study may be simpler.

A rough estimate based on the iso-shielding lines diagram given in Johnson and Bovey's paper<sup>19</sup> yields a shift of the order of 0.1 p.p.m., for acetone oxime, compatible with the shifts observed. An analysis of the experimental data based on an extension of Johnson and Bovey's table<sup>19</sup> and taking

- (18) J. Pople, *J. Chem. Phys.*, **24**, 1111 (1956).
- (19) J. S. Waugh and R. W. Fessenden, *J. Am. Chem. Soc.*, **70**, 846 (1957); J. S. Waugh, *ibid.*, **80**, 6697 (1958); C. E. Johnson and F. A. Bovey, *J. Chem. Phys.*, **29**, 1012 (1958).
- (20) See e.g., S. Califano and W. Lüttke, *Z. physik. Chem. (Frankfurt) [N.F.]*, **5**, 240 (1955); **6**, 83 (1956), and references given therein.

into account self-association of acetone oxime, is under way.

The case of diisopropyl ketoxime (III, see Table I) is exceptional, not only because two septets appear in  $\text{CCl}_4$  solution also, but because two  $(\text{CH}_3)_2\text{CH}$ -doublets, 2.5 c./sec. apart, are observed. Steric hindrance of some kind may be invoked to explain the non-equivalence of isopropyl groups or positions; the spectrum of diisopropyl ketone exhibits a single septet and a single doublet.

Another group of observations concerns spectra of oximes in the presence of acid or base. Some of the preliminary results are: 10% acetoxime solutions in 10 *N* HCl, 10 *N* NaOH and pyridine have spectra with methyl doublets of 2.1, 5.3 and 4.7 c./sec., respectively. Presumably, the chemical shifts in the aqueous solutions are caused by the non-equivalence of methyl groups in the corresponding ions  $(\text{CH}_3)_2\text{C}=\text{NOH}_2^+$  or  $(\text{CH}_3)_2\text{C}=\text{NHOH}^+$ , and  $(\text{CH}_3)_2\text{C}=\text{NO}^-$ . In pyridine solutions, both the ring and the presence of the anion may be responsible for the shift. In the aqueous solutions, the peak separation decreases with decreasing concentration of acid or base. Additional work is planned on oximes in aqueous solutions of different *pH* and in non-aqueous solutions of acids and bases such as acetic acid and triethylamine.

In unsymmetrical ketoximes, similar separations were observed (see Table III) under the conditions described for the symmetrical ketoximes. It is assumed that the  $\text{CH}_3\text{-C}(=\text{NOH})$ - resonance of an isomer consists of just one peak, due to the absence of any resolved spin-spin coupling across the  $\text{C}=\text{NOH}$  group. Hence, oximes of the  $\text{CH}_3\text{-C}(=\text{NOH})$ -R type are believed to represent a class of compounds favorable for the study of *syn-anti* isomerism. In fact, no such coupling was observed<sup>21</sup> in oximes or ketones of this type, except for  $\text{CH}_3\text{-CO-CF}_3$ . In this case, the proton resonance consists of a well-resolved quadruplet (with  $J = 1.0$  c./sec.) caused by H-F coupling across the carbonyl carbon atom.

The relevant part of the butanone oxime (VIII) spectrum consists of two overlapping quartets for  $-\text{CH}_2-$  having an intensity ratio of about 1:3, and a pair of singlets for  $\text{CH}_3-$  having an intensity ratio of about 3:1. It is reasonable to assume that the components with relative intensity of 1 are displayed by one of the possible geometrical isomers (*syn* or *anti* with respect to methyl), and that with relative intensity 3 by the other. The reversed sequence of intensities in the spectrum may be rationalized as follows. Let  $p_g$  and  $q_g$  be the shifts of a group in *syn* and *anti* positions, respectively, and let  $F_g$  be the resonance frequency characteristic for the "unshifted" group. Then for *syn*-(methyl)-butanone oxime, the spectrum will be  $(F_{\text{CH}_2} + q_{\text{CH}_2})_{\text{syn}}$  and  $(F_{\text{CH}_3} + p_{\text{CH}_3})_{\text{syn}}$ , and for *anti*-(methyl)-butanone oxime  $(F_{\text{CH}_2} + p_{\text{CH}_2})_{\text{anti}}$  and  $(F_{\text{CH}_3} + q_{\text{CH}_3})_{\text{anti}}$ . If one assumes that  $p_g > q_g$ , the lines of a mixture of *syn* and *anti* forms appear in this order:  $(F_{\text{CH}_2} + q_{\text{CH}_2})_{\text{syn}}$ ,  $(F_{\text{CH}_2} + p_{\text{CH}_2})_{\text{anti}}$ ,  $(F_{\text{CH}_3} + q_{\text{CH}_3})_{\text{anti}}$ ,  $(F_{\text{CH}_3} + p_{\text{CH}_3})_{\text{syn}}$ . Such a sequence was also observed by Phillips<sup>3</sup> in

the spectrum of benzyl methyl nitrosamines. An analogously reversed sequence of lines would also occur for  $p_g < q_g$ . Incidentally, in all spectra of the unsymmetrical ketoximes examined which indicate the presence of both isomers, the intensity ratio is approximately 3:1. Any intensity ratio in a spectrum reflects, of course, the isomeric ratio in the presence of the solvent used, which may not necessarily be the same as that of the oxime in the pure state.

The case of phenylacetone oxime (IX) is of some interest. The material used at first was not crystalline, although the viscous oil obtained contained the stoichiometric proportions of C and H for the oxime. The melting point reported<sup>22</sup> for this compound is 70°. The spectrum (see Fig. 1) shows that it consists of a mixture of two isomers. As in the case of 1,3-diphenyl-2-propanone oxime (V), no external aromatic agent is required to produce the separation of peaks which belong to non-equivalent groups. The sequence of intensities is the same as for butanone oxime, that is 1:3 for  $\text{CH}_2$  (singlets) and 3:1 for  $\text{CH}_3$  (singlets). Further experiments with oily and crystalline material revealed that the oil is a non-equilibrium mixture of the form which melts at 70° and gives rise to the stronger components of the doublets, and the other form not stable at room temperature. The isomerization behavior of phenylacetone oxime is still under investigation.

4-Methyl-3-penten-2-one oxime (XV) is reported<sup>11</sup> to exist in two separate forms (solid and liquid) at room temperature. As suggested by the presence of two methyl peaks in the ratio of about 6:1, the spectrum of the liquid used indicates the presence in the liquid of 15% of the solid form as solute. In this connection, it should be pointed out that those ketoximes which have been known to exist in two isomeric forms,<sup>1</sup> may be valuable compounds for further study; not many, however, appear to be suited for n.m.r. spectroscopy.

The spectra of some oximes listed in Table III indicate only one isomer, presumably the *syn* (methyl). Internal hydrogen-bonding may be the cause for the preferential formation of only one isomer in the case of oximes (XII) and (XVIII), and crowding about the  $\text{R-C}(=\text{NOH})$  bond may account for the others.

These findings may be compared with results on the Beckman rearrangement of oximes, which so far has been the method most widely used for the investigation of *syn-anti* isomerism. These results are tabulated and discussed in a forthcoming volume of "Organic Reactions."<sup>23</sup> Compounds VIII and X seem to be a mixture of the two isomers, whereas compounds IX, XIII and XVII apparently exist in a single form.

Single peaks were also found for the resonance of the corresponding nuclei in the spectra of  $\text{CH}_3\text{-C}(=\text{NOH})\text{-C}_6\text{H}_5$ ,  $\text{CF}_3\text{-C}(=\text{NOH})\text{-C}_6\text{H}_5$ , and  $\text{C}_2\text{H}_5\text{-C}(=\text{NOH})\text{-C}_6\text{H}_5$ .<sup>24</sup> The Beckmann rearrange-

(21) Cf. also L. M. Jackman, "Applications of Nuclear Magnetic Resonance Spectroscopy in Organic Chemistry," Pergamon Press, New York, N. Y., 1959, p. 83.

(22) D. H. Hey, *J. Chem. Soc.*, 18 (1930); R. M. Jaeger and J. A. van Dijk, *Koninkl. Ned. Akad. Wetenschap. Proc.*, 44, 26 (1941).

(23) L. G. Donaruma and W. Z. Heldt in "Organic Reactions," Vol. 11, John Wiley and Sons, Inc., New York, N. Y.



ment of  $\text{CH}_3\text{-C(=NOH)-C}_6\text{H}_5$  yields products whose properties suggest the presence of the two isomers, whereas only one isomer was found in the case of  $\text{C}_2\text{H}_5\text{-C(=NOH)-C}_6\text{H}_5$ . Since, as has been pointed out,<sup>22</sup> the experimental conditions of the Beckmann rearrangement can be conducive to isomerization, and not all the rearrangement products are always accounted for in the literature, the conclusions drawn from reports on Beckmann rearrangement studies as to the isomeric composition of the original oxime may not always be valid.

### Appendix

To check Phillips' assignment<sup>3</sup> of the two  $-\text{CH}=\text{NOH}$

(24) For the preparation of  $\text{C}_2\text{H}_5\text{-C(=NOH)-C}_6\text{H}_5$ , see K. N. Campbell, B. K. Campbell and E. P. Chaput, *J. Org. Chem.*, **8**, 99 (1943).

multiplets arising from *syn-anti* isomerism, the spectra of the two *p*-chlorobenzaldoximes<sup>25</sup> in dimethyl sulfoxide solution were examined. The significant portions of the spectra consisted of the following lines (c./sec.), with the center of the benzene ring multiplet taken as the origin. (With  $(\text{CH}_3)_2\text{SO}$  as reference, the origin of this multiplet in the *anti* oxime lies at higher field by about 6 c/s than of the *syn* oxime.)

Compound	Ring proton peaks				$-\text{CH}=\text{NOH}$ peak
	1	2	3	4	
<i>syn</i> oxime	-12	-3	+3	-12	-27
<i>anti</i> oxime	-21	-13	+13	+21	+17

Thus, the  $-\text{CH}=\text{NOH}$  resonance of the *anti* oxime indeed appears at higher field, and Phillips' assignment<sup>3</sup> seems to be correct. The *syn-anti* shift is, in the present case, of the order of 0.7 p.p.m., as compared to 0.6 p.p.m. for propionaldoximes.<sup>3</sup>

(25) H. Erdmann and E. Schwechten, *Ann.*, **260**, 53 (1890).

## LOW TEMPERATURE THERMODYNAMIC PROPERTIES OF SIX ISOMERIC HEPTANES

BY H. M. HUFFMAN,<sup>1</sup> M. E. GROSS, D. W. SCOTT AND J. P. McCULLOUGH

Contribution No. 94 from the Thermodynamics Laboratory, Petroleum Research Center, Bureau of Mines, U. S. Department of the Interior, Bartlesville, Oklahoma

Received September 21, 1960

In a continuing program of studies of thermodynamic properties of aliphatic hydrocarbons, low-temperature thermal measurements were made on the nine isomeric heptanes, but definitive results could be obtained for the following six compounds only: *n*-heptane, 2-methylhexane, 3-ethylpentane, 2,2-dimethylpentane, 2,4-dimethylpentane and 2,2,3-trimethylbutane. Values of heat capacity in the solid and liquid states and of the latent heats and temperatures of isothermal phase changes were determined for each of these six isomers. Also, the vapor pressure of 2-methylhexane was measured in the ranges, 0–45°, 17–159 mm. From the observed data were calculated values of the free energy function, heat content function, heat content, entropy and heat capacity of the condensed phases at selected temperatures between 10 and 300°K. These results and literature values of heat of formation, heat of vaporization and vapor pressure were used to compute values of the chemical thermodynamic properties for the liquid and ideal gas states at 298.15°K.

The preparation of comprehensive tables of thermodynamic property values for important homologous series of hydrocarbons requires knowledge of the variation of such properties with both molecular size and structure. The Bureau of Mines has a continuing program to determine part of the needed fundamental information by low temperature calorimetric studies of selected groups of hydrocarbons. For acyclic hydrocarbons, previous publications have reported low temperature thermal data for nine *n*-paraffins,<sup>2</sup> five isomeric hexanes,<sup>3</sup> seven 1-olefins,<sup>4</sup> six isomeric pentenes,<sup>5</sup> and several others. This paper describes an investigation of the isomeric heptanes. Studies of all nine isomers were attempted, but for reasons discussed in a following section, definitive results could be obtained for only six isomers: *n*-Heptane, 2-methylhexane, 3-ethylpentane, 2,2-dimethylpentane, 2,4-dimethylpentane and 2,2,3-trimethylbutane. Values of heat capacity in the solid and liquid states in the range 12–300°K. and of the latent heats and temperatures of isothermal

phase changes were determined for each of these six compounds. Also, the vapor pressure of 2-methylhexane was measured in the ranges, 0–45°, 17–159 mm. From the observed data were calculated values of the free energy function, heat content function, heat content, entropy and heat capacity of the condensed phases at selected temperatures between 10 and 300°K. These results and literature values of heat of formation, heat of vaporization and vapor pressure were used to compute values of the chemical thermodynamic properties for the liquid and ideal gas states at 298.15°K. Detailed results of these studies are in the Experimental section.

### Discussion of Results

**Chemical Thermodynamic Properties at 298.15°K.**—Table I lists the chemical thermodynamic properties of the six heptanes at 298.15°K. The tabulated values are based only on experimental data from this investigation and earlier studies of heats of formation and vaporization and vapor pressure cited in text and in the footnotes to Table I. Current tabulations of American Petroleum Institute Research Project 44<sup>6</sup> also give

(6) American Petroleum Institute Research Project 44, "Selected Values of Physical and Thermodynamic Properties of Hydrocarbons and Related Compounds," Carnegie Press, Carnegie Institute of Technology, Pittsburgh, Pennsylvania, 1953.

(1) Deceased.

(2) H. L. Finke, M. E. Gross, Guy Waddington and H. M. Huffman, *J. Am. Chem. Soc.*, **76**, 333 (1954).

(3) D. R. Douslin and H. M. Huffman, *ibid.*, **68**, 1704 (1946).

(4) J. P. McCullough, H. L. Finke, M. E. Gross, J. F. Messerly and Guy Waddington, *J. Phys. Chem.*, **61**, 289 (1957).

(5) S. S. Todd, G. D. Oliver and H. M. Huffman, *J. Am. Chem. Soc.*, **69**, 1519 (1947).



TABLE I  
 MOLAL THERMODYNAMIC PROPERTIES AT 298.15°K.

Compound	State	$\Delta H_v^\circ, ^a$ kcal.	$\Delta S_v^\circ, ^a$ cal. deg. <sup>-1</sup>	$S^\circ, ^b$ cal. deg. <sup>-1</sup>	$\Delta H_f^\circ, ^b, ^c$ kcal.	$\Delta F^\circ, ^b, ^c$ kcal.	log $K_f, ^b, ^c$
<i>n</i> -Heptane	Liq.	8.749	23.74	78.53	-53.63 <sup>d</sup>	0.24	-0.18
	Gas			102.27	-44.88	1.91	-1.40
2-Methylhexane	Liq.	8.343	23.10	77.28	-54.93 <sup>d</sup>	-0.69	+0.51
	Gas			100.38	-46.59	+ .77	- .56
3-Ethylpentane	Liq.	8.436	23.17	75.18	-53.77 <sup>d</sup>	1.10	- .81
	Gas			98.35	-45.33	2.63	-1.93
2,2-Dimethylpentane	Liq.	7.776	22.13	71.77	-57.05 <sup>d</sup>	-1.16	+0.85
	Gas			93.90	-49.27	+0.02	- .01
2,4-Dimethylpentane	Liq.	7.885	22.36	72.46	-56.17 <sup>d</sup>	- .49	+ .36
	Gas			94.82	-48.28	+ .73	- .54
2,2,3-Trimethylbutane	Liq.	7.682	21.76	69.85	-56.63 <sup>d</sup>	- .17	+ .12
	Gas			91.61	-48.95	+1.02	- .75

<sup>a</sup> The standard heat and entropy of vaporization. <sup>b</sup> The entropy, heat of formation, free energy of formation and logarithm of the equilibrium constant of formation in the standard liquid or gas state at 298.15°K. <sup>c</sup> For the reaction  $7C(c, \text{graphite}) + 8H_2(g) = C_7H_{16}(l \text{ or } g)$ . <sup>d</sup> E. J. Prosen and F. D. Rossini, *J. Research Natl. Bur. Standards*, **34**, 263 (1945).

values of the properties in Table I. Some of the results in the API tabulations, which are based on preliminary data from this work, differ slightly from the values reported here. Although the differences are minor, the values in Table I are considered more accurate than the earlier results.

Huffman, Parks and Thomas<sup>7</sup> made low temperature thermal studies of these compounds over 30 years ago. Their results for the entropy increment between 90 and 298°K. (the range of their measurements) agree with those of this work within 1%. However, because they had to compute the increment between 0 and 90°K. by an uncertain extrapolation, some of their values of  $S_{298}$  are in error by several per cent.

**Thermal Behavior of the Heptanes in the Solid State.**—Normal heptane, 3-ethylpentane and 2,4-dimethylpentane have regular heat capacity curves in the solid state; 2-methylhexane and 2,2-dimethylpentane have peaks in the heat capacity curves, designated as Type H transitions in the empirical classification of McCullough.<sup>8</sup> Much more complicated behavior is shown by 2,2,3-trimethylbutane: two non-isothermal transitions (either Type 2N or Type H<sup>8</sup>) are followed by an isothermal transition (Type I<sup>8</sup>) as the crystals are heated from 80 to 125°K. Of the heptane isomers not studied completely, 3,3-dimethylpentane has at least three crystalline modifications, and 3-methylhexane and 2,3-dimethylpentane form glasses.<sup>9</sup> The plots of heat capacity *vs.* temperature in Fig. 1 depict the thermal behavior of the crystalline heptanes. For reference purposes in the discussion that follows, the heat capacity curve of *n*-heptane is superimposed on the curves of each of the other five isomers.

Crystal structure and other information needed for detailed understanding of the results shown in Fig. 1 are unavailable, but the results afford an unusual demonstration of the effect of isomeric differences on the thermal behavior of organic crystals. In addition to the occurrence of phase transformations, three points are to be noted:

First, the heat capacity of *n*-heptane is the lowest of all isomers in the region below 50°K., undoubtedly because the branched hydrocarbons form "softer" crystals. That is, the lattice contribution to the heat capacity becomes fully excited at lower temperatures for a branched heptane than it does for *n*-heptane. The fact that the heat capacity of 3-ethylpentane is only a little higher than that of *n*-heptane below 50°K. suggests that this symmetrically branched compound forms a more compact crystal than the less symmetrically branched isomers.

Second, the heat capacity curve of *n*-heptane is higher than those of the other isomers in at least part of the region from 50 to 120°K. This crossing of heat capacity curves is caused in part by the delayed excitation of the lattice contribution of *n*-heptane. However, as unbranched compounds usually have more low-lying internal energy levels than branched compounds, the more rapid increase in the heat capacity of *n*-heptane above 50°K. also is due in part to increased contributions from internal degrees of freedom.

Third, the heat capacity of each branched isomer again becomes higher than that of *n*-heptane at some temperature above 100°K. For some of the branched isomers, the heat capacity curve has pronounced positive curvature in the region below the melting point. This effect undoubtedly is due to increased libration, or "prerotation",<sup>10</sup> of molecules at the lattice sites, as in the higher *n*-paraffins.<sup>2</sup> The heat capacity of *n*-heptane also may be affected by "prerotation", but at higher temperatures and probably to a lesser extent. The "softer" crystals of 2-methylhexane, 2,2-dimethylpentane and 2,4-dimethylpentane evidently allow appreciable libration of molecules about a crystal lattice site as the melting point is approached, perhaps including some degree of restricted rotation. The results for 3-ethylpentane do not provide evidence of significant "prerotation" effects, in keeping with the observation that this compound must form relatively compact crystals.

With thermal evidence only, it is not practical to speculate about the details of the solid-phase transformations that occur in 2-methylhexane,

(7) H. M. Huffman, G. S. Parks and S. B. Thomas, *J. Am. Chem. Soc.*, **52**, 3241 (1930).

(8) J. P. McCullough, Proceedings of the Symposium on Chemical Thermodynamics, Watten, Austria, August, 1959; to be published.

(9) Further attempts to study these three compounds are planned.

(10) C. P. Smyth, *Trans. Faraday Soc.*, **42A**, 175 (1946).

2,2-dimethylpentane and 2,2,3-trimethylbutane. Because of slow thermal equilibration, the shapes of the heat capacity curves could not be defined precisely in the regions a few degrees above and below the temperatures at which the peaks occur. However, the curves drawn are consistent with continuous enthalpy measurements made over the ranges of anomalous behavior and, therefore, are generally correct.

Two of the isomeric hexanes—2,2-dimethylbutane and 2,3-dimethylbutane—also exhibit phase transformations in the solid state.<sup>3</sup> Nuclear magnetic resonance<sup>11</sup> and X-ray diffraction<sup>12</sup> studies have shown that the high-temperature phase of 2,2-dimethylbutane is highly disordered; that is, the molecules as a whole undergo restricted rotation at crystal lattice sites. The three transformations in 2,2,3-trimethylbutane undoubtedly result in a high-temperature phase with a comparable degree of orientational disorder. However, as the entropy of fusion of 2,2,3-trimethylbutane (2.17 cal. deg.<sup>-1</sup> mole<sup>-1</sup>) is significantly larger than those of the two dimethylbutanes,<sup>3</sup> the high-temperature crystals of this heptane probably are not so completely disordered as those of the branched hexanes.

On the basis of the thermal evidence, the crystals of the less symmetrically shaped molecules of 2-methylhexane and 2,2-dimethylpentane do not obtain a high degree of orientational disorder in the solid phase. Perhaps the transitions that occur in these two compounds result in slight changes in crystal structure that allow the increased librational freedom discussed before. Apparently, 2,4-dimethylpentane is symmetrical enough that increased librational freedom occurs without a transition, but it is not symmetrical enough to form a highly disordered, or "rotating,"<sup>11</sup> crystal at temperatures below its melting point. As a result, this last compound shows no anomaly other than the effects of "prerotation."

In general terms, the thermal behavior of the heptanes in the solid phase may be summarized as follows. The compact crystals of *n*-heptane and 3-ethylpentane undergo no phase transformation, although they may show slight effects of "prerotation." ("Prerotation" is used here as a term to describe the increased librational freedom, possibly including restricted over-all rotation about one axis, gained by molecules of some organic crystals at temperatures below the melting point.) The less compact crystals of 2-methylhexane, 2,2-dimethylpentane and 2,4-dimethylpentane show more pronounced effects of "prerotation." The onset of "prerotation" in 2-methylhexane and 2,2-dimethylpentane is preceded by phase transformations that are evidenced by peaks in the heat capacity curves. The more symmetrical (ellipsoidal) molecule, 2,4-dimethylpentane, also exhibits "prerotation" effects, but without a preparatory phase change. The still more symmetrical (globular) molecule, 2,2,3-trimethylbutane undergoes three transformations in the solid phase,

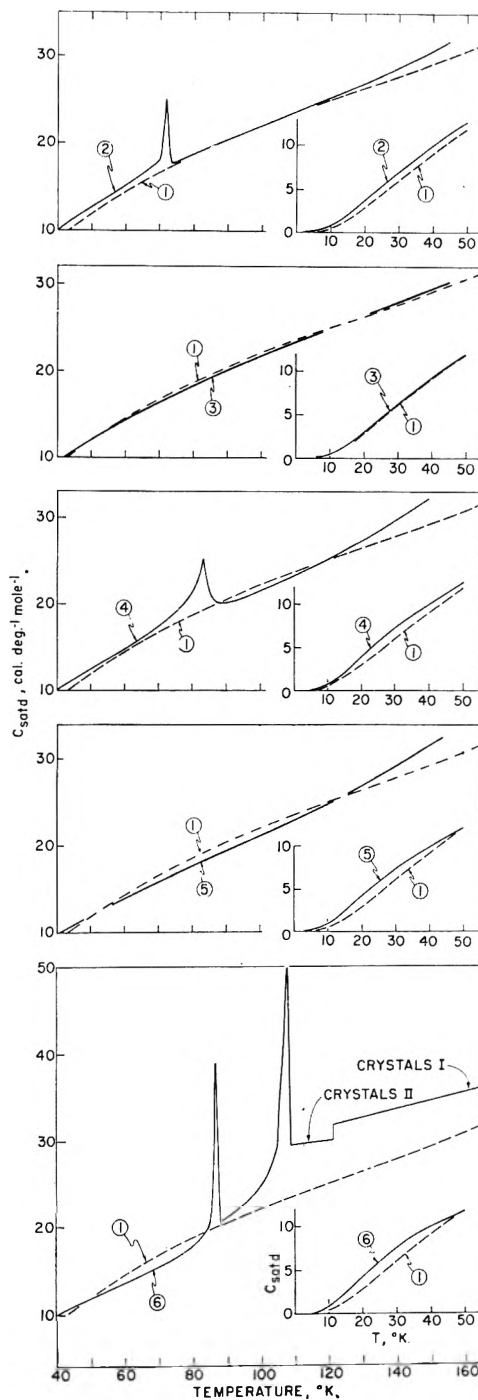


Fig. 1.—Heat capacity curves for six isomeric heptanes in the solid state: (1) *n*-heptane; (2) 2-methylhexane; (3) 3-ethylpentane; (4) 2,2-dimethylpentane; (5) 2,4-dimethylpentane; and (6) 2,2,3-trimethylbutane.

with the high temperature crystalline phase having a much higher degree of orientational disorder than usually implied by the term "prerotation."

### Experimental

**Apparatus and Physical Constants.**—The low temperature calorimetric<sup>13</sup> and vapor pressure<sup>14</sup> measurements were

(11) J. G. Aston, B. Bolger, R. Trambarulo and H. Segall, *J. Chem. Phys.*, **22**, 460 (1954).

(12) B. Post, R. S. Schwartz and I. Fankuchen, *J. Am. Chem. Soc.*, **73**, 5113 (1951).

(13) H. M. Huffman, *Chem. Revs.*, **40**, 1 (1947); H. M. Huffman, S. S. Todd and G. D. Oliver, *J. Am. Chem. Soc.*, **71**, 584 (1949); D. W. Scott, D. R. Douslin, M. E. Gross, G. D. Oliver and H. M. Huffman, *ibid.*, **74**, 883 (1952).

made with apparatus described by Huffman and co-workers. The 1951 International Atomic Weights<sup>16</sup> and values of the fundamental physical constants<sup>16</sup> were used. Measurements of temperature were made with platinum-resistance thermometers calibrated in terms of the International Temperature Scale of 1948<sup>17</sup> from 90 to 400°K.; and Celsius temperatures were converted to Kelvin temperatures by addition of 273.15°.<sup>18</sup> From 11 to 90°K., temperature measurements were made in terms of the provisional scale of the National Bureau of Standards.<sup>19</sup> Energy was measured in joules and converted to calories by the relation, 1 cal. = 4.184 (exactly) joules. Measurements of mass, electrical potential and resistance were made in terms of standard devices calibrated at the National Bureau of Standards.

The results in this paper originally were calculated with physical constants and temperatures related to the definition 0° = 273.16°K. Temperatures reported here are in terms of the newer definition,<sup>18</sup> but only some of the experimental results were recalculated. Numerical inconsistencies less than the *precision* of the experimental data may have been introduced by this procedure.

**Materials.**—The samples of the branched isomers were API Research hydrocarbons.<sup>20</sup> As described in detail in another publication,<sup>21</sup> extensive measurements were made on four different samples of *n*-heptane, two of which were API Research samples<sup>20</sup> and two of which were Calorimetry Conference samples.<sup>22</sup> Because the detailed results for *n*-heptane are to be published elsewhere,<sup>21</sup> only a summary of the data for this compound is given here for comparison with results for the other isomers.

**Heat Capacities in the Solid and Liquid States.**—The heat capacity of each heptane was measured in the solid and liquid states in the approximate range 12 to 300°K. Observed values of heat capacity at saturation pressure,  $C_{\text{satd}}$ , are recorded for each isomer, except *n*-heptane, in Table II. The temperature increments used in the measurements were small enough to obviate corrections for non-linear variation of  $C_{\text{satd}}$  with  $T$ , except as noted in Table II. The precision of the results was, in general,  $\pm 0.1\%$ , and above 30°K., the accuracy uncertainty should not exceed 0.2%, except in the regions of phase transformations. Near phase changes data for the solid state may be less precise and less accurate because of rapid changes of  $C_{\text{satd}}$  with  $T$ , slow equilibration, or uncertainties caused by the presence of impurities. The results in Table II have not been corrected for premelting caused by impurities.

Empirical equations were obtained to represent the heat capacity of each compound in the liquid state. The constants of these equations are listed in Table III.

**Solid-state Phase Transformations.**—So far as could be determined, the phase transformations in 2-methylhexane and 2,2-dimethylpentane and two of those in 2,2,3-trimethylbutane were non-isothermal. From the heat capacity data and enthalpy measurements including the entire temperature range of a transformation, the following peak values of heat capacity were computed: 2-Methylhexane, 25.17 cal. deg.<sup>-1</sup> mole<sup>-1</sup> at 71.5°K.; 2,2-dimethylpentane, 25.17 cal. deg.<sup>-1</sup> mole<sup>-1</sup> at 83.2°K.; and 2,2,3-trimethylbutane, 39.00 cal. deg.<sup>-1</sup> mole<sup>-1</sup> at 86.8°K. and 50.13 cal. deg.<sup>-1</sup> mole<sup>-1</sup> at 108.0°K.

TABLE II  
THE MOLAL HEAT CAPACITIES OF FIVE ISOMERIC HEPTANES  
IN THE SOLID AND LIQUID STATE, CAL. DEG.<sup>-1</sup>

$T$ , °K. <sup>a</sup>	$\Delta T$ <sup>b</sup>	$C_{\text{satd}}$ <sup>c</sup>	$T$ , °K. <sup>a</sup>	$\Delta T$ <sup>b</sup>	$C_{\text{satd}}$ <sup>c</sup>
2-Methylhexane					
Crystals					
			100.12	8.550	22.162
			109.71	10.626	23.713
12.61	1.190	1.385	119.97	9.911	25.385
14.12	1.828	1.792	129.59	9.337	27.007
16.35	2.656	2.438	137.60	6.677	28.439
19.11	2.871	3.349			
19.62	3.628	3.518			
22.31	3.538	4.437			
23.66	4.446	4.887	160.41	6.594	43.134
25.90	3.632	5.636	169.29	11.150	43.543
27.99	4.225	6.345	181.70	13.686	44.176
29.64	3.859	6.891	194.69	8.954	44.879
32.22	4.218	7.722	204.46	10.590	45.474
36.79	4.931	9.121	215.40	11.283	46.183
41.83	5.144	10.602	226.58	11.095	46.954
46.64	4.471	11.856	237.59	10.904	47.816
51.26	4.768	13.064	248.80	11.532	48.678
56.51	6.668	14.387	260.23	11.319	49.665
62.32	4.956	15.830	269.33	9.549	50.467
66.27	2.954	16.858	271.84	11.899	50.693
68.88	2.252	17.736	277.70	8.636	51.258
70.90	1.786	23.577	278.81	9.396	51.356
72.85	2.113	18.720	283.62	11.669	51.781
76.39	4.973	18.150	286.66	9.279	52.122
83.29	8.832	19.366	294.35	6.104	52.880
85.56	4.472	19.748	295.18	11.442	52.913
91.78	8.131	20.842	301.17	7.540	53.564
2,2-Dimethylpentane					
Crystals					
			83.65	1.112	24.492
			84.41	2.088	22.625
14.30	1.244	1.893	84.81	1.209	21.802
14.90	1.501	2.086	86.58	2.240	20.371
15.89	1.943	2.414	88.82	2.248	20.042
16.80	2.270	2.742	91.28	2.659	20.209
18.25	2.833	3.247	93.90	8.847	20.550
19.57	3.262	3.733	102.45	5.123	21.848
21.38	3.425	4.409	102.45	8.266	21.895
22.99	3.593	4.988	108.52	7.025	22.985
24.92	3.660	5.638	110.46	7.751	23.383
26.86	4.133	6.292	115.77	7.463	24.387
28.62	3.749	6.854	123.03	7.057	25.886
31.00	4.155	7.607 <sup>d</sup>	129.91	6.697	27.399
32.44	3.895	8.045 <sup>d</sup>	132.80	5.932	28.058
35.17	4.182	8.792	136.79	7.065	29.065
39.40	4.270	9.904	139.06	6.578	29.765
44.30	5.544	11.109	143.57	6.494	32.192
49.88	5.617	12.441			
54.93	4.310	13.596			
55.53	5.669	13.731			
59.70	5.221	14.714	154.68	4.475	39.554
65.08	5.545	16.062	159.28	9.690	39.872
65.75	4.077	16.207	159.81	5.798	39.916
69.95	4.333	17.332	166.52	7.622	40.413
71.18	6.653	17.714	168.89	9.515	40.572
73.64	3.048	18.464	175.02	9.367	41.056
76.37	2.411	19.466	178.77	10.258	41.325
78.61	2.066	20.583	184.75	10.093	41.805
80.61	1.942	22.123	194.74	9.891	42.626
82.48	1.794	24.327	204.98	10.581	43.488
82.54	1.117	24.467	215.45	10.366	44.405
Liquid					

(14) G. Waddington, J. W. Knowlton, D. W. Scott, G. D. Oliver, S. S. Todd, W. N. Hubbard, J. C. Smith and H. M. Huffman, *J. Am. Chem. Soc.*, **71**, 797 (1949).

(15) E. Wichers *ibid.*, **74**, 2447 (1952).

(16) F. D. Rossini, F. T. Gucker, Jr., H. L. Johnston, L. Pauling and G. W. Vinal, *ibid.*, **74**, 2699 (1952).

(17) H. F. Stimson, *J. Research Natl. Bur. Standards*, **42**, 209 (1949).

(18) H. F. Stimson, *Am. J. Phys.*, **23**, 614 (1955).

(19) H. J. Hoge and F. G. Brickwedde, *J. Research Natl. Bur. Standards*, **22**, 351 (1939).

(20) These samples of API Research hydrocarbons were made available through the American Petroleum Institute Research Project 44 on the "Collection, Analysis and Calculation of Data on Properties of Hydrocarbons" and were purified by the American Petroleum Institute Research Project 6 on the "Analysis, Purification and Properties of Hydrocarbons," both at the Carnegie Institute of Technology.

(21) J. P. McCullough and J. F. Messerly, *U. S. Bur. Mines Bull.*, to be published.

(22) D. R. Stull, *Chem. Eng. News*, **27**, 2772 (1949).

225.71	10.162	45.341	271.13	9.317	49.911	61.70	6.365	14.657	186.35	12.183	43.230	
235.78	9.964	46.304	280.37	9.151	50.880	63.18	6.226	14.985	190.99	11.251	43.548	
242.38	9.869	46.941	289.44	8.994	51.902	68.23	6.689	15.992	198.87	12.852	44.053	
252.15	9.672	47.932	298.36	8.841	52.876	69.58	6.583	16.275	202.13	11.046	44.294	
261.73	9.490	48.917				74.63	6.120	17.262	211.59	12.587	44.951	
2,4-Dimethylpentane												
Crystals						Liquid						
12.82	0.921	1.769	160.81	5.780	40.556	80.93	6.475	18.480	223.82	10.660	45.880	
14.03	1.488	2.182	162.71	7.759	40.695	83.19	6.866	18.906	224.05	12.327	45.901	
15.91	2.291	2.807	167.98	8.556	41.086	87.56	6.782	19.706	234.05	10.471	46.674	
16.46	3.230	2.971	171.33	9.492	41.356	90.34	7.450	20.183	234.82	11.335	46.759	
18.37	2.628	3.632	176.93	9.340	41.774	94.49	7.077	20.868	236.25	12.080	46.847	
19.96	3.777	4.164	186.18	9.167	42.511	97.57	7.005	21.382	237.27	10.344	46.902	
21.37	3.357	4.653	195.46	8.984	43.268	101.87	7.701	22.081	244.43	10.291	47.519	
24.28	4.871	5.592	195.71	9.896	43.289	104.85	7.563	22.550	246.05	11.126	47.657	
25.33	4.572	5.895	205.32	10.746	44.111	109.81	8.164	23.349	248.18	11.843	47.832	
29.05	4.670	7.034	205.52	9.706	44.136	112.66	8.052	23.804	248.36	11.848	47.837	
29.87	4.498	7.263	215.13	9.529	44.988	118.18	8.576	24.684	254.63	10.121	48.385	
34.06	5.340	8.402	215.89	10.378	45.048	120.51	7.651	25.062	257.07	10.915	48.644	
39.50	5.530	9.756	224.99	10.192	45.922	126.54	8.149	25.999	259.68	10.787	48.851	
45.10	5.666	10.993	227.00	11.847	46.104	128.00	7.318	26.227	259.93	11.597	48.872	
50.81	5.760	12.216	230.42	10.104	46.427	134.51	7.790	27.249	265.07	10.754	49.349	
56.10	4.425	13.289	235.09	9.994	46.872	135.17	7.029	27.555	268.29	11.518	49.648	
56.61	5.850	13.379	238.71	11.578	47.248	141.71	6.039	28.369	271.17	12.195	49.894	
61.01	5.402	14.231	240.42	9.905	47.415	142.15	7.487	28.417	271.69	11.274	49.926	
66.61	5.791	15.296	250.16	11.322	48.384	146.80	5.142	29.206	272.23	13.008	49.978	
72.61	6.214	16.383	250.23	9.716	48.444				275.74	10.579	50.312	
78.59	5.750	17.478	260.25	10.318	49.477				279.30	10.512	50.670	
84.53	6.136	18.603	262.14	12.642	49.638				283.25	11.963	51.017	
90.43	5.750	19.662	270.48	10.115	50.574	145.19	8.123	40.792 <sup>e</sup>	283.64	12.632	51.051	
90.84	6.475	19.730	272.57	9.250	50.779	153.25	8.004	41.228 <sup>e</sup>	285.09	12.715	51.181	
96.71	6.812	20.730	274.63	12.342	50.987	161.20	7.890	41.670	286.21	10.395	51.308	
97.47	6.779	20.861	275.89	10.650	51.140	163.92	9.739	41.806	289.33	9.538	51.628	
102.90	5.575	21.811	277.95	7.626	51.388	165.92	9.647	41.912	295.48	12.497	52.205	
104.54	7.365	22.090	280.48	9.927	51.672	170.00	9.713	42.195	296.14	12.363	52.269	
109.23	7.076	22.944	281.74	9.084	51.792	174.52	11.476	42.449	296.14	9.435	52.287	
112.54	8.641	23.561	285.80	8.053	52.245	176.42	11.369	42.547	297.66	12.413	52.417	
116.12	6.709	24.258	286.44	10.430	52.314	180.11	10.502	42.828	298.79	9.386	52.568	
119.89	4.933	24.888	286.84	12.059	52.327							
120.92	8.119	25.137	290.34	9.738	52.761							
123.46	7.959	25.639	290.74	8.922	52.772							
126.28	7.846	26.221	293.53	7.407	53.078							
129.55	9.142	26.964	296.77	10.228	53.450							
131.19	7.513	27.343	299.59	8.769	53.758							
133.90	7.403	27.982 <sup>*</sup>	300.00	9.563	53.824							
138.41	8.570	29.009	301.15	7.819	53.925							
141.11	7.013	29.776	307.09	7.180	54.596							
146.65	7.925	31.993										
2,2,3-Trimethylbutane												
Crystals II										83.57	2.537	19.181
										85.79	1.898	27.854
						13.08	0.975	1.731	87.43	1.367	41.373	
						14.34	1.514	2.225	88.25	2.977	27.490	
						16.32	2.282	2.930	89.28	2.336	20.900	
						16.89	3.178	3.136	91.58	2.272	21.509	
						18.75	2.575	3.847	91.86	4.244	21.579	
						19.99	3.035	4.314	94.04	2.638	22.285	
						22.16	4.237	5.110	96.63	2.542	23.223	
						23.99	4.955	5.740	96.82	5.695	23.320	
						25.93	3.300	6.339	99.12	2.443	24.296	
						29.22	5.519	7.479 <sup>d</sup>	101.51	2.329	25.713	
						29.82	4.474	7.655 <sup>d</sup>	102.24	5.142	26.278	
						34.90	5.843	9.044 <sup>d</sup>	103.77	2.203	27.498	
						41.12	6.583	10.135	105.87	1.989	31.240	
						47.25	5.675	11.337	107.61	1.483	44.805	
						52.62	5.075	12.395	109.37	2.041	29.966	
						53.63	4.157	12.500	111.41	2.050	29.658	
						54.55	4.888	12.643	113.36	6.119	29.677	
						58.38	5.334	13.327	113.63	2.378	29.766	
						59.60	5.209	13.546	114.90	3.763	29.836	
						64.23	6.456	14.403	115.01	3.646	30.291	
						64.92	5.433	14.544	115.27	3.710	29.609	
						69.87	4.432	15.444	116.12	2.619	30.066	
						70.87	6.819	15.644				
						74.17	4.164	16.317				
						77.94	3.377	17.177				
						80.97	2.681	18.040				
									129.29	7.558	32.673	
Crystals I												

TABLE II (continued)

$T$ , °K. <sup>a</sup>	$\Delta T$ <sup>b</sup>	$C_{\text{satd}}$ <sup>c</sup>	$T$ , °K. <sup>c</sup>	$\Delta T$ <sup>b</sup>	$C_{\text{satd}}$ <sup>c</sup>
137.66	9.176	33.522	241.74	5.407	44.924
147.15	9.802	34.422	241.89	5.396	44.967
156.80	9.512	35.403	242.93	6.302	45.088
166.60	10.087	36.388			
176.55	9.815	37.418			
186.24	9.567	38.434			
195.69	9.323	39.446	253.03	5.250	46.319
203.10	7.968	40.211	255.09	6.110	46.557
204.91	9.116	40.457	258.69	6.066	46.916
211.95	9.718	41.244	262.02	7.749	47.273
214.29	9.645	41.519	270.54	9.296	48.187
218.49	9.577	41.995	279.77	9.157	49.077
221.55	9.536	42.385	288.85	8.998	50.088
227.95	9.342	43.161	298.17	9.654	51.015
230.00	7.367	43.439	306.95	7.917	51.913
235.83	6.410	44.139	313.26	4.696	52.610
236.45	5.486	44.175			

<sup>a</sup>  $T$  is the mean temperature of each heat capacity measurement. <sup>b</sup>  $\Delta T$  is the temperature increment in each measurement. <sup>c</sup>  $C_{\text{satd}}$  is the heat capacity of the condensed phase under its own pressure. <sup>d</sup> Curvature corrections applied. <sup>e</sup> Undercooled liquid.

Heats of Fusion, Triple Point Temperatures and Purity of Samples.—The heats of fusion,  $\Delta H_m$ , were determined from the heat capacity data and enthalpy measurements made over finite temperature intervals including the triple point temperatures. The results of two or more determinations for each isomer are in Table IV.

The triple point temperature and sample purity for each compound were determined from studies of the equilibrium melting temperature as a function of the fraction of sample melted.<sup>23</sup> The results for 2-methylhexane, 3-ethylpentane, 2,2-dimethylpentane and 2,4-dimethylpentane are given in Table V. For these four compounds, the equilibrium temperatures,  $T_{\text{obsd}}$ , were plotted as functions of  $1/F$ , the reciprocal of the fraction of total sample in the liquid phase. The triple point temperatures,  $T_{\text{T.P.}}$ , were determined by linear extrapolations to zero value of  $1/F$ . If the impurities form ideal solutions in the liquid phase and are insoluble in the solid phase, the relation between mole fraction of total impurity,  $N_2^*$ , and melting point depression,  $\Delta T = T_{\text{T.P.}} - T_{\text{obsd}}$ , is<sup>24</sup>

$$-\ln(1 - N_2) = \Delta \Delta T (1 \times B \Delta T + \dots) \quad (1)$$

where  $N_2 = N_2^*/F$ . The cryoscopic constants,  $A = \Delta H_m / RT_{\text{T.P.}}$  and  $B = 1/T_{\text{T.P.}} - \Delta C_m / 2\Delta H_m$ , were calculated from the values of  $\Delta H_m$  and  $T_{\text{T.P.}}$  in Table IV and values of  $\Delta C_m$  obtained from data in Table VII (discussed in the following section). Values of  $A$  and  $B$  are included in Table IV. The impurity values given in Table V were cal-

TABLE III

EMPIRICAL EQUATIONS FOR THE MOLAL HEAT CAPACITY IN THE LIQUID STATE

$$C_{\text{satd}}(\text{liq.}) = a + bT + cT^2 + dT^3, \text{ cal. deg.}^{-1} \text{ mole}^{-1}$$

Compound	$a$	$b \times 10^2$	$c \times 10^4$	$d \times 10^7$	Range, °K. <sup>a</sup>
<i>n</i> -Heptane	56.582	-14.490	5.7813	-4.1667	240-370
2-Methylhexane	41.850	-2.6750	2.1531	+0.10417	160-300
3-Ethylpentane	34.578	+3.2850	0.41562	1.6667	155-300
2,2-Dimethylpentane	33.582	0.4340	2.4200	-1.3333	155-300
2,4-Dimethylpentane	37.049	-4.2300	4.4188	-4.0364	160-310
2,2,3-Trimethylbutane	21.854	+9.0867	0.23333	.....	250-310

<sup>a</sup> The temperature range in which the equations represent the observed heat capacity data within about  $\pm 0.05\%$ .

The "isothermal" transition in 2,2,3-trimethylbutane was studied by observing the temperature as a function of fraction transposed (fraction of sample in the form of crystals I) with the results

% Transposed	22	48	86
$T$ , °K.	120.88	121.18	121.38

The sample did not reach true thermal equilibrium during these observations, although the point at 86% transposed was observed for about 15 hours. Nevertheless, the transition was assumed to be essentially isothermal, and the transition temperature was taken as 121.4°K.

TABLE IV

TRIPLE POINT TEMPERATURES, HEATS OF FUSION AND CRYOSCOPIC CONSTANTS

Compound	$T_{\text{T.P.}}$ <sup>a</sup> °K.	$\Delta H_m$ cal. mole <sup>-1</sup>	$A$ , deg. <sup>-1</sup>	$B$ , deg. <sup>-1</sup>
<i>n</i> -Heptane	182.55	$3355 \pm 2^b$	0.05065	0.00347
2-Methylhexane	154.90	$2195 \pm 1^b$	.04603	.00398
3-Ethylpentane	154.58	$2282 \pm 1^b$	.04805	.00408
2,2-Dimethylpentane	149.43	$1392.2 \pm 0.5^b$	.03137	.00419
2,4-Dimethylpentane	153.97	$1636 \pm 1^b$	.03472	.00425
2,2,3-Trimethylbutane	248.57	$540.4 \pm 0.1^b$	.00440	.00244

<sup>a</sup> Estimated accuracy uncertainty,  $\pm 0.05^\circ\text{K}$ . <sup>b</sup> Maximum deviation from the mean of two or more determinations.

The heat of transition of 2,2,3-trimethylbutane at 121.4°K. was determined from measurements of the enthalpy increase over the temperature interval from about 117 to 127°K. The average value of four determinations and maximum deviation from the mean are  $585.8 \pm 4.0$  cal. mole<sup>-1</sup>. This relatively poor precision is due to difficulty in obtaining reproducible crystals in the range 108-121°K., as evidenced by the poor precision of the heat capacity data in that region.

culated using eq. 1 in its simplified form (for  $N_2^* \ll 1$ ),  $N_2^* = A\Delta T$ . The plot of  $T_{\text{obsd}}$  vs.  $1/F$  for 2,2,3-trimethylbutane departs markedly from linearity, probably because the impurity is partly soluble in the solid phase. Because the cryoscopic constant  $A$  is less than 0.01 deg.<sup>-1</sup>, the solid-solution treatment of Mastrangelo and Dornte<sup>25</sup> is applicable.<sup>23</sup> The application of this treatment to the results for 2,2,3-trimethylbutane is shown in Table VI.

Chemical Thermodynamic Properties in the Solid and Liquid States.—The low temperature calorimetric data for each of the six heptanes were used in calculating values of the free energy function, heat content function, heat content and entropy in the solid and liquid states at selected temperatures from 10 to 300°K., or higher. The values at 10°K. were calculated from Debye functions, the parameters of which were evaluated from the heat capacity data between about 12 and 20°K.<sup>26</sup> The thermodynamic properties above 10°K. were calculated from the values of heat and temperature of phase changes and from appropriate numerical integration of values of  $C_{\text{satd}}$  read from large scale plots of the data in Table II. The results are in Table VII. Corrections for the effects of premelting were applied as necessary in computing the "smoothed" data in the last table.

The Vapor Pressure of 2-Methylhexane.—Osborne and Ginnings<sup>27</sup> have reported accurate experimental values of

(23) J. P. McCullough and Guy Waddington, *Anal. chim. Acta*, **17**, 80 (1957).

(24) A. R. Glasgow, Jr., A. J. Streiff and F. D. Rossini, *J. Research Natl. Bur. Standards*, **35**, 355 (1945).

(25) S. V. R. Mastrangelo and R. W. Dornte, *J. Am. Chem. Soc.*, **77**, 6200 (1955).

(26) The number of degrees of freedom and characteristic temperatures, respectively, of these Debye functions are: *n*-heptane, 5.5 and 121.0°; 2-methylhexane, 5 and 101.3°; 3-ethylpentane, 7 and 133.0°; 2,2-dimethylpentane, 6 and 108.2°; 2,4-dimethylpentane, 5 and 92.5°; 2,2,3-trimethylbutane, 6 and 101.7°.

TABLE V  
MELTING POINT SUMMARIES

Melted, %	1/F	T, °K.	
		Obsd.	Graph. <sup>b</sup>
2-Methylhexane (impurity = 0.16 mole %)			
10.68	9.363	154.6223	154.57
22.50	4.444	154.7664	154.75
51.41	1.945 <sup>a</sup>	154.8341 <sup>a</sup>	154.8341
75.56	1.323	154.8555	154.8559
92.48	1.081 <sup>a</sup>	154.8644 <sup>a</sup>	154.8644
100	1.000	154.8672	154.8672
Pure	0		154.9024
2,2-Dimethylpentane (impurity 0.17 mole %)			
13.58	7.364	149.1742	149.0
27.36	2.655	149.2814	149.24
45.35	2.205	149.3264	149.314
67.20	1.488 <sup>a</sup>	149.3522 <sup>a</sup>	149.3522
89.05	1.123 <sup>a</sup>	149.3715 <sup>a</sup>	149.3715
100	1.000		149.3780
Pure	0		149.4309

2,4-Dimethylpentane (impurity = 0.09 mole %)			
7.72	12.95	153.6604	153.644
27.40	3.650 <sup>a</sup>	153.8762 <sup>a</sup>	153.8762 <sup>a</sup>
52.13	1.918	153.9200	153.9195
76.91	1.300	153.9360	153.9349
92.42	1.082 <sup>a</sup>	153.9404 <sup>a</sup>	153.9404 <sup>a</sup>
100	1.000		153.9424
Pure	0		153.9674
3-Ethylpentane (impurity = 0.005%)			
6.30	15.87	154.5733	154.568
24.25	4.124 <sup>a</sup>	154.5800 <sup>a</sup>	154.5800
51.15	1.955	154.5823	154.5823
71.32	1.402	154.5826	154.5829
91.47	1.093 <sup>a</sup>	154.5832 <sup>a</sup>	154.5832
100.00	1.000		154.5833
Pure	0		154.5844

<sup>a</sup> Straight lines through these points were extrapolated to 1/F = 0 to obtain the triple point temperatures. <sup>b</sup> Temperatures read from the straight lines of footnote a.

TABLE VI  
2,2,3-TRIMETHYLBUTANE: MELTING POINT SUMMARY<sup>a</sup>  
T<sub>T.P.</sub> = 248.568 ± 0.05°K.; impurity = 0.053 mole %;  
distribution coefficient, K = 0.333

Melted, %	$\frac{1}{[F + K/(1 - K)]}$	T <sub>obsd.</sub> , °K.	T <sub>calcd.</sub> , °K.
12.88	1.590	248.369	248.376
26.84	1.301	248.412	248.411
50.46	0.995	248.448	248.448
69.47	.837	248.466	248.467
88.51	.722	248.481	248.481

<sup>a</sup> Values of T<sub>T.P.</sub>, T<sub>calcd.</sub>, K and impurity were calculated with the expressions given in ref. 25.

TABLE VII  
THE MOLAL THERMODYNAMIC PROPERTIES IN THE SOLID AND LIQUID STATES<sup>a</sup>

T, °K.	$-\frac{(F_{\text{solid}} - H^{\circ}_{\text{solid}})/T_{\text{cal.}}}{\text{deg.}^{-1}}$	$\frac{(H_{\text{solid}} - H^{\circ}_{\text{solid}})/T_{\text{cal.}}}{\text{deg.}^{-1}}$	H <sub>solid</sub> - H <sup>o</sup> <sub>o</sub> , cal.	S <sub>solid</sub> , cal., deg. <sup>-1</sup>	C <sub>solid</sub> , cal., deg. <sup>-1</sup>
<i>n</i> -Heptane					
Crystals					
10	0.039	0.119	1.189	0.158	0.473
15	.132	.386	5.797	.518	1.464
20	.299	.823	16.450	1.122	2.836
25	.540	1.380	34.493	1.920	4.399

30	.848	2.017	60.51	2.865	6.014
35	1.210	2.704	94.65	3.914	7.622
40	1.617	3.414	136.56	5.031	9.135
45	2.060	4.131	185.88	6.191	10.583
50	2.533	4.846	242.27	7.379	11.956
60	3.541	6.242	374.51	9.783	14.462
70	4.604	7.581	530.6	12.185	16.694
80	5.700	8.846	707.7	14.546	18.711
90	6.812	10.048	904.3	16.860	20.566
100	7.930	11.181	1118.1	19.111	22.173
110	9.047	12.250	1347.5	21.297	23.700
120	10.156	13.266	1591.9	23.422	25.164
130	11.257	14.235	1850.6	25.492	26.567
140	12.346	15.165	2123.1	27.511	27.945
150	13.423	16.064	2409.5	29.487	29.346
160	14.488	16.940	2710.4	31.428	30.863
170	15.540	17.809	3027.4	33.349	32.599
180	16.584	18.684	3363.1	35.268	34.536
182.55	16.848	18.909	3451.8	35.757	35.037
Liquid					
182.55	16.848	37.288	6806.8	54.136	48.520
190	18.34	37.72	7167	56.07	48.27
200	20.29	38.24	7649	58.54	48.15
210	22.17	38.71	8130	60.89	48.23
220	23.98	39.15	8614	63.14	48.49
230	25.73	39.57	9101	65.30	48.88
240	27.42	39.96	9592	67.39	49.38
250	29.06	40.35	10089	69.42	49.98
260	30.65	40.74	10592	71.39	50.66
270	32.20	41.12	11102	73.32	51.39
273.15	32.68	41.24	11264	73.92	51.64
280	33.70	41.50	11620	75.20	52.19
290	35.16	41.88	12146	77.05	53.04
298.15	36.33	42.19	12581	78.53	53.76
300	36.59	42.27	12681	78.86	53.93
310	37.98	42.66	13225	80.64	54.85
320	39.34	43.05	13778	82.40	55.78
330	40.67	43.45	14340	84.13	56.75
340	41.98	43.86	14913	85.84	57.76
350	43.26	44.27	15495	87.53	58.79
360	44.51	44.69	16089	89.20	59.89
370	45.74	45.11	16694	90.86	61.04

2-Methylhexane

Crystals

10	0.062	0.184	1.843	0.246	0.726
15	.203	.576	8.635	.779	2.024
20	.443	1.137	22.746	1.580	3.653
25	.766	1.810	45.23	2.576	5.338
30	1.160	2.538	76.12	3.698	7.002
35	1.608	3.290	115.16	4.898	8.585
40	2.096	4.047	161.86	6.143	10.088
45	2.617	4.794	215.74	7.411	11.441
50	3.160	5.523	276.16	8.683	12.734
60	4.293	6.937	416.2	11.230	15.230
70	5.465	8.311	581.7	13.776	18.300
80	6.674	9.679	774.2	16.353	18.773
90	7.879	10.787	970.8	18.666	20.509
100	9.070	11.842	1184.1	20.912	22.141
110	10.247	12.851	1413.6	23.098	23.755
120	11.406	13.828	1659.3	25.234	25.378
130	12.551	14.779	1921.2	27.330	27.039
140	13.681	15.720	2200.7	29.401	28.884
150	14.798	16.665	2499.8	31.463	30.942
154.90	15.342	17.135	2654.3	32.477	32.010





Liquid						Liquid					
153.97	15.109	27.244	4195.0	42.353	40.048	248.57	29.44	31.61	7858.7	61.05	45.88
160	16.16	27.73	4437	43.89	40.49	250	29.62	31.69	7923	61.32	46.02
170	17.86	28.50	4846	46.37	41.24	260	30.88	32.26	8388	63.14	47.05
180	19.51	29.23	5262	48.75	42.01	270	32.10	32.83	8864	64.94	48.08
190	21.11	29.93	5686	51.04	42.81	273.15	32.49	33.01	9017	65.50	48.41
200	22.67	30.59	6118	53.26	43.65	280	33.31	33.39	9350	66.70	49.12
210	24.17	31.23	6559	55.41	44.51	290	34.49	33.95	9847	68.45	50.17
220	25.64	31.86	7009	57.50	45.42	298.15	35.44	34.41	10260	69.85	51.03
230	27.07	32.47	7468	59.54	46.38	300	35.65	34.51	10354	70.16	51.22
240	28.47	33.07	7937	61.54	47.37	310	36.79	35.07	10871	71.86	52.26
250	29.83	33.66	8415	63.49	48.38	320	37.91	35.62	11399	73.54	53.32
260	31.16	34.25	8904	65.41	49.43						
270	32.46	34.83	9404	67.30	50.51						
273.15	32.87	35.01	9564	67.89	50.85						
280	33.74	35.41	9915	69.15	51.60						
290	34.99	35.98	10436	70.98	52.70						
298.15	36.00	36.45	10870	72.46	53.59						
300	36.22	36.56	10969	72.79	53.79						
310	37.43	37.13	11512	74.57	54.87						

## 2,2,3-Trimethylbutane

Crystals II					
10	0.074	0.218	2.184	0.292	0.861
15	.240	.680	10.193	.920	2.442
20	.525	1.351	27.025	1.876	4.312
25	.908	2.124	53.09	3.032	6.080
30	1.365	2.922	87.65	4.287	7.719
35	1.875	3.706	129.69	5.581	9.040
40	2.419	4.436	177.44	6.855	10.027
45	2.981	5.107	229.82	8.088	10.922
50	3.552	5.734	286.71	9.286	11.823
60	4.701	6.899	413.9	11.600	13.620
70	5.847	7.992	559.4	13.839	15.474
80	6.984	9.060	724.8	16.044	17.725
82	7.210	9.280	760.9	16.490	18.421
84	7.437	9.508	798.7	16.945	19.420
90	8.129	10.542	948.8	18.671	21.098
100	9.302	11.761	1176.1	21.063	24.743
101	9.419	11.894	1201.2	21.313	25.375
102	9.538	12.028	1226.8	21.566	26.060
103	9.655	12.170	1253.4	21.825	26.823
104	9.774	12.313	1280.5	22.087	27.670
105	9.892	12.469	1309.2	22.361	29.600
110	10.497	13.620	1498.1	24.117	29.575
115	11.119	14.319	1646.7	25.438	29.838
120	11.743	14.971	1796.5	26.714	30.096
121.4	11.918	15.145	1838.7	27.063	30.170

## Crystals I

121.4	11.918	19.971	2424.5	31.889	31.880
130	13.31	20.78	2702.3	34.09	32.73
140	14.88	21.67	3034.6	36.56	33.72
150	16.41	22.51	3376.8	38.92	34.72
160	17.88	23.30	3729.1	41.19	35.72
170	19.32	24.06	4091.4	43.39	36.73
180	20.72	24.79	4463.8	45.52	37.76
190	22.08	25.51	4846.8	47.59	38.82
200	23.40	26.20	5240.4	49.60	39.90
210	24.70	26.88	5645.1	51.58	41.02
220	25.96	27.55	6061.0	53.51	42.18
230	27.20	28.21	6488.9	55.42	43.40
240	28.42	28.87	6929.4	57.29	44.69
248.57	29.44	29.44	7318.3	58.88	45.87

<sup>a</sup> The values tabulated are the free energy function, heat content function, heat content, entropy and heat capacity of the condensed phases at saturation pressure.

heat of vaporization at 298.15°K.,  $\Delta H_{v298.15}$ , for all of the heptanes studied except 2-methylhexane. Forziati, Norris and Rossini<sup>28</sup> determined the vapor pressure of 2-methylhexane from 18 to 91°, but to allow more accurate calculation of the heat of vaporization by the Clapeyron equation, the results of these authors were extended by measurements in the range 0–45°. The results, determined by the static method described previously,<sup>14</sup> are in Table VIII. These data and those of Forziati, *et al.*,<sup>28</sup> were combined to obtain the following Cox equation for the vapor pressure of 2-methylhexane. In eq. 2  $T$  is in °K. and  $p$  is in mm. Values

$$\log(p/760) = A(1 - 363.202/T) \quad (2)$$

$\log A = 0.860881 - 8.4898 \times 10^{-4}T + 8.9539 \times 10^{-7}T^2$  of vapor pressure calculated with eq. 2 are included in Table VIII. This Cox equation represents the data of Forziati, *et al.*,<sup>28</sup> about as well as their Antoine equation.

TABLE VIII

## VAPOR PRESSURE OF 2-METHYLHEXANE

$T$ , °K.	$p$ , mm.	$\frac{p(\text{obsd.}) - p(\text{calcd.})}{p(\text{calcd.})}$ , %
273.15	17.56	0.00
288.15	40.09	-.03
293.15	51.63	-.04
298.15	65.83	-.04
303.15	83.15	-.01
308.15	104.05	.00
313.15	129.07	+.01
318.15	158.79	-.01

<sup>a</sup> Calculated with eq. 2. The deviations in this range are predominantly negative as a result of using both the data reported here and those in ref. 28 in obtaining eq. 2

**The Standard Heats and Entropies of Vaporization at 298.15°K.**—By using the Clapeyron equation, eq. 2 and an estimate of the second virial coefficient ( $2.53 \text{ l. mole}^{-1}$ ),<sup>29</sup> the heat of vaporization of 2-methylhexane at 298.15°K. was calculated to be  $8.32_5 \text{ kcal. mole}^{-1}$ . This value and values for the other isomers given by Osborne and Ginnings<sup>27</sup> were used in calculating the values of standard heat,  $\Delta H_v^\circ_{298.15}$ , and entropy,  $\Delta S_v^\circ_{298.15}$ , of vaporization given in Table I. In these calculations, values of the entropy of compression to one atm. were calculated from eq. 2 and the results of Forziati, *et al.*<sup>28</sup> Small but significant corrections for the effect of gas imperfection were determined from an unpublished correlation of the results of previous investigations in this Laboratory. These values of  $\Delta H_v^\circ_{298.15}$  and  $\Delta S_v^\circ_{298.15}$  were used with experimental values of entropy and heat of formation in the liquid state to obtain the values of the thermodynamic properties in the ideal gas state given in Table I.

**Acknowledgments.**—The assistance of G. D. Oliver, W. N. Hubbard and R. E. Robinson in some of the experiments is gratefully acknowledged.

(27) N. S. Osborne and D. C. Ginnings, *J. Research Natl. Bur. Standards*, **39**, 543 (1947).

(28) A. F. Forziati, W. R. Norris and F. D. Rossini, *ibid.*, **43**, 555 (1949).

(29) D. W. Scott, H. L. Finke, M. E. Gross, G. B. Guthrie and H. M. Huffman, *J. Am. Chem. Soc.*, **72**, 2424 (1950).

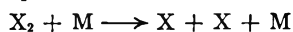
## THE KINETICS OF DISSOCIATION OF A DIATOMIC GAS

BY H. O. PRITCHARD

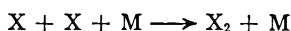
*Chemistry Department, University of Manchester, Manchester 13, England**Received September 21, 1960*

The collision theory of chemical reactions is developed to a point where it is capable of describing the mechanics of the dissociation and recombination of a diatomic gas. The experimental observation of activation energies for dissociation which are substantially less than the heat of dissociation appears to be due to a failure to maintain an equilibrium population amongst the highest vibrational energy levels. Since the dissociation process is thermodynamically irreversible, there is no simple relation between the dissociation and recombination rate constants and therefore no correspondence between the heat of dissociation and the activation energies for the two processes.

One of the most unsatisfactory aspects of the theory of chemical kinetics has been the failure to describe reasonably the simplest of all reactions, the dissociation of a diatomic gas. The rates of dissociation (and their temperature dependences) have been measured at high temperatures for three diatomic molecules,  $I_2$ ,  $Br_2$  and  $O_2$  by the shock-wave technique.<sup>1</sup> The reactions are bimolecular and may be represented as



It is convenient to define a *standard rate constant for dissociation*,  $\kappa = N z_0 e^{-D_0/RT}$  where  $N$  is the total number of  $X_2$  molecules,  $z_0$  is the number of collisions with  $M$  per second suffered by an individual  $X_2$  molecule in its zeroth vibrational state, and  $D_0$  is the dissociation energy of  $X_2$ ; this is the usual simple collision theory rate. The experimentally observed rates of dissociation are  $3.4\kappa$  for  $I_2$  at  $1300^\circ K.$ ,  $3.8\kappa$  for  $Br_2$  at  $1600^\circ K.$ , and  $\sim 150\kappa$  for  $O_2$  at  $3000^\circ K.$  Furthermore, the temperature dependences of these rate constants (*i.e.*, activation energies) are in all cases *substantially less than* the respective dissociation energies: for  $I_2$  the discrepancy ranges from 4.2 to 9.5 kcal. according to the nature of  $M$ , for  $Br_2$  from 5.9 to 15.5 kcal., and for  $O_2$  it is about 11 kcal. In addition, the rates of the reverse processes have been measured for  $I_2$  and  $Br_2$ : as is well known, the recombinations are third order *i.e.*



and the rates vary substantially with the nature of  $M$ .<sup>2</sup> In both cases the recombination proceeds more slowly at higher temperatures<sup>3</sup> and we have an apparent negative activation energy. In a reversible system, the difference between the recombination and dissociation activation energies should equal the heat of the reaction, but as the observed recombination temperature dependences are only about  $-2$  kcal., there is still a large discrepancy between them and the high-temperature dissociation results.

Simple collision theory accounts for none of these facts. Nevertheless, the ultimate description of such reactions can only be given in terms of collision processes, and it is therefore necessary,

under pressure of experimental observation, to develop a more detailed form of collision theory.

**A Simple Extension of Collision Theory.**—The normal collision treatment of a diatomic dissociation reaction has no fine structure, *i.e.*, it makes no assumptions about the mechanism by which the ground-state molecule  $X_2$  eventually breaks up into  $X + X$ . The diatomic molecule has  $n$  bound vibrational states, and their populations are  $N_0 e^{-E_i/RT}$  where  $i$  runs from 0 to  $n$  and all energies are measured relative to the ground state. If we make the naive assumption that dissociation may take place from any vibrational state, then the relative motion of  $X_2$  and the third body  $M$  must supply the remainder of the dissociation energy ( $D_0 - E_i$ ); the probability of the relative energy along the line of centres being in excess of this value is  $e^{-(D_0 - E_i)/RT}$ . If  $P_{i\infty}$  is an *a priori* probability which tells us what fraction of the *suitably energetic collisions* will lead to dissociation, then the rate of dissociation from any state  $i$  will be

$$P_{i\infty} \cdot N_0 e^{-E_i/RT} \cdot z_i e^{-(D_0 - E_i)/RT} = P_{i\infty} N_0 z_i e^{-D_0/RT}$$

where  $z_i$  is calculated using the collision diameter of  $X_2$  in its  $i$ th vibrational state. However, we cannot write the total rate of dissociation as the sum over all  $i$  from 0 to  $n$  since if any significant dissociation takes place from the low-lying states, this will have the effect of depopulating the higher states and thereby reducing their contribution to the rate-sum. It is fairly well established that the appropriate value of  $P_{i\infty}$  is only appreciably for small energy jumps (*e.g.*, see later) so that dissociation is going to be most favourable for the  $n$ th state, less so for the  $(n - 1)$ th state, and so on. Hence, the activation of  $X_2$  from its ground state to the dissociated state takes place by a predominantly step-wise process and the rate constant for the reaction, provided the Boltzmann distribution is maintained, will be of the order of  $P_{n\infty} N_0 z_n e^{-D_0/RT}$ ; it will not be exactly equal to this expression because of the effects of some dissociation from lower energy states. Thus, the maximum rate that we can expect to get is with  $P_{n\infty} = 1$ , *i.e.*,  $k = N_0 z_n e^{-D_0/RT}$ , and since a diatomic molecule in its topmost vibrational state is considerably bigger than the normal molecule, this can be greater than the standard rate  $\kappa$ . It is not easy to calculate the appropriate value of  $z_n$ , but some idea of its magnitude can be assessed by considering  $H_2$ : in the ground state, the bond length is  $0.74 \text{ \AA}$ . whereas in the topmost vibrational state (according to the calculation described below), the bond length is about  $3.5 \text{ \AA}$ .; in heavier molecules having lower force constants, the length of the

(1) (a) D. Britton, N. Davidson, W. Gehman and G. Schott, *J. Chem. Phys.*, **25**, 804 (1956); (b) D. Britton and N. Davidson, *ibid.*, **25**, 810 (1956); (c) H. B. Palmer and D. F. Hornig, *ibid.*, **26**, 98 (1957); (d) D. Britton, *J. Phys. Chem.*, **64**, 742 (1960); (e) S. A. Losev, *Doklady Translations, Phys. Chem. Section*, **120**, 467 (1959).

(2) K. E. Russell and J. Simons, *Proc. Roy. Soc. (London)*, **A217**, 271 (1953).

(3) (a) D. L. Bunker and N. Davidson, *J. Am. Chem. Soc.*, **80**, 5085 (1958); (b) W. G. Givens and J. E. Willard, *ibid.*, **81**, 4773 (1959).

bond in the topmost state will be relatively somewhat greater than this, but in any event, it is unlikely that  $z_n$  would exceed  $z_0$  by more than an order of magnitude. Thus we could account for rates up to say  $10\kappa$ , covering the experimental data for  $I_2$  and  $Br_2$ , but not the value of 150 for  $O_2$ . However, we would still predict a temperature dependence equal to  $D_0$  and we are not, therefore, much nearer the solution of this problem. For this reason, a more detailed description of the activation process is put forward in this paper, based on an attempt to calculate the probability per collision of a vibrational transition  $v = i \rightarrow j$ , for all  $i$  and  $j$  including the continuum.

**The Elements of the Calculation.**—The model chosen for consideration was the reaction



because the hydrogen molecule has only 15 bound vibrational levels. The molecules of experimental interest have many more, *i.e.*,  $I_2$  has 125–175,  $Br_2$  has 100–145 and  $O_2$  has 50–60, making the necessary calculations impracticably long. The molecule was assumed to be a Morse oscillator, and the necessary constants were chosen to make the spacings of the topmost levels approximately correct (*i.e.*,  $D_e = 38284 \text{ cm.}^{-1}$ ,  $\alpha = 1.942 \times 10^8 \text{ cm.}^{-1}$  and  $k = 15.25$ ); the energy of the  $v = 0 \rightarrow 1$  transition  $\Delta_{01}$  is then overestimated by about 6%. The probability of transition between any two states  $v = i \rightarrow j$  was then calculated using the equations given by Jackson and Mott<sup>4</sup> for the treatment of the collision of an atom with an oscillator, *i.e.*

$$p_{ij}(w) = \frac{1}{4\pi^2} (Y_{ij})^2 \sinh u_i \sinh u_j \left[ \frac{u_i^2 - u_j^2}{\cosh u_i - \cosh u_j} \right]^2$$

where  $Y_{ij}$  is the matrix element of the collisional perturbation potential over the Morse wave functions  $\xi_i$  and  $\xi_j$  of the two states, and  $u = 4\pi^2 \times mv/ah$  with  $m =$  the reduced mass of the colliding pair,  $w =$  the relative velocity of approach of the pair, and  $h =$  Planck's constant:  $a$  is a constant defining the perturbation potential as discussed below. The two subscripts  $i$  and  $j$  refer to the values of  $u$  before and after the transition from  $v = i \rightarrow j$ .

The probability  $p_{ij}(w)$  is a function of the relative approach velocity  $w$  and therefore, to give the required probability  $P_{ij}$ , this function has to be integrated over the Maxwell distribution of approach velocities  $w$  appertaining to the particular temperature under consideration. For downward transitions, the integral was taken over all energies of approach from 0 to  $\infty$ , but for the upward transitions, the integral can only run from  $\Delta_{ij}$  to  $\infty$ : note that  $p_{ij}$  refers to a fraction of all collisions, whereas  $P_{ij}$  refers only to sufficiently energetic collisions. In this way, an array of transition probabilities can, in principle, be built up for all transitions between states  $i$  and  $j$ , whether bound or unbound. In the case of a dissociation process, it is necessary to integrate again over all possible transitions into the continuum, and in the case of a recombination, the second integration must be performed over all values of the approach energies

of the recombining pair. Knowing this matrix of probabilities, one can then calculate the number of transitions per unit time taking place at equilibrium, and it is an easy matter to see whether or not equilibrium is likely to be maintained: if it is, the calculation of the over-all rate is straightforward, but if it is not, one can only draw qualitative conclusions because an adequate description of the real situation would then require an exact knowledge of the various probabilities.

It should be pointed out that the application of the Jackson and Mott procedure to a light molecule is subject to severe limitations. Some of these have been discussed by Schwartz and Herzfeld,<sup>5</sup> and others will be mentioned in this paper. The present treatment therefore contains many drastic approximations, but in all cases these have been made with due consideration to the physics of the situation. These approximations have been made in order to try to make progress. More sophisticated treatments have been given of the  $v = 0 \rightarrow 1$  transition, and more formal treatments of dissociation by collisional excitation have been examined; however it is so much easier to understand the mechanics of a complex process like this when numerical magnitudes can be assigned to the basic steps which contribute to the over-all dissociation.

**The Neglect of Angular Momentum.**—In a gas at a temperature of several thousand degrees, there are many molecules having high angular quantum numbers and it is necessary to consider the effect of rotation on the dissociation process, and what errors are likely to be introduced by using wave functions corresponding to zero angular momentum. In the first place, if we consider only first-order terms in the angular perturbation, there will be a selection rule limiting changes in angular quantum number to  $\pm 1$ ; in the real case therefore we can expect changes of angular momentum by  $\pm 1$  unit to predominate. Hence we are justified in neglecting dissociation by the acquiring of a large increment in rotational energy, and can reduce the problem essentially to one of vibrational excitation.

We may then consider two separate cases. The first of these is when the molecules have so much rotational energy that a positive energy barrier is present between the bound and the dissociated states. Consideration of these states is ruled out of the present discussion on the grounds that the net energy required for these molecules to dissociate is larger than  $D_0$ ; tunnelling through the barrier will be infinitesimal,<sup>6</sup> particularly for  $Br_2$  and  $I_2$ , and so these processes will tend to increase the activation energy whereas we are trying to account for the experimental reduction of  $E$  below  $D_0$ . We may therefore confine ourselves to a consideration of the second case, *i.e.*, to molecules having only moderate amounts of rotational energy. Here, the vibrational wave functions are qualitatively similar to those for zero angular momentum, and as we have ruled out large changes in rotational energy, the over-all

(5) R. N. Schwartz and K. F. Herzfeld, *J. Chem. Phys.*, **22**, 767 (1954).

(6) D. E. Stogryn and J. O. Hirschfelder, *ibid.*, **31**, 1531 (1959); **33**, 942 (1960).

(4) J. M. Jackson and N. F. Mott, *Proc. Roy. Soc. (London)*, **A137**, 703 (1932).

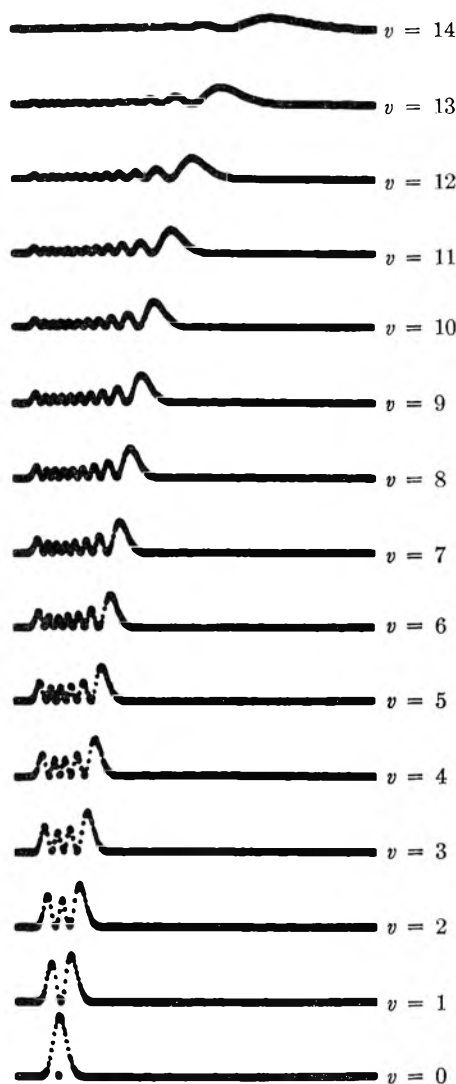


Fig. 1.—Morse wave functions ( $\rho^2\xi_i^2$ ) for the bound states of  $H_2$  (all functions shown to the same scale). This diagram was constructed using the Graphical Output of the Manchester University Mercury Computer. The functions extend over 5 Å. from  $\rho = -0.6$  Å. to  $\rho = +4.4$  Å.; the point  $\rho = 0$  is marked by a dot below the zeroth order wave function.

description of the dissociation process will not be grossly wrong if we use the simple Morse wave functions.

**Details of the Calculation.**—The Jackson and Mott treatment assumes that the interaction potential between the colliding particles is exponential and purely repulsive, *i.e.*,  $\phi = Ce^{-a\rho}$ . The constant  $a$  was chosen from the best fit of the experimental data for  $H_2/He$  collisions<sup>7</sup> to an exponential over the range of  $\phi/k$  from 0 to 2000°K. A reasonable value of  $a$  is about  $5 \times 10^8$  cm.<sup>-1</sup>. A further assumption of the Jackson and Mott treatment is that one member of the vibrating pair has an infinite mass, but of necessity we are limited to a consideration of  $H_2$ . The principal effect of violating this assumption will be to alter  $a$  in some unknown way and therefore we can only expect to get, at best, a semi-quantitative description of the situation: we cannot expect the sum of the transition

probabilities for any individual state to add up to unity, and we must accept that they are correct relative to each other, and obtain their absolute magnitudes by suitable renormalization.

The matrix elements

$$Y_{ij} = \int_{-\infty}^{\infty} e^{a(\rho - \rho_i)} \xi_i(\rho) \xi_j(\rho) \rho^2 d\rho$$

where  $\rho$  is  $(r - r_e)$  and  $\rho_i$  is the average value of  $\rho$  for the  $i$ th state, were calculated by a 250-strip Simpson's Rule quadrature. The wave functions are shown as a plot of  $\rho^2\xi_i^2$  in Fig. 1; note that for the state  $v = 14$ , the left-hand maximum is almost non-existent and the wave function virtually has one large peak near 3.3 Å. internuclear separation. The only difficulty arose in the cases of  $Y_{14,14}$  and  $Y_{13,14}$  which diverged (as they must since  $a > \alpha$ ), but it was found that logarithmic plots of  $Y_{m,m}$ ,  $Y_{m-1,m}$ , etc. against  $m$  gave straight lines, and suitable values for the divergent cases were chosen by extrapolation. Morse wave functions are not known for the continuum, and although various approximations were tried they were unsatisfactory and the following very crude assumption was made: since only small energy jumps are favored, the important part of the continuum will be very close to the discrete states, and so the wave functions will not be too unlike that for the topmost bound state; therefore the matrix elements involving the continuum were taken to be the same as those for the state  $v = 14$ .

The probabilities  $p_{ij}(w)$  were integrated over the three-dimensional Maxwell distribution of approach velocities using a 10-point Laguerre quadrature<sup>8</sup>; this integration yielded directly the over-all  $p_{ij}$  for discrete transitions, but for transitions into the continuum, the total probability was found by integration of the resulting  $p_{i\epsilon}$  over all possible continuum energies  $\epsilon$ . The individual rates for various processes were then found by applying these probabilities to the collision numbers appropriate to the individual initial states, the collision diameters  $\sigma_i$  being estimated from the  $\rho_i$ . The reason for using the three-dimensional Maxwell distribution was to obtain the maximum possible value for the rate of dissociation, having the value of  $150\kappa$  for  $O_2$  in mind; however, in no case was an increase in rate of excitation of more than about 50% found over that which would be obtained using the normal two-dimensional distribution.

Since we have to renormalize the relative transition probabilities, it is necessary to know the probability that no transition will take place upon collision. This was taken to be

$$p_{ii}(w) = \lim_{u_j \rightarrow u_i} p_{ij}(w) = \frac{1}{\pi^2} (Y_{ii})^2 u_i^2$$

and integrated over the Maxwell distribution as before. The transition probabilities were then renormalized so that  $\sum_j p_{ij} = 1$  with the added condition

at high temperatures that none of the  $\int p_{i\epsilon} d\epsilon$  should exceed  $e^{-(D_0 - E)/R_i T}$ ; this latter condition is due to an overestimate of the probability of

(7) E. A. Mason and W. E. Rice, *J. Chem. Phys.*, **22**, 522 (1954).

(8) H. E. Salzer and R. Zucker, *Bull. Am. Math. Soc.*, **55**, 1004 (1949).



per sec., about  $2 \times 10^6$  are sufficiently energetic and  $3.2 \times 10^6$  transitions occur, *i.e.*, we have an efficiency of 1 in 50 of all collisions, and 1 in 6 of sufficiently energetic collisions. In other words, the number of transitions taking place from  $v = i \rightarrow j$  is  $P_{ij} N_{iz} e^{-\Delta_{ij}/RT}$  and both  $P_{ij}$  and  $e^{-\Delta_{ij}/RT}$  increase as  $\Delta_{ij}$  decreases.

As evidence of the second rule, we observe that at 3000°K., transitions appear to take place over a much wider difference between  $i$  and  $j$ , *e.g.*, transitions can take place from  $v = 0$  up to as far as  $v = 9$ ; on the other hand, at 300°K., only the  $v = 0 \rightarrow 1$  transition takes place. At 3000°K., molecules in the state  $v = 0$  suffer  $2.0 \times 10^{27}$  collisions per sec., of which about  $2 \times 10^{26}$  are sufficiently energetic for the  $v = 0 \rightarrow 1$  transition, and  $7 \times 10^{23}$  transitions take place, *i.e.*, an efficiency of 1 in  $3 \times 10^2$  of the sufficiently energetic collisions; at 300°K., the corresponding fraction is 1 in  $3.5 \times 10^4$ . Thus,  $P_{ij}$ , like  $e^{-\Delta_{ij}/RT}$  increases with temperature, and should really be regarded as some function of  $e^{-\Delta_{ij}/RT}$  (*cf.* ref. 9).

These results are in qualitative agreement with experimental findings on energy transfer. The  $v = 0 \rightarrow 1$  transition for several molecules has been studied by ultrasonic methods,<sup>9</sup> and it is known that the probability of transfer for sufficiently energetic collisions increases with temperature, although the present calculation seems to overestimate the probability and underestimate its temperature variation. At the other end of the scale, we have evidence from the dissociation rates for Br<sub>2</sub> and I<sub>2</sub> that for high vibrational levels, most of the sufficiently energetic collisions lead to dissociation, so that  $P_{ij}$  must certainly increase as  $\Delta_{ij}$  decreases. Furthermore, I<sub>2</sub> molecules formed in their 26th vibrational state only make observable transitions on collision to the 24th, 25th, 27th and 28th states<sup>10</sup>: this is what would be expected from the results in Table I, remembering that these excited states of I<sub>2</sub> are energetically quite close together.

In addition, the rate of the  $v = 0 \rightarrow 2$  transition has been studied for carbon monoxide in a shock wave<sup>11</sup>; however, owing to experimental inaccuracies, it was not possible to distinguish between the two processes  $v = 0 \rightarrow 1 \rightarrow 2$  and  $v = 0 \rightarrow 2$ . If we consider our mixture suddenly heated from 300 to 1000°K., we can see what is likely to happen. At 300°K., there are about  $6 \times 10^6$  molecules in the  $v = 1$  state, and none in the  $v = 2$  state. This gas is suddenly raised to 1000°K. where the populations should be  $4 \times 10^{13}$  in  $v = 1$  and  $8 \times 10^{10}$  in  $v = 2$ . Thus, the  $v = 1$  state will populate in the order of  $10^{-7}$  seconds, according to the data in Table I. Population of the  $v = 2$  state will take place by two processes,  $v = 0 \rightarrow 2$  and  $v = 1 \rightarrow 2$ : the former will predominate until such time as the  $v = 1$  state becomes sufficiently populated, *i.e.*, about  $3 \times 10^{-8}$  of its equilibrium value which will take of the order of  $3 \times 10^{-12}$  seconds; then the latter process will take over and be complete in the order of another

$10^{-7}$  seconds. As was pointed out above, these rates are rather fast, but there is no doubt that the over-all process is predominantly stepwise—it is a consequence of the fact that the calculated probabilities come out to be  $p_{02} \approx p_{01} p_{12}$ , etc.; similarly then,  $P_{02} \approx P_{01} P_{12}$ , etc.

**Dissociation.**—If we simply take the total number of molecules dissociating at equilibrium (as in Table I) for each temperature, we get an activation energy of about 104 kcal./mole, as expected. However, if we inspect Table I more closely, we note that the number of molecules dissociating, assuming equilibrium, is about  $3 \times 10^6$  per sec.; this number, despite the fact that it would be immeasurably low, is more than the number of transitions from state  $v = 11 \rightarrow 12$ , *i.e.*, above  $v = 11$ , the Boltzmann distribution breaks down. Inspection of the results for 2000 and 3000°K. shows that the higher the temperature, the sooner the breakdown occurs, *i.e.*,  $v = 9 \rightarrow 10$  at 2000°K. and  $v = 7 \rightarrow 8$  at 3000°K. In other words, the higher the temperature, the worse the departure from the Boltzmann equilibrium distribution, and since the deficient states are those from which dissociation may take place, the rate of dissociation will not increase with temperature as quickly as it should have done; this causes a low “activation energy” to be observed.

With the numbers at our disposal, we can make no quantitative analysis of the situation, and will therefore proceed in an empirical manner. In Fig. 2 is plotted an approximate population distribution for the vibrational energy levels of H<sub>2</sub> for the various temperatures, with disequilibrium setting in at successively lower levels. To simplify matters we can assume without any loss of generality that dissociation takes place from only one state,  $v = 14$ , and since the energy gap is small,  $P_{14,\infty}$  is roughly one. Then, from the usual Arrhenius relationship, the “activation energy” is proportional to the relative population of the  $v = 14$  state for a given pair of temperatures. To illustrate how this disequilibrium can affect the observed Arrhenius parameters, let us assume that the population of  $v = 14$  is 95% Boltzmann at 1000°K., 25% at 2000°K. and 15% at 3000°K.; the over-all rate in the middle of the range would then be about 25% of what is expected, still somewhat greater than  $\kappa$ , and the activation energy would be 98 kcal., *i.e.*, a deficit of 6 kcal./mole. There is no need for the activation energy to be constant over such a wide temperature range—the rate would only be measurable well above 2000°K., and the activation energy of 98 kcal. could equally well result from a distribution of, say, 90% Boltzmann at 2000°K. and 55% Boltzmann at 3000°K. with an over-all rate only slightly less than the expected equilibrium value.

If this is the true explanation of the anomalous Arrhenius parameters measured in diatomic dissociation reactions, the observed activation energy must depend critically on the energy-transfer properties of the colliding particle  $M$ , a conclusion which is in full accord with the experimental data for both Br<sub>2</sub> and I<sub>2</sub>. Furthermore, it must be emphasized that we cannot predict from dissociation measurements anything about the corresponding

(9) K. F. Herzfeld and T. A. Litovitz, “Absorption and Dispersion of Ultrasonic Waves,” Academic Press, New York, N. Y., 1959.

(10) (a) C. Arnot and C. A. McDowell, *Can. J. Chem.*, **36**, 114, 1322 (1958); (b) J. C. Polanyi, *ibid.*, **36**, 121 (1958).

(11) M. W. Windsor, N. Davidson and R. Taylor, *J. Chem. Phys.*, **27**, 315 (1957).



recombination because such a system is thermodynamically irreversible.

**Recombination.**—The rate of recombination was calculated assuming a mixture of  $3.5 \times 10^{16}$  H atoms per cc. and  $3.5 \times 10^{19}$  He atoms per cc.—a mixture of the sort which might be produced with  $I_2$  using a very intense flash. It was also assumed that whenever two H atoms approached each other within 6 Å., they were in effect a "latent"  $H_2$  molecule, and could be knocked down from the continuum into a bound state (the square of the wave function for the state  $v = 14$  has its principal maximum near 3.3 Å. and falls off to about 0.05 of this value at 6 Å., where the depth of the potential well is 2.8 cm.<sup>-1</sup>). At equilibrium, the number of such unbound pairs is<sup>12</sup>

$$N_{AB} = 4\pi N_A N_B \int_0^{r^*} \left\{ 1 - \frac{E(r)}{kT} \right\} r^2 dr$$

where  $E(r)$  is the (Morse) potential energy function and  $r^*$  is the critical separation, *i.e.*, 6 Å. Each of these latent pairs was estimated to have a mean collision diameter of about 5 Å., and the chance of recombination from any part of the continuum was calculated from the number of collisions suffered by any pair and the probability per collision of the necessary transition. To obtain the total rate, these partial rates were integrated over the Maxwell distribution of approach velocities of the H atom pairs, and, for purposes of renormalization, the numbers of transitions from one part of the continuum to any other part of the continuum were likewise estimated and integrated. The calculations showed that at all temperatures, about 80% of the recombinations took place into the state  $v = 14$ , and that the rate decreased with increasing temperature; the distribution of the remaining recombinations was about 20% to  $v = 13$ , 0.1% to  $v = 12$  and  $10^{-4} - 10^{-6}\%$  to lower states. The relevant data for recombination into the  $v = 14$  state are given in Table II. It will be seen that the rate of recombination at 300°K. is equivalent to a rate constant of  $10^{-32}$  molecules<sup>-2</sup> cm.<sup>3</sup>sec.<sup>-1</sup>, which is of the order of observed rates for such processes.<sup>2</sup> And although the number of suitable collisions goes through a minimum around 1000°K., the rate continues to decrease as the temperature rises because of a progressive decrease in  $p_{\infty,14}$ . This decrease in  $p_{\infty,14}$  with increasing temperature arises largely because of the increase in the average amount of energy which has to be removed from the latent pair by the third body.<sup>13</sup> The over-all activation energy for the *initial* recombination into  $v = 14$  is about -1.2 kcal.; the figures in Table II suggest that the activation energy is not constant over the whole temperature range, but we would not be justified in putting much weight on this conclusion because a small change in rate could cause a large change in  $E$  for any individual temperature increment without altering the over-all value very much.

To obtain the real rate of recombination, it is necessary to take account of the redissociation

(12) L. S. Kassel, "The Kinetics of Homogeneous Gas Reactions," Chem. Catalog Co., New York, N. Y., 1932.

(13) (a) D. Husain and H. O. Pritchard, *J. Chem. Phys.*, **30**, 1101 (1959). (b) H. O. Pritchard, *Quart. Revs.*, **14**, 46 (1960).

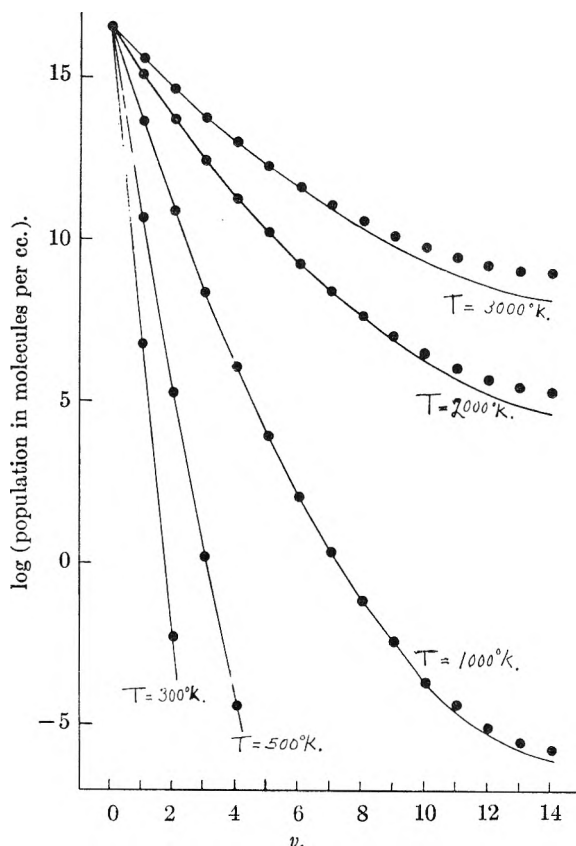


Fig. 2.—Relative populations of the vibrational states of  $H_2$ : ●, equilibrium population; —, disturbed population.

TABLE II

RATE OF RECOMBINATION IN A MIXTURE OF  $3.5 \times 10^{16}$  H ATOMS PER CC. AND  $3.5 \times 10^{19}$  He ATOMS PER CC.

Temp., °K.	No. of pairs of H atoms within 6 Å., $\times 10^{-19}$	No. of $H_2^*/He$ collisions per sec. $\times 10^{-23}$	Probability of recombination per collision	Rate of recombination in molecules of $H_2$ formed per sec.
300	6.03	3.66	$1.04 \times 10^{-3}$	$3.81 \times 10^{20}$
500	4.07	3.19	$7.64 \times 10^{-4}$	$2.44 \times 10^{20}$
1000	2.60	2.88	$4.71 \times 10^{-4}$	$1.36 \times 10^{20}$
2000	1.87	2.93	$2.75 \times 10^{-4}$	$8.06 \times 10^{19}$
3000	1.62	3.11	$1.97 \times 10^{-4}$	$6.13 \times 10^{19}$

which may occur on subsequent collisions, as pointed out recently by Polanyi.<sup>14</sup> If we consider a simplified system, where recombination takes place only into  $v = 14$  and the molecule is considered "safe" once it has been knocked down to  $v = 13$ , then the total rate of formation of stable molecules is

$$k' p_{14,13} (1 + p_{14,14} + p_{14,14}^2 + \dots) = k' p_{14,13} \sum_{c=0}^{\infty} p_{14,14}^c = \frac{k' p_{14,13}}{1 - p_{14,14}}$$

where  $k'$  is the *initial* rate of formation of  $v = 14$ , and the terms in the summation give the chance of stabilization on each successive collision of the newly formed  $v = 14$  molecule. Since  $p_{14,\infty} + p_{14,14} + p_{14,13} \approx 1$  and  $p_{14,\infty}$  increases with temperature, the effect as the temperature rises is to cause a small progressive reduction in the over-all rate of recom-

(14) J. C. Polanyi, *J. Chem. Phys.*, **31**, 1338 (1959).



bination below the initial rate of formation of the state  $v = 14$ . With the numbers at our disposal, it is not possible to calculate the magnitude of this effect because it is quite sensitive to the relative values of the three probabilities concerned. In the dissociation calculation, they were normalized so that  $P_{14,\infty} = 1$ , but it is apparent that the observed temperature dependence for recombination would be much too large if this were so, and a value of  $P_{14,\infty}$  of about  $1/2$  would lead to more reasonable results.

### Conclusion

As a result of this calculation, we see that collision theory must be amplified somewhat. We have found that activation occurs almost entirely by single steps, and the number of transitions  $N_{ij}$  taking place from  $v = i \rightarrow j$  may be represented by

$$N_{ij} = N_{i\infty} P_{ij} e^{-\Delta_{ij}/RT}$$

where  $P_{ij}$  is shown by the calculation (and confirmed by experiment) to be very small if  $\Delta_{ij}/RT$  is large, and tends to the order of  $1/2$  as  $\Delta_{ij}/RT$  approaches zero. When the molecules have been sufficiently activated, dissociation may take place from any of several states which lie within  $RT$  of the dissociation limit, with the topmost level dominating slightly. Because  $P_{ij}$  is substantially less than unity except for processes near the dissociation limit, there must be some point on the activation ladder where  $N_{ij}$  is less than the equilibrium value of  $N_{i\infty}$  and the Boltzmann distribution amongst the vibrational levels fails above this point. If the failure to maintain the distribution is worst at the low temperatures, we would have a high value of  $E$  (and a high value of the frequency factor<sup>15</sup>), but the calculation suggests that the failure is worst at the highest temperatures, leading to a low value of  $E$  in accord with experiment; the

value of  $E$  will depend on the energy-transfer characteristics of the molecules concerned, again in agreement with experiment.

A satisfactory calculation of the kinetics of recombination cannot be obtained within the Jackson and Mott framework. The cause of the divergence in the topmost matrix elements ( $Y_{ij}$ ) must be removed, and satisfactory wave functions for the continuum must be found, so that it would be possible to calculate accurately the relative values of the relevant probabilities. One could then set up a generalized scheme of recombination from the continuum, principally into  $v = 13$  and  $v = 14$ , with redissociation on subsequent collision from several of the topmost states. Having achieved these aims, it would be worth while to examine more rigorously the number of latent  $H_2$  pairs in the system, either along the lines discussed by Bunker,<sup>16</sup> or by following on from the work of Stogryn and Hirschfelder.<sup>6</sup> It appears, however, that a negative temperature coefficient will be guaranteed, partly because of an increase in the average energy jump, and partly because of the increased effect of redissociation as the temperature rises.

The idea of this calculation arose out of discussions of the carbon monoxide problem with Professor Norman Davidson in 1957, during the author's stay at the California Institute of Technology. It is a pleasure to acknowledge my indebtedness to those who made this visit possible, and to many friends and colleagues for helpful discussions, both in Manchester and in Pasadena.

(15) An alternative explanation of high frequency factors in unimolecular reactions may possibly be as follows: there is failure to maintain an equilibrium distribution of energy in the critical coordinate because transfer from other modes of vibration in the molecule is relatively slow; but as the temperature rises, these vibrations become more anharmonic and this transfer takes place more readily, so that the equilibrium could be least important at the highest temperatures.

(16) D. L. Bunker, *J. Chem. Phys.*, **32**, 1001 (1960).

## THE PALLADIUM-CHLORINE SYSTEM AT HIGH TEMPERATURE<sup>1</sup>

BY WAYNE E. BELL, ULRICH MERTEN AND M. TAGAMI

*John Jay Hopkins Laboratory for Pure and Applied Science, General Atomic Division of General Dynamics Corporation, San Diego, California*

*Received September 26, 1960*

The palladium-chlorine system has been studied over the range 500 to 1500° and at chlorine pressures up to 1 atm.  $PdCl_2$  is the only solid chloride that is stable in this range, and its melting point was determined as  $680 \pm 2^\circ$ . The solubility of palladium in liquid  $PdCl_2$  is small near the melting point of the compound, but increases with temperature. At 980°, the liquid in equilibrium with palladium contains 61 at.-% chlorine and has a dissociation pressure of 1 atm. Studies of the effect of chlorine pressure on vapor pressure indicate that the important gaseous species are  $PdCl_2$  and a gaseous polymer  $Pd_3Cl_{10}$ . At 1-atm. chlorine pressure,  $Pd_3Cl_{10}(g)$  is the principal species below 980°, reaching a maximum partial pressure of  $12 \times 10^{-3}$  atm. at 850°. Above 980°,  $PdCl_2(g)$  becomes the main species, and at 1506° it has a partial pressure of 0.1 atm. at 1-atm. chlorine pressure. Thermodynamic quantities were determined from the dissociation-pressure and vapor-pressure data.

### Introduction

The palladium-chlorine system has been studied over the range 500 to 1500° in order to identify condensed phases and vapor species, to measure dissociation pressures and vapor pressures, and to determine thermodynamic values from these pressure data.

Little information has been reported on the high-temperature chemistry of the palladium-chlorine system. According to Brewer,<sup>2</sup>  $PdCl_2$  is the only solid chloride of importance. Puche<sup>3</sup> found the melting point of  $PdCl_2$  to be 678° and reported

(2) L. Brewer, "The Chemistry and Metallurgy of Miscellaneous Materials: Thermodynamics," National Nuclear Energy Series, Div. IV, Vol. 19B, McGraw-Hill Book Co., Inc., New York, N. Y., 1950 p. 232.

(3) F. Puche, *Ann. Chem.*, **9**, 233 (1938).

(1) This work was supported in part by the U. S. Atomic Energy Commission under Contract AT(04-3)-164.

dissociation-pressure data for the chloride over the range 605 to 995°. He found the dissociation pressure to be 1 atm. at 920° and from a difference in slopes calculated a value of 9.7 kcal./mole for the heat of fusion. Krustinsons<sup>4</sup> reported dissociation-pressure data over the range 721 to 738° and, in disagreement with Puche, found the dissociation pressure to be 1 atm. at 738°. Krustinsons observed volatility of the chloride at 590°, and Brewer<sup>2</sup> estimated its boiling point to be 1300°K. Recently, Oranskaya and Mikhailova<sup>5</sup> reported dissociation-pressure and vapor-pressure data measured over the range 610 to 757°. They reported values for  $\Delta H^\circ$  and the heat of fusion; however, these values are not consistent with values which one may calculate from their expressions for dissociation pressure and vapor pressure as a function of temperature.

### Experimental Procedure

**Condensed-phase Studies.**—To determine the effect of temperature and chlorine pressure on the composition of palladium chloride, samples of the chloride (made in a separate experiment) were placed in a dead-end, quartz sample tube. The sample tube was mounted in a furnace and connected through a constriction in the tubing to a vacuum system, a mercury manometer, and a chlorine gas supply. The sample tube was first evacuated at about 100° to remove adsorbed material and then was heated under an appropriate chlorine pressure. At temperature, the sample was allowed to reach equilibrium with the chlorine gas; the sample tube was then sealed off at the constriction and immediately quenched. The palladium content of the sample was determined gravimetrically by hydrogen reduction.

Melting temperatures were determined by thermal analysis. The palladium-chloride melt was contained in a quartz tube that was mounted in a furnace and connected to a mercury manometer and a chlorine supply. A thermocouple was mounted on the outside of the tube for measuring the ambient temperature in the furnace. A measuring thermocouple inside a small-diameter, dead-end quartz tube was positioned in the center of the melt. The composition of the chloride was varied by changing the chlorine pressure. Melting temperatures were taken to be the average of the heating and cooling plateaus, which differed by about two degrees.

**Dissociation-pressure Studies.**—In measuring dissociation pressures, both static and dynamic (transpiration) methods were used as described by Bell, Garrison and Merten.<sup>6</sup> For convenience and accuracy, the static method was used for pressures above about 0.1 atm., and the transpiration method was used for lower pressures. The apparatus for the static method consisted essentially of a dead-end quartz reaction tube mounted in a furnace and connected through a small sulfuric acid manometer to a chlorine supply and a mercury manometer. At each temperature, the chlorine pressure was adjusted until equilibrium conditions, as indicated by the sulfuric acid manometer, were obtained. The dissociation pressure was taken to be the reading on the mercury manometer corrected for the pressure across the sulfuric acid manometer and for the pressure of the palladium-chloride vapor species.

For the transpiration method, a quartz reaction tube, shown in Fig. 1, was used. Argon was the carrier gas. Flow rates were 1 to 3 ml. STP/min., which is in the range where the calculated pressures were found to be independent of flow rate. The effluent argon was collected in an inverted volumetric flask and the chlorine was collected in KI solution. The dissociation pressure was then calculated from the relative quantities of argon and chlorine. Several determinations were made at each temperature and averaged.

(4) J. Krustinsons, *Z. Elektrochem.*, **44**, 537 (1938).

(5) M. A. Oranskaya and N. A. Mikhailova, *Zhur. Neorg. Khim.*, **5**, 12 (1960).

(6) W. E. Bell, M. C. Garrison and U. Merten, *J. Phys. Chem.*, **64**, 145 (1960).

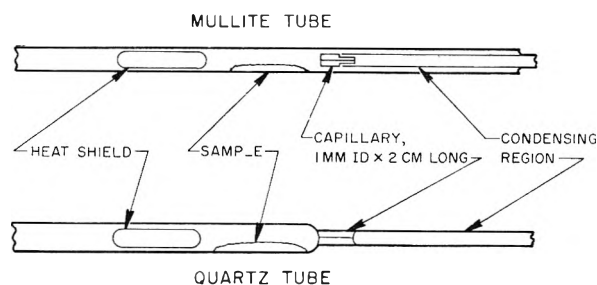


Fig. 1.—Reaction tubes: quartz used to 1000°, mullite used above this temperature.

**Vapor-pressure Studies.**—Vapor pressures were determined by the transpiration method with the reaction tubes shown in Fig. 1. In general, quartz tubes were used up to 1000° and mullite tubes were used above this temperature. The reaction tubes were mounted in tube furnaces and were connected to a vacuum system, a mercury manometer, and a chlorine gas supply.

In each experiment, a palladium-metal sample was placed in the reaction tube and heated to temperature under vacuum. Chlorine was admitted to the system to a desired pressure under flow conditions which prevented premature vapor deposition in the condensing region. Where the chlorine gas pressure was above the dissociation pressure, time was allowed for the chloride to form. Chlorine served as the carrier gas.

During the experiment, the vapor condensed in the tube at the edge of the furnace. When quartz reaction tubes were used, the condensing region was cut out and the palladium chloride condensed was analyzed gravimetrically by hydrogen reduction. At temperatures above 1000°, when mullite reaction tubes were used, the material that condensed on the inside of the tube was dissolved in aqua regia, and the palladium was determined as the dimethylglyoximate. Gravimetric analysis by hydrogen reduction could not be performed (1) because of the difficulty in removing the metal from the inside of the mullite condenser tube after reduction, and (2) because appreciable contamination resulted from chlorine corrosion of the mullite. In the neighborhood of 1500°, this contamination, which contained aluminum and silicon, amounted to 10 to 15% of the material condensed.

In experiments conducted at 1-atm. chlorine pressure, the effluent chlorine gas was collected in KI solution and was determined volumetrically with a standard thiosulfate solution. In the experiments conducted at chlorine pressures below 1 atm., the effluent chlorine gas was collected in a liquid nitrogen trap held under vacuum, and pressure in the reaction tube was maintained by supplying chlorine to the system at a rate sufficient to offset the outflow. At the end of the experiment, the chlorine was transferred from the cold trap into KI solution.

**Flow-rate Studies.**—For the vaporization experiments, the flow rates at the lower temperatures ranged from 0.01 to 0.03 mmole (Cl<sub>2</sub> + Pd)/min., depending on pressure conditions, and at the higher temperatures they varied from 0.03 to 0.2 mmole/min. The results given in Table I show that these flow rates were in the range where the mole ratio (moles Pd/mole Cl<sub>2</sub>) was independent of flow rate; i.e., that equilibrium conditions existed and that diffusion effects were negligible.

A further check on the effect of vapor diffusion under these flow-rate conditions can be obtained by using Merten's treatment<sup>7</sup> of diffusion effects in the transpiration method. A knowledge of  $D$ , the interdiffusion coefficient for vapor and gas, is required in this treatment, and from static (zero flow rate) experiments, we found  $D$  for the palladium chloride-chlorine system to be in the range 0.1 to 9 cm.<sup>2</sup>/sec., depending on conditions of pressure and temperature. Using the highest value for  $D$  (i.e., the value at 1500° and 0.2 atm.), the flow rate of 0.03 mmole/min. cited above, and the capillary dimensions 2 cm. long by 0.1 cm. in diameter, we calculated the value of the term  $\exp(-v\lambda/DA)$  to be 10<sup>-4</sup> (see eq. 1 of Ref. 7). This is negligible compared to unity and shows further that diffusion effects may be neglected under our experimental conditions.

(7) U. Merten, *ibid.*, **63**, 443, (1959).

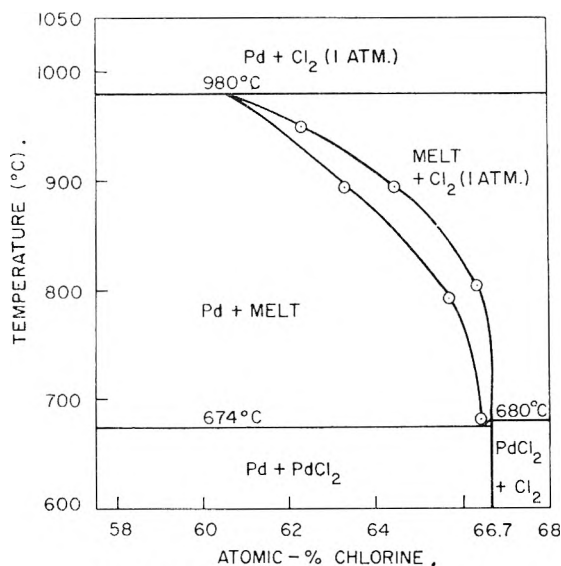


Fig. 2.—The palladium-chlorine system.

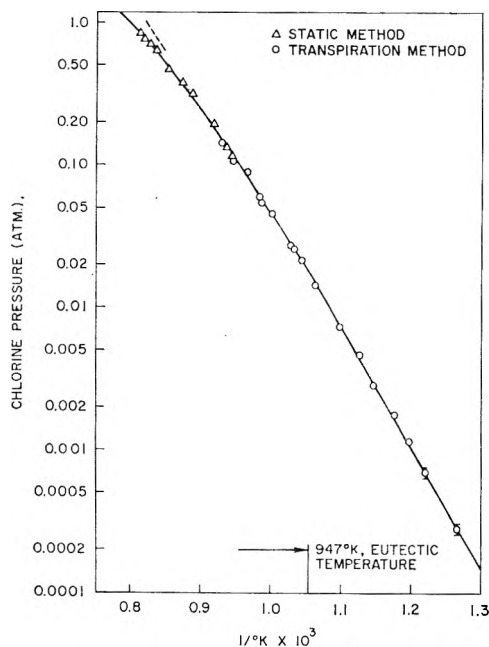


Fig. 3.—Dissociation pressure of condensed chlorides in palladium-chlorine system.

TABLE I

EFFECT OF FLOW RATE ON MOLE RATIO (MOLES Pd/MOLE  $\text{Cl}_2$ )

Temp. °C.	System pressure, atm.	Flow rate, mmoles ( $\text{Cl}_2 + \text{Pd}$ )/min.	Mole ratio, Pd: $\text{Cl}_2$ ( $\times 10^2$ )
800	0.65	0.0096	8.4
800	.66	.019	8.1
800	.66	.034	7.9
800	.66	.111	8.0
1304	1.0	.03	3.5
1304	1.0	.185	3.6
1304	1.0	.455	3.7

**Materials.**—Pulverized palladium sponge (99.995% purity, Johnson Matthey) was employed for all work except the melting-point determinations. For the latter, palladium chloride (60% metal content, metal of 99.95% purity, Engelhard Industries, Inc.) was used. The chlo-

rine gas (99.85% minimum purity, Matheson Co.) flowed through a sulfuric acid bubbler and  $\text{P}_2\text{O}_5$  powder before entering the reaction tube. The argon gas (99.9% minimum purity, Liquid Carbonic) flowed through a sulfuric acid bubbler,  $\text{P}_2\text{O}_5$  and hot calcium metal.

**General.**—The stopcocks were lubricated with Kel-F grease. Monel needle valves were used to regulate the gas flow and were found to behave satisfactorily in contact with chlorine gas. The corrosive action of chlorine on the mercury manometer was retarded by a layer of sulfuric acid on top of the mercury. Tube furnaces were used—nichrome wound for temperatures up to  $1000^\circ$  and platinum-rhodium wound for higher temperatures. Auxiliary heaters were placed at the ends of the furnaces to minimize temperature gradients. The main winding of each furnace was controlled by a time-proportioning controller, and the auxiliary heaters were controlled either manually or by controllers. With this arrangement, temperatures could be held constant to  $\pm 1^\circ$  or less below  $1000^\circ$  and to  $\pm 3^\circ$  or less up to  $1500^\circ$ . Temperatures were measured with Pt, Pt-10% Rh thermocouples located at intervals in a tube mounted alongside the reaction tube. The thermocouples were calibrated against standard Pt, Pt-10% Rh thermocouples certified by the National Bureau of Standards.

### Results and Discussion

**Condensed-phase Behavior.**—In agreement with others,<sup>2,3</sup> we found the solid chloride to be  $\text{PdCl}_2$ . Using thermal-analysis techniques, we determined a melting point of  $680 \pm 2^\circ$  for this compound under 1-atm. chlorine pressure. This is in good agreement with Puche's value of  $678^\circ$ .<sup>3</sup>

Early in the work, we noted anomalous behavior of the temperature dependence of the vapor pressure in the region  $800$  to  $950^\circ$ . We suspected that this behavior was due to the existence of either a lower chloride of definite composition or a liquid Pd-Pd $\text{Cl}_2$  solution of variable composition. The latter was found to be the case. The possibility that a stable lower chloride exists appears to be eliminated by the fact that the degree of chlorination had no effect on dissociation pressures obtained by either the static or the transpiration method.

The data obtained from the condensed-phase studies are summarized in Fig. 2. The palladium-rich limit of the existence range was determined by measuring the palladium content of quenched melts which had been held at temperature in contact with a chlorine pressure very slightly in excess of the Pd(s)-Pd $\text{Cl}_2$ (l)- $\text{Cl}_2$  equilibrium pressure at that temperature. The chlorine-rich limit was determined from similar analyses of melts held in contact with 1-atm. chlorine pressure. Above  $980^\circ$ , the liquid is not stable at chlorine pressures of 1 atm. or less.

Although the liquidus data were obtained at total pressures below 1 atm., they should be valid in this isobaric section within experimental error. The eutectic temperature,  $674 \pm 2^\circ$ , was obtained by a thermal analysis of Pd(s)-Pd $\text{Cl}_2$ (l) mixtures. It is believed that the temperatures and compositions given in Fig. 2 are accurate to within  $\pm 2^\circ$  and  $\pm 0.2$  at.-%, respectively.

**Dissociation Pressures.**—Dissociation pressures were measured over the range 517 to  $958^\circ$ . The results are plotted in Fig. 3. Temperatures are believed to be accurate to within  $\pm 2^\circ$  and pressures to within  $\pm 5\%$ , except at the lower pressures where larger uncertainties are shown. Extrapolation of the curve shows the dissociation pressure to

be 1 atm. at 980°. A slight break in the curve occurs at the eutectic temperature, 674°.

Above the eutectic temperature, the slope of the curve changes with temperature. This is a result of the variable composition of the liquid, and the magnitude of the effect may be discerned by noting the difference between the curve and the dashed line. The latter is a continuation of the linear portion of the curve immediately above the eutectic temperature.

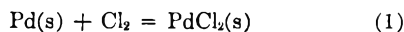
From the slope of the curve taken immediately below the eutectic temperature (947°K.), we calculate

$$\Delta H_{947}^0 = -38.6 \pm 1.0 \text{ kcal./mole}$$

and from this we find

$$\Delta S_{947}^0 = \frac{\Delta H^0}{T} - R \ln P = -32.6 \pm 1.0 \text{ e.u.}$$

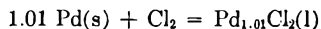
for the reaction



From the slope taken immediately above the eutectic temperature, we calculate

$$\Delta H_{947} = -34.2 \pm 1.0 \text{ kcal./mole}$$

for the reaction



The liquid composition was obtained from Fig. 2.

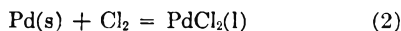
The heat of formation of  $\text{Pd}_{1.01}\text{Cl}_2(\text{l})$  at the eutectic temperature is undoubtedly equal to the heat of formation of  $\text{PdCl}_2(\text{l})$  at the melting point (953°K.), within the uncertainty of the data. Therefore

$$\Delta H_{953}^0 = -34.2 \pm 1.0 \text{ kcal./mole}$$

and from this we find

$$\Delta S_{953}^0 = -28.0 \pm 1.0 \text{ e.u.}$$

for the reaction



Combining  $\Delta H^0$  values for reactions 1 and 2, we obtain

$$\Delta H_{f, 953} = +4.4 \pm 2.0 \text{ kcal./mole}$$

for the heat of fusion of  $\text{PdCl}_2$ .

Puche<sup>3</sup> reported dissociation-pressure data obtained by the static method over the range 605 to 995°. In agreement with our results, his  $\log P_{\text{Cl}_2}$  vs.  $1/T$  plot shows an inflection at about 950°K. (the eutectic temperature); but, for unknown reasons, his pressures are higher than ours by at least a factor of two. From the difference in slopes, Puche calculated 9.7 kcal./mole for the heat of fusion. This does not agree with our value of  $4.4 \pm 2.0$  kcal./mole cited above.

Oranskaya and Mikhailova<sup>6</sup> reported dissociation-pressure data, measured by the transpiration method over the range 610 to 757°, which for the most part fall between ours and Puche's. They reported  $\Delta H^0$  values; however, these are not consistent with their equations relating dissociation pressure and temperature.

**Thermodynamic Properties of  $\text{PdCl}_2(\text{g})$ .**—The vaporization data obtained in the range 1100 to 1500° can be interpreted in a straightforward fashion. Palladium metal is the stable condensed phase under the chlorine pressures studied, and the solid-vapor equilibrium is simply

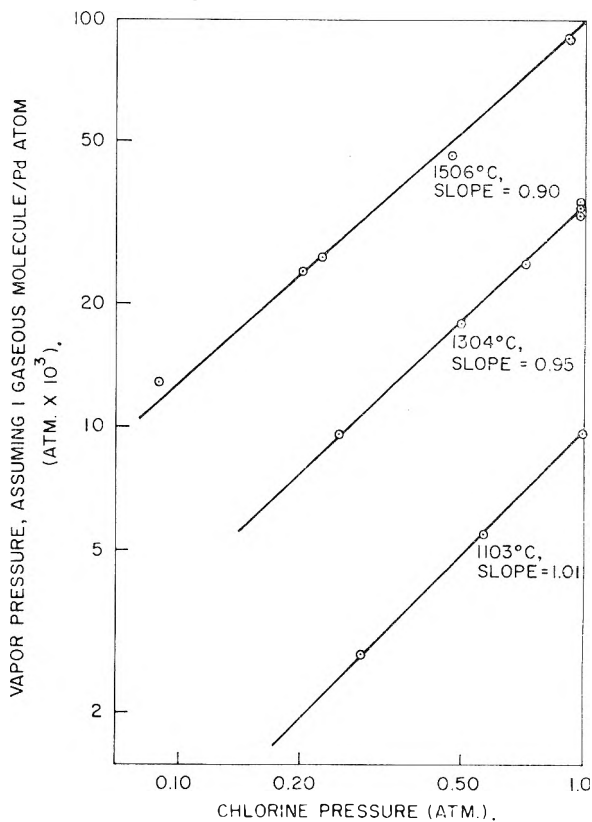


Fig. 4.—Effect of chlorine pressure on vapor pressure.

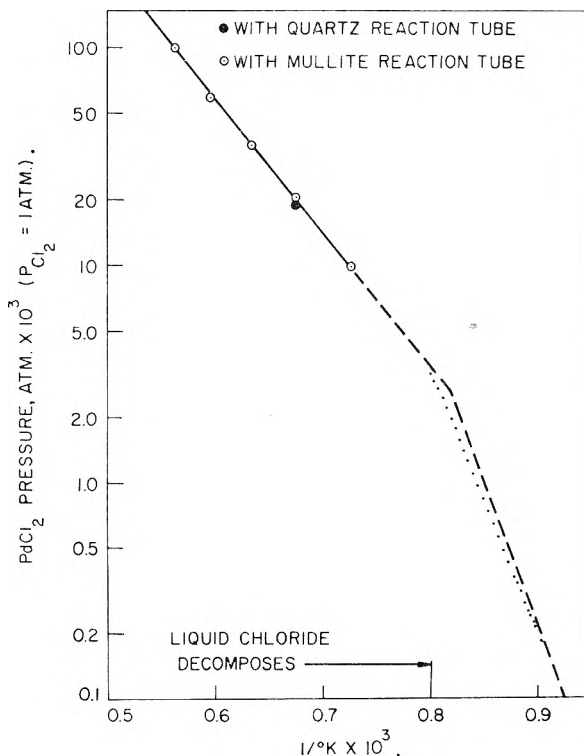
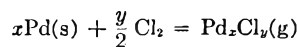


Fig. 5.—Temperature dependence of  $\text{PdCl}_2$  pressure at 1 atm. chlorine pressure.



Using the equilibrium constant for this reaction, we can write

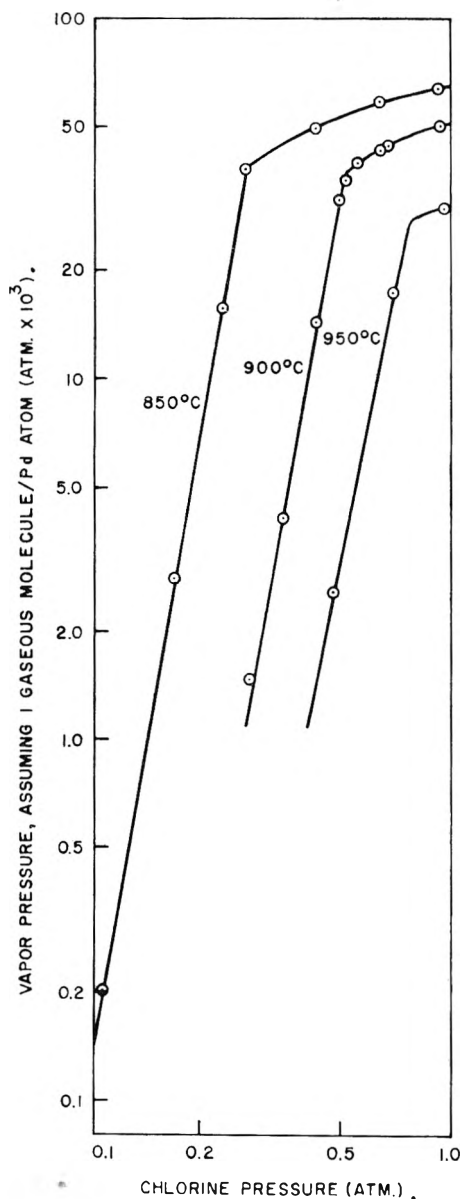


Fig. 6.—Effect of chlorine pressure on vapor pressure. Data were corrected for palladium derived from  $\text{PdCl}_2(\text{g})$ .

$$\log P_{\text{Pd}_x\text{Cl}_y} = \frac{y}{2} \log P_{\text{Cl}_2} + \log K$$

Thus, the chlorine content of the vapor molecule can be determined from the chlorine pressure dependence of the vapor pressure.

Figure 4 includes chlorine-pressure-dependence curves at 1103, 1304 and 1506°. The slopes are 1.01, 0.95 and 0.90, respectively; thus,  $y \approx 2$ , which shows that the principal vapor species is  $\text{Pd}_x\text{Cl}_2$ . The data do not permit an unambiguous evaluation of  $x$ ; however, since palladium occurs very commonly with an oxidation number of two and, indeed, the only stable solid chloride is  $\text{PdCl}_2$ , it seems probable that  $x = 1$ . This identity will be assumed in the discussion which follows.

The curves in Fig. 4 decrease in slope with increasing temperature to an extent which seems to be outside of experimental error, at least at the highest temperature. We suspected that this

effect was the result of small contributions from  $\text{PdCl}(\text{g})$  or  $\text{Pd}(\text{g})$ ; however, the curves do not change slope in a manner indicative of  $\text{PdCl}$ , and the vapor pressure of palladium is insufficient to cause the effect.<sup>8</sup> It is possible that chlorine corrosion of the mullite contaminated the gas stream and resulted in the formation of a small amount of another palladium-bearing vapor species at the highest temperatures.

Figure 5 shows the temperature dependence of the  $\text{PdCl}_2$  pressure at 1-atm. chlorine pressure. The points at 10<sup>3</sup>/°K. = 0.562, 0.634 and 0.727 were taken from the curves in Fig. 4. The three remaining points were obtained from additional experiments. A quartz tube was used in one of the experiments (normally, mullite tubes were used above 1000°) to show that the composition of the reaction tube had little, if any, influence on the results.

From the slope of the solid curve in Fig. 5, we calculate at the mean temperature (1573°K.)

$$\Delta H_{1573}^0 = +27.9 \pm 2.0 \text{ kcal./mole}$$

and from this we find

$$\Delta S_{1573}^0 = +11.1 \pm 2.0 \text{ e.u.}$$

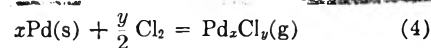
for the reaction



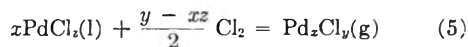
The dashed curve in Fig. 5 is an extrapolation of the experimentally determined vapor-pressure curve to 10<sup>3</sup>/°K. = 0.820, the hypothetical point at which  $\text{PdCl}_2(\text{l})$  decomposes at 1-atm. chlorine pressure (see Fig. 3); and at this point the slope changes by 34.2 kcal./mole, the heat of formation of  $\text{PdCl}_2(\text{l})$ .

The dotted curve in Fig. 5 reflects the effect of change in liquid composition on the vapor pressure and represents the actual pressure of  $\text{PdCl}_2$  over the Pd– $\text{PdCl}_2$  solution in the region between 10<sup>3</sup>/°K. = 0.800 and 0.900. The method of obtaining the dotted curve will be described below.

**Thermodynamic Properties of  $\text{Pd}_x\text{Cl}_y(\text{g})$ .**—In the temperature range where the condensed chloride is stable over a portion of our chlorine-pressure range, it is possible to identify the vapor species by studying the solid–vapor equilibrium



and, at the same temperature but at higher chlorine pressures, the equilibrium



where  $z$  is the number of chlorine atoms per palladium atom in the Pd– $\text{PdCl}_2$  solution.

Using the equilibrium constant for reaction 4, we can write

$$\log P_{\text{Pd}_x\text{Cl}_y} = \frac{y}{2} \log P_{\text{Cl}_2} + \log K$$

A similar relationship is obtained for reaction 5, and we evaluate  $y/2$  or  $(y - xz)/2$  from the slope of the  $\log P_{\text{Pd}_x\text{Cl}_y}$  vs.  $\log P_{\text{Cl}_2}$  curve.

There is one difficulty in interpreting the data

(8) (a) J. F. Haefling and A. H. Daane, *Trans. Met. Soc. AIME*, **212**, 115 (1958); (b) L. H. Dreger and J. L. Margrave, *J. Phys. Chem.*, **64**, 1323 (1960).

in this fashion. The experimental measurements of the quantity of palladium condensed give only a value of  $xP_{\text{Pd}_2\text{Cl}_y}$ , rather than a direct measure of  $P_{\text{Pd}_2\text{Cl}_y}$ . This in itself does not affect the observed slope since  $x$  is presumably a constant, but  $P_{\text{Cl}_2}$  must be calculated by subtracting the measured  $\text{Pd}_2\text{Cl}_y$  pressure from the system pressure. This cannot be done with certainty until  $x$  has been determined. Fortunately,  $P_{\text{Pd}_2\text{Cl}_y} \ll P_{\text{Cl}_2}$ , and we can evaluate  $y/2$  and  $(y - xz)/2$  with small error by assuming that  $x = 1$  (one gaseous molecule for each palladium atom condensed) as a first approximation. The  $\log P_{\text{Pd}_2\text{Cl}_y}$  vs  $P_{\text{Cl}_2}$  curves in Fig. 6 were obtained in this manner. The points have been corrected for the  $\text{PdCl}_2$  vapor contribution.<sup>9</sup> The breaks in the curves represent equilibrium dissociation pressures of the Pd-PdCl<sub>2</sub> solution and agree with the data of Fig. 3. At these points the products of reactions 4 and 5 must be the same.

From slopes taken immediately above and below the breaks and from values of  $z$  at the breaks obtained from the left-hand curve in Fig. 2, we calculate the values of  $x$  and  $y$  given in Table II. From the averages of these values, we see that  $x$  and  $y$  approximate 5 and 10, respectively, and that the vapor species appears to be  $\text{Pd}_5\text{Cl}_{10}$ .

TABLE II

EVALUATION OF  $x$  AND  $y$  FROM THE SLOPES OF THE PRESSURE-DEPENDENCE CURVES

Temp., °C.	$z$	$x$	$y$
850	1.82	4.8	11.0
900	1.70	5.0	11.0
950	..	..	9.6
	Average values		
..	..	4.9	10.5

Assuming the vapor species to be  $\text{Pd}_5\text{Cl}_{10}$ , we can now recalculate the vapor pressures and chlorine pressures. These data are shown in Fig. 7. The linear portion of each curve was drawn with a slope of 5.0, and it can be seen that the data fit within experimental error.

Figure 8 shows chlorine-pressure-dependence data at 700 and 800°. Because of the low pressures involved, we did not attempt to obtain data below the dissociation pressure at these temperatures. Assuming the vapor species to be  $\text{Pd}_5\text{Cl}_{10}$ , we calculate from the data of Figs. 7 and 8 the values shown in Table III for the composition of the liquid. Slopes taken at 1-atm. chlorine pressure and immediately above the dissociation pressure were used in the calculations. The calculated values agree within experimental error with the independent values of Fig. 2 and provide a further check on  $\text{Pd}_5\text{Cl}_{10}$  as the vapor species.

Having identified the vapor species, we now calculate from our measurements the  $\text{Pd}_5\text{Cl}_{10}$  vapor pressure at 1-atm. chlorine pressure as a function of temperature. These data are plotted in Fig. 9, and the  $\text{PdCl}_2$  vapor pressure data (from Fig. 5) are included for comparison. The  $\text{Pd}_5\text{-}$

(9) Values for  $P_{\text{PdCl}_2}$  were taken from the dotted curve in Fig. 5 and corrected to the appropriate chlorine pressure.

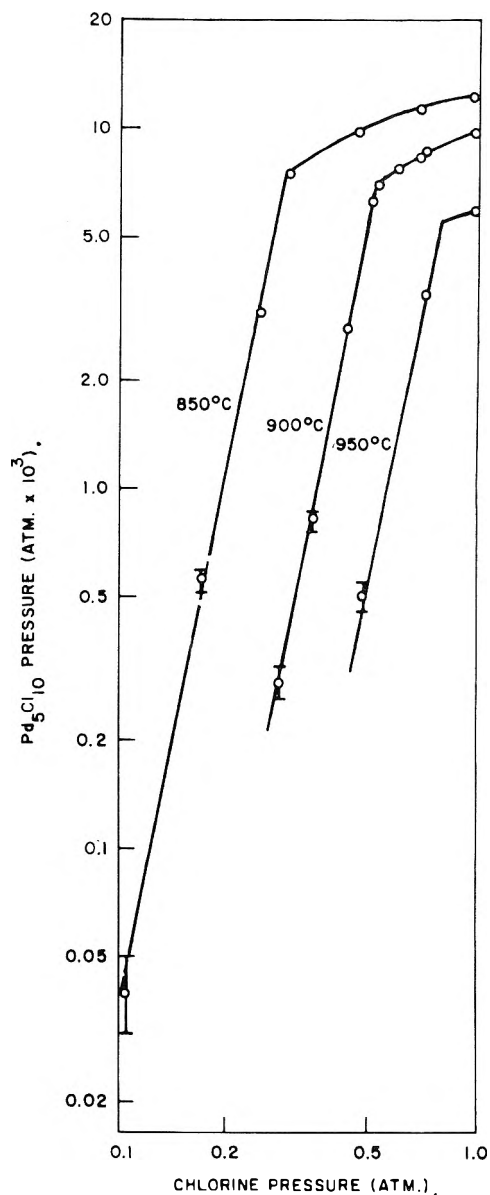


Fig. 7.—Effect of chlorine pressure on  $\text{Pd}_5\text{Cl}_{10}$  pressure. Linear portions were drawn with a slope of 5.0.

TABLE III

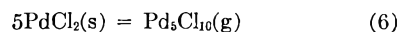
COMPOSITION OF LIQUID Pd-PdCl<sub>2</sub> SOLUTION

Temp., °C.	Chlorine pressure	Composition (at.-%)	
		Taken from Fig. 2	Calcd. from vapor-pressure data of Figs. 7 and 8
700	1 atm.	66.7	66.7
800	1 atm.	66.2	66.2
850	D.p. <sup>a</sup>	64.5	63.5
850	1 atm.	65.6	65.8
900	D.p. <sup>a</sup>	63.0	63.2
900	1 atm.	64.3	64.8

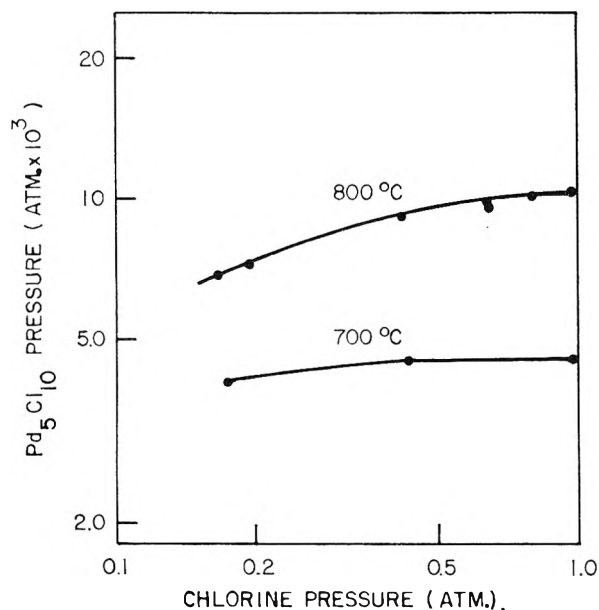
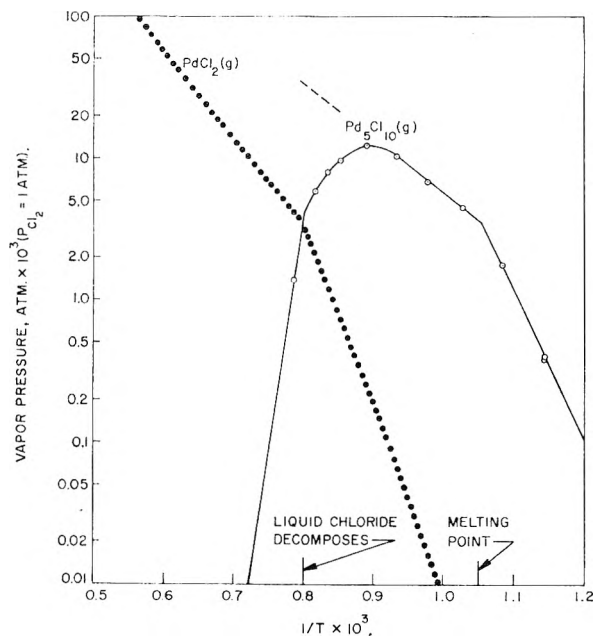
<sup>a</sup> Dissociation pressure.

$\text{Cl}_{10}$  data were corrected for the  $\text{PdCl}_2$  vapor contribution.

The vaporization reaction at temperatures below the melting point (953°K.) of  $\text{PdCl}_2$  is



assuming, of course, the vapor species to be  $\text{Pd}_5\text{Cl}_{10}$ ,

Fig. 8.—Effect of chlorine pressure on  $\text{Pd}_5\text{Cl}_{10}$  pressure.Fig. 9.—Temperature dependence of partial pressure of  $\text{Pd}_5\text{Cl}_{10}$  and  $\text{PdCl}_2$  at 1-atm. chlorine pressure.

as it was found to be above the melting point. From the slope of the curve taken below the melting point, we calculate

$$\Delta H^0_{953} = +47.3 \pm 2.0 \text{ kcal./mole}$$

and from this we obtain

$$\Delta S^0_{953} = +38.6 \pm 2.0 \text{ e.u.}$$

for reaction 6.

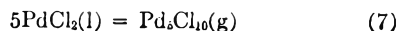
From the slope of the curve taken immediately above the melting point, we calculate

$$\Delta H^0_{953} = +17.6 \pm 1.0 \text{ kcal./mole}$$

and from this we obtain

$$\Delta S^0_{953} = +7.3 \pm 1.0 \text{ e.u.}$$

for the reaction



On the basis of the data in Fig. 2, the condensed state was taken to be  $\text{PdCl}_2(\text{l})$ .

Combining  $\Delta H^0$  values for reactions 6 and 7, we obtain

$$\Delta H_{f,953} = \frac{29.7 \pm 3.0}{5} = +5.9 \pm 0.6 \text{ kcal./mole}$$

for the heat of fusion per mole of  $\text{PdCl}_2$ . This value agrees within experimental error with the value  $4.4 \pm 2.0$  kcal./mole obtained above from the dissociation-pressure data.

The curved section of the  $\text{Pd}_5\text{Cl}_{10}$  curve in Fig. 9 represents the partial pressure of  $\text{Pd}_5\text{Cl}_{10}(\text{g})$  in equilibrium with chlorine at 1-atm. pressure and with liquid of variable composition. The effect of the variability of the liquid composition on the vapor pressure can be discerned by noting the difference between the solid curve and the dashed line in Fig. 9. The latter is a continuation of the linear portion of the curve above the melting point.

We are now in a position to calculate the dotted curve in Fig. 5. It can be shown that

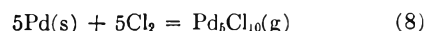
$$\left(\frac{P_5}{P_5'}\right)^{1/5} = \frac{P_1}{P_1'}$$

where  $P_5$  and  $P_1$  are hypothetical vapor pressures of  $\text{Pd}_5\text{Cl}_{10}$  and  $\text{PdCl}_2$ , respectively, over  $\text{PdCl}_2(\text{l})$ , and where  $P_5'$  and  $P_1'$  are corresponding vapor pressures over the liquid  $\text{Pd}-\text{PdCl}_2$  solution. Using values of  $P_5$  and  $P_5'$  taken from the dashed and solid curves in Fig. 9 and values of  $P_1$  from the dashed curve in Fig. 5, we calculated values of  $P_1'$  and obtained the dotted curve in Fig. 5.

Combining  $\Delta H^0$  values for reactions 2 and 7, we obtain

$$\Delta H^0_{953} = 5(-34.2 \pm 1.0) + (17.6 \pm 1.0) = -153 \pm 6.0 \text{ kcal./mole}$$

for the reaction



The  $\text{Pd}_5\text{Cl}_{10}$  curve through the point at  $10^3/^\circ\text{K.} = 0.785$  was drawn with a slope equivalent to this value of  $\Delta H^0$ , since the vaporization reaction in this region is represented by reaction 8.

There are very few related data in the literature on which one might base estimates of the heat capacities of the various palladium-chlorine species encountered in this work. As a result, no attempt has been made to calculate thermodynamic quantities at  $298^\circ\text{K.}$

The existence of the gaseous polymer  $\text{Pd}_5\text{Cl}_{10}$  is an interesting result, but not an entirely unexpected one, since solid palladium chloride is known to exist in a polymer-like crystal structure.<sup>10</sup>

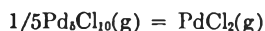
The low-temperature vapor pressure data reported here are best fit by  $\text{Pd}_5\text{Cl}_{10}$ , but  $\text{Pd}_6\text{Cl}_{12}$  or a mixture of it and  $\text{Pd}_5\text{Cl}_{10}$  are alternative assignments which cannot be completely excluded. It does seem clear, however, that lower polymers do not appear in the vapor phase in significant concentrations. This suggests that the higher polymer has a closed structure which is not stable for shorter chain lengths. Such a closed structure might be preferred, because it permits all the palladium atoms in the molecule to have a co-

(10) A. F. Wells, *Z. Krist.*, **100**, 189 (1938).



ordination number of four as well as an oxidation number of two.

The vapor pressure data yield some additional qualitative information about the liquid state of the system. The heat of the reaction



is about 58 kcal./mole; this is very close to the 62 kcal./mole heat required for the evaporation of the monomer from the liquid and is much larger than the 4 kcal./mole  $\text{PdCl}_2$  value required for the evaporation of the pentamer. Thus, the bonding between  $\text{PdCl}_2$  units in the pentamer is qualitatively equal in strength to their bonding to the liquid.

This suggests that  $\text{PdCl}_2$  forms a closed structure or a very long chain polymer in the liquid state.

Oranskaya and Mikhailova<sup>5</sup> reported vapor-pressure data measured by the transpiration method over the range 610 to 757°. If we take into account that they considered  $\text{PdCl}_2$ , rather than  $\text{Pd}_5\text{Cl}_{10}$ , to be the vapor species, their data roughly agree with ours. Their temperatures were not high enough to permit observation of the effect of change in liquid composition on vapor pressure.

**Acknowledgments.**—The authors are indebted to R. C. Jensen, M. C. Garrison and R. E. Inyard for performing some of the experimental work.

## THERMODYNAMIC PROPERTIES OF GASEOUS RUTHENIUM CHLORIDES AT HIGH TEMPERATURE<sup>1</sup>

BY WAYNE E. BELL, M. C. GARRISON AND ULRICE MERTEN

John Jay Hopkins Laboratory for Pure and Applied Science, General Atomic Division of General Dynamics Corporation, San Diego, California

Received September 26, 1960

The thermodynamic properties of the gaseous ruthenium chlorides have been studied over the range 650 to 1500° and at chlorine pressures from 0.1 to 1.5 atm. The effect of chlorine pressure on vapor pressure indicates that the important vapor species are  $\text{RuCl}_4$  and  $\text{RuCl}_3$ . Over  $\text{RuCl}_3(\text{s})$  at a chlorine pressure of 1 atm.,  $\text{RuCl}_4(\text{g})$  is the principal species, reaching a maximum partial pressure of 0.065 atm. at 853°—the temperature at which  $\text{RuCl}_3(\text{s})$  decomposes. Above 853°, where  $\text{Ru}(\text{s})$  is the stable condensed phase, the partial pressure of  $\text{RuCl}_4(\text{g})$  decreases with increasing temperature, and  $\text{RuCl}_3(\text{g})$  becomes the principal species. At 1500°, the partial pressure of  $\text{RuCl}_3(\text{g})$  in equilibrium with  $\text{Ru}(\text{s})$  and 1-atm.  $\text{Cl}_2$  is 0.16 atm. Thermodynamic quantities were determined for the reactions and species studied.

### Introduction

Several investigators<sup>2</sup> have observed the volatility of ruthenium chloride in the region 600 to 800°. Shchukarev, Kolbin and Ryabov<sup>3</sup> reported vapor pressures measured over the range 575 to 727° and assumed  $\text{RuCl}_3$  to be the vapor species. Recently, these authors presented evidence indicating that a higher chloride, probably  $\text{RuCl}_4$ , may have been involved.<sup>4</sup>

The present work was undertaken for the purpose of identifying the important gaseous species and determining their thermodynamic properties over the range 600 to 1500° and at chlorine pressures from 0.1 to 1.0 atm.

### Experimental

**Procedure.**—The transpiration method was used as described in a previous paper.<sup>5</sup> Quartz reaction tubes were used up to 1000°, and mullite reaction tubes were used above that temperature. Flow rates ranged from 0.01 to 0.1 mmole/min., depending on temperature and pressure conditions. In this range, studies showed vapor pressures to be independent of flow rate. Chlorine was normally used as the carrier gas; in a few experiments, however, chlorine-argon mixtures, made in stainless steel cylinders, were used. In the latter experiments, the total system pressure was 1

atm. Temperatures were measured with standardized Pt, Pt-10% Rh thermocouples and are believed to be accurate to within  $\pm 2^\circ$  below 1000 and to within  $\pm 4^\circ$  above that temperature.

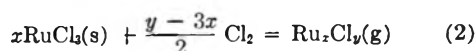
Pulverized ruthenium sponge (99.995% purity, Johnson Matthey) was employed. The purity of the other materials was the same as in the earlier experiments.<sup>5</sup>

**Analyses.**—When quartz reaction tubes were used, the condensing region was cut out and the ruthenium chloride that had condensed was analyzed gravimetrically by hydrogen reduction. When mullite tubes were used, a more complicated analytical procedure was necessary because of appreciable contamination of the condensate resulting from chlorine corrosion of the mullite. Therefore, the technique was to break up the condensing region and to dissolve the material condensed with a KOH- $\text{KNO}_3$  fusion. The ruthenium was then separated as the volatile oxide, precipitated as the hydrated oxide, reduced with hydrogen and weighed as the metal.

### Results

The important vapor species were identified by determining the dependence of vapor pressure on chlorine pressure. Thermodynamic quantities for the species were determined by studying the vapor pressures as a function of temperature.

**Pressure Dependence.**—In the temperature range where  $\text{RuCl}_3(\text{s})$  is stable over a portion of our chlorine-pressure range, the solid-vapor equilibria to be considered are



We assume the vapor species to be the same over the metal and the chloride. It should be noted

(1) This work was supported in part by the U. S. Atomic Energy Commission under Contract AT(04-3)-164.

(2) H. Remy and M. Kohn, *Z. anorg. allgem. Chem.*, **137**, 365 (1924); L. Wöhler and P. Balz, *ibid.*, **137**, 411 (1924); M. A. Hill and F. E. Beamish, *J. Am. Chem. Soc.*, **72**, 4855 (1950).

(3) S. A. Shchukarev, N. I. Kolbin and A. N. Ryabov, *Zhur. Neorg. Khim.*, **3**, 1721 (1958).

(4) S. A. Shchukarev, N. I. Kolbin and A. N. Ryabov, *ibid.*, **4**, 1692 (1959).

(5) W. E. Bell, U. Merten and M. Tagami, *J. Phys. Chem.*, **65**, 510 (1961).

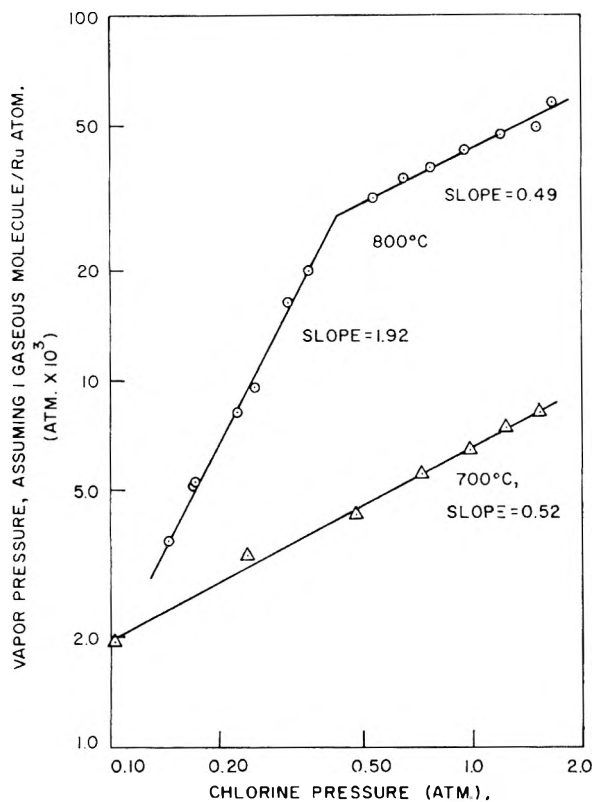


Fig. 1.—Effect of chlorine pressure on vapor pressure at 700 and 800°.

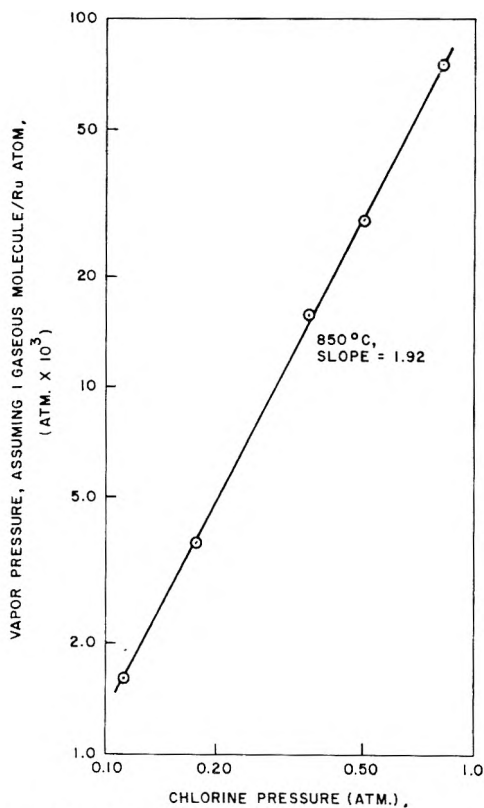


Fig. 2.—Effect of chlorine pressure on vapor pressure at 850°.

that previous studies<sup>6</sup> have shown  $\text{RuCl}_3$  to be the

(6) W. E. Bell, M. C. Garrison and Ulrich Merten, *J. Phys. Chem.*, **64**, 145 (1960).

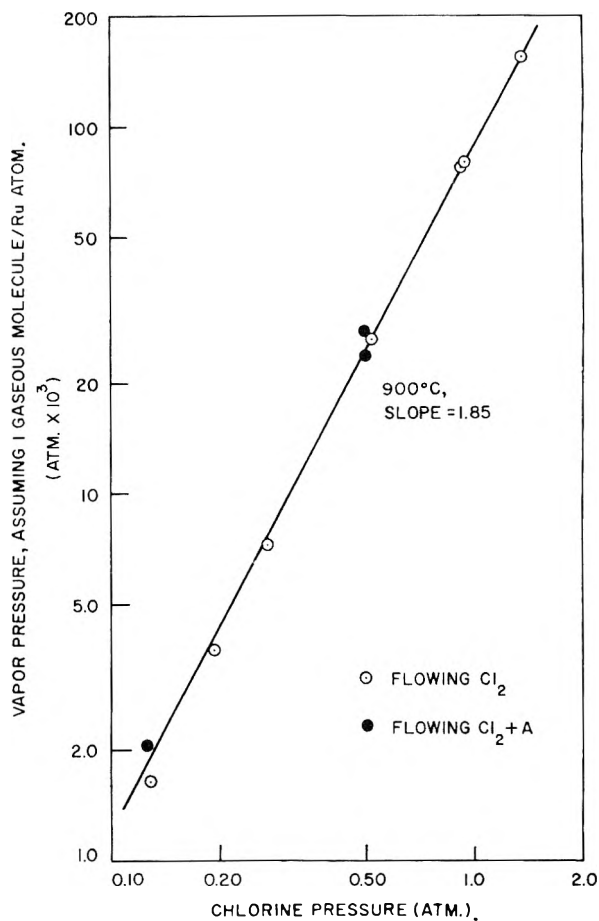


Fig. 3.—Effect of chlorine pressure on vapor pressure at 900°.

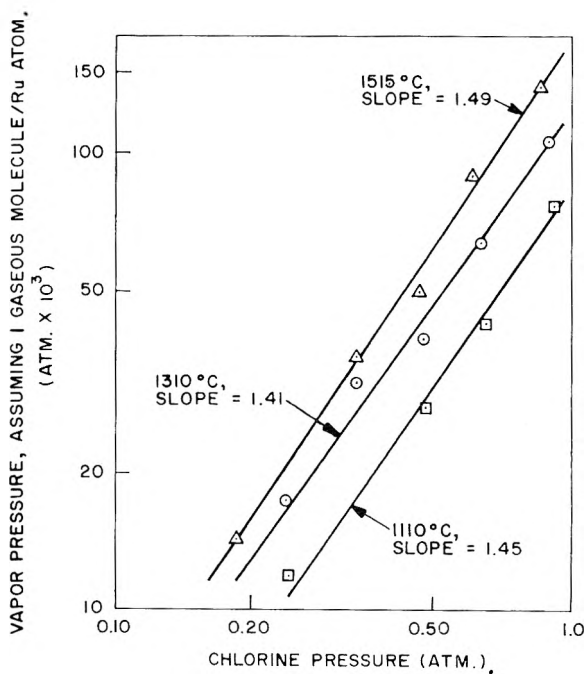


Fig. 4.—Effect of chlorine pressure on vapor pressure at three different temperatures.

only stable solid chloride under our conditions.

From the equilibrium constant for reaction 1, we obtain

$$\log P_{\text{Ru}_x\text{Cl}_y} = \frac{y}{2} \log P_{\text{Cl}_2} + \log K$$

A similar expression is obtained for reaction 2, and we evaluate  $y/2$  and  $(y - 3x)/2$  by studying the effect of chlorine pressure on vapor pressure.

Isotherms obtained at 700 and 800, 850 and 900° are shown in Figs. 1, 2 and 3, respectively. The break in the 800° isotherm at 0.43 atm. fixes the equilibrium dissociation pressure of  $\text{RuCl}_3(\text{s})$ , and the result agrees with dissociation-pressure data reported earlier.<sup>6</sup>

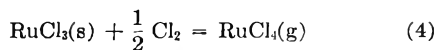
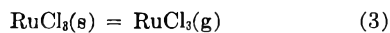
From the observed slopes, we see that  $y/2 \cong 2$  and  $(y - 3x)/2 \cong 0.5$ . Thus,  $y = 4$  and  $x = 1$ , and it is apparent that the principal vapor species in the temperature range (700 to 900°) and chlorine-pressure range investigated is  $\text{RuCl}_4$ .

In calculating the data in Figs. 1, 2 and 3, account was taken of the chlorine produced when the  $\text{RuCl}_4(\text{g})$  condensed to form  $\text{RuCl}_3(\text{s})$ .<sup>7</sup> The data were plotted assuming one gaseous molecule per ruthenium atom. In three of the experiments conducted at 900°, a mixture of argon and chlorine was used as the carrier gas (undiluted chlorine was normally used) with no apparent effect on the results. The consistently low values of  $y/2$  are the result of a contribution from  $\text{RuCl}_3(\text{g})$ .

Pressure-dependence data obtained in the range 1100 to 1500° are shown in Fig. 4. Ruthenium metal is the condensed phase under the chlorine pressures used, and reaction 1 is the vaporization reaction. The observed slopes are 1.45, 1.41 and 1.49; thus,  $y \cong 3$ , and the principal vapor species is  $\text{Ru}_x\text{Cl}_3$ . The data do not permit an evaluation of  $x$ . However, since the stable solid chloride is  $\text{RuCl}_3$ , it seems probable that  $x = 1$ , and we shall assume the vapor species to be  $\text{RuCl}_3$ . It should be noted that the data in Fig. 4 show no trend which is suggestive of a still lower chloride.

The data in Fig. 4 were not corrected for the contribution of  $\text{RuCl}_4(\text{g})$ , nor were the data in Figs. 1, 2 and 3 corrected for the contribution of  $\text{RuCl}_3(\text{g})$ . Therefore, the isotherms shown represent total vapor pressures.

**Temperature Dependence.**—Since  $\text{RuCl}_3$  and  $\text{RuCl}_4$  are the important vapor species under our experimental conditions, the solid-vapor equilibria which must be considered are



When  $\text{RuCl}_3(\text{s})$  is the stable condensed phase at a chlorine pressure of 1 atm., the observed vapor pressure must be the sum of contributions from (3) and (4); and when  $\text{Ru}(\text{s})$  is the stable condensed phase, the observed pressure must be the sum of contributions from (5) and (6).

Reaction 3 is related to (5) and reaction 4 is related to (6) by the reaction

(7) During a transpiration experiment  $\text{RuCl}_4(\text{g})$  decomposes to  $\text{RuCl}_3(\text{s})$  on condensation, and the additional chlorine produced must be subtracted from the total quantity of chlorine collected to obtain the quantity which passed over the sample as chlorine.

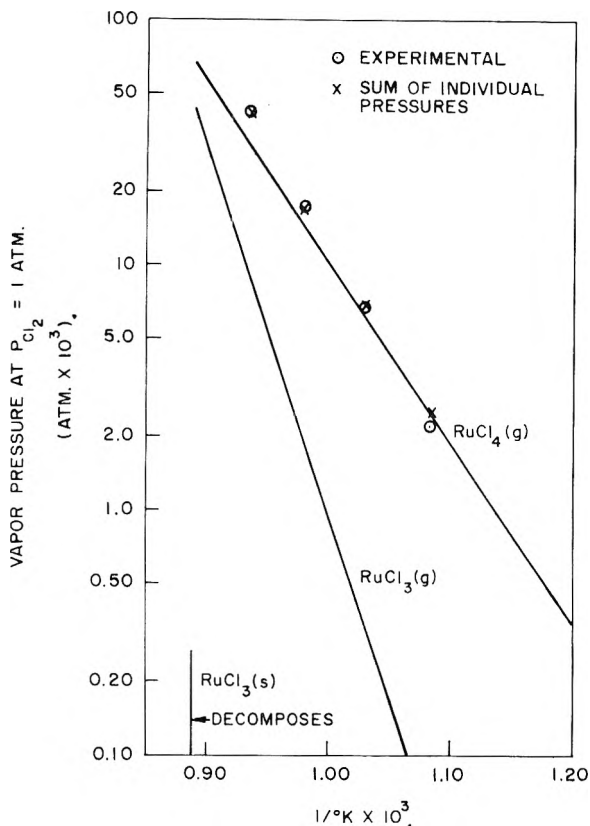


Fig. 5.—Observed vapor pressures over  $\text{RuCl}_3(\text{s})$  resolved into individual partial pressures of  $\text{RuCl}_3(\text{g})$  and  $\text{RuCl}_4(\text{g})$ .

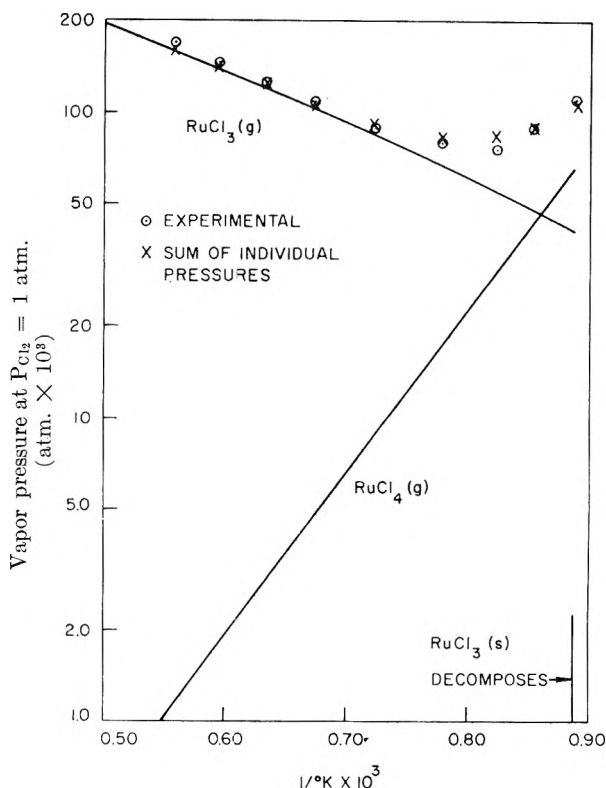


Fig. 6.—Observed vapor pressures over ruthenium metal resolved into individual partial pressures of  $\text{RuCl}_3(\text{g})$  and  $\text{RuCl}_4(\text{g})$ .

TABLE I  
THERMODYNAMIC DATA FOR VAPORIZATION REACTIONS

$\text{RuCl}_3(\text{s}) = \text{RuCl}_3(\text{g})$	$\text{RuCl}_3(\text{s}) + \frac{1}{2}\text{Cl}_2 = \text{RuCl}_4(\text{g})$
$\Delta H_{1000}^0 = +67.4 \pm 3.0$ kcal./mole	$\Delta H_{1000}^0 = +33.4 \pm 2.0$ kcal./mole
$\Delta S_{1000}^0 = +53.6 \pm 3.0$ e.u.	$\Delta S_{1000}^0 = +24.2 \pm 2.0$ e.u.
$\Delta C_p = -9.2$ cal./mole/°K. (estimated)	$\Delta C_p = -6.6$ cal./mole/°K. (estimated)
$\Delta H_{298}^0 = +73.9 \pm 4.0$ kcal./mole	$\Delta H_{298}^0 = +38.0 \pm 3.0$ kcal./mole
$\Delta S_{298}^0 = +64.7 \pm 4.0$ e.u.	$\Delta S_{298}^0 = +32.2 \pm 3.0$ e.u.
$\text{Ru}(\text{s}) + 3/2\text{Cl}_2 = \text{RuCl}_3(\text{g})$	$\text{Ru}(\text{s}) + 2\text{Cl}_2 = \text{RuCl}_4(\text{g})$
$\Delta H_{1400}^0 = +8.2 \pm 2.0$ kcal./mole	$\Delta H_{1400}^0 = -24.6 \pm 3.0$ kcal./mole
$\Delta S_{1400}^0 = +1.0 \pm 2.0$ e.u.	$\Delta S_{1400}^0 = -27.2 \pm 3.0$ e.u.
$\Delta C_p = -4.7$ cal./mole/°K. (estimated)	$\Delta C_p = -2.1$ cal./mole/°K. (estimated)
$\Delta H_{298}^0 = +13.4 \pm 3.0$ kcal./mole	$\Delta H_{298}^0 = -22.3 \pm 4.0$ kcal./mole
$\Delta S_{298}^0 = +8.3 \pm 3.0$ e.u.	$\Delta S_{298}^0 = -24.0 \pm 4.0$ e.u.



In the dissociation-pressure work reported earlier,<sup>6</sup> we found that for reaction 7

$$\begin{aligned} \Delta H_{1020}^0 &= -57.2 \pm 1.0 \text{ kcal./mole} \\ \Delta S_{1020}^0 &= -50.9 \pm 1.0 \text{ e.u.} \end{aligned}$$

and, using an estimated value of 4.5 cal./mole/°K. for  $\Delta C_p$ , we calculated that

$$\begin{aligned} \Delta H_{298}^0 &= -60.5 \pm 2.0 \text{ kcal./mole} \\ \Delta S_{298}^0 &= -56.4 \pm 2.0 \text{ e.u.} \end{aligned}$$

We found also in the earlier work that  $\text{RuCl}_3(\text{s})$  decomposes at 853° under a chlorine pressure of 1 atm.

Figure 5 shows the observed vapor pressures and individual partial pressures of  $\text{RuCl}_3$  and  $\text{RuCl}_4$  in equilibrium with  $\text{RuCl}_3(\text{s})$  and 1-atm. chlorine pressure, and Fig. 6 shows the pressure data for  $\text{Ru}(\text{s})$  and 1-atm. chlorine pressure. Where possible, the observed pressure points were taken from the pressure-dependence curves; the remaining points came from additional experiments. The chlorine released on condensation of  $\text{RuCl}_4$  vapor was taken into account in calculating the observed pressures.<sup>7</sup>

The individual partial-pressure curves were arrived at by successive approximations and are drawn so that the sum of the partial pressures best fits the observed pressures. At 853° (see above), the curves change slope by -56.7 kcal./mole—the heat of reaction 7 at 853°. The curves are in accord with the equation

$$\ln p = -\frac{\Delta H^0}{RT} + \frac{\Delta C_p}{R} \ln T + I$$

Thermodynamic values for reactions 3 through 6 are summarized in Table I. The  $\Delta H^0_T$  values represent the slopes of the individual partial pressure curves in Figs. 5 and 6 at the mid-point of the temperature range studied. The  $\Delta S^0_T$  values were calculated by using the relationship

$$\Delta S^0 = \frac{\Delta H^0}{T} + R \ln p$$

The  $\Delta C_p$  values were estimated by means of rough rules given by Kubaschewski and Evans.<sup>8</sup>  $C_p$  for  $\text{RuCl}_4(\text{g})$  was taken to be 22 cal./mole/°K. on the basis of Doerner's selection<sup>9</sup> for  $\text{CrCl}_4(\text{g})$ .

(8) O. Kubaschewski and E. L. Evans, "Metallurgical Thermochemistry," 3rd ed., Pergamon Press, New York, N. Y., 1958.

(9) H. A. Doerner, Bur. of Mines Tech. Paper, 577 (1937).

The  $\Delta H_{298}^0$  and  $\Delta S_{298}^0$  values were calculated by assuming  $\Delta C_p$  to be constant over the temperature range involved.

Combining  $\Delta S_{298}^0$  values for reactions 5 and 6 with standard entropies ( $S_{298}^0$  of  $\text{Ru} = 6.9 \pm 0.5$  e.u. and  $S_{298}^0$  of  $\text{Cl}_2 = 53.3 \pm 0.92$  e.u., given by Kelley<sup>10</sup>) we obtain  $S_{298}^0$  of  $\text{RuCl}_3(\text{g}) = 95.1 \pm 4.0$  e.u. and  $S_{298}^0$  of  $\text{RuCl}_4(\text{g}) = 89.5 \pm 5.0$  e.u.<sup>11</sup>

### Discussion

The evidence that  $\text{RuCl}_4$  is a vapor species appears to be conclusive; the pressure-dependence data used for the identification were clear cut and were obtained without experimental difficulty. In addition to our findings, Shchukarev, *et al.*,<sup>4</sup> reported evidence of a higher chloride and assumed it to be  $\text{RuCl}_4$ . They reported preliminary vapor-pressure data, but their data are insufficient to permit a comparison with our data.

Evidence for a species containing three chlorine atoms per molecule, probably  $\text{RuCl}_3$ , also appears conclusive. Our pressure-dependence data taken above 1100° indicate the presence of this species, and Shchukarev, *et al.*,<sup>4</sup> also found evidence for it.

The pressure-dependence data taken above 1100° were more uncertain than the low-temperature data (compare the data in Fig. 4 with those in Figs. 1, 2 and 3). This increased uncertainty at the higher temperatures was partly the result of chlorine corrosion of the mullite reaction tubes, which may have resulted in the formation of small quantities of additional ruthenium-bearing species, and partly due to the nature of the high-temperature apparatus, which caused larger uncertainties in the analytical procedure. The uncertainty in these data may have obscured evidence of a gaseous lower chloride, such as  $\text{RuCl}_2(\text{g})$ , which, if it exists, would be most important at the highest temperatures.

The  $S_{298}^0$  values of  $95.1 \pm 4.0$  and  $89.5 \pm 5.0$  e.u. for  $\text{RuCl}_3(\text{g})$  and  $\text{RuCl}_4(\text{g})$ , respectively, may be compared with estimated values of 82.9 and 85.3 e.u., which were calculated from an empirical equation give by Kubaschewski and Evans.<sup>12</sup> The

(10) K. K. Kelley, Bull. U. S. Bur. of Mines, 477 (1950).

(11) It has been suggested that, based on  $C_p$  values for  $\text{TiCl}_4(\text{g})$ ,  $\text{ZrCl}_4$ ,  $\text{HfCl}_4(\text{g})$  and  $\text{SnCl}_4(\text{g})$  given in K. K. Kelley, Bureau of Mines Bulletin 584 (1960),  $C_p = 25$  cal./mole/°K. for  $\text{RuCl}_4(\text{g})$  may be a better estimate than the value 22 cal./mole/°K. which we selected. Using  $C_p = 25$  cal./mole/°K., we calculate  $S_{298}^0$  of  $\text{RuCl}_4(\text{g}) = 85.3 \pm 5.0$  e.u.

(12) Ref. 8, p. 195.

value for  $\text{RuCl}_4(\text{g})$  seems reasonable; however, the value for  $\text{RuCl}_3(\text{g})$  is about 10 e.u. higher than one might expect.

TABLE II

COMPARISON OF  $\Delta S_{298}^0$  VALUES FOR THE RUTHENIUM-CHLORINE SYSTEM AND THE CHROMIUM-CHLORINE SYSTEM

Reaction	$\Delta S_{298}^0$ (e.u.)	
	Ruthenium <sup>a</sup>	Chromium <sup>b</sup>
$\text{MCl}_3(\text{s}) = \text{MCl}_3(\text{g})$	$+64.7 \pm 4.0$	$+55.1$
$\text{MCl}_3(\text{s}) + \frac{1}{2} \text{Cl}_2 = \text{MCl}_4(\text{g})$	$+32.2 \pm 3.0$	$+30.7$
$\text{M}(\text{s}) + 3/2 \text{Cl}_2 = \text{MCl}_3(\text{g})$	$+8.3 \pm 3.0$	$+0.5$
$\text{M}(\text{s}) + 2\text{Cl}_2 = \text{MCl}_4(\text{g})$	$-24.0 \pm 4.0$	$-24.0$

<sup>a</sup> This work. <sup>b</sup> H. A. Doerner.<sup>9</sup>

The chromium-chlorine system at high temperature, which was thoroughly studied by Doerner,<sup>9</sup>

is similar in many ways to the ruthenium-chlorine system:  $\text{CrCl}_3(\text{g})$  and  $\text{CrCl}_4(\text{g})$  are important vapor species, and reactions analogous to those in Table I occur. Doerner found standard entropies for  $\text{CrCl}_3(\text{g})$  and  $\text{CrCl}_4(\text{g})$  to be 86.1 and 88.3 e.u., respectively, which may be compared with the above values for  $\text{RuCl}_3(\text{g})$  and  $\text{RuCl}_4(\text{g})$ . Table II gives a comparison of  $\Delta S_{298}^0$  values for analogous reactions involved in the two systems. In our studies of the dissociation pressure of  $\text{RuCl}_3(\text{s})$ ,<sup>6</sup> we found the standard entropy for  $\text{RuCl}_3(\text{s})$  to be  $30.5 \pm 2.5$  e.u., which may be compared to a value of 31.0 e.u. for  $\text{CrCl}_3(\text{s})$  found by Doerner.

**Acknowledgments.**—The authors are indebted to R. C. Jensen, M. Tagami and R. E. Inyard for performing part of the experimental work.

## THE EQUILIBRIUM $2/3\text{Bi}(\text{l}) + 1/3\text{BiI}_3(\text{g}) = \text{BiI}(\text{g})$ <sup>1</sup>

BY DANIEL CUBICCIOTTI

Stanford Research Institute, Menlo Park, California

Received September 26, 1960

The equilibrium  $2/3 \text{Bi}(\text{l}) + 1/3 \text{BiI}_3(\text{g}) = \text{BiI}(\text{g})$  was studied by a transpiration technique over the temperature range 545 to 735° and the pressure range 0.1 to 50 mm. The enthalpy change for the reaction was 21 kcal. and the standard entropy 16 e.u. at mid-temperature. An excess pressure of reduced Bi species in the higher pressure range was interpreted as due to the formation of a polymer,  $\text{Bi}_n\text{I}_n$ .

### Introduction

The equilibria of liquid Bi with gaseous  $\text{BiX}_3$  and  $\text{BiX}$ , in which X was Cl or Br, have recently been studied.<sup>2,3</sup> For those systems rather appreciable percentages of the monohalide were found in the equilibrium vapor, but no evidence of a dihalide (whether as  $\text{BiX}_2$  or as  $\text{Bi}_2\text{X}_2$ ). The iodide system was investigated as a companion study, with the results reported below.

### Experimental

The same transpiration method was used as in the chloride work<sup>2</sup>; however, it was found necessary to envelop the exit tube of the apparatus with an inert atmosphere box because of the strong susceptibility of the products to air oxidation. The Bi-I samples obtained were analyzed for Bi by conversion to  $\text{Bi}_2\text{O}_3$  as in the Bi-Br system.<sup>3</sup> The  $\text{BiI}_3$  was made from  $\text{Bi}_2\text{O}_3$  and aqueous HI, dried and doubly distilled in an  $\text{N}_2$  stream.

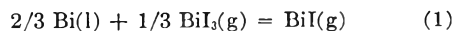
The transpiration experiments were made at five different temperatures: 543–547; 592–596; 639–642; 683–687; 734–736°, although the temperature of each run was constant to 1°. The pressures finally calculated were adjusted (with very small corrections) to the temperatures: 545, 595, 640, 685 and 735°, respectively. The flow rates were such that from 0.005 to 0.2 mole of  $\text{N}_2$  was passed in 8 hours and from 0.1 to 0.2 g. Bi-I sample collected. From the results of experiments to evaluate diffusion effects a correction of from 0 to 6% was made on the results, the larger corrections applying to the experiments made with smaller flow rates and higher pressures of Bi species in the gas stream.

### Results and Discussions

The data obtained were treated like those of the earlier systems<sup>2,3</sup>; that is, the results of each ex-

periment were reduced to the pressures of  $\text{BiI}$  and  $\text{BiI}_3$  required to account for the amount and composition of the transpired material. Then these pressures were plotted as logarithm of pressure of  $\text{BiI}$  vs. logarithm of pressure of  $\text{BiI}_3$ . In such a plot consistency of results with a single equilibrium is indicated by the concordance of the points with a straight line, and the relative stoichiometry of the gaseous species in the equilibrium is given by the slope of the line.

The log plots of the present data are given in Fig. 1. For the lower half of the diagram (pressures below about 3 mm. of  $\text{BiI}_3$ ) the points fall reasonably well on the straight lines drawn at each temperature. Those lines were drawn at a slope of 3.0, so that the equilibrium obtained in that region was



The equilibrium constants for that reaction were calculated from the data on the straight lines and these were plotted vs. reciprocal of absolute temperature, as in Fig. 2, to give the enthalpy change for that reaction. Since a straight line represents the data well, the enthalpy change reaction 1 was constant in the temperature range studied and equal to  $21.1 \pm 0.8$  kcal. The standard free energy changes for the reaction derived from the equilibrium constants at 545 and 735° were  $7.80 \pm 0.1$  and  $4.76 \pm 0.1$  kcal., respectively. Thus the standard entropy change for reaction 1 at the mid-temperature (640°) was  $16 \pm 1$  e.u. Kelley<sup>4</sup> gives values for the absolute entropies of  $\text{Bi}(\text{l})$  and  $\text{BiI}$

(1) This work was made possible by the financial support of the Research Division of the United States Atomic Energy Commission.

(2) D. Cubicciotti, *J. Phys. Chem.*, **64**, 791 (1960).

(3) D. Cubicciotti, *ibid.*, **64**, 1506 (1960).

(4) K. K. Kelley, U. S. Bur. Mines Bull. No. 477 (1950) and No. 584 (1960).

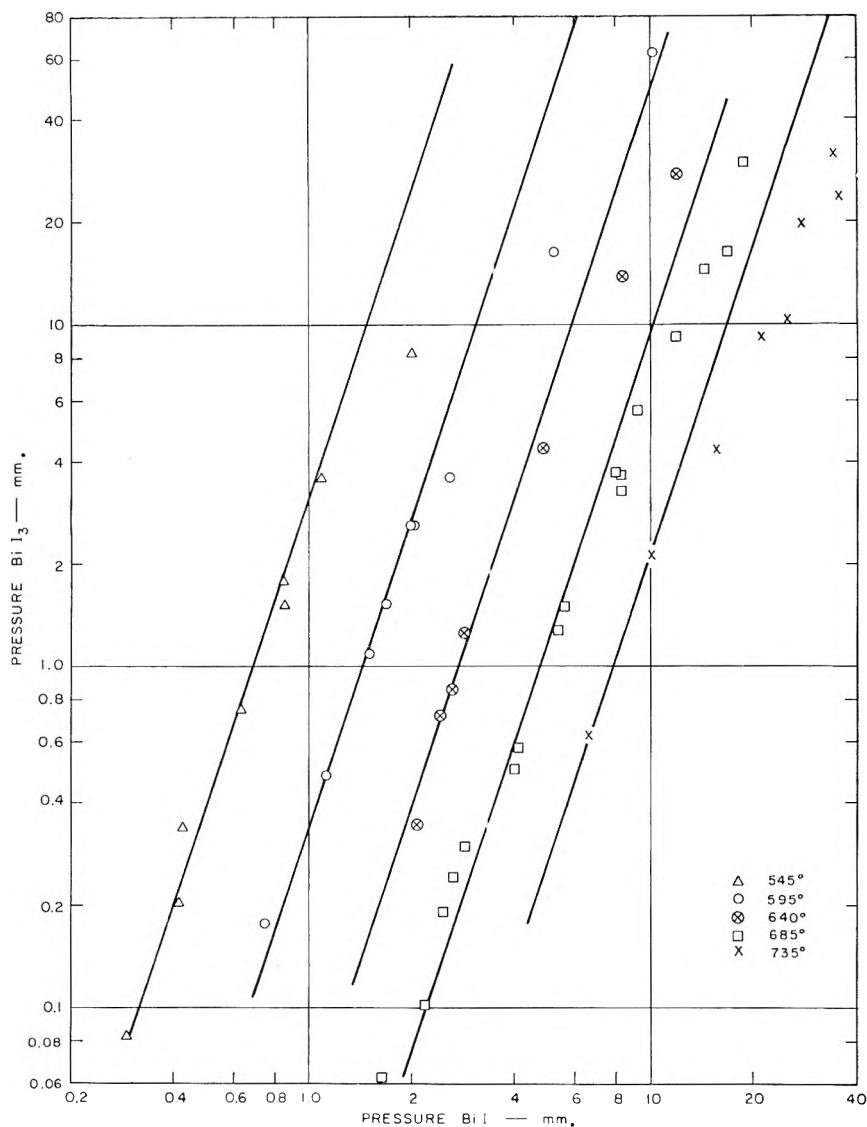


Fig. 1.—Logarithmic plot of pressure of  $\text{BiI}_3$  vs.  $\text{BiI}$  at 545, 595, 640, 685 and 735°. The straight lines were drawn with slope 3.0 through the lower pressure values.

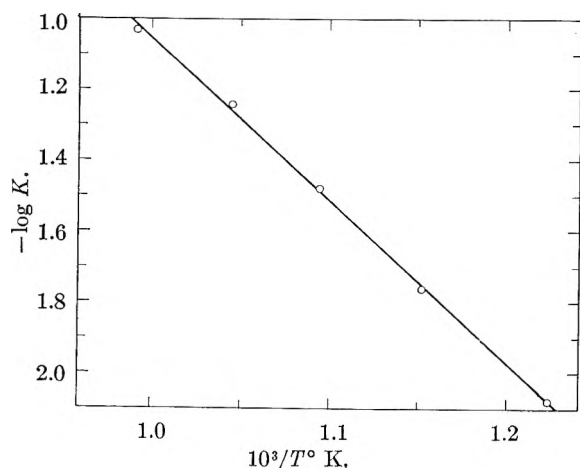


Fig. 2.—Logarithm of the equilibrium constant of reaction 1 vs. reciprocal of absolute temperature.

$\text{I}(\text{g})$ ; so the absolute entropy of  $\text{BiI}_3(\text{g})$  at 640° can be calculated to be  $126 \pm 5$  e.v. At present there are no reliable enthalpies of formation for

either iodide on which to base a calculation of the other. The dissociation energies of  $\text{BiI}(\text{g})$  reported<sup>5</sup> by Gaydon ( $2.5 \pm 1$  e.v.) and Herzberg (2.7 e.v.) are too doubtful to use for this purpose and there are no measured values for  $\text{BiI}_3$ .

In the higher pressure region (above about 3 mm.  $\text{BiI}_3$ ) it was apparent that the results were departing systematically from the lines representing the equilibrium of equation 1 (see Fig. 1). The departures were in the direction of an excess of lower-valent Bi over that expected from equation 1. They increased as the pressure increased and, when expressed as  $\text{BiI}$  in excess of equilibrium 1, became as large as 25% of the  $\text{BiI}$  pressure.

This excess of lower-valent Bi was felt to be an indication of polymerization of the  $\text{BiI}$  to form one or more new species of formula  $\text{Bi}_n\text{I}_n$ . Therefore, the difference between the experimental value of the pressure of  $\text{BiI}$  and the value calculated from the equilibrium constant derived from the low pressure values (*i.e.*, the value given by the straight lines in Fig. 1) was plotted on a log-log plot. The results were quite scattered since they represented small differences between large

numbers. Because of the scatter it was not possible to decide unequivocally on a value for  $n$ , the degree of polymerization. A value of three seemed best to the author but values of two and four were not unreasonable. This degree of polymerization could probably be derived better from some other type of experiment.

Attempts to fit the higher pressure data with equilibria involving  $\text{BiI}_2$  as well as  $\text{BiI}$  and  $\text{BiI}_3$  were unsuccessful. At a given temperature it was possible to account for the amount of Bi and I in each sample on this basis; however, it was not possible to fulfill the requirement of constancy of two concentration quotients among the three species from one sample to another.

An experiment to observe the species in the vapor with a mass spectrometer was made.  $\text{BiI}_3$  was passed over a heated Bi surface and then through a small orifice into the ionization chamber of a Bendix mass spectrometer. The temperature of

(5) See T. L. Cottrell, "The Strengths of Chemical Bonds," Butterworths, London, 2nd Ed., 1958.

the Bi and the pressure of the  $\text{BiI}_3$  were both varied. Peaks corresponding to  $\text{BiI}_3^+$ ,  $\text{BiI}_2^+$ ,  $\text{BiI}^+$  and  $\text{Bi}^+$  were observed. The relative intensities of these peaks for  $\text{BiI}_3$  only were: weak, medium, strong, medium, respectively; and for  $\text{BiI}_3$  passed over hot Bi they were: weak, medium, very strong and strong. The  $\text{BiI}^+$  and  $\text{Bi}^+$  peaks increased relative to the  $\text{BiI}_3^+$  as the temperature of the Bi in the cell was increased. There were no peaks at masses greater than 600 so that no polymers of BiI were observed, although the mass spectrometer was capable of detecting masses as great as 1000. Thus the experiment confirmed the presence of BiI in the vapor, and its increase as the Bi temperature was increased. It was felt that the polymer of BiI was not observed in this experiment because the vapor did not come to equilibrium with the Bi metal; therefore, the pressure of BiI was much lower than the equilibrium pressure, and that of the polymer was so much lower as not to be observable. It was estimated that the  $\text{BiI}_3$  in this experiment was in contact with the Bi for only one hundredth the time of contact found necessary in the transpiration experiments, so that presumably the equi-

librium concentration of BiI and  $\text{Bi}_n\text{I}_n$  did not have enough contact time to be formed.

A comparison of the three Bi-halide systems studied shows some regularities. The equilibrium constants for the formation of the monohalide (*cf.* reaction 1) tend to increase slightly in going from Cl to Br and from Br to I (*i.e.*, at  $600^\circ$ :  $K_{\text{Cl}} = 0.011$ ;  $K_{\text{Br}} = 0.014$ ;  $K_{\text{I}} = 0.019$ ). This increase is due to a progressively more favorable enthalpy change for the reaction which just barely overrides the progressively less favorable entropy change. In the iodide system there was evidence for a polymer of the monohalide at pressures of  $\text{BiI}_3$  above about 3 mm. In the chloride and bromide systems no evidence for polymers was observed; however, those systems were investigated at lower  $\text{BiX}_3$  pressures. It may well be that at higher pressures measurable amounts of polymers may be formed.

**Acknowledgments.**—The author is indebted to Mr. William E. Robbins, who performed the transpiration experiments, to Dr. Thomas A. Milne, who did the mass spectrometer experiment, and to Dr. Francis J. Keneshea, Jr. for fruitful discussions.

## HEAT OF SOLUTION OF ORTHOPHOSPHORIC ACID

BY EDWARD P. EGAN, JR., AND BASIL B. LUFF

*Division of Chemical Development, Tennessee Valley Authority, Wilson Dam, Alabama*

*Received October 6, 1960*

From measurements of the heat of solution of orthophosphoric acid over the range 0 to 89.13%  $\text{H}_3\text{PO}_4$ , tables were derived relating the relative apparent molal heat content ( $\phi_L$ ) and the partial molal heat contents ( $\bar{L}_2$ ,  $\bar{L}_1$ ) to concentration at intervals of 5%  $\text{H}_3\text{PO}_4$ . The molal heat of formation from the elements at  $25^\circ$  was calculated as a function of moles of water in solution.

The heat of solution of phosphoric acid in water was summarized by the National Bureau of Standards<sup>1</sup> from scattered values appearing before 1915. Another summary tabulation,<sup>2</sup> which drew upon unpublished work by TVA, had among its shortcomings a gap between 35 and 45%  $\text{H}_2\text{PO}_4$ .

This paper describes a redetermination of the heat of solution over the range 0 to 89.13%  $\text{H}_3\text{PO}_4$ . Measurements at higher concentrations would have been complicated by the presence of non-ortho forms of acid,<sup>3</sup> with their heats of hydrolysis.

**Materials and Apparatus.**—Reagent grade phosphoric acid was recrystallized twice as the hemihydrate. Stock solutions were prepared from the drained, unwashed crystals.

A solution calorimeter from earlier work<sup>4,5</sup> was modified in a few details. The capsule-type platinum resistance thermometer was exposed directly to the solution. The head of the thermometer was sealed into a small glass support tube with Apiezon W wax. The thermometer was suspended in the glass draft tube of the stirrer with the tip of the capsule a few millimeters above the impeller. A 100-ohm heater was wound directly on the outside of the draft tube.

Assembly and disassembly of the calorimeter were facilitated by attaching the head to the body by means of six small parallel-jawed spring clamps of a type used in sheet metal assembly. The clamps were completely covered by the water-bath and were without observable effect on the heat leak.

The initial bulk charge of liquid for each measurement (850 ml.) was weighed. Each incremental addition to the bulk liquid in the calorimeter was suspended inside the stirrer shaft in a thinwalled glass bulb which was crushed against the bottom of the Dewar to start the solution period.

The calorimeter system was calibrated electrically immediately before and after each measurement. One defined calorie was taken as 4.1840 abs. j. Temperatures were recorded to four decimal places, as small differences were important.

The conditions of measurement ensured a temperature rise of at least  $0.15^\circ$  for every observation. The temperature at the end of each measurement was  $25 \pm 0.05^\circ$ , and no temperature corrections were necessary. As the water-bath around the calorimeter was held at  $26 \pm 0.02^\circ$ , heat leaks were always in the same direction.

**Heats of Solution.**—The concentration range 0 to 83.6 molal (89.13%)  $\text{H}_3\text{PO}_4$  was covered in five series of measurements: Series 1:  $\text{H}_2\text{O}$  plus successive increments of 75.14%  $\text{H}_3\text{PO}_4$ ; final concentration, 49.4%  $\text{H}_3\text{PO}_4$ ; Series 2: same; Series 3:  $\text{H}_2\text{O}$  plus successive increments of 49.86%  $\text{H}_3\text{PO}_4$ ; final concentration, 17.0%  $\text{H}_3\text{PO}_4$ ; Series 4: 44.58%  $\text{H}_3\text{PO}_4$  plus successive increments of 89.13%  $\text{H}_3\text{PO}_4$ ; final concentration, 75%  $\text{H}_3\text{PO}_4$ ; Series 5: 89.13%  $\text{H}_3\text{PO}_4$  plus successive increments of  $\text{H}_2\text{O}$ ; final concentration, 72%  $\text{H}_3\text{PO}_4$ . Incremental

(1) National Bureau of Standards Circular 500, U. S. Govt. Printing Office, Washington, D. C., 1952.

(2) T. D. Farr, Tennessee Valley Authority, *Chem. Eng. Rept.*, No. 8 (1950).

(3) E. P. Egan, Jr., and Z. T. Wakefield, *J. Phys. Chem.*, **61**, 1500 (1957).

(4) E. P. Egan, Jr., B. B. Luff and Z. T. Wakefield, *ibid.*, **62**, 1091 (1958).

(5) E. P. Egan, Jr., Z. T. Wakefield and K. L. Elmore, *J. Am. Chem. Soc.*, **78**, 1811 (1956).



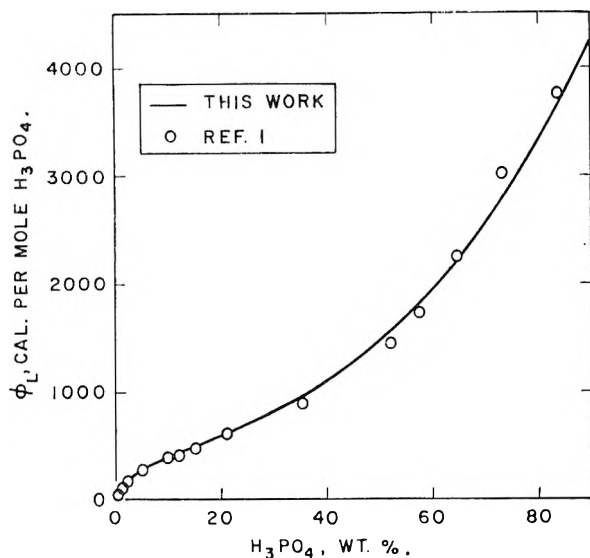


Fig. 1.—Relative apparent molal heat content of phosphoric acid solutions.

dilution of 90%  $\text{H}_3\text{PO}_4$  with water to a concentration approaching infinite dilution would have been more straightforward, but the construction of the calorimeter limited each addition to 35 ml. Dilution of 850 ml. of phosphoric acid solution with 35-ml. portions of water soon would have run into undesirably small increments of concentration and of heat.

The observed heat effects on a molal basis are shown in Table I. (For internal consistency, more significant figures were used in calculation than are shown in Table I.) The average deviation of the measured heats of solution was 0.3%.

Manipulative details in adjusting the end solution from a measurement to a weighed fixed volume of 850 ml. for the next measurement entailed loss of 1 to 2% of the solution. Linear corrections were made in sample weights and in heat effects to put initial and final solutions for each run on the same basis.

When small portions of 75.14 or 49.86%  $\text{H}_3\text{PO}_4$  were diluted with various amounts of water, the observed heat effects became increasingly exothermic with decrease in the final concentration. When plotted against final concentration, the heat of solution approached the axis at  $m = 0$  almost asymptotically. Unpublished calculations at TVA suggest that the degree of dissociation of  $\text{H}_3\text{PO}_4$  goes through a minimum at about 1.2 molal, then rises sharply to 1.0 at the axis where  $m = 0$ . A parallel behavior of the heats of solution in dilute solution indicates that the measured heats of solution in dilute solutions included heats of ionization.

The integral heats of solution in calories per mole  $\text{H}_3\text{PO}_4$  at the observed final concentrations are shown in Table II.

When the integral heats of solution of 75.14%  $\text{H}_3\text{PO}_4$  at final concentrations between 0.2 and 1.3 molal were plotted against  $m^{1/2}$ , the resultant straight line indicated a value of  $-2913$  cal. per mole  $\text{H}_3\text{PO}_4$  for the heat of solution at infinite dilution of 75.14%  $\text{H}_3\text{PO}_4$ . This value was subtracted from values of  $\Delta H$  at each final concentration to

yield values of  $\phi_L$ . From a similar plot between 0.5 and 1.6 molal, a value of  $-1497$  cal. per mole  $\text{H}_3\text{PO}_4$  was obtained for the heat of solution at infinite dilution of 49.86%  $\text{H}_3\text{PO}_4$ . Values of  $\phi_L$  calculated from the series 3 measurements with 49.86%  $\text{H}_3\text{PO}_4$  agreed with those calculated from series 1 and 2 with 75.14%  $\text{H}_3\text{PO}_4$ .

In series 4, the integral heats of solution resulting from solution of 89.13%  $\text{H}_3\text{PO}_4$  in an initial solution of 44.58%  $\text{H}_3\text{PO}_4$  were too far from the axis at  $m = 0$  for a satisfactory extrapolation against  $m^{1/2}$ . The intercept was calculated to be  $-4250$  cal. per mole  $\text{H}_3\text{PO}_4$  by successive approximations in the region where series 1 and 2 overlapped series 4.

In series 5, calculation of the heats of solution per mole of  $\text{H}_3\text{PO}_4$  for 89.13%  $\text{H}_3\text{PO}_4$  was straightforward. Two of the final solutions overlapped series 4. The measured heats of dilution were combined with values of  $\phi_L$  as calculated at the concentrations in the region of overlap between series 4 and 5 to obtain  $\phi_L$  between 70 and 89%  $\text{H}_3\text{PO}_4$ .

Calculated values of  $\phi_L$  in calories per mole  $\text{H}_3\text{PO}_4$  at the observed final concentrations are shown in Fig. 1 and Table II. The abscissas in Fig. 1 are expressed in weight per cent. instead of molality to avoid compression of the data at low molalities. The data summarized by NBS<sup>1</sup> agree reasonably well with the present measurements up to 20%  $\text{H}_3\text{PO}_4$ ; above 20%, the earlier data are somewhat scattered. The earlier TVA data<sup>2</sup> above 45%  $\text{H}_3\text{PO}_4$  are roughly parallel to the present data and about 120 cal. per mole higher.

The heats of formation of  $\text{H}_3\text{PO}_4$  at the lowest concentrations cited by NBS<sup>1</sup> were plotted against  $m^{1/2}$  and extrapolated to yield  $-309,440$  cal. per mole  $\text{H}_3\text{PO}_4$  as the heat of formation at infinite dilution. This value was combined with the smoothed values of  $\phi_L$  to relate heat of formation to concentration in handbook-type Table III.

TABLE I OBSERVED HEATS OF SOLUTION OF $\text{H}_3\text{PO}_4$ SOLUTIONS					
$m_1(\text{H}_3\text{PO}_4 \cdot n_1 \text{H}_2\text{O}) + m_2(\text{H}_3\text{PO}_4 \cdot n_2 \text{H}_2\text{O}) = m_3(\text{H}_3\text{PO}_4 \cdot n_3 \text{H}_2\text{O})$					
$m_1$	$n_1$	$m_2$	$n_2$	$n_3$	Q, cal.
Series 1, 75.14% $\text{H}_3\text{PO}_4$ stock soln. ( $n_2 = 1.80$ )					
0	(46.998)	0.2787	0.2787	170.426	761.56
0.2720	170.426	.3005	.5724	81.915	758.15
.5568	81.915	.3858	.9426	49.125	929.03
.9094	49.125	.3028	1.2121	37.304	701.13
1.1792	37.304	.2908	1.4700	30.281	648.47
1.4299	30.281	.3100	1.7400	25.206	664.92
1.6910	25.206	.2938	1.9449	21.741	605.96
1.9310	21.741	.2992	2.2302	19.065	593.41
2.1684	19.065	.2829	2.4512	17.073	538.36
2.3885	17.073	.2976	2.6861	15.381	543.89
2.6102	15.381	.3534	2.9636	13.761	615.13
2.8647	13.761	.3049	3.1696	12.610	504.95
3.0806	12.610	.2597	3.3403	11.770	409.99
3.2533	11.770	.3266	3.5799	10.860	499.46
3.4681	10.860	.2478	3.7160	10.256	364.33
3.6340	10.256	.3131	3.9470	9.585	435.07
3.8315	9.585	.3498	4.1814	8.934	461.58
4.0432	8.934	.2839	4.3271	8.466	355.51
4.2149	8.466	.3236	4.5385	7.990	387.17
4.3696	7.990	.2883	4.6580	7.607	327.65
4.5640	7.607	.3149	4.8789	7.232	340.37

$m_1$	$n_1$	$m_2$	$m_3$	$n_3$	Q, cal.
4.7308	7.232	.3548	5.0855	6.853	362.65
4.9228	6.853	.3170	5.2398	6.547	306.79
5.0802	6.547	.3324	5.4126	6.256	303.22
5.2428	6.256	.3003	5.5432	6.015	259.59
5.3836	6.015	.2977	5.6814	5.794	245.19
5.5260	5.794	.3421	5.8681	5.561	266.24

Series 2, 75.14% H<sub>3</sub>PO<sub>4</sub> stock soln. ( $n_2 = 1.800$ )

0	46.980	0.1948	0.1949	242.833	538.49
0.1917	242.833	.3490	.5408	87.243	889.86
.5235	87.243	.1779	.7014	65.573	436.29
.6899	65.573	.3599	1.0497	43.711	853.77
1.0155	43.711	.3423	1.3577	33.147	775.17
1.3153	33.147	.3293	1.6447	26.870	716.20
1.5940	26.870	.3330	1.9270	22.537	693.90
1.8686	22.537	.3226	2.1912	19.485	641.47
2.1260	19.485	.3530	2.4790	16.967	671.33
2.3993	16.967	.3459	2.7452	15.055	627.55
2.6573	15.055	.3060	2.9634	13.686	528.03
2.8781	13.686	.2808	3.1589	12.630	465.02
3.0768	12.630	.3260	3.4028	11.592	514.41
3.2989	11.592	.3049	3.6038	10.764	459.20
3.5016	10.764	.3129	3.8146	10.028	446.97
3.7037	10.028	.2947	3.9984	9.422	401.80
3.8878	9.422	.3678	4.2556	8.763	474.74
4.1105	8.763	.3466	4.4571	8.221	421.93
4.3115	8.221	.3819	4.6934	7.699	439.45
4.5256	7.699	.3732	4.8989	7.249	401.96
4.7283	7.249	.3592	5.0874	6.865	364.06
4.9192	6.865	.3759	5.2951	6.505	356.98
5.1060	6.505	.3550	5.4610	6.199	317.58
5.2811	6.199	.3633	5.6444	5.916	306.41
5.4521	5.916	.3466	5.7987	5.670	276.17
0	(46.971)	.0083	0.0083	5633.8	29.45
0	(46.979)	.0093	.0093	5042.5	31.48
0	(46.965)	.0105	.0105	4478.9	35.55
0	(47.001)	.0128	.0128	3668.0	41.70
0	(46.990)	.0145	.0145	3247.0	48.54
0	(46.994)	.0149	.0149	3164.3	49.22
0	(47.009)	.0218	.0218	2153.2	69.85
0	(47.002)	.0349	.0349	1347.4	108.09
0	(46.984)	.0427	.0427	1101.6	127.55
0	(47.009)	.0640	.0640	736.0	190.71
0	(46.990)	.0737	.0737	639.6	215.63
0	(47.028)	.0904	.0904	522.2	257.82
0	(46.971)	.1290	.1290	365.8	368.27

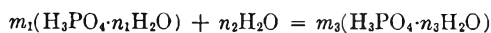
Series 3, 49.86% H<sub>3</sub>PO<sub>4</sub> stock soln. ( $n_2 = 5.470$ )

0	(47.031)	0.1831	0.1831	263.047	252.20
0.1771	263.047	.1981	.3751	127.039	229.57
.3629	127.039	.1873	.5502	85.644	202.44
.5330	85.644	.1890	.7221	64.658	194.20
.6995	64.658	.1854	.8849	52.256	180.76
.8575	52.256	.1809	1.0384	44.105	167.03
1.0070	44.105	.1940	1.2010	37.866	171.37
1.1619	37.866	.2009	1.3629	33.090	167.88
1.3172	33.090	.1894	1.5066	29.618	149.79
1.4594	29.618	.1816	1.6410	26.946	138.00

Series 4, 89.13% H<sub>3</sub>PO<sub>4</sub> stock soln. ( $n_2 = 0.663$ )

4.9700	6.761	0.4742	5.4442	6.230	976.02
5.2614	6.230	.4657	5.7271	5.777	915.11
5.5376	5.777	.4638	6.0014	5.382	853.92
5.8047	5.382	.4619	6.2666	5.034	805.35
6.0625	5.034	.4740	6.5365	4.717	782.23
6.3176	4.717	.4372	6.7548	4.455	678.59
6.5430	4.455	.4713	7.0143	4.200	695.45

6.7775	4.200	.4936	7.2711	3.960	686.99
7.0158	3.960	.4732	7.4890	3.752	618.93
7.2438	3.752	.4577	7.7015	3.568	566.76
7.4438	3.568	.4791	7.9229	3.393	558.22
7.6502	3.393	.4106	8.0608	3.254	453.94
7.8278	3.254	.4888	8.3166	3.101	512.13
8.0189	3.101	.4530	8.4719	2.971	445.44
8.1989	2.971	.5016	8.7005	2.838	466.00
8.3965	2.838	.4703	8.8768	2.713	410.69
8.5728	2.713	.4491	9.0219	2.611	369.05
8.7295	2.611	.4219	9.1514	2.521	328.31
8.8669	2.521	.4296	9.2965	2.435	317.36
9.0187	2.435	.4545	9.4732	2.350	316.24
9.1537	2.350	.4821	9.6358	2.266	314.39
9.3126	2.266	.4961	9.8087	2.185	304.15
9.4508	2.185	.4316	9.8824	2.118	250.40
9.4876	2.118	.4482	9.9358	2.053	245.73
9.6957	2.053	.4611	10.1568	1.990	238.22
9.8216	1.990	.4816	10.3032	1.928	233.04
9.9369	1.928	.4654	10.4023	1.871	211.33
10.0559	1.871	.4015	10.4574	1.825	173.76



Series 5, dilution of 89.13% H<sub>3</sub>PO<sub>4</sub>

13.2810	0.663	1.3050	13.2810	0.762	2038.38
12.9221	.762	1.5105	12.9221	.879	2200.66
12.5948	.879	1.4451	12.5948	.993	1934.59
12.2280	.993	1.3368	12.2280	1.103	1655.98
11.9247	1.103	1.4463	11.9247	1.224	1674.98
11.5815	1.224	1.6910	11.5815	1.370	1794.70
11.2086	1.370	1.7677	11.2086	1.528	1710.00
10.8277	1.528	1.5545	10.8277	1.671	1375.51
10.4902	1.671	1.5267	10.4902	1.817	1244.86
10.1673	1.817	1.5641	10.1673	1.970	1172.55
9.8638	1.970	1.5249	9.8638	2.125	1055.80

**Partial Molal Heat Contents.**—Values of  $\phi_L$  from Table II were fitted to polynomials in molality and weight fraction over various ranges of concentration and with various functions of the variables. The equations giving the best fit were

$$\phi_L = 369.50m^{1/2} \quad m = 0 \text{ to } 1.5 \quad (1)$$

$$\phi_L = 180.46 + 185.45m + 22.08m^2 - 22.33m^3 + 4.03m^4 \quad m = 1.5 \text{ to } 2.5 \quad (2)$$

$$\phi_L = 292.06 + 923.79w + 3374.87w^2 - 2478.92w^3 + 3473.99w^4 \quad m = 2.5 \text{ to } 85.0 \quad (3)$$

where  $m$  = molality and  $w$  = weight fraction of H<sub>3</sub>PO<sub>4</sub>. The mean probable error in equations 1 and 3 is 2.5 cal. per mole H<sub>3</sub>PO<sub>4</sub>—in equation 2, 0.2 cal. per mole.

A deviation of 2.5 cal. per mole is well within the error of observation, but smooth slopes at the point of overlap of two equations require first differences with deviations of 0.1 cal. per mole or less. The slopes at the points of overlap thus show slight breaks that seem unavoidable without resort to a more elaborate method of representation.

Relative partial molal heat contents at molalities up to 2.5 were calculated by conventional methods.<sup>5</sup> Above 2.5 molal, the slope  $\partial\phi_L/\partial m$  was converted analytically to the slope in terms of weight fraction,

(5) S. Glasstone, "Thermodynamics for Chemists," D. Van Nostrand Co., Inc., New York, N. Y., 1947.

TABLE II

HEAT OF SOLUTION AND RELATIVE APPARENT MOLAL HEAT CONTENT AT OBSERVED FINAL CONCENTRATION, CAL. PER

Molality	MOLE H <sub>3</sub> PO <sub>4</sub>		Molality	-ΔH	φ <sub>L</sub>
	-ΔH	φ <sub>L</sub>			
Series 1, 75.14% H <sub>3</sub> PO <sub>4</sub>					
0	2931	0	5.1110	2007	924
0.3257	2733	198	5.4122	1971	960
0.6776	2623	308	5.7908	1925	1006
1.1299	2535	396	6.2131	1874	1057
1.4880	2480	451	6.5567	1833	1098
1.8330	2431	500	6.9469	1788	1143
2.2021	2380	551	7.2969	1748	1183
2.5531	2333	598	7.6750	1705	1226
2.9114	2286	645	8.0993	1657	1274
3.2511	2242	689	8.4776	1615	1316
3.6088	2196	735	8.8726	1572	1359
4.0336	2141	789	9.2287	1534	1397
4.4016	2095	836	9.5806	1497	1434
4.7160	2055	876	9.9818	1455	1476
Series 2, 75.14% H <sub>3</sub> PO <sub>4</sub>					
0	2931	0	4.7882	2042	889
0.2252	2763	168	5.1568	1996	935
.6362	2625	306	5.5350	1949	982
.8465	2581	349	5.8913	1906	1025
1.2698	2510	421	6.3342	1853	1078
1.6746	2448	483	6.7514	1804	1127
2.0658	2394	537	7.2096	1751	1180
2.4628	2340	591	7.6686	1699	1232
2.8486	2288	643	8.0858	1651	1280
3.2715	2233	698	8.5327	1601	1330
3.6868	2180	751	8.9538	1556	1375
4.0555	2134	797	9.3823	1509	1422
4.3949	2091	840	9.7894	1467	1464
Series 3, 49.86% H <sub>3</sub> PO <sub>4</sub>					
0	1497	0	1.2589	1084	413
0.2116	1378	119	1.4663	1051	446
.4374	1262	235	1.6779	1020	477
.6486	1201	296	1.8745	991	506
.8589	1155	342	2.0603	965	532
1.0626	1118	379			
Series 4, 89.13% H <sub>3</sub> PO <sub>4</sub>					
0	4250	0	19.5570	1944	2306
8.9080	2884	1366	20.3856	1887	2363
9.6060	2809	1441	21.1841	1834	2416
10.3115	2734	1516	21.9403	1785	2465
11.0240	2661	1589	22.7155	1737	2513
11.7648	2588	1662	23.5391	1687	2563
12.4578	2521	1729	24.4179	1635	2615
13.2135	2451	1799	25.3257	1583	2667
14.0147	2379	1871	26.1219	1539	2711
14.7929	2311	1939	26.9590	1495	2755
15.5539	2247	2003	27.8157	1450	2800
16.3593	2182	2068	28.7123	1405	2845
17.0584	2127	2123	29.5822	1362	2888
17.8959	2064	2186	30.3356	1327	2923
18.6811	2006	2244			
Series 5, diln. 89.13% H <sub>3</sub> PO <sub>4</sub>					
83.671	0	4240	40.520	908	3332
72.878	154	4086	36.337	1061	3179
63.181	324	3916	33.216	1188	3052
55.881	478	3762	30.555	1307	2933
50.340	613	3627	28.170	1422	2818
44.445	753	3487	25.599	1539	2701

TABLE III

HEATS OF FORMATION OF PHOSPHORIC ACID SOLUTIONS, KCAL. PER MOLE H<sub>3</sub>PO<sub>4</sub> AT 298.16°K.

n <sub>H<sub>2</sub>O</sub>	-ΔH <sub>f</sub> <sup>o</sup>	n <sub>H<sub>2</sub>O</sub>	-ΔH <sub>f</sub> <sup>o</sup>
1	+305.68	100	309.16
2	306.64	200	309.25
3	307.21	300	309.28
4	307.59	400	309.30
5	307.84	500	309.32
6	308.04	700	309.34
8	308.29	1000	309.35
10	308.46	2000	309.38
12	308.57	3000	309.39
15	308.69	4000	309.40
20	308.81	5000	309.40
25	308.88	7000	309.41
30	308.94	10,000	309.41
40	309.00	20,000	309.42
50	309.05	50,000	309.43
75	309.12	100,000	309.43
		∞	309.44

$\partial\phi_L/\partial w$ . Table IV, in concentration increments of 5%, was derived from the results.

TABLE IV

RELATIVE PARTIAL MOLAL HEAT CONTENTS OF H<sub>3</sub>PO<sub>4</sub> SOLUTIONS, CAL. PER MOLE H<sub>3</sub>PO<sub>4</sub>

H <sub>3</sub> PO <sub>4</sub> , wt. %	φ <sub>L</sub>	$\bar{L}_2$	$-\bar{L}_1$
0	0	0	0
5	271	406	1.313
10	346	590	4.020
15	498	754	8.288
20	598	931	15.35
25	709	1152	27.15
30	834	1392	43.92
35	975	1651	66.91
40	1144	1929	100.2
45	1308	2229	138.5
50	1505	2549	192.0
55	1727	2889	261.3
60	1976	3247	350.6
65	2258	3619	464.9
70	2576	3998	609.9
75	2937	4374	792.7
80	3345	4733	1021
85	3807	5059	1305
90	4328	5328	1653

The measurements were not extrapolated to 100% H<sub>3</sub>PO<sub>4</sub>. The heat of formation of H<sub>3</sub>PO<sub>4</sub>(aq) is taken as -309,440 cal. per mole, the heat of formation of H<sub>3</sub>PO<sub>4</sub>(c)<sup>1</sup> as -306,200 cal. per mole. If the heat of fusion is taken as 3100 cal. per mole,<sup>3</sup> then the increment H<sub>3</sub>PO<sub>4</sub>(1-aq) should be 6340 cal. per mole H<sub>3</sub>PO<sub>4</sub>. The equation for φ<sub>L</sub> at high molalities extrapolates smoothly to 5585 cal. at 100% H<sub>3</sub>PO<sub>4</sub>. It is not clear whether the curve for φ<sub>L</sub> should turn up sharply above 90% H<sub>3</sub>PO<sub>4</sub> to an intercept of 6340 or whether the value for the heat of formation of H<sub>3</sub>PO<sub>4</sub>(aq) or that for H<sub>3</sub>PO<sub>4</sub>(c) is in error by about 800 cal., which is within the accuracy with which they are known.

The present results affect the values reported in an article<sup>4</sup> on the heat capacity of phosphoric acid solutions. Revisions of Tables V through VIII in that article will be submitted for publication.

## HYDROGEN ATOM EXCESSES IN SOME PROPANE FLAMES

BY ROBERT REID<sup>1</sup> AND ROBERT WHEELER*Department of Chemistry, Queen's University, Kingston, Ontario*

Received October 7, 1960

Concentrations of atomic hydrogen have been determined at various heights in some pre-mixed propane-air flames. Excesses were noted early in the burnt gases, these being relatively larger for lean (fuel) flames and smaller for rich flames, the direct reverse of observations in hydrogen flames. The rise-velocities of the burnt gases have been measured and used to establish reaction velocity parameters consistent with ternary recombination of the excesses.

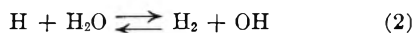
## Introduction

Sugden and co-workers,<sup>2-5</sup> have applied various emission spectrophotometric techniques to measure the atomic hydrogen and hydroxyl radical concentrations in the burnt gases of atmospheric hydrogen-air flames. Their results show that [H] becomes increasingly excessive of the equilibrium amount, as the flames are made more hydrogen rich. This is paralleled by similar excesses in [OH] and [O] measured by independent means.<sup>6,7</sup> Fenimore and Jones<sup>8,9</sup> have sampled through a fine quartz probe the combustion products of organic as well as inorganic fuels. Adding small quantities of heavy water to the gas supply, they analyzed samples from the burnt gases mass-spectrographically and were able to determine [H] at several positions. Their results for H<sub>2</sub>-air mixtures corroborate those of Sugden's group. In contrast, their findings for the very fuel-rich, low-temperature, hydrocarbon flames showed the theoretical equilibrium or lower concentration throughout. Apparently, the carrying over of an excess of organic fuel into the burnt gases is not accompanied by large amounts (greater than equilibrium) of atomic hydrogen.

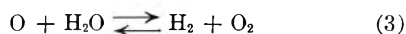
Whether or not the value of [H] entering the burnt gases is above its thermodynamic equilibrium value, [H]<sub>e</sub>, a similar relationship to its equilibrium concentration is expected for each member of the group, OH, O<sub>2</sub> and O. Very soon after departing the primary zone, a partial chemical equilibrium should establish to a degree that

$$\frac{[H]}{[H]_e} = \frac{[OH]}{[OH]_e} = \frac{[O_2]^{1/4}}{[O_2]_e^{1/4}} = \frac{[O]^{1/2}}{[O]_e^{1/2}} \quad (1)$$

[H] and [OH] are equilibrated by the fast reaction<sup>2,9</sup>

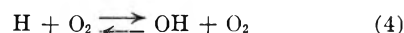


while the reaction



should be balanced<sup>10</sup> through the very fast bi-

molecular exchange<sup>9</sup>



In flames of organic fuels, the quasi-equilibrium of equation 1 will certainly be assisted by the reaction



this<sup>11</sup> being only somewhat slower than 2.

A photometric technique developed by Sugden and collaborators has been applied here to some propane-air flames burning at atmospheric pressure. These results show some evidence that [H] is initially in excess even in very rich mixtures.

## Experimental

**Burner and Supply.**—Metered quantities of propane and air with added nitrogen or argon were mixed and burned at a Meker type burner of 7.8 cm. diameter. This burner was mounted on a telescoping brass tube, permitting movement in the vertical direction. Very small but equal amounts of lithium and sodium chloride solutions were atomized into an isolated gas supply to the very center of the flame (3.8 cm. diam.). This resulted in a uniform flame with respect to the fuel and air supply but in the very center of which appeared minute quantities of evaporated sodium and lithium atoms whose partial pressures in the burnt gases were each approximately 10<sup>-7</sup> atm. The outer annular flame acted as thermal shield against self-absorption of the radiation at the flame edge.

**Photometric System.**—Radiation from selected heights in the very center of the flame was focused at the entrance slit of a direct reading Farrand grating monochromator. The width of the entrance slit was 0.01 cm. and its height for the flames investigated was found to be maximally 0.05 cm. At a magnification of 1.0 the source of radiation was limited to 0.04 cm.<sup>2</sup> by suitably situated optical stops. A 1P 21 electron multiplier photo-tube operating at about 100 v. per stage was mounted behind the exit slit. A sectored disc operating at 465 c./sec. chopped the radiation falling on the entrance slit with provision made to prevent draughts. The resulting alternating signal was amplified, rectified and measured on a damped sensitive but selective voltmeter. Because the flame front was not totally flat, attention was directed to the burnt gases at some distance above the burner top and upwards on the central flame axis. Measurements of the intensities of the sodium-d-lines at 5893 Å. and the lithium red lines at 6707 Å. were made at identical points and the ratio of these used with the measured temperature to deduce [H] at each point.

**Temperature Measurements.**—Flame temperatures were measured by the usual sodium-d line reversal method,<sup>12</sup> using a tungsten strip filament background source. The reversal point was determined by a photometric scanning technique rather than by eye. The burnt gas temperatures measured in this manner, ranging from 1850–2400°K., were verified by a similar reversal of the lithium doublet.

**Rise-Velocity Determinations.**—In order to convert observations of intensity from a distance to a time scale, a measure of the velocity with which the burnt gases ascend vertically from the reaction zone was made. A simple rotating drum camera was used to photograph the traces of small

(1) Department of Physical Chemistry, University of Cambridge, England.

(2) E. M. Bulewicz, C. G. James and T. M. Sugden, *Proc. Roy. Soc. (London)*, **A235**, 89 (1956).

(3) P. J. Padley and T. M. Sugden, *ibid.*, **A248**, 248 (1958).

(4) E. M. Bulewicz and T. M. Sugden, *Trans. Faraday Soc.*, **54**, 1855 (1958).

(5) C. G. James and T. M. Sugden, *Proc. Roy. Soc. (London)*, **A248**, 238 (1958).

(6) E. M. Bulewicz and T. M. Sugden, *Trans. Faraday Soc.*, **52**, 1481 (1956).

(7) C. G. James and T. M. Sugden, *Nature*, **175**, 252 (1955).

(8) C. P. Fenimore and G. W. Jones, *J. Phys. Chem.*, **62**, 693 (1958).

(9) C. P. Fenimore and G. W. Jones, *ibid.*, **63**, 1834 (1959).

(10) C. P. Fenimore and G. W. Jones, *ibid.*, **62**, 178 (1958).

(11) C. P. Fenimore and G. W. Jones, *ibid.*, **62**, 1578 (1958).

(12) A. G. Gaydon and H. G. Wolfhard, "Flames, Their Structure, Radiation and Temperature," Chapman and Hall, London, 1960.

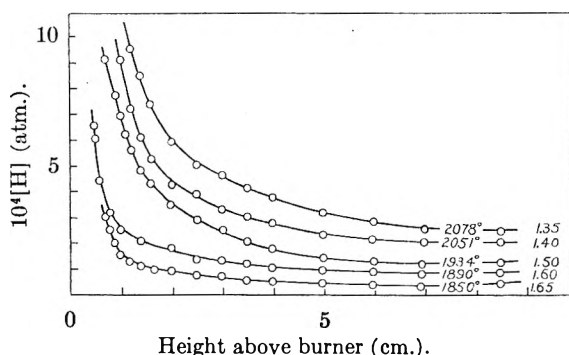


Fig. 1.—Axial hydrogen atom concentrations in flames of various pre-burnt mixture strengths (propane/stoichiometric propane), absolute temperatures are shown for the steady state.

quantities of aluminum particles introduced in the flame gas supply to the very center of the burner only. The drum of the camera was 64 cm. in circumference and rotated at 78 rev./min. with its surface in the focal plane of the camera. A vertical slit system was used to record only those traces of particles ascending near the center of the flame. The velocity  $V_m$  of the traces can be calculated from  $V_m = (64 \pi T \tan \theta) / s$  cm./sec., where  $r$  = the distance between the camera lens and the flame,  $s$  = the distance between the lens and the film,  $T$  = the angular speed of the drum in rev./sec., and  $\theta$  = the angle between the trace marks and the perpendicular to the axis of rotation of the drum.

Four different grades of aluminum particles were used in a series of experiments. Three of the samples were graded flat particles with surface areas of  $1.5 \times 10^4$ ,  $2.8 \times 10^4$ ,  $5 \times 10^4$  cm.<sup>2</sup>/g., the fourth was an atomized sample of considerably smaller specific surface. Particles were introduced in the gas supply by suspending them on a wire gauze fitted to a detachable Pyrex container just beneath the burner. Slight vibrations of the container were sufficient to carry the particles into the flame.

In the measurements, we found no variations in  $\tan \theta$  with particle size, indicating that the particles employed were sufficiently small to obviate a size factor correction. A simple graphical method was used to establish the most frequently occurring value of  $\tan \theta$  for each flame. Values of  $\theta$  were distributed over about  $5^\circ$  in each flame, the error of measurement in this angle being about 1%. Both this and the systematic error resulting from the effect of gravitational force on the aluminum particles (<1%) are small considered to the distribution in  $\theta$ . Alkemade<sup>13</sup> has made similar particle-track measurements in various hydrocarbon flames and invariably obtained measured gas velocities lower than the calculated theoretical values ( $V_m \sim 72\%$  of the calculated value). He attributes the extent of the angular distribution to a real dispersion of the flame gases. The precautions taken here of careful shielding and the use of a slit device to isolate the central column of gases make it appear more likely that the slower particles result from collisions at and near the burner top.

Results for a series of flame families of varying total gas flow show that  $\tan \theta$  is very nearly linearly dependent on the total initial gas flow. For most flames, maximum values of  $\theta$  were observed when the mixture strength approached stoichiometry, *i.e.*, the hottest flames. When we calculated the rise-velocity,  $V_T$ , based on gaseous thermal expansion and the maximum flame diameter, experimentally determined by the use of incandescent platinum probes, reasonably good agreement was found between  $V_T$  and  $V_m$ . On the other hand, the use of the burner diameter in the calculation usually leads to values of  $V_T$  greater than, but in some rare cases less than,  $V_m$ . This scatter and unpredictability is largely removed by measuring the actual flame diameter, in which case the calculated gas velocity seems reliable.

[H] from Intensity Measurements.—When equal quantities of sodium and lithium salts are atomized into identical flames, the intensity of the lithium resonance radiation is usually much reduced from that of the sodium. Bulewicz, James and Sugden<sup>2</sup> show how [H] may be deduced from the measurement of the ratio of these intensities. We used 0.004

$M$  solutions of lithium and sodium chlorides at which dilution the effect of self-reversal of the radiation was negligible in a shielded flame.

The free lithium atom population is depleted by



forming stable gaseous LiOH and reducing the intensity of the red lines. Moreover, this reaction is expected to be equilibrated in the burnt gas region. Therefore

$$[\text{H}] = K_6[\text{H}_2\text{O}] \frac{[\text{Li}]}{[\text{LiOH}]}, \quad K_6 = \frac{[\text{LiOH}][\text{H}]}{[\text{Li}][\text{H}_2\text{O}]}$$

The measured ratio of line intensity  $I(\text{Na})/I(\text{Li})$  at any point is equal to  $m(1 + [\text{LiOH}]/[\text{Li}])$ , with  $m$  being an easily determined instrument factor. The value of  $K_6$  at any temperature may be calculated from equilibria data<sup>14,15</sup> for the dissociation of (a)  $\text{H}_2\text{O} \rightarrow \text{H} + \text{OH}$ , (b)  $\text{LiOH} \rightarrow \text{Li} + \text{OH}$ .  $[\text{H}_2\text{O}]$  is sufficiently large in these flames that the calculated equilibrium values may be used.

## Results and Discussion

[H] Excesses.—Figure 1 is a representative set of results for the determination of [H] at numerous heights for various mixture strengths on the rich side of stoichiometry (mixture strength = actual propane/stoichiometric propane). The flames in the set have differing final temperatures but all have the same pre-burnt gas flow, 20 l./min. Other data at different flow rates showed similar form and nature. These fuel-rich flames provide the closest approach to isothermicity in the burnt gases; the flame with the lowest over-all temperature and smallest numerical gradient (1940–1850°K.) over 8 cm. of flame height had a mixture strength of 1.65. Small quantities of argon were added to the gas supply to obtain the lowest temperatures.

Initially [H] is in excess of its theoretical value but after a few milliseconds, an almost constant minimum value is reached with which persists throughout most of the flame's height. The constancy of the steady-state value suggests that this is the equilibrium value  $[\text{H}]_e$ . The flame front was not ideally flat, having a typical "waffle-like" surface and measurements made close to the top of the front were scattered and not totally reproducible. Nevertheless, it is evident that excesses in [H] are present just entering the burnt gases, but these are not large. In the lowest temperature flame in the set shown in Fig. 1, the value of [H] just above the flame front is very close to that of  $[\text{H}]_e$  while a  $\text{H}_2$ -air flame of approximately the same temperature (1800°K.) shows<sup>2</sup>  $[\text{H}] \sim 30[\text{H}]_e$ . A cross comparison of any one set of flames in a family at the same height illustrates an interesting trend. The relative degree of excess in [H] as it leaves the reaction zone, as expressed by  $[\text{H}]/[\text{H}]_e$  is least for the richest of flames and increases as the gas supply is made leaner. This is displayed in Table I where the above ratio is calculated at the near equivalent flame point of 1 cm. for the family in Fig. 1. This is the direct reverse of the behavior in  $\text{H}_2$ -air flames and is in accordance with the expectations of Fenimore and Jones.<sup>9</sup>

Burnt equilibrium concentrations were calcu-

(14) B. Lewis and G. von Elbe, "Combustion, Flames and Explosions of Gases," Academic Press, New York, N. Y., 1951.

(15) H. Smith and T. M. Sugden, *Proc. Roy. Soc. (London)*, **A219**, 204 (1953).

(13) C. T. J. Alkemade, Dissertation, University of Utrecht, 1954.

lated by the procedure of Gaydon and Wolfhard<sup>12</sup> using our measured temperatures combined with their data, and equilibrium constants from Lewis and von Elbe.<sup>14</sup> The theoretical values,  $[H]_T$ , so calculated were of the same order but characteristically higher than  $[H]_e$ . For the family in Fig. 1,  $[H]_e = 0.44 [H]_T$  throughout. This is not thought to be entirely the result of errors in the temperature measurement or in the calibration of the optical pyrometer used to measure the brightness temperatures of the tungsten strip filament. In most flames above, the temperature would have to alter by 100°K. in order to close the difference.  $[H]_e$  was, of course, measured well up the flame (7 cm.) where shielding by the outer flame is least efficient. However, removal of the shield leads to erroneously high estimates of  $[H]_e$ . Unshielded low-temperature flames have, in fact, shown a minimum in  $[H]$  at a point well up in the burnt gases. This has been attributed<sup>15</sup> to self absorption of the resonance radiation at the flame edges, mainly the D-lines. Figure 2 further argues for the measured value  $[H]_e$ , being accepted as the true equilibrium value. In these flames, the variation in  $[H_2]$  is almost insignificant and the plot of  $\log [H]_e$  against  $1/T$  is reasonably linear and has  $\epsilon$  slope corresponding to an energy of dissociation,  $H_2 \rightarrow 2H$ , of 103 kcal./mole.

The results obtained in some leaner flames are shown in Fig. 3. These faster burning mixtures were visibly inadequately shielded beyond 4 or 5 cm. above the burner top. Secondary combustion with entrained air at the edges caused a peak in both temperature and  $[H]$  on the rich side of stoichiometry. Rather steep temperature gradients up these flames brought about a decay of  $[H]$  beyond about 3 cm. and therefore no leveling off to a steady-state value was observed. Nevertheless, the lean flames do show excesses in  $[H]$  and these excesses are found to decay at similar rates to those in the more isothermal fuel-rich flames.

The existence of excesses of carbon-containing radicals in the burnt gases of organic flames is a matter for conjecture at the moment. The quantities of C, CH and  $C_2$  required for full equilibrium in this region are extremely small, being, respectively, some  $10^{12}$ ,  $10^{13}$  and  $10^{23}$  times smaller than  $[H]_e$  or  $[OH]_e$ . An excess of several orders of magnitude in any or all of the organic radicals would still result in a minute concentration and be difficult to detect. There is a suggestion here however, that this group and the inorganic group OH, H and O are closely linked in their primary zone reactions. The trend in Table I shows that where an excess of organic free radicals might be expected to issue forth into the burnt gases (high fuel/oxidant ratio), near equilibrium concentrations of the inorganics H, OH, and O are actually found. Certain fuel fragments are then probably oxidized by OH and O in preference to  $H_2O$ ,  $CO_2$  or CO. The work of Fenimore and Jones supports the view that CO, in hydrocarbon flames, is only formed from the reaction of the

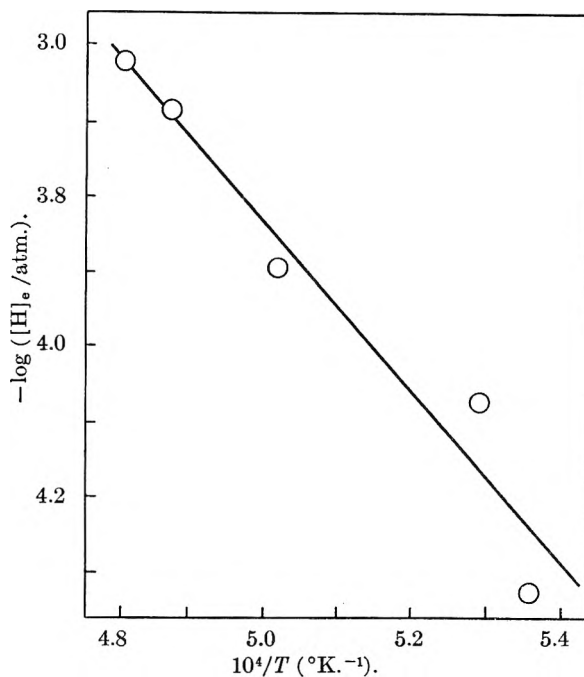


Fig. 2.—A plot of  $\log [H]_e$  against  $1/T$  for the flames in Fig. 1.

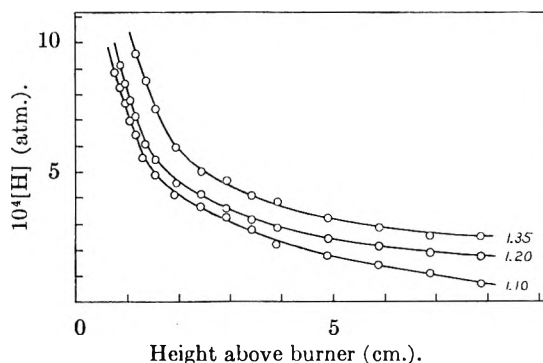


Fig. 3.—Axial hydrogen atom concentrations in some leaner flames.

fuel fragments with members of the species OH, O or  $H_2O$  and not directly with  $O_2$ , although an oxidation with  $O_2$  cannot be ruled out here if the equality of equation 1 is established quickly.

Mixture (propane/stoichiometric propane)	$[H]_1$ cm./ $[H]_e$
1.65	3.0
1.60	2.4
1.50	5.4
1.40	6.0
1.35	~6.8

**Recombination of Excesses.**—In view of the near equilibrium values of  $[H]$  leaving the reaction zone of the very rich flames, it is pertinent to follow the decay of any measureable excess as some means of confirmation of its existence. Bulewicz, James and Sugden<sup>2,4</sup> have shown that large excesses in  $[H]$ , and by independent means those in  $[OH]$  also, decay by three-body collisions in the burnt gases of  $H_2$ -air flames. The system of reactions

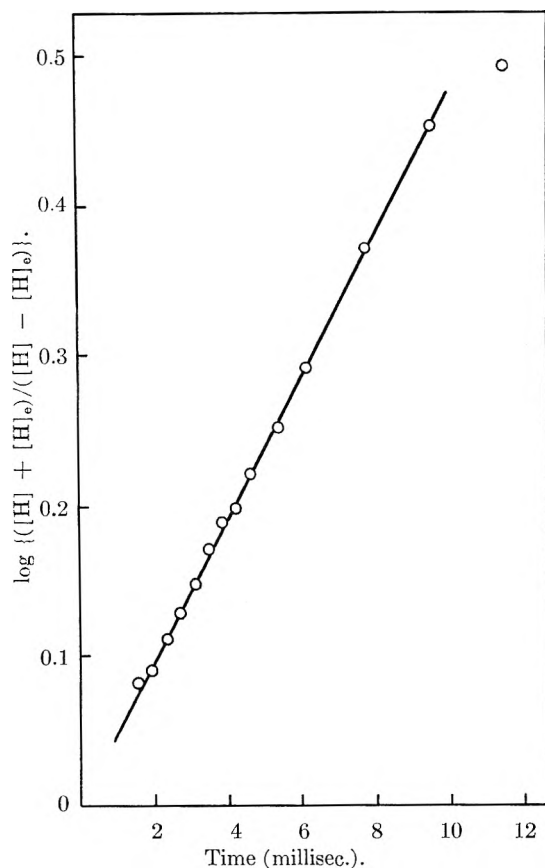
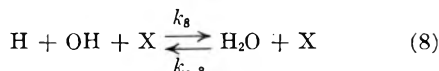
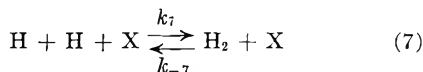


Fig. 4.—The recombination rate of H excesses in a flame of pre-burnt ratio (propane/stoichiometric propane) = 1.35. Times are above the burner top.



with X being predominately  $\text{H}_2\text{O}$ , its efficiency 10 times that of either  $\text{H}_2$  or  $\text{N}_2$ , are by far the most important removers of supra-equilibrium concentrations. It may be readily shown that

$$-\frac{d[\text{H}]}{dt} = a[\text{H}]^2 - b$$

where the constants

$$a = \frac{2(k_7 + k_8 K_2 [\text{H}_2\text{O}]/[\text{H}_2])}{1 + K_2 [\text{H}_2\text{O}]/[\text{H}_2]}$$

$$b = \frac{2(k_{-7}[\text{H}_2] + k_{-8}[\text{H}_2\text{O}])}{1 + K_2 [\text{H}_2\text{O}]/[\text{H}_2]}$$

$$\text{and } K_2 = \frac{[\text{H}_2][\text{OH}]}{[\text{H}_2\text{O}][\text{H}]}$$

and the concentrations of the third-bodies are included in the velocity constants. This has the solution

$$t = \frac{1}{2(ab)^{1/2}} \ln \left\{ \frac{[\text{H}] + (b/a)^{1/2}}{[\text{H}] - (b/a)^{1/2}} \right\} + \text{a constant}$$

If  $-d[\text{H}]/dt = 0$  at  $t = \infty$ , then  $(b/a)^{1/2} = [\text{H}]_e$  and  $(ab)^{1/2} = a[\text{H}]_e$ . For the decay of the very small excesses we measured, it is also necessary to measure  $[\text{H}]_e$  and treat the data in the following manner. Calculate and plot  $\log \{([\text{H}] + [\text{H}]_e)/([\text{H}] - [\text{H}]_e)\}$  against  $t$ , which should be linear and of slope  $0.868 a[\text{H}]_e$ . Such a plot for a flame of mixture strength 1.35 and in which  $t$  has been calculated from experimental rise-velocity measurements is shown in Fig. 4. In this case, the parameter  $a$  takes the value,  $0.59 \times 10^{-13} \text{ cm}^3 \text{ molecule}^{-1} \text{ sec}^{-1}$  at  $2078^\circ\text{K}$ . This is only somewhat lower than the value of the over-all recombination parameter  $2.0 \times 10^{-13}$  measured by Padley and Sugden in  $\text{H}_2$  flames at  $2085^\circ\text{K}$ . Furthermore, despite the fact that the measurement of  $a$  is subject to largest error in the lowest temperature flames where  $[\text{H}] \sim [\text{H}]_e$ , the set shown in Fig. 1 displays an increase in  $a$  as the temperature is lowered ( $10^{15} a$  takes the following values at  $2051^\circ$ , 0.69;  $1934^\circ$ , 0.79;  $1890^\circ$ , 1.11). This similar trend is found in  $\text{H}_2$  flames,<sup>3,4</sup> and the rates of recombination measured here infer that excesses in H, OH and O do exist.

We are indebted to the National Research Council of Canada for a grant in aid of this research and we are grateful to the Aluminium Laboratories, Ltd., Kingston, Ont., for gifts of graded aluminum particles.

## THE KINETICS OF THE REACTIONS OF AROMATIC HYDROCARBONS IN SULFURIC ACID. II. TOLUENE, THE XYLENES, PSEUDOCUMENE AND HEMIMELLITENE

BY MARTIN KILPATRICK AND MAX W. MEYER

*Department of Chemistry, Illinois Institute of Technology, Chicago, Ill.*

*Received October 7, 1960*

Kinetic data are reported for the sulfonation of certain methylbenzenes under conditions where the reaction goes to completion. The data, together with kinetic data for the disulfonation of mesitylene, support the rate law presented in a previous paper.

This paper reports the sulfonation of toluene and the di- and trimethyl-substituted benzenes which under our experimental conditions react completely to monosulfonates leaving no residual hydrocarbon. The rate law

$$\frac{d[\Sigma \text{ArSO}_3\text{H}]}{dt} = k_{\text{obs}} [\text{ArH}] \quad (1)$$

holds for each concentration of excess sulfuric acid, and as shown in Fig. 1, a plot of  $\log k_{\text{obs}}$  vs. stoichiometric sulfuric acid concentration is linear over



the range of acid concentration studied. Table I gives the least squares intercepts and slopes from which the velocity constants may be calculated.

TABLE I

VELOCITY CONSTANTS FOR THE SULFONATION OF METHYLBENZENES AT 12.3°

Hydrocarbon	Range of concn. H <sub>2</sub> SO <sub>4</sub> , mole/l.	Intercept	Slope
Benzene	16.9-15.8	-18.957	1.3797
Toluene	15.5-14.6	-16.607	1.3385
<i>p</i> -Xylene	15.2-14.4	-16.349	1.3600
<i>o</i> -Xylene	15.2-14.2	-14.221	1.2168
Pseudocumene (1,2,4-methyl)	14.4-13.4	-12.517	1.1361
<i>m</i> -Xylene	14.4-13.6	-12.365	1.1286
Hemimellitene (1,2,3-methyl)	14.4-13.4	-10.800	1.0296

An examination of the slopes in Fig. 1 and Table I shows that the lines are not parallel to the benzene line, which means that the relative rates are not independent of the sulfuric acid concentration. There is not, however, much difference between benzene and *p*-xylene which form only one monosulfonate. The other methylbenzenes give a mixture of monosulfonates.

Our knowledge of the concentration of molecular sulfuric acid in vitriol is limited to the range 15-18.6 *M* at 25° so that the equation of the previous paper<sup>1</sup>

$$\frac{d[\Sigma \text{ArSO}_3\text{H}]}{dt} = k \frac{[\text{H}_2\text{SO}_4]_{\text{sp}}^2 [\text{ArH}]}{c_{\text{H}_2\text{O}}} \times F \quad (2)$$

cannot be tested directly. However, a plot of  $2 \log [\text{H}_2\text{SO}_4]_{\text{sp}} - \log a_{\text{H}_2\text{O}}$  at 25° vs. the stoichiometric concentration of sulfuric acid has a slope of 1.13 which is practically the same as those for  $\log k_{\text{obs}}$  at 25° vs. stoichiometric sulfuric acid for benzene (1.14)<sup>1</sup> and toluene (1.17).<sup>2</sup>

A further indication that equation 2 is the correct kinetic equation is provided by the sulfonation of mesitylenesulfonic acid to the disulfonic acid. Due to the rapid decrease in the activity of water beyond 18 *M* the plot of  $2 \log [\text{H}_2\text{SO}_4]_{\text{sp}} - \log a_{\text{H}_2\text{O}}$  vs. stoichiometric sulfuric acid rises steeply. All of the hydrocarbons themselves sulfonate too rapidly for measurement in this range, but mesitylenesulfonic acid, which desulfonates below 15 *M* H<sub>2</sub>SO<sub>4</sub>, forms the stable disulfonic acid at 18.51 *M*, the half-time being 383 minutes. At 18.55 *M*, the half-time is 28 minutes which illustrates the steepness of the curve. Figure 2 shows this relationship graphically, the line for the sulfonation of benzene being included for reference. The data are presented in Table II. The velocity constant recorded as  $k_{\text{obs}}$  is the first-order constant calculated using decadic logarithms, *i.e.*, 0.4343 times the true constant. The inconsistencies in the table are not due to the kinetic measurements, but to the difficulty in determining the acid concentrations in the narrow range of concentration employed.

The graph shows that the line  $\log (k_{\text{obs}} \times 10^6)$  vs.

(1) M. Kilpatrick, M. W. Meyer and M. L. Kilpatrick, *J. Phys. Chem.*, **64**, 1433 (1960).

(2) C. Eaborn and R. Taylor, *J. Chem. Soc.*, 1480 (1960).

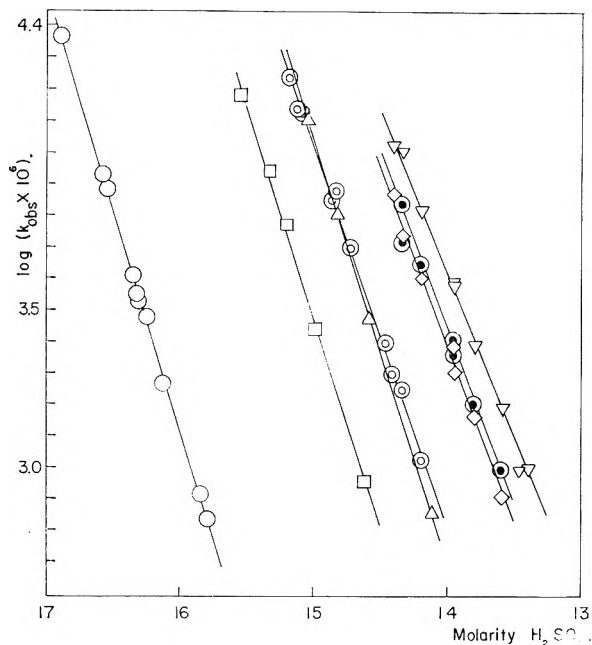


Fig. 1.—The sulfonation of methylbenzenes at 12.3°,  $\log (k_{\text{obs}} \times 10^6)$  vs. molarity sulfuric acid: ○, benzene; □, toluene; △, *p*-xylene; ⊙, *o*-xylene; ◇, pseudocumene; ▽, hemimellitene.

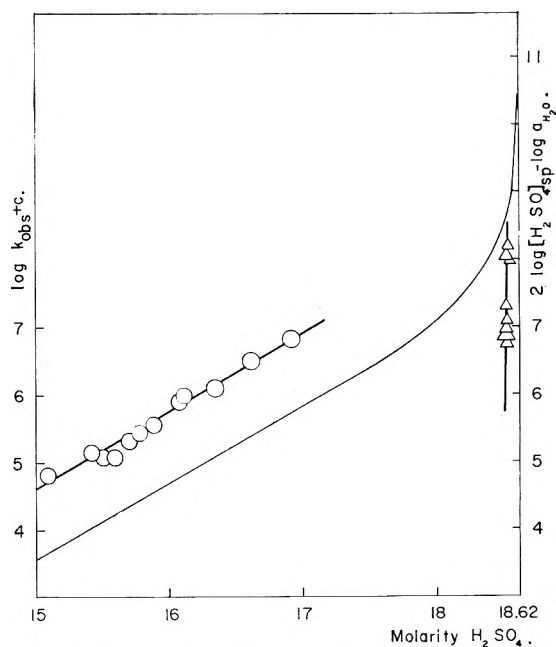


Fig. 2.— $2 \log [\text{H}_2\text{SO}_4]_{\text{sp}} - \log a_{\text{H}_2\text{O}}$  at 25° vs. molarity sulfuric acid: ○,  $\log k_{\text{obs}}$  for sulfonation of benzene at 25°,  $c = 8$ ; △,  $\log k_{\text{obs}}$  for sulfonation of mesitylenesulfonic acid at 12.5°,  $c = 10$ .

mole % SO<sub>3</sub> is extremely steep. Least squares treatment gives

$$\log (k_{\text{obs}} \times 10^6) = -216.286 + 4.457 [\text{mole } \% \text{ SO}_3]$$

or in terms of molarity

$$\log (k_{\text{obs}} \times 10^6) = -690.04 + 37.42 [\text{molarity H}_2\text{SO}_4]$$

In the acid region 49.1 to 49.5 mole % SO<sub>3</sub>, the value of  $[\text{H}_2\text{SO}_4]_{\text{sp}}$  varies from 17.80 to 18.20 moles/l, that is, it remains essentially constant. A test of equation 2 would be, therefore

TABLE II  
SULFONATION OF MESITYLENESULFONIC ACID IN H<sub>2</sub>SO<sub>4</sub> AT  
12.5°

Mole % SO <sub>3</sub>	$k_{\text{obs}} \times 10^4, \text{min.}^{-1}$	Half-time, min.
49.45	107	28
49.42	169	18
49.26	22.2	136
49.28	7.38	408
49.10	7.85	383
49.32	120	25
49.20	6.22	484
49.29	14.2	212
49.24	10.2 <sup>a</sup>	295

<sup>a</sup> The hydrocarbon was used as the starting material.

$$k_{\text{obs}} \times a_{\text{H}_2\text{O}} = \text{constant}$$

The values of  $a_{\text{H}_2\text{O}}$  for sulfuric acid solutions as given by Giauque and co-workers<sup>3</sup> are not experi-

(3) W. F. Giauque, E. W. Hornung, J. E. Kunzler and T. R. Rubin, *J. Am. Chem. Soc.*, **82**, 62 (1960).

mentally defined in the acid region 49.1 to 49.5 mole % SO<sub>3</sub>, so that no more than a qualitative agreement can be obtained. From 48.7 mole % SO<sub>3</sub> to 50.0 mole % SO<sub>3</sub>, the decrease of  $a_{\text{H}_2\text{O}}$  is of the order of 10<sup>3</sup>;  $k_{\text{obs}}$ , therefore, must rise steeply with the mole fraction of SO<sub>3</sub>, which it does, confirming qualitatively the rate equation found valid for the monosulfonation of benzene at lower sulfuric acid concentrations.<sup>1</sup>

Since the isomer distribution for the sulfonation of toluene is somewhat sensitive to the ratio of toluene to acid, and to temperature,<sup>4</sup> it does not appear worthwhile to include calculations of the partial rate factors.

**Acknowledgment.**—This research was supported in part by a grant from the Petroleum Research Fund, administered by the American Chemical Society. Grateful acknowledgment is hereby made to the donors. Thanks are also due to the Simoniz Company for yearly grants to the department.

(4) A. F. Holleman and P. Caland, *Ber.*, **44**, 2054 (1911).

## THE RATE OF REACTION OF HYDROGEN WITH NITROGEN DIOXIDE<sup>1</sup>

BY W. A. ROSSER, JR., AND H. WISE

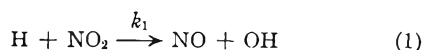
Stanford Research Institute, Menlo Park, California

Received October 7, 1960

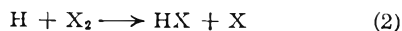
The rate of the reaction  $\text{H} + \text{NO}_2 \xrightarrow{k_1} \text{NO} + \text{OH}$  has been measured relative to that of  $\text{H} + \text{Cl}_2 \xrightarrow{k_2} \text{HCl} + \text{Cl}$  in a system containing H<sub>2</sub>, Cl<sub>2</sub> and NO<sub>2</sub>. In the temperature range between 500 and 540°K. the ratio  $k_1/k_2$  is given by the expression  $k_1/k_2 = 2.6 \times e^{3130/t}$ . Therefrom the value for  $k_1$  is found to be 10<sup>13.6</sup> cc./mole sec. The rate is independent of temperature in the region 500 to 540°K. and corresponds to a collision efficiency of about 1 in 20.

### Introduction

Molecular hydrogen and nitrogen dioxide react at a conveniently measurable rate at moderate temperatures. Recent studies<sup>2,3</sup> revealed that the kinetic mechanism probably involves the reaction



Although the system of reactions is too complicated for determination of individual rate constants, the rate constant  $k_1$  may be indirectly measured by comparison with the known rate constant for the reaction



where X<sub>2</sub> is either Br<sub>2</sub> or Cl<sub>2</sub>.

Under conditions where NO<sub>2</sub> does not interact with X<sub>2</sub> or with the products of the reactions, the comparison may be made in the following way. The molecules NO<sub>2</sub> and X<sub>2</sub> each react directly or indirectly with H<sub>2</sub> to produce hydrogen atoms. For long reaction chains resulting from the hydrogen atoms so produced, the ratio  $k_1/k_2$  is given by

$$\frac{k_1}{k_2} = \frac{-\frac{d}{dt}(\text{NO}_2)}{-\frac{d}{dt}(\text{X}_2)} \frac{(\text{X}_2)}{(\text{NO}_2)} \quad (3)$$

and can be determined by experimental measurement of the pertinent quantities. Also, since  $k_2$  is known for both Cl<sub>2</sub> and Br<sub>2</sub>,  $k_1$  may be obtained.

### Experimental

The apparatus used in this kinetic study has been described in a preceding publication.<sup>4</sup> The essential elements of the system are: (a) a quartz reaction vessel housed in a cylindrical resistance furnace; (b) a tungsten lamp; (c) a Beckman DU monochromator to select light of the desired wave length, whose intensity is detected by a photomultiplier tube and displayed on a recording instrument.

In order to obtain temperature uniformity within the reaction vessel, the furnace was heated by four separate resistance windings, each independently regulated by hand adjustment of a variable voltage-supply. Further, the reaction vessel was housed within a heavy-walled, aluminum liner.

Initial experiments were made with the three-component system H<sub>2</sub>-NO<sub>2</sub>-Br<sub>2</sub>. However, it was found that NO<sub>2</sub> reacts rapidly with HBr, the product of the reaction between H atoms and Br<sub>2</sub>. Consequently, no HBr accumulates in the system until NO<sub>2</sub> has disappeared. The essential features of the kinetics of the NO<sub>2</sub>-HBr reaction have already been reported.<sup>5</sup> The analogous reaction between NO<sub>2</sub> and HCl was also studied<sup>6</sup> and found to be slow enough to neglect.

(1) Sponsorship of this work by the Physical and Biological Sciences Division of Stanford Research Institute is gratefully acknowledged.

(2) W. A. Rosser, Jr., and H. Wise, *J. Chem. Phys.*, **26**, 571 (1957).

(3) P. A. Ashmore and B. P. Levitt, *Trans. Faraday Soc.*, **53**, 835 (1956).

(4) W. A. Rosser, Jr., and H. Wise, *J. Phys. Chem.*, **63**, 1753 (1959).

(5) W. A. Rosser, Jr., and H. Wise, *ibid.*, **64**, 602 (1960).

The present study is therefore concerned with the system  $H_2-Cl_2-NO_2$ .

The initial concentrations of each reactant and the temperature of reaction were varied in the indicated ranges:  $(NO_2)_i$  from  $3 \times 10^{-8}$  to  $8 \times 10^{-8}$  moles/cc.;  $(Cl_2)_i$  from  $7 \times 10^{-8}$  to  $2 \times 10^{-7}$  moles/cc.;  $(H_2)_i$  from  $2 \times 10^{-7}$  to  $6 \times 10^{-7}$  moles/cc.; ratios  $(Cl_2)_i/(NO_2)_i$  from 1 to 4; and temperature from 500 to 540°K. Commercial  $NO_2$ ,  $Cl_2$  and  $H_2$ , obtained from the Matheson Co., Inc., were used in all experiments. Purified  $H_2$  was used as supplied. Chlorine was used after removal (by vacuum distillation) of impurities non-condensable at the temperature of liquid nitrogen. The traces of NO present in commercial  $NO_2$  were converted to  $NO_2$  by dry  $O_2$  and the excess  $O_2$  subsequently removed by vacuum evaporation at the temperature of liquid nitrogen.

The rate of reaction in the system  $H_2-Cl_2-NO_2$  may be conveniently measured by optical means inasmuch as both  $NO_2$  and  $Cl_2$  absorb light in the visible or near ultraviolet region of the spectrum. At any wave length  $\lambda$  in this region the rate of change of the optical density may be represented by the equation

$$(-\log T_\lambda) = \alpha_\lambda(\dot{NO}_2) + \beta_\lambda(\dot{Cl}_2) \quad (4)$$

where  $T$  is the optical transmission, and the dot represents time derivatives. Measurements at two suitable wave lengths are necessary in order to solve for  $(\dot{NO}_2)$  and  $(\dot{Cl}_2)$ . In these experiments the two wave lengths chosen were 4200 and 3300 Å. The relevant absorption constants  $\alpha_\lambda$  and  $\beta_\lambda$  were determined empirically at the temperature of operation. At 4200 Å. the ratio  $\beta_{42}/\alpha_{42} \approx 2 \times 10^{-2}$ . Consequently, for comparable concentrations of  $Cl_2$  and of  $NO_2$ , the  $Cl_2$  contributes only slightly to the total optical density. At 3300 Å. the ratio of  $\beta_{33}/\alpha_{33} \sim 1/2$  and both  $Cl_2$  and  $NO_2$  contribute to the optical density.

### Results

In all experiments reaction was initiated by adding an excess of  $H_2$  to the reaction vessel already containing the other reactants,  $NO_2$  and  $Cl_2$ . During the course of reaction the optical density was measured at one or the other of the two monitoring wave lengths, 4200 or 3300 Å. Two or three duplicate experiments were carried out at each monitoring wave length.

A comparison of the results of separate but identical experiments was complicated by the following two factors. The admission of  $H_2$  to the reaction vessel created an optical disturbance, associated with mixing, which required up to twenty seconds to subside. Moreover, the onset of reaction was frequently preceded by an induction period of short but variable length. For each experiment the experimental procedure required that a virtual time origin be established in such a manner that the effects of induction and mixing had been eliminated. For this purpose various simple functions of the optical density,  $(-\log T_\lambda)$ , such as  $-\log T_\lambda$ ,  $(-\log T_\lambda)^{1/2}$ , and  $\log(-\log T_\lambda)$ , were plotted *versus* time and the one selected which appeared to vary linearly during the course of reaction. By linear extrapolation of this function to its initial value a virtual time origin was established. An example of the procedure is shown in Fig. 1.

During the course of each experiment the time derivatives,  $(-\log T_\lambda)$ , were determined graphically at various time intervals. The maximum extent of reaction corresponded to about 25% reaction. At each wave length the results of duplicate experiments were averaged. Finally, the two equations of the type shown in eq. 4 were solved for

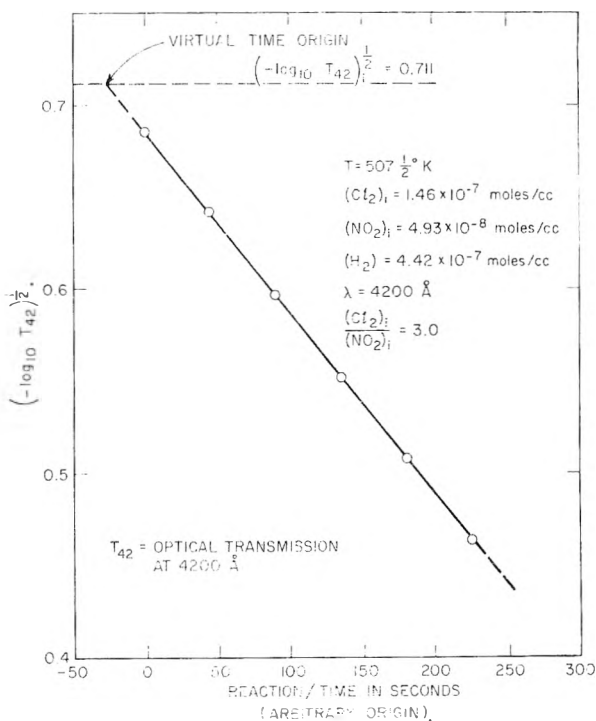


Fig. 1.—Example of method used to determine virtual beginning of reaction.

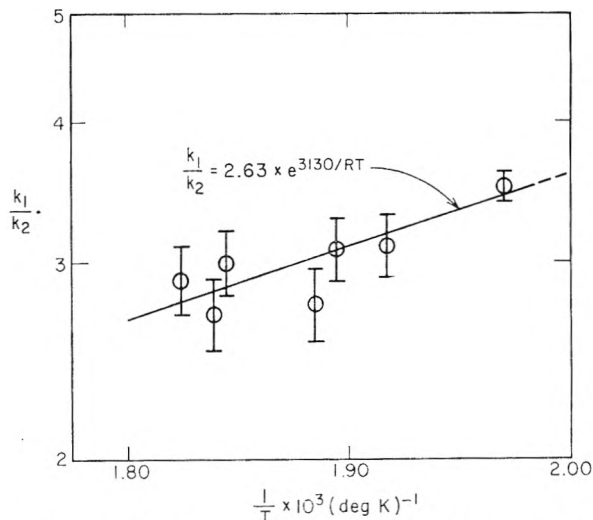


Fig. 2.—Specific reaction rate as a function of temperature.

$(\dot{NO}_2)$  and  $(\dot{Cl}_2)$  at various values of the reaction time.

Solution of eq. 3 involves the ratio  $(Cl_2)/(NO_2)$ , which changes during the course of reaction. For long reaction chains the cited ratio may be cast in the form

$$\frac{(Cl_2)}{(NO_2)} = \frac{(Cl_2)_i}{(NO_2)_i} e^{(k_2/k_1 - 1) \ln [(NO_2)/(NO_2)_i]} \quad (5)$$

Equation 5 may be substituted in eq. 3 to give

$$\frac{k_1}{k_2} = \frac{(\dot{NO}_2)}{(\dot{Cl}_2)} \frac{(Cl_2)_i}{(NO_2)_i} e^{(k_2/k_1 - 1) \ln [(NO_2)/(NO_2)_i]} \quad (6)$$

Equation 6 is a convenient expression for  $k_1/k_2$  because the absorption by  $NO_2$  at 4200 Å. is much

greater than that by  $\text{Cl}_2$ . Consequently,  $-\log T_{42} \approx \alpha_{42}(\text{NO}_2)$  and

$$\frac{(\text{NO}_2)}{(\text{NO}_2)_i} = \frac{-\log T_{42}}{(-\log T_{42})_i} + \delta \quad (7)$$

where the small correction factor  $\delta$  can be evaluated with acceptable accuracy from the initial reaction conditions. Equation 6 may be finally solved by iteration, using the initial reactant concentrations, the experimental values of  $(\dot{\text{NO}}_2)$  and  $(\dot{\text{Cl}}_2)$ , eq. 7, and a preliminary value of  $k_1/k_2$ . A preliminary value can be determined from eq. 6 by ignoring the exponential term. In this way  $k_1/k_2$  was obtained for each set of reaction conditions at the various selected values of reaction time. No systematic variation in  $k_1/k_2$  with time was observed. The ratio  $k_1/k_2$ , obtained as described, was found to be  $3 \pm 3/4$  for all experimental variables in the ranges cited earlier. In particular, the temperature variation of  $k_1/k_2$  in the temperature range 500 to 540°K. is less than the limits of error given above.

A temperature coefficient for  $k_1/k_2$  was obtained by using only the results of experiments in which the initial ratio  $(\text{Cl}_2)_1/(\text{NO}_2)_i$  was about 3, and  $(\text{NO}_2)_i \sim 5 \times 10^{-8}$  moles/cc. These concentrations resulted in comparable rates of disappearance of  $\text{NO}_2$  and  $\text{Cl}_2$ , and were chosen with the intention of minimizing experimental error. The results of experiments which satisfied the above restrictions are shown in Fig. 2. The estimated limits of error are shown by the symbols used in the figure. The data were fitted visually by a straight line which corresponds to the Arrhenius equation

$$\frac{k_1}{k_2} = 2.63 \times e^{3130/RT} \quad (8)$$

The individual rate constants  $k_1$  and  $k_2$  may be represented by eq. 9 and 10

$$k_1 = A_1 e^{-Q_1/RT} \quad (9)$$

$$k_2 = A_2 e^{-Q_2/RT} \quad (10)$$

Then eq. 8 implies that  $A_1/A_2 = 2.63$  and  $Q_2 - Q_1 = 3130$  cal. It is known<sup>6</sup> that  $Q_2$  lies between 2 and 3 kcal., consequently one obtains  $Q_1 \approx 0$  kcal. and  $A_1/A_2 = 2.6$ .

An explicit expression for  $k_2$  has been reported<sup>7</sup> which in conjunction with eq. 8 leads to the value  $k_1 = 10^{13.5}$  cc./mole sec. in the temperature range 500 to 540°K. This value for  $k_1$  corresponds to a collision efficiency of about 1 in 20. The results are consistent with the fact that reaction 1 involves two free radicals and may be expected to proceed at a rate comparable to the collision rate.

The procedure used in deriving  $k_1/k_2$  is critically dependent on the assumption that the reaction chains are long. For the two-component system  $\text{H}_2\text{-Cl}_2$  such a condition undoubtedly obtains. In the case of the system  $\text{H}_2\text{-NO}_2$  the reaction chains are probably shorter than in the case of the system  $\text{H}_2\text{-Cl}_2$ . The ternary system  $\text{H}_2\text{-Cl}_2\text{-NO}_2$  would be expected to involve chain lengths intermediate between the values for the individual binary systems. Very long chain lengths for  $\text{H}_2\text{-Cl}_2$  will consequently tend to validate the method used in our calculations of  $k_1/k_2$ .

(6) A. F. Trotman-Dickenson, "Gas Kinetics," Butterworths, London, 1955, p. 185.

(7) M. Bodenstein and W. Jost, "Katalyse bei Homogenen Gas Reaktionen," Handbuch der Katalyses (ed. G. M. Schwab) Springer-Verlag, Vienna, Vol. I, 1941, p. 301.

## VISCOELASTIC PROPERTIES OF POLYETHYLENE OXIDE IN THE RUBBER-LIKE STATE\*

BY THEODORE P. YIN, STUART E. LOVELL AND JOHN D. FERRY

*Department of Chemistry, University of Wisconsin, Madison, Wisconsin*

*Received October 10, 1960*

The viscoelastic properties of a sample of polyethylene oxide, molecular weight  $1.15 \times 10^4$ , have been studied in the rubber-like state above the melting point. The real and imaginary parts of the complex compliance were measured between 0.04 and 1000 cycles/sec. in the temperature range from 68 to 120°; the creep compliance was measured at 80 to 100°, including creep recovery at 100°. The method of reduced variables gave superposed curves for all the data with shift factors which followed the Arrhenius equation with an activation energy of 11.7 kcal./mole. The creep was represented by the Andrade equation with an additional term for steady-state flow, from which the steady flow viscosity was calculated. The relaxation and retardation spectra comprised the plateau and terminal zones. The average spacing between coupling entanglement points was estimated in two ways to be about 200 chain atoms, of normal magnitude. However, the extremely wide plateau of the relaxation spectrum indicates that the entanglements are unusually tight. Since the transition zone lies at shorter times than those covered in the present experiments, the logarithm of the monomeric friction coefficient at 100° must be less than  $-6.4$ .

### Introduction

Most investigations of time-dependent mechanical properties of amorphous polymers have been confined to polyvinyl derivatives whose chain backbones consist solely of carbon atoms and carry pendant side groups. The present study is concerned with polyethylene oxide, whose repeating

unit is  $-\text{CH}_2\text{-CH}_2\text{-O}-$ . The expectation of a high degree of mobility in configurational rearrangements, due to the oxygen chain atoms and the absence of side groups, has been confirmed. Measurements on the amorphous polymer were limited to a temperature range between 65 (the melting point) and 120° (where degradation set in if the experiments continued more than a day). At the lowest temperature and highest frequency of measure-

\* Part XXXIV of a series on Mechanical Properties of Substances of High Molecular Weight.

ment (1000 cycles/sec.), the transition zone between rubber-like and glass-like consistency was not reached. However, the measurements served to define the viscoelastic properties in the rubber-like plateau and terminal zones.

### Material and Methods

The polymer was kindly furnished by Dr. F. E. Bailey of Union Carbide Chemicals Company.<sup>1</sup> It was a specially selected sample (138,541-6307) with a viscosity-average molecular weight of  $1.15 \times 10^6$  as estimated from the intrinsic viscosity in water at 30°,  $[\eta] = 1.11$ , using the equation of Bailey, Kucera and Imhof.<sup>2</sup> The melting point was determined by observation under a microscope to be 65°, the density of the amorphous polymer at 70° was 1.077 g./ml., and the thermal expansion coefficient was  $6.2 \times 10^{-4}$  deg.<sup>-1</sup>.

The granular polymer was dried *in vacuo* for 5 weeks at room temperature. Samples for mechanical measurements were molded at 78° and annealed for about 3 hours at 70°. To avoid oxidative degradation, which can be rapid at higher temperatures, all measurements were made in a continuous stream of nitrogen. In the Fitzgerald-Ferry transducer apparatus,<sup>3</sup> the level of oxygen was thus reduced to <0.01%, the limit of detection by a Beckman Oxygen Analyzer. In the Plazek torsion pendulum,<sup>4</sup> the removal of oxygen was less effective. However, the condition of each sample was monitored by repeated check runs, and if there was any evidence of degradation (to which the loss tangent is quite sensitive<sup>5</sup>) the data were rejected.

The Fitzgerald-Ferry transducer<sup>5</sup> was used for measurements between 24 and 1000 cycles/sec., the upper limit being curtailed by the driving tube impedance with this very compliant material. Since the last description of the instrument,<sup>6</sup> an improved driving tube as described by Fitzgerald<sup>7</sup> had been installed. Three pairs of disc-shaped samples were employed. Samples 120, 5/16 in. diameter by 1/8 in. thick, were measured successively at 67.9, 73.1, 77.8, 82.7, 67.9 and 65.0°; samples 123, 11/16 in. by 1/8 in., at 80.5, 82.7, 88.9 and 80.5°; and samples 124, 11/16 in. by 1/32 in., at 88.9, 100.0, 110.7 and 11.9°. Values of the components of the complex compliance,  $J'$  and  $J''$ , agreed very well for 123 and 124 at the overlapping temperature. Those for 120 were higher by about 11%; the discrepancy was attributed to an error in the sample coefficient due to a slight bulging, and the data were corrected by a constant factor in the customary manner.<sup>3</sup>

The Plazek torsion pendulum<sup>4</sup> was used for measurements between 0.04 and 2.5 cycles/sec. Two disc-shaped samples were employed. Sample 45, 3/4 in. diameter by 5/16 in. thick, was measured successively at 68.6, 73.1, 77.8, 82.6, 88.8, 100.1 and 73.1°. Sample 48, 5/16 in. by 3/16 in., was measured at 88.8, 100.9, 110.5, 120.0 and 88.8°. The values of the storage modulus,  $G'$ , were all about 13% lower for sample 48 at overlapping temperatures; since this sample showed a slight distortion in shape, the latter data were corrected by a constant factor to bring them into agreement with those of sample 45.

The torsion pendulum was also used for creep measurements at 80.5, 88.8 and 100.0° up to 6.3 hr., with creep recovery at 100.0°. The sample had the same dimensions as sample 45; when dynamic measurements at low frequencies were converted to creep compliance by the approximation method of Ninomiya and Ferry,<sup>8</sup> the values agreed closely at overlapping times, so no empirical corrections were applied to the creep data.

### Results

The creep compliance at three temperatures is

- (1) F. N. Hill, F. E. Bailey, Jr., and J. T. Fitzpatrick, *Ind. Eng. Chem.*, **50**, 5 (1958).
- (2) F. E. Bailey, Jr., J. L. Kucera and L. G. Imhof, *J. Polymer Sci.*, to be published.
- (3) E. R. Fitzgerald and J. D. Ferry, *J. Colloid Sci.*, **8**, 1 (1953).
- (4) D. J. Plazek, M. N. Vrancken and J. W. Berge, *Trans. Soc. Rheology*, **2**, 39 (1958).
- (5) H. Högberg, S. E. Lovell and J. D. Ferry, *Acta Chem. Scand.*, **14**, 1424 (1960).
- (6) D. J. Plazek, W. Dannhauser and J. D. Ferry, *J. Colloid Sci.* (in press).
- (7) E. R. Fitzgerald, *J. Chem. Phys.*, **27**, 1180 (1957).
- (8) K. Ninomiya and J. D. Ferry, *J. Colloid Sci.*, **14**, 36 (1959).

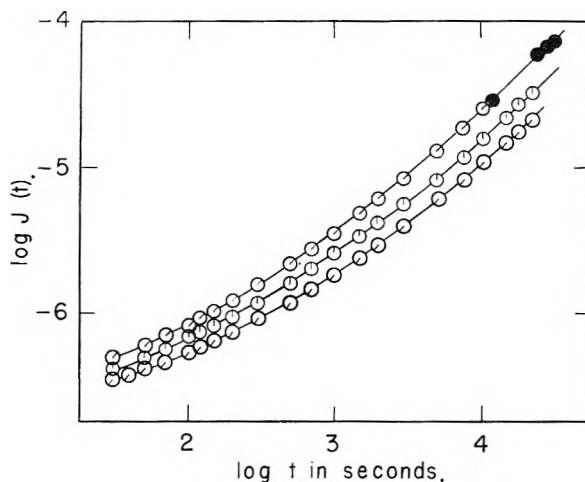


Fig. 1.—Creep compliance plotted logarithmically at (top to bottom) 100.0, 88.8 and 80.5°. Black circles calculated from creep recovery by equation 1.

plotted logarithmically in Fig. 1. The recovery measurements were converted to creep by the equation

$$J(t) = J_r(t) + J(t - \theta) \quad (1)$$

where  $\theta$  is the time of load removal and  $J_r(t)$  is the creep compliance measured during recovery at a time  $t$  elapsed since the load was first applied. Where this calculation almost overlaps the part of the curve directly measured, it provides a test of the Boltzmann superposition principle, and beyond this it gives an extension of  $J(t)$  somewhat beyond the longest times of direct measurement.

To save space, the original dynamic data are not reported, but only after reduction to a reference temperature of 100° by the method of reduced variables.<sup>9</sup> The reduced compliances  $J'_p (= J'T \rho/T_0 \rho_0)$ , where  $\rho$  and  $\rho_0$  are the densities at  $T$  and at the reference temperature  $T_0$ ),  $J''_p$ , and  $J_p(t)$  could be superposed with the customary shift factors  $a_T$ . The temperature dependence of  $a_T$  did not follow the WLF equation,<sup>9</sup> however, but rather an equation of the Arrhenius form

$$\log a_T = (\Delta H_a/2.303R)(T - T_0)/TT_0 \quad (2)$$

with  $\Delta H_a = 11.7$  kcal./mole. This is not surprising, since the WLF equation is expected<sup>9,10</sup> to be replaced by the Arrhenius equation at temperatures far above the glass transition temperature  $T_g$ . Although  $T_g$  is probably inaccessible experimentally because of the high degree of crystallinity below the melting point, in principle it must lie far below the temperature range of the present measurements. The magnitude of  $\Delta H_a$  is entirely reasonable compared with those of other polymers at elevated temperatures.

The reduced dynamic data are shown in Fig. 2, covering a frequency scale of about 5 logarithmic decades. The reduced creep compliance is plotted in Fig. 3. Interpolated values are listed in Table I. Here the units of  $\omega$  are rad/sec.;  $t$ , sec.; and  $J'$ ,  $J''$ ,  $J(t)$ , cm.<sup>2</sup>/dyne.

(9) M. L. Williams, R. F. Landel and J. D. Ferry, *J. Am. Chem. Soc.*, **77**, 3701 (1955).

(10) F. Bueche, *J. Chem. Phys.*, **30**, 748 (1959).

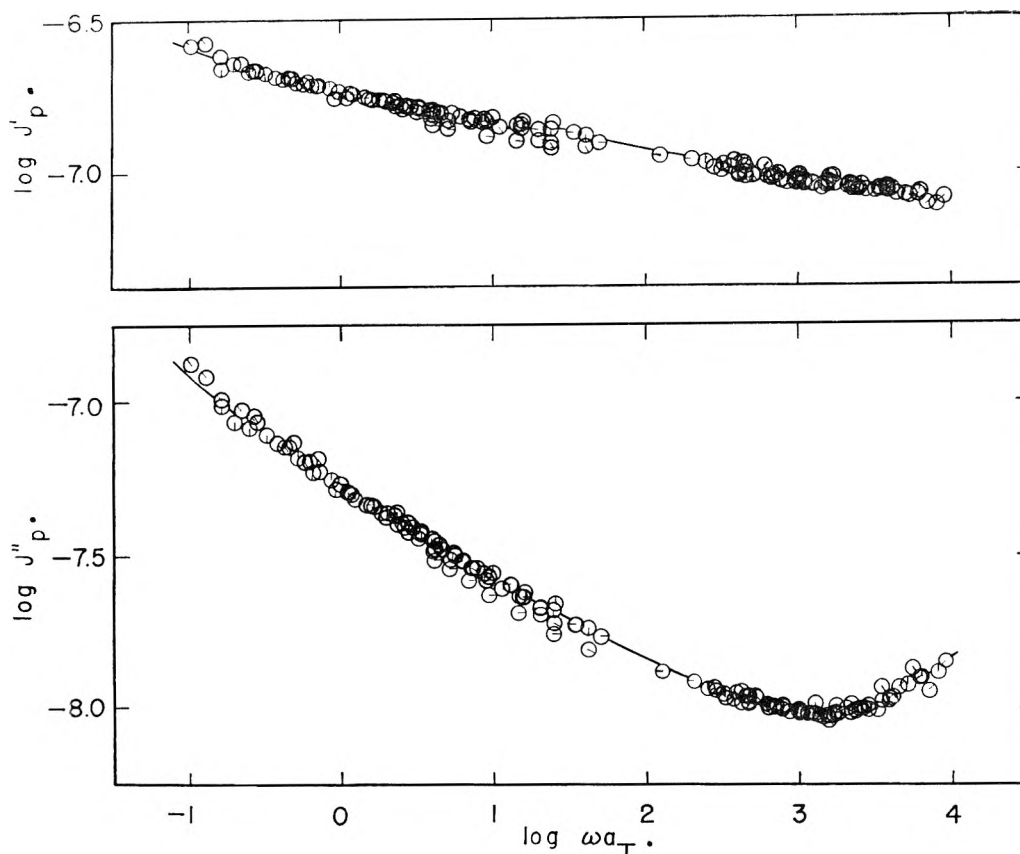


Fig. 2.—Real ( $J'$ ) and imaginary ( $J''$ ) parts of the complex compliance of polyethylene oxide, plotted logarithmically against circular frequency after reduction to a reference temperature of  $100^\circ$  by equation 2. Points left of 2 on abscissa scale are from torsion pendulum measurements; right of 2, from transducer measurements. Pips denote ten different temperatures from  $65.0$  to  $120.0^\circ$ .

TABLE I

DYNAMIC AND CREEP COMPLIANCES REDUCED TO $100^\circ$				
$\log \omega$	$\log J'$	$\log J''$	$\log t$	$\log J(t)$
-1	-6.58	-6.92	1.0	-6.52
0	-6.73	-7.29	2.0	-6.09
1	-6.83	-7.58	3.0	-5.46
2	-6.92	-7.83	4.0	-4.61
3	-7.03	-8.02	4.5	-4.12
4	-7.10	-7.83		

### Discussion

**Analysis of Creep and Flow.**—For certain polymers of very high molecular weight, Plazek<sup>6,11</sup> has shown that the creep at long times can be described by the equation

$$J(t) = J_g + J_0\psi(t) + \beta t^{1/3} + t/\eta \quad (3)$$

where  $\beta$  is the Andrade coefficient and  $\eta$  the steady flow viscosity. The first two terms are negligible in the range of very long times where equation 3 can be profitably used to estimate  $\eta$  even if steady-state flow has not quite been attained. Plots of  $J(t)$  against  $t^{1/3}$  gave short linear segments followed by upward divergence due to the  $t/\eta$  term; from the linear segments,  $\beta$  was roughly estimated to be  $0.90$ ,  $1.71$  and  $13.9 \times 10^{-7}$   $\text{cm}^2 \text{ dyne}^{-1} \text{ sec}^{-1/3}$  at  $80.5$ ,  $88.8$  and  $100.0^\circ$ , respectively. Plots of  $J(t) - \beta t^{1/3}$  against  $t$  were then found to be accurately linear, as shown in Fig. 4, and from their slopes  $\eta$  was calculated to be  $12.4$ ,  $8.8$  and  $5.1 \times 10^8$  poises,

(11) D. J. Plazek, *J. Colloid Sci.*, **15**, 50 (1960).

respectively, at the three temperatures given. The temperature dependence of  $\eta$  is in excellent agreement with equation 2, further confirming the value chosen for  $\Delta H_a$ .

**Relaxation and Retardation Spectra.**—The retardation spectrum  $L$  was calculated from  $J'$  and  $J''$  by the Williams-Ferry approximation<sup>12</sup> except for a region near  $\log \omega = 0$ , where the Schwarzl-Staverman<sup>13</sup> and Fujita<sup>14</sup> approximations were employed, as described in previous publications.<sup>15</sup> From creep,  $L$  was calculated by a modified equation of Schwarzl and Staverman in which subtraction of the flow contribution is unnecessary.<sup>15</sup> To calculate the relaxation spectrum  $H$ , the complex modulus was first converted to the complex modulus by the usual reciprocal relationship, and the creep data were converted to the stress relaxation modulus  $G(t)$  by the approximation given by Smith<sup>16</sup>

$$G(t) = (\sin m\pi)/m\pi J(t) \quad (4)$$

where  $m$  is the slope of  $\log J(t)$  vs.  $\log t$ . Then the Williams-Ferry approximations<sup>11</sup> were applied to  $G'$ ,  $G''$  and  $G(t)$ .

(12) M. L. Williams and J. D. Ferry, *J. Polymer Sci.*, **11**, 169 (1953).

(13) F. Schwarzl and A. J. Staverman, in H. A. Stuart, "Die Physik der Hochpolymeren," Vol. IV, Springer, Berlin, 1956, p. 44.

(14) H. Fujita, *J. Appl. Phys.*, **29**, 943 (1958).

(15) J. W. Berge, P. R. Saunders and J. D. Ferry, *J. Colloid Sci.*, **14**, 135 (1959).

(16) T. L. Smith, *Trans. Soc. Rheol.*, **2**, 131 (1959).

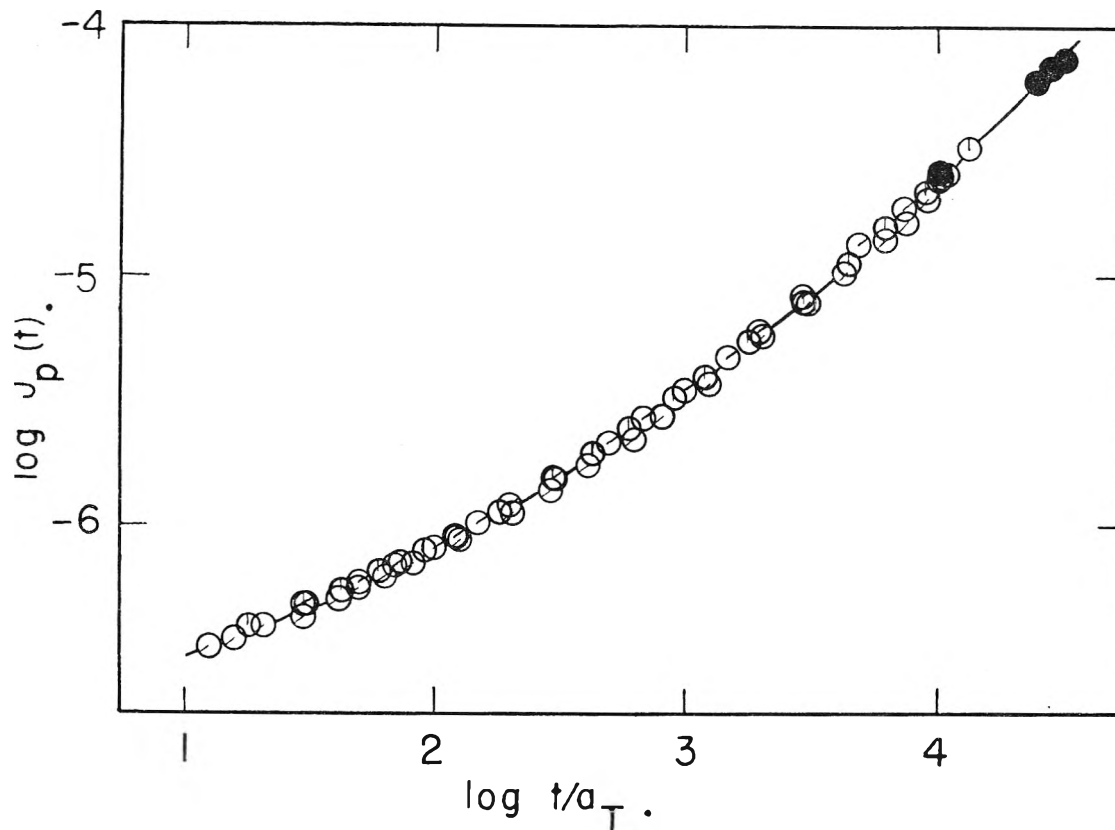


Fig. 3.—Data of Fig. 1 reduced to 100.0° by equation 2.

Values of  $\log H$  and  $\log L$  are given in Tables II and III and plotted in Fig. 5. The agreement between calculations from different experimental sources is in most cases very good. The relaxation spectrum, unfortunately, does not extend to short enough times to enter the transition zone where the monomeric friction coefficient can be calculated by the Rouse theory.<sup>17</sup> It exhibits a remarkably long plateau zone for such a moderate molecular weight, indicating strong coupling of the type described as long-range entanglement,<sup>18</sup> followed by the terminal zone which normally accompanies the onset of flow. The retardation spectrum passes through a maximum in the terminal zone. This is not the maximum associated with the entanglement network, from the location of which the spacing between coupling points can be calculated by the theory of Marvin<sup>19,20</sup>; the network maximum in  $L$  normally appears at the bottom of the transition zone in  $H$  and must be to the left of the logarithmic time scale encompassed by these experiments.

**Spacing between Entanglement Points.**—The average molecular weight between entanglement points,  $M_e$ , can be estimated from the present data in two ways.

In the plateau zone, the loss tangent ( $\tan \delta = J''/J'$ ) passes through a distinct minimum as a function of either frequency<sup>5</sup> or temperature,<sup>21</sup> and

(17) J. D. Ferry and R. F. Landel, *Kolloid-Z.*, **148**, 1 (1956).

(18) J. D. Ferry, R. F. Landel and M. L. Williams, *J. Appl. Phys.*, **26**, 359 (1955).

(19) R. S. Marvin, in J. T. Bergen, "Viscoelasticity-Phenomenological Aspects," Academic Press, New York, N. Y., 1960, p. 27.

(20) T. P. Yin and J. D. Ferry, *J. Colloid Sci.*, (in press).

TABLE II  
RELAXATION AND RETARDATION SPECTRA REDUCED TO 100°,  
FROM DYNAMIC MEASUREMENTS

$\log \tau$	$\log H$		$\log L$	
	from $G'$	from $G''$	from $J'$	from $J''$
-4.0	5.84	5.94	-8.25	-8.20
-3.5	5.92	5.79	-8.19	-8.24
-3.0	5.88	5.77	-8.15	-8.26
-2.5	5.82	5.82	-8.02	-8.19
-2.0	5.82	5.80	-7.97	-8.07
-1.5	5.80	5.80	-7.91	-7.95
-1.0	5.83	5.83	-7.88 <sup>a</sup>	-7.86 <sup>b</sup>
-0.5	5.89 <sup>a</sup>	5.90 <sup>b</sup>	-7.71 <sup>a</sup>	-7.72 <sup>b</sup>
0	5.90 <sup>a</sup>	5.93 <sup>b</sup>	-7.63 <sup>a</sup>	-7.60 <sup>b</sup>
0.5	5.92 <sup>a</sup>	5.98 <sup>b</sup>	-7.43 <sup>a</sup>	-7.42 <sup>b</sup>
1.0	5.90	5.97	-7.33	-7.24

<sup>a</sup> From Schwarzl-Staverman approximation. <sup>b</sup> From Fujita approximation.

TABLE III  
RELAXATION AND RETARDATION SPECTRA REDUCED TO 100°.  
FROM CREEP MEASUREMENTS

$\log \tau$	$\log H$	$\log \tau$	$\log L$
1.6	5.90	0.8	-7.35
2.1	5.70	1.3	-7.14
2.6	5.36	1.8	-6.83
3.1	4.93	2.3	-6.53
3.6	4.42	2.8	-6.43
		3.3	-6.51
		3.8	-6.59

the depth is sensitive to the ratio  $M/M_e$ . From the theory of Marvin,<sup>19</sup> the relation can be approxi-

(21) W. P. Cox, R. A. Isaksen and E. H. Merz, *J. Polymer Sci.*, **44**, 149 (1960).



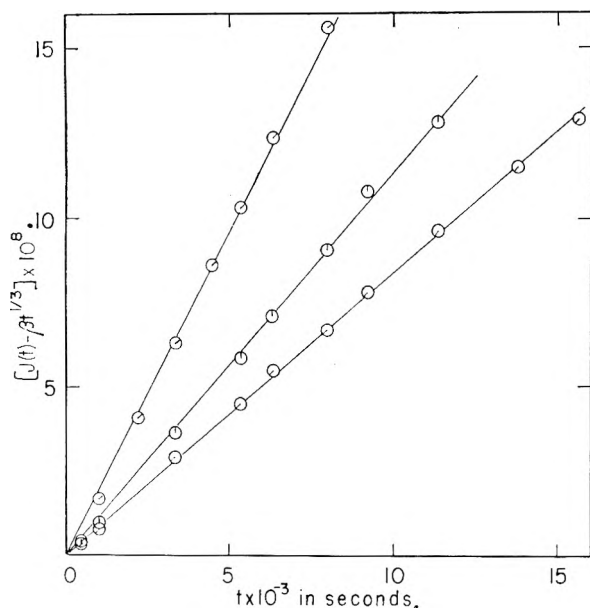


Fig. 4.—Linear creep plots after subtraction of Andrade contribution to determine viscosity.

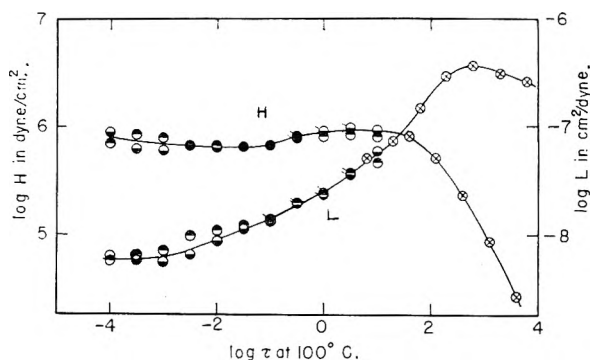


Fig. 5.—Relaxation ( $H$ ) and retardation ( $L$ ) spectra reduced to  $100^\circ$ . Points top black, from  $G'$  or  $J'$ ; bottom black, from  $G''$  or  $J''$ ; crossed, from creep.

mated<sup>5</sup> by

$$\tan \delta = 1.02(M/2M_e)^{-0.80} \quad (5)$$

for a polymer of uniform molecular weight. The loss tangent calculated from the data of Table I passes through a minimum of 0.10 at  $\log \omega = 2.9$ . Assumption of a uniform molecular weight of  $1.15 \times 10^5$  thus gives  $M_e = 3200$ . Molecular weight distribution would imply<sup>5,21</sup> a lower value of  $M_e$ .

A rough estimate can also be made from the magnitude of  $J'$  in the plateau region, which is about  $10^{-7}$  cm.<sup>2</sup>/dyne, using the theory of rubber-like elasticity for cross-linked networks. The result is  $M_e = 3100$ , in fortuitously good agreement.

A molecular weight of 3000 between entanglement points corresponds to approximately 200 chain bonds per network strand. This may be compared with values of 130 to 500 for Hevea rubber, 250 to 400 for polyisobutylene, and 200 to 600 for polystyrene, the ranges depending on the

method of estimation.<sup>22</sup> Thus the spacing appears to be of normal magnitude though relatively small.

**Terminal Relaxation Time and Plateau Width.**—From the measured viscosity and molecular weight, the terminal relaxation time of the Rouse theory can be calculated as  $\tau_1 = 6\eta M/\pi^2\rho RT = 1.08 \times 10^3$  sec. This conforms to the steep drop in  $H$  seen in Fig. 5 in the neighborhood of  $\log \tau = 3$ , and indicates that the relation of  $\tau_1$  to  $\eta$  is normal. However, both  $\tau_1$  and  $\eta$  are very much higher than would be expected for a polymer with this molecular weight whose transition zone lies so far to the left on the time scale.

The preceding statement is equivalent to saying that the plateau zone is abnormally broad. From Fig. 5 there are evidently at least 7 logarithmic decades between the regions of the transition and terminal zones where the slope of  $H$  with logarithmic coordinates reaches  $-1/2$ . The width calculated from the formula<sup>18</sup>  $\Delta = 2.4 \log (M/2M_e)$ , which is satisfactory for several vinyl polymers,<sup>22</sup> is only 3.0 decades. It would appear that the entanglements in polyethylene oxide, though relatively normal in spacing, are unusually tight, corresponding to a very low slippage factor in Bueche's picture<sup>23</sup> of entanglement coupling. Such abnormally tight coupling has also been postulated in aqueous solutions of a styrene-maleic acid copolymer<sup>24</sup> and demonstrated in polydimethyl siloxane<sup>6</sup> of very high molecular weight, though it is unlikely that the same mechanism can account for all cases. It seems evident that there are types of widely spaced intermolecular coupling intermediate in character between the entanglement coupling described by Bueche<sup>23</sup> and permanent cross-links.

Failure to reach the transition zone makes it impossible to calculate the monomeric friction coefficient  $\zeta_0$  in the usual manner.<sup>17,18</sup> It cannot be obtained either by the indirect procedure recently used for polydimethyl siloxane of intermediate molecular weights,<sup>6</sup> because of the abnormal character of the entanglement coupling. An upper limit for  $\log \zeta_0$  based on the position of  $H$  in Fig. 5 would be  $-6.4$  at  $100^\circ$ , corresponding to the monomer unit  $-\text{CH}_2\text{-CH}_2\text{-O}$  (units dyne-sec./cm.<sup>2</sup>). This is comparable with that of  $-6.8$  for Hevea rubber<sup>22</sup> and  $-7.3$  for polydimethyl siloxane<sup>6</sup> at  $25^\circ$ , and reflects a high degree of local chain mobility.

**Acknowledgments.**—This work was supported in part by a grant from the National Science Foundation, and in part by the Research Committee of the Graduate School of the University of Wisconsin from funds supplied by the Wisconsin Alumni Research Foundation. We are much indebted to Mrs. W. C. Frazier and Mrs. A. Rossol for help with the calculations.

(22) J. D. Ferry, "Viscoelastic Properties of Polymers," John Wiley and Sons, New York, N. Y., 1961, Chapter 13.

(23) F. Bueche, *J. Chem. Phys.*, **20**, 1959 (1952).

(24) G. E. Heckler, T. E. Newlin, D. M. Stern, R. A. Stratton, J. R. Witt and J. D. Ferry, *J. Colloid Sci.*, **15**, 294 (1960).

# AN INFRARED AND ISOPIESTIC INVESTIGATION OF THE INTERACTION BETWEEN TRI-*n*-BUTYL PHOSPHATE AND MONO-(2-ETHYLHEXYL)-PHOSPHORIC ACID<sup>1</sup>

BY J. R. FERRARO AND D. F. PEPPARD

Argonne National Laboratory, Argonne, Illinois

Received October 13, 1960

The interaction between tri-*n*-butyl phosphate<sup>2</sup> and mono-(2-ethylhexyl)-phosphoric acid<sup>3</sup> was investigated. The method of continuous variations utilizing changes in infrared absorption and changes in the freezing point depression of the mixtures was used. Isopiestic measurements also were made. Results gave evidence that an association product had resulted at a ratio of 2 moles of TBP per hexamer unit of H<sub>2</sub>MEHP.

Several new terms have recently appeared in the solvent extraction literature such as: "synergism" and "antisynergism." The term "synergism" pertains to an enhancement of the extraction of a cation from an aqueous phase by a mixture of solvents (generally a neutral and an acidic organophosphorus compound); the mixture giving better extraction than either solvent alone. "Antisynergism" would be the reverse of this. Such an antisnergistic effect is observed for the extraction of Np(IV) and Th(IV) into H<sub>2</sub>MEHP when TBP is added.<sup>4</sup> The purpose of the present study was to determine the nature of the interaction between TBP and H<sub>2</sub>MEHP, and this has been accomplished by the use of several techniques including infrared studies, cryoscopic studies and isopiestic measurements. Baes<sup>5</sup> has similarly studied the interaction of bis-(2-ethylhexyl)-phosphoric acid and tri-*n*-octylphosphine oxide in *n*-octane. Our laboratory is presently investigating other interactions which give both synergistic and antisynergistic effects in the solvent extraction of various cations.<sup>6</sup> Other laboratories<sup>7-9</sup> have similarly been engaged in a study of these effects.

## Experimental

The infrared studies were made with a Beckman IR-4 spectrophotometer. The method of continuous variations<sup>10</sup> was used. Beer's law was found to hold in the concentration ranges used in this study ( $\Sigma M = 0.075$  and  $0.10 M$ ). "Spectral Grade" cyclohexane from Fisher Scientific Co. was used throughout the investigation.

For the freezing point studies "Spectral Grade" benzene was used (Eastman Organic Chemicals Co.). The method of continuous variations was again employed.

Molecular weight determinations were obtained by the Signer method<sup>11</sup> of isothermal distillation, and by isothermal distillation in an evacuated chamber.<sup>12</sup> The solvents employed in these association studies, in addition to

benzene and cyclohexane, were *n*-hexane (Matheson Coleman & Bell Co., b.p. 68-69°), carbon tetrachloride (Spectral Grade—Eastman Organic Chemicals Co.), chloroform (Reagent Grade—Merck Co.), absolute methanol (Anal. Reagent—Mallinckrodt Co.), and acetone (Reagent—Fisher Scientific Co.), which was dried by anhydrous CaCl<sub>2</sub>. The solvents, TBP and H<sub>2</sub>MEHP, were purified as reported in a previous publication.<sup>13</sup>

## Results

**Molecular Weight Studies.**—In the course of preliminary freezing point studies it became apparent that H<sub>2</sub>MEHP was highly aggregated and that the molecular weight varied with the solvent used. In order to perform precise continuous variation studies it was imperative that a study be made of the molecular weight of H<sub>2</sub>MEHP in various solvents. The method of isothermal distillation was used, utilizing Signer tubes,<sup>11</sup> as well as a method involving distillation in an evacuated chamber.<sup>12</sup> The results from both methods were comparable, and errors are estimated to be in the vicinity of  $\pm 5\%$ . Solvents capable of hydrogen bonding, such as CHCl<sub>3</sub>, CH<sub>3</sub>COOH<sup>13</sup> and CH<sub>3</sub>OH tend to reduce the degree of aggregation of H<sub>2</sub>MEHP; the latter two solvents reducing the substance to a monomer, probably through solute-solvent interaction. Chloroform reduces the aggregation to about 3.5. Acetone possessing a basic oxygen also reduces the aggregation, but only to a dimer. In the concentration ranges used in these studies H<sub>2</sub>MEHP is hexameric in benzene and is aggregated further in cyclohexane. (Molecular weight is close to 12 times the simple formula weight.)

The results of isopiestic studies of mixtures of H<sub>2</sub>MEHP and TBP in benzene are shown in Table I. In all of the solutions at equilibrium the sum of the concentrations of the mixtures are always greater than the concentration of the reference. In the solution with a TBP/(H<sub>2</sub>MEHP)<sub>6</sub> ratio of 0.97 the solvent distills from the mixture to reference. In the solution with a TBP/(H<sub>2</sub>MEHP)<sub>6</sub> ratio of 1.98 there is virtually no distillation of solvent. In the last two solutions with TBP/(H<sub>2</sub>MEHP)<sub>6</sub> ratios greater than 2 the distillation occurs from the reference to the mixture. Thus there is indicated an interaction occurring, which decreases the total number of particles in solution. This appears to occur at a ratio of TBP/(H<sub>2</sub>MEHP)<sub>6</sub> of 2.

## Freezing Point Depression Studies (Benzene).—

(13) D. F. Peppard, J. R. Ferraro and G. W. Mason, *J. Inorg. Nucl. Chem.*, **7**, 231 (1958).

(1) Based on work performed under the auspices of the U. S. Atomic Energy Commission. Presented at 138th American Chemical Society Meeting, New York, September 12-16, 1960.

(2) Henceforth abbreviated as TBP.

(3) Henceforth abbreviated as H<sub>2</sub>MEHP.

(4) D. F. Peppard, G. W. Mason and R. J. Sironen, *J. Inorg. Nucl. Chem.*, **10**, 117 (1959).

(5) H. T. Baker and C. F. Baes, Jr., USAEC Unclassified Document, ORNL-2443 (1957); 2486 (1957); 2451 (1957); 2737 (1959).

(6) D. F. Peppard, unpublished data.

(7) H. Irving and D. N. Edgington, *Proc. Chem. Soc.*, 360 (1960).

(8) C. A. Blake, D. E. Horner and J. M. Schmitt, USAEC Unclassified Document ORNL-2259 (1959).

(9) J. Kennedy, U.K.A.E.A., Doc. No. AERE C/M 369 (1958).

(10) P. Job, *Ann. Chim.*, [10] **9**, 113 (1928).

(11) E. P. Clark, *Ind. Eng. Chem., Anal. Ed.*, **13**, 820 (1941).

(12) J. E. Morton, A. D. Campbell and T. S. Ma, *The Analyst*, **78**, 722 (1953); G. Scatchard, W. J. Hamer and S. E. Wood, *J. Am. Chem. Soc.*, **60**, 3061 (1938).

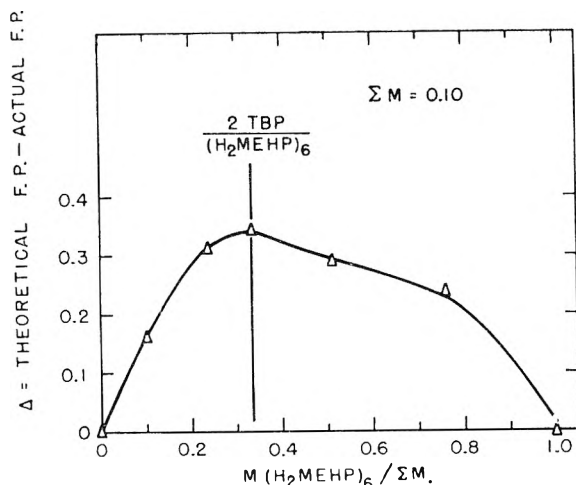


Fig. 1—Continuous variations study of TBP and  $(\text{H}_2\text{MEHP})_6$  in benzene at  $5^\circ$ .

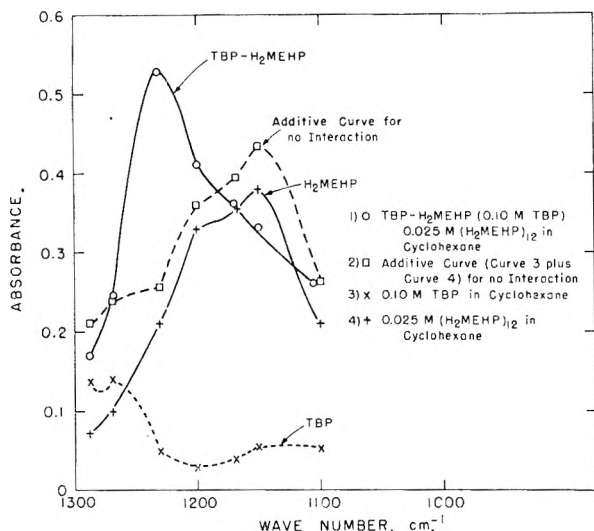


Fig. 2—Infrared spectra of tri-*n*-butyl phosphate, mono-(2-ethylhexyl)-phosphoric acid and mixture of each solute in cyclohexane at  $25^\circ$ ; ratio  $\text{TBP}/(\text{H}_2\text{MEHP})_{12} = 4$ .

Continuous variation studies using the difference between a theoretical freezing point depression ( $\Delta T_i$ ) for no interaction, and the actual freezing point depression ( $\Delta T$ ) in benzene ( $\Sigma M = 0.10$ ), show a maximum at the ratio  $2\text{TBP}/(\text{H}_2\text{MEHP})_6$  (Fig. 1). Thus the results from the isopiestic studies and freezing point depression studies are all consistent with the above ratio for the interaction between TBP and  $\text{H}_2\text{MEHP}$  and with equilibrium 1.

**Infrared Studies.**—Continuous variation studies in cyclohexane also indicate an association product between the  $\text{H}_2\text{MEHP}$  polymer and TBP at a ratio of  $2\text{TBP}$  per  $(\text{H}_2\text{MEHP})_6$ . Figure 2 illustrates the infrared spectra in cyclohexane of the pure components and of the mixture:  $4\text{TBP}/(\text{H}_2\text{MEHP})_{12}$ . The additive curve for no interaction is also included. It is observed that the TBP doublet in the region of  $1270\text{ cm}^{-1}$  (corresponding to the unbonded phosphoryl absorption) disappears. The region of  $1150\text{ cm}^{-1}$  in  $\text{H}_2\text{MEHP}$  (corresponding to the hydrogen bonded  $\text{P}\rightarrow\text{O}$  absorption) diminishes, and the appear-

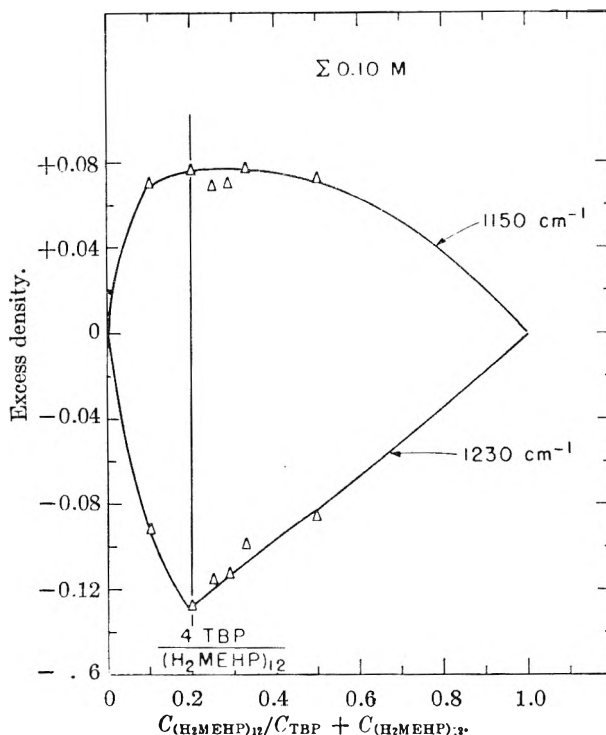
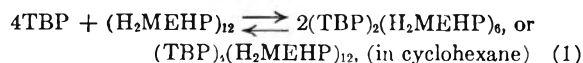
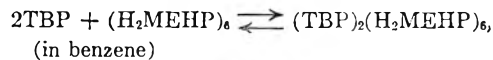


Fig. 3—Continuous variations study of  $(\text{H}_2\text{MEHP})_{12}$  and TBP in cyclohexane at  $25^\circ$ ;  $\Sigma 0.10\text{ M}$ .

ance of a new peak at about  $1230\text{ cm}^{-1}$  is observed for the complex. A continuous variation plot for  $(\text{H}_2\text{MEHP})_{12}$  and TBP in cyclohexane at  $25^\circ$  is illustrated in Fig. 3. Results have been obtained for total molarity ( $\Sigma M = 0.075$  and  $0.10\text{ M}$ ) where Beer's law has been shown to hold. Results are plotted at two wave lengths,  $1230\text{ cm}^{-1}$  and  $1150\text{ cm}^{-1}$ . Maxima in excess density at  $1150\text{ cm}^{-1}$  and minima at  $1230\text{ cm}^{-1}$  are obtained for a ratio  $4\text{TBP}/(\text{H}_2\text{MEHP})_{12}$  at  $\Sigma M$  concentrations equal to  $0.075$  and  $0.10\text{ M}$ .

The results point to a reaction between TBP and  $(\text{H}_2\text{MEHP})_6$  maximizing at the ratio of  $2\text{TBP}/(\text{H}_2\text{MEHP})_6$ . The results are consistent with the following proposed equilibrium



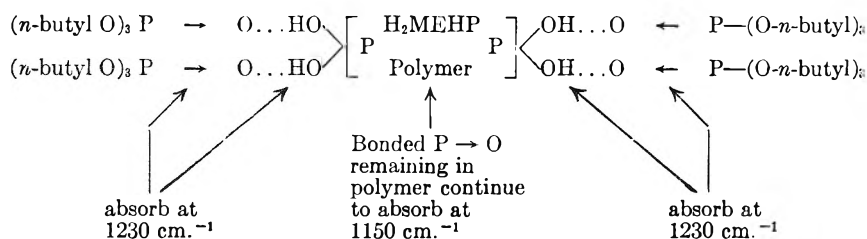
### Discussion

From the infrared spectra in cyclohexane it is observed that the doublet  $\text{P}\rightarrow\text{O}$  absorption for TBP at about  $1270\text{ cm}^{-1}$  appears to change as  $\text{H}_2\text{MEHP}$  is added. A new peak at  $1230\text{ cm}^{-1}$  begins to form. When the ratio reaches  $2\text{TBP}$  per hexamer of  $\text{H}_2\text{MEHP}$  the  $\text{P}\rightarrow\text{O}$  absorption at  $1270\text{ cm}^{-1}$  has disappeared, and the peak at  $1230\text{ cm}^{-1}$  is at a maximum. This would appear to indicate that the phosphoryl oxygen in TBP is being bonded, since it has shifted to lower frequency, and is probably bonded to the hydrogen in the  $\text{H}_2\text{MEHP}$  polymer. The bonded  $\text{P}\rightarrow\text{O}$  absorption at  $1150\text{ cm}^{-1}$  in the  $\text{H}_2\text{MEHP}$  polymer diminishes in intensity as TBP is added, but never entirely disappears. Apparently some of the phos-

TABLE I  
ISOPIESTIC EQUILIBRATIONS OF TBP AND (H<sub>2</sub>MEHP)<sub>6</sub> IN BENZENE AT 25°

Ref. $C_{(TBP)}$ (moles/l.)	Soln. of (H <sub>2</sub> MEHP) <sub>6</sub> and TBP, $C_{(TBP)}$ (moles/l.)	$C_{(H_2MEHP)_6}$ (moles/l.)	$\frac{C_{(TBP)}}{C_{(H_2MEHP)_6}}$	$\frac{C_{(TBP)} + C_{(H_2MEHP)_6}}{C_{(H_2MEHP)_6}}$	Particles indicated in mixtures if ref. is considered as 1 particle
0.041	0.032	0.033	0.97	0.035	>1
.033	.037	.019	1.98	.056	= or <1
.032	.040	.011	3.64	.051	<1
.031	.036	.005	7.40	.041	<1

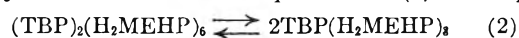
phoryl oxygens remain bonded as they are in the pure polymer of H<sub>2</sub>MEHP. The other oxygens (hydroxyl oxygens) are probably involved in the bonding to the TBP, and they appear to be less strongly bonded than those oxygens bonded in the polymer. Since the structure of the H<sub>2</sub>MEHP polymer is not known, it is very difficult to assign a structure for the complex. However, the schematic illustration (below) will help to visualize a possible explanation of the experimental facts. Experimental support for such a postulate comes from a study of the P→O absorption at 1150 cm.<sup>-1</sup> for H<sub>2</sub>MEHP (Fig. 2).



An 0.038 M (H<sub>2</sub>MEHP)<sub>12</sub> in cyclohexane shows an absorbance of 0.580 at 1150 cm.<sup>-1</sup>. If only 0.075 M of TBP is present in such a solution, it would be expected that since only 2 of the 24 hydroxyls in the H<sub>2</sub>MEHP polymer are involved in bonding to the TBP, the absorbance would be expected to be reduced to  $[22/24 (0.580)] = 0.53$ . The experimental absorbance is found to be 0.523. Likewise when 0.10 M TBP is added to 0.025 M (H<sub>2</sub>MEHP)<sub>12</sub> (absorbance at 1150 cm.<sup>-1</sup> is 0.380) it would be expected that 4 of the 24 hydroxyls would now be involved in bonding and that the absorbance should be reduced to  $[20/24 (0.380)] = 0.32$ . The experimental absorbance is found to be 0.330.

As a result of the above data and of the cryoscopic and isopiestic measurements it is believed that the TBP merely adds on to the H<sub>2</sub>MEHP hexamer in benzene. Cryoscopic studies made on a fixed concentration of H<sub>2</sub>MEHP (e.g., 1 mole of hexamer), and adding varying amounts of TBP (e.g., 1 mole, 2 moles, 3 moles) showed little change in the freezing point depression

until the TBP was in excess of a 2:1 ratio. Isopiestic studies were made by diluting the concentrations of the reference and mixture solutions by one-half the concentration used in Table I, in an effect to see if the number of particles in the mixtures could be changed. The results were the same as those obtained for the higher concentrations. Thus it would appear that the TBP adds directly and that the primary equilibrium is (1), with little if any contribution from equilibrium (2). It ap-



pears that this interaction between a neutral phos-

phate and mono-alkyl phosphoric acids is a general type of interaction for these classes of compounds<sup>14</sup> rather than an isolated case.

### Conclusion

The interaction between TBP and H<sub>2</sub>MEHP gives an association product at a ratio (TBP)<sub>2</sub>/(H<sub>2</sub>MEHP)<sub>6</sub>. Since the structures of both the H<sub>2</sub>MEHP polymer and the complex remain unknown, explanation of the reasons for this system giving an antisnergistic effect is difficult. It is obvious that the true explanation is not a simple one, but the results can be accounted for rather simply, since in the interaction between TBP and H<sub>2</sub>MEHP some of the potential sites for cation extraction are no longer available to the complex. The sites are tied up in forming the complex between TBP and H<sub>2</sub>MEHP, thus causing a decrease in the extraction of the cation into the organic phase. It is evident that these complex systems giving synergism or antisnergism behavior in metal extractions merit more attention.

(14) J. R. Ferraro, unpublished data.

## POTASSIUM HEXAFLUOROPHOSPHATE—AN ASSOCIATED ELECTROLYTE

By R. A. ROBINSON,\* J. M. STOKES AND R. H. STOKES

*Chemistry Department of the University of New England, Armidale, N.S.W., Australia**Received October 20, 1960*

The densities, viscosities and conductances of aqueous solutions of potassium fluorophosphate have been determined at 25 and 50°. Isopiestic vapor pressure measurements have been made at 25° and the osmotic and activity coefficients computed. The equivalent conductances at infinite dilution are 132.83 and 203.25 cm.<sup>2</sup> int. ohm<sup>-1</sup> equiv.<sup>-1</sup> at 25 and 50°, respectively, and the association constants are 2.42 and 1.43 liter mole<sup>-1</sup>.

Our attention was drawn to the interesting salt, potassium hexafluorophosphate, KPF<sub>6</sub>, by the work of Randles<sup>1</sup> on the surface potential of its solutions. We have studied some properties of aqueous solutions of the fluorophosphate, in particular the conductance and vapor pressure, and have concluded that it exhibits marked association to ion pairs and even higher aggregates.

## Experimental

Potassium fluorophosphate was obtained from the Ozark-Mahoning Company and recrystallized from water, using polythene vessels throughout; for most purposes one recrystallization sufficed, but for the conductance measurements three or even four recrystallizations were found necessary. In preliminary work, oven-drying of the recrystallized material in glass weighing bottles resulted in slight etching of the glass, suggesting some decomposition of the moist material at temperatures as low as 80°; this oven-dried material gave considerable scatter of data in conductance measurements. For all the measurements reported in this paper the recrystallized material was dried to constant weight in vacuum desiccators over sodium hydroxide.

**Density.**—The following densities of aqueous solutions were measured at 25°

<i>m</i>	0.1010	0.1334	0.1901	0.2078
<i>d</i>	1.00860	1.01217	1.01840	1.02048
<i>m</i>	0.2806	0.3951	0.4121	
<i>d</i>	1.02830	1.04062	1.04211	

These data can be represented by

$$d = 0.99707 + 0.1153m - 0.0139m^2$$

where *m* is the molality of the solution. Densities were measured at three concentrations at 50°

<i>m</i>	0.1862	0.3482	0.4479
<i>d</i>	1.00834	1.02512	1.03512

**Viscosity.**—Viscosities of aqueous solutions at 25° were determined as

<i>m</i>	0.1010	0.2033	0.2806	0.3879	0.4459
$\eta/\eta^0$	0.9985	0.9968	0.9952	0.9925	0.9918

Two measurements were made at 50°

<i>m</i>	0.1849	0.3451
$\eta/\eta^0$	1.0019	1.0024

The saturated solution at 25° was found to be 0.497 *M* by measuring the conductivity of a diluted aliquot and 0.501 *M* by the isopiestic method.<sup>2</sup> The saturated solution at 25° has a refractive index identical with that of water as closely as could be measured with an Abbe refractometer.

**Conductance.**—Solutions were prepared by weight from the vacuum-dried salt and conductivity-water in equilibrium with the atmosphere. The cells had fairly high constants of 10–20 cm.<sup>-1</sup>, being of tubular form with the electrodes in bulbs at the ends, in order that an accurate calculation of the cell constant change between 25 and 50° could be made.<sup>3</sup> They were calibrated with the Jones and Bradshaw 0.01 *D*

and 0.1 *D* potassium chloride standards; the equivalent conductances of Table I are therefore given in cm.<sup>2</sup> int. ohm<sup>-1</sup> equiv.<sup>-1</sup>. Frequency-dependence in the range 500–2000 c./sec. was negligible. The conductivity-bridge was a Leeds and Northrup Jones bridge; the cells were immersed in oil thermostats held at 25 and 50° within  $\pm 0.002^\circ$ . The temperatures were checked by a platinum resistance thermometer and may be taken as correct within 0.005°. Volume-concentrations of the solutions (*c*) were calculated using the above density data.

TABLE I

EQUIVALENT CONDUCTANCE OF POTASSIUM FLUOROPHOSPHATE AT 25 AND 50°

<i>c</i> × 10 <sup>3</sup> , mole l. <sup>-1</sup>	$\Lambda$ , cm. <sup>2</sup> int. ohm <sup>-1</sup> equiv. <sup>-1</sup>	<i>c</i> × 10 <sup>3</sup> , mole l. <sup>-1</sup>	$\Lambda$ , cm. <sup>2</sup> int. ohm <sup>-1</sup> equiv. <sup>-1</sup>
	25°		25°
0.8123	130.04	46.80	111.93
1.3889	129.18	49.86	111.38
2.5135	127.81	55.04	110.40
2.5192	127.81	55.86	110.32
4.005	126.43	69.37	108.05
5.672	125.24	70.64	107.84
5.854	125.13	84.16	105.93
7.715	124.00		50°
10.642	122.44	0.8049	198.81
14.821	120.65	1.3764	197.51
14.964	120.57	3.969	193.38
15.940	120.24	5.621	191.56
18.292	119.32	5.801	191.35
20.438	118.62	7.645	189.73
21.284	118.33	10.546	187.44
30.729	115.63	14.829	184.75
38.213	113.80	18.127	182.96
		49.14	171.63

**Vapor Pressures.**—Isopiestic vapor pressure measurements were made at 25°, using sodium chloride as reference electrolyte; the results are given in Table II.

TABLE II

ISOPIESTIC MEASUREMENTS AT 25°

<i>m</i> <sub>1</sub>	<i>m</i> <sub>2</sub>	<i>m</i> <sub>1</sub>	<i>m</i> <sub>2</sub>	<i>m</i> <sub>1</sub>	<i>m</i> <sub>2</sub>
0.09001	0.09513	0.2781	0.3249	0.3739	0.4578
.1363	.1479	.2903	.3426	.3777	.4651
.1747	.1954	.3261	.3949	.3987	.5010
.1799	.1999	.3412	.4168	.4143	.5240
.1831	.2043	.3452	.4205		
.2713	.3158	.3693	.4551		

<sup>a</sup> (1) = NaCl; (2) = KPF<sub>6</sub>.

## Discussion

From the density data at 25°, the partial molal volume of the salt at infinite dilution is calculated as 68.7 ml. mole<sup>-1</sup> and if the limiting partial molal volume of the potassium ion<sup>4</sup> is 1.5<sub>0</sub> ml. mole<sup>-1</sup>, that of the hexafluorophosphate ion is 67.2 ml.

(4) R. H. Stokes and R. A. Robinson, *Trans. Faraday Soc.*, **53**, 301 (1957).

\* National Bureau of Standards, Washington, D. C.

(1) J. E. B. Randles, *Disc. Faraday Soc.*, **24**, 194 (1957).

(2) G. Scatchard, W. G. Hamer and S. E. Wood, *J. Am. Chem. Soc.*, **60**, 3061 (1938).

(3) R. A. Robinson and R. H. Stokes, "Electrolyte Solutions," Second Edition, Butterworths Scientific Publications, London, 1959, p. 97.

mole<sup>-1</sup>. With the same choice for the potassium ion, the partial molal volumes of the halide ions are:  $\bar{V}_{\text{Cl}}^0 = 25.3_1$ ,  $\bar{V}_{\text{Br}}^0 = 32.2_3$  and  $\bar{V}_{\text{I}}^0 = 43.8_5$  ml. mole<sup>-1</sup>. The  $\text{PF}_6^-$  ion is known from X-ray studies<sup>5</sup> to be octahedral, with a P-F internuclear distance of 1.73 Å.; taking the van der Waals radius of the fluorine atom as 1.22 Å., the maximum diameter of the  $\text{PF}_6^-$  ion is 5.9 Å. A monovalent ion of this size is unlikely to cause appreciable electrostriction of water molecules in its vicinity, and its apparent volume in solution should be near to its actual physical volume. Spheres of 5.9 Å. diameter would have a molal volume of 64.8 ml.

The viscosity results at 25° can be represented by

$$\eta/\eta^0 = 1 + 0.0057\sqrt{c} - 0.028c$$

0.0057 being the coefficient of the Falkenhagen and Vernon<sup>6</sup> term calculated with the ion-mobilities given below. The linear coefficient,  $-0.028$ , includes a contribution of  $-0.007$  for the potassium ion<sup>7</sup>; thus the  $\text{PF}_6^-$  ion, in spite of its large size, diminishes the viscosity of water. The small numerical value of the linear coefficient must represent a balance between the "obstructive" effect of the large anion and the "structure-breaking" effect on the solvent; that the former must be large can be argued by analogy with the effect of pentaerythritol, with a molar volume of 101 ml., on the viscosity of water, where it has been found<sup>8</sup> that the coefficient of the linear term is  $+0.353$ .

The conductivity results (Fig. 1) are typical of an electrolyte showing pronounced ion-pair association, a conclusion which is supported by comparing the activity coefficients (Fig. 5) with those of normal 1-1 electrolytes. The method of Fuoss<sup>9</sup> was therefore adapted to determine the values of  $\Lambda^0$  and the association constant,  $K_A$ . The Fuoss-Onsager equation for a completely dissociated 1:1 electrolyte is

$$\Lambda_\eta = \Lambda^0 - S\sqrt{c} + Ec \log c + Jc$$

where  $S$  and  $E$  are parameters depending on  $\Lambda^0$  but not on the ion size and  $J$  depends on both  $\Lambda^0$  and the ion size.  $\Lambda_\eta$  is the experimental equivalent conductance corrected for the viscosity of the solution. In the case of very large ions, this correction takes the form of simple multiplication by the relative viscosity, but work in this Laboratory<sup>10</sup> on the mobility of ions in solutions of non-electrolytes suggests that this is an over-correction for ions of less than 5 Å. radius. In any event, it is doubtful if relative viscosities of less than unity can be appropriately used in this way since the argument depends on the use of Einstein's equation for the viscosity of a continuum containing spherical obstructions.<sup>11</sup> However, the maximum viscosity

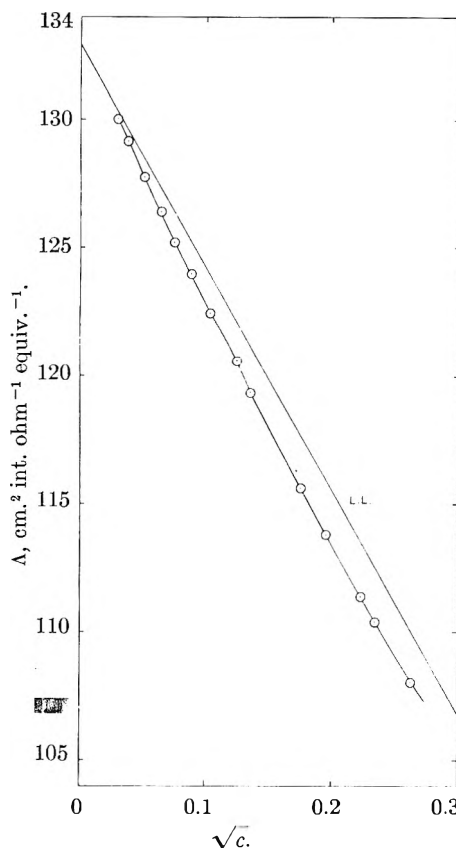


Fig. 1.—Equivalent conductance of potassium fluorophosphate solution at 25° as a function of concentration.

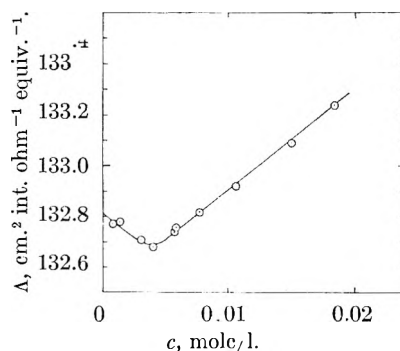


Fig. 2.—Change of  $\Lambda'$  ( $\equiv \Lambda + S\sqrt{c} - Ec \log c$ ) with concentration.

effect involved in the present work would be only 0.05% at  $c = 0.02$ , the highest concentration used in evaluating  $K_A$  from the conductance data.

For an associated electrolyte, we have

$$\bar{K}_\Lambda = \frac{(1 - \alpha)c\gamma_u}{\alpha^2 c^2 \gamma_i^2}$$

where  $\alpha$  is the fraction of free ions,  $c$  is the stoichiometric concentration,  $\gamma_i$  is the mean activity coefficient of the ions at the ionic concentration,  $\alpha c$ , and  $\gamma_u$  is the activity coefficient of the ion pairs (which for the present, we shall regard as unity). The denominator may more conveniently be replaced by  $c^2 \gamma^2$  where  $\gamma$  is the stoichiometric activity coefficient, known from the vapor pressure measurements. We then have

(5) H. Bode and G. Teufer, *Acta Cryst.*, **8**, 611 (1955); H. Bode and H. Clausen, *Z. anorg. Chem.*, **265**, 229 (1951); **268**, 20 (1952).

(6) H. Falkenhagen and E. L. Vernon, *Physik. Z.*, **33**, 140 (1932).

(7) M. Kaminsky, *Disc. Faraday Soc.*, **24**, 71 (1957).

(8) F. J. Kelly, R. Mills and J. M. Stokes, *J. Phys. Chem.*, **64**, 1448 (1960).

(9) R. M. Fuoss and F. Accascina, "Electrolytic Conductance," Interscience Publishers, New York, N. Y., 1959, Chap. 16.

(10) J. M. Stokes and R. H. Stokes, *J. Phys. Chem.*, **62**, 497 (1958); B. J. Steel, J. M. Stokes and R. H. Stokes, *ibid.*, **62**, 1514 (1958).

(11) A. Einstein, *Ann. Phys.*, **19**, 289 (1906).

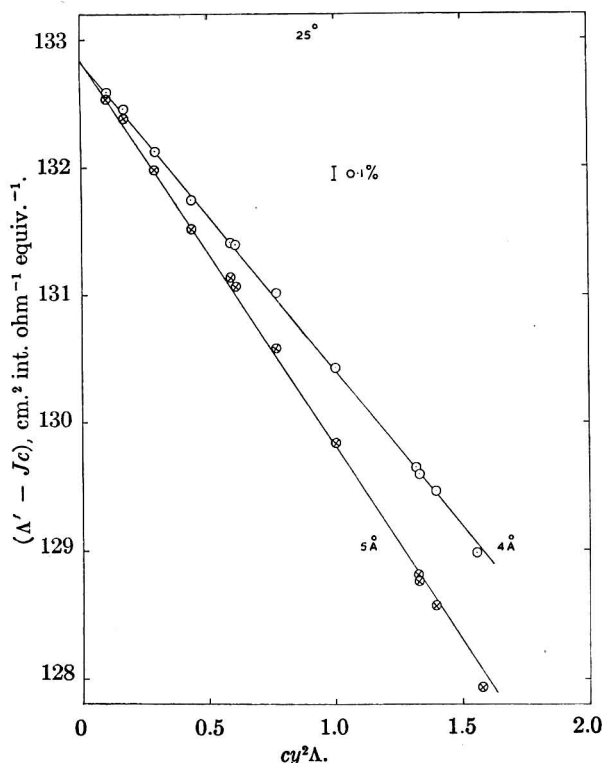


Fig. 3.— $(\Lambda' - Jc)$  vs.  $cy^2\Lambda$ . Temperature,  $25^\circ$ . The  $J$  function is calculated with  $a = 4 \text{ \AA}$ . (upper curve) and  $a = 5 \text{ \AA}$ . (lower curve).

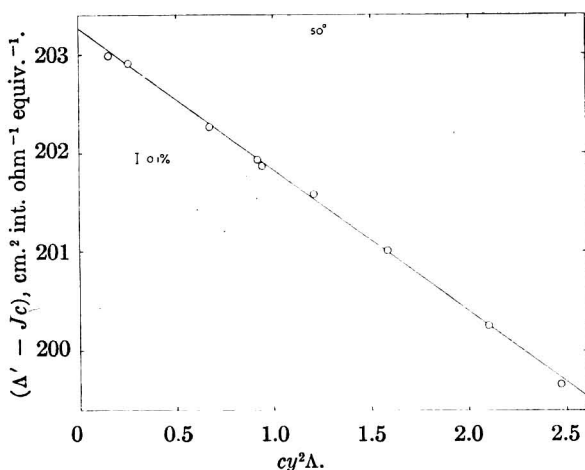


Fig. 4.— $(\Lambda' - Jc)$  vs.  $cy^2\Lambda$  at  $50^\circ$ ;  $a = 4 \text{ \AA}$ .

$$\alpha = 1 - K_A c y^2$$

from which ionic concentrations,  $c_i = \alpha c$ , can be evaluated once  $K_A$  is known. The Fuoss equation now becomes

$$\Lambda = \alpha[\Lambda^0 - S\sqrt{c_i} + Ec_i \log c_i + Jc_i]$$

In very dilute solutions where  $c_i \approx c$ , this may be approximated by

$$\Lambda = \Lambda^0 - S\sqrt{c} + Ec \log c + Jc - K_A c y^2 \Lambda$$

Following Fuoss, we first calculate

$$\Lambda' (\equiv \Lambda + S\sqrt{c} - Ec \log c)$$

using as preliminary values of  $\Lambda^0 = 132.9$  and  $203.1 \text{ cm.}^2 \text{ ohm}^{-1} \text{ equiv.}^{-1}$  which give  $S = 91.22$  and  $149.47$  and  $E = 49.79$  and  $83.55$  at  $25$  and  $50^\circ$ , respectively. However, a plot of  $\Lambda'$  vs.  $c$  (Fig. 2),

suggested by Fuoss, is not in this instance linear at low concentrations. To overcome this difficulty, we write

$$\Lambda' - Jc = \Lambda^0 - (K_A y^2 c \Lambda)$$

so that, since  $J$  is known as a function of ion size, a plot of the left-hand side against  $y^2 c \Lambda$  should extrapolate to  $\Lambda^0$  with slope  $K_A$ .

In the cases of association discussed by Fuoss, who used the results of Mercier and Kraus<sup>12</sup> on tetrabutylammonium bromide in water-dioxane mixtures, the ion size parameter,  $a$ , was determined by measurements in mixtures of low dielectric constant and the value so found used to determine  $J$ . In the present work we have calculated  $a$  from the potassium ion radius of  $1.33 \text{ \AA}$ . and the  $\text{PF}_6^-$  ion radius which we have taken as  $2.67 \text{ \AA}$ . (slightly less than the "maximum" radius of  $2.95 \text{ \AA}$ . on the grounds that some approaches of the ions could be slightly closer because of the octahedral shape of the  $\text{PF}_6^-$  ion). For the resulting ion size parameter,  $a = 4.0 \text{ \AA}$ ., we calculate  $J = 233$  and  $334$  at  $25$  and  $50^\circ$ , respectively. Values of  $\Lambda'$  and  $y^2 \Lambda c$  are given in Table III, which also includes values of  $\Lambda^0$  calculated for each experimental point by the equation

$$\Lambda^0 = \Lambda' - Jc + K_A y^2 \Lambda c$$

The function  $(\Lambda' - Jc)$  is plotted against  $cy^2\Lambda$  in Fig. 3, where it will be seen that the average deviation of the points from the straight line does not exceed  $0.03 \text{ \AA}$  units. Thus we can with confidence use this plot to give  $\Lambda^0 = 132.83 \text{ cm.}^2 \text{ int. ohm}^{-1} \text{ equiv.}^{-1}$  and  $K_A = 2.42 \text{ liter mole}^{-1}$ . An improved approximation may be made by using this value of  $K_A$  to calculate true ionic concentrations and re-evaluating  $\Lambda'$ , using these in place of the total concentrations, but this will not change the value of  $K_A$  by more than  $2\%$  and leaves  $\Lambda^0$  unaffected. The value of  $K_A$  is, however, quite sensitive to the choice of ion size parameter. Figure 3 includes a plot which leads to  $K_A = 3.02 \text{ liter mole}^{-1}$  with  $a = 5 \text{ \AA}$ ., but the fit of this straight line is not quite so good at concentrations above  $0.01 \text{ M}$ . The value of  $a = 3 \text{ \AA}$ . was also tried but gave deviations from the straight line several times larger.

The same calculation was carried out with the  $50^\circ$  data (Fig. 4) where an ion size of  $4 \text{ \AA}$ . leads to  $\Lambda^0 = 203.25 \text{ cm.}^2 \text{ int. ohm}^{-1} \text{ equiv.}^{-1}$  and  $K_A = 1.43 \text{ liter mole}^{-1}$ . The ratio  $K_A^{25}/K_A^{50}$  is  $1.69$ . Using an ion size of  $5 \text{ \AA}$ . at both temperatures the ratio is  $1.51$ ; thus there is no doubt that the ratio is close to  $1.6$  even if the correct value of  $a$  is somewhat uncertain. Hence the mean enthalpy change on association is  $-4.0 \text{ cal. mole}^{-1}$ . Fuoss<sup>13</sup> has proposed the equation

$$K_A = \frac{4\pi}{3000} N a^3 e^b$$

where  $b = e^2/(\epsilon k T a)$  for the molar scale association constant. With  $a = 4 \text{ \AA}$ ., this equation gives  $K_A = 0.97$  and  $1.03 \text{ liter mole}^{-1}$  at  $25$  and  $50^\circ$ , respectively, and the mean enthalpy change would be  $+0.46 \text{ kcal. mole}^{-1}$ . Thus the experimental enthalpy change is not only of different magnitude

(12) P. L. Mercier and C. A. Kraus, *Proc. Natl. Acad. Sci.*, **41**, 1033 (1955).

(13) R. M. Fuoss, *J. Am. Chem. Soc.*, **80**, 5059 (1958).



TABLE III  
CALCULATION OF  $\Lambda^0$  AND  $K_A$   
 $\Lambda' - Jc = \Lambda^0 - K_A \Lambda y^2 c$   
 $\Lambda' = \Lambda + S\sqrt{c} - Ec \log c$

25°				50°			
$S = 91.22$				$S = 149.47$			
$E = 49.79$				$E = 83.55$			
$J = 233 (a = 4 \text{ \AA.})$				$J = 354 (a = 4 \text{ \AA.})$			
$K_A = 2.42$				$K_A = 1.43$			
$10^3 c$	$\Lambda'$	$\Lambda y^2 c$	$\Lambda^0$	$10^3 c$	$\Lambda'$	$\Lambda y^2 c$	$\Lambda^0$
0.8123	132.77	0.0983	132.82	0.8049	203.26	0.151	203.21
1.3889	132.78	.163	132.85	1.3764	203.38	.251	203.28
2.5135	132.71	.282	132.81	3.969	203.59	.668	203.23
2.5192	132.71	.282	132.81	5.621	203.82	.912	203.24
4.005	132.68	.430	132.79	5.801	203.82	.936	203.22
5.672	132.74	.585	132.84	7.645	204.15	1.207	203.32
5.854	132.76	.601	132.85	10.546	204.53	1.581	203.28
7.715	132.82	.766	132.87	14.829	205.22	2.099	203.27
10.642	132.92	1.001	132.86	18.127	205.72	2.471	203.20
14.821	133.10	1.322	132.85				
14.964	133.09	1.328	132.81				
15.940	133.18	1.398	132.85				
18.292	133.24	1.558	132.75				

Mean  $\Lambda^0 = 132.83 \pm 0.03$       Mean  $\Lambda^0 = 203.25 \pm 0.03$

but of different sign; this discrepancy may perhaps be due to the neglect of entropy terms in the derivation of Fuoss' equation.

The limiting ionic mobilities of the  $\text{PF}_6^-$  ion are 59.28 and 91.85  $\text{cm}^2 \text{int. ohm}^{-1} \text{equiv.}^{-1}$  at 25 and 50°, respectively. The  $(\lambda^0 \eta^0)$  product therefore changes from 0.5278 at 25° to 0.5021 at 50°: in this respect the ion is intermediate in behavior between the halide ions for which the  $(\lambda^0 \eta^0)$  product diminishes more rapidly with temperature and the calcium ion for which the product decreases by about 1%.

From the isopiestic vapor pressure measurements, the osmotic and activity coefficients given in Table IV were calculated. Figure 5 compares these activity coefficients with those of potassium chloride and potassium nitrate, and shows that the data for the fluorophosphate conform with the limiting Debye-Hückel equation up to saturation! In contrast with normal salts such as potassium chloride and iodide and with the somewhat less associated potassium nitrate, the association is so marked that it should be possible to calculate the association constant from the thermodynamic data alone. For this purpose we use the equation

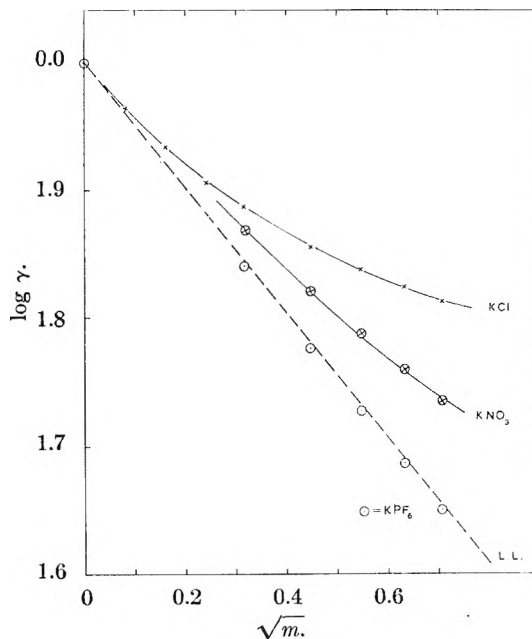


Fig. 5.—The activity coefficient of potassium fluorophosphate compared with those of potassium chloride and potassium nitrate and with the values computed by the limiting Debye-Hückel equation.

TABLE IV

OSMOTIC AND ACTIVITY COEFFICIENTS OF POTASSIUM FLUOROPHOSPHATE AT 25°

$m$	0.1	0.2	0.3	0.4	0.5
$\psi$	.878	.829	.795	.763	.735
$\gamma$	.693	.597	.535	.486	.447

TABLE V

CALCULATION OF  $K_A$  AT 25° FROM ACTIVITY COEFFICIENT DATA

$m$	$\gamma$	$\gamma$	$\alpha$	$\frac{\log(K_A/\gamma\psi)}{(K_A/\gamma\psi)}$
0.1	0.693	0.774	0.895	0.340
.2	.597	.728	.820	.402
.3	.535	.700	.764	.439
.4	.486	.681	.714	.481
.5	.447	.667	.670	.519

TABLE VI

CALCULATION OF  $K_Q$  AT 25° USING  $K_A = 2.09 \text{ LITER MOLE}^{-1}$

$m$	"Apparent" $K_A$	$\beta'$	$\alpha'$	$K_Q$
0.1	2.19	0.0024	0.900	2.4
.2	2.52	.015	.850	3.3
.3	2.75	.028	.820	2.6
.4	3.03	.044	.802	2.8
.5	3.30	.061	.791	2.8

$$K_A = \frac{\alpha_{\text{KPF}_6}}{\alpha_{\text{K}} + \alpha_{\text{PF}_6^-}} = \frac{(1 - \alpha)m\gamma_u}{\alpha^2 m^2 \gamma_i^2}$$

where now we are calculating a molality scale  $K_A$ . As above, we can reduce this to

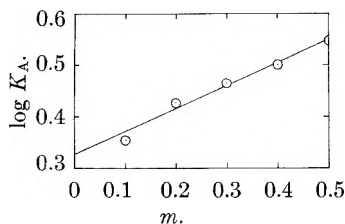


Fig. 6.— $K_A/\gamma_U$  vs.  $m$  and the extrapolation to obtain  $K_A$ .

$$K_A/\gamma_U = (1 - \alpha)/(m\gamma^2)$$

where  $\gamma$  is the stoichiometric activity coefficient of Table IV. Also  $\gamma = \alpha \gamma_i$  where  $\gamma_i$  is the mean ionic activity coefficient of the unassociated part,<sup>14</sup> which we shall take as given by

$$-\log \gamma_i = \frac{A\sqrt{m_i}}{1 + Ba\sqrt{m_i}} + \log(1 + 0.036m_i)$$

with  $A = 0.511$  liter<sup>1/2</sup> mole<sup>-1/2</sup>,  $B = 0.328$  liter<sup>1/2</sup> mole<sup>-1/2</sup> and  $a = 4$  Å, *i.e.*, a fully dissociated but unhydrated electrolyte with an ion size consistent with the physical dimensions of the ions. The details of the calculation are shown in Table V in which only the final stages in the successive approximations for  $\alpha$  and  $\gamma_i$  are given. A plot (Fig. 6) of  $\log K_A/\gamma_U$  against  $m$  is a straight line and, since  $\gamma_U \rightarrow 1$  as  $m \rightarrow 0$ , Fig. 6 gives the limiting value of  $K_A$  as 2.0, which is in reasonable agreement with the value of 2.42 from conductance data. However, the slope of the line implies that  $\log \gamma_U = -0.4m$ . At first sight, this means a surprisingly rapid decrease in the activity coefficient of the ion pairs but it must be remembered that an ion pair with  $a = 4$  Å. constitutes a dipole of moment  $19D$  which will interact strongly with both neighboring ions and neighboring ion pairs leading to the formation of triple and quadruple ions. In this connection we might note that Roberts and Kirkwood<sup>15</sup> found that the activity coefficient of glycine in potassium chloride solution is given by

(14) Ref. 3, p. 37.

(15) R. M. Roberts and J. G. Kirkwood, *J. Am. Chem. Soc.*, **63**, 1373 (1941).

$$\log \gamma_U = -0.1789m_{KCl}$$

(omitting higher terms in  $m_{KCl}$ ).

Assuming that quadruple ions are formed, let the concentrations of ion pairs and quadruple ions be denoted by  $m_U$  and  $m_Q$ , respectively; then at a stoichiometric molality  $m$ , the concentrations of potassium and fluorophosphate ions are each  $[m - m_U - 2m_Q]$ . The relation  $\gamma = \alpha \gamma_i$ , used above, now becomes

$$\gamma = \gamma_i[\alpha' - 2\beta']$$

where

$$\alpha' = \frac{m - m_U}{m} \text{ and}$$

$$\beta' = m_Q/m$$

Hence, if quadruple ions are formed, the quantity  $\alpha$  should be replaced by  $(\alpha' - 2\beta')$  and

$$\begin{aligned} K_A(\text{apparent}) &= \frac{1 - \alpha' + 2\beta'}{m\gamma^2} \\ &= K_A + \frac{2\beta'}{m\gamma^2} \end{aligned}$$

and the equilibrium constant for quadruple ion formation is

$$K_Q = \frac{m_Q}{m_U^2} = \frac{\beta'}{(1 - \alpha')^2 m}$$

assuming that the activity coefficients of both uncharged species are unity.

Thus  $\beta'$  can be calculated from the variation in the "apparent"  $K_A$  with concentration. These values of  $\beta'$  can then be substituted to give  $K_Q$ . The results of this calculation are given in Table VI. It is evident that the lack of constancy in  $K_A$  calculated from the activity coefficient data by the first method can be explained by assuming a small amount of quadruple ion formation. Similar calculations showed that the assumption of triple ion formation was inadequate.

We thank the Ozark-Mahoning Company of Tulsa, Oklahoma, for providing potassium fluorophosphate.

## DI-*t*-BUTYL ETHER: STRAIN ENERGY AND PHYSICAL PROPERTIES

BY E. J. SMUTNY AND A. BONDI

Shell Development Co., Emeryville, California

Received October 24, 1960

Di-*t*-butyl ether was synthesized and several physical properties recorded: the heat of formation, the heat of vaporization, the vapor pressure, density and viscosity. The strain of di-*t*-butyl ether, consequent to the crowding of the opposed methyl groups, was determined as approximately 7.6 kcal./mole.

The synthesis of di-*t*-butyl ether has remained for several years a vexing and frustrating problem. Many futile attempts have been made. Reboul<sup>1</sup> observed that the conventional Williamson technique gave only isobutylene and *t*-butyl alcohol. Henry<sup>2</sup> was no more successful. These early failures led some authors<sup>3</sup> to point out that it would be

impossible to place two tertiary butyl groups on the same oxygen atom. It was not until the relatively unusual methods of Erickson and Ashton<sup>4</sup> and more recently of Horner<sup>5</sup> and of Lawesson and Yang<sup>6</sup> that authors claimed success.

(1) E. Reboul, *Compt. rend.*, **108**, 162 (1889).

(2) L. Henry, *Rec. trav. chim.*, **23**, 324 (1904).

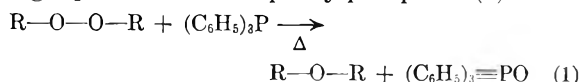
(3) W. A. Hare and E. Mack, *J. Am. Chem. Soc.*, **54**, 4272 (1932).

(4) J. L. E. Erickson and W. Ashton, *ibid.*, **63**, 1769 (1941).

(5) L. Horner, *Ann.*, **591**, 138 (1955).

(6) S. Lawesson and N. C. Yang, *J. Am. Chem. Soc.*, **81**, 4230 (1959).

Horner's method<sup>5</sup> depends on an elegant means of removing a peroxidic oxygen atom, namely treating a peroxide with triphenylphosphine (1).

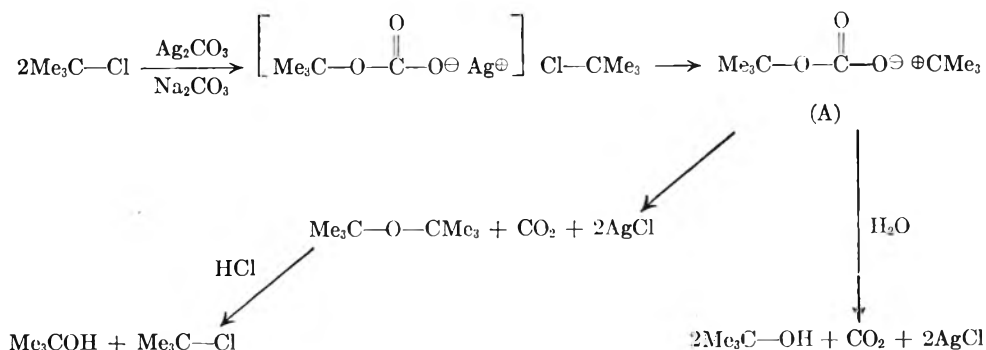


Horner claims that when di-*t*-butyl peroxide (R = Me<sub>3</sub>C-) is heated to 110–120° with triphenylphosphine for 30 hours an 81% yield of di-*t*-butyl ether is obtained.

This method was repeated several times with triphenylphosphine and no detectable amount of di-*t*-butyl ether was isolated. Triethylphosphite was tried as well with no more success.<sup>7</sup> As will become evident later, the properties of di-*t*-butyl ether and di-*t*-butyl peroxide are so similar as to be easily confused. A reaction does occur but since the desired product was not formed the reaction was not investigated further.<sup>8</sup> Horner's method which relies on the oxophilic character of phosphines has been employed with hydroperoxides and acyl peroxides<sup>9</sup> with notable success.

The method of Erickson and Ashton<sup>4</sup> was found to be more reliable, though sensitive to conditions. *t*-Butyl chloride was stirred with freshly prepared silver carbonate<sup>10</sup> in dry ether over anhydrous sodium carbonate. Distillation of the mixture gave a 31% yield of ether.

This rather unorthodox synthesis of an ether can be rationalized as below. *t*-Butyl chloride and silver carbonate react to give silver *t*-butyl carbonate which immediately reacts with another molecule of *tert*-butyl chloride. The resultant ion pair (A)<sup>11</sup> then decomposes in one of two ways; in the presence of water only *t*-butyl alcohol is formed, but under anhydrous conditions the ether results. The solution must be kept neutral otherwise the ether is degraded as fast as formed to *t*-butyl alcohol and *t*-butyl chloride. It is consequently evident why dry and neutral (or alkaline) conditions are essential to the success of the reaction.



Di-*t*-butyl ether is a clear mobile liquid boiling at 108–109°. Owing to its nearly spherical structure

(7) Recently Dr. H. E. De La Mare of These Laboratories has used tributylphosphite and did not observe di-*t*-butyl ether.

(8) C. Walling, O. Basedow and E. Savas, *J. Am. Chem. Soc.*, **82**, 2181 (1960).

(9) M. Greenbaum, D. Denny and A. Hoffmann, *ibid.*, **78**, 2563 (1956).

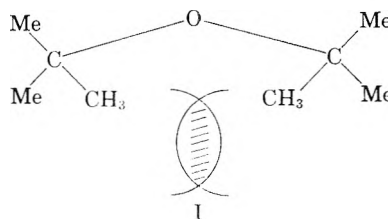
(10) *Org. Syntheses*, **25**, 54 (1945).

(11) An ion pair is preferred only because it is not immediately apparent why di-*t*-butyl carbonate should be unstable. Were this an intermediate, isolation of the dialkyl carbonate should be possible under these relatively mild conditions.

it has an odor reminiscent of camphor. It is readily cleaved by acids and gives an immediate Lucas test with dilute hydrochloric acid. It is quite stable to base and should be stored over potassium hydroxide or sodium. In Table I the properties of the ether are compared with those of di-*t*-butyl peroxide.

A curious fact about the ease of hydrolysis of di-*t*-butyl ether was observed. When a sample was resolved on a GLC column, the number of peaks observed depended on the age of the column. For example, when a sample was examined on an old or frequently used TEG (triethylene glycol) column two peaks appeared—one very sharp and quite early in the spectrum (presumably isobutylene) and the other characteristic of TBA. If a new TEG column was used only the peak for di-*t*-butyl ether was observed. It thus appears that the acid sites uncovered by the bleeding of a frequently used column hydrolyze the ether.

**Strain Energy in Di-*t*-butyl Ether.**—The crowding of methyl groups in the structure I has generally been held responsible for the difficult synthesis of this compound.



A quantitative estimate of the destabilization of this compound by the mutual repulsion of the *t*-butyl groups can now be made from the experimental heat of combustion data ( $\Delta H_c$ ) assembled in Table II. The heat of formation data ( $\Delta H_f$  and  $\Delta H_f^\circ$ ) derived therefrom are found in Table III.<sup>12</sup> The literature value of the standard heat of formation of dimethyl ether has been added as it will be

required to develop a more general picture of the relations to molecular structure.

In the absence of strain one can predict the standard heat of formation,  $\Delta H_f^\circ$ , of di-*t*-butyl ether from the above data as follows:  $\Delta H_f^\circ$  (di-*t*-butyl ether) =  $2[\Delta H_f^\circ$  (Me-O-(*t*-Bu)) -  $\frac{1}{2}\Delta H_f^\circ$  (Me<sub>2</sub>O)], or  $\Delta H_f^\circ$  (di-*t*-butyl ether) =  $2[\Delta H_f^\circ$  (*i*-pr-O-(*t*-Bu)) -  $\frac{1}{2}\Delta H_f^\circ$  (*i*-Pr<sub>2</sub>O)]. Interestingly enough both

(12) The calculating methods employed in the conversion of the experimental data to  $\Delta H_f^\circ$  can be found in "Experimental Thermochemistry" by F. D. Rossini, 1955.

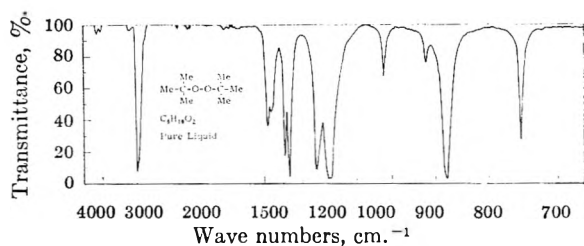
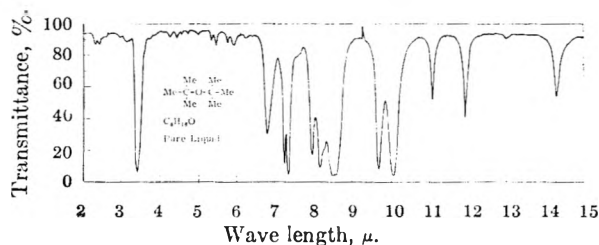
Fig. 1.—Di-*t*-butyl peroxide.Fig. 2.—Di-*t*-butyl ether.

TABLE I

PROPERTIES OF DI-*t*-BUTYL PEROXIDE AND DI-*t*-BUTYL ETHER

	DTBP <sup>a</sup>	DTBE
B.p., °C.	111	108-109
$n_D^{20}$	1.3890	1.3946
$d_{20}$	0.7940	0.7622
Infrared	Fig. 1	Fig. 2
GLC (TEG 100°)	3 min.	3.5 min.

<sup>a</sup> H. Tobolsky and R. Mesrobian "Organic Peroxides," Interscience Pub., New York, N. Y., 1954, p. 164.

TABLE II

HEATS OF COMBUSTION (AT CONSTANT VOLUME, AT 25°) OF SEVERAL ETHERS

Ether	$H_c$ , kcal./mole
Methyl <i>t</i> -butyl	801.5 ± 1.15
Isopropyl <i>t</i> -butyl	1108.9 ± 0.66
Di- <i>t</i> -butyl	1268.7 ± 0.25

TABLE III

HEATS OF FORMATION (AT CONSTANT PRESSURE, AT 25°) OF SEVERAL ETHERS

Ether	$-\Delta H_f^\circ$ (gas), kcal./mole	$-\Delta H_f^\circ$ (liq.), kcal./mole
Dimethyl	45.3 ± 0.3 <sup>a</sup>	...
Diisopropyl	76.4 ± 0.2 <sup>b</sup>	83.88
Methyl <i>t</i> -butyl	70.0 ± 1.2	77.2
Isopropyl <i>t</i> -butyl	85.6 ± 0.6	94.0
Di- <i>t</i> -butyl	87.2 ± 0.3	96.1

<sup>a</sup> Natl. Bur. Stand. Circular 500, 1952. <sup>b</sup> G. S. Parks and K. E. Manchester, *IUPAC Bull. Thermodyn.*, 2, 8 (1956).

calculations yield exactly the same result, 94.8 kcal./mole. This may mean either that there is just as little strain in isopropyl *t*-butyl ether as one has reason to expect in methyl *t*-butyl ether, or that the strain effect is hidden in the uncertainties of the heat of formation of the two *t*-butyl ethers. The upper limit of the strain in isopropyl *t*-butyl ether would then be 1.8 kcal./mole, but the probable value is rather less as there is independent chemical evidence for the absence of strain in isopropyl *t*-butyl ether.

Subtraction of the observed from the calculated (strain-free) heat of formation of di-*t*-butyl ether yields for the strain energy 7.6 with a maximum

uncertainty of ± 1.2 kcal./mole and a probable uncertainty of ± 0.6 kcal./mole. For the strain energy of the homomorph, di-*t*-butyl methane one obtains

$$\Delta H_f^\circ(\text{di-}t\text{-butylmethane})^{13} - 2[\Delta H_f^\circ(2,2\text{-dimethylbutane}) - \frac{1}{2}\Delta H_f^\circ(\text{propane})] = 6.1 \text{ kcal./mole}$$

OR

$$\Delta H_f^\circ(\text{di-}t\text{-butylmethane}) - [\Delta H_f^\circ(2,2\text{-dimethylbutane}) + \Delta H_f^\circ(2,2\text{-dimethylpentane}) - \Delta H_f^\circ(n\text{-butane})] = 5.7 \text{ kcal./mole}$$

or an average of 5.9 kcal./mole.

Assuming the usual bond angles and covalent bond distances, the distance between the quaternary carbons in the hydrocarbon should be 2.54 Å. compared with 2.36 Å. for the ether. The direction of the instability difference between the two compounds is therefore in agreement with expectations. A quantitative assessment could be made through detailed consideration of the molecular geometry and the use of an appropriate potential function.

Further credence in the data of Tables II and III can be obtained from heats of reaction. The heat of addition of alcohols to olefins (Table IV) has been calculated from the heat of formation data. In one case, the formation of methyl *t*-butyl ether in liquid phase, the calculated heat of reaction could be compared with the datum obtained from the temperature coefficient of the equilibrium constant.<sup>14</sup> Assuming perfect solution of the product and reactants one obtains, from the heats of formation and vaporization, the heat of reaction 1 in Table IV the value  $\Delta H(\text{liq.}) = -10.7$  kcal./mole. From the equilibrium constants the value  $\Delta H-$

TABLE IV

HEAT OF REACTION FOR THE VAPOR PHASE ADDITION OF ALCOHOLS TO VARIOUS OLEFINS (AT 25°)

Reaction	$\Delta H^\circ$ , kcal./mole
1. MeOH + <i>i</i> -butene → methyl <i>t</i> -butyl ether	-17.9 ± 1.2
2. <i>t</i> -BuOH + <i>i</i> -butene → di- <i>t</i> -butyl ether	- 8.6
3. <i>i</i> -PrOH + <i>i</i> -butene → <i>i</i> -propyl <i>t</i> -butyl ether	-16.5
4. <i>i</i> -PrOH + propene → di- <i>i</i> -propyl ether	-16.2

(liq.) = -11.2 kcal./mole for reaction is obtained. Since the heat of mixing in this process is probably no more than 0.5 kcal./mole the agreement is quite satisfactory. This lends considerable support to the data of Tables II and III and the strain calculation therefrom.

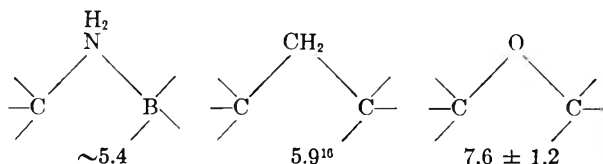
It should be noted that Brown<sup>15</sup> has proposed molecules which are closely related structurally will possess very similar steric strains. Homomorphs of the di-*t*-butylmethane variety were postulated to have strains of ~5.4 kcal./mole. This value was derived largely from the heat of dissociation of trimethylamine-trimethylboron. Obviously the geom-

(13) Calcd. from heat of combustion data by Johnson, Prosen and Rossini, *J. Research Natl. Bur. Standards*, 38, 419 (1947) and  $\Delta H_{\text{vap}}$  in API-44 tables as  $\Delta H_f^\circ = -57.8$  kcal./mole.

(14) Private communication from R. Hawthorne; data by J. Fetterly.

(15) H. C. Brown, *J. Am. Chem. Soc.*, 78, 1248 (1956); H. C. Brown, G. Barbaras, H. Berneis, W. Bonner, R. Johannesen, M. Grayson and K. Nelson, *ibid.*, 75, 1 (1953).

eries of the systems are sufficiently distinct that the strain in the ether is almost 50% in excess of that of the amine-boron complex.



Though strain energy values may show considerable differences between homomorphs, other physical properties of the compounds are very similar. This fact is demonstrable in heat of vaporization, density, viscosity and vapor pressure as tabulated below.

**Heat of Vaporization.**—The heat of vaporization of ethers is essentially equal to that of their hydrocarbon homomorph as long as the ether oxygen is shielded by a group larger than methyl, as is shown by the data of Table V. If one of the groups is a methyl group, 0.5 kcal./mole has to be added to the heat of vaporization of the hydrocarbon homomorph.

TABLE V

COMPARISON OF THE HEAT OF VAPORIZATION (AT 25°) OF ETHERS WITH THAT OF THE HYDROCARBON HOMOMORPHS

	$\Delta H_v$ , kcal./mole	Ref. <sup>a</sup>
Methyl <i>t</i> -butyl ether	7.5	S
2,2-Dimethylbutane	6.62	A
Diisopropyl ether	7.9	S
2,4-Dimethylpentane	7.86	A
Di- <i>t</i> -butyl ether	9.0	M
2,2,4,4-Tetramethylpentane	9.1	A

<sup>a</sup> Ref. A = API-44 Tables; M = this work; S = unpublished data, Shell Development Co.

TABLE VI

VAPOR PRESSURE OF DI-*t*-BUTYL ETHER (DETERMINED BY DYNAMIC METHOD)

<i>t</i> , °C.	$p_{obs}$ , mm.	$p_{calc}$ , mm. <sup>a</sup>
4.0	9.8	10.0
14.0	18.4	18.05
18.0	22.4	22.5
22.0	28.3	27.9
26.0	34.5	34.2
30.0	42.3	41.8
34.0	50.8	50.7
38.0	59.2	61.0
109.0	760	(760)

<sup>a</sup> Calculated with the equation given in the text.

The vapor pressure equation for the range 4 to 109° is  $\log p$  (mm.) = 29.7859 - 2947.95/*T* - 7.43  $\log T$ . From this equation one can derive the heat of vaporization (given above) and its temperature coefficient, the heat capacity difference between liquid and vapor,  $\Delta C_p$ . The latter is 14.7 ± 2 cal./mole °K., compared with 13.5 cal./mole °K. predicted from a correlation for the hydrocarbon homomorph. Considering the accuracy of the data this is a reasonable agreement.

**Density.**—The density of ethers (diethyl ether and above) nearly equals that of their hydrocarbon homomorph when expressed in the reduced form  $V_w/V$  where  $V_w$  is the van der Waals volume of the

molecule.<sup>17</sup> This result is not surprising since  $V/V_w$  is a simple function of  $RT/\Delta H_{vap}$ .<sup>17</sup> Typical data are presented in Table VII. Extrapolation of ether densities to other temperatures requires therefore only the readily available hydrocarbon data (API-44 tables).

TABLE VII

DENSITY AND REDUCED VOLUME OF ETHERS AND THEIR HYDROCARBON HOMOMORPHS

Substance	$d^{20}_4$ , g./cm. <sup>3</sup>	$V_w$ , cm. <sup>3</sup> /mole ( $V_{70}/V_w$ )
Methyl <i>t</i> -butyl ether	0.7418	63.5 1.87
2,2-Dimethylbutane	.6492	68.2 1.94
Di- <i>t</i> -butyl ether	.7622	94.0 1.813
2,2,4,4-Tetramethylpentane	.7195	98.9 1.801

**Viscosity.**—The viscosity of the ethers has been measured over a wide temperature range (Table VIII). No unexpected phenomena were observed. The near identity of the viscosity of the ethers and that of their hydrocarbon homomorphs is apparent from the comparison of Table IX. This similarity extends to the respective activation energies for flow ( $\Delta H^*$ ) which in the case of di-*t*-butyl ether and 2,2,4,4-tetramethylpentane is 2.45 and 2.34 kcal./mole, respectively, for the range from 20 to 50°. The corresponding value for di-*n*-butyl ether (or *n*-nonane) is 2.1 kcal./mole. The difference is presumably due to the relative rigidity of the *t*-butyl ether.

TABLE VIII

KINEMATIC VISCOSITY OF VARIOUS ETHERS

<i>t</i> , °C.	-53.9	-40	+20	+50	+60	+98.9
Methyl <i>t</i> -butyl ether: $\nu$ , cs.	1.332	1.028	0.471	0.367	...	...
<i>t</i> -Propyl <i>t</i> -butyl ether: $\nu$ , cs.	2.734	1.949	0.669	.491	0.449	...
Di- <i>t</i> -butyl ether: $\nu$ , cs.	6.37	4.109	1.068	.722	0.636	0.427

TABLE IX

DYNAMIC VISCOSITY OF VARIOUS ETHERS AND OF THEIR HYDROCARBON HOMOMORPHS

Substance	Viscosity (centipoise) at °C.	
	15	20
Di- <i>n</i> -butyl ether	0.74	
<i>n</i> -Nonane	0.766	
Methyl <i>t</i> -butyl ether		0.35
2,2-Dimethylbutane		.375
<i>i</i> -Propyl <i>t</i> -butyl ether		.497
2,2,4-Trimethylpentane		.503
Di- <i>t</i> -butyl ether		.815
2,2,4,4-Tetramethylpentane		.88

**Acknowledgment.**—The authors wish to acknowledge the assistance of Mr. R. B. McConaughy in the calculations, and of Dr. J. H. Badley who determined the vapor pressure of di-*t*-butyl ether.

### Experimental

Methyl *t*-butyl and isopropyl *t*-butyl ethers were obtained commercially and purified before use.

**Di-*t*-butyl Ether.**—In a 2-liter 3-neck flask equipped with a mechanical stirrer, a condenser and a means for observing gas evolution was placed 135 g. (0.49 mole) of silver carbonate, 100 g. (~1 mole) of sodium carbonate and 500 ml. of dry ether. To this slurry was added 92.6 g. (1 mole) of

(17) A. Bondi and D. J. Simkin, *AIChE J.*, 6, 191 (1960), and Preprint No. 22, A.I.Ch.E. Meeting, St. Paul, Minn., Sept., 1959.

*t*-butyl chloride in 500 ml. of dry ether. The solution was stirred and shielded from light for ~60 hours. Gas evolution was at first sluggish but then was steady for some time. The ethereal solution was decanted and the rose colored precipitate washed with ether. The combined extracts were distilled over sodium through a glass helices column and finally through a Piro-Glover spinning band. Di-*t*-butyl ether: b.p. 108–109° (759.1 mm.),  $n_D^{20}$  1.3946, yield 20 g. (31%).

Properties.—The heat of combustion was determined in a

300-ml. Parr (oxygen) bomb calorimeter. The completeness of the reaction was judged visually. The repeatability of the data is indicated with the results given in Table II. The maximum inaccuracy of the results is within 0.2%. Corrections to constant pressures, etc., followed ref. 12. The vapor pressures were determined by means of a dynamic (gas carrier) method. The data are believed to be accurate within  $\pm 1\%$ . The viscosities were determined according to ASTM D-445.

## HIGH TEMPERATURE THERMODYNAMICS OF THE IRON OXIDE SYSTEM

BY OLIVER N. SALMON<sup>1</sup>

*Electronics Laboratory, General Electric Company, Schenectady, N. Y.*

*Received November 4, 1960*

A high temperature thermodynamic study has been carried out on the iron oxide system. Chemical activities have been related to defects in the solid state structures. Fundamental thermodynamic results have been calculated by application of the activity expressions to experimental oxygen dissociation pressure-composition-temperature data.

### Introduction

The purpose of this study was to establish the relationship between thermodynamic properties, composition and structure of iron oxide at elevated temperatures. This study was a precursor to work on the development of ferrites of desired microwave, electrical, magnetic and ceramic properties by control of composition and structure.

The theoretical approach to obtaining activity expressions was first developed. Then activity expressions were derived and applied to the experimental data for the wüstite, magnetite and hematite phases of the iron oxide system.

### Experimental

The oxygen dissociation pressure measurements on the iron oxide system were made in a Pyrex vacuum system. For a typical run, a sample of powdered hematite (obtained either by oxidation of reagent grade iron wire or as Fe<sub>2</sub>O<sub>3</sub>, Mapico 110-2, from the Columbian Carbon Co.) weighing 5 to 10 g. was loaded into a platinum cup (2.2 cm. tall  $\times$  2.7 cm. o.d.  $\times$  .025 cm. wall) enclosed within a stabilized ZrO<sub>2</sub> cell. The cell was inserted into a Vycor reaction chamber. The reaction chamber was then connected to the vacuum means of a 65/40 ball joint. The male part of the ball joint is made of Vycor while the female part is of Pyrex to avoid the use of graded glass seals. After connecting to the vacuum system the reaction chamber was pumped out to a pressure of less than  $10^{-6}$  atmospheres and then isolated from the vacuum pumps.

The platinum cup containing the sample was then heated inductively by an induction coil around the Vycor reaction chamber in the region of the sample. The 500 kc. r-f power to the induction coil was supplied by a 20-kva General Electric Induction Heater. More uniform heating of the reaction cell was obtained by attaching a 0.050 cm. thick platinum disc to the inside top surface of the cell by means of platinum wires spot welded to the disc and leading through small holes in the cell top. A 0.025 cm. thick platinum disc was placed in the bottom of the platinum cup to protect the cup from possible chemical attack by the sample and to aid in achieving uniform heating of the sample. The two platinum discs along with the platinum cup act as susceptors for converting the r-f power from the Induction Heater to heat in the reaction cell.

The sample temperature was determined with an optical pyrometer by focusing on the sample through a 0.65 cm. diameter opening in the top of the reaction cell *via* an optical glass window in the top of the reaction chamber and a flat

glass mirror mounted above the window. The pyrometer was calibrated for the particular experimental set-up against a platinum-platinum rhodium (13% Rh) thermocouple.

Oxygen dissociation pressure measurements were made at equilibrium at elevated temperatures by reading a mercury manometer with a Gaertner cathetometer for oxygen pressures of  $5 \times 10^{-3}$  to 1 atmosphere and by means of a double McLeod gauge for pressures of  $10^{-8}$  to  $5 \times 10^{-3}$  atmosphere. The oxygen content of the sample was determined from knowing the initial oxygen content (*e.g.*, fully oxidized iron in the form of Fe<sub>2</sub>O<sub>3</sub>) and by keeping a careful account of the oxygen either removed from the sample by evolution into a known volume or added to the sample from this known volume (by pressure-temperature measurements on the gas in the known volume).

Early in the experimental work it was observed that oxygen gas, at pressures of about  $10^{-6}$  to  $3 \times 10^{-3}$  atmosphere, became activated by the combination of high temperature near the reaction cell and the r-f magnetic field in the Vycor reaction chamber generated by the induction heater. This was displayed visually by the blue color in gas in reaction chamber. The activated region extended up into the neighborhood of ball and socket joint. The activated oxygen reacted with the Apiezon grease at the joint to generate CO<sub>2</sub> gas which was condensed in cold traps. This caused oxygen to be used up and thus made it difficult to measure the oxygen pressure and to keep account of the correct oxygen content of the sample. This problem was solved by wrapping a copper sheet around the outside of the Vycor tube between the induction coil and the ball joint and electrically grounding the sheet. This eliminated the r-f magnetic field in the upper portion of the Vycor tube and allowed the activation in the oxygen gas to be quenched before reaching the stop-cock grease.

Whenever the reaction cell was hot, the sample and other contents of the Vycor reaction chamber were protected from mercury vapors and other condensable vapors such as H<sub>2</sub>O and CO<sub>2</sub> by cold traps maintained at liquid nitrogen temperature (about  $-193^\circ$ ).

Sample temperatures of up to 1450° can be obtained when using the reaction cell as described. At higher temperatures hot spots sometimes develop in the platinum cup and result in holes. Temperatures of greater than 1500° probably could be obtained by replacing the platinum cup with a cup containing 60% platinum and 40% rhodium. The stabilized ZrO<sub>2</sub> cell which contains the platinum cup begins to act as a susceptor for the r-f power at temperatures somewhat above 1300° due to increased electrical conductivity. This takes some of the power load off the platinum cup susceptor at high temperature and consequently diminishes the incidence of hot spots in the platinum cup. With the arrangement described above, iron oxide samples have been heated for several weeks at elevated temperatures (1100 to 1400°) without holes developing in the platinum cup.

<sup>1</sup> Now with the Central Research Laboratory of the Minnesota Mining and Manufacturing Company, St. Paul, Minnesota.

### Results and Discussion

Before detailing the theoretical development, the following expressions will be defined for clarity and assistance to those readers who are unfamiliar with this particular subject matter.

$\mu_i$ —chemical potential of component  $i$ ; defined

$$\left[ \frac{\partial F}{\partial n_i} \right]_{T, P, \text{ other } n_i}$$

where  $F$  = total Gibbs free energy of the given phase

$n_i$  = no. of moles of component  $i$  in a given phase

$P$  = pressure

$T$  = absolute temp.

$a_i$ —activity of component  $i$ ; defined by  $RT \ln a_i = \mu_i - \mu_i^0$

where  $R = 1.9864 \text{ cal./}^\circ\text{K. per mole (gas constant)}$

$\mu_i^0$  = chemical potential of component  $i$  in its chosen standard state

$\mu_i - \mu_i^0$ —partial molal free energy of mixing of component  $i$  defined also by  $[\bar{H}_i - H_i^0] - T[\bar{S}_i - S_i^0]$

where  $\bar{H}_i - H_i^0$  = partial molal heat of mixing

$\bar{S}_i - S_i^0$  = partial molal entropy of mixing

From these definitions, the activity  $a_i$  of component  $i$  can be defined by

$$RT \ln a_i = [\bar{H}_i - H_i^0] - T[\bar{S}_i - S_i^0] \quad (1)$$

The expressions  $[\bar{H}_i - H_i^0]$  and  $[\bar{S}_i - S_i^0]$  are usually not very dependent on temperature but are functions of composition of a given phase. With these two functions established, the  $a_i$ 's can be expressed as functions of composition and temperature by use of the above equation.

In the work on the iron oxide system, an attempt will be made to select standard states of components in a given phase in such a way that  $\bar{H}_i - H_i^0$  is very small. As a first approximation, then,  $\bar{H}_i - H_i^0$  will be assumed to be zero. Also the volume change in mixing will be assumed zero. For this case

$$R \ln a_i = -[\bar{S}_i - S_i^0]$$

The partial molal entropy of mixing,  $\bar{S}_i - S_i^0$ , is related to the total entropy of mixing  $S_M$  for a given phase by

$$\bar{S}_i - S_i^0 = \left[ \frac{\partial \Delta S_M}{\partial n_i} \right]_{T, P, \text{ other } n_i} \quad (2)$$

For the case of athermal mixing which is being assumed in this treatment, the total entropy of mixing can be related to the number of distinguishable arrangements of ions in the mixed phase and in the standard states of various components.<sup>2</sup>

The resulting relation is

$$\Delta S_M = k \left[ \ln \Omega_M - \sum_i \ln \Omega_i^0 \right] \quad (3)$$

where

$k$  is Boltzmann's constant

$\Omega_M$  is the no. of distinguishable arrangements of ions in the given solid phase

$\Omega_i^0$  is the no. of distinguishable arrangements of ions in the chosen standard state of component  $i$

In the derivation of the activity expressions to follow it was observed that better agreement with experiments was obtained if the  $\Omega_i^0$ 's were all assumed to be one. This means that perfect

order was assumed to exist in the standard states selected for the solid iron oxide components.

Thus, by use of equations 1, 2 and 3, the activity  $a_i$  of component  $i$  in a solid phase can be related to the number of arrangements of ions in the phase. The number of arrangements can in turn be related to composition of the phase in a manner to be described below for the iron-oxygen system.

The chemical activity of oxygen in the gas phase is assumed to be equal to its partial pressure expressed in atmospheres. In the derivations to follow, subscripts 1, 2 and 3 refer to  $\text{Fe}_2\text{O}_3$ ,  $\text{Fe}_3\text{O}_4$  and  $\text{FeO}$ , respectively.  $\alpha$  refers to the hematite solid phase, and  $\gamma$  refers to the magnetite solid phase and  $w$  refers to the wüstite phase.

**A. Derivation of Activity Expressions for the Magnetite Phase.**—Consider the mixing of  $N_1$  molecules of  $\text{Fe}_2\text{O}_3$  and  $N_2$  molecules of  $\text{Fe}_3\text{O}_4$  in the magnetite phase. The standard states will be chosen as the magnetite structure for both stoichiometric  $\text{Fe}_2\text{O}_3$  and stoichiometric  $\text{Fe}_3\text{O}_4$  for this case. It will be assumed that the standard state  $\text{Fe}_2\text{O}_3(\gamma)$  has  $\text{Fe}^{2+}$  vacancies<sup>3</sup> in the octahedral<sup>4</sup> positions in the lattice, which positions for  $\text{Fe}_3\text{O}_4$  would be filled by  $\text{Fe}^{2+}$  ions.

The  $N_1$  molecules of  $\text{Fe}_2\text{O}_3(\gamma)$  contribute  $3N_1\text{O}^{2-}$  ions to the solid phase, 2.25 iron ion positions, of which 1.5 $N_1$  are octahedral and 0.75-  $N_1$  tetrahedral, 1.5 $N_1$   $\text{Fe}^{3+}$  ions, 0.5 $N_1$   $\text{Fe}^{2+}$  and 0.25 $N_1$   $\text{Fe}^{2+}$  vacancies. The 0.25 $N_1$   $\text{Fe}^{2+}$  vacancies are assumed to be in the octahedral sites. The  $N_2$  molecules of  $\text{Fe}_3\text{O}_4$  contribute  $4N_2\text{O}^{2-}$  ions to the solid phase, 3 $N_2$  iron ion positions, of which 2 $N_2$  are octahedral and  $N_2$  are tetrahedral, 2 $N_2$   $\text{Fe}^{3+}$  ions, and  $N_2$   $\text{Fe}^{2+}$  ions. The  $N_2$   $\text{Fe}^{2+}$  ions are assumed to be in octahedral sites. It will be assumed that the only new ionic arrangements resulting from mixing the  $N_1$   $\text{Fe}_2\text{O}_3$  molecules and  $N_2$   $\text{Fe}_3\text{O}_4$  molecules in the magnetite phase are due to the random mixing of the  $N_2$   $\text{Fe}^{2+}$  ions with the 0.25 $N_1$   $\text{Fe}^{2+}$  vacancies. The number of distinguishable arrangements  $\Omega_M$  in the mixture is, therefore

$$\Omega_M = \frac{[0.25N_1 + N_2]!}{[0.25N_1]![N_2]!}$$

The number of arrangements in the chosen standard state of  $\text{Fe}_2\text{O}_3(\gamma)$  considering only the  $\text{Fe}^{2+}$  vacancies is

$$\Omega_1^0 = \frac{[0.25N_1]!}{[0.25N_1]!} = 1$$

The number of arrangements in the chosen standard state of  $\text{Fe}_3\text{O}_4(\gamma)$  considering only the  $\text{Fe}^{2+}$  ions is

$$\Omega_2^0 = \frac{[N_2]}{[N_2]} = 1$$

Hence by equation 3

$$\Delta S_M = k \ln \frac{[0.25N_1 + N_2]!}{[0.25N_1]![N_2]!} \quad (4)$$

Making use of the Stirling Approximation (*i.e.*,  $\ln(A!) = A \ln A - A$ ) and letting  $N_1 + N_2 =$

(2) J. H. Hildebrand and R. L. Scott, "Solubility of Non-Electrolytes," Third Edition. Reinhold Publ. Corp., New York, N. Y., 1950, pp. 109-112.

(3) H. Flood and D. G. Hill, *Z. Elektrochem.*, **61**, 18 (1957).

(4) E. J. W. Verwey and P. W. Haayman, *Physica*, **VIII**, 979 (1941).



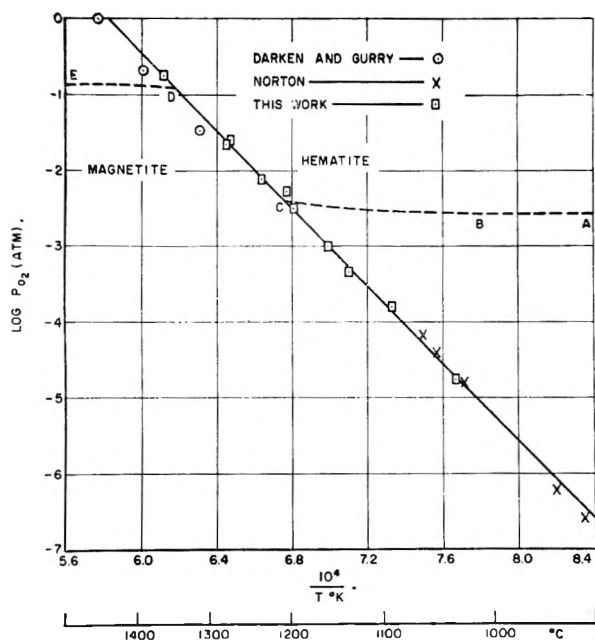


Fig. 1.—Relation between oxygen dissociation pressure and temperature at equilibrium between magnetite and hematite.

$N_0$ , where  $N_0$  is Avogadro's number (*i.e.*,  $6.023 \times 10^{23}$ ) Equation 4 becomes

$$\Delta S_M = -R \left[ 0.25n_1 \ln \frac{0.25n_1}{0.25n_1 + n_2} + n_2 \ln \frac{n_2}{0.25n_1 + n_2} \right] \quad (5)$$

where  $R = kN_0$  the gas constant  
 $n_1 = N_1/N_0$  moles of  $\text{Fe}_2\text{O}_3$   
 $n_2 = N_2/N_0$  moles of  $\text{Fe}_3\text{O}_4$

Now differentiate  $\Delta S_M$  in equation 5 with respect to  $n_1$  and  $n_2$ , respectively, and substitute in the equations

$$R \ln a_1 = - \left[ \frac{\partial \Delta S_M}{\partial n_1} \right]_{T,P,n_2} \quad \text{and}$$

$$R \ln a_2 = - \left[ \frac{\partial \Delta S_M}{\partial n_2} \right]_{T,P,n_1}$$

to obtain

$$a_1(\gamma) = \left[ \frac{0.25n_1}{0.25n_1 + n_2} \right]^{0.25}$$

$$a_2(\gamma) = \frac{n_2}{0.25n_1 + n_2}$$

dividing the numerators and denominators by  $n_1 + n_2$

$$a_1(\gamma) = \left[ \frac{0.25X_1}{0.25X_1 + X_2} \right]^{0.25} \quad (6)$$

$$a_2(\gamma) = \frac{X_2}{0.25X_1 + X_2} \quad (7)$$

where  $X_1$  and  $X_2$  are the mole fractions of  $\text{Fe}_2\text{O}_3$  and  $\text{Fe}_3\text{O}_4$ , resp., in the magnetite phase and  $\gamma$  denotes the magnetite phase.

It should be pointed out that it was not necessary to assume the  $\text{Fe}^{2+}$  from the  $\text{Fe}_3\text{O}_4(\gamma)$  and the  $\text{Fe}^{2+}$  vacancies from the  $\text{Fe}_2\text{O}_3(\gamma)$  were located in octahedral positions to derive the above activity expressions. It is only necessary to assume that the entropy of mixing results from the random mixing of these  $\text{Fe}^{2+}$  ions and vacancies.

**B. Application of Activity Expressions to the Experimental Results for the Magnetite Phase.**—Equation 7 has been used to calculate  $a_2(\gamma)$  for  $\text{Fe}_3\text{O}_4$  in the magnetic phase. The calculated results from equation 7 are compared with the experimental results of Darken and Gurry<sup>5</sup> for  $a_2(\gamma)$  at  $1575^\circ$  in Table I. Their experimental values for  $a_2(\gamma)$  were determined from oxygen dissociation pressure *versus* composition of the magnetite solid solution at  $1575^\circ$  by application of the Gibbs-Duhem equation. Their values of  $a_2(\gamma)$  were relatively independent of temperature in the range studied ( $1400$  to  $1575^\circ$ ).

TABLE I  
ACTIVITY OF  $\text{Fe}_3\text{O}_4$  IN MAGNETITE

Mole fraction of $\text{Fe}_3\text{O}_4$	Activity of $\text{Fe}_3\text{O}_4$	
	Calcd. by eq. 7	Exptl. value of Darken and Gurry
1	1	1
0.9	0.98	0.97
.8	.95	.94
.7	.90	.90
.6	.85	.86

The agreement in Table I gives considerable support to the validity of equation 7 for  $a_2(\gamma)$ , and in so doing also supports the validity of equation 6 for  $a_1(\gamma)$ . This follows from the Gibbs-Duhem equation by which it can be shown that if equation 7 is correct, then the true activity of  $\text{Fe}_2\text{O}_3$  in the magnetite solid solution is directly proportional to the  $a_1(\gamma)$  given by equation 6.

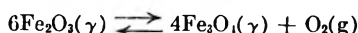
Oxygen dissociation pressures have been measured at various temperatures and oxygen contents for magnetite (*i.e.*,  $\text{Fe}_3\text{O}_4(\gamma)$ ) containing some  $\text{Fe}_2\text{O}_3$  in solid solution. A typical run is illustrated by line ABCDE in Fig. 1. The iron oxide was heated to some given temperature and oxygen allowed to evolve from the iron oxide into a known volume of the vacuum system until the pressure stopped changing. This pressure was then considered to be the equilibrium pressure for the given temperature and oxygen content of the iron oxide. Then the temperature of iron oxide was raised to a new value and the new equilibrium oxygen pressure measured. The oxygen content could be calculated by considering the amount of oxygen which had evolved from the iron oxide to give the measured oxygen pressure in the known volume. The oxygen content at point A on Fig. 1 corresponded to stoichiometric  $\text{Fe}_2\text{O}_3$ . The compositions were expressed as mole fractions of  $\text{Fe}_3\text{O}_4$  (*i.e.*,  $X_2$ ), the other component being  $\text{Fe}_2\text{O}_3$ .

Along line AB in Fig. 1 the  $\alpha$ - $\text{Fe}_2\text{O}_3$  (hematite) was in contact with excess oxygen gas. As the temperature was raised the  $\alpha$ - $\text{Fe}_2\text{O}_3$  did not lose any oxygen until a temperature corresponding to point B was reached. Along line BC the  $\alpha$ - $\text{Fe}_2\text{O}_3$  started losing oxygen to the gas phase and the concentration of  $\text{Fe}^{2+}$  or  $\text{Fe}_3\text{O}_4$  in solution in the hematite phase began to increase from zero at point B to the saturation value at point C. At point C a magnetite phase began to separate from the  $\alpha$ - $\text{Fe}_2\text{O}_3$  phase. Along line CD the magnetite phase<sup>7</sup> and hematite phase coexist in equilibrium

(5) L. S. Darken and R. W. Gurry, *J. Am. Chem. Soc.*, **68**, 798 (1946).

with each other and with the oxygen gas phase. As the temperature is raised along CD and more oxygen evolves into the gas phase, point D is reached where all the  $\alpha$ -Fe<sub>2</sub>O<sub>3</sub> phase has just disappeared to form magnetite and oxygen gas. Along line DE the magnetite is losing oxygen and hence the concentration of Fe<sup>3+</sup> or Fe<sub>2</sub>O<sub>3</sub> in solution in the magnetite phase is decreasing.

A series of runs were made of the type illustrated by line ABCDE at various contents of oxygen in the iron oxide at the start of each run. A careful account had to be kept of the oxygen added to or removed from the vacuum system for the entire series of runs. From the DE portion of the various ABCDE curves data on oxygen dissociation pressure, oxygen composition and temperature were compiled for the magnetite phase. For this composition region the reaction involved in the dissociation of the oxide is



where  $\gamma$  refers to the magnetite phase, and  $\text{g}$  refers to the gas phase

The standard heat of reaction  $\Delta H^0(\gamma)$  and standard entropy of reaction  $\Delta S^0(\gamma)$  for this reaction are related to the activities  $a_1$  and  $a_2$  and oxygen dissociation pressure  $P_{\text{O}_2}$  by

$$\Delta H^0(\gamma) - T\Delta S^0(\gamma) = -RT \ln \left[ \frac{P_{\text{O}_2} a_2^4}{a_1^6} \right] \quad (8)$$

Hence by substituting  $X_1$  and  $X_2$  for  $a_1$  and  $a_2$  from equations 6 and 7  $\Delta H^0(\gamma)$  and  $\Delta S^0(\gamma)$  can be related to  $P_{\text{O}_2}$ ,  $X_1$ ,  $X_2$  and  $T$  which are all measured data. The relation is expressed by

$$\Delta H(\gamma) - T\Delta S^0(\gamma) = -RT \ln \left[ P_{\text{O}_2} \left[ \frac{X_2}{0.25X_1 + X_2} \right]^4 \left[ \frac{0.25X_1 + X_2}{0.25X_1} \right]^{1.6} \right] \quad (9)$$

The data on  $P_{\text{O}_2}$ ,  $X_1$ ,  $X_2$  and  $T$  are shown in Table II. The values of  $\Delta H^0(\gamma)$  and  $\Delta S^0(\gamma)$  have been computed by application of the least-squares method to the data in Table II and to equation 9. The resulting values of  $\Delta H^0(\gamma)$  and  $\Delta S^0(\gamma)$  and the corresponding probable errors are

$$\begin{aligned} \Delta H^0(\gamma) &= 78,000 \pm 4200 \text{ cal.} \\ \Delta S^0(\gamma) &= 47.0 \pm 4.0 \text{ cal./}^\circ\text{K.} \end{aligned}$$

The corresponding values calculated from Darken and Gurry's<sup>5</sup> data on  $P_{\text{O}_2}$ ,  $X_1$ ,  $X_2$  and  $T$  for the magnetite phase are

$$\begin{aligned} \Delta H^0(\gamma) &= 84,500 \pm 1600 \text{ cal.} \\ \Delta S^0(\gamma) &= 52.5 \pm 0.9 \text{ cal./}^\circ\text{K.} \end{aligned}$$

Thus the thermodynamic results of the present work using vacuum technique agree fairly well with those of Darken and Gurry using a gas flow method at known partial pressures of oxygen and using chemical analysis to determine equilibrium oxygen content of magnetite containing excess Fe<sub>2</sub>O<sub>3</sub> in solid solution.

**C. Derivation of Activity Expressions for the Wüstite Phase.**—W. L. Roth of the General Electric Research Laboratory has recently completed a neutron diffraction study of wüstite containing some Fe<sub>3</sub>O<sub>4</sub> in solid solution.<sup>6</sup> He found cation vacancies in the octahedral sites and interstitial

(6) W. L. Roth. General Electric Research Laboratory Report No. 58RL-2128.

TABLE II  
OXYGEN DISSOCIATION PRESSURE, COMPOSITION AND TEMPERATURE DATA FOR THE MAGNETITE PHASE OF IRON OXIDE

Temp., °K.	Oxygen pressure, at.	Mole fraction Fe <sub>2</sub> O <sub>3</sub>	Mole fraction Fe <sub>3</sub> O <sub>4</sub>
1551	$1.47 \times 10^{-2}$	0.3979	0.6021
1617	$1.80 \times 10^{-2}$	.2090	.7910
1697	$1.89 \times 10^{-2}$	.1518	.8482
1621	$3.33 \times 10^{-2}$	.3068	.6932
1664	$3.46 \times 10^{-2}$	.2291	.7709
1585	$3.20 \times 10^{-2}$	.3801	.6199
1680	$1.255 \times 10^{-1}$	.3587	.6413
1700	$1.264 \times 10^{-1}$	.3068	.6932
1504	$3.59 \times 10^{-3}$	.3418	.6582
1541	$6.18 \times 10^{-3}$	.1886	.8114
1483	$2.17 \times 10^{-3}$	.3255	.6745
1526	$4.42 \times 10^{-3}$	.1918	.8082
1430	$4.45 \times 10^{-4}$	.2315	.7685
1492	$1.47 \times 10^{-3}$	.1679	.8321
1576	$2.37 \times 10^{-3}$	.1107	.8893
1375	$1.00 \times 10^{-4}$	.1380	.8620
1495	$5.86 \times 10^{-4}$	.1065	.8935
1581	$1.01 \times 10^{-3}$	.0777	.9223
1435	$3.0 \times 10^{-6}$	.0114	.9886
1525	$2.41 \times 10^{-5}$	.0096	.9904

iron ions in tetrahedral sites. These occurred in a ratio of about two octahedral vacancies for each tetrahedral iron ion. On the basis of these observations, it will be assumed that the wüstite structure has the same charge distribution as magnetite structure and also that an Fe<sub>3</sub>O<sub>4</sub> molecule is arranged in the same manner in wüstite will place two iron ions in octahedral positions and one iron ion in a tetrahedral position in the face centered cubic arrangement of oxygen ions. In the following treatment (w) will refer to the wüstite phase.

Let  $N_3$  molecules of FeO and  $N_2$  molecules of Fe<sub>3</sub>O<sub>4</sub> mix in solid solution in the wüstite phase. The standard states will be chosen as the wüstite structure for both stoichiometric FeO and Fe<sub>3</sub>O<sub>4</sub>. The wüstite standard state of Fe<sub>3</sub>O<sub>4</sub> will thus have the same ionic arrangement as the magnetite structure, but will have a slightly expanded lattice constant to match the wüstite structure. The wüstite standard state of FeO will have the same charge distribution as the standard state of Fe<sub>3</sub>O<sub>4</sub>, and hence will have interstitial Fe<sup>0</sup> atoms in octahedral positions and iron ion vacancies in tetrahedral positions.

The  $N_3$  molecules of FeO(w) contribute  $N_3\text{O}^{2-}$  sites filled by  $N_3\text{O}^{2-}$  ions,  $N_2$  octahedral positions,  $0.5N_3$  Fe<sup>0</sup> atoms in octahedral positions,  $0.25N_3$  Fe<sup>2+</sup> ions in octahedral positions,  $0.25N_3$  Fe<sup>3+</sup> ions in octahedral positions and  $0.25N_3$  Fe<sup>3+</sup> holes in tetrahedral positions each with a 3+ charge. The  $N_2$  molecules of Fe<sub>3</sub>O<sub>4</sub>(w) contribute  $4N_2$  O<sup>2-</sup> sites filled by  $4N_2$  O<sup>2-</sup> ions,  $4N_2$  octahedral positions,  $N_2$  Fe<sup>2+</sup> ions in octahedral positions,  $N_2$  Fe<sup>3+</sup> ions in octahedral positions,  $2N_2$  neutral octahedral holes, and  $N_2$  Fe<sup>3+</sup> ions in tetrahedral positions. In deriving the expression for the entropy of mixing, only the random mixing of the  $0.5N_3$  Fe<sup>0</sup> atoms with  $2N_2$  neutral octahedral holes will be considered. The mixing of the 0.25

tetrahedral holes with the  $N_2$   $\text{Fe}^{3+}$  ions in tetrahedral positions is neglected because Roth found that in wüstite each pair of neutral octahedral holes has in general one interstitial iron ion in a tetrahedral position associated with it. Thus, the mixing of  $\text{Fe}^{3+}$  ions in tetrahedral sites with tetrahedral holes is not independent of the mixing of  $\text{Fe}^0$  atoms with octahedral holes. The existence of an association of iron ions with vacancies and consequent decrease of entropy is supported by the thermodynamic treatment of wüstite solid solution by Brynstad and Flood,<sup>7</sup> but their model for the structure is different from that suggested by Roth's work. The number of distinguishable arrangements  $\Omega_M$  in the solid solution mixture is, therefore

$$\Omega_M = \frac{[0.5N_3 + 2N_2]!}{[0.5N_3]![2N_2]!}$$

$\Omega_2^0$  and  $\Omega_3^0$  will both be assumed equal to unity. Consequently, following the general procedure outlined in the theoretical development earlier in the paper, the activities  $a_3$  and  $a_2$  of  $\text{FeO}$  and  $\text{Fe}_3\text{O}_4$ , respectively, in the wüstite phase are given by

$$a_3(w) = \left[ \frac{0.5X_3}{0.5X_3 + 2X_2} \right]^{0.5} \quad (10)$$

$$a_2(w) = \left[ \frac{2X_2}{0.5X_3 + 2X_2} \right]^2 \quad (11)$$

where  $X_3$  and  $X_2$  are the mole fractions of  $\text{FeO}$  and  $\text{Fe}_3\text{O}_4$ , resp.

**D. Application of the Activity Expressions to the Experimental Results for the Wüstite Phase.**—Equation 10 has been used to calculate the chemical activity  $a_3(w)$  of  $\text{FeO}$  in the wüstite phase for various mole fractions of  $\text{Fe}_3\text{O}_4$  in solid solution in the wüstite. The other component was  $\text{FeO}$ . The calculated results from equation 10 are compared with the experimental results of Darken and Gurry<sup>8</sup> for  $a_3(w)$  at 1200° in Table III. Their experimental values for  $a_3(w)$  were determined from oxygen dissociation pressure *vs.* compositions of the wüstite solid solution at 1200° by application of the Gibbs–Duhem equation. The experimental values of  $a_3(w)$  appear to be quite independent of temperature in the range studied (1100 to 1400°).

TABLE III  
ACTIVITY OF  $\text{FeO}$  IN WÜSTITE

Mole fraction of $\text{Fe}_3\text{O}_4$	Activity of $\text{FeO}$	
	Calcd. by eq. 10	Exptl. value of Darken and Gurry <sup>8</sup>
0.053	0.90	0.90
.062	.89	.90
.081	.86	.87
.110	.82	.84
.141	.78	.79
.194	.71	.71
.235	.67	.66
.248	.66	.64

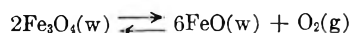
In Table III, the experimental values of  $a_3(w)$  of Darken and Gurry have each been multiplied by the same constant factor which was selected

(7) J. Brynstad and H. Flood, *Z. Elektrochem.*, **62**, 953 (1958).

(8) L. S. Darken and R. W. Gurry, *J. Am. Chem. Soc.*, **67**, 1407 (1945).

so as to cause the calculated and experimental values of  $a_3(w)$  to be equal at a composition of 0.053 mole fraction  $\text{Fe}_3\text{O}_4$ . This operation is equivalent to changing one of the limits of integration in the application of the Gibbs–Duhem equation to the raw experimental data and does not alter the self-consistency of the results. It is also equivalent to selecting a new standard state composed of stoichiometric  $\text{FeO}$  for wüstite rather than the one used in arriving at the experimental activities.

The dissociation of oxygen from wüstite (*i.e.*,  $\text{FeO}(w)$ ) containing some  $\text{Fe}_3\text{O}_4$  in solid solution may be represented by



By application of the activity expressions 10 and 11 to this equation the expression for the equilibrium constant  $K(w)$  becomes

$$K(w) = P_{\text{O}_2} \left[ \frac{0.5X_3}{0.5X_3 + 2X_2} \right]^3 \left[ \frac{0.5X_3 + 2X_2}{2X_2} \right]^4 \quad (12)$$

By application of equation 12 to the data of Darken and Gurry<sup>8</sup> on oxygen dissociation pressure *vs.* composition of the wüstite phase, the average value of  $K(w)$  was found to be  $3.75 \times 10^{-10}$  and  $6.74 \times 10^{-8}$  at 1200 and 1400°, respectively. These values for  $K(w)$  were substituted into equation 12 and  $P_{\text{O}_2}$  *vs.* mole fraction  $\text{Fe}_3\text{O}_4$  were calculated at 1200 and 1400°. These calculated results are shown as solid curves in Fig. 2. The experimental results of Darken and Gurry are shown as small circles in the Fig. 2. The agreement is considered good.

Values of the standard heat of reaction  $\Delta H^0(w)$  and standard entropy of reaction  $\Delta S^0(w)$  for above oxygen dissociation reaction were calculated from the value of  $K(w)$  at 1200 and 1400° by use of the relation,  $RT \ln K(w) = -\Delta H^0(w) + T \Delta S^0(w)$

$$\Delta H^0(w) = 127000 \text{ cal.}$$

$$\Delta S^0(w) = 43.2 \text{ cal./}^\circ\text{K.}$$

**E. Derivation of the Activity Expressions for the Hematite Phase.**—No satisfactory data on oxygen dissociation pressure, composition and temperature for the hematite phase are available in the scientific literature for calculating the activity of  $\text{Fe}_2\text{O}_3$  as a function of concentration of  $\text{Fe}_3\text{O}_4$  in solid solution in hematite. Consequently, an experimental study was carried out to obtain such data. These data are represented by the BC portions of a series of ABCDE curves of the type shown in Fig. 1 and are listed in Table IV. In the course of this study the oxygen dissociation pressure *versus* temperature relation was established for the two solid phase system having a magnetite phase in equilibrium with a hematite phase. This relationship is shown as the solid curve in Fig. 1.

The experimental study indicated that  $\text{Fe}_3\text{O}_4$  had a very low solubility in the hematite ( $\text{Fe}_2\text{O}_3(\alpha)$ ) phase at temperatures as high as 1300 to 1400°. Hence, the concentration range in hematite is too short to be able to give postulated activity expressions a very thorough testing. However, the analysis of the data in Table IV by application of thermodynamic principles and the least-squares

TABLE IV

OXYGEN DISSOCIATION PRESSURE, COMPOSITION AND TEMPERATURE DATA FOR THE HEMATITE PHASE OF IRON OXIDE

Temp., °K.	Oxygen pressure, atm.	Mole fraction Fe <sub>2</sub> O <sub>3</sub>	Mole fraction Fe <sub>3</sub> O <sub>4</sub>
1462	3.88 × 10 <sup>-3</sup>	0.9936	0.0064
1436	3.57 × 10 <sup>-3</sup>	.9952	.0048
1475	5.01 × 10 <sup>-3</sup>	.9875	.0125
1458	4.20 × 10 <sup>-2</sup>	.9920	.0080
1436	3.63 × 10 <sup>-3</sup>	.9948	.0052
1419	3.36 × 10 <sup>-3</sup>	.9964	.0036
1411	3.22 × 10 <sup>-3</sup>	.9972	.0028
1430	3.29 × 10 <sup>-3</sup>	.9968	.0032
1432	3.35 × 10 <sup>-3</sup>	.9964	.0036
1450	3.62 × 10 <sup>-3</sup>	.9952	.0048
1469	4.59 × 10 <sup>-3</sup>	.9899	.0101
1486	7.11 × 10 <sup>-3</sup>	.9769	.0231
1458	4.13 × 10 <sup>-3</sup>	.9924	.0076
1447	3.71 × 10 <sup>-3</sup>	.9944	.0056
1422	3.32 × 10 <sup>-3</sup>	.9968	.0032
1506	2.053 × 10 <sup>-2</sup>	.9968	.0032
1523	2.086 × 10 <sup>-2</sup>	.9952	.0048
1523	2.125 × 10 <sup>-2</sup>	.9932	.0068
1510	2.072 × 10 <sup>-2</sup>	.9960	.0040
1505	2.079 × 10 <sup>-2</sup>	.9956	.0044
1521	2.118 × 10 <sup>-2</sup>	.9936	.0064
1509	2.112 × 10 <sup>-2</sup>	.9940	.0060
1486	2.039 × 10 <sup>-2</sup>	.9976	.0024
1479	1.187 × 10 <sup>-1</sup>	.9900	.0100
1598	1.211 × 10 <sup>-1</sup>	.9814	.0186
1588	1.202 × 10 <sup>-1</sup>	.9927	.0073
1580	1.195 × 10 <sup>-1</sup>	.9883	.0117
1570	1.190 × 10 <sup>-1</sup>	.9912	.0088
1537	1.18 × 10 <sup>-1</sup>	.9932	.0068
1474	1.178 × 10 <sup>-1</sup>	.9944	.0056
1604	1.195 × 10 <sup>-1</sup>	.9891	.0109
1606	1.206 × 10 <sup>-1</sup>	.9835	.0165
1580	1.190 × 10 <sup>-1</sup>	.9912	.0088
1527	1.178 × 10 <sup>-1</sup>	.9960	.0040

method indicated that the activity of Fe<sub>3</sub>O<sub>4</sub> over the narrow solid solution range in hematite was very nearly directly proportional to mole fraction X<sub>2</sub> of Fe<sub>3</sub>O<sub>4</sub> in solid solution. This means that each Fe<sub>3</sub>O<sub>4</sub> molecule dissolved in hematite is contributing one independent defect to the structure. It will be assumed that this defect is an interstitial Fe<sup>0</sup> atom. The Fe<sub>3</sub>O<sub>4</sub> molecules will also supply some 3+ vacancies in iron ion positions but the location of the vacancies will be assumed to be dependent on the location of the interstitial atoms of Fe<sup>0</sup>.

The entropy of mixing N<sub>1</sub> Fe<sub>2</sub>O<sub>3</sub> molecules and N<sub>2</sub> Fe<sub>3</sub>O<sub>4</sub> molecules will be obtained from the random mixing of N<sub>2</sub> interstitial Fe<sup>0</sup> atoms supplied by the Fe<sub>3</sub>O<sub>4</sub> molecules with N<sub>1</sub> neutral interstitial holes supplied by the Fe<sub>2</sub>O<sub>3</sub> molecules. This leads to the simple activity expressions for the hematite phase

$$a_1(\alpha) = X_1 \quad (13)$$

$$a_2(\alpha) = X_2 \quad (14)$$

F. Application of the Activity Expressions to the Experimental Results for the Hematite Phase.— Activity expressions 13 and 14 when applied to the reaction

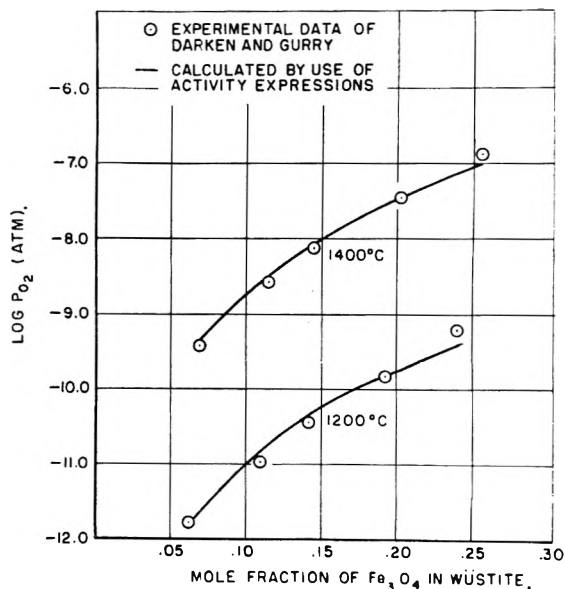
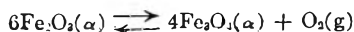


Fig. 2.—Isotherms at 1200 and 1400° for oxygen dissociation pressure vs. content of Fe<sub>3</sub>O<sub>4</sub> in solid solution in wüstite.

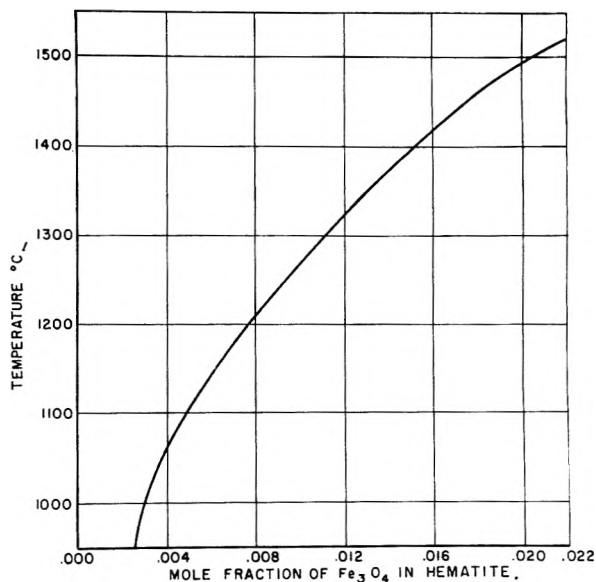


Fig. 3.—Composition of hematite in equilibrium with magnetite.

lead to the following relation between P<sub>O<sub>2</sub></sub>, X<sub>1</sub>, X<sub>2</sub>, T, ΔH<sup>0</sup>(α) and ΔS<sup>0</sup>(α)

$$RT \ln P_{\text{O}_2} \frac{X_2^4}{X_1^6} = -\Delta H^0(\alpha) + T\Delta S^0(\alpha) \quad (15)$$

where ΔH<sup>0</sup>(α) and ΔS<sup>0</sup>(α) are the standard heat and entropy, resp., for above oxygen dissociation reaction

Equation 15 has been applied by the least-squares method to the data in Table IV, to obtain the value of ΔH<sup>0</sup>(α) and ΔS<sup>0</sup>(α) and the corresponding probable errors. These are

$$\Delta H^0(\alpha) = 187,000 \pm 17,000 \text{ cal.}$$

$$\Delta S^0(\alpha) = 77 \pm 11 \text{ cal./°K.}$$

The data in Table IV were obtained by progressing in a forward and reverse direction over curve ABCDE (Fig. 1) for each run. A different run would, of course, have a different ABCDE curve.

The large probable errors in  $\Delta H^0(\alpha)$  and  $\Delta S^0(\alpha)$  are not unreasonable because slight departure from equilibrium would cause the mole fraction of  $\text{Fe}_3\text{O}_4$  to be in error by relatively large percentages in such a dilute solid solution region.

The solid curve in Fig. 1 shows the relationship between oxygen dissociation pressure and temperature when a hematite phase is in equilibrium with a magnetite phase. The corresponding data of Norton<sup>9</sup> and Darken and Gurry<sup>6</sup> are also shown. When values of  $P_{\text{O}_2}$  and  $T$  from this curve are substituted along with the above values of  $\Delta H^0(\alpha)$  and  $\Delta S^0(\alpha)$  into equation 15, the composition (*i.e.*,  $X_1$  and  $X_2$ ) of the hematite phase in equilibrium with the magnetite phase can be calculated at temperature  $T$ . This has been done and the results are plotted in Fig. 3. It is evident from the curve in Fig. 3 that the solubility of  $\text{Fe}_3\text{O}_4$  in the hematite phase is very slight.

**G. Conclusions.**—The pressure-composition-temperature relationships at high temperature for the wüstite, magnetite and hematite phases of the iron oxide system have been successfully explained by consideration of the entropy of mixing of lattice defects in the lattice. In this study the

(9) F. J. Norton, General Electric Research Laboratory Report No. 55RL-1248.

heat of mixing of the defects with the lattice has been assumed to be zero. The experimental results agree with this assumption. Another helpful assumption has been that the charge distribution in a given phase such as wüstite is independent of the composition of that phase. This has been a valuable guide in postulating how the defects are positioned in the lattice.

By knowing the expression for entropy of mixing of defects as a function of oxygen content, it is possible, by applying thermodynamic principles to the experimental data on oxygen dissociation pressure, composition and temperature, to obtain standard heats and entropies of oxygen dissociation from the wüstite, magnetite and hematite phases. By use of the values for the standard heat and entropy of oxygen dissociation and the corresponding expression for entropy of mixing of defects as a function of composition, one can readily calculate the oxygen dissociation pressure for any oxygen content and temperature of wüstite, magnetite and hematite phases.

**Acknowledgment.**—The author gratefully acknowledges the support of this work by the U. S. Army Signal Corps Engineering Laboratories, Fort Monmouth, New Jersey, under SC Contract No. DA-36-039-sc-74904.

## KINETICS OF THE REACTION BETWEEN HYDROGEN PEROXIDE AND AQUO-(ETHYLENEDIAMINETETRAACETO)-COBALT(II) AND EVIDENCE FOR THE FORMATION OF A PEROXODICOBALT(III,III) COMPLEX<sup>1</sup>

BY RICHARD G. YALMAN

*Department of Chemistry, Antioch College, Yellow Springs, Ohio*

*Received November 8, 1967*

A peroxodicobalt(III,III) intermediate is formed during the oxidation of aquo-(ethylenediaminetetraaceto)-cobalt(II) to cobalt(III) by hydrogen peroxide. In the presence of a large excess of cobalt(II) the oxidation is stoichiometric. Otherwise oxygen is formed. The kinetics of these reactions were determined by manometric, spectrophotometric and polarographic techniques. The mechanisms of these reactions are discussed.

When hydrogen peroxide is added to solutions of aquo-(ethylenediaminetetraaceto)-cobalt(II),  $\text{YCoH}_2\text{O}^{-2}$ , cobalt(III) complexes are formed.<sup>2</sup> At the same time hydrogen peroxide is decomposed. The purpose of this investigation was to examine the kinetics of these reactions.

Preliminary experiments showed that the evolution of oxygen could be studied by manometric techniques in the pH range of 6.5–8.5 at 30°. Under these conditions there is an equilibrium between aquo-(ethylenediaminetetraaceto)-cobalt(III),  $\text{YCoH}_2\text{O}^{-}$ , and hydroxo-(ethylenediaminetetraaceto)-cobalt(III),  $\text{YCoOH}^{-}$ ,<sup>2</sup> and both of these complexes form ethylenediaminetetraaceto-cobalt(III),  $\text{YCo}^{-2}$ .<sup>3</sup> At 576  $\mu\text{m}$ .<sup>3,4</sup> these complexes have the same molecular absorption coefficient and the spectrophotometric study of the

oxidation of cobalt(II) to cobalt(III) is independent of the product(s) at this wave length.

### Experimental

**Reagents.**—Dihydrogen aquo-(ethylenediaminetetraaceto)-cobalt(II) was prepared by the method of Shimi and Higginson.<sup>3</sup> This complex was the only source of cobalt(II) and ethylenediaminetetraacetic acid used in these experiments. Crystalline catalase was obtained from Nutritional Biochemicals Corp., Cleveland, Ohio. All other chemicals were C.P., A.C.S. reagent grade. All salt solutions were carefully filtered and, where necessary, analyzed by standard volumetric procedures.

Reaction mixtures were prepared by rapidly mixing solutions of the cobalt(II) complex with solutions of hydrogen peroxide. The latter contained sufficient phosphate buffer and sodium perchlorate so that on dilution to volume each reaction mixture was 0.1 M in phosphate and had a total ionic strength of 0.5 M. In a number of experiments excess hydrogen peroxide was destroyed after 5 minutes by chilling the reaction mixture and adding catalase. Solutions treated in this way will be called *catalase* treated reaction mixtures. In one series of experiments to determine stoichiometry dilute solutions of hydrogen peroxide were added dropwise with continuous stirring to buffered solutions of the cobalt(II) complex. The pH's of all solutions were measured periodically with a Beckman Model G pH meter.

(1) Part of the material in this paper was presented before the Division of Physical Chemistry at the 134th meeting of the American Chemical Society, Chicago, 1958.

(2) G. Schwarzenbach, *Helv. Chim. Acta*, **32**, 839 (1949).

(3) I. A. Shimi and W. C. E. Higginson, *J. Chem. Soc.*, 260 (1958).

(4) S. M. Jorgensen, *Acta Chem. Scand.*, **9**, 1362 (1955).

**Oxygen Experiments.**—The amount and rate of oxygen evolution was determined with an Acme Equipment Co. Warburg Apparatus using Summerson manometers and one-arm Warburg flasks. The latter were calibrated by the reaction between hydrogen peroxide and potassium permanganate in dilute sulfuric acid. The reaction mixture was generated by dumping solutions of the cobalt(II) complex from the side arm into buffered hydrogen peroxide solutions. The thermobars contained similar solutions, but no cobalt(II). After a short induction period straight line curves were obtained by plotting  $\log(H_\infty - H_t)$  against  $t$ , where  $H_\infty$  is the total change in the height of the manometer. First-order rate constants were calculated from the slopes of these lines.

In a few experiments catalase treated reaction mixtures were placed in Warburg flasks and, after equilibrating for 15 minutes, the evolution of oxygen was observed. Although the amount of oxygen formed in these experiments was only about 40% of that formed in the original reaction mixtures, the rate of oxygen evolution was nearly twice as great, indicating a reaction involving catalase. In duplicate experiments the same amount of oxygen was formed almost instantaneously when potassium triiodide was added from the side arm to catalase treated reaction mixtures.

**Spectrophotometric Experiments.**—Optical density measurements were made with a Beckman Model DU Spectrophotometer with a photomultiplier attachment using 1 cm. silica cells. The cell compartment was maintained at  $29.7 \pm 0.1^\circ$  by circulating water from a constant temperature bath through coils in the cell housing. A number of measurements were made at  $0.5^\circ$  by circulating water from an ice-bath through the cell housing. In these experiments Drierite was placed in the cell housing to prevent fogging.

The absorption spectra of  $\text{YCoH}_2\text{O}^-$ ,  $\text{YCoH}_2\text{O}^-$  and  $\text{YCo}^-$  were determined from 320 to 660  $\mu$ . The results were in agreement with those reported in the literature.<sup>3,4</sup> The concentration of cobalt(III) was determined from measurements at 576  $\mu$ , where the complexes have the same molar absorption coefficient. In the experiments to determine stoichiometry corrections were made for the amount of unreacted cobalt(II).

At 576  $\mu$  the optical density of the reaction mixtures increases rapidly and then more slowly. From plots of  $\log(D_\infty - D_t)$  against  $t$  it was found that these changes corresponded to two rate-determining steps following consecutive first-order kinetics. The rate constant for the first step was then calculated from semilog plots of the initial measurements corrected for the optical densities due to the second reaction.

Somewhat different results were obtained in the ultraviolet region. Thus in the region 340 to 365  $\mu$ , where minima occur in the absorption spectra of the cobalt(III) complexes,<sup>3,4</sup> the optical densities of the reaction mixtures increase rapidly, pass through a maxima and then decrease slowly following first-order kinetics. Extrapolation of the data of Shimi and Higginson<sup>3</sup> to  $30^\circ$  indicates that the rate of conversion of equilibrium mixtures of  $\text{YCoH}_2\text{O}^-$  and  $\text{YCoOH}^-$  to  $\text{YCo}^-$  increases from approximately  $1 \times 10^{-1}$  l. moles<sup>-1</sup> min.<sup>-1</sup> at pH 8 to  $2 \times 10^{-1}$  l. moles<sup>-1</sup> min.<sup>-1</sup> at pH 6-7. Preliminary experiments showed that this is faster than the decrease in the optical density of the reaction mixtures. Therefore subsequent measurements were made at 340  $\mu$ , the minimum in the absorption spectrum of  $\text{YCo}^-$ .

In a number of experiments the reaction mixtures were allowed to stand at  $30^\circ$  until their optical density reached a maximum at 340  $\mu$ . The solutions were then quickly chilled and their absorption spectra measured at  $0.5^\circ$ . From time to time the measurements were repeated with freshly prepared solutions. The range 320 to 600  $\mu$  was examined.

**Polarograph Experiments.**—Catalase treated reaction mixtures were de-oxygenated with nitrogen and examined with a Sargeant Model XXI Polarograph using Lingane-type H cells placed in a constant temperature bath. The effect of the height of the mercury column on the diffusion current of these solutions and of solutions of  $\text{YCo}^-$  were determined at  $0^\circ$  by packing the cells in ice.

## Results

**Stoichiometry.**—The amount of oxygen evolved and the total amount of cobalt(III) formed in

various reaction mixtures are given in column four of Table I. In the first set of experiments an excess of hydrogen peroxide was used and the reaction was performed in the Warburg apparatus. In the second set an excess of  $\text{YCoH}_2\text{O}^-$  was used and the solutions were analyzed spectrophotometrically.

Values of the consumption ratio  $n$

$$n = \frac{\Delta[\text{H}_2\text{O}_2]}{\Delta[\text{Co(II)}]}$$

are given in column five. At constant ratios of  $\text{H}_2\text{O}_2:\text{Co(II)}$   $n$  increases with increasing pH. The increase is particularly rapid in the neighborhood of pH 7, but above this the increase is more gradual. In the presence of an excess of hydrogen peroxide  $n$  is essentially independent of the total amount of hydrogen peroxide present. However, in the presence of excess  $\text{YCoH}_2\text{O}^-$   $n$  decreases and approaches a value of 0.5, corresponding to the stoichiometric oxidation of cobalt(II) to cobalt(III). When  $n$  has a value of 1.5, one mole of hydrogen peroxide is decomposed for each gram-atom of cobalt(II) oxidized to cobalt(III).

TABLE I  
STOICHIOMETRY OF THE  $\text{YCoH}_2\text{O}^-$ - $\text{H}_2\text{O}_2$  REACTION

pH	Reagents, mmoles		Products, mmoles O <sub>2</sub> or Co(III)	n
	$\text{YCoH}_2\text{O}^-$	$\text{H}_2\text{O}_2$		
A. Oxygen <sup>a</sup>				
6.9	0.025	0.3558	0.0085	1.18
7.0	.049	.544	.0196	1.30
7.0	.0294	.544	.0125	1.35
7.2	.0375	.356	.0158	1.37
7.4	.0125	1.068	.0065	1.54
7.4	.0125	2.136	.0066	1.55
7.4	.0250	0.7116	.0140	1.62
7.4	.0250	1.068	.0136	1.59
8.15	.025	0.356	.0143	1.65
8.5	.025	.356	.0151	1.71
B. Cobalt(III) <sup>b</sup>				
7.4	1.347	0.507	0.343	1.48
7.4	1.347	.101	.123	0.82
7.4	1.347	.0507	.074	.69
7.4	1.347	.0253	.048	.53
7.4	1.347	.0127	.025	.51

<sup>a</sup> Average of quadruplicate experiments. <sup>b</sup> Average of duplicate experiments.

**Kinetics.**—In buffered solutions containing a high ratio of  $\text{H}_2\text{O}_2:\text{YCoH}_2\text{O}^-$  the evolution of oxygen was preceded by an induction period which decreased with increasing pH and disappeared above pH 8. After the induction period and above pH 8 the evolution of oxygen obeyed the rate law

$$d[\text{O}_2]/dt = k_{\text{obs}}([\text{O}_2]_\infty - [\text{O}_2])$$

where  $[\text{O}_2]_\infty$  is the total amount of oxygen formed in the experiment.

At constant hydrogen peroxide concentration the observed rate constant increased linearly with increasing  $[\text{OH}^-]$  and at constant pH it increased linearly with increasing  $[\text{H}_2\text{O}_2]$ . The rate law is given by

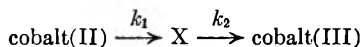
$$k_{\text{obs}} = k_a + k_b[\text{OH}^-] + k_c'[\text{OH}^-][\text{H}_2\text{O}_2]$$

or

$$k_{\text{obs}} = k_a + k_b[\text{OH}^-] + k_c[\text{OOH}^-] \quad (\text{I})$$

and at 30°  $k_a = 3 \times 10^{-3} \text{ min.}^{-1}$ ,  $k_b = 7.4 \times 10^4 \text{ l. moles}^{-1} \text{ min.}^{-1}$  and  $k_c = 2.3 \times 10^3 \text{ l. moles}^{-1} \text{ min.}^{-1}$ . The latter was calculated from the relationship  $k_c = k_c' K_w / K_{\text{H}_2\text{O}_2}$  using the value of  $2.6 \times 10^{-12} \text{ moles/l.}$  for the ionization of hydrogen peroxide at 30°.<sup>5</sup> All experiments were performed at a constant ionic strength of 0.5 *M* and no corrections were made for activity coefficients.

**Kinetics of Cobalt(III) Formation.**—The oxidation of  $\text{YCoH}_2\text{O}^{-2}$  to cobalt(III) complexes was followed spectrophotometrically in buffered solutions containing a large excess of either  $\text{YCoH}_2\text{O}^{-2}$  or hydrogen peroxide. At 576  $m\mu$  the increase in the optical density occurred in two steps paralleling the induction period and the formation of oxygen in the manometric experiments. From plots of  $\log(D_\infty - D_t)$  against  $t$  the rate-determining reactions were found to obey first-order kinetics, indicating the formation of at least one reaction intermediate



From these experiments it was found that  $k_2$  obeyed the same rate law as the rate constant for the formation of oxygen (equation I) and that  $k_a = 3.3 \times 10^{-3} \text{ min.}^{-1}$ ,  $k_b = 5.6 \times 10^4 \text{ l. moles}^{-1} \text{ min.}^{-1}$  and  $k_c = 2.9 \times 10^3 \text{ l. moles}^{-1} \text{ min.}^{-1}$ . The agreement between these two sets of experiments indicates that the formation of oxygen and the second step in the oxidation of cobalt(II) to cobalt(III) occur simultaneously.

As the results in Table IIA show the rate constant  $k_1$  for the first step in the oxidation of cobalt(II) to cobalt(III) is first order with respect to both cobalt(II) and hydrogen peroxide. On the other hand measurements over a twenty-fold range of  $[\text{OH}^-]$  show (Table IIB) that at constant hydrogen peroxide concentration the quotient  $k_1/[\text{OH}^-]$  increases slowly with increasing hydroxyl ion concentration. A straight line was obtained by plotting  $[\text{OH}^-]/k_1$  against  $[\text{H}_3\text{O}^+]$  and the rate law for  $k_1$  was found to be

$$k_1 = k_f[\text{OOH}^-]/(1 + k_r[\text{H}_3\text{O}^+]) \quad (\text{II})$$

At 30°  $k_f$  and  $k_r$  have the values of  $8.5 \times 10^4$  and  $1.1 \times 10^6 \text{ l. moles}^{-1} \text{ min.}^{-1}$ , respectively.

Optical density measurements in the ultraviolet region show that an intermediate is formed during the oxidation of cobalt(II) to cobalt(III). Thus at 340  $m\mu$  the optical density of the reaction mixtures increased rapidly, passed through a maximum and then decreased slowly. Again these changes parallel the induction period and the evolution of oxygen in the manometric experiments and the changes in optical density at 576  $m\mu$ . The time required for the optical density to reach a maximum at 340  $m\mu$  decreased with increasing *pH* and above *pH* 7.5 it could not be determined experimentally.

The occurrence of the maxima at 340  $m\mu$  was calculated from the equation<sup>6</sup>

TABLE II

RATE CONSTANT  $k_1$  FROM MEASUREMENTS AT 576  $m\mu$ 

A. <i>pH</i> 7.34			
$[\text{YCoH}_2\text{O}^{-2}]$	$[\text{H}_2\text{O}_2]$	$k_1, \text{ min.}^{-1}$	$k_1[\text{YCoH}_2\text{O}^{-2}], \text{ l. mole}^{-1} \text{ min.}^{-1}$
0.0108	0.000914	0.0483	4.47
.0216	.000914	.105	4.86
.0270	.000914	.120	4.43
.0540	.000914	.231	4.27
.00098	.02295	.118	
.00098	.0459	.218	5.15
.00098	.06885	.310	4.75
.00098	.0925	.435	4.71
B. 0.00098 <i>M</i> $\text{YCoH}_2\text{O}^{-2}$ , 0.0925 <i>M</i> $\text{H}_2\text{O}_2$			
<i>pH</i>	$k_1, \text{ min.}^{-1}$	$k_1[\text{OH}^-], \text{ l. mole}^{-1} \text{ min.}^{-1}$	
6.18	0.0168	$1.2 \times 10^6$	
6.63	.069	1.61	
6.72	.092	1.74	
6.84	.121	1.74	
6.93	.154	1.83	
7.26	.356	1.95	
7.34	.435	1.98	
7.44	.550	1.99	
..	...	2.07 <sup>a</sup>	

<sup>a</sup> Limiting value from plot of  $[\text{OH}^-]/k_1$  against  $[\text{H}_3\text{O}^+]$ .

$$T = \frac{\ln k_1/k_2}{k_1 - k_2}$$

where  $k_1$  and  $k_2$  are the observed rate constants at 576  $m\mu$ . The calculated values of  $T$  for solutions containing 0.0925 *M*  $\text{H}_2\text{O}_2$  and 0.00098 *M*  $\text{YCoH}_2\text{O}^{-2}$  are given in column four of Table III. The good agreement between these values and the observed values of  $T$  (column five) indicate that the kinetics of the formation and decomposition of the intermediate is the same as the kinetics of the oxidation of cobalt(II) to cobalt(III) and that the decomposition of this material follows the same rate laws as the evolution of oxygen.

TABLE III

OCCURRENCE OF THE MAXIMUM AT 340  $m\mu$   
0.0925 *M*  $\text{H}_2\text{O}_2$ ; 0.00098 *M*  $\text{YCoH}_2\text{O}^{-2}$ 

<i>pH</i>	$k_1, \text{ min.}^{-1}$	$k_2, \text{ min.}^{-1}$	$T, \text{ min.}$	Obsd.
6.63	0.069	0.0089	34.2	35.5
6.72	.092	.0102	25.8	26.0
6.84	.121	.0120	21.0	22.0
6.93	.154	.0169	16.2	17.0
7.26	.356	.0278	8.2	8.5
7.34	.435	.0320	6.5	7.5
7.44	.550	.0366	5.3	6.0

<sup>a</sup> From changes in the optical density at 576  $m\mu$ .

**Identification of the Intermediate.**—The absorption spectrum of the intermediate was determined in the following way. The optical density of the reaction mixtures is given by

$$D = \beta_2[\text{Co(II)}] + \beta_3[\text{Co(III)}] + \beta_X[\text{X}]$$

where  $\beta_2$  and  $\beta_3$  are the molar absorption coefficient of cobalt(II) and cobalt(III), respectively, and  $\beta_X$  is the molar absorption coefficient of the intermediate whose concentration is  $[\text{X}]$ . Optical

(6) A. A. Frost and R. G. Pearson, "Kinetics and Mechanism," John Wiley and Sons, New York, N. Y., 1953, p. 155.



density measurements at various wave lengths were made on reaction mixtures which were chilled when the value of  $D$  reached a maximum at 340  $m\mu$ . The concentrations of the reactants were calculated from the usual exponential expressions for consecutive first-order kinetics. In making these calculations it was assumed that the intermediate contained one atom of cobalt. Upon substituting into the above expression and rearranging values of  $\beta_X$  were calculated.

If the intermediate is a polymer, then from

$$[\text{Co(II)}]_i = [\text{Co(II)}] + [\text{Co(III)}] + n[\text{X}]$$

where  $n$  is the number of cobalt atoms in the polymer and  $[\text{Co(II)}]_i$  is the initial concentration of cobalt(II), it can be shown that there will be no change in the values of  $[\text{Co(II)}]$  and  $[\text{Co(III)}]$ , but that  $[\text{X}]$  will be reduced by the factor  $n$  and that  $\beta_X$  will be increased by the same factor. However there will be no change in the general nature of the absorption spectrum of the intermediate.

In the optical region the absorption spectrum of the intermediate could not be distinguished from that of  $\text{YCo}^-$ . Because of the experimental errors involved this can only be interpreted as indicating that the intermediate has a band in the visible region similar in location and intensity to that of the cobalt(III) complexes. On the other hand, there is a rapid increase in the molar absorption coefficient in the ultraviolet region typical of peroxodicobalt(III,III) complexes.<sup>7,8</sup> In view of this and the greater stability of binuclear peroxo cobalt complexes<sup>9</sup> compared to aqueous solutions of peroxocobalt(III)<sup>10</sup> the intermediate observed here is probably the binuclear complex,  $\text{YCoOOC}_2\text{Y}^{-4}$ .

The formation of a peroxo intermediate was confirmed by the polarographic experiments. When *catalase* treated reaction mixtures are reduced at the dropping mercury electrode, two waves were observed. The first varied from  $-0.050$  v. vs. S.C.E. at pH 7 to  $-0.170$  v. at pH 9. No difference could be detected between this wave and that of  $\text{YCo}^-$ .<sup>11</sup> The value of the diffusion current at  $-0.30$  v. vs. S.C.E. was determined for different heights of the mercury column at 0.5°. As the results in Table IV show, the reduction at the first wave for the reaction mixtures and for  $\text{YCo}^-$  is diffusion controlled.

The second wave was typical of that obtained in solutions of hydrogen peroxide<sup>12</sup> and identical to that obtained with diaquotetrakis-(glycino)- $\mu$ -peroxodicobalt(III,III).<sup>8</sup> It had a broad band beginning at  $-0.7$  v. vs. S.C.E. and extended to  $-1.1$  v. The half-wave potential was  $-0.9$  v. and its diffusion current, which could be measured from  $-1.2$  to  $-1.6$  v., was 33–50% greater than that observed at  $-0.3$  v. At 30° the diffusion

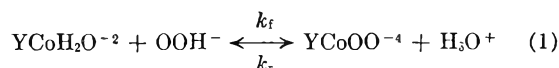
TABLE IV  
EFFECT OF COLUMN HEIGHT ON DIFFUSION CURRENT  
0.0001225  $M$  cobalt, pH 9.33, 0.5°

Height, cm.	$i_d$ , $\mu\text{a.}$	$t$ , sec./drop open circuit	$m$ , mg./sec.	$i_d/h^{1/2}$ , $\mu\text{a. cm.}^{-1/2}$
A. Ethylenediaminetetraacetocobalt(III)				
68.3	2.37	4.53	1.53	2.85
58.3	2.18	5.30	1.33	2.86
48.3	1.98	6.40	1.08	2.85
38.3	1.78	8.06	0.84	2.88
B. <i>Catalase</i> treated reaction mixtures				
68.3	2.14	4.53	1.53	2.59
58.3	1.97	5.30	1.33	2.59
48.3	1.76	6.40	1.08	2.53
38.3	1.57	8.06	0.84	2.54

current decreased until the second wave disappeared. Simultaneously there was a 0.0–33% decrease in the diffusion current due to the first reduction step, the amount of decrease increasing with increasing pH. Although no systematic relationship between the net change of the diffusion current for the two steps was observed, the rate of change was nearly twice as great as that observed in the untreated reaction mixtures. These results also suggest that the intermediate may be decomposed by catalase itself.

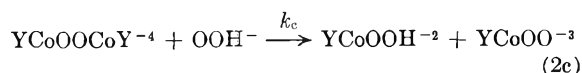
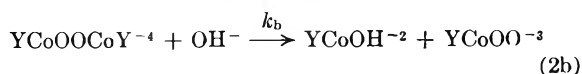
### Discussion

Although the results observed here can be interpreted by the intermediate formation of bis-(ethylenediaminetetraaceto)- $\mu$ -peroxodicobalt(III,III), other intermediates are also formed. Thus the rate law for  $k_1$  (equation I) suggests the reversible formation of a peroxocobalt(II) complex<sup>13</sup>



Subsequent fast reactions include the reaction of this complex with additional cobalt(II) to form a dimer which is then oxidized by hydrogen peroxide to the peroxodicobalt(III,III) complex. The latter two-electron reaction is preferable to either the formation of cobalt(IV) (also requiring two electrons) or to the formation of free radicals by a one-electron reaction, particularly in the initial reaction mixtures which contain a large excess of hydrogen peroxide.

The observed kinetics for the decomposition of the intermediate would be satisfied by



Both reactions 2 and 2a would contribute to the rate constant  $k_a$ . No attempt was made to distinguish between them. Because of the size of the ligand and the general instability of peroxo com-

(13) Both  $\text{YCoOOH}^{-3}$  and  $\text{YCoOOH}^{-2}$  will be stronger acids than the corresponding aquo ions.

(7) L. Michaelis, *Federation Proc.*, **7**, 509 (1948).

(8) R. G. Yalman and M. Warga, *J. Am. Chem. Soc.*, **80**, 1011 (1958).

(9) A. Werner, *Ann.*, **375**, 1 (1910).

(10) J. H. Baxendale and C. F. Wells, *Trans. Faraday Soc.*, **53**, 800 (1957).

(11) P. Souchay and J. Faccherre, *Anal. Chim. Acta*, **3**, 252 (1949).

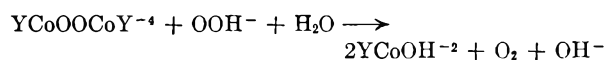
(12) I. M. Kolthoff and J. J. Lingane, "Polarography," Interscience Publishers, New York, N. Y., 1952, p. 557.

plexes these reactions would be expected to have a type  $S_N1$  mechanism. There would then be a competition between coordination of the remaining carboxylate group on the ligand and solvation by a water molecule for the cobalt atom with coordination number five.

Reactions 2a and 2b are the acid and base hydrolysis of the intermediate,  $YCoOOCY^{-4}$ . If (2) is ignored or if the rate constants for (2) and (2a) are of the same order of magnitude, then the observed rate constants,  $k_a$  and  $k_b$ , are of the same orders of magnitude as the acid and base hydrolysis constants of other ethylenediamine complexes of cobalt(III) and reaction 2b may also be of type  $S_N1CB$ .<sup>14</sup>

Reaction 2c satisfies the observed kinetics with respect to  $OOH^-$  for the formation of oxygen and the second step in the formation of cobalt(III). Although some doubt has been raised as to whether substitution by reagents other than hydroxyl ion occurs in reactions with cobalt(III) complexes,<sup>14</sup> there had been a recent report of such a substitution by cyanide ion.<sup>15</sup> Also observations in this Laboratory indicate that  $Co(NH_3)_5Cl^{+2}$  can be formed directly from  $(NH_3)_5CoOOC(NH_3)_5^{+4}$ .

An alternate reaction to (2c) is



However, experiments in this laboratory show that  $(NH_3)_5CoOOC(NH_3)_5^{+4}$  is not involved in the catalytic decomposition of hydrogen peroxide by ammoniacal solutions of cobalt(II) sulfate.

In reactions (2)–(2c) the reactive product is  $YCoOO^{-3}$  which is in equilibrium with  $YCoOOH^{-2}$ .

(14) F. Basolo and R. G. Pearson, "Mechanisms of Inorganic Reactions," John Wiley and Sons, Inc., New York, N. Y., 1958, p. 128 and 130.

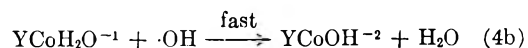
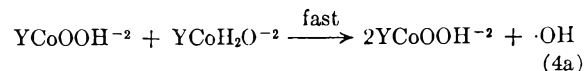
(15) D. A. L. Hope and J. E. Prue, *J. Chem. Soc.*, 2782 (1960).

This substance could then react rapidly with hydrogen peroxide to form oxygen



Reaction 3 is analogous to one proposed for the decomposition of hydrogen peroxide by catalase<sup>16</sup> and to the reaction between  $Co(NH_3)_5C_2O_4^+$  and hydrogen peroxide.<sup>17</sup> Reaction 3 also satisfies the observed stoichiometry ( $n = 1.5$ ) in the presence of excess hydrogen peroxide.

On the other hand the stoichiometric reaction ( $n = 0.5$ ) between cobalt(II) and hydrogen peroxide in the presence of a large excess of cobalt(II) suggests the occurrence of



The formation of free radicals in reaction 4a and their subsequent reaction with hydrogen peroxide would also account for the variations in the amount of hydrogen peroxide decomposed at different  $pH$ 's.

**Acknowledgment.**—The author wishes to acknowledge support of this project by Research Grant RG-4458 from the U. S. Public Health Service. The author also wishes to thank the Fels Institute, Yellow Springs, Ohio, for the use of the Warburg apparatus and the Kettering Institute, Yellow Springs, Ohio, for the use of the polarograph. Others who have contributed to the experimental work include Margaret Warga and Roger Bakeman.

(16) B. Chance and R. R. Ferguson in "The Mechanism of Enzyme Action," edited by W. D. McElroy and B. Glass, The Johns Hopkins Press, 1954, p. 389.

(17) P. Saffir and H. Taube, *J. Am. Chem. Soc.*, **82**, 13 (1960).

## NOTES

### ICE VIII—AN ACETONE HYDRATE?

BY ARVIN S. QUIST AND HENRY S. FRANK

Department of Chemistry, University of Pittsburgh, Pittsburgh 13, Pennsylvania

Received August 10, 1960

In 1938 Cohen and van der Horst<sup>1</sup> described a solid material prepared by cooling acetone–water solutions to temperatures near  $-35^\circ$ . X-Ray powder patterns, density determinations and chemical analyses of their finely divided crystals led these authors to conclude that they had obtained a new solid phase of water, which they called Ice VIII. They reported that this ice belonged to the cubic system, with  $a = 9.68 \text{ \AA}$ . at  $-35^\circ$  and a density of 1.05 g./cc. at  $-30^\circ$ .

(1) E. Cohen and C. J. G. van der Horst, *Z. physik. Chem.*, **B40**, 231 (1938).

We have also prepared crystals belonging to the cubic system by the slow cooling of 60 weight % solutions of acetone in water. In contrast to the tiny crystals obtained by Cohen and van der Horst, our procedure yielded relatively large, well-formed, octahedral crystals (usually obtained in a range of sizes, up to approximately 1 mm. in edge length) which were suitable for single crystal X-ray studies.

**Preparation of Sample and Procedure for X-Ray Measurements.**—The octahedral crystals were best prepared when the acetone–water solution was contained in a triple-walled glass vessel (two air spaces) which was immersed in a cold bath, the temperature of which usually was kept near  $-40^\circ$ . Suitable crystals seemed to be obtained more readily if the acetone–water solution was first frozen solid and then melted before the slow cooling to near  $-40^\circ$  was carried out. These crystals could be isolated by pouring the suspension of the crystals in the mother liquor onto an absorbent paper in a cold box held to a temperature near  $-35^\circ$ . Single crystals

were placed (without being permitted to warm up) in glass capillary tubes which were then mounted on the goniometer head of an X-ray camera. Weissenberg photographs were taken, using copper  $K\alpha$  radiation. The X-ray camera was enclosed in a specially constructed, double-walled, Plexiglass box which could be cooled to approximately  $-35$  to  $-40^\circ$  by the use of solid carbon dioxide. Several different single crystals were studied, all of them freshly prepared and most of them approximately 0.5 mm. in diameter. Measurements on one crystal usually required 10 to 12 hours.

**Unit Cell and Space Group.**—Weissenberg photographs obtained with the morphological twofold and fourfold as rotation axes showed diffraction patterns that were consistent with  $m\bar{3}m$  Laue symmetry. When indexed on the basis of a cubic cell, these data contained only reflections of the type  $h + k = 2n$ ,  $k + l = 2n$ , and  $h + l = 2n$  for the general ( $hkl$ ) class, and only reflections of the type  $k + l = 4n$  for the ( $0kl$ ) zone, thereby uniquely fixing the space group as  $Fd\bar{3}m$  within the assumed octahedral system. All observable powder diffraction lines were consistent with the above extinctions and were indexable on the basis of a cubic cell with the dimensions 17.16 Å., which was determined from oscillation and Weissenberg photographs.

These diffraction data indicate that the structure under investigation is isostructural, at least in its water framework, with one of the "liquid hydrates" described by von Stackelberg.<sup>2,3</sup> The cell dimensions, which are presumably determined by the water structure alone, are identical within experimental error in the two cases.

In order to extend the comparison between this structure and the "liquid hydrate" of von Stackelberg, representative three dimensional intensity data for the crystal were qualitatively estimated and compared with the spectral intensities calculated from the model described<sup>2</sup> by von Stackelberg for the oxygen framework of the "liquid hydrates." Lorentz and polarization corrections were applied to the square of the calculated structure factor amplitudes, in order that the calculated quantity might be more realistically compared to the observed values. The intensity distribution for the calculated and observed spectra were remarkably similar, further substantiating the isostructural relationship that appears to exist between this crystal and the hydrates of chloroform, dichloromethane, ethyl chloride, etc., that were studied by von Stackelberg. The unit cell of these crystals contains 136 water molecules, which form a framework of slightly deformed pentagonal dodecahedra. These pentagonal dodecahedra share faces to form a unit cell containing 8 large voids (in the form of hexadecahedra, with 12 pentagonal faces and 4 hexagonal faces) and 16 small voids (spaces inside the pentagonal dodecahedra). If each large void contains a molecule of acetone, the formula of the hydrate will be  $(CH_3)_2CO \cdot 17H_2O$ .

**Density and Composition of the Crystals.**—The crystal density was determined by flotation in organic liquids. The measured density was found to be quite variable, decreasing as the period of time increased between the isolation of the crystal and the density measurement. The maximum observed value of the density, found when freshly prepared crystals were used, was 0.95 g./cc., which corresponds to what would be observed if all eight molecules of the acetone were present per unit cell. Crystals which had been allowed to stand for several hours in a partial vacuum near temperatures of  $-30$  to  $-40^\circ$  gave a density of 0.80 g./cc., corresponding to the density of the framework, i.e., to the complete "evaporation" of acetone.

The composition of the crystals was determined by the use of a gas chromatograph (Burrell Kromo-Tog, Model K2). A column consisting of Tween on Celite separated the acetone and water peaks completely, with only a slight tailing of the water peak. For complete filling of the large voids in the crystal, a value of 15.9 weight % acetone would be expected. No value as large as this was observed, whether the crystals were relatively fresh, or had been standing for some time at Dry Ice temperatures, the usual result being between 9 and 14 weight % acetone. This result is to be expected for well-drained crystals, considering the fact that the crystals lose acetone readily, and that when the crystal is melted for analysis, acetone is the more volatile component and would tend to be lost preferentially. Therefore,

although the experimental results do not give the expected value, one may conclude that the value 15.9% probably would be approached under the most favorable conditions.

From the density determinations and the chromatographic analyses, it was concluded that the crystal structure under consideration was that of an acetone hydrate,  $(CH_3)_2CO \cdot 17H_2O$ . Because the crystals seemed to lose acetone so readily, it was of interest to determine whether the loss of the acetone had any effect upon the structure of the crystal. Crystals that had lost most of their acetone (as determined from density measurements) retained their sharp, octahedral appearance, but were then opaque. This opacity could be due either to frost coating the crystal, or to changes in the interior of the crystal, or to both factors.

In order to determine the effect of the loss of acetone upon the crystal structure, the following experiments were carried out: Dry, cold nitrogen gas was passed slowly over a collection of these crystals held at a temperature between  $-35$  and  $-40^\circ$ . After 7 hours, the density and composition of some of them were measured, and X-ray photographs taken of others. For 10 crystals, the range of densities corresponds to 0 to 1 acetone molecule per unit cell. Gas chromatographic analyses on another sample corresponded to 1% by weight acetone present, or less than 0.5 molecule of acetone per unit cell. The X-ray photographs of the crystals, however, showed the powder pattern of hexagonal ice, and contained only a few spots corresponding to the acetone hydrate structure, indicating that the framework structure was not stable at  $-35^\circ$  when most of the acetone molecules had been lost.

This does not necessarily mean, however, that a small amount of acetone cannot be lost without destroying the structure. As stated above, the X-ray measurements which showed good hydrate structure usually required a single crystal to stand for 10 to 12 hours, and other crystals which had stood as long as this typically showed densities corresponding to the loss of, say, 20% of their acetone. This may have been responsible for the small amount of diffraction from hexagonal structure always present on the X-ray photographs, but the latter also might have come (as we imagined) from the unavoidable frost on the capillaries. We are therefore unable either to affirm or to deny that the structure can survive small losses of acetone. The fact that fresh crystals seem to have their full complement of acetone is in keeping with Glew's finding,<sup>4</sup> that the hydrate of bromochlorodifluoromethane, which has the same 17 Å. framework, displays essentially complete occupancy of the interstitial sites.

## Discussion

X-Ray powder photographs obtained in this Laboratory for the acetone hydrate correspond quite closely to the powder photographs published by Cohen and van der Horst. Since the acetone hydrate crystal has a face-centered cubic lattice, if its X-ray powder pattern were interpreted as resulting from a primitive cubic lattice, one could possibly obtain a value of  $a = 9.7$  Å. The analytical results of Cohen and van der Horst, indicating the absence of acetone in the crystal, were probably the result of the ease with which acetone escapes from the crystal preparations. The high density they reported may have arisen from some replacement of acetone by  $CCl_4$ , which was a component of the mixtures they used for density comparisons (we succeeded in producing a little replacement of this kind, and the much larger surface-to-volume ratio in their material would have favored such a process). The fact that they also obtained cubic crystals from solutions of acetaldehyde, propionaldehyde or pyridine doubtless is accounted for by the generality of the phenomenon of hydrate formation.

It is also possible that the isotropic cubes, octahedra and tetrahedra obtained by Rau<sup>5</sup> on con-

(2) M. von Stackelberg and H. R. Müller, *J. Chem. Phys.*, **19**, 1319 (1951); *Z. Elektrochem.*, **58**, 25 (1954).

(3) W. F. Claussen, *J. Chem. Phys.*, **19**, 259 (1951).

(4) D. N. Glew, *Can. J. Chem.*, **38**, 208 (1960).

densing water vapor onto a metal mirror at  $-72^\circ$  are "liquid hydrate" type crystals, since other researchers<sup>6,7</sup> who sought to repeat Rau's results could do so only when they used water contaminated with organic compounds, such as ethyl alcohol.

Although double hydrates of acetone with some of the inert gases have been prepared,<sup>8</sup> giving cubic crystals with  $a = 17.3 \text{ \AA}$ , this is the first time, so far as we can find, that the acetone hydrate has been reported.

**Acknowledgment.**—We are grateful to Dr. Richard K. McMullan of the Crystallography Laboratory for his help with the X-ray diffraction studies. A.S.Q. wishes to thank the National Science Foundation for financial support.

(5) W. Rau, *Schr. Deut. Akad. Luft.*, **8**, 65 (1944).

(6) B. M. Cwilong, *J. Glaciol.*, **1**, 53 (1947).

(7) A. W. Brewer and H. P. Palmer, *Proc. Phys. Soc.*, **648**, 765 (1951).

(8) J. G. Waller, *Nature*, **186**, 429 (1960).

## INTERPRETATION OF THE MAGNETIC RESONANCE SPECTRUM OF THE METHYLENE GROUP IN CERTAIN UNSYMMETRICALLY SUBSTITUTED COMPOUNDS

By J. S. WAUGH AND F. A. COTTON

*Department of Chemistry and Laboratory for Chemical and Solid State Physics, Massachusetts Institute of Technology, Cambridge, Massachusetts*

Received November 11, 1960

Finegold has recently reported and commented on some apparently anomalous features of the methylene proton resonance in dialkyl sulfites<sup>1</sup> and in O,O'-diethylmethylphosphonothioate,<sup>2</sup> and similar peculiarities have been noted recently by other investigators.<sup>3,4</sup> These may conveniently be discussed with specific reference to the situation in diethyl sulfite. Instead of the 1:3:3:1 quartet expected for the splitting of the methylene resonance by the adjacent methyl group, Finegold observed *two* such quartets, slightly displaced from one another and showing slightly different coupling constants with the methyl group. That is, one pair of methylene protons in the molecule is clearly not equivalent to the other. Finegold made the natural assumption that each of these pairs is in fact one of the methylene groups, and was thus forced to conclude that the two ethyl groups are somehow chemically different, *i.e.*, that the two sulfur-ethoxy bonds are differently hybridized.

We feel it appropriate to point out that the above assumption is not necessary, and that an alternative interpretation can be made and supported which does less violence to accepted theories of chemical bonding. It simply involves the observation that the two methylene protons of the *same* methylene group are not stereochemically equivalent, because of the lack of symmetry of the (non-planar) substituted sulfur atom with respect to internal rotation about the S-O-C linkage.

(1) H. Finegold, *Proc. Chem. Soc.*, 283 (1960).

(2) H. Finegold, *J. Am. Chem. Soc.*, **82**, 2641 (1960).

(3) J. D. Roberts (to be published).

(4) B. I. Shapiro, private communication.

The situation is more complicated than, but not essentially different from, that which is possible in simple substituted ethanes, as pointed out by Pople.<sup>5</sup> The non-equivalence in question persists when a time average is performed over all (nine) staggered (or eclipsed) rotational isomers. Phenomena of this type which depend on the energetic non-identity of rotational isomers have been reported by a number of investigators.<sup>5-8</sup> However, it has perhaps not been adequately recognized that when the symmetry of substitution is sufficiently low, the non-equivalence of methylene protons can in principle still persist when the isomers are all accidentally of *equal* energy, or even when the internal rotation is *free*.<sup>5</sup> (This statement depends entirely on a symmetry argument. It seems unlikely that in practice the asymmetry with respect to internal rotation required to produce magnetic non-equivalence would not also be reflected in some angular dependence of potential energy.)

If the phenomena observed by Finegold are to be explained in this way, it is clearly not necessary that the molecule contain *two* methylene groups. In fact, similar compounds containing only one methylene group should give "normal" methylene resonances if Finegold's interpretation is correct, but should continue to show non-equivalences if our alternative description is valid. To decide between these possibilities, we have observed the proton resonance spectrum of  $C_6H_5-S(O)-OCH_2-CH_3$ ,<sup>9</sup> which differs from diethyl sulfite only in replacement of one of the ethoxy groups by a phenyl group. The methylene resonance, shown in Fig. 1, is readily recognized as attributable to a pair of non-equivalent protons, in this case split to almost exactly the same extent by the methyl protons. An analysis of the spectrum shows that the chemical shift between these protons is  $0.434 \pm 0.005$  p.p.m. and the spin-spin coupling between them is  $10.0 \pm 0.5$  c.p.s. Each of them is coupled to the methyl protons with a coupling constant of  $7.1 \pm 0.5$  c.p.s. All the coupling constants are within the normal ranges<sup>10,11</sup> for structures of this type. It is to be expected that the coupling constants will be approximately the same as in diethyl sulfite, but the chemical shift between the methylene protons is probably quite sensitive to the substituents on the sulfur and may well be different.

It is to be noted that a non-equivalence such as Finegold proposed should lead to a simpler methylene spectrum, inasmuch as the spin coupling between non-equivalent hydrogens would be vanishingly small because of the large separation

(5) J. A. Pople, *Mol. Phys.*, **1**, 1 (1958).

(6) P. M. Nair and J. D. Roberts, *J. Am. Chem. Soc.*, **79**, 4565 (1957).

(7) J. N. Shoolery and B. L. Crawford, Jr., *J. Mol. Spectro.*, **1**, 270 (1957).

(8) D. M. Graham and J. S. Waugh, *J. Chem. Phys.*, **27**, 968 (1957).

(9) This compound was kindly prepared by Dr. A. Blake following the procedure of R. Otto and A. Rössing, *Ber.*, **18**, 2495 (1885), and was characterized by C, H and S analyses.

(10) R. E. Glick and A. A. Bothner-By, *J. Chem. Phys.*, **25**, 362 (1956).

(11) H. S. Gutowsky, M. Karplus and D. M. Grant, *ibid.*, **31**, 1278 (1959).

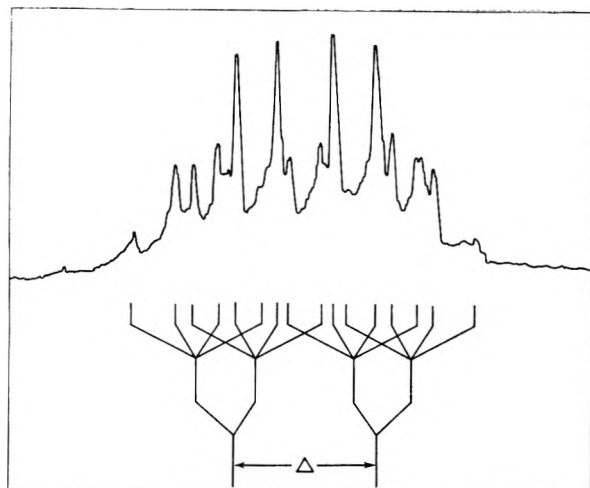


Fig. 1.

of the proton pairs from one another. Thus it is at first sight surprising that Finegold would not have been forced into our interpretation by the complexity of his spectrum. Unfortunately, in diethyl sulfite, the chemical shift seems accidentally to be so small that the additional lines are vanishingly weak, so that the two possible kinds of non-equivalence are not readily distinguishable from one another. From his figure it would appear that the relevant chemical shift is in the vicinity of 0.05 p.p.m. If we assume the spin-spin coupling between the non-equivalent protons to be 10 c.p.s., as it is in our compound, it is easy to predict<sup>12</sup> that the satellite lines should have intensities of only 1–2% of the central components.<sup>13</sup>

Similar phenomena are observed in many other molecules.<sup>3,4</sup> In diethyl acetal, for example, we have observed a complex methylene multiplet which has been analyzed to give a chemical shift difference of  $0.152 \pm 0.005$  p.p.m., an internal spin coupling of  $9.2 \pm 0.3$  c.p.s., and couplings of about 6.7 and 7.2 c.p.s. between the non-equivalent methylene protons and the methyl group.<sup>14</sup> It is significant that the spectrum of ethylal, which differs from acetal only in the substitution of a hydrogen atom for the central methyl group, contains a perfectly normal methylene quartet.<sup>14</sup> This circumstance is completely in accord with the arguments presented here, since the ethylal molecule possesses too much symmetry to allow non-equivalence of the protons in the same methylene group.

We wish to thank the National Science Foundation for support of this work.

(12) J. S. Waugh, "Proceedings of the IV International Meeting on Molecular Spectroscopy," 1959, Pergamon Press, London, in press.

(13) Dr. Finegold (private communication) has agreed to the probable correctness of the interpretation proposed here. He has stated that in many other phosphorus compounds he had studied (e.g.,  $(\text{EtO})_2\text{P}(\text{O})\text{Me}$ ,  $(\text{EtO})_2\text{PMe}$ ,  $(\text{EtO})_2\text{P}(\text{S})\text{Cl}$ ,  $(\text{EtO})_2\text{P}(\text{O})\text{H}$  and  $(\text{EtO})_2\text{P}(\text{O})\text{SMe}$  all methylene protons appeared to be equivalent and that these observations caused him to choose his previously published explanation for his observations on  $(\text{EtO})_2\text{P}(\text{S})\text{Me}$  rather than the one proposed here.

(14) C. S. Johnson, Jr., J. P. Fackler, Jr., J. S. Waugh and F. A. Cotton, unpublished work.

## D<sub>2</sub>O ISOTOPE EFFECTS IN THE CATALYTIC ACTIVATION OF MOLECULAR HYDROGEN BY METAL IONS

BY J. F. HARROD AND J. HALPERN

Department of Chemistry, The University of British Columbia, Vancouver Canada

Received December 22, 1960

With a view to gaining further insight into the role of the solvent in the catalytic activation of molecular hydrogen in solution,<sup>1</sup> the rates of reaction of hydrogen with a number of metal ions and complexes, in H<sub>2</sub>O and D<sub>2</sub>O, have been compared. Our results are summarized in Table I.

TABLE I

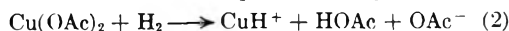
Metal ion	Rate law	Temp., °C.	$k_{\text{H}_2\text{O}}/k_{\text{D}_2\text{O}}$ ( $\pm 0.1$ )	Ref. <sup>a</sup>
Cu <sup>2+</sup>	$k[\text{H}_2][\text{Cu}^{2+}]$	110	1.20	<sup>e</sup>
Ag <sup>+</sup> <sup>b</sup>	$k[\text{H}_2][\text{Ag}^+]^2$	50	1.23	<sup>d</sup>
Hg <sup>2+</sup>	$k[\text{H}_2][\text{Hg}^{2+}]$	75	1.26	<sup>e</sup>
Hg <sub>2</sub> <sup>2+</sup>	$k[\text{H}_2][\text{Hg}_2^{2+}]$	75	1.33	<sup>e</sup>
Cu(OAc) <sub>2</sub>	$k[\text{H}_2][\text{Cu}(\text{OAc})_2]$	100	0.93	<sup>f</sup>
PdCl <sub>4</sub> <sup>2-</sup>	$k[\text{H}_2][\text{PdCl}_4^{2-}]$	80	0.90	<sup>g</sup>
RhCl <sub>6</sub> <sup>3-</sup>	$k[\text{H}_2][\text{RhCl}_6^{3-}]$	80	1.00	<sup>h</sup>
MnO <sub>4</sub> <sup>-</sup>	$k[\text{H}_2][\text{MnO}_4^-]$	50	0.99	<sup>i</sup>
Ag <sup>+</sup> + MnO <sub>4</sub> <sup>-</sup>	$k[\text{H}_2][\text{Ag}^+][\text{MnO}_4^-]$	40	0.93	<sup>i</sup>

<sup>a</sup> Earlier measurements in H<sub>2</sub>O are described in the quoted reference. The same procedures were used in the present measurements and the results in H<sub>2</sub>O agree well with the earlier ones. <sup>b</sup> While at higher temperatures, the reaction of H<sub>2</sub> with Ag<sup>+</sup> follows a rate law and mechanism similar to those for Cu<sup>2+</sup>, the predominant contribution under the conditions of this comparison is from the "termolecular" path which is believed to involve homolytic splitting of H<sub>2</sub> according to equation 3 (ref. d, this Table). <sup>c</sup> E. Peters and J. Halpern, *J. Phys. Chem.*, **59**, 793 (1955); J. Halpern, E. R. Macgregor and E. Peters, *ibid.*, **60**, 1455 (1956). <sup>d</sup> A. H. Webster and J. Halpern, *ibid.*, **60**, 280 (1956); **61**, 1239, 1245 (1957). <sup>e</sup> G. J. Korinek and J. Halpern, *ibid.*, **60**, 285 (1956). <sup>f</sup> E. Peters and J. Halpern, *Can. J. Chem.*, **33**, 356 (1955). <sup>g</sup> J. Halpern, J. F. Harrod and P. E. Potter, *ibid.*, **37**, 1446 (1959). <sup>h</sup> J. F. Harrod and J. Halpern, *ibid.*, **37**, 1933 (1959). <sup>i</sup> A. H. Webster and J. Halpern, *Trans. Faraday Soc.*, **33**, 51 (1957).

It was hoped, in particular, that these measurements would provide a criterion for distinguishing those mechanisms<sup>2</sup> in which H<sub>2</sub> is split heterolytically, transferring a proton to a water molecule, e.g.



from those in which a ligand other than water is believed to serve as the proton acceptor, e.g.



or in which H<sub>2</sub> is split homolytically without proton transfer



The results in Table I fail, however, to provide any clear-cut indication of such mechanistic differences. All the aquo ions included in the comparison (Cu<sup>2+</sup>, Ag<sup>+</sup>, Hg<sup>2+</sup> and Hg<sub>2</sub><sup>2+</sup>) show modest reductions in rate, ranging from 20 to 30%, on passing from H<sub>2</sub>O to D<sub>2</sub>O, while the rates for complexes containing ligands other than water in

(1) J. Halpern, *J. Phys. Chem.*, **63**, 398 (1959); *Advances in Catalysis*, **9**, 302 (1957); **11**, 301 (1959).

(2) Refs. c. d. Table I.

their inner coordination shells are nearly equal in the two solvents. This pattern, including the similarity of the isotope effects for  $\text{Cu}^{2+}$  and  $\text{Ag}^+$ , suggests that differences in the coordinating properties of  $\text{H}_2\text{O}$  and  $\text{D}_2\text{O}$  (for which other evidence has been cited<sup>3</sup>), rather than specific participation of water in the reaction, are largely responsible for the isotope effect in the case of the aquo ions. This is of interest in view of the many other studies<sup>4</sup> of  $\text{H}_2\text{O}$ - $\text{D}_2\text{O}$  isotope effects aimed at elucidating the role of solvent in the mechanisms of various reactions of metal ions.

Grateful acknowledgement is made to the National Research Council of Canada and to the donors of the Petroleum Research Fund administered by the American Chemical Society for support of this work.

(3) J. Halpern and A. C. Harkness, *J. Chem. Phys.*, **31**, 1147 (1959).

(4) J. Hudis and R. W. Dodson, *J. Am. Chem. Soc.*, **78**, 911 (1956); F. B. Baker and T. W. Newton, *J. Phys. Chem.*, **61**, 381 (1957); A. Zwickel and H. Taube, *J. Am. Chem. Soc.*, **81**, 1288 (1959).

## POLAROGRAPHIC AND COULOMETRIC INVESTIGATIONS ON THE REDUCTION RATE OF COBALT(II) IN THE PRESENCE OF CYSTINE

By EMILIAN B. WERONSKI

Department of Chemistry, University of Warszawa, Warszawa, Poland  
Received June 28, 1960

Enhancement of the diffusion current has been found in "Brdicka's electrolyte" and other cobalt solutions in the presence of some proteins and amino acids containing sulfhydryl or disulfide groups. This phenomenon has been attributed to the catalytic reduction of hydrogen,<sup>1</sup> but the mechanism has not been elucidated.<sup>2</sup> In the case of copper(II) or bismuth(III) ions in 1 *N* sulfuric acid, the author observed a similar "catalytic current" in the presence of very small concentrations of hydrocarbons, *e.g.*, benzene, toluene, the xylenes, *n*-pentane, *n*-hexane and cyclohexane.<sup>3</sup> Since the latter "catalytic current" is due to an increase in the reduction of copper(II) or bismuth(III) ions, not to catalytic reduction of hydrogen, the following experiments were carried out to re-examine the current of cobalt ions in the presence of cystine.

### Experimental

The solution studied was a modified Brdicka's electrolyte: 0.0025 *M* cobalt(II) chloride and 0.00001 *M* cystine in a 0.1 *M* ammonium chloride-0.1 *M* ammonium hydroxide buffer.

Polarographic measurements, which followed standard practice, were made with a Cambridge Polarograph (No. C 466573). The capillary had an *m*-value of 2.06 mg. sec.<sup>-1</sup> and a drop time of 4.5 sec. in twice distilled water at a height of the mercury reservoir of 60 cm. (closed circuit) at 18°.

(1) R. Brdicka, *Coll. Czechoslov. Chem. Commun.*, **5**, 148 (1933).

(2) R. Brdicka, *ibid.*, **11**, 614 (1939); *Chem. Listy*, **34**, 59 (1940); Klumpar, *Coll. Czechoslov. Chem. Commun.*, **13**, 11 (1948); A. G. Stromberg, *Zhur. Fiz. Khim.*, **20**, 409 (1946); J. Heyrovsky, *Coll. Czechoslov. Chem. Commun.*, **9**, 273 (1937); M. von Stackelberg and H. Faasbender, *Z. Elektrochem.*, **62**, 834 (1958).

(3) Some of the experimental results submitted in partial fulfillment of the requirements for the degree of Doctor, E. B. Weronski, Department of Chemistry, University Warszawa. 1957.

The solution (0.5 ml.) was electrolyzed in millicoulometric cell. The reference electrode was a layer of mercury on the bottom of the cell connected by a plastic tube to the mercury reservoir. The anodic mercury was moved slowly up and down at one minute intervals by movement of the mercury reservoir. Owing to this agitation of the mercury layer, to the large diameter of the cathode capillary, and to the narrowness of the electrolytic cell, the solution was continuously but gently stirred during the electrolysis. Before electrolysis the solutions were freed from dissolved oxygen by bubbling hydrogen through them, and during the electrolysis hydrogen gas was passed very slowly over the surface of the electrolyte. The hydrogen was partially saturated with ammonia by treatment with ammonium chloride-ammonia buffer of the same concentration as the electrolyte solution.

Polarographic curves were recorded before and after electrolysis.

### Results

The effect of electrolysis on the diffusion current of Co(II) ions is shown in Fig. 1. The solutions

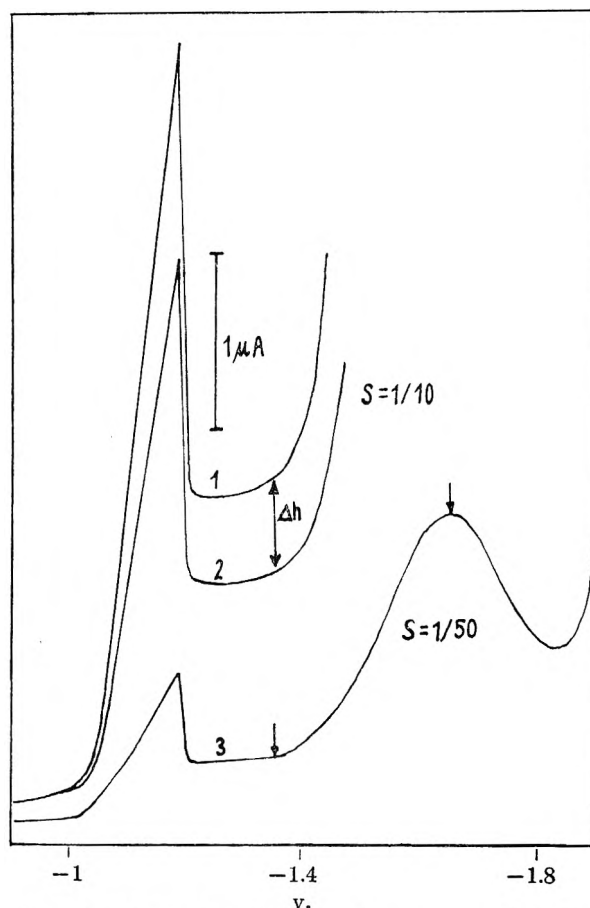


Fig. 1.—Curves 1 and 3 are polarograms of Brdicka's electrolyte before electrolysis; S denotes the sensitivity of the galvanometer. Curve 2 is the polarogram of aliquots of Brdicka's electrolyte after  $t_{-1.35}$  min. of electrolysis at  $-1.35$  v., or after  $t_{-1.65}$  min. of electrolysis at  $-1.65$  v.

were electrolyzed at either  $-1.35$  v. (where the diffusion current of cobalt is not distorted) or at  $-1.65$  v. (where the enhancement of current is maximal) until the diffusion current measured at  $-1.35$  v. decreased by about 30%. Aliquots electrolyzed at  $-1.35$  v. for  $t_{-1.35}$  minutes, or at  $-1.65$  v. for  $t_{-1.65}$  minutes gave identical polarograms (curve 2).

We found that the amounts of electricity in-



volved in the two electrolyses are approximately the same: *i.e.*,  $h_{-1.35} \times t_{-1.35}$  is about equal to  $h_{-1.65} \times t_{-1.65}$ , where  $h_{-1.35}$  and  $h_{-1.65}$  are the heights of the polarographic steps measured at  $-1.35$  and  $-1.65$  v., respectively, before the electrolysis. The decrease in the diffusion current of Co(II) ions at  $-1.35$  v. ( $\Delta h$ ) is proportional to this quantity. If  $t_{-1.35}$  is determined experimentally,  $t_{-1.65}$  can be estimated within a 10% error.

These results suggest that the second wave (at  $-1.65$  v.) of Brdicka's electrolyte is due to an increase in the reduction rate of cobalt(II) ions rather than to the catalytic reduction of hydrogen. It follows that the reaction is no more diffusion controlled and probably cobalt ions are provided to the electrode surface in a transport process similar to that observed in the case of polarographic maxima.

## SECONDARY PROCESSES IN GAS PHASE RADIOLYSIS OF HYDROCARBONS

BY JEAN H. FUTRELL

Aeronautical Research Laboratories, Wright-Patterson AFB, Ohio

Received August 15, 1960

In recent publications Back and Miller<sup>1</sup> and Back<sup>2</sup> have shown that irradiation studies of hydrocarbon vapors must be conducted at very low conversion if meaningful results are to be obtained. They have demonstrated that unsaturated products formed with very high yield initially in  $\alpha$ -particle and  $\gamma$ -radiolysis act as internal scavengers; thus a very low steady-state concentration of unsaturates is measured at conversions of a few per cent. This is very reasonably attributed to hydrogen atom scavenging by the unsaturated products.

We have confirmed these observations in recent studies in this Laboratory of gas phase radiolysis of *n*-pentane with cobalt-60  $\gamma$ -rays.<sup>3</sup> Such behavior, however, is distinctly different from that observed in an earlier study of normal hexane with 2 Mev. electrons from a Van de Graaff accelerator.<sup>4</sup> Several exploratory experiments were performed in an attempt to resolve this discrepancy and the results are reported in this communication.

In  $\gamma$ -radiolysis of gases in glass ampoules of modest dimensions, the major process of photon degradation is the ejection of secondary electrons from the walls of the container. Hence in our experiments using cobalt-60  $\gamma$ -rays the gas was exposed to a homogeneous flux of high energy electrons of 1 Mev. energy or less. Thus in both series of experiments the gases were irradiated with electrons, and the principal difference in the radiation sources employed is that the electrons from the Van de Graaff are initially mono-energetic while those from cobalt-60 have a broad distribution of energies. We are therefore reluctant to attribute the difference in radiolysis behavior to a simple difference in radiation quality.

The electron and  $\gamma$ -ray irradiations differed significantly with respect to two other experimental

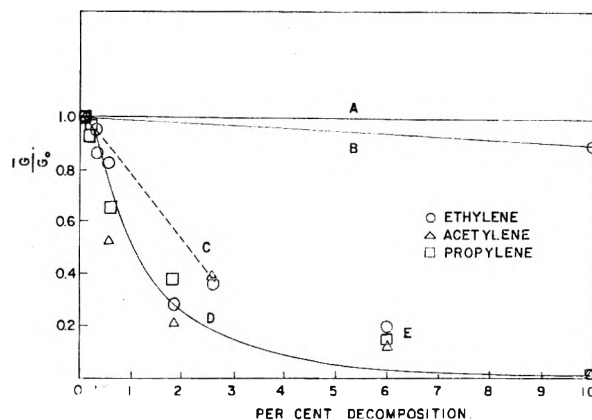


Fig. 1.—Yields of selected products from radiolysis of *n*-paraffin hydrocarbons: A, ethane under all experimental conditions; B, ethylene from Van de Graaff electron irradiation using cylindrical reactors; C, inhomogeneous flux  $\gamma$ -irradiation; D, homogeneous flux irradiation; E, pseudo-homogeneous flux electron irradiation.

parameters—radiation intensity and distribution—and the presently reported experiments attempted to separate these parameters. The yields of unsaturated products as measured in four different types of experiments are presented in the accompanying figure. The data are presented as the quantity  $G/G_0$  for convenience in presentation.  $\bar{G}$  is the apparent 100 electron volt yield of a given product at some particular dose, while  $G_0$  is the yield of that product obtained by extrapolating the yield curves to zero conversion in each case.

Curve D presents the data from  $\gamma$ -radiolysis of *n*-pentane in the low conversion region and affirms the conclusions of Back and Miller<sup>1</sup> for  $\alpha$ -particle radiolysis of this compound. It illustrates the rapid attainment of a steady-state concentration of unsaturates undetectable by usual analytical methods at conversions which have been used in many previous studies. Curve A presents the same quantity for saturated products ethane and propane at these conversion levels for both the radiolysis of pentane and electron radiolysis of hexane. Curve B presents the yield of ethylene from hexane decomposition with Van de Graaff electrons.<sup>4</sup>

The Van de Graaff studies were conducted with cylindrical Pyrex vessels 2.5 cm. in diameter and 80 cm. in length with the beam incident on a thin window (1 mm.) at one end of the vessel. Because of scattering of the incident beam in passage through the window, most of the radiolysis occurred in the first few centimeters of the tube. In an attempt to simulate the flux gradient of the Van de Graaff reactors, a special ampoule 4.5 feet in length by 2.5 centimeters in diameter was constructed. When pointed at the center of the cobalt-60 source the dose at the most intense region was a factor of  $50 \pm 20$  higher than the dose at the other end of the reactor compared to the analogous ratio of intensities of the order of 1000 for the electron experiments. The dotted curve C presents the data obtained in this experiment.

These data suggested that the inhomogeneous flux might be responsible for the anomalous behavior in the Van de Graaff irradiations. Unfortu-

(1) R. A. Back and N. Miller, *Trans. Faraday Soc.*, **55**, 911 (1959).

(2) R. A. Back, *J. Phys. Chem.*, **64**, 124 (1960).

(3) J. H. Futrell, *ibid.*, **64**, 1634 (1960).

(4) J. H. Futrell, *J. Am. Chem. Soc.*, **81**, 5921 (1959).



nately, however, size limitations in using the special target required the use of a more intense  $\gamma$ -source, so that there still remained the possibility that source intensity is the major factor. Accordingly, spherical one-liter Pyrex reactors with thin bubble windows were constructed for use in Van de Graaff irradiations. While the radiation flux is still not homogeneous in these reactors, this condition is much more closely approached than with the cylindrical reactors. With the same incident current of 10 microamperes used in the earlier hexane experiments, the cluster of points designated E was obtained for *n*-pentane radiolysis.

These experiments indicate that a significant factor in radiolysis experiments is what may be termed target geometry or flux geometry in the radiation vessel. The observations are consistent with the interpretation that in the earlier Van de Graaff experiments using cylindrical reactors unsaturated products which are formed in the reaction zone diffuse into the low radiation flux region of the reactor where they are not exposed to reactive intermediates formed in radiolysis. Thus the steady-state concentration of unsaturated products is much higher than under homogeneous irradiation; and as a result of "poor" target geometry, the measured *G*-values at conversions of a few per cent may approach the zero dose values. In systems approaching homogeneous flux of particles we find that  $\bar{G}/G_0$  curves asymptotically approach 1 in the region below 0.15% conversion. A limited number of experiments conducted at such low conversions indicates that values previously reported for unsaturated products from *n*-hexane radiolysis<sup>4</sup> were low by 20–30% because of the phenomenon described in this note.<sup>5</sup>

(5) NOTE ADDED IN PROOF.—*G*-values for products from *n*-hexane radiolysis determined in recent experiments at conversions of ca. 0.1% are H<sub>2</sub>,  $\geq 5.2$  (4.3); CH<sub>4</sub>, 0.6 (0.5); C<sub>2</sub>H<sub>6</sub>, 0.3 (0.2); C<sub>2</sub>H<sub>4</sub>, 1.4 (1.1); C<sub>2</sub>H<sub>2</sub>, 0.9 (0.9); C<sub>3</sub>H<sub>6</sub>, 0.6 (0.3); C<sub>3</sub>H<sub>4</sub>, 1.5 (1.4); C<sub>4</sub>H<sub>6</sub>, 0.1 (0.1); C<sub>4</sub>H<sub>2</sub>, 1.4 (1.1); C<sub>4</sub>H<sub>2</sub>, 0.2 (0.2). Values in parentheses are from reference 4.

## REMARKS ON THE ARCHIBALD METHOD OF MOLECULAR WEIGHT DETERMINATION IN THE ULTRACENTRIFUGE

BY JAMES M. PETERSON AND ROBERT M. MAZO

Contribution No. 2608 from the Gates and Crellin Laboratories of Chemistry, California Institute of Technology, Pasadena, California

Received August 16, 1960

The Archibald method for the determination of molecular weights in the ultracentrifuge involves the measurement of  $(\partial c/\partial r)^1$  at the boundary of the ultracentrifuge cell.<sup>2,3</sup> This measurement is effected by the extrapolation of interior measurements to the boundary. There is some uncertainty in this extrapolation, and so we began to investigate numerical solutions of the Lamm differential equation<sup>3,4</sup> in order to determine

(1) The symbols used in this article have the same meaning as those of ref. 6.

(2) W. J. Archibald, *J. Phys. Chem.*, **51**, 1204 (1947).

(3) H. K. Schachman, "Ultracentrifugation in Biochemistry," Academic Press, Inc., New York, N. Y., 1959.

(4) C. Lamm, *Arkiv Mot; Astron. Fysik*, **B1B**, No. 2 (1920);

the shape of the gradient curve near the boundary for some typical operating conditions.

The Lamm equation was converted into a difference equation, in the standard way,<sup>5</sup> and a program for the solution of the difference equation was written for the Burroughs 220 Datatron Digital Computer. When the program was substantially complete, we discovered previous work by Fujita and MacCosham,<sup>6</sup> who present an analytical solution to the Lamm equation based on an approximation which seems to be quite innocuous. We therefore decided to use our program to check whether the approximation is, in fact, innocuous. For this purpose we used the following parameters, some of which are derived from experiments in these laboratories on a hemoglobin sample:  $\omega = 977.9$  rad./sec.;  $r_1 = 5.7$  cm.; mol. wt. =  $6.68 \times 10^4$ ;  $S = 4.5 \times 10^{-13}$  sec.<sup>-1</sup>;  $D = 6.56 \times 10^{-7}$  cm.<sup>2</sup>/sec. The grid spacing for the difference equation was  $\Delta r/r_1 = 2.4 \times 10^{-4}$ ,  $\Delta t = 1$  sec. The numerical integration was begun at the meniscus and continued into the cell.

Equation 23 of ref. 6 should have a multiplicative factor  $\exp(-z/2)$ , which was omitted by the authors since it is approximately unity. If we include this factor, for the sake of completeness, our numerical results agree with the predictions of the so amended equation 23 with a maximum error of 0.01% for a time of 45 minutes over the entire range of *r* for which  $\partial c/\partial r$  is not negligible. A time of 45 minutes was chosen because it is a standard time for Archibald technique measurements carried out in these laboratories.

The conclusion is that further numerical work is superfluous. The formula of Fujita and MacCosham is a perfectly adequate solution of the Lamm equation under the conditions relevant to the Archibald method.

Curves of  $\partial c/\partial r$  versus *r* obtained from the numerical work showed a linear region extending appreciably into the cell. In our example at 45 minutes, the curve was quite linear for about 10% of the cell ( $r/r_1 = 1.02$ ). In order to see more generally how far this linear region should extend we have expanded  $\partial^2(c/c_0)/\partial(r/r_1)^2$  as a function of  $(r/r_1 - 1) = \delta$  up to terms of order  $\delta^4$ . This function should, of course, be a constant if  $\partial c/\partial r$  is linear in *r*. The general form of the coefficient is rather complicated, and we do not display them here, giving only the numerical results for 45 minutes.

$$\frac{\partial^2(c/c_0)}{\partial(r/r_1)^2} = -1048 - 4.870 \times 10^4 \delta + 7.408 \times 10^8 \delta^2 + 1.208 \times 10^8 \delta^3 - 3.314 \times 10^{10} \delta^4 + \dots$$

It can be seen from this example that the non-constant terms are not small. The linearity extends further into the cell than one has any right to expect from the size of the coefficients of  $\delta$ , apparently because the higher terms approximately cancel, being of the same order of magnitude and of varying sign.

Thus there does not seem to be any general rule

(5) K. S. Kunz, "Numerical Analysis," McGraw-Hill Book Co., Inc., New York, N. Y., 1957, Chapter 14.

(6) H. Fujita and V. J. MacCosham, *J. Chem. Phys.*, **30**, 291 (1959).

(7) W. D. Hutchinson, private communication.

about the range over which a linear extrapolation will be valid. If an accurate extrapolation is desired, we suggest that a molecular weight determined by the best extrapolation one can make be used to compute the constants in the Fujita-MacCosham formula. The formula then can be used to compute  $\partial c/\partial r$ , and the molecular weight can be adjusted until a self-consistent result is contained. The Fujita-MacCosham formula is relatively easy to evaluate numerically.

We wish to thank Dr. J. Vinograd for helpful discussions of the experimental aspects of this problem.

## SELF-DIFFUSION OF LIQUID MERCURY

BY ROBERT E. MEYER

Chemistry Division, Oak Ridge National Laboratory,<sup>1</sup> Oak Ridge Tennessee, and University of Illinois, Urbana, Illinois

Received August 17, 1960

Self-diffusion measurements in liquid mercury already have been reported twice.<sup>2</sup> However, these two investigations disagreed in that the values of Hoffman<sup>2b</sup> were 11 to 16% greater than those reported by Nachtrieb and Petit.<sup>2a</sup> Furthermore, both investigations were carried out in the rather limited temperature range of 0 to 100°. This temperature range is sufficient to determine  $D_0$  and  $E_{\text{diff}}$  in the equation usually assumed,  $D = D_0 \exp(-E_{\text{diff}}/RT)$ , where  $D$  is the diffusion coefficient,  $D_0$  is an essentially temperature-independent constant, and  $E_{\text{diff}}$  is the experimental activation energy. However, a temperature range of 100° is not sufficient to determine whether this equation actually represents the data if the data are accurate to only a few per cent. The Stokes-Einstein<sup>3</sup> and Eyring<sup>4</sup> expressions for  $D$  give equations of the form  $D = kT/a\eta$  where "a" is a constant and  $\eta$  is the viscosity. This equation, when combined with the experimentally observed equation  $\eta = \eta_0 \exp(E_{\text{vis}}/RT)$ , leads directly to the equation

$$D = (\text{constant})T \exp(-E_{\text{vis}}/RT) \quad (1)$$

in which the temperature appears in the pre-exponential term. It also has been suggested<sup>5</sup> that the expression for  $D$  should be  $D = bT^2$ , where  $b$  is a constant, and that diffusion in liquid metals is an essentially non-activated process. It was therefore of some interest to determine experimentally the temperature dependence of  $D$  over a wide temperature range. Mercury was chosen because the determinations could be made at relatively low temperatures and because mercury has a small value of  $E_{\text{vis}}$  (~500 cal./mole) so that small changes in the pre-exponential term will not be masked by large changes in the exponential term.

The capillary-reservoir technique<sup>6</sup> was chosen

(1) Operated by Union Carbide Corp. for the U. S. Atomic Energy Commission.

(2) (a) N. H. Nachtrieb and J. Petit, *J. Chem. Phys.*, **24**, 746 (1956); (b) R. E. Hoffman, *ibid.*, **20**, 1567 (1952).

(3) A. E. Einstein, *Ann. Physik*, **17**, 549 (1905); **19**, 371 (1906); *Z. Elektrochem.*, **14**, 235 (1908).

(4) C. M. Carlson, H. Eyring and T. Ree, *Proc. Nat. Acad. Sci.*, **46**, 649 (1960).

(5) R. A. Swalin, *Acta Met.*, **7**, 736 (1959).

(6) J. S. Anderson and K. Saddington, *J. Chem. Soc.*, S381 (1949).

and the experimental procedure was essentially the same as that used for liquid sodium.<sup>7</sup> Diffusion coefficients were calculated from the equation

$$\ln \pi^2 C_{\text{av}}/8C_0 = -\pi^2 Dt/4L^2 \quad (2)$$

where  $C_{\text{av}}$  is the average activity of the tracer ( $\text{Hg}^{203}$ ) in the capillary after the run,  $C_0$  is the initial activity,  $t$  is the elapsed time, and  $L$  is the length of the capillary. The capillaries were made from 0.5 mm. i.d. precision bore Pyrex tubing. Temperatures were maintained with an ice-bath, an oil-bath for the 42 to 108° runs, and a furnace for the high temperature runs (including two of the 108° runs). As shown in Table I, the lengths of the capillaries and  $t$  were varied for different runs at the same temperature.

TABLE I  
SELF-DIFFUSION COEFFICIENTS OF MERCURY

$T$ , °K.	$D$ cm. <sup>2</sup> sec. <sup>-1</sup> $\times 10^5$	$t$ , sec. $\times 10^{-5}$	$L$ , cm.
273.2	1.50	3.301	3.28
273.2	1.51	1.962	3.28
315.4	1.88	1.556	4.39
315.4	1.88	2.358	3.28
315.4	1.89	3.371	3.87
352.6	2.44	1.484	3.28
352.6	2.33	2.698	3.28
381.6	2.69	1.636	3.87
381.6	2.71	1.815	3.28
381.6	2.72	1.359	3.28
381.6	2.77	1.039	3.87
414.2	3.26	1.962	3.87
415.1	3.23	0.8802	3.28
452.9	3.80	.8874	3.28
497.6	4.42	.8865	3.28
512.5	4.70	.6264	3.87

The data are given in Table I and are plotted in Fig. 1 along with the results of the two previous investigations. Also shown in the graph are two theoretical curves, the one calculated from the relation  $D = kT/1.59 \times 10^{-7} \eta$  and the other from the relation  $D = 1.86 \times 10^{-10} T^2$ . In each case the numerical constant was calculated from the average of the experimental value of  $D$  at 108°. The viscosity values were experimental.<sup>8</sup>

Examination of Table I shows that the results are reproducible enough to preclude any significant random error in the measurement. Figure 1 shows that the results are quite close to Hoffman's,<sup>2b</sup> who also used a capillary-reservoir technique. The suggestion was made by Nachtrieb and Petit<sup>2a</sup> that the high stirring rate used by Hoffman<sup>2b</sup> (250 r.p.m.) caused convective losses from the capillary orifice and therefore raised the apparent values of  $D$ . In the present work, the capillary was rotated about a radius of about  $3/4$  cm. at speeds of 3-4 r.p.m. This could account for the fact that Hoffman's values of  $D$  are slightly higher, but it is difficult to see how this effect could account for the 10-12% discrepancy between these data and those of Nachtrieb and Petit. In view of the fact that Nachtrieb and Petit used a shear-cell technique in their measurements, it appears that

(7) R. E. Meyer and N. H. Nachtrieb, *J. Chem. Phys.*, **23**, 1851 (1955).

(8) S. Erk, *Z. Physik*, **47**, 886 (1928).

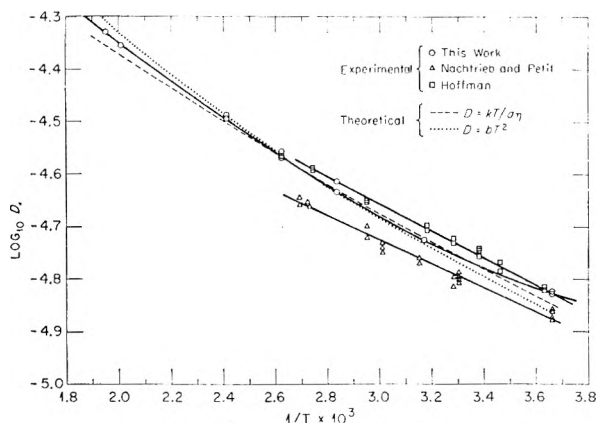


Fig. 1.—Self-diffusion in liquid mercury.

there must be a systematic error inherent in one or both of these techniques.

Reference to Fig. 1 shows that the expression  $D = D_0 \exp(-E_{\text{diff}}/RT)$  is not a good representation of the data since the plot of  $\log D$  vs.  $1/T$  does not give a straight line. The two theoretical curves represent the data equally well, although neither one is completely satisfactory. Swalin's theory<sup>5</sup> predicts a value of the constant equal to  $1.99 \times 10^{-10}$  as compared to the value of  $1.86 \times 10^{-10}$  used in Fig. 1. Eyring's theory<sup>4</sup> gives the expression  $D = kT/\xi(V_s/N)^{1/3}\eta$  where  $V_s$  is the molar volume of the solid at the melting point (14.13 cc. for Hg),  $N$  is Avogadro's number, and  $\xi$  is a constant equal to the number of nearest neighbors about a given atom in a plane. In a close packed structure,  $\xi$  should be six and for liquids somewhat less than six. The expression  $\xi(V_s/N)^{1/3}$ , when set equal to the numerical constant  $1.59 \times 10^{-7}$  cm. used in Fig. 1, yields a value of 5.6 for  $\xi$ . Thus both Swalin's and Eyring's equation predict the values of their respective constants quite closely.

Actually, a very good representation of the data is provided by the empirical equation  $\log D = 1.854 (\pm 0.018) \log T - 9.349 (\pm 0.045)$ . In liquid sodium<sup>7</sup> the analogous equation is  $\log D = 2.92 (\pm 0.10) \log T - 11.90 (\pm 0.25)$ . The fact that the coefficient of  $\log T$  for liquid Na is not near two but close to three, argues against Swalin's theory.

A possible source of error in these experiments is convection and this is most likely to occur at the highest temperatures. The presence of convection errors would therefore tend to favor the equation  $D = kT/a\eta$ , because the experimental points are above the theoretical line for this equation.

## THE HEAT STABILITIES OF BISACETYLACETONEETHYLENEDIIMINE AND ITS METAL CHELATES

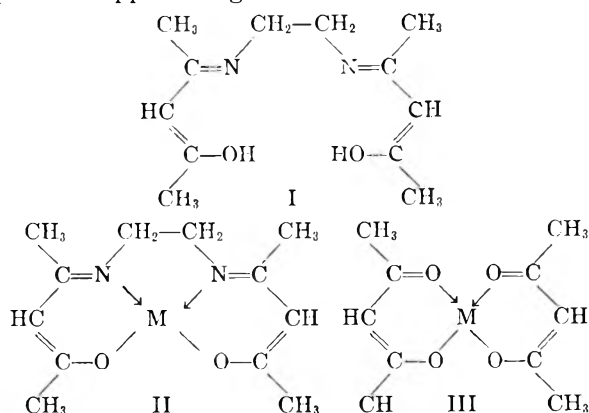
BY ROBERT G. CHARLES

Westinghouse Research Labs., Pittsburgh 35, Pa.

Received August 19, 1960

The metal chelates (II) derived from bisacetylacetonethylenediimine (I) and divalent metal ions have been reported to have remarkable thermal stability.<sup>1</sup> According to Morgan and Main Smith

the copper chelate II boils undecomposed at a "high temperature" while the corresponding nickel compound "boils without decomposition at a temperature approaching a red heat."<sup>1</sup>



Such heat stability is surprising in view of the much lower stabilities which have been found for the similarly constituted metal acetylacetonates III.<sup>2</sup> It has seemed worthwhile, therefore, to re-investigate the heat stabilities of the metal chelates II. For comparison we have also studied the heat stability of the chelating agent I.

The principal experimental method adopted for the present work involved heating weighed samples of the compounds in sealed evacuated glass tubes. The tubes were cooled and broken open, the contents dissolved in a known volume of methanol, and the ultraviolet absorption spectra determined. Any significant pyrolysis of the tube contents should result in detectable changes in the spectra when compared with the spectra of the pure compounds in the same solvent.

In Fig. 1 are given the spectra of the pure substances and of the tube contents after heating for four hours at the temperatures indicated. It is evident that bisacetylacetonethylenediimine itself and its copper chelate decompose to a detectable degree even at 200° and are largely destroyed at 250°. The nickel chelate II is more stable and shows no changes in the spectrum when heated to 300°. At 350°, however, the latter compound is almost completely pyrolyzed.

It can be seen from Fig. 1 that the chelates II are much less stable than hitherto supposed. The copper chelate II is very similar in heat stability to copper acetylacetonate while the nickel chelate II is somewhat more stable than is nickel acetylacetonate.<sup>2</sup> The chelating agent I and the copper chelate II appear to be very similar in stability to each other.

To supplement the sealed tube experiments we have also studied the weight loss as a function of temperature as each of the compounds I, II(Cu), and II(Ni) was heated, in an atmosphere of argon (at atmospheric pressure) on a thermobalance. Figure 2 is a plot of the results obtained. Each of the three curves shown is characterized by an initial region of constant weight at the lower temperatures, followed by a region of large weight loss

(1) G. T. Morgan and J. D. Main Smith, *J. Chem. Soc.*, 912 (1926).

(2) J. Von Hoene, R. G. Charles and W. M. Hickam, *J. Phys. Chem.*, 62, 1099 (1958).

in the temperature range 175 to 350°. Without information supplemental to Fig. 2 it would not be possible to tell whether the weight losses observed result from (a) volatilization of unchanged compound, (b) pyrolysis, with the formation of volatile products, or (c) some combination of these two effects. For each of the thermogravimetric runs a considerable amount of apparently amorphous material was observed to deposit on the cool tube above the furnace throughout the temperature region 175 to 350°. A significant amount of solid residue remained in the sample container after the copper chelate run, but only a few tenths of a mg. of residue remained from the other two experiments.

To determine the extent to which pyrolysis had occurred during the thermogravimetric runs the total volatilized materials from each experiment were collected, dissolved in methanol, and their ultraviolet absorption spectra determined. The absorption curve obtained for the volatilized material from the nickel compound was nearly identical with that for the undecomposed chelate shown in Fig. 1. The weight loss shown in Fig. 2 for this compound is therefore due almost entirely to volatilization of unchanged nickel chelate. The absorption curve for the volatile matter from the copper chelate resembled that for the pure copper compound II but the absorbance values of the absorption peaks at 229 and 307 m $\mu$  were reduced to 0.27 and 0.57, respectively. In addition, a shoulder appeared at about 325 m $\mu$  which did not appear in the spectrum of the pure copper compound. The weight loss in Fig. 2 for the copper compound must be due partially to pyrolysis and partially to volatilization of unchanged chelate. The shoulder at 325 m $\mu$  may be due to the formation of some compound I as a pyrolysis product since the spectrum of this substance has a strong absorption peak in this wave length region (Fig. 1). The production of I through the pyrolysis of copper chelate II would be completely analogous to the known formation of acetylacetone as a pyrolysis product from copper acetylacetonate.<sup>2</sup>

The absorption curve for the volatilized materials from the chelating agent I was also similar to that of the pure compound. The absorption peak at 322 m $\mu$  was, however, reduced in intensity (absorbance = 0.35) and a new absorption peak (absorbance = 0.27) appeared at 215 m $\mu$ . The weight loss in Fig. 2 for the chelating agent must, like that for the copper compound, result partially from volatilization of pyrolysis products and partially from evaporation of unchanged compound.

A brief study was made of the non-volatile pyrolysis residue remaining from the copper chelate II when this material was heated for 4 hours at 350° in argon, at atmospheric pressure, in an open container. An X-ray diffraction powder pattern showed that copper metal was the only detectable crystalline component. Elemental analysis showed the presence of copper (53.5%), carbon (30.6%), hydrogen (2.4%), nitrogen (3.0%), and oxygen (10.5%, by difference).

The statements of the earlier workers<sup>1</sup> relative to the heat stabilities of the compounds studied

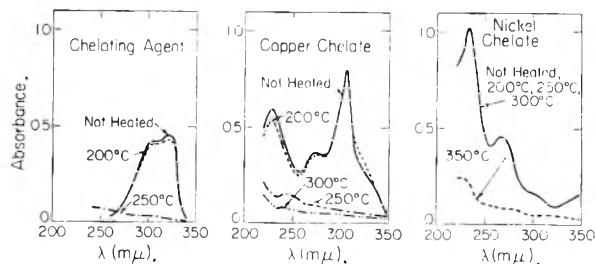


Fig. 1.—Ultraviolet absorption spectra of bisacetylacetonethylenediimine, its copper and nickel chelates and their pyrolysis products, in methanol.

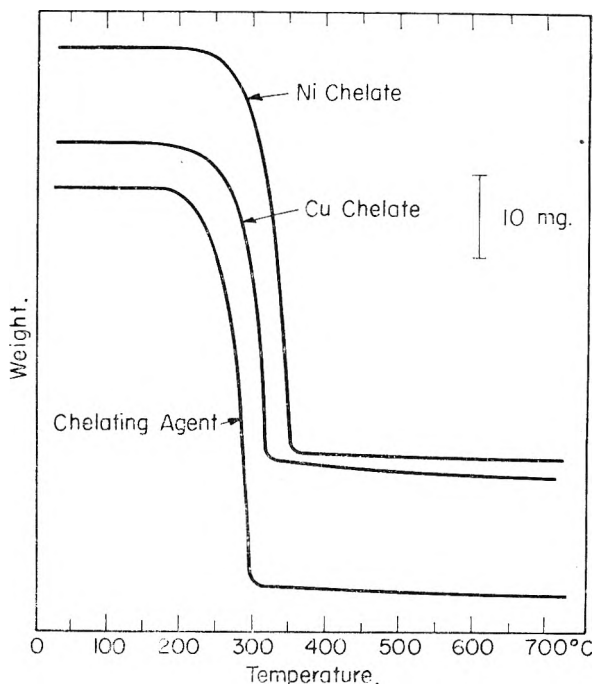


Fig. 2.—Weight loss curves for bisacetylacetonethylenediimine and its copper and nickel chelates in an atmosphere of argon. Fifty-mg. samples were used.

here apparently were based entirely on visual observation. Since the chelates are deeply colored it would be difficult to determine that decomposition was occurring by visual inspection. It is apparent from the results obtained here that, at the temperatures used by these authors, complete decomposition must occur in a very short time.

#### Experimental

**Preparation of Compounds. Bisacetylacetonethylenediimine.**—This compound was prepared by the method of McCarthy, Hovey, Ueno and Martell<sup>3</sup> and recrystallized twice from water. The compound was dried in a vacuum desiccator; m.p. 111–111.5°; reported<sup>3</sup> 111–111.5°.

**Bisacetylacetonethylenediiminonickel(II).**—Eleven and two tenths g. (0.05 mole) of recrystallized bisacetylacetonethylenediimine was dissolved in 200 ml. of water by gentle heating. To the warm solution was added, slowly with stirring, a solution of 12.4 g. (0.05 mole) of nickel acetate tetrahydrate in 200 ml. of water. One hundred ml. of 1 M aqueous NH<sub>3</sub> was then added slowly. The resulting mixture was heated nearly to boiling, maintained at this temperature for a few minutes, and finally cooled in a refrigerator for several hours. The red crystalline product was filtered off, washed several times with water and air-dried to give 10.3 g. of crude product.

(3) P. J. McCarthy, R. J. Hovey, K. Ueno and A. E. Martell, *J. Am. Chem. Soc.*, **77**, 5820 (1955).

The chelate was recrystallized twice by the following procedure. Ten g. of the compound was dissolved in 100 ml. of methanol by gentle heating. The warm solution was filtered and 30 ml. of water added. The mixture was cooled several hours in the refrigerator and the product filtered off, air-dried and finally dried for four hours at 100°. The recovery was 80% of the crude product taken; m.p. 198–199° (lit. 195–196°,<sup>3</sup> 200°<sup>1</sup>). *Anal.* Calcd. for C<sub>12</sub>H<sub>18</sub>N<sub>2</sub>Ni: Ni, 20.89. Found: Ni, 20.9.

**Bisacetylacetonediiminocopper(II).**—This compound was prepared by essentially the same method as that used for the nickel compound above. Ten g. (0.05 mole) of copper acetate monohydrate was substituted for the nickel acetate. The yield of crude violet product was 11.1 g.

The product was twice recrystallized by dissolving in methanol (75 ml. for each 11 g.) by gentle warming. The solution was cooled to room temperature and filtered through filter paper. About 2 g. of blue copper acetylacetonate remained on the filter paper during the first recrystallization and was discarded. To the filtrate was added, a little at a time, 75 ml. of water. The mixture was cooled for two hours in the refrigerator. The product was filtered off, air-dried, and finally dried for four hours at 100°. The yield of recrystallized product was 60 to 80% of the amount of crude product taken; m.p. 137–138° (lit. 141.5°,<sup>3</sup> 137°<sup>1</sup>). *Anal.* Calcd. for C<sub>12</sub>H<sub>18</sub>O<sub>2</sub>N<sub>2</sub>Cu: Cu, 22.24. Found: Cu, 21.9.

The ultraviolet absorption spectra (in methanol) of the three compounds prepared here were essentially identical with those reported by Ueno and Martell.<sup>4</sup> The infrared spectra of the solid compounds (in KBr pellets) also agreed well with the published wave length values of Ueno and Martell.<sup>5</sup>

**Sealed Tube Experiments.**—Exactly 100-mg. samples of each of the compounds above were weighed into 2 ml. Pyrex glass tubes. These were connected to a vacuum pump, evacuated to a pressure of about 5  $\mu$  and sealed with an oxygen-gas torch. (The tube contents remained at room temperature during this process.) The tubes were heated for four hour intervals in a special electric furnace designed to minimize temperature gradients. The temperature was held constant to  $\pm 1^\circ$  during the runs. At the end of the heating intervals the tubes were cooled rapidly in the air. Each tube was then wrapped in polyethylene film and pulverized with a hammer.

The pulverized tube and polyethylene was stirred with 100 ml. of spectral grade methanol and the resulting solution filtered through acid-washed filter paper into a 250-ml. volumetric flask. The residue and filter paper were washed repeatedly with additional portions of methanol until the contents of the flask were brought to the mark. Five-ml. aliquots of the solutions from the copper and nickel chelates were each diluted further to 200 ml. with methanol. Two-ml. aliquots of the solutions from the chelating agent (I) were diluted to 200 ml.

The spectra of these dilute solutions were recorded at room temperature with a Cary model 14 spectrophotometer using 1 cm. quartz cells, and methanol as the reference liquid. Solutions of the pure compounds were obtained by dissolving 0.100-g. samples in methanol and diluting in the same manner as above.

**Thermogravimetric Runs.**—Thermogravimetric curves for each of the three compounds were obtained with a thermobalance constructed in these laboratories and described elsewhere.<sup>6</sup> It was possible with the balance employed to exclude air from the sample with a stream of high purity argon. Each of the experiments was performed in a 50 ml./min. stream of argon at atmospheric pressure (ca. 730 mm.). A 50.0-mg. sample of the compound was contained in a 1-ml. open platinum crucible. The temperature of the furnace surrounding the sample was increased linearly with time at 2.1°/min. and the weight was recorded automatically with time.

A trap surrounded with solid CO<sub>2</sub> was connected to the outlet tube for the argon to trap any vaporized material which did not condense on the inside of the furnace tube, immediately outside the furnace. The combined volatilized material from each run was dissolved in methanol. The resulting solutions were diluted to half the volumes re-

ferred to above (to compensate for the smaller samples used in the thermogravimetric runs) and ultraviolet absorption spectra were obtained as described in the earlier section.

**Acknowledgments.**—The writer is grateful to Mrs. M. A. Dolan for help in the experimental portion of this work and to Dr. J. H. Lady and his group for the infrared spectra.

## REACTIONS OF TRITIUM ATOMS WITH FROZEN HYDROCARBONS<sup>1</sup>

BY R. D. SHORES AND H. C. MOSER

*Department of Chemistry, Kansas State University of Agriculture and Applied Science, Manhattan, Kansas*

*Received September 2, 1960*

Several experimental techniques have yielded hydrogen atoms of different energies, and variations in their reactions have been observed. Hydrogen and deuterium atoms produced at a hot tungsten ribbon reacted readily with some solid olefins at  $-195^\circ$  but did not undergo exchange reactions with solid propane.<sup>2</sup> Deuterium atoms produced by the discharge method<sup>3</sup> were found to exchange with hydrogen atoms in benzene, normal alkanes and cycloalkanes above cyclobutane. No exchange was observed with cyclopropane or cyclobutane. On the other hand, exchange of tritium for hydrogen occurred when tritium was generated by He<sup>3</sup>(n, p)H<sup>3</sup> reactions in the presence of cyclopropane.<sup>4</sup> Similarly, exchange was the principal reaction observed for recoil tritons in a number of other instances.<sup>5</sup> The present study was undertaken to examine some of the reactions of tritium atoms of intermediate energy.

### Experimental

Tritium atoms were generated from molecular hydrogen containing tritium at a tungsten filament maintained at 1750°. The atoms were allowed to react with frozen hydrocarbons (0.1 to 0.25 cc.) which were uniformly deposited on the inside wall of a 250-ml. flask immersed in liquid air. The tungsten filament was suspended at the center of the flask. Hydrogen containing tritium was released into the reaction flask by desorption from titanium metal; hydrogen pressures of less than 10  $\mu$  were maintained during the reactions.

The tritium content of the hydrogen was approximately 0.9 mc. per millimole. From 0.1 to 0.2 microcurie was released into the system (reaction flask and pressure gauge) at a time. Several times during a reaction, the system was evacuated and fresh hydrogen was released into the system. The total reaction time was usually less than one hour.

Labeled products (liquid at room temperature, or 0° in the case of *n*-pentane) were separated by gas chromatography using a 140 cm. Ucon non-polar column. Two methods of radioassay were used: the gas stream from the chromatography column was passed through an ionization chamber or proportional counter, or fractions from the effluent stream were trapped in toluene-phosphor solution cooled to 0° and counted in a Tri-Carb scintillation spectrometer.

### Results

Table I summarizes the results of tritium atom reactions with six hydrocarbons. Use of carriers

(1) Work performed under contract AT (11-1)-584 with the U. S. Atomic Energy Commission. Contribution No. 608, K.A.E.S., Manhattan.

(2) R. Klein and M. D. Scheer, *J. Phys. Chem.*, **62**, 1011 (1958).

(3) H. I. Schiff and E. W. R. Steacie, *Canad. J. Chem.*, **29**, 1 (1951).

(4) J. K. Lee, B. Musgrave and F. S. Rowland, *J. Am. Chem. Soc.*, **81**, 3803 (1959).

(5) See, for example, F. S. Rowland and R. Wolfgang, *Nuclonics*, **14**, No. 8. 58 (1956).

(4) K. Ueno and A. E. Martell, *J. Phys. Chem.*, **61**, 257 (1957).

(5) K. Ueno and A. E. Martell, *ibid.*, **59**, 998 (1955).

(6) R. G. Charles and A. Langer, *ibid.*, **63**, 603 (1959).

was made in some instances; the carriers indicated were added prior to the gas chromatographic separations.

TABLE I

Compound	Compd. reacted	Distribution of tritium, %		Carrier
		Light <sup>a</sup> fraction	Heavy <sup>a</sup> fraction	
Benzene	21	1	4	Cyclohexane-35, cyclohexene-39
Cyclohexane	81	6	13	.....
Cyclohexene	22	4	5	Cyclohexane-69
1-Hexene	27	1	3	<i>n</i> -Hexane-69
<i>n</i> -Hexane	83	5	12	.....
<i>n</i> -Pentane	83	13	4	.....

<sup>a</sup> Light and heavy fractions were those collected before and after the emergence of the compound reacted, respectively, but do not include the activity in a carrier when one was present.

Both methods of radioassay showed the presence of minor amounts of tritiated compounds which had chromatographic retention times different from either the compound reacted or the carriers. Identification of these compounds has not been completed. Tritiated hexadiene, if present in reacted benzene, was eluted with one of the other components.

The pressure dropped from 10 to less than 1  $\mu$  within a few seconds during reactions with unsaturated compounds and decreased slowly during reactions with saturated compounds. Providing the tungsten filament was sufficiently outgassed, a pressure of less than 1  $\mu$  could be maintained in the closed system with the filament heated to 1750°. Therefore, evaporation of hydrocarbon as a result of radiation was not extensive.

### Discussion

With unsaturated compounds, both addition and substitution were observed; with saturated compounds, substitution was the principal reaction that occurred. Unlike previous results,<sup>2</sup> the hydrogen atoms reacted with both *n*-pentane and 1-hexene. This probably was due to a change in experimental conditions. In the present study a smaller reaction vessel was used as well as lower hydrogen pressures. Conditions were chosen such that the distance between the filament and wall of the vessel was less than the mean free path of hydrogen atoms. Therefore the atoms reached the walls with more energy than in the previous experiments.

The high yields of labeled target compounds observed indicate that this method might be used for labeling organic molecules with tritium. Furthermore, the amount of sample degradation should be less than with either the gas exposure or recoil labeling technique.

Results of reactions with alcohols and carbonyl compounds will be reported when these studies are more complete. Reaction rates were not determined in the present study. These and the effects of variation of pressure and temperature are being investigated.

**Acknowledgment.**—The authors express thanks to Dr. R. H. McFarland for his advice in constructing the experimental equipment.

## THE RATE OF THERMAL DECOMPOSITION OF DIMETHYL 2,2'-AZO-BIS-ISOBUTYRATE

BY HORACE A. ORY<sup>1</sup>

*Monsanto Chemical Company, Plastics Division, Texas City, Texas*

*Received August 22, 1960*

Many azo compounds have been studied and found useful for thermal and photo-initiation of polymerization. Among these, dimethyl 2,2'-azo-bis-isobutyrate (DAIB) has favorable solubility properties and is especially applicable in circumstances which involve solubility problems.<sup>2</sup> To complement and extend the dilatometric kinetic data which have been reported,<sup>3,4</sup> the rate of thermal decomposition of DAIB has been studied by a spectrophotometric technique. The decompositions were allowed to proceed within the heated cell compartment of a spectrophotometer and the concentration of DAIB was followed by absorbance measurements. With this method time delays, temperature changes, and other disadvantages associated with sample handling were avoided, and the advantages of direct and accurate spectrophotometry were obtained.

### Experimental

The walls and bottom of the cell compartment of a Cary Model 11 spectrophotometer were lined with a quarter-inch thickness of asbestos. The top of the compartment was fitted with an asbestos cover which accepted a calibrated thermometer and a heating unit by which air within the compartment was circulated over a nichrome heated ribbon. An electronic temperature controller, which used a thermister within the cell compartment for sensing temperature and a thyatron tube for regulating current through the nichrome ribbon, maintained temperature constant within  $\pm 0.2^\circ$ .

For each determination of decomposition rate, the cell compartment was allowed to reach thermal equilibrium before the sample was introduced. A 10 mm. quartz cell was filled with a solution of DAIB in isoöctane (0.05 mole/l.), purged with nitrogen, and covered with a rubber cap which was slit to permit nitrogen to escape under slight pressure as it was produced during the reaction. The cell was placed in the heated compartment, where it quickly reached equilibrium temperature. At time intervals the DAIB absorbance was measured at its 3620 Å. maximum, against pure isoöctane. To avoid photochemical complications, no light was allowed to strike the sample except briefly during the absorbance measurements.

Adherence to Beer's law was verified for DAIB absorbance at 3620 Å., over the concentration range studied. Absorption at 3620 Å. by reaction products was measured after 24 hours reaction at 84.5°, and proved to be too small to affect measurements of DAIB absorbance at this wave length.

### Results and Discussion

Plots of the logarithms of absorbances against times of decomposition of DAIB were linear with very little scattering of points. Least squares treatments were used to determine the first-order

(1) E. H. Plesset Associates, Inc., 1281 Westwood Blvd., Los Angeles 24, Calif.

(2) W. M. Padgett and E. Perry, *J. Polymer Sci.*, **37**, 543 (1959).

(3) F. M. Lewis and M. S. Matheson, *J. Am. Chem. Soc.*, **71**, 747 (1949).

(4) K. Ziegler, W. DeParade and W. Meye, *Ann.*, **567**, 141 (1950).



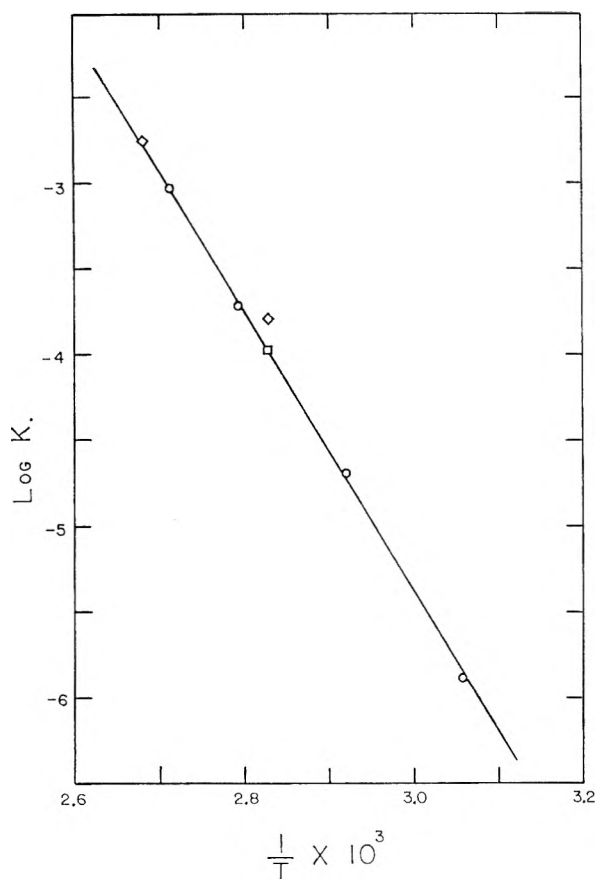


Fig. 1.—The temperature dependence of the rate of thermal decomposition of dimethyl 2,2'-azo-bis-isobutyrate: □, Lewis and Matheson; ◇, Ziegler, Deparade and Meyer; ○, this work.

rates of thermal decomposition. At temperatures of 53.6, 68.9, 84.5 and 95.3°, the decomposition rates were  $1.31 \times 10^{-6}$ ,  $2.07 \times 10^{-5}$ ,  $1.96 \times 10^{-4}$  and  $9.31 \times 10^{-4}$  sec.<sup>-1</sup>, respectively. These results are comparable to those that have been reported for similar azo compounds.

The data were used to construct the Arrhenius plot shown in Fig. 1. The results of dilatometric rate determinations by earlier workers<sup>3,4</sup> also are indicated. The following rate expression is obtained

$$K(\text{sec.}^{-1}) = 1.17 \times 10^{19} e^{-37,300/RT}$$

The activation energy obtained here, 37.3 kcal., agrees within experimental error with that reported by Lewis and Matheson,<sup>3</sup> 35.8 kcal. However, neither of these values agrees well with that reported by Ziegler, Deparade and Meyer,<sup>4</sup> 30.9 kcal. By reference to Fig. 1 it can be seen that the discrepancy in activation energy might be regarded simply as a discrepancy in the rate of decomposition at 80°. However, a preferable explanation is that it results from the influence of the solvent. The activation energies reported here, and by Lewis and Matheson, were determined using hydrocarbon solvents, while that low value was determined using nitrobenzene as solvent. Ziegler, Deparade and Meyer give the result of a determination of the decomposition rate at 80°

in a hydrocarbon solvent, undecane; that result falls squarely on the line shown in Fig. 1.

The pre-exponential factor obtained here is  $1.17 \times 10^{19}$ . The corresponding entropy of activation, under the assumption that the reacting solution is ideal, is 28.2 e.u. While not unprecedented, these values are uncommonly large. They are entirely plausible, however, upon consideration that (1) they apply to the decomposition of an unstable compound, (2) resulting in an increased number of molecules, (3) including nitrogen, which has a high molar entropy.

## THE EFFECT OF ANILINE AND ITS DERIVATIVES ON OXANILIC ACID

BY LOUIS WATTS CLARK<sup>1</sup>

Department of Chemistry, Saint Mary of the Plains College, Dodge City, Kansas

Received September 19, 1960

It has long been known that the first two members of the homologous series of dicarboxylic acids, oxalic acid and malonic acid, readily undergo decarboxylation when heated either alone or in certain solvents. Recently the mechanisms of both reactions have been established on the basis of kinetic studies.<sup>2</sup> It appears highly probable that the rate-determining step of both reactions is essentially the same, namely, the formation, prior to cleavage, of a transition complex involving coordination between one of the polarized, electrophilic, carbonyl carbon atoms of the un-ionized diacid with an unshared pair of electrons on a nucleophilic atom of a solvent molecule. Since only one carboxyl group is involved in the rate-determining step it would be deduced that mono-derivatives of both acids also should be capable of undergoing decarboxylation in polar solvents according to the same mechanism. This deduction has been confirmed already in the case of the decarboxylation of oxamic acid in several aromatic amines.<sup>3</sup>

Preliminary experiments in this Laboratory recently revealed that oxanilic acid, another mono-derivative of oxalic acid, likewise undergoes decarboxylation when warmed in polar solvents. Since this compound, apparently, has never been the subject of any kind of kinetic study, it was thought worthwhile to carry out an investigation of the kinetics of the reaction in order to ascertain whether or not it proceeded by the same mechanism as that of the other related acids. For this purpose kinetic studies were carried out in this Laboratory on the decarboxylation of oxanilic acid in aniline, *o*-toluidine and *o*-ethylaniline. The results of this investigation are reported herein.

### Experimental

**Reagents.**—(1) The oxanilic acid used in this research was 100.0% pure as revealed by the fact that in every decarboxylation experiment the theoretical volume of CO<sub>2</sub> was obtained. (2) The solvents were reagent grade. Each sample of each solvent was distilled at atmospheric pressure directly into the dried reaction flask immediately before the beginning of each decarboxylation experiment.

- (1) Western Carolina College, Cullowhee, N. C.
- (2) (a) G. Fraenkel, R. L. Belford and P. E. Yankwich, *J. Am. Chem. Soc.*, **76**, 15 (1954); (b) L. W. Clark, *J. Phys. Chem.*, **61**, 699 (1957).
- (3) L. W. Clark, *ibid.*, **65**, 180 (1961).



**Apparatus and Technique.**—The kinetic experiments were conducted in a constant-temperature oil-bath ( $\pm 0.01^\circ$ ) by measuring the volume of  $\text{CO}_2$  evolved at constant pressure. Details are given in a previous paper.<sup>4</sup> Temperatures were determined by means of a thermometer calibrated by the U. S. Bureau of Standards. In each experiment a 0.2948-g. sample of oxanilic acid (the amount required to yield 40.0 ml. of  $\text{CO}_2$  at STP on complete reaction) was introduced in the usual manner into the reaction flask containing about 60 ml. of solvent saturated with dry  $\text{CO}_2$  gas. All atmospheric oxygen was flushed out of the apparatus with a stream of the dry  $\text{CO}_2$  gas, and the experiments were carried out in an atmosphere of  $\text{CO}_2$  in order to prevent oxidation of the solvents during the kinetic experiments.

### Results

In studies on the decarboxylation of oxamic acid in aniline and in *o*-toluidine<sup>3</sup> some experimental difficulties were experienced due to the tendency of the reverse reaction to occur,  $\text{CO}_2$  and formamide recombining to give oxamic acid. In the present studies on the decarboxylation of oxanilic acid no such difficulties were experienced, there being no observable tendency for the reverse reaction to occur. The theoretical volume of  $\text{CO}_2$  was obtained in each decarboxylation experiment. No difference in the rate of reaction at a fixed temperature could be detected when the quantity of solvent used was varied from 50 to 135 g. In the case of each of the solvents used in this investigation the  $\log(V_\infty - V_t)$  was a linear function of time over practically the entire course of the reaction. Results of a typical experiment are shown graphically in Fig. 1.

Duplicate experiments were performed in each solvent at three or four temperatures over about a  $20^\circ$  range. The average rate constants, calculated in the usual manner from the slopes of the experimental logarithmic plots, are brought together in Table I. The parameters of the Eyring equation, based upon the data in Table I, are shown in Table II, along with corresponding data previously obtained for the decarboxylation of oxamic acid.

TABLE I

APPARENT FIRST-ORDER RATE CONSTANTS FOR THE DECARBOXYLATION OF OXANILIC ACID IN THREE AROMATIC AMINES

Solvent	Temp., °C.	$k \times 10^4$ , sec. <sup>-1</sup>	Av. dev.
Aniline	132.46	0.51	$\pm 0.004$
	142.34	2.16	$\pm .01$
	151.78	8.44	$\pm .02$
<i>o</i> -Toluidine	130.47	0.59	$\pm .008$
	141.14	3.20	$\pm .01$
	148.96	8.23	$\pm .02$
<i>o</i> -Ethylaniline	131.66	0.75	$\pm .01$
	142.14	3.18	$\pm .01$
	146.55	5.76	$\pm .03$
	149.80	9.10	$\pm .01$

TABLE II

KINETIC DATA FOR THE DECARBOXYLATION OF OXANILIC ACID AND OXAMIC ACID IN SEVERAL AROMATIC AMINES

Solvent	Oxanilic acid		Oxamic acid <sup>3</sup>	
	$\Delta H^\ddagger$ , kcal./ mole	$\Delta S^\ddagger$ , e.u.	$\Delta H^\ddagger$ , kcal.	$\Delta S^\ddagger$ , e.u.
Aniline	49.8	+46.3	59.7	+68.0
<i>o</i> -Toluidine	47.8	+39.9	53.7	+57.1
<i>o</i> -Ethylaniline	45.5	+34.3		

(4) L. W. Clark, *J. Phys. Chem.*, **60**, 1150 (1956).

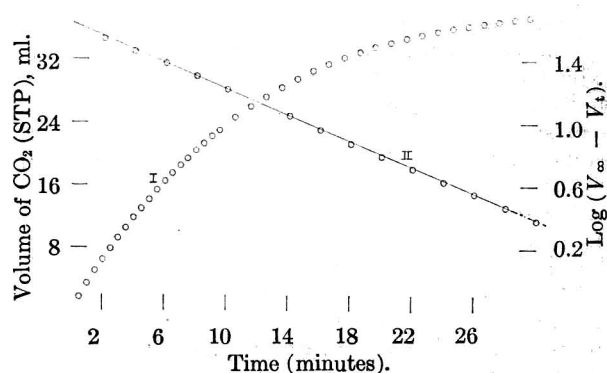


Fig. 1.—Experimental data: decarboxylation of 0.2948 g. of oxanilic acid in 130 g. of aniline at  $160.58^\circ$  (cor.): I, volume of  $\text{CO}_2$  (ml.); II,  $\log(V_\infty - V_t)$ .

### Discussion

Oxamic acid represents the substitution of an amine group for one of the terminal hydroxyl groups of oxalic acid. Inasmuch as the +M effect of the amide group is greater than that of the hydroxyl,<sup>5</sup> the carbonyl carbon atom of oxamic acid which becomes involved in coordination with the nucleophilic atom of the solvent molecule will have a lower effective positive charge than will that of oxalic acid.<sup>3</sup> On the basis of the principle that the activation energy or enthalpy decreases as the attraction between two reagents increases,<sup>6</sup> it would be deduced that, in a given solvent, the  $\Delta H^\ddagger$  for the decarboxylation of oxalic acid would be less than that of oxamic acid, in the event both reactions proceed by the same mechanism. The experimental data shown in lines 2 and 3 of Table III confirm this deduction.

TABLE III

KINETIC DATA FOR THE DECARBOXYLATION OF SEVERAL UNSTABLE ACIDS IN ANILINE SOLUTION

Reactant	$\Delta H^\ddagger$ , kcal./mole	$\Delta S^\ddagger$ , e.u.	$k_{140} \times 10^4$ , sec. <sup>-1</sup>
Malonic acid <sup>7</sup>	26.9	-4.45	50.0
Oxalic acid <sup>2</sup>	40.3	+16.2	1.5
Oxamic acid <sup>3</sup>	59.7	+68.0	0.25
Oxanilic acid	49.8	+46.3	1.5

Oxanilic acid represents the substitution of a phenyl group for one of the amide hydrogen atoms of oxamic acid. Since the phenyl group exerts a strong -I effect its presence will tend to reduce the +E effect on the amide nitrogen atom; therefore, the effective positive charge on the antipodal, polarized, carbonyl carbon atom of oxanilic acid will not be neutralized to as great an extent as it is in oxamic acid. This will mean that oxanilic acid will be a stronger acid than oxamic acid, and the effective positive charge on the carbonyl carbon atom involved in solvation will be higher in oxanilic acid than in oxamic acid. It would be predicted therefore, that, in a given solvent, the  $\Delta H^\ddagger$  would be less for the decarboxylation of oxanilic acid than for that of oxamic acid, provided the two reactions proceed by the same mechanism. Con-

(5) A. E. Remick, "Electronic Interpretations of Organic Chemistry," John Wiley and Sons, Inc., New York, N. Y., 2nd Ed., 1949, p. 57.

(6) K. J. Laidler, "Chemical Kinetics," McGraw-Hill Book Co., Inc., New York, N. Y., 1950, p. 138.

(7) L. W. Clark, *J. Phys. Chem.*, **62**, 79 (1958).

sidering also the greater bulk of the phenyl group as compared with the hydrogen atom, it would be expected that, in the approach of the attacking molecule to the nitrogen atom of the amine, oxanilic acid should encounter more steric hindrance than would oxamic acid—in other words, for the reaction in a given solvent, the  $\Delta S^*$  for the reaction should be less for oxanilic acid than for oxamic acid. Both these predictions are seen to be confirmed by the data in Table III.

In the studies of the decarboxylation of oxamic acid in aniline and in *o*-toluidine<sup>3</sup> it was shown that the presence of a methyl group *ortho* to the amino group has two effects, namely, (1) a +I effect which increases the electron density on the nitrogen atom of the amine giving rise to a decrease in  $\Delta H^*$ , and (2) an *ortho* or steric effect<sup>9</sup> which hinders the approach of the oxamic acid to the nitrogen atom, resulting in a decrease in  $\Delta S^*$ . Analogy suggests that oxanilic acid should behave in this respect in a manner similar to oxamic acid. The experimental data in Table II confirms this expectation. It is seen that, on passing from aniline to *o*-toluidine, a progressive decrease in both  $\Delta H^*$  and  $\Delta S^*$  takes place for both the oxamic acid and the oxanilic acid reactions. A further decrease in the parameters takes place in the oxanilic acid reaction on going from *o*-toluidine to *o*-ethylaniline. For each solvent it will be noted, also, that both  $\Delta H^*$  and  $\Delta S^*$  are lower for the decarboxylation of oxanilic acid than for that of oxamic acid. This is due to the fact that, in the first place, the effective positive charge on the coordinating carbonyl carbon atom of oxanilic acid is greater than it is on that of oxamic acid, and, secondly, the molecule of the former is the more complex.

These circumstances leave little doubt but that oxanilic acid decomposes in polar solvents by the same mechanism as does oxamic acid, oxalic acid and malonic acid.

In aniline solution, the  $\Delta S^*$  for the decarboxylation of oxanilic acid is 18.5 e.u. smaller than it is for that of oxamic acid (see Table III, lines 3 and 4). This difference in  $\Delta S^*$  is commensurate with the increased steric hindrance which would be expected from the substitution of a phenyl group for one of the amide hydrogen atoms of oxamic acid. Since oxanilic acid is considerably larger than oxalic acid the  $\Delta S^*$  for the reaction in aniline would be expected to be larger for oxalic acid than for that of oxanilic acid provided the same number of molecules of each acid were involved in the solvation step. We find, however, that, in aniline, the  $\Delta S^*$  for the oxalic acid reaction is actually 30 e.u./mole less than it is for that of oxanilic acid. It is well known that the dicarboxylic acids in solution associate through hydrogen bonding to form a cluster composed of at least 3–4 molecules.<sup>9</sup> When one of the hydroxyl groups of a dicarboxylic acid is replaced by some other group such as the N-phenyl amide group association evidently can no longer take place past the dimer stage. In view of the great differences in the activation entropies of

these two reactions it may be deduced that, in the case of oxanilic acid, probably only a single molecule coordinates with the solvent, whereas, in the case of oxalic acid, a supermolecule consisting of an association cluster of 3–4 single molecules coordinates. A similar interpretation has been advanced for the oxamic acid data.<sup>3</sup>

In Table III it will be observed that, at 140°, oxalic acid and oxanilic acid decompose in aniline at about the same rate. This evidently is due to the circumstance that, even though the  $\Delta H^*$  for the decarboxylation of oxalic acid is nearly 10 kcal./mole less than it is for that of oxanilic acid, the improved entropy factor in the case of oxanilic acid exactly compensates for this disadvantage.

Further work on this problem is contemplated.

**Acknowledgment.**—The support of this research by the National Science Foundation, Washington, D. C., is gratefully acknowledged.

## HEAT OF NEUTRALIZATION OF STRONG ACIDS BY STRONG BASES IN MIXED WATER-DIOXANE SOLUTIONS<sup>1</sup>

By HIDEHIKO KIDO AND W. CONARD FERNELIUS

Department of Chemistry, The Pennsylvania State University, University Park, Pa.

Received August 4, 1960

In determining formation constants of complexes of organic ligands with metal ions, it is common practice to use the mixed solvent water–dioxane to secure the necessary solubility.<sup>2–7</sup> A careful analysis of this mixed solvent has shown that measurements made with ordinary glass and calomel electrodes and a pH meter can be used to calculate thermodynamic dissociation constants of weak electrolytes and formation constants of complexes.<sup>8</sup> This signifies that even a 75 volume % dioxane–water mixture (mole fraction of dioxane = 0.388) is functioning essentially as a “water” solvent. Indeed, the activity of water at 25° in a 75% dioxane solution differs by only 10% from that of pure water.<sup>9</sup> Nevertheless, many are concerned that the state of hydration of ions in this

(1) This investigation was carried out under contract AT(30-1)-907 between The Pennsylvania State University and the U. S. Atomic Energy Commission.

(2) M. Calvin and K. W. Wilson, *J. Am. Chem. Soc.*, **67**, 2003 (1945).

(3) D. P. Mellor and L. E. Maley, *Nature*, **159**, 370 (1947); L. E. Maley and D. P. Mellor, *Australian J. Sci. Research*, **2A**, 92 (1949).

(4) H. Freiser, R. G. Charles and W. D. Johnston, *J. Am. Chem. Soc.*, **74**, 1383, 1385 (1952); W. D. Johnston and H. Freiser, *Anal. Chem. Acta*, **11**, 201 (1954); T. R. Harkins and H. Freiser, *J. Am. Chem. Soc.*, **77**, 1374 (1955); **78**, 1143 (1956); **80**, 1132 (1958); G. E. Cheney, H. Freiser and Q. Fernando, *ibid.*, **81**, 2611 (1959).

(5) F. Basolo, Y. T. Chen and R. Kent Murmann, *ibid.*, **76**, 956 (1954).

(6) L. G. Van Uitert, C. G. Haas, W. C. Fernelius and B. E. Douglas, *ibid.*, **75**, 455 (1953); L. G. Van Uitert, W. C. Fernelius and B. E. Douglas, *ibid.*, **75**, 457, 2736, 2739 (1953); L. G. Van Uitert and W. C. Fernelius, *ibid.*, **75**, 3862 (1953); **76**, 375 (1954); C. M. Callahan, W. C. Fernelius and B. P. Block, *Anal. Chim. Acta*, **16**, 101 (1957); D. F. Martin and W. C. Fernelius, *J. Am. Chem. Soc.*, **81**, 1509 (1959); B. B. Martin and W. C. Fernelius, *ibid.*, **81**, 2342 (1959).

(7) H. Irving and H. Rossotti, *Acta Chem. Scand.*, **10**, 87 (1956).

(8) L. G. Van Uitert and C. G. Haas, *J. Am. Chem. Soc.*, **75**, 451 (1953); L. G. Van Uitert and W. C. Fernelius, *ibid.*, **76**, 5887 (1954).

(9) F. Hovorka, R. A. Schaefer and D. Dreisbach, *J. Am. Chem. Soc.*, **58**, 2264 (1936).

(8) L. P. Hammett, “Physical Organic Chemistry,” McGraw-Hill Book Co., Inc., New York, N. Y., 1940, p. 204.

(9) W. Hückel, “Theoretical Principles of Organic Chemistry,” Vol. II, Elsevier Pub. Co., New York, N. Y., 1958, p. 329 *et seq.*

solvent may be different from that in water.<sup>10</sup> Determinations of the heat of neutralization of strong acids by strong bases in solutions of dioxane-water varying from 0 to 75 volume % dioxane show a variation of only 2.4%. The condition of solvation of the proton and hydroxide ion must thus differ only by very little in the two solvents.

#### Experimental

The apparatus and procedures for enthalpy titrations are essentially those described by Jordan and Alleman.<sup>11</sup> For each run, 100 ml. of 0.01 M sodium hydroxide in the given solvent was titrated with 1.0M hydrochloric acid in the same solvent. The results assembled in Table I are the average of 5-9 determinations at each mole fraction of dioxane.

TABLE I

#### HEATS OF NEUTRALIZATION IN WATER-DIOXANE

Dioxane		$\Delta H_{\text{neut.}}$
Vol. %	Mole fr.	
0	0.00	13.57 $\pm$ 0.02
25	0.066	13.65 $\pm$ 0.14
50	0.174	13.70 $\pm$ 0.04
75	0.388	13.89 $\pm$ 0.04

(10) Private communications.

(11) J. Jordan and T. G. Alleman, *Anal. Chem.*, **29**, 9 (1957).

## SOLUBILITY AND THERMODYNAMIC FUNCTIONS OF ETHYLENE IN DIETHYL SULFATE

BY A. M. TRUCHARD, H. G. HARRIS AND  
D. M. HIMMELBLAU

Department of Chemical Engineering, The University of Texas, Austin  
12, Texas

Received October 24, 1960

As part of a study of the reaction of olefins with sulfuric acid, a thorough investigation of the solubility of ethylene in diethyl sulfate has been made. From the solubility data the partial molal heats and entropies of solution have been calculated.

(a) **Apparatus.**—The experimental apparatus consisted of two calibrated volumetric bulbs which contained approximately equal volumes of gas after 200 ml. of diethyl sulfate had been added to the larger bulb. The flasks were immersed in a thermostat (good to  $\pm 0.05^\circ$ ) and attached to a mercury manometer. The system was evacuated by prolonged pumping, and ethylene at about 2 atm. pressure was added to the empty smaller flask. Pressures in the system were measured, and then the ethylene was admitted to the bulb containing the diethyl sulfate. The system was allowed to reach equilibrium while being stirred.

For each temperature successive additions of ethylene were brought into contact with the diethyl sulfate at pressures ranging from 50 to 1300 mm. Plots of corrected partial pressure of ethylene vs. mole fraction ethylene dissolved in diethyl sulfate could be fit with excellent precision by straight lines. The diethyl sulfate was Eastman practical grade purified by washing with  $\text{Na}_2\text{CO}_3$  solution and drying with  $\text{CaCl}_2$ . At temperatures much higher than  $100^\circ$  diethyl sulfate begins to degrade so the maximum temperature reported is  $80^\circ$ .

(b) **Results.**—Table I shows the Henry's law constants from 0 to  $80^\circ$  computed as  $\mathcal{K} = p$  (atm.)/ $x$  (mole fraction). Since the logarithms of the Henry's law constants were not exactly a linear function of temperature, a curve to fit the values of  $\mathcal{K}$  of the form

$$\log \mathcal{K} = 3.04666 - 0.132845 \times 10^3 \left(\frac{1}{T}\right) - 5.9302 \times 10^{-4} \left(\frac{1}{T}\right)^2 \quad (1)$$

was calculated by the least squares technique to give an excellent fit (maximum deviation from 0 to  $80^\circ$  was 1.51%). With the aid of this equation, the partial molal heats of solution were calculated as

$$(\bar{H}_L^0 - \bar{H}_G) = 2.303R \left[ \frac{\partial \log \mathcal{K}}{\partial (1/T)} \right] \quad (2)$$

and the partial molal entropies of solution were calculated as

$$(\bar{S}_L - \bar{S}_G) = -R \left( \frac{\partial \ln a_L}{\partial \ln x_L} \right)_T \left( \frac{\partial \log \mathcal{K}}{\partial \log T} \right) \quad (3)$$

The calculated thermodynamic values are listed in Table I. Nomenclature and discussion related to equations 2 and 3 is in reference 1.

TABLE I

#### HENRY'S LAW CONSTANTS AND THERMODYNAMIC DATA FOR ETHYLENE

$t$ , $^\circ\text{C}$ .	$\mathcal{K}$ (atm./ mole fr.) In $\text{Et}_2\text{SO}_4$	$-(\bar{H}_L^0 - \bar{H}_G)$ , cal./g. mole <sup>a</sup> In $\text{Et}_2\text{SO}_4$		$-(\bar{S}_L - \bar{S}_G)$ , cal./ (g. mole)( $^\circ\text{K}$ ) <sup>b</sup> In $\text{Et}_2\text{SO}_4$	
		2430	5260	17.9	36.4
0	68.71	2430	5260	17.9	36.4
20	92.24	2300	4390	16.8	33.3
25	98.73 <sup>c</sup>	2270	4170	16.7	32.6
30	105.1	2240	3880	16.6	31.7
40	117.3	2180	3340	16.4	29.9
60	144.2	2080	2100	16.1	26.0
80	172.8	1995	850	15.9	22.3

<sup>a</sup> Standard State: "infinite dilution." <sup>b</sup> Standard State: mole fraction = 1.0. <sup>c</sup> Calculated.

#### Discussion

The reliability of the Henry's law constants was excellent since the standard deviation for  $\mathcal{K}$  for any temperature was less than 0.01. The accuracy of the apparatus was tested by measuring the solubility of ethylene in water at  $0^\circ$ .  $\mathcal{K}$  was determined to be  $5.28 \times 10^3$ , which is 4.5% less than the value of Winkler.<sup>2</sup> Winkler's value may be high, however, since the data of Davis and McKetta<sup>3</sup> and Bradbury, McNulty, Savage and McSweeney,<sup>4</sup> when extrapolated to lower temperatures, yields a lower value (less than  $5 \times 10^3$ ) for  $\mathcal{K}$ .

The partial molal heats and entropies of solution of ethylene in diethyl sulfate do not change as much with temperature as do corresponding values for ethylene dissolved in water, which have been calculated from the data in reference 5, although the trend with temperature is the same. The values of  $(\bar{S}_L - \bar{S}_G)$  in diethyl sulfate are one-half as negative as those in water and correspond closely to the values shown in Table II for other non-polar compounds. The values in Table II have been computed from the data of Horiuti.<sup>6</sup>

(1) D. M. Himmelblau, *J. Phys. Chem.*, **63**, 1863 (1959).

(2) L. W. Winkler, *Z. physik. Chem.*, **55**, 350 (1906).

(3) J. E. Davis and J. J. McKetta, *J. Chem. Eng. Data*, **5**, 374 (1960).

(4) E. J. Bradbury, D. McNulty, R. L. Savage and E. E. McSweeney, *Ind. Eng. Chem.*, **44**, 211 (1952).

(5) D. M. Himmelblau and E. Arends, *Chem. Ing. Tech.*, **31**, 791 (1959).

An interpretation of the thermodynamic data is that the quasi-ice-like structures caused by the dissolution of ethylene in water are more rigid or penetrate to a greater distance from the ethylene molecule than those created in diethyl sulfate and other non-polar compounds. Presumably this is due to the hydrogen bonding in water. Furthermore, the type of structure in the non-polar compounds is quite stable as the temperature changes; the thermodynamic functions for the compounds listed in Table II have essentially constant values over the temperature range for which data are available. The arrangement of the structure surrounding the ethylene molecule in diethyl sulfate appears to be independent of the nature of the solvent for both diethyl sulfate and those compounds listed in Table II.

(6) J. Horiuti, *Bull. Inst. Phys. Chem. Research (Tokyo)*, **9**, 697 (1930); *Sci. Papers Inst. Phys. Chem. Research (Tokyo)*, **17**, 125 (1931).

TABLE II

PARTIAL MOLAL HEATS AND ENTROPIES OF SOLUTION FOR ETHYLENE DISSOLVED IN NON-POLAR SOLVENTS<sup>a</sup> (0 TO 40°)

Solvent	$-(\bar{H}_L^0 - \bar{H}_G)$ , cal./g. mole <sup>b</sup>	$-(\bar{S}_L - \bar{S}_G)$ , cal./ (g. mole) <sup>(°K.)<sup>c</sup></sup>
CCl <sub>4</sub>	2420	16.5
CH <sub>3</sub> COOCH <sub>3</sub>	2260	16.5
C <sub>6</sub> H <sub>6</sub>	2220	16.2
(CH <sub>3</sub> ) <sub>2</sub> CO	2130	16.1

<sup>a</sup> Calculated from data of reference 6. <sup>b</sup> Standard State: "infinite dilution." <sup>c</sup> Standard State: mole fraction = 1.0.

**Acknowledgment.**—This research was supported by a grant from the Petroleum Research Fund administered by the American Chemical Society. Grateful acknowledgment is hereby made to the donors of this fund.

## COMMUNICATION TO THE EDITOR

### SPECIFIC REFRACTIVE INCREMENT OF POLYPROPYLENE IN $\alpha$ -CHLORONAPHTHALENE

Sir:

We have determined the specific refractive increment for solutions of isotactic polypropylene in  $\alpha$ -chloronaphthalene at 125°. Our weighted average value is  $dn/dc = -0.189 \pm 0.005$  cc./g. for mercury green (5460 Å.) light. The measurements were made using a differential refractometer of the Debye<sup>1</sup> design as modified by Schulz.<sup>2</sup> The instrument was calibrated with aqueous solutions of potassium chloride using the data of Stamm.<sup>3</sup>

The value obtained is consistent, as expected, with measured values of  $dn/dc$  for the system polyethylene- $\alpha$ -chloronaphthalene.<sup>4-6</sup> It is also in good agreement with that reported by Chiang,<sup>7</sup>  $-0.188$  cc./g. at 140°. (Chiang's value becomes  $-0.191$  cc./g. at 125° using a temperature coefficient equal to that for the polyethylene- $\alpha$ -chloronaphthalene system, approximately  $+0.0002$  cc./g.°C.)

However, our results do not support the value of  $-0.216$  cc./g. at 145° reported by Parrini<sup>8</sup> (which becomes  $-0.220$  cc./g. when similarly corrected

to 125°) or the value of  $-0.227$  cc./g. at 125° reported by Kinsinger and Hughes.<sup>9</sup> Although Parrini's value was measured directly, that of Kinsinger and Hughes was obtained from an extrapolation to 125° of values measured at 25° and 50°, and was supported by calculations based on the Gladstone-Dale relationship which, as the authors noted, is highly unlikely to be applicable to hydrocarbon polymer- $\alpha$ -chloronaphthalene systems. Kinsinger<sup>10</sup> also used a value of 1.532 for the refractive index of  $\alpha$ -chloronaphthalene at 125°. The correct value for this quantity for mercury green light is  $1.594 \pm 0.0002$ , as measured several times in our laboratory over the past decade, and supported by calculation from the data of Auwers and Frühling.<sup>11</sup>

Until the apparent discrepancy is resolved between values of  $dn/dc$  reported by ourselves and Chiang and those reported by Parrini and Kinsinger, it would appear advisable to apply with caution the viscosity-molecular weight relations published for the system polypropylene- $\alpha$ -chloronaphthalene.<sup>7-9,12</sup>

POLYCHEMICALS DEPARTMENT  
E. I. DU PONT DE NEMOURS AND CO., INC.  
DU PONT EXPERIMENTAL STATION  
WILMINGTON 98, DELAWARE  
F. W. BILLMEYER, JR.  
RECEIVED DECEMBER 6, 1960

- (1) P. P. Debye, *J. Applied Phys.*, **17**, 392 (1946).
- (2) G. V. Schulz, O. Bodmann and H.-J. Cantow, *J. Polymer Sci.*, **10**, 73 (1953).
- (3) R. F. Stamm, *J. Opt. Soc. Am.*, **40**, 788 (1950).
- (4) F. W. Billmeyer, Jr., *J. Am. Chem. Soc.*, **75**, 6118 (1953).
- (5) R. Chiang, *J. Polymer Sci.*, **36**, 91 (1959).
- (6) V. Kokle, F. W. Billmeyer, Jr., L. T. Muus and E. J. Newitt, presented at the 139th National Meeting of the American Chemical Society, St. Louis, Mo., April 23, 1961.
- (7) R. Chiang, *J. Polymer Sci.*, **28**, 235 (1958).
- (8) P. Parrini, F. Sebastiano and G. Messina, *Makromol. Chem.*, **38**, 27 (1960).

- (9) J. B. Kinsinger and R. E. Hughes, *J. Chem. Phys.*, **63**, 2002 (1959).
- (10) J. B. Kinsinger, Ph.D. Thesis, University of Pennsylvania, 1958.
- (11) K. V. Auwers and A. Frühling, *Liebig's Ann.*, **422**, 192 (1921), reproduced in part in the "International Critical Tables," Vol. VII, p. 49.
- (12) S. Shyluk, paper presented at the 138th National Meeting of the American Chemical Society, New York, N. Y., September, 1960.

BOND ALTERNATION IN CYCLOOCTADECANON  
 BOND AND ITS INFLUENCE ON THE ELECTR  
 BOND FISSION IN THE OXIDATIONS OF 2-  
 BOND IN ACID SILICATES AND PHOSPHATE  
 BOND LENGTHS IN LONG CONJUGATED MOLE  
 BOND REFRACTIONS.\*  
 BOND. ASSOCIATION IN ETHER SOLUTION  
 BOND.\*  
 BONDING AND RELATED PHENOMENA BY ULT  
 BONDING AND SEMICONDUCTIVITY RELATIO  
 BONDING IN ACETYLENE AND CARBON DIOX  
 BONDING IN ANILINES AND PHENOLS.\*  
 BONDING IN MONO-ANIONS OF STERICALLY  
 BONDING OF ACRIDONE AND 9- AMINO ACR  
 BONDING. (GER.)  
 BONDING.\* DIMETHYL PHOSPHINO- ALUMIN  
 BONDS AND ELECTRONEGATIVITY OF SILYL  
 BONDS BY ISOTOPIIC EXCHANGE.\*  
 BONDS CARBON- CARBON AND CARBON- OXY  
 BONDS IN COMPLEXES.\*  
 BONDS.\*  
 BORANES WITH OLEFINES AND DIENE HYDR  
 BORATE MINERALS.\*  
 BORATE.\*  
 BORATE.\*  
 BORATE.\*  
 BORATES AND THEIR CONVERSION  
 BORIC ACID ESTERS.  
 BORIC ANHYDRIDE.\*  
 BORIC OXID

BOND ON THAT OF TURBULENT BURNING.\*  
 CONDENSATIONS OF 1- ALKYL BUTADIENES WITH UNSYMMETRICAL DIENOP  
 LID-3-YLI-1+1- DIPHENYL BUTAN-2-ONE.\*  
 ATION OF TRACE WATER IN BUTANE BY GAS CHROMATOGRAPHY.\*  
 CTS AND THE KINETICS OF BUTANE CRACKING INITIATED BY ADDING  
 F BROMINE ON 2- PHENYL- BUTANOL-2 OR 2- PHENYL- BUTENE-2.\*  
 ROGENATION OF 2- METHYL BUTENE-1 IN THE PRESENCE OF PLATINUM  
 BUTANOL-2 OR 2- PHENYL- BUTENE-2.\*  
 -(2-ETHYLHEXYL) MONO-S-BUTOXIDE IN HYDROCARBONS. PREPARATI  
 ON OF CHROMIUM TETRA-T-BUTOXIDE WITH ALCOHOLS.\*  
 ENE. CHROMIUM TETRA-T-BUTOXIDE. REACTION OF CHROMIUM TETR  
 FARED SPECTRA OF TERT- BUTYL ALCOHOL AND TERT- BUTYL ALCOHO  
 BUTYL ALCOHOL AND TERT- BUTYL ALCOHOL.\*  
 ETHYL BUTYRATE WITH T- BUTYL CHROMATE.\*  
 NES TRANS-2- BROMO-5-T- BUTYL CYCLOHEXANONE.\*  
 EPOXIDATION OF BUTYL OLEATE BY HYDROGEN PEROXIDE.\*  
 REACTIONS OF T- BUTYL PERESTERS. REACTIONS OF PERES  
 HENYL ETHANOL AND A- T- BUTYL- BENZYL ALCOHOL.\*  
 ENCE OF POLY-PARA-TERT- BUTYL- PHENYL METHACRYLATE SOLUTIONS  
 RESINS SOLUBLE IN OIL. BUTYL- PHENYL- FORMALDEHYDIC RESINS.  
 ZATION OF 1,4- DICHLORO BUTYNE-2 AND SYNTHESIS EFFECTED ON I  
 ROXIDE ON 1,4- DICHLORO BUTYNE-2.\*  
 REACTION OF ETHYL BUTYRATE WITH T- BUTYL CHROMATE.\*  
 AND OF PROPIONATES AND BUTYRATES OF COPPER, MERCURY, AND LE  
 OXO-GAMMA-2- XANTHENYL BUTYRIC ACID INTO 2+3- BENZO XANTHON  
 BY-PRODUCTS FROM RICE BENEFICIATION  
 C- FLUORO CLRARINE. CONSTITUTION OF  
 DESFORMYL COMPOUNDS OF C- NITROSO COMPOUNDS IN SOLUTION.\*  
 ASSOCIATION OF TRANS- DIMERIC C- NITROSO COMPOUNDS IN SOLUTION.\*  
 E OF CAP...

YOUNJR-60-EGI  
 GOUTH -60-BAC  
 SHIGDN-60-NMB  
 JONEJR-60-QOC  
 RYSKYJ-60-SIH  
 SALEL -60-ABL  
 GILLRG-60-CBR  
 BRANJC-60-EMB  
 YAMAT -60-PST  
 DEARJC-60-SHB  
 GOODCH-60-BSR  
 MCLCAD-60-CDH  
 DEARJC-60-SHB  
 EBERL -60-PHR  
 ZANKV -60-LAF  
 BAERN -60-HEA  
 BURGAB-60-PAB  
 PONOVA-60-VFS  
 VASIVG-60-TSC  
 VUKSMF-60-PTC  
 VLCEAA-60-PSB  
 SHIGDN-60-NSC  
 MKHBM-60-CCS  
 CHRICL-60-CCS  
 STRUUT-60-CND  
 HOLLAK-60-RAT  
 BIENA -60-RDS  
 MOSSKC-60-TAT  
 MKHBM-60-DBC  
 -60-DBC  
 -MSV

SAMPLE OF  KEYWORD INDEX

announcing a new publication

# CHEMICAL TITLES

*the express service for increasing "current awareness" of new chemical research*

● Starting in January 1961, CHEMICAL TITLES will be issued twice each month with each issue reporting approximately 3000 titles from the most recent chemical research. This service provides a current author and keyword index to selected chemical journals and is intended to fill the void between primary publication and the appearance of abstracts.

Taken from 575 journals—110 Russian—of pure and applied chemistry, these titles are listed for maximum convenience of use. The first part is a permuted title index in which keywords from

each title are arranged alphabetically with each keyword in full or partial context. The second part is an alphabetical index of authors together with full titles of papers and journals in which they appear. You can find a source in a minute.

Timeliness matches ease of use. All titles are found in the listing *within two weeks of the time they are received* in the offices of The Chemical Abstracts Service, the publisher. No other index or alerting service provides such prompt and complete coverage.

Prices and discounts follow:

	Base Rate	Rate per Volume College and University	ACS Member
1st-10th subscriptions (each)	\$65	\$50	\$50*
Additional 11th-25th subscriptions (each)	45	45	...
26th and each succeeding subscription	30	30	...

\* Single subscription only

ORDER FROM: CIRCULATION DEPARTMENT • AMERICAN CHEMICAL SOCIETY  
1155 SIXTEENTH STREET, N.W. • WASHINGTON 6, D.C.



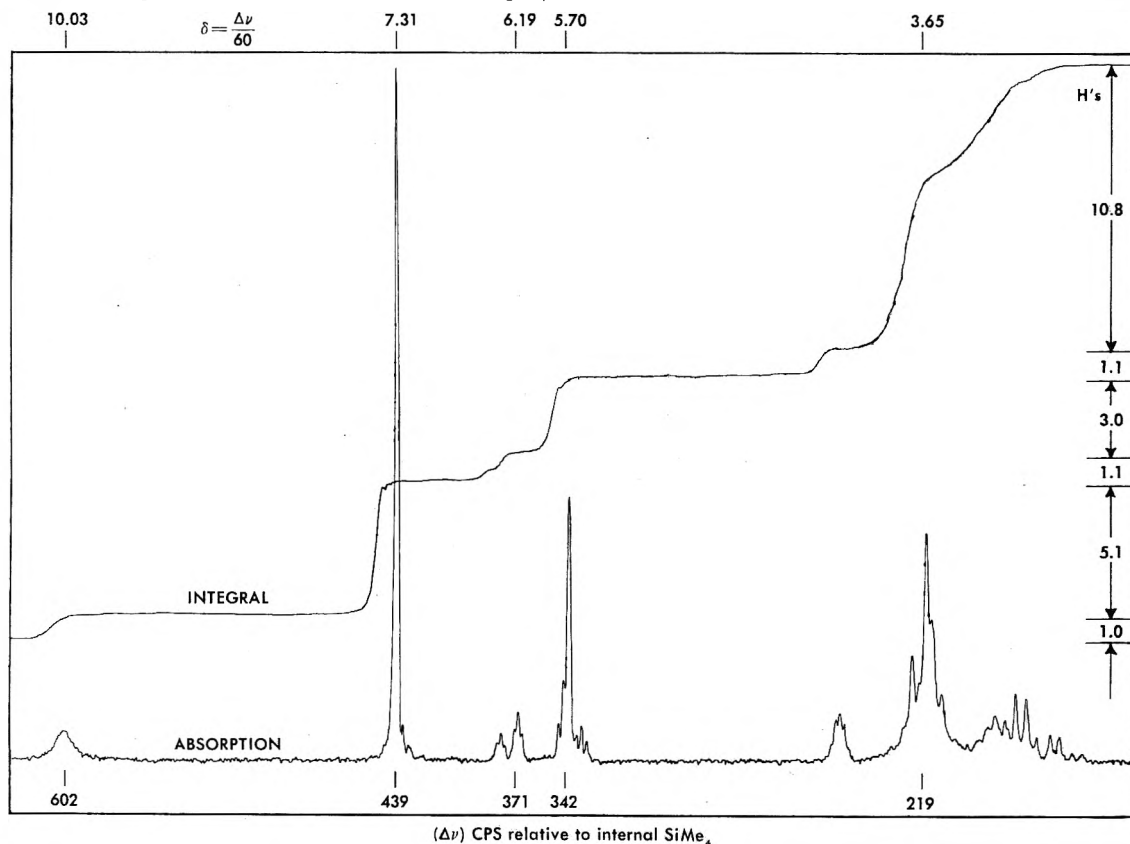
# PROTON COUNTING IN COMPLEX MOLECULES BY NMR SPECTROSCOPY

A total count of protons in a molecular species can now be accomplished by high resolution NMR spectroscopy, using electronically integrated spectra. This promises to be of great value in chemical structure work because it allows the number to be fixed to the nearest proton. By contrast, calculations made solely from molecular weight determinations and hydrogen analyses are frequently accurate only within several hydrogen atoms.

## STRUCTURAL INFORMATION FROM PROTON COUNTING

**Interpretation:** An organic compound known to be a monocarboxylic acid was examined as a  $\text{CDCl}_3$  solution. The 60 mc spectrum exhibits the signal from the carboxylic acid hydrogen at  $\delta = 10.03$ . Using this signal as an internal standard corresponding to one proton, the integral curve reveals that the peak at  $\delta = 7.31$ , characteristic of hydrogen on aromatic rings, is equivalent to five protons. The signals around  $\delta = 6.19$  and those in the group

around  $\delta = 5.70$  correspond to four protons and are typical of olefinic hydrogen. The remaining signals are in the region of the spectrum which is characteristic of protons on aliphatic carbon and are equivalent to twelve hydrogens making the total proton count equal to 22. This confirms the empirical formula  $\text{C}_{21}\text{H}_{22}\text{O}_2$  obtained from combustion data.



For literature which fully explains the 100 mc EPR Spectrometer and its application to basic and applied research in physics, chemistry, biology and medicine, write the Instrument Division.



**VARIAN associates**  
PALO ALTO 52, CALIFORNIA